

BULGARIAN CHEMICAL COMMUNICATIONS

2017 Volume 49 / Special Issue B

Commemorative Issue in Honor of Acad. Bogdan Kurtev on the occasion
of his 100th birth anniversary

*Journal of the Chemical Institutes
of the Bulgarian Academy of Sciences
and of the Union of Chemists in Bulgaria*

Professor Bogdan Jordanov Kurtev, Member of BAS - Builder of Modern Organic Chemistry in Bulgaria



16.06.1917-03.12.1995

The career of Professor Bogdan J. Kurtev as a leading chemist in Bulgaria began in 1958 when at the age of 41 he was appointed to the responsible post of Director of the Chemical Institute at the Bulgarian Academy of Sciences (BAS). In 1960 this institute was split into two: Institute of General and Inorganic Chemistry and Institute of Organic Chemistry (IOC). B. Kurtev became the first Director of the latter and remained on this post till 1989. Upon his appointment B. Kurtev had the experience of seven years teaching organic chemistry as Docent at the Chair of Organic Chemistry, Vice Dean of the Physical Mathematical Faculty and a Ph.D. degree (1950) obtained in the prestigious Moscow Chemical Technological Institute “D. I. Mendeleev” under Acad. V. M. Rodionov on the synthesis of β -naphthyl- β -amino acids by means of the Rodionov reaction and uracils derived from the amino acids.



Prof. Vladimir Rodionov with collaborators.

His scientific capacity is illustrated by his appointment as assistant in organic chemistry by Professor D. Ivanov in Nov 1940 immediately following his graduation taking into account the limited number of positions at the time.

In the first postwar decades several challenges faced Bulgarian Chemistry. The sheer increase of number of students trained was dramatic. Before the war Sofia University the single provider of chemical education had an input per annum of *ca.* 20 students, in 1953 the number increased to 120, larger numbers were taught in the new Higher Institute of Chemical Technology and many other institutions. The scope of research fields rapidly increased with the demands of fast growing industry in socialist Bulgaria.

Organic chemistry itself underwent a great transformation. The perception of organic chemists as skillful experimenters of exceptional memory changed with the development of theoretical methods of explaining and predicting chemical behavior of organic compounds. No less was the importance of the new “physical” or “instrumental” methods. The handicap of Stalin’s purging science of “idealistic” theories in the early 1950’s, such as Linus Pauling’s resonance theory, took more than a decade to shake off in organic chemistry education. Feeling the importance of modern interpretation of organic chemistry, in 1957 B. Kurtev developed and taught the advanced course “Structure and Reactivity of Organic Compounds” - first of its kind in Bulgaria. It encompassed stereochemistry, conformational analysis, mechanisms of organic reactions, quantitative correlations of reactivity (the basis of QSAR in more recent times).

B. Kurtev proved exceptionally suitable to meet these challenges as person of very high intelligence, well versed in most fields of chemistry besides organic, of sound administrative skills. As Director of IOC he interviewed each appointee; an important characteristic for him was the dedication towards research which he tested by inquiring about their Master’s Thesis even the m.p. of compounds obtained. His integrity and sense of justice were beyond dispute. The following example was typical - in 1962 in Prague the IUPAC Conference on Natural Products was attended by elite of organic chemistry. The lab of organic synthesis suggested

the participation of B. Kurtev, J. Stefanovsky and I. Pojarlieff. The central management of BAS approved a grant for the Director; the two young scientists were permitted to attend on their own expenses. B. Kurtev said this was unfair and shared his grant in three equal parts. Witness of the enthusiasm of our lab remain the autographs of Nobel Prize winners Ruzicka, Prelog, Woodward, Robinson, Todd, Barton written on the book *Perspectives in Organic Chemistry* edited by Sir Alexander Todd. More importantly he used contacts with distinguished scientists from the other side of the iron curtain to obtain grants for talented young researchers interested in a particular field. Personal applications/invitations were forbidden by default. B. Kurtev would ask for a nameless invitation to IOC and had the authority to make the Party bureau nominate the prearranged person. Upon rare occasions the Party changed the nomination which, however, destroyed the deal. B. Kurtev could be successful in his policies even at the expense of by-passing rules because of his authority and trust by the Party. I believe loyalty to socialism was predetermined by the fact that his father Jordan Kurtev was executed without trial in September 1923 as a communist. This happened during the uprising against the fascist coup d'état, shot and thrown from the rocks over river Iskar at the railway station Lakatnik. The father, Jordan Kurtev, worked in the analytical laboratory of the copper mines in nearby Eliseina. He had a degree in chemistry from Sofia University and further education in Germany and Toronto, Canada.

Characteristically B. Kurtev and his coworkers were open to the world, joint research was carried out with labs in Hungary, France, Germany, England, Latvia, Lithuania to mention some.

B. Kurtev was instrumental in much of the rapid development of the chemical sciences in BAS as Head of the Department of Chemical Sciences of BAS since 1962 while holding his Directorship of IOC simultaneously. The Department evolved into Unified Center of Chemical Sciences in BAS (1973), unified referring to closer links with the Chemical Faculty of Sofia University. B. Kurtev served also as Vice-president of BAS 1971-73. One of the biggest achievements was the generous UNESCO grant for creating a Centre of Phytochemistry (CP) based on the existing powerful labs researching ethereal oils, alkaloids, lipids, proteins, enzymes. This provided the IOCCP with a new building and modern infrastructure e.g. the first mass spectrometer in Bulgaria.

Before and after the war organic chemistry research in Sofia was dominated by the outstanding figure of Professor D. Ivanov elaborating on the "officially named" Ivanov reaction, the theme of the Ph.D. theses of many future professors. Professor B. Kurtev never published a paper with D. Ivanov; after being appointed as assistant at the end of 1940 he was soon conscripted first in the cavalry regiment at Breznik and then in an antiaircraft artillery unit in Dedeagach (now Alexandroupoli) on the Aegean. After the war he was transferred as assistant to the Chair of Medical Chemistry at the Higher Institute of Medicine under Professor Alexander Spassow with whom in 1946 he published in German his first two papers on the preparation of 3-pyrazolidones from phenylhydrazides of β -hydroxy acids.

Most broadly the scientific contributions of Professor Kurtev can be grouped in the following fields:

A. Mechanisms, stereochemistry, and synthetic applications of aldol type reactions where-by a C-C bond is formed by base or acid catalysed addition of a C-H to a carbonyl or imine double bond

The following list is in roughly chronological order. The names in parenthesis are the main coworkers. In many cases the products contain a 1,2-diphenylethane skeleton disubstituted in the 1 and 2 positions.

Reaction of Schiff bases and hydramides with esters of phenylacetic acids catalyzed by anhydrous $AlCl_3$ (N. Mollov). Kurtev and Mollov first used this catalyst for such condensations creating a convenient method of preparing the *erythro* esters in good yields. The stereoselectivity was shown to be due to equilibration of the diastereomers and lower solubility of the preferred isomer.

Base catalysis by alkaline alcoholates, amides and hydrides of the above reaction including the dimethylamides of phenylacetic acid (E. Simova, J. Stefanovski) has afforded high yields and *erythro/threo* selectivities in cases ranging from 10:1 to 1:10.

The Rodionov reaction (I. Pojarlieff) provides β -amino acids by heating an aromatic aldehyde (aliphatic give lower yields) with malonic acid in an ethanol solution of ammonia. The new pair acetaldehyde and methylmalonic acid was chosen to obtain a 1,2-dimethyl analogues to the 1,2-diphenyl system. Low yields and low selectivity prompted a stereospecific synthesis from the isomeric 2,3-dimethylsuccinic acid *via* the

Hoffmann rearrangement of the monoamides – yielding relative configurations and high yields of the pure isomers.

The Perkin Reaction (C. Krachanov) yields cinnamic acid upon heating an aromatic aldehyde in acetic anhydride in the presence of base. The reaction goes through the aldol intermediate - the respective β -hydroxy anhydride. Kinetic results of Kurtev and Krachanov for the elimination stage of the *erythro/threo* isomers of the product from benzaldehyde and phenylacetic acid indicated larger activation energy (larger temperature coefficient) for the elimination stage, *i.e.* at low temperatures the elimination would be arrested which led to the discovery of a new method of preparing β -hydroxy- α,β -diphenylpropionic acids. It showed *erythro* selectivity opposite to the Ivanov reaction.



With Prof. Christo Kratchanov.

Significant contributions to the mechanism and synthetic applications were also made to important organic reaction: Reformatski (M. Mladenova, B. Blagoev), Ivanov reagents and reaction (M. Mladenova, B. Blagoev), Low temperature Claisen Condensation (C. Kratchanov, N. Kirtchev), Erlenmeyer-Plöchl (I. Kavrakova, E. Simova).

B. Cyclization reactions

The above reactions yielded as products open-chain diastereomer derivatives which could be readily converted into heterocycles of interest *per se* (β -lactams, dihydouracils, tetrahydro-1,3-oxazines, and 1,3-oxazin-2-ones, to name a few). Such cyclizations were also studied to assign the relative configurations (*erythro/threo*). In cases of stereospecific ring closure the *cis-trans* isomerism of heterocycles obtained present direct proof of the configuration of initial open-chain diastereomers.

In many cases the configuration had to be deduced from the rate of ring-closure presuming different stabilities of transition or ground states. The formation of β -lactams from β -phenylamino- α,β -diphenylpropionic acids (N. Mollov, E. Simova, J. Stefanovski), N \rightarrow O benzoyl migration in 3-aminopropanols (N. Mollov, A. Orahovats), dihydouracils (M. Lyapova, I. Pojarlieff), present such examples.



A part of Lab. Mechanism of Organic and Enzyme Reactions and Organic Synthesis, 1980. The first row from left to right: Prof. Blagoy Blagoev, Prof. Nina Berova, Prof. Bogdan Kurtev, Assoc. Prof. Iva Blagoeva, Prof. Jury Stefanovsky.

This research stimulated the interest of Professor Kurtev into the factors governing reactivity in cyclization reactions. As early as 1959 with Mollov and Simova he applied the concept of favoured conformations along the lines of what became known as the Winstein-Holness equation to assign configurations of β -aniline- α,β -diphenylpropionic acids. The reactivities were quantified by measuring kinetics of cyclization and their activation parameters (I. Pojarlieff, I. Blagoeva, A. Orahovats, V. Fodor).

Expanding the substituent pattern in the open chain compounds allowed important contributions to be made in understanding the *gem*-dimethyleffect (I. Pojarlieff, I. Blagoeva). This steric effect is readily understood in small ring formation, but puzzling in six or five membered rings because hindrance by substituents instead of decreasing increases the rates of cyclizations. The driving force is actually the fact that *syn* interactions between the substituents in the open chain actually decrease in the ring since they become interactions of the members of the ring itself, *e.g.* the *syn* interaction of two methyl groups of 0.8 kcal/mol compared to the *anti* form is

relieved if butane is incorporated in the cycle chain. That enthalpy is the driving force of the effect was confirmed by successful correlations of seven reaction series of the *gem* effect with steric strain energies and following more precise molecular mechanics studies of P. Ivanov.

Stereoelectronic effect in N→O and O→N acyl migrations (M. Lyapova, I. Pojarlieff) were nicely demonstrated by means of the 1,2,3-triphenylpropane system developed by Kurtev and Lyapova where *N*-methylation in 1,3-aminopropanols inversed reactivities of the stereoisomers. The examples were included in Deslongchamps's book on stereoelectronic effects. These effects were later shown to apply in the case of 1,3-aminopropan-thiols by V. Kurteva, M. Lyapova, I. Pojarlieff.



With Assoc. Prof. Maria Lyapova and Prof. Jury Stefanovsky.

C. Stereochemistry

Characteristically B. Kurtev demanded precision in experiment and interpretation. To this end the configuration of a wide range of derivatives was ultimately proven by chemical transformations. Thus the *erythro/threo* assignments of the β -amino- α,β -diphenylpropionic acids were unequivocally established by stereospecific conversion into *meso* and racemic stilbenediamines (J. Stefanovsky). The link between the amino and phenylamino series was established by phenylation of the amino group in a stereospecific reaction (N. Berova, E. Simova).

The resolution of the 1-menthyl esters of β -amino- α,β -diphenylpropionic acids into the four optically active isomers opened a new line of research (N. Berova, J. Stefanovski). The chiral aminopropanols obtained upon reduction proved useful substrates for structure/optical rotation relationships based on the contributions of chiral segments in the various conformations. The

unexpected result transpired that preferred in the *threo* diastereomers were conformations with *syn* phenyl groups which ran against Cram's rule that the two large substituents, *i.e.* the phenyl groups will prefer the *anti* conformation. In 1966 ^1H NMR (G. Fodor, R. E. Reavill, J. Stefanovsky, H. J. Bernstein) obtained large J_{23} for both epimers reliably showing preferred *syn* phenyls in the *threo* isomer. Later this was found to be quite universal *e.g.* work of S. Spassov and gave rise to a host of studies to explain this phenomenon. The extensive and elaborate computational studies of P. Ivanov answered most of the problems.

A versatile branch of the studies of optical activity was the work on Circular Dichroism and Absolute Configuration of key compounds with phenylsubstituents (N. Berova, P. Ivanov, G. Snatzke).



With Prof. Nina Berova



Prof. Gunter Snatzke and Prof. Carl Djerassi in front of IOCCP, Sofia.

The chromatographic behaviour of diastereomers (M. Palamareva, L. Snyder) of great importance for practical purposes was extensively studied from the view point of chromatographic theory and structure of substrates creating rules and computer programs for successful separation of open chain and cyclic compounds.

The geometry and conformations of many heterocyclic systems have been examined by means of NMR (S. Spassov, I. Pojarlieff, A. R. Katritzky). A study of the biologically important dihydrouacil, including dihydroorotic acid, has been widely cited.



With Prof. Katritzky and collaborators; Norwich 1965.

The existence of allylic strain in six-membered heterocycles with an endocyclic *N*-substituted amide group and a neighbouring substituent (I. Pojarlieff, M. Lyapova, A. Orahovats) could explain the significant effects of *N*-substitution on conformational equilibria in tetrahydro-1,3-oxazin-2-ones, hexahydropyrimidine-2-ones and hexahydropyrimidine-2,4-diones. A contribution to atropisomerism (S. Simova, Z. Beresnevičiu) was the assignment of the solution conformations of the atropisomers of some 1-(1-naphthyl)-hexahydro-2,4-dioxo(or 2-thio-4-oxo)-pyrimidines.

D. Applied research

B. Kurtev took active interest and was involved in practically almost all such projects in IOC (with a Centre of Phytochemistry) as well as many projects of the Unified Centre of Chemical Sciences. I will illustrate his activity with one of largest industrial projects of BAS in the 1970's "Bright Acid Copper Plating Agent B-7211" – carried out by a joint team from IOC and IPC (Institute of Physical Chemistry) (I. Juchnovski, I. Pojarlieff, S. Rashkov). For five years the whole

road was undergone from research, developing and implementing the manufacturing of the additive in the dye factory in Kostenetz, Bulgaria. B-7211 was used for the production of ca. 1 500 000 cars annually (Lada, Moskvich, Škoda, Wartburg, Volga, Zaporozhietz) between 1975-1990.



From left to right: Prof. Ivan Juhnovsky, Prof. Ivan Pojarlieff, Prof. Stefan Rashkov.

Our consultations with B. Kurtev were almost weekly and involved both administrative matters and scientific problems. Contrary to the common practice of leading managers to participate as authors of patents only on the merit of their administrative position motivated by financial awards, Professors B. Kurtev and R. Kaishev (Director of IPC) refused to participate as authors. They were forced to break their rules for parity reasons with the Directors from the Lithuanian AS and Soviet Industry Directors in just three patents concerning subsequent versions (BS-1 and BS-2) of the additive B-7211 developed by a joint Bulgarian-Soviet team.

CONCLUSION

The above non exhaustive overview of the work of B. Kurtev, I believe, suffices to name him as a builder of modern organic chemistry in Bulgaria bringing the inheritance of D. Ivanov, A. Zlatarov, and P. Raykov to a higher, more advanced level in the second half of the 20th century.

Professor DSc Ivan Pojarlieff,
Corr. Member of BAS

Institute of Organic Chemistry with Centre of Phytochemistry, Bulgarian Academy of Sciences, Acad. G. Bonchev str., bl. 9, 1113 Sofia, Bulgaria; E-mail: ipjarli@orgchm.bas.bg

Diastereoselective addition of functionalized organolithium compounds to (-)-menthone – synthesis of chiral ligands for enantioselective addition of diethylzinc to aldehydes

I. Zagranjarska, K. Kostova*, A. Chimov, V. Dimitrov*

Institute of Organic Chemistry with Center of Phytochemistry, Bulgarian Academy of Sciences, Acad. G. Bonchev 9, Sofia 1113, Bulgaria

Received March 08, 2017; Revised March 13, 2017

Dedicated to Acad. Bogdan Kurtev on the occasion of his 100th birth anniversary

The addition of N- and S-functionalized organolithium compounds to (-)-menthone was studied and a series of new chiral substituted neomenthol derivatives has been isolated. The new chiral compounds have been applied as precatalysts for addition of diethylzinc to aldehydes and enantioselectivity of up to 80% ee was achieved.

Key words: (-)-menthone; organolithium compounds; diethylzinc; enantioselectivity

INTRODUCTION

The enantioselective addition of dialkylzinc compounds to aldehydes catalyzed by different types of chiral ligands has attracted in recent years significant interest because the resulting enantiomerically pure or enriched alcohols are important intermediates for the synthesis of bioactive compounds and natural products [1–4]. Aminoalcohols have been shown to act as highly efficient chiral ligands in this reaction and therefore a large number of aminoalcohols has been synthesized and tested as ligands [1, 2, 5–12]. One of the most potent ligand applied by Noyori as a catalyst is the dimethylamino-isoborneol Noyori prepared from camphor [13–19]. Considering the variety of the aminoalcohols synthesized so far, it is important to note that most commonly natural sources of chirality (*e.g.* terpenoids, aminoacids and alkaloids) have been used for their synthesis. The natural ketone (-)-menthone has been successfully used to prepare chiral aminoalcohols applied in the asymmetric addition of organozinc reagents to carbonyl compounds [20–26]. In our previous studies a series of aminoalcohols has been synthesized and applied as ligands through the highly diastereoselective addition of functionalized organolithium compounds to natural terpenoid ketons as chirality sources [27–30].

In this work we are describing the synthesis of set of neomenthol derivatives bearing N- and S-

heteroatom functionalities, which are able to serve as chiral ligands for enantioselective addition of dialkylzinc reagents to aldehydes. The key step in the synthetic approach is the highly selective equatorial addition of N- and S-functionalized organolithium reagents to (-)-menthone leading to aminoalcohols and sulfur containing structural analogues.

EXPERIMENTAL

General

The reactions with air and moisture sensitive reagents were carried out in flame-dried Schlenk flasks under an argon atmosphere. The solvents were dried (sodium/benzophenone for ether and THF; Na[Et₄Al] for toluene and hexane) and distilled under an argon atmosphere prior to use. Thin layer chromatography (TLC) was performed on aluminum sheets pre-coated with silica gel 60 F₂₅₄ (Merck). Flash column chromatography was carried out using silica gel 60 (230–400 mesh, Merck). Optical rotations ($[\alpha]_D^{20}$) were measured on a Perkin Elmer 241 polarimeter. The NMR spectra were recorded in CDCl₃ on a Bruker DRX 250 (250.13 MHz for ¹H NMR, 62.9 MHz for ¹³C NMR) spectrometer with TMS as the internal standard for chemical shifts (δ , ppm). ¹H and ¹³C NMR data are reported as follows: chemical shift, multiplicity (s = singlet, d = doublet, t = triplet, q = quartet, br = broad, m = multiplet), coupling constants (Hz), integration, and identification. C-multiplicities were assigned by DEPT techniques.

* To whom all correspondence should be sent:
E-mail: kalina@orgchm.bas.bg

EI-MS (70 eV) were recorded on a Hewlett Packard 6890/5973 and reported as fragmentation in m/z with relative intensities (%) in parentheses. High performance liquid chromatography (HPLC) separations were performed with an Agilent 1100 System fitted with a diode array detector and a manual injector with a 20 μ L injection loop. Gas chromatography (GC) was performed with a Shimadzu GC-17A. Elemental analyses were performed by the Microanalytical Service Laboratory of the Institute of Organic Chemistry, Bulgarian Academy of Sciences.

The following starting materials were used (commercially available or prepared according to the literature): (-)-menthone, N,N-dimethylbenzylamine, N,N-dimethylaniline, TMEDA, *n*-BuLi (1.6 M or 2.5 M in hexane, *Fluka*), Et₂Zn (1 M in hexane or heptane, *Fluka*), anhydrous CeCl₃.

(1S,2S,5R)-2-isopropyl-5-methyl-1-(thiophen-2-yl)cyclohexan-1-ol 7

To a solution of thiophene (0.21 ml, 2.605 mmol) in THF (2 ml) *n*-BuLi (1.3 ml, 2.084 mmol, 1.6 M solution in hexane) was added at -10 °C under Ar atmosphere. The reaction mixture was stirred for 1 h at 20 °C and then (-)-menthone (0.3 ml, 1.74 mmol) was added. After 24 h the reaction mixture was hydrolyzed with water, extracted with Et₂O and the organic layer was dried (Na₂SO₄). After evaporation of the solvent, the crude product was chromatographed (\varnothing = 18 mm, h = 540 mm, 24 g silica gel, PE:Et₂O = 100:1). Compound **7** was isolated (0.333 g, 80%) as colorless oil. Compound **7** was additionally purified by Kugelrohr-distillation (120 °C, 0.001 Torr). $[\alpha]_{\text{D}}^{20}$ = -11.80 (c 1.00, CHCl₃). ¹H NMR: δ 0.71 (d, J = 6.8, 3H, CH₃), 0.78 (d, J = 6.8, 3H, CH₃), 0.80 (d, J = 6.1, 3H, CH₃), 1.82–1.25 (m, 8H), 1.04–0.88 (m, 1H), 1.86 (s, 1H, OH), 6.79 (dd, J = 3.4, 1.2, 1H, H-3'), 6.86 (dd, J = 5.1, 3.4, 1H, H-4'), 7.05 (dd, J = 5.1, 1.2, 1H, H-5'). ¹³C NMR: 18.25 (q, CH₃), 21.14 (t, CH₂), 22.00 (q, CH₃), 23.71 (q, CH₃), 26.69 (d, CH), 28.38 (d, CH), 34.88 (t, CH₂), 51.77 (d, C-2), 52.86 (t, C-6), 78.20 (s, C-1), 121.28* (d, C-4'), 122.80* (d, C-3'), 126.68 (d, C-5'), 154.82 (s, C-2'). MS (EI): 238 (M⁺, >1), 225 (13), 183 (3), 167 (3), 153 (100), 139 (5), 126 (19), 111 (23), 97 (7), 69 (11), 55 (11). Anal. Calcd for C₁₄H₂₂OS (238.39): C 70.54, H 9.30, S 13.45; Found: C 70.60, H 9.29, S 13.26.

(1S,2S,5R)-2-isopropyl-5-methyl-1-(5-trimethylsilylthiophen-2-yl)cyclohexan-1-ol 8

To a solution of trimethyl(thiophen-2-yl)silane (0.56 ml, 3.490 mmol) in THF (2 ml) *n*-BuLi (1.1 ml, 2.792 mmol, 2.5 M solution in hexane) was added at -10 °C under Ar atmosphere. The reaction mixture was stirred for 1 h at 20 °C and then (-)-menthone (0.4 ml, 2.327 mmol) was added. After 24 h the reaction mixture was hydrolyzed with water, extracted with Et₂O and the organic layer was dried (Na₂SO₄). After evaporation of the solvent, the crude product was chromatographed (\varnothing = 17 mm, h = 550 mm, 51 g silica gel, PE:Et₂O = 20:1). It were isolated 0.051 g (14%) unreacted (-)-menthone (**1**) and 0.529 g (73%) of pure product **8** as colorless oil. The product was additionally purified by Kugelrohr-distillation (120 °C, 0.001 Torr). $[\alpha]_{\text{D}}^{20}$ = -11.60 (c 1.00, CHCl₃). ¹H NMR: δ 0.30 (s, 9H, Si(CH₃)₃), 0.81 (d, J = 6.8 z, 3H, CH₃), 0.87 (d, J = 6.8, 3H, CH₃), 0.89 (d, J = 6.1, 3H, CH₃), 1.92–1.37 (m, 10H), 6.93* (d, J = 3.4, 1H, H-4'), 7.10* (d, J = 3.4, 1H, H-3'). ¹³C NMR: -0.01 (3q, Si(CH₃)₃), 18.34 (q, CH₃), 21.20 (t, CH₂), 22.05 (q, CH₃), 23.80 (q, CH₃), 26.76 (d, CH), 28.51 (d, CH), 34.95 (t, CH₂), 51.61 (d, C-2), 53.10 (t, C-6), 78.61 (s, C-1), 122.80* (d, C-4'), 133.82* (d, C-3'), 137.43 (s, C-5'), 160.28 (s, C-2'). MS (EI): 310 (M⁺, 31), 295 (18), 277 (5), 237 (4), 225 (100), 198 (29), 183 (34), 167 (3), 141 (4), 115 (4), 91 (4), 73 (23), 55 (6). Anal. Calcd for C₁₇H₃₀OSSi (310.57): C 65.74, H 9.74, S 10.32, Si 9.04; Found: C 66.18, H 9.86, S 10.22, Si 9.49.

(1S,2S,5R)-1-(2-((dimethylamino)methyl)phenyl)-2-isopropyl-5-methylcyclohexan-1-ol 9

Procedure A: To a solution of N,N-dimethylbenzylamine (0.58 ml, 3.890 mmol) in Et₂O (15 ml) *n*-BuLi (1.24 ml, 3.112 mmol, 2.5 M solution in hexane) was added at 20 °C under Ar atmosphere. The reaction mixture was refluxed for 4.5 h. After cooling to 20 °C (-)-menthone (0.45 ml, 2.593 mmol) was added, the reaction mixture was stirred for 96 h and then was hydrolyzed with water, extracted with Et₂O, and the organic layer was dried (Na₂SO₄). After evaporation of the solvent, the crude product was chromatographed (\varnothing = 23 mm, h = 580 mm, 95g silica gel, CH₂Cl₂:CH₃OH:NH₄OH = 100:0.5:0.05). It were isolated 0.184 g (46%) unreacted (-)-menthone (**1**) and 0.160 g (21%) of pure product **9** as colorless oil. The product was purified by Kugelrohr-distillation (120 °C, 0.001 Torr).

Procedure B: To a solution of N,N-dimethylbenzylamine (0.58 ml, 3.890 mmol) in

Et₂O (17 ml) *n*-BuLi (1.24 ml, 3.112 mmol, 2.5 M solution in hexane) was added at 20 °C under Ar atmosphere. The reaction mixture was refluxed for 4.5 h. Activation of (-)-menthone (**1**) was performed separately as follows. To a suspension of anhydrous CeCl₃ (0.640 g, 2.593 mmol) in THF (10 ml) (-)-menthone (**1**) (0.45 ml, 2.593 mmol) was added and the mixture was stirred at room temperature until a yellow gel-like suspension was formed (40 min). The *in situ* prepared organolithium reagent **4** was added to the activated (-)-menthone and the mixture was stirred for a further 96 h at 20 °C under Ar atmosphere. The reaction mixture was hydrolyzed with saturated NH₄Cl solution, extracted with Et₂O, washed with water and the organic layer was dried (Na₂SO₄). After evaporation of the solvent, the crude product was chromatographed (∅ = 17 mm, *h* = 550 mm, 54 g silica gel, CH₂Cl₂:CH₃OH:NH₄OH = 100:0.5:0.05). It was isolated 0.513 g (68%) of pure product **9** as colorless oil. The product was additionally purified by Kugelrohr-distillation (120 °C, 0.001 Torr). [α]_D²⁰ = -3.90 (c 1.00, CHCl₃). ¹H NMR: δ 0.71 (d, *J* = 6.8, 3H, CH₃), 0.86 (d, *J* = 6.6, 3H, CH₃), 0.88 (d, *J* = 6.8, 3H, CH₃), 0.94–1.11 (m, 1H), 1.40–2.06 (m, 8H), 2.22 (2s, 6H, (H₃C)₂N), 3.65 (bs, 2H, H₂C-N), 7.02–7.14 (m, 2H, Ph), 7.23–7.30 (m, 2H, Ph). ¹³C NMR: 18.40 (q, CH₃), 21.24 (t, CH₂), 22.39 (q, CH₃), 23.98 (q, CH₃), 27.34 (d, CH), 28.00 (d, CH), 35.48 (t, CH₂), 43.97 (2q, N(CH₃)₂), 51.42 (d, C-2), 53.18 (t, C-6), 65.46 (t, N-CH₂), 80.82 (s, C-1), 125.44 (d, Ph), 127.74 (d, Ph), 127.79 (d, Ph), 132.78 (d, Ph), 135.17 (s, C-2'), 148.71 (s, C-1'). MS (EI): 289 (M⁺, 21), 274 (21), 225 (34), 204 (100), 183 (19), 159 (40), 145 (16), 119 (32), 105 (9), 91 (33), 69 (19), 58 (29), 46 (18). Anal. Calcd for C₁₉H₃₁NO (289.463): C 78.84, H 10.79, N 4.84; Found: C 78.74, H 10.83, N, 4.68.

(1S,2S,5R)-1-(2-((dimethylamino)methyl)-3-(trimethylsilyl)phenyl)-2-isopropyl-5-methylcyclohexan-1-ol 10

To a solution of N,N-dimethyl-1-(2-trimethylsilyl)phenylmethanamine (0.807 g, 3.890 mmol) in Et₂O (18 ml) *n*-BuLi (1.24 ml, 3.112 mmol, 2.5 M solution in hexane) was added at 20 °C under Ar atmosphere. The reaction mixture was refluxed for 4.5 h. After cooling to 20 °C (-)-menthone (0.45 ml, 2.593 mmol) was added. After 48 h the reaction mixture was hydrolyzed with water, extracted with Et₂O and the organic layer was dried (Na₂SO₄). After evaporation of the

solvent, the crude product was chromatographed (∅ = 24 mm, *h* = 520 mm, 85 g silica gel, CH₂Cl₂:CH₃OH:NH₄OH = 100:0.5:0.05). It was isolated 0.170 g (43%) unreacted (-)-menthone (**1**) and 0.426 g (45%) of pure product **10** as colorless oil. The product was purified by Kugelrohr-distillation (50–120 °C, 0.001 Torr). [α]_D²⁰ = +7.30 (c 1.00, CHCl₃). ¹H NMR: δ 0.35 (s, 9H, (H₃C)₃Si), 0.71 (d, *J* = 7.1, 3H, CH₃), 0.85 (d, *J* = 6.4, 3H, CH₃), 0.86 (d, *J* = 6.8, 3H, CH₃), 0.90–1.00 (m, 1H), 1.40–2.10 (m, 8H), 2.22 (s, 6H, (H₃C)₂N), 3.88 (d, *J* = 12.2, 1H, HC-N), 3.96 (d, *J* = 12.2, 1H, HC-N), 7.18–7.25 (m, 1H, Ph), 7.31–7.38 (m, 2H, Ph), 8.57 (br s, 1H, OH). ¹³C NMR: 2.01 (3q, Si(CH₃)₃), 18.45 (q, CH₃), 21.42 (t, CH₂), 22.46 (q, CH₃), 24.03 (q, CH₃), 27.45 (d, CH), 28.14 (d, CH), 35.58 (t, CH₂), 43.35 (2q, N(CH₃)₂), 51.63 (d, C-2), 53.38 (t, C-6), 63.18 (t, N-CH₂), 81.05 (s, C-1), 126.60 (d, Ph), 129.58 (d, Ph), 132.52 (d, Ph), 140.87* (s, C-3'), 141.45* (s, C-2'), 148.66 (s, C-1'). MS (EI): 361 (M⁺, 24), 346 (31), 318 (10), 304 (26), 276 (100), 243 (13), 231 (21), 206 (17), 191 (35), 147 (9), 73 (50), 58 (20), 46 (10). Anal. Calcd for C₂₂H₃₉NOSi (361.645): C 73.07, H 10.87, N 3.87, Si 7.77; Found: C 72.96, H 11.07, N 3.65, Si 7.92.

(1S,2S,5R)-1-(2-(dimethylamino)phenyl)-2-isopropyl-5-methylcyclohexan-1-ol 11

Procedure A: To a solution of *n*-BuLi (1.55 ml, 3.889 mmol, 2.5 M solution in hexane) TMEDA (0.58 ml, 3.889 mmol) was added in one portion at 0 °C under Ar atmosphere. The reaction mixture was stirred for 30 min at 20 °C and then N,N-dimethylaniline (0.62 ml, 4.862 mmol) was added. The reaction mixture was refluxed for 4.5 h. After cooling to 0 °C (-)-menthone (**1**) (0.56 ml, 3.241 mmol) was added, the reaction mixture was stirred at 20 °C for 96 h and it was hydrolyzed with water, extracted with Et₂O, and dried (Na₂SO₄). After evaporation of the solvent, the crude product was chromatographed (∅ = 30 mm, *h* = 577 mm, 80 g silica gel, petroleum ether/Et₂O = 100:1). It was isolated 0.142 g (28%) unreacted (-)-menthone and 0.262 g (29%) of pure product **11** as colorless crystals. Mp 117–118 °C (methanol). [α]_D²⁰ = -19.70 (c 1.00, CHCl₃).

Procedure B: To a solution of *n*-BuLi (1.55 ml, 3.889 mmol, 2.5 M solution in hexane) TMEDA (0.58 ml, 3.889 mmol) was added in one portion at 0 °C under Ar atmosphere. The reaction mixture was stirred for 30 min at 20 °C and then N,N-

dimethylaniline (0.62 ml, 4.862 mmol) was added and it was refluxed for 4.5 h. Activation of the (-)-menthone (**1**) was performed separately as follows. To a suspension of anhydrous CeCl₃ (0.800 g, 3.241 mmol) in THF (10 ml) (-)-menthone (**1**) (0.56 ml, 3.241 mmol) was added and the reaction mixture was stirred at room temperature until a yellow gel-like suspension was formed (40 min). The *in situ* prepared organolithium reagent **6** was added to the activated (-)-menthone and the mixture was stirred for further 96 h at 20 °C under Ar atmosphere. It was hydrolyzed with saturated NH₄Cl solution, extracted with Et₂O, washed with water and the organic layer was dried (Na₂SO₄). After evaporation of the solvent, the crude product was chromatographed ($\varnothing = 30$ mm, $h = 577$ mm, 57g silica gel, petroleum ether/Et₂O = 100:1; 20:1; 5:1). It were isolated 0.009 g (2%) unreacted (-)-menthone and 0.315 g (35%) pure product as colorless crystals. Mp 117–118 °C (methanol). $[\alpha]_D^{20} = -19.70$ (c 1.00, CHCl₃). ¹H NMR: δ 0.73 (d, $J = 7.1$, 3H, CH₃), 0.88 (d, $J = 6.6$, 3H, CH₃), 0.86–1.05 (m, 1H), 0.91 (d, $J = 7.1$, 3H, CH₃), 1.45–2.08 (m, 8H), 2.67 (s, 3H, H₃C-N), 2.68 (s, 3H, H₃C-N), 7.14–7.36 (m, 4H, Ph), 10.40 (s, 1H, OH). ¹³C NMR: 18.40 (q, CH₃), 21.14 (t, CH₂), 22.44 (q, CH₃), 23.79 (q, CH₃), 27.58 (d, CH), 28.16 (d, CH), 35.50 (t, CH₂), 45.84 (q, N-CH₃), 46.89 (q, N-CH₃), 50.96 (d, C-2), 53.54 (t, C-6), 81.15 (s, C-1), 123.31 (d, Ph), 126.20 (d, Ph), 127.12 (d, Ph), 127.37 (d, Ph), 142.63 (s, C-1'), 151.74 (s, C-2'). MS (EI): 275 (M⁺, 31), 260 (17), 232 (8), 214 (30), 204 (5), 190 (100), 160 (9), 148 (87), 134 (18), 120 (22), 106 (10), 91 (11), 77 (13), 55 (13). Anal. calcd for C₁₈H₂₉NO (275.436): C 78.49, H 10.61, N, 5.09; Found: C 78.26, H 10.76, N, 4.99.

General procedure for enantioselective addition of diethylzinc to aldehydes

To a solution of the corresponding ligand **7–11** (3 mol %) in hexane or toluene (10 ml) Et₂Zn (1.7 mmol, 1 M solution in hexane) was added dropwise at 0 °C under Ar atmosphere. The mixture was stirred for 30 min at 0 °C and then the corresponding aldehyde (1 mmol) was added at -20 °C. The reaction mixture was stirred at the appropriate temperature (see Table 1) and monitored by TLC (petroleum ether/Et₂O = 4:1) until the aldehyde was consumed or no further consumption was observed. The mixture was quenched (aq. NH₄Cl), extracted with Et₂O and dried (Na₂SO₄). After evaporation of the solvent, the crude product was purified by column

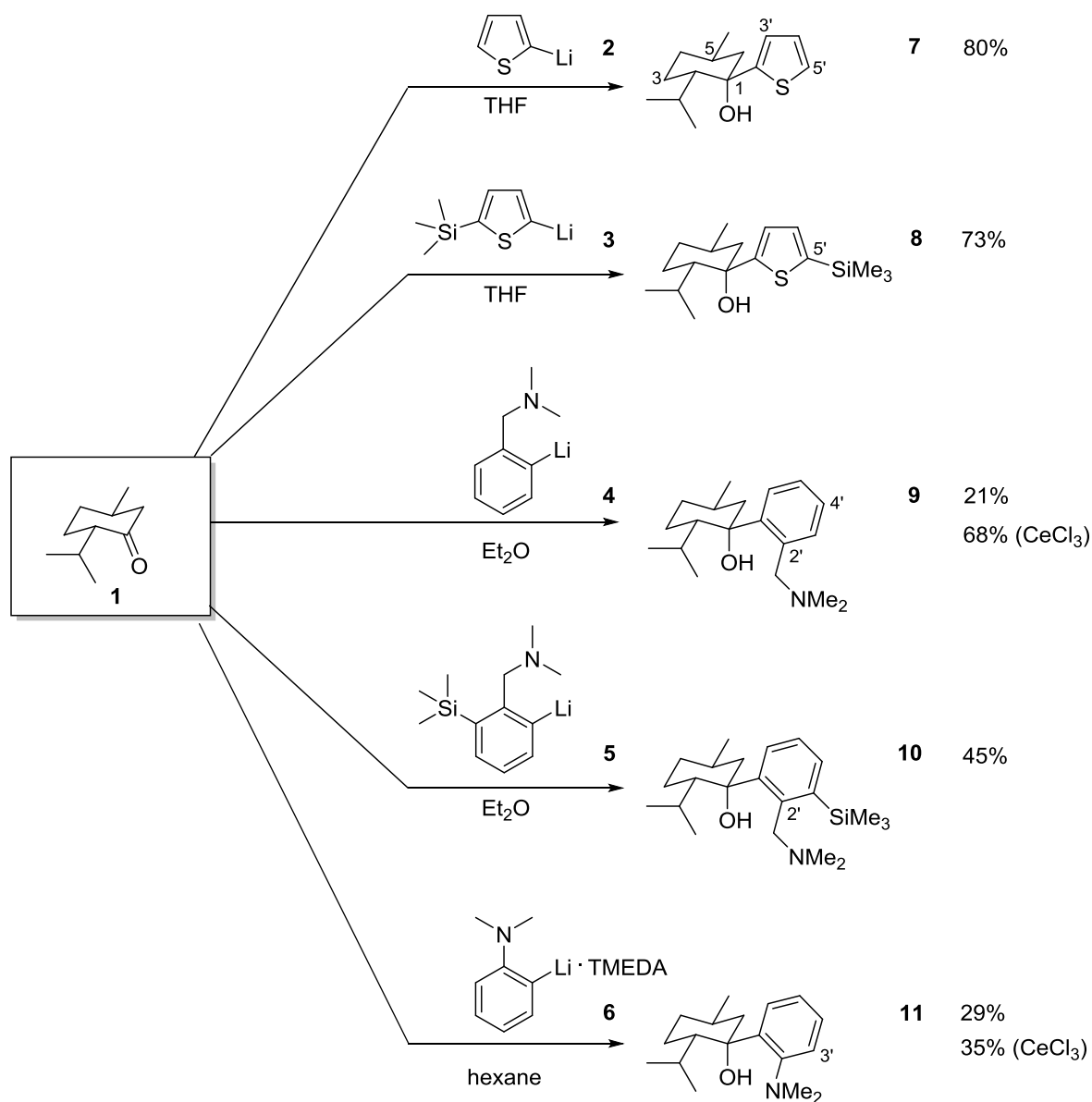
chromatography (petroleum ether/Et₂O = 20:1 or 10:1).

RESULTS AND DISCUSSION

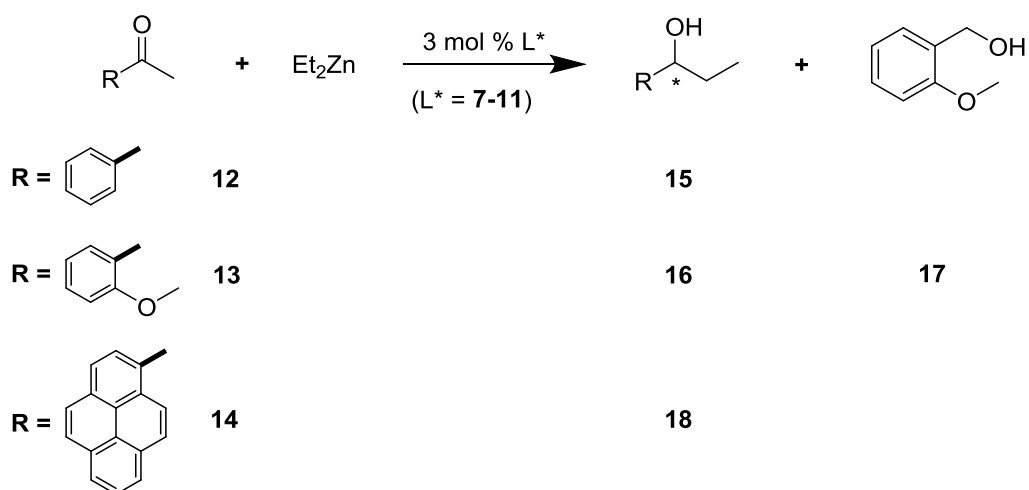
For the synthesis of neomenthol derivatives bearing N- and S-heteroatom functionalities, a set of lithium reagents was selected, which are based on the thiophene and amino-substituted phenyl moieties. The addition of the lithium reagents **2–6** (Scheme 1) was performed according previous experience [31]. The reagents **2** and **3** were chosen with the purpose to synthesize sulfur analogues of aminoalcohols, in which the bulky trimethylsilyl-group modifies in the case of **3** the stereochemical environment next to the sulfur coordinating center. With the reagents **4** and **5** was aimed to prepare δ -aminoalcohols, which incorporate the aromatic phenyl group in the side chain and in addition to study the sterical influence of the trimethylsilyl-group as in the case of **5**. The reagent **6** possess the dimethylamino group directly attached to the aromatic moiety and was planned to provide for comparison γ -aminoalcohol after the addition to (-)-menthone.

The addition of *in situ* generated thiophen-2-yl-lithium (**2**) [32] to (-)-menthone occurred readily at room temperature in THF as a solvent and the thiophene substituted neomenthyl derivative was isolated in excellent yield (80%) after purification by column chromatography. The analogous 5-trimethylsilyl-thiophen-2-yl-lithium (**3**) [32] was reacted with (-)-menthone under the same conditions as in the above case providing after hydrolytic work up and column chromatography product **8** in 73% yield and 14% unreacted menthone.

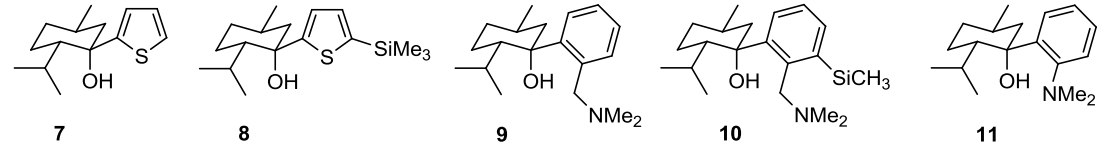
The formation of reagent **4** from N,N-dimethylbenzylamine with *n*-BuLi is known to proceed in THF *in situ* highly efficient [33]. Menthone was added to the generated solution of **4** and the mixture was stirred for 4 days at room temperature, monitored by TLC. The reaction was slow and incomplete. After hydrolytic work up and column chromatography the desired δ -aminoalcohol **9** was isolated in low yield (21%) together with 46% unreacted (-)-menthone. With the purpose to realize higher yield the own procedure [34–36] for activation of the ketone with anhydrous CeCl₃ in THF was applied. The addition of reagent **4** to the activated (-)-menthone occurred in this case in 68% yield (19% unreacted menthone was also recovered).



Scheme 1 Addition of organolithium reagents to (-)-menthone (**1**).



Scheme 2. Enantioselective addition of diethylzinc to the aldehydes **12**, **13** and **14** catalyzed by chiral ligands **7–11**.

Table 1. Enantioselective addition of Et₂Zn to the aldehydes **12**, **13** and **14** catalyzed by chiral ligands (L*) **7–11**.**Ligands L*:**


No	Ligand	Aldehyde	Solvent	Reaction time [h]	Reaction temp. [°C]	Yield ^a [%]	ee ^b [%]	Yield ^a 17 [%]
1	7	12	Hexane	168	20	70 (15)	0	-
2	8	12	Hexane	216	20	18 (15)	0	-
3	9	12	Hexane	45	20	92 (15)	66 (<i>S</i>)	-
4	9	12	Toluene	5	20	73 (15)	68 (<i>S</i>)	-
5	9	12	Toluene	5	60	83 (15)	58 (<i>S</i>)	-
6	9	12	Toluene	2	100	71 (15)	42 (<i>S</i>)	-
7	10	12	Hexane	24	20	83 (15)	18 (<i>S</i>)	-
8	11	12	Hexane	24	20	83 (15)	60 (<i>S</i>)	-
9	11	12	Toluene	5	20	68 (15)	80 (<i>S</i>)	-
10	11	12	Toluene	5	60	66 (15)	74 (<i>S</i>)	-
11	11	12	Toluene	5	100	64 (15)	66 (<i>S</i>)	-
12	7	13	Hexane	240	20	6 (16)	0	24
13	7	13	Toluene	72	20	73 (16)	0	9
14	8	13	Hexane	240	20	6 (16)	0	28
15	8	13	Toluene	48	20	62 (16)	0	6
16	9	13	Hexane	216	20	5 (16)	28 (<i>S</i>)	32
17	9	13	Toluene	48	20	81 (16)	46 (<i>S</i>)	4
18	9	13	Toluene	4	60	74 (16)	56 (<i>S</i>)	6
19	9	13	Toluene	2	100	75 (16)	38 (<i>S</i>)	10
20	10	13	Hexane	24	20	83 (16)	26 (<i>S</i>)	2
21	11	13	Hexane	24	20	82 (16)	54 (<i>S</i>)	5
22	11	13	Toluene	5	20	61 (16)	74 (<i>S</i>)	-
23	11	13	Toluene	3	60	69 (16)	62 (<i>S</i>)	7
24	11	13	Toluene	2	100	71 (16)	45 (<i>S</i>)	15
25	9	14	Hexane	24	20	84 (18)	68 ^c	-
26	9	14	Toluene	6	60	68 (18)	52 ^c	-
27	11	14	Hexane	24	20	74 (18)	60 ^c	-
28	11	14	Toluene	4	60	60 (18)	64 ^c	-

^aYields are given after column chromatography. ^bEnantiomeric excess of **15** determined by GC analysis (Hydrodex-β-TBDAC column, 122 °C isothermal, 1 ml/min He, split 21, T_{det} = 230 °C, T_{inj} = 220 °C); retention times: t_{minor} (*R*) = 9.4 min and t_{major} (*S*) = 9.8 min; enantiomeric excess of **16** determined by HPLC with chiral column (Nucleodex β PM column, 0.8 ml/min, acetonitrile/water = 20:80 to acetonitrile/water = 43:57, for 17 min; 205 nm DAD detector); retention times: t_{major} = 11.3 min and t_{minor} = 12 min. ^cOptical purity determined by polarimetry based on the maximum values for the specific rotations of the corresponding enantiomer for **18** [α]_D²⁰ = -60.1 (c 0.72, CHCl₃) for 95% ee of unknown configuration [38].

The trimethylsilyl-substituted lithium reagent **5** was formed and applied using the same conditions as in the case of reagent **4**. The δ-aminoalcohol **10** was isolated in 45% yield after chromatography purification. This yield was sufficient to obtain

enough quantity for the further experiment and therefore it was abandoned to perform further optimization. For the synthesis of γ-aminoalcohol **11** the formation of lithium reagent **6** was performed from *N,N*-dimethylaniline and *n*-

BuLi-TMEDA in THF, refluxing the mixture within 4.5 h [32]. The addition of **6** to (-)-menthone occurred in low yield (29%) by using the standard conditions. After activation of the ketone with anhydrous CeCl₃ in THF the yield could be enhanced to 35%.

The newly synthesized aminoalcohols and sulfur containing analogues **7–11** were applied as ligands, in catalytic quantities (3 mol%), for enantioselective addition of diethylzinc (Scheme 2) to benzaldehyde (**12**), *o*-methoxybenzaldehyde (**13**) and pyrenecarbaldehyde (**14**). In almost all cases the ligands studied were active catalysts that provide the additional reaction in good to high yields (Table 1). The sulfur containing ligands **7** and **8** were poor catalysts in respect of both providing chemical yields and enantioselectivity, although the reaction with benzaldehyde (in the case of **7**) realized acceptable yields (entries 1 vs. 12 and 14). Similar results were obtained with ligand **9** for the addition of Et₂Zn to aldehyde **13** in hexane as solvent (entry 16). Changing the solvent from hexane to toluene improved significantly the addition of Et₂Zn to *o*-methoxybenzaldehyde (**13**) in the case of ligand **9** (entries 16, 17), but also in the case of ligands **7** and **8** (entries 12, 13 and 14, 15). It should be pointed out that in the course of the Et₂Zn addition to *o*-methoxybenzaldehyde a competing reduction reaction takes place with formation of product **17**. This reaction may occur if prolonged reaction times are applied [14, 37] and in the case of aldehyde **13** the coordinating ability of the methoxy group provides favourable conditions. In most other cases suitable conditions have been optimized to obtain the corresponding secondary alcohols **15**, **16** and **18** in good yields.

In respect of the enantioselectivity in general the best results were obtained with ligand **11**, considering the additions to aldehydes **12–14** – enantioselectivities between 45 and 80% ee. Ligand **9** provided acceptable degree of enantioselectivity compared with the poor result of **10** bearing the bulky trimethylsilyl group. It is interesting to note that increasing the reaction temperature from 20 °C to 60 °C and 100 °C brought shortening of the reaction time, but in general moderate change of yields and lowering of the enantioselectivity. In all studied cases the configuration of the predominant enantiomer of **15**, **16** and **18** was *S*.

CONCLUSION

A series of aminoalcohols and sulfur containing analogues has been synthesized by addition of

functionalized organolithium compounds to (-)-menthone. The new chiral compounds have been applied as precatalysts in the enantioselective addition of diethylzinc to aldehydes. Moderate enantioselectivity was observed and in some cases acceptable degrees of enantioselectivity could be achieved (up to 80% ee).

Acknowledgements: Support by the National Science Fund of Bulgaria (projects UNA 17/2005 and DRNF 02/13/2009) is gratefully acknowledged.

REFERENCES

1. R. Noyori, *Asymmetric Catalysis in Organic Chemistry*, Chapter 5, John Wiley and Sons: New York, 1994.
2. R. Noyori, M. Kitamura, *Angew. Chem., Int. Ed.*, **30**, 49 (1991).
3. K. Soai, S. Niwa, *Chem. Rev.*, **92**, 833 (1992).
4. M. Avalos, R. Babiano, P. Cintas, J. L. Jiménez, J. C. Palacios, *Tetrahedron: Asymmetry*, **8**, 2997 (1997).
5. N. Oguni, T. Omi, *Tetrahedron Lett.*, **25**, 2823 (1984).
6. L. Pu, H.-B. L. Yu, *Chem. Rev.*, **101**, 757 (2001).
7. K. Soai, T. Shibata, in: *Catalytic Asymmetric Synthesis*, I. Ojima (ed.), Wiley-VCH, New York, 2000, p. 699.
8. K. Mikami, M. Lautens, *New Frontiers in Asymmetric Catalysis*, Wiley-Interscience: Hoboken, 2007.
9. R. G. Arrayás, J. Adrio, J. C. Carretero, *Angew. Chem. Int. Ed.*, **45**, 7674 (2006).
10. V. Dimitrov, K. Kostova, *Lett. Org. Chem.*, **3**, 176 (2006).
11. C. Cardellicchio, M. A. M. Capozzi, F. Naso, *Tetrahedron: Asymmetry*, **21**, 507 (2010).
12. I. Szatmári, F. Fülöp, *Tetrahedron*, **69**, 1255 (2013).
13. M. Kitamura, S. Suga, K. Kawai, R. Noyori, *J. Am. Chem. Soc.*, **108**, 6071 (1986).
14. M. Kitamura, S. Okada, S. Suga, R. Noyori, *J. Am. Chem. Soc.*, **111**, 4028 (1989).
15. R. Noyori, S. Suga, K. Kawai, S. Okada, M. Kitamura, N. Oguni, M. Hayashi, T. Kaneko, Y. Matsuda, *J. Organomet. Chem.*, **382**, 19 (1990).
16. M. Kitamura, S. Suga, M. Niwa, R. Noyori, *J. Am. Chem. Soc.*, **117**, 4832 (1995).
17. M. Yamakawa, R. Noyori, *J. Am. Chem. Soc.*, **117**, 6327 (1995).
18. M. Yamakawa, R. Noyori, *Organometallics*, **18**, 128 (1999).
19. R. Noyori, *Angew. Chem., Int. Ed. Engl.*, **41**, 2008 (2002).
20. G. Chelucci, F. Soccolini, *Tetrahedron: Asymmetry*, **3**, 1235 (1992).
21. T. Shono, N. Kise, T. Fujimoto, A. Yamanami, R. Nomura, *J. Org. Chem.*, **59**, 1730 (1994).

22. H.-L. Kwong, W.-S. Lee, *Tetrahedron: Asymmetry*, **10**, 3791 (1999).
23. Y. Q. Xu, T. X. Wu, X. F. Pan, *Chinese Chemical Letters*, **12**, 1055 (2001).
24. Q. Xu, X. Wu, X. Pan, A. S. C. Chan, T.-K. Yang, *Chirality*, **14**, 28 (2002).
25. D. Le Goanvic, M. Holler, P. Pale, *Tetrahedron: Asymmetry*, **13**, 119 (2002).
26. M. Leven, N. E. Schlörer, J. M. Neudörfl, B. Goldfuss, *Chem. Eur. J.*, **16**, 13443 (2010).
27. M. Genov, V. Dimitrov, V. Ivanova, *Tetrahedron: Asymmetry*, **8**, 3703 (1997).
28. M. Genov, K. Kostova, V. Dimitrov, *Tetrahedron: Asymmetry*, **8**, 1869 (1997).
29. I. Philipova, V. Dimitrov, S. Simova, *Tetrahedron: Asymmetry*, **10**, 1381 (1999).
30. S. Panev, A. Linden, V. Dimitrov, *Tetrahedron: Asymmetry*, **12**, 1313 (2001).
31. M. Kamenova-Nacheva, G. M. Dobrikov, V. Dimitrov, *Tetrahedron: Asymmetry*, **27**, 852 (2016).
32. L. Brandsma, H. D. Verkruisje in: *Preparative Polar Organometallic Chemistry*, Springer-Verlag, Berlin, Heidelberg, **1987**, Vol 1.
33. C. T. Viswanathan, C. A. Wilkie, *J. Organometallic Chem.*, **54**, 1 (1973).
34. V. Dimitrov, S. Bratovanov, S. Simova, K. Kostova, *Tetrahedron Lett.*, **35**, 6713 (1994).
35. V. Dimitrov, K. Kostova, M. Genov, *Tetrahedron Lett.*, **37**, 6787 (1996).
36. S. Panev, V. Dimitrov, *Tetrahedron: Asymmetry*, **11**, 1517 (2000).
37. K. Dikova, M. Kamenova-Nacheva, K. Kostova, V. Dimitrov, *Bulg. Chem. Commun.*, **46** (Special Issue A), 33 (2014).
38. A. Pfaltz, M. Genov, unpublished results.

**ДИАСТЕРЕОСЕЛЕКТИВНО ПРИСЪЕДИНЯВАНЕ НА ФУНКЦИОНАЛИЗИРАНИ
ОРГАНОЛИТИЕВИ СЪЕДИНЕНИЯ КЪМ (-)-МЕНТОН – СИНТЕЗ НА ХИРАЛНИ
ЛИГАНДИ ЗА ЕНАНТИОСЕЛЕКТИВНО ПРИСЪЕДИНЯВАНЕ НА ДИЕТИЛЦИНК КЪМ
АЛДЕХИДИ**

И. Загранярска, К. Костова*, А. Чимов, В. Димитров*

Институт по Органична химия с Център по Фитохимия, ул. Акад. Г. Бончев, бл. 9, София 1113, България

Постъпила на 08 март 2017 г.; Коригирана на 13 март 2017 г.

(Резюме)

Изучено е присъединяването на N- и S-функционализирани органолитиетови съединения към (-)-ментон и е синтезирана серия от хирални заместени неоментолови производни. Новите хирални съединения са приложени като пре-катализатори за присъединяване на диетилцинк към алдехиди и е постигната енантиоселективност до 80% ee.

Stereoselective functionalization strategy of 2,5-diketopiperazine derived from L-proline and glycine

A. Petrova, M. Pancheva, K. Kostova*, I. Zagranjarska, M. Tavlinova-Kirilova,
V. Dimitrov*

Institute of Organic Chemistry with Centre of Phytochemistry, Bulgarian Academy of Sciences, Acad. G. Bonchev street, bl. 9, 1113 Sofia, Bulgaria

Received March 15, 2017; Revised March 22, 2017

Dedicated to Acad. Bogdan Kurtev on the occasion of his 100th birth anniversary

The functionalization of diketopiperazine Cyclo(Gly-Pro) by using suitable deprotonation reagent and electrophile offers the opportunity for synthesis of structurally diverse series of compounds (libraries) possessing bioactivity. This synthetic approach has been proved as feasible in respect to use different electrophiles and in particularly concerning the observed very high stereoselectivity.

Key words: 2,5-diketopiperazines; alkylation; acylation; LHMDS; LDA

INTRODUCTION

Diketopiperazines (DKPs) are the smallest cyclic peptides in which the two nitrogen atoms of a piperazine 6-membered ring are part of amide linkages. Three regioisomers are possible, differing in the locations of the two carbonyl groups around the ring. All of these three isomeric diketopiperazines, the 2,5-derivatives (Fig. 1) have attracted the greatest interest.

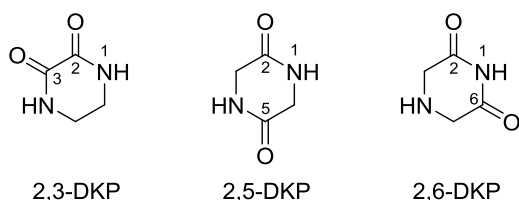
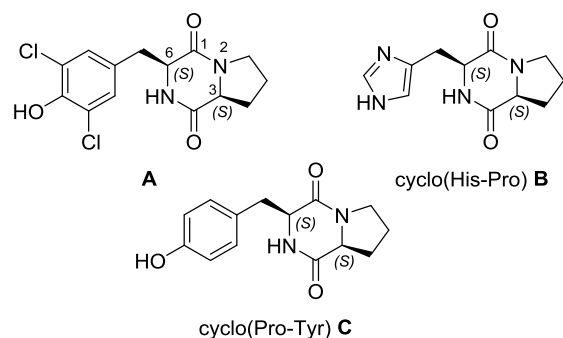


Fig. 1. Isomers of diketopiperazines.

The 2,5-DKPs occur in numerous natural products isolated from fungi, bacteria, plants and animals. Diketopiperazines are important for drug discovery due to their properties, such as conformationally constrained scaffolds, stability to proteolysis, ability to simulate peptidic pharmacophore groups and to bind to a wide range of biological targets. It is important to note that within the DKP framework, diversity can be introduced at up to six positions with

stereochemical control at up to four positions. Recently published review articles describe their properties, biological activity and methods of synthesis [1–4]. Most of the natural and synthetic 2,5-DKPs exhibit different kinds of biological activity, e.g. antitumor [5–9], antiviral [10, 11], antifungal [12] and antibacterial [13, 14]. Important is their potential to be applied as neuroprotective agents [3, 15].

Our interest in the chemistry of diketopiperazines has been attracted by the recently isolated compound **A** (Fig. 2), which was isolated from the fungal culture *Leptoxyphium* sp. [16]. This compound has been evaluated as very promising inhibitor of monocyte chemotactic protein-1, which has been implicated in both acute and chronic inflammatory and autoimmune diseases, associated with infiltration of monocytes. Therefore, this compound has the potential to serve as a model for development of small molecular weight chemokine receptor antagonists as anticancer agents.



* To whom all correspondence should be sent:
E-mail: vdim@orgchem.bas.bg

Fig. 2. 2,5-Diketopiperazines containing L-proline structural motif.

The importance of the proline containing DKPs in the development of bioactive agents could be further demonstrated with the examples of Cyclo(His-Pro) **B** (obtained by enzymatic cleavage of the hypothalamic TRH (thyrotropin releasing hormone) [17], intensively investigated for its role in the CNS (central nervous system) [18–20]) and the fungal host-specific phytotoxin maculosin-1, cyclo(Pro-Tyr) **C**, produced by *Alternaria alternata* on spotted knapweed (*Centaurea maculosa*) (possible template for creating a safe and environmentally friendly specific bioherbicides [21]).

Inspired by this results we are describing our feasibility studies to develop approach for the preparation of compound **A**, which could be of general applicability for the synthesis of a series of structurally diverse analogues with control of the stereochemistry. Thus the synthesis of the N-benzyl protected diketopiperazine cyclo(Gly-Pro) was obtained from L-proline and glycine and the introduction of suitable substituents at 6-position of the ring was studied by means of deprotonation-coupling methodology.

EXPERIMENTAL

General

The reactions with air and moisture sensitive reagents were carried out in flame-dried Schlenk flasks under an argon atmosphere. The organic solvents were distilled prior to use. The THF was dried by refluxing over sodium/benzophenone and distilled under an argon atmosphere. Thin layer chromatography (TLC) was performed on aluminium sheets pre-coated with silica gel 60 F₂₅₄ (Merck). Flash column chromatography was carried out using silica gel 60 (230–400 mesh, Merck). The melting points of the compounds were determined by using BOETIUS, type PHMK 05 (uncorrected). The NMR spectra were recorded in CDCl₃ on a Bruker Avance II+ 600 (600.13 MHz for ¹H NMR, 150.92 MHz for ¹³C NMR) spectrometer with TMS as the internal standard for chemical shifts (δ, ppm). ¹H and ¹³C NMR data are reported as follows: chemical shift, multiplicity (s = singlet, d = doublet, t = triplet, q = quartet, br = broad, m = multiplet), coupling constants (Hz), integration, and identification. The assignment of the ¹H and ¹³C NMR spectra was made on the basis of DEPT, HSQC, and NOESY experiments. All assignments marked with an asterisk are tentative. Mass spectra

(MS) were recorded on a Thermo Scientific DFS (Double Focusing Magnetic Sector) mass spectrometer using chemical ionization and reported as fragmentation in *m/z* with relative intensities (%) in parentheses and reported as fragmentation in *m/z* with relative intensities (%) in parentheses. Elemental analyses were performed by the Microanalytical Service Laboratory of the Institute of Organic Chemistry, Bulgarian Academy of Sciences.

The following commercially available starting materials were used: Benzyl bromide (*Aldrich*), NaH (60% dispersion in mineral oil, *Aldrich*), LHMDS (1 M solution in THF/ethylbenzene, *Acros*), LDA (2 M solution in THF/*n*-heptane/ethylbenzene, *Acros*), 3,5-dimethoxybenzyl bromide (*Aldrich*), 3-methylbenzoyl chloride (*Aldrich*).

(*S*)-2-benzylhexahydropyrrolo[1,2-*a*]pyrazine-1,4-dione **7**

To a suspension of (*S*)-hexahydropyrrolo[1,2-*a*]pyrazine-1,4-dione (**6**) (0.647 g, 4.196 mmol) in acetonitrile (220 ml) NaH (6.294 mmol) was added. The reaction mixture was stirred for 40 min. at 50 °C after that benzyl bromide (0.35 ml, 5.035 mmol) was added. After 24 h the solvent was evaporated, the residue was dissolved with CH₂Cl₂, the organic phase was washed with saturated solution of NaCl and dried over Na₂SO₄. After evaporation of the solvent, the crude product was purified by column chromatography (φ = 28 mm, *h* = 530 mm, 70 g silica gel, eluent: CH₂Cl₂/CH₃OH = 40:1) to give 0.801 g (78%) of **7** as colorless crystals. R_f = 0.48 (eluent: EtOAc/CH₃OH = 10:1); mp 112–114 °C (Et₂O/petroleum ether). ¹H NMR (CDCl₃): δ = 7.23–7.38 (m, 5H, H_{ar}), 4.74 (d, *J* = 14.6, 1H, H-10), 4.46 (d, *J* = 14.4, 1H, H-10), 4.13 (m, 1H, H-3), 3.98 (d, *J* = 16.6, 1H, H-6), 3.76 (d, *J* = 16.6, 1H, H-6), 3.48–3.67 (m, 2H, H-9), 2.39–2.51 (m, 1H, H-7), 1.93–2.21 (m, 3H, H-7, H-8). ¹³C NMR: δ = 167.15 (s, NC=O), 163.00 (s, NC=O), 135.44 (s, C-11), 128.91 (2d, C_{ar}), 128.33 (2d, C_{ar}), 128.06 (d, C-14), 59.08 (d, C-3), 51.13 (t, CH₂), 49.51 (t, CH₂), 45.20 (t, CH₂), 29.00 (t, CH₂), 22.56 (t, CH₂).

(*8aS*)-2-benzyl-3-(3,5-dimethoxybenzyl)hexahydropyrrolo[1,2-*a*]pyrazine-1,4-dione **8**

Method A: To a solution of **7** (0.200 g, 0.819 mmol) in dry THF (10 ml) LHMDS (1.23 ml, 1.228 mmol) was added at -78 °C through a septum under

Ar atmosphere. After 1 h 3,5-dimethoxybenzyl bromide (0.227 g, 0.982 mmol) dissolved in THF (2 ml) was added. After stirring for 3 h at -78 °C the temperature was allowed to rise to room temperature (20 °C) for 24 h. The mixture was quenched (aq. NH₄Cl), extracted with CH₂Cl₂, washed with water, and the organic phase was dried over Na₂SO₄. After evaporation of the solvent, the crude product was purified by column chromatography (φ = 20 mm, h = 530 mm, 50 g silica gel, eluent: EtOAc) to give 0.230 g (71%) of **8** as a light yellow oil. The isolated product **8** is a mixture of two diastereoisomers (**A** and **B**) in a ratio 95:5 (NMR data). The oil was crystallized from Et₂O/ petroleum ether to give colorless crystals, which are again mixture of two diastereoisomers (**A** and **B**) in a ratio 96:4 (NMR data).

Method B: To a solution of **7** (0.180 g, 0.737 mmol) in dry THF (10 ml) LDA (0.74 ml, 1.474 mmol) was added at -78 °C through a septum under Ar atmosphere. After 1 h 3,5-dimethoxybenzyl bromide (0.227 g, 0.982 mmol) dissolved in THF (2 ml) was added. After stirring for 4 h at -78 °C the temperature was allowed to rise to room temperature (20 °C) for 24 h. The mixture was quenched (aq. NH₄Cl), extracted with CH₂Cl₂, washed with water, and the organic phase was dried over Na₂SO₄. After evaporation of the solvent, the crude product was purified by column chromatography (φ = 20 mm, h = 530 mm, 50 g silica gel, eluent: EtOAc) to give 0.134 g (55%) of the **8** as a light yellow oil. The isolated product **8** is a mixture of two diastereoisomers (**A** and **B**) in a ratio 95:5 (NMR data). R_f = 0.53 (eluent: EtOAc, the two diastereoisomers have the same R_f -value in different solvents or mixture of solvents), mp = 106–108 °C (PE/Et₂O; mixture of two diastereoisomers in ratio 96:4). ¹H NMR: δ = 7.23–7.33 (m, 3H, H-12, H-14, H-16), 7.20–7.21 (m, 2H, H-13, H-15), 6.39 (t, J = 2.3, 1H, H-21_{isomer A}), 6.35 (t, J = 2.3, 1H, H-21_{isomer B}), 6.25 (d, J = 2.2, 2H, H-19_{isomer A}, H-23_{isomer A}), 6.23 (d, J = 2.2, 2H, H-19_{isomer B}, H-23_{isomer B}), 5.70 (d, J = 14.7, 1H, H-10_{isomer B}), 5.27 (d, J = 14.8, 1H, H-10_{isomer A}), 4.2 (t, J = 3.8, 1H, H-6_{isomer B}), 4.15 (t, J = 4.7, 1H, H-6_{isomer A}), 4.02 (d, J = 14.7, 1H, H-10_{isomer B}), 3.87 (d, J = 14.7, 1H, H-10_{isomer A}), 3.74 (s, 6H, 2OCH₃), 3.58 (dt, J = 12.2, 8.5, 1H, H-9), 3.36 (m, 1H, H-9), 3.07 (d, J = 4.90, 2H, H-17), 2.90 (dd, J = 10.7, 6.4, 1H, H-3), 2.20–2.25 (m, 1H, H-7), 1.92–1.96 (m, 1H, H-8), 1.80–1.85 (m, 1H, H-7), 1.65–1.69 (m, 1H, H-8). ¹³C NMR: δ = 167.65 (s, NC=O), 164.87 (s, NC=O), 160.89 (2s, C-20, C-22), 137.44* (s, C-

11), 135.89* (s, C-18), 128.92 (2d, C-12, C-16), 128.45 (2d, C-13, C-15), 128.05 (d, C-14), 107.48 (2d, C-19, C-23), 99.99 (d, C-21), 62.45 (d, C-6), 57.92 (d, C-3), 55.43 (2q, 2OCH₃), 47.38 (t, C-10), 44.98 (t, C-9), 37.22 (t, C-17), 29.38 (t, C-7), 21.94 (t, C-8). MS (CI) m/z = 395 (100, [M+1]⁺), 243 (90), 90 (55). Anal. Calcd for C₂₃H₂₆N₂O₄ (394.471): C 70.03, H 6.64, N 7.10; Found: C 69.74, H 6.95, N 7.19.

(8*aS*)-2-benzyl-3-(3-methylbenzoyl)hexahydro-pyrrolo[1,2-*a*]-pyrazine-1,4-dione **9** and 2-benzyl-8*a*-(3-methylbenzoyl)hexahydro-pyrrolo[1,2-*a*]-pyrazine-1,4-dione **10**

Method A: To a solution of **7** (0.200 g, 0.819 mmol) in dry THF (10 ml) LHMDs (1.23 ml, 1.228 mmol) was added at -78 °C through a septum under Ar atmosphere. After 1 h 3-methylbenzoyl chloride (0.13 ml, 0.982 mmol) was added portion wise for a period of 15 min. After stirring for 3 h at -78 °C the temperature was allowed to rise to room temperature (20 °C) for 24 h. The mixture was quenched (aq. NH₄Cl), extracted with CH₂Cl₂, washed with water, and the organic phase was dried over Na₂SO₄. After evaporation of the solvent, the crude product was purified by column chromatography (φ = 20 mm, h = 530 mm, 50 g silica gel, eluent: CH₂Cl₂/Et₂O = 15:1) to give 0.075 g (25%) of **9** (colorless crystals), as single diastereoisomer. R_f = 0.54 (eluent: EtOAc/CH₃OH = 40:1); mp = 153–155 °C (PE/Et₂O). ¹H NMR: δ = 7.89 (d, J = 7.80, 1H, H-23), 7.86 (s, 1H, H-19), 7.41 (dt, J = 8.22, 0.66, 1H, H-21), 7.34 (t, J = 7.68, 1H, H-22), 7.23–7.25 (m, 3H, H-13, H-14, H-15), 7.15 (m, 2H, H-12, H-16), 5.50 (s, 1H, H-6), 5.03 (d, J = 14.80, 1H, H-10), 4.33 (dd, J = 10.26, 6.84, 1H, H-3), 4.06 (d, J = 14.80, 1H, H-10), 3.58–3.62 (m, 1H, H-9), 3.39–3.43 (m, 1H, H-9), 2.48–2.52 (m, 1H, H-7), 2.40 (s, 3H, H-24), 2.07–2.14 (m, 1H, H-7), 1.99–2.05 (m, 1H, H-8), 1.81–1.89 (m, 1H, H-8). ¹³C NMR: δ = 191.17 (s, C=O), 169.44 (s, NC=O), 159.51 (s, NC=O), 138.63* (s, C-11), 135.42 (d, C-21), 135.00* (s, C-18), 133.85* (s, C-20), 130.03 (d, C-19), 128.89 (4d, C-12, C-13, C-15, C-16), 128.63 (d, C-22), 128.16 (d, C-14), 127.09 (d, C-23), 67.91 (d, C-6), 59.46 (d, C-3), 49.08 (t, C-10), 46.13 (t, C-9), 29.47 (t, C-7), 22.60 (t, C-8), 21.35 (q, CH₃). MS (CI) m/z = 363 (78, [M+1]⁺), 119 (100). Anal. Calcd for C₂₂H₂₂N₂O₃ (362.429): C 72.91, H 6.12, N 7.73; Found: C 73.15, H 6.33, N 7.97.

Method B: To a solution of **7** (0.150 g, 0.614 mmol) in dry THF (10 ml) LDA (0.61 ml, 1.228

mmol) was added at $-78\text{ }^{\circ}\text{C}$ through a septum under Ar atmosphere. After 1 h 3-methylbenzoyl chloride (0.18 ml, 1.351 mmol) was added portion wise for a period of 10 min. After stirring for 3 h at $-78\text{ }^{\circ}\text{C}$ the mixture was quenched (aq. NH_4Cl), extracted with CH_2Cl_2 , and washed with water and the organic phase was dried over Na_2SO_4 . After evaporation of the solvent, the crude product was purified by column chromatography ($\varphi = 20\text{ mm}$, $h = 530\text{ mm}$, 50 g silica gel, eluent: PE/ $\text{Et}_2\text{O} = 1:4$). It was isolated 0.058 g (26%) of product **9** and 0.019 g (9%) of product **10** as light yellow oil. The data of **9** are identical with those obtained using LHMDS as a deprotonating agent.

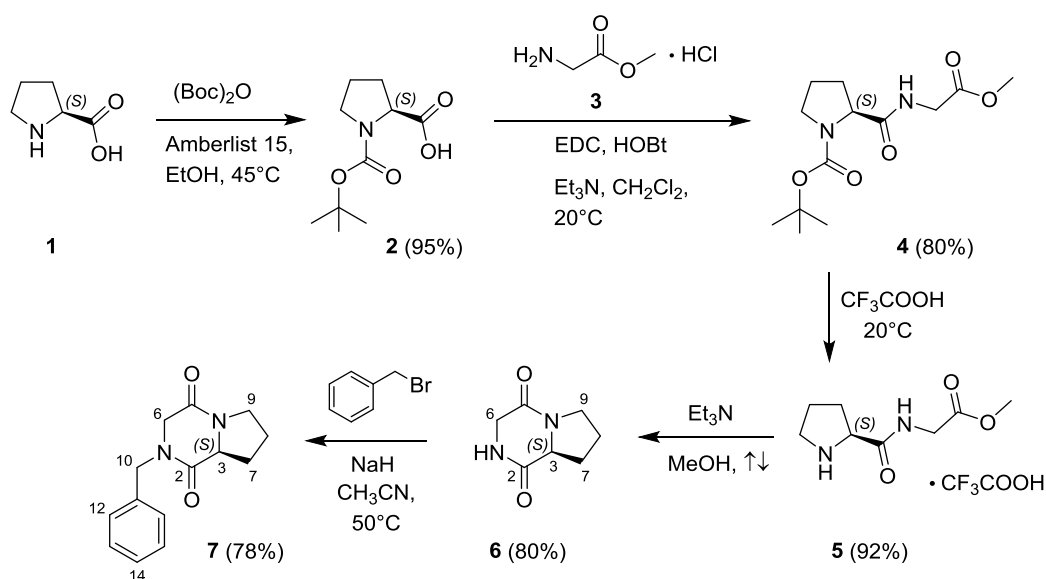
Data for **10**: $R_f = 0.45$ (eluent: $\text{EtOAc}/\text{CH}_3\text{OH} = 40:1$). $^1\text{H NMR}$: $\delta = 8.15$ (d, $J = 7.80$, 1H, H-23), 8.04 (d, 1H, H-19), 7.44 (d, $J = 7.56$, 1H, H-21), 7.38 (t, $J = 7.74$, 1H, H-22), 7.19–7.22 (m, 1H, H-14), 7.15–7.19 (m, 2H, H-13, H-15), 6.93–6.94 (m, 2H, H-12, H-16), 4.71 (d, $J = 14.70$, 1H, H-10), 4.35 (d, $J = 14.70$, 1H, H-10), 3.82 (d, $J = 17.04$, 1H, H-6), 3.72–3.76 (m, 1H, H-9b), 3.69 (d, $J = 17.04$, 1H, H-6), 3.47–3.51 (m, 1H, H-9), 3.01–3.06 (m, 1H, H-7), 2.68–2.72 (m, 1H, H-7), 2.43 (s, 3H, H-24), 1.95–2.01 (m, 1H, H-8), 1.73–1.81 (m, 1H, H-8). $^{13}\text{C NMR}$: $\delta = 193.02$ (s, C=O), 165.09 (s, NC=O), 165.05 (s, NC=O), 138.60* (s, C-11), 135.20* (s, C-18), 134.91 (d, C-21), 132.71* (s, C-20), 130.65 (d, C-19), 128.88 (2d, C-13, C-15), 128.51 (d, C-22), 127.98 (d, C-14), 127.82 (2d, C-12, C-16), 127.60 (d, C-23), 77.39 (s, C-3), 51.77 (t, C-6), 50.53 (t, C-10), 44.81 (t, C-9), 33.71 (t, C-7), 21.99 (t, C-8), 21.45 (q, CH_3). MS (CI) $m/z = 363$ (100, $[\text{M}+1]^+$), 243 (47), 119 (68), 91 (47). Anal. Calcd for $\text{C}_{22}\text{H}_{22}\text{N}_2\text{O}_3$

(362.429): C 72.91, H 6.12, N 7.73; Found: C 72.64, H 5.89, N 7.53.

RESULTS AND DISCUSSION

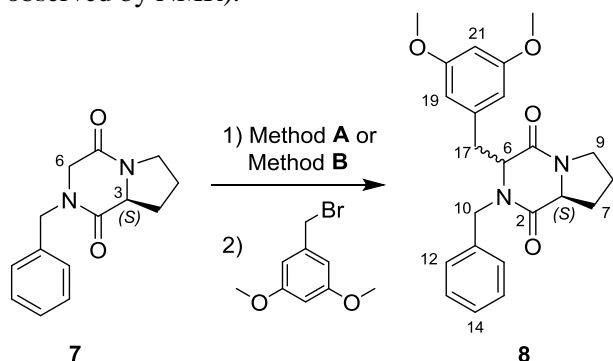
The unsubstituted diketopiperazine Cyclo(Gly-Pro) **6** was synthesized according published procedure over 4 steps (Scheme 1) without purification of the intermediates [22]. However, we could significantly improve the overall yield of **6** to 56% starting with L-proline **1**, compared with the published yield of 38% for the reaction sequence from **2** to **6**. The N-benylation of **6** occurred by using NaH, benzylbromide in acetonitrile in 78% yield and it was curious that we could not find this procedure in the literature. The synthesis of compound **7** has been described to proceed in 56% yield by multicomponent Ugi-reaction, however without taking into account the yield for preparation of one of the starting compounds that needs 5-step procedure [23].

The N-benzylated DKP **7** was used as starting compound for the planned experiments. For the deprotonation of **7** the reagents lithium hexamethyldisilazide (LHMDS) and lithium diisopropyl amide (LDA) were used (Scheme 2). The alkylation of the generated enolate was realized with 3,5-dimethoxybenzyl bromide as a model compound, since 3,5-dichloro-4-hydroxybenzyl bromide, needed for the synthesis of DKP **A** was not commercially available. The reaction sequence using LHMDS leading to DKP **8** was high yielding, whereas with LDA a moderate yield could be realized.



Scheme 1. Synthesis of the Cyclo(Gly-Pro) **6** and the N-benzylated DKP **7**.

In both cases an excellent diastereoselectivity was observed. One crystallization from diethyl ether/petroleum ether could not improve the diastereoisomeric ratio (**8a**:**8b** = 96:4-ratio was observed by NMR).



Method A: LHMDS 71% **8a**:**8b** = 95:5 (90% de)
Method B: LDA 55% **8a**:**8b** = 95:5 (90% de)

Scheme 2. Alkylation of **7** with 3,5-dimethoxybenzyl bromide using LHMDS (Method A) or LDA (Method B) as deprotonating agents (the numbering of the C-atoms is presented to support the assignment of the NMR spectra).

The configuration of the newly formed stereogenic center in the major diastereoisomer **8a** was determined by using advanced NMR experiments. Important prerequisite was the rigid structure of the 2,5-diketopiperazine ring fused to the cyclic five-membered proline-ring resulting in a stable boat conformation of the DKP [24, 25]. For determining the configuration at the stereogenic center C-6 it was necessary to identify the relative position of the 3,5-dimethoxybenzyl moiety attached. By means of NOESY spectra the proton proximities shown with arrows in Fig. 3 were observed (only most important proton-proton NOE interdependencies are presented). The observed proximities between the formal proline proton at the C-3 position of the DKP-ring and the *ortho*-proton of the 3,5-dimethoxybenzyl moiety, as well as the positions of protons from the both benzylic CH₂-groups relative to those of the C-6 proton, allowed to deduce the configuration of C-6 stereogenic center as *R* taking into account the known *S* configuration of C-3. Consequently, the major diastereoisomer of compound **8** is formed as a result of the reaction between deprotonated DKP **7** and 3,5-dimethoxybenzyl bromide approaching from the less hindered opposite direction relative to the tilt between the proline and DKP fused rings.

As next aim in the feasibility study was proved and tested the reaction of deprotonated **7** with 3-methylbenzoyl chloride (Scheme 3). Irrespective of

the deprotonation agent (LHMDS or LDA) the expected product **9** could be isolated after chromatography purification in low yield (25%).

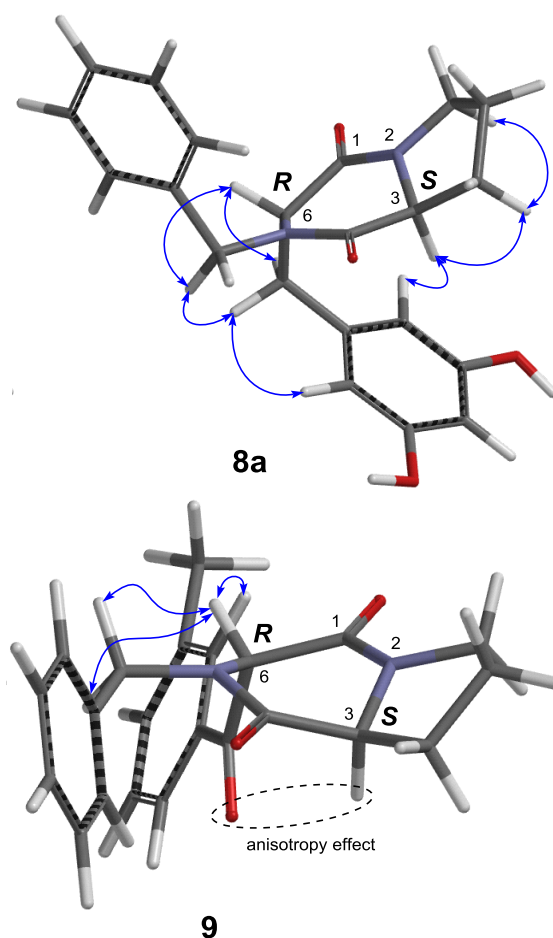
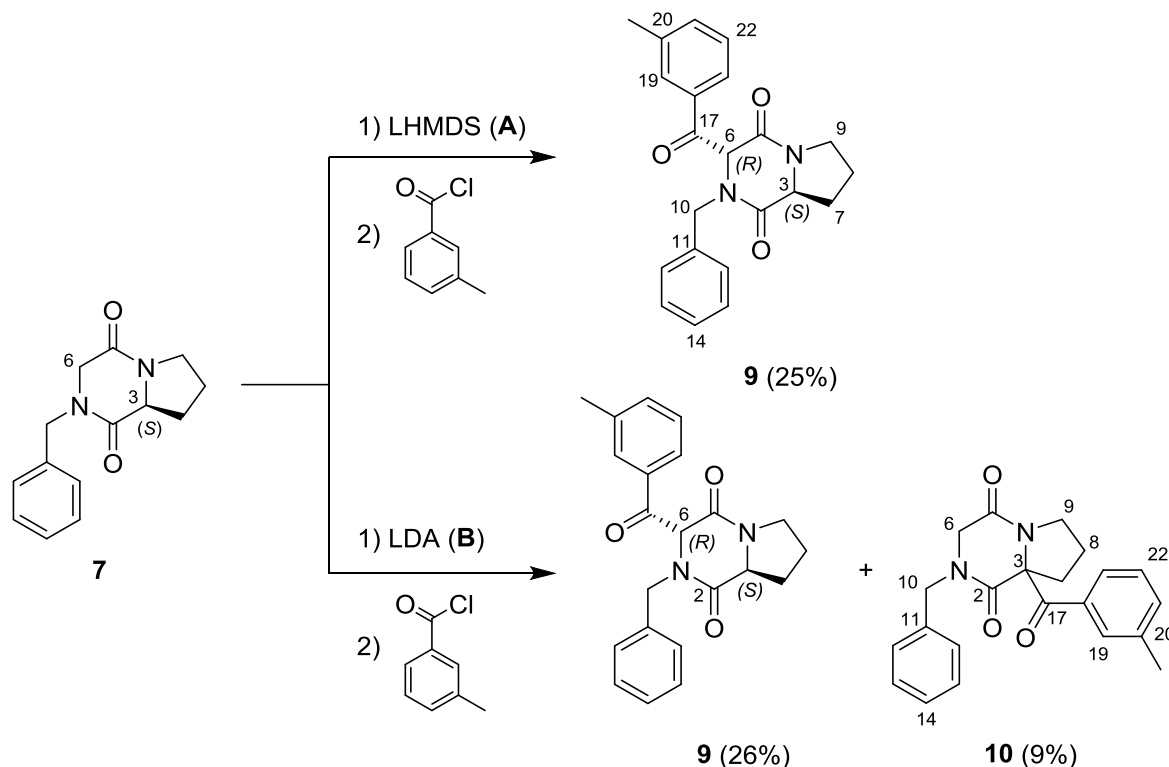


Fig. 3. The observed proton proximities by means of NOESY spectra used for determination of the configuration of compounds **8a** (major diastereoisomer) and **9**.

Surprisingly, in the reaction performed with LDA the formation of the by-product **10** was observed (9% yield of isolated compound). Compounds **9** and **10** could be separated by column chromatography and isolated in pure form. It is noteworthy that compound **9** was formed as a single diastereoisomer. The stereoselectivity was expected to be the same as in the case of compound **8**. The most significant argument for the configuration of **9** was the chemical shift of the C-3 proton (4.33 ppm), which was downfield shifted compared with the same proton in compound **8a** (2.90 ppm). This observation was obviously a result of the anisotropy effect and the corresponding deshielding of C-3 proton. The observed proton proximities in the NOESY spectra (Fig. 3) supported the suggested configuration for the C-6 stereogenic center as *R*. The NMR spectra of



Scheme 3. Acylation of **7** with 3-methylbenzoyl chloride using LHMDS (Method **A**) or LDA (Method **B**) as deprotonating agents (the numbering of the C-atoms is presented to support the assignment of the NMR spectra).

compound **10** (1D and 2D) clearly supported the structure presented in Scheme 3. At this moment the discussion about the formation of **10** would be speculative.

CONCLUSION

The feasibility of the reaction sequence deprotonation of diketopiperazine Cyclo(Gly-Pro) followed by reaction with electrophiles proved to be a promising strategy for synthesis of libraries of structurally diverse compounds possessing biological activity. The observed stereoselectivity is significant advantage in the synthesis of compounds with definite configuration.

Acknowledgements: Support by the National Science Fund of Bulgaria (projects UNA 17/2005 and DRNF 02/13/2009) is gratefully acknowledged.

REFERENCES

- M. B. Martins, I. Carvalho, *Tetrahedron*, **63**, 9923 (2007).
- P. J. Milne, G. Kilian, in: *Comprehensive Natural Products II*, L. Mander, H.-W. Liu (eds), Elsevier Ltd., 2010, p. 658.
- C. Cornacchia, I. Cacciatore, L. Baldassarre, A. Mollica, F. Feliciani, F. Pinnen, *Mini. Rev. Med. Chem.*, **12**, 2 (2012).
- A. D. Borthwick, *Chem. Rev.*, **112**, 3641 (2012).
- C. J. M. Graz, G. D. Grant, S. C. A. Brauns, A. Hunt, H. Jamie, P. J. Milne, *J. Pharm. Pharmacol.*, **52**, 75 (2000).
- S. Zhao, K. S. Smith, A. M. Deveau, C. M. Dieckhaus, M. A. Johnson, T. L. Macdonald, J. M. Cook, *J. Med. Chem.*, **45**, 1559 (2002).
- H. Woehlecke, H. Osada, A. Herrmann, H. Lage, *Int. J. Cancer*, **107**, 721 (2003).
- J. F. Sanz-Cervera, E. M. Stocking, T. Usui, H. Osada, R. M. Williams, *Bioorg. Med. Chem.*, **8**, 2407 (2000).
- K. Kanoh, S. Kohno, J. Katada, J. Takanashi, I. Uno, *J. Antibiot.*, **52**, 134 (1999).
- H. Habashita, M. Kokubo, S. Hamano, N. Hamanaka, M. Toda, S. Shibayama, H. Tada, K. Sagawa, D. Fukushima, K. Maeda, H. Mitsuya, *J. Med. Chem.*, **49** (2006).
- V. Mas, A. Falco, I. Brocal, L. Perez, J. M. Coll, A. Estepa, *Antiviral Res.*, **72**, 107 (2006).
- L. Yang, R.-X. Tan, Q. Wang, W.-Y. Huang, Y.-X. Yin, *Tetrahedron Lett.*, **43**, 6545 (2002).
- M. P. De Carvalho, W. R. Abraham, *Curr. Med. Chem.*, **19**, 3564 (2012).
- I. R. Shimi, N. Abedallah, S. Fathy, *Antimicrob. Agents Chemother.*, **11**, 373 (1977).

15. P. W. Baures, W. H. Ojala, W. J. Costain, M. C. Ott, A. Pradhan, W. B. Gleason, R. K. Mishra, R. L. Johnson, *J. Med. Chem.*, **40**, 3594 (1997).
16. P. Klausmeyer, O. M. Z. Howard, S. M. Shipley, T. G. McCloud, *J. Nat. Prod.*, **72**, 1369 (2009).
17. C. Prasad, A. Peterkofsky, *J. Biol. Chem.*, **251**, 3229 (1976).
18. A. Peterkofsky, F. Battaini, *Neuropeptides*, **1**, 105 (1980).
19. A. Peterkofsky, F. Battaini, Y. Koch, Y. Takahara, P. Dannies, *Mol. Cell. Biochem.*, **42**, 45 (1982).
20. A. Minelli, I. Bellezza, S. Grottelli, F. Pinnen, L. Brunetti, M. Vacca, *Peptides*, **27**, 105 (2006).
21. R. Ortiz-Castro, C. Díaz-Pérez, M. Martínez-Trujillo, R. E. del Río, J. Campos-García, J. López-Bucio, *Proc. Nat. Acad. Sci. USA*, **108**, 7253 (2011).
22. B. R. de Costa, X. He, J. T. M. Linders, C. Dominguez, Z. Q. Gu, W. Williams, W. D. Bowen, *J. Med. Chem.*, **36**, 2311 (1993).
23. C. R. B. Rhoden, D. G. Rivera, O. Kreye, A. K. Bauer, B. Westermann, L. A. Wessjohann, *J. Comb. Chem.*, **11**, 1078 (2009).
24. V. Madison, P. E. Young, E. R. Blout, *J. Am. Chem. Soc.*, **98**, 5358 (1976).
25. Z. Li, S. Mukamel, *J. Phys. Chem. A*, **111**, 11579 (2007).

СТРАТЕГИЯ ЗА СТЕРЕОСЕЛЕКТИВНО ФУНКЦИОНАЛИЗИРАНЕ НА 2,5-ДИКЕТОПИПЕРАЗИН ПОЛУЧЕН ОТ L-ПРОЛИН И ГЛИЦИН

А. Петрова, М. Панчева, К. Костова*, И. Загранярска, М. Тавлинова-Кирилова, В.
Димитров*

*Институт по Органична Химия с Център по Фитохимия, Българска Академия на Науките, ул. Акад. Г. Бончев,
бл. 9, 1113 София, България*

Постъпила на 15 март 2017 г.; Коригирана на 22 март 2017 г.

(Резюме)

Функционализирането на дикетопиперазин Cyclo(Gly-Pro) чрез използване на подходящ депротониращ реагент и електрофил предлага възможността за синтез на структурно разнообразни серии от съединения (библиотеки), притежаващи биоактивност. Този синтетичен подход беше доказан, че е осъществим по отношение на използване на разнообразни електрофили и особено относно наблюдаваната висока стереоселективност.

Bifunctionalized allenes. Part XX. A convenient and efficient regioselective synthesis of phosphorylated 3-(α -hydroxyalkyl)allenes

H. H. Hasanov, I. K. Ivanov, V. Ch. Christov*

Department of Chemistry, Faculty of Natural Sciences, Konstantin Preslavsky University of Shumen, 115 Universitetska St., 9712 Shumen, Bulgaria

Received February 08, 2017; Revised March 16, 2017

Dedicated to Acad. Bogdan Kurtev on the occasion of his 100th birth anniversary

A convenient and efficient regioselective synthesis of phosphorylated 3-(α -hydroxyalkyl)allenes by an atom-economical [2,3]-sigmatropic rearrangement of the mediated propargyl phosphites or phosphinites which can be readily prepared *via* reaction of (tetrahydro-2*H*-pyran-2-yloxy)-alkynols with dimethyl chlorophosphite or chlorodiphenyl phosphine respectively in the presence of a base is described.

Key words: synthesis; protection of hydroxy group; [2,3]-sigmatropic rearrangement; phosphorylated 3-(α -hydroxyalkyl)allenes

INTRODUCTION

The synthesis and application of allene derivatives has had a great influence in preparative organic chemistry during the last three decades. The crucial structural characteristic of allenes is the presence of two π electron clouds separated by a single sp-hybridized carbon atom. Due to that very unique structural and electronic arrangement allenic compounds have an extraordinary reactivity profiles. Moreover, functionalized allenes have also attracted growing attention due to their versatility as key building blocks for organic synthesis. The synthetic potential of functionalized allenes has been thoroughly explored in recent years. The research in that area has led to the development of novel methods for the construction of a variety of functionalized heterocyclic and carbocyclic systems [1–6].

There are variety of methods for the construction of hydroxyallenes that include prototropic rearrangement of propargylic alcohols [7, 8], metal-catalyzed nucleophilic addition of propargylic derivatives to aldehydes [9–15], Cu(I)-catalyzed reaction of propargylic chlorides with Grignard reagents [16, 17], metal-catalyzed reaction of propargylic oxiranes with organometallic compounds [18–22] and ketones [23, 24], reduction of alcohols, ethers, oxiranes *etc.* with aluminium reagents [25–27], Pd(0)-catalyzed reaction of cyclic carbonates with acetylenic compounds [28, 29], S_N2' [30, 31] and A_N [32, 33] reactions of metallated alkoxy-allenes

with oxiranes and ketones [34], and other routes [35].

In addition, there are methods [36–39] for the synthesis of phosphorus-containing allenes (phosphonates [40–43], phosphinates [44, 45], and phosphine oxides [46–51]) including reactions of α -alkynols with chloride-containing derivatives of phosphorus acids followed by [2,3]-sigmatropic rearrangement. Several diethylphosphono-substituted α -allenic alcohols were prepared by Brel [52, 53] directly from alcohols by Horner-Mark rearrangement of unstable propargylic phosphites.

As a part of our research program on the chemistry of the bifunctionalized allenes, we required a convenient method to introduce a phosphorus-containing group such as phosphonate or phosphine oxide group as well as a α -hydroxy group in the third position to the allenic system of double bonds. The above mentioned groups provoke organic researchers' interest because of their useful functionalities in organic synthesis. The emphasis is particularly on the applications of these groups as temporary transformers of chemical reactivity of the allenic system in the synthesis of eventually heterocyclic compounds.

Our scientific interest on the synthesis [54, 55] and electrophilic cyclization [56, 58] and cycloisomerisation reactions [57, 58] of phosphorylated 1-(α -hydroxyalkyl)allenes [54, 56, 57], 1-(β -hydroxyalkyl)allenes [55, 58], 4-hydroxy-1,3,4-triphenyl-buta-1,2-dienes [63] and 3-(β -hydroxyalkyl)allenes [64] reported in our previous articles led to the discovery of a convenient and efficient

* To whom all correspondence should be sent:
E-mail: vchristo@shu.bg

regioselective synthesis of phosphorylated 3-(α -hydroxyalkyl)allenes by an atom economical [2,3]-sigmatropic rearrangement of the mediated (tetrahydro-2H-pyran-2-yloxy)-propargyl phosphite or phosphinite.

EXPERIMENTAL

General Information

All new synthesized compounds were purified by column chromatography and characterized on the basis of NMR, IR, and microanalytical data. NMR spectra were recorded on DRX Bruker Avance-250 (Bruker BioSpin, Karlsruhe, Germany) (^1H at 250.1 MHz, ^{13}C at 62.9 MHz, ^{31}P at 101.2 MHz) and Bruker Avance II+600 (Bruker BioSpin GmbH, Karlsruhe, Germany) (^1H at 600.1 MHz, ^{13}C at 150.9 MHz, ^{31}P at 242.9 MHz) spectrometers for solutions in CDCl_3 . All ^1H and ^{13}C NMR experiments were measured referring to the signal of internal TMS and ^{31}P NMR experiments were measured referring to the signal of external 85% H_3PO_4 . J values are given in hertz. IR spectra were recorded with an FT-IRAffinity-1 Shimadzu spectrophotometer (Shimadzu, Tokyo, Japan). Elemental analyses were carried out by the Microanalytical Service Laboratory of Faculty of Chemistry and Pharmacy, University of Sofia, Bulgaria, using Vario EL3 CHNS(O) (Elementar Analysensysteme, Hanau, Germany). Column chromatography was performed on Kieselgel 60 F_{254} (70–230 mesh ASTM, 0.063–0.200 nm, Merck). Et_2O and THF were distilled from Na wire/benzophenone, CH_2Cl_2 was distilled over CaH_2 , and other organic solvents used in this study were dried over appropriate drying agents by standard methods and distilled prior to use. All other chemicals used in this study were commercially available and were used without additional purification unless otherwise noted. Reactions were carried out in oven dried glassware under an argon atmosphere and exclusion of moisture. All compounds were checked for purity on TLC plates Kieselgel 60 F_{254} (Merck).

General procedure [59-62] for synthesis of (tetrahydro-2H-pyran-2-yloxy)-alkanone 2

A solution of the α -hydroxy-alkanones **1** (120 mmol) and DHP (3,4-dihydro-2H-pyran) (15.14 g, 180 mmol) in dry methylene chloride (100 mL) containing PPTS (pyridinium *p*-toluenesulfonate) (3 g, 12 mmol) is stirred for 10 h at room

temperature. Then the reaction was quenched with saturated NaHCO_3 and extracted with methylene chloride. The organic layer was dried over anhydrous sodium sulfate. After evaporation of the solvent, the residue was chromatographed on a column (silica gel, Kieselgel Merck 60 F_{254}) with a mixture of ethyl acetate and hexane as an eluent. The pure products **2** had the following properties:

1-(Tetrahydro-2H-pyran-2-yloxy)-propan-2-one (2a). Pale yellow oil, yield: 95%. Eluent for TLC: ethyl acetate:hexane = 1:1, R_f 0.59; IR (neat, cm^{-1}): 1120 (C-O-C), 1721 (C=O). $^1\text{H-NMR}$ (250.1 MHz): δ_{H} 1.45-1.83, 3.55-3.71, 4.37-4.46 (overlapping multiplets, 9H, OTHP), 2.07 (s, 3H, Me), 4.11-4.27 (m, 2H, CH_2). $^{13}\text{C-NMR}$ (62.9 MHz) δ_{C} 19.5 (CH_2), 25.3 (CH_2), 26.7 (CH_3), 30.1 (CH_2), 62.1 (CH_2), 74.4 (CH_2), 99.0 (CH), 205.7 (C). Anal. Calcd. for $\text{C}_8\text{H}_{14}\text{O}_3$: C 60.74, H 8.92; found: C 60.68, H 8.87.

3-(Tetrahydro-2H-pyran-2-yloxy)-butan-2-one (2b). Pale yellow oil, yield: 96%. Eluent for TLC: ethyl acetate:hexane = 1:2, R_f 0.53; IR (neat, cm^{-1}): 1125 (C-O-C), 1721 (C=O). $^1\text{H-NMR}$ (250.1 MHz): δ_{H} 1.20 (d, $J=6.3$ Hz, 3H, Me-CH), 1.49-1.71, 3.60-3.73, 4.59-4.67 (overlapping multiplets, 9H, OTHP), 2.19 (s, 3H, Me), 4.03-4.11 (m, 2H, CH). $^{13}\text{C-NMR}$ (62.9 MHz) δ_{C} 16.5 (CH_3), 19.5 (CH_2), 25.0 (CH_3), 25.7 (CH_2), 30.7 (CH_2), 63.1 (CH_2), 77.0 (CH), 95.4 (CH), 211.5 (C). Anal. Calcd. for $\text{C}_9\text{H}_{16}\text{O}_3$: C 62.77, H 9.36; found: C 62.72, H 9.40.

Phenyl-[1-(tetrahydro-2H-pyran-2-yloxy)-cyclohexyl]-methanone (2c). Colourless oil, yield: 93%. Eluent for TLC: ethyl acetate:hexane = 1:4, R_f 0.44; IR (neat, cm^{-1}): 1123 (C-O-C), 1442, 1489 (Ph), 1680 (C=O). $^1\text{H-NMR}$ (250.1 MHz): δ_{H} 1.35-2.11, 3.49-3.79, 5.15-5.24 (overlapping multiplets, 19H, OTHP, cyclohexyl), 7.34-8.02 (m, 5H, Ph). $^{13}\text{C-NMR}$ (62.9 MHz) δ_{C} 20.2 (CH_2), 24.0 (2x CH_2), 25.2 (CH_2), 26.0 (CH_2), 31.6 (CH_2), 35.2 (2x CH_2), 62.4 (CH_2), 82.7 (C), 97.2 (CH), 128.1-133.0 (Ph), 201.4 (C). Anal. Calcd. for $\text{C}_{18}\text{H}_{24}\text{O}_3$: C 74.97, H 8.39; found: C 75.02, H 8.43.

Synthesis and spectral data of *diphenyl-2-(tetrahydro-2H-pyran-2-yloxy)-ethanone 2d* were described in our previous paper [63].

General procedure for synthesis of (tetrahydro-2H-pyran-2-yloxy)-alkynols 3

Ethylmagnesium bromide [prepared from magnesium (1.22 g, 50 mmol) and ethyl bromide (5.50 g, 50 mmol) in dry THF (50 mL)] is added dropwise under stirring to the phenylacetylene (50

mmol) and then the mixture is refluxed for 2 h. The solution of the prepared ethynyl magnesium bromide is added dropwise under stirring to the (tetrahydro-2H-pyran-2-yloxy)-alkanones **2** (100 mmol). The mixture is refluxed for 16 h and after cooling is hydrolyzed with a saturated aqueous solution of ammonium chloride. The organic layer is separated, washed with water, and dried over anhydrous sodium sulfate. Solvent and the excess of ketone are removed by distillation. Purification of the residue is achieved by column chromatography (silica gel, Kieselgel Merck 60 F₂₅₄) with ethyl acetate-hexane. The pure products **3** had the following properties:

2-Methyl-4-phenyl-1-(tetrahydro-2H-pyran-2-yloxy)-but-3-yn-2-ol (3a). Yellow oil, yield: 75%. Eluent for TLC: ethyl acetate:hexane = 1:4, R_f 0.52; IR (neat, cm⁻¹): 1123 (C-O-C), 1443, 1489 (Ph), 3420 (OH). ¹H-NMR (600.1 MHz): δ_H 1.58 (s, 3H, Me), 1.63-1.92, 3.99-4.09, 4.67-4.78 (overlapping multiplets, 9H, OTHP), 3.31 (s, 1H, OH), 3.60-3.90 (m, 2H, CH₂), 7.26-7.43 (m, 5H, Ph). ¹³C-NMR (150.9 MHz) δ_C 19.4 (CH₂), 25.3 (CH₂), 26.2 (CH₃), 30.6 (CH₂), 62.8 (CH₂), 67.6 (C), 76.2 (CH₂), 83.7 (C), 99.9 (C), 105.5 (CH), 122.6-131.4 (Ph). Anal. Calcd. for C₁₆H₂₀O₃: C 73.82, H 7.74; found: C 73.76, H 7.78.

3-Methyl-1-phenyl-4-(tetrahydro-2H-pyran-2-yloxy)-pent-1-yn-3-ol (3b). Yellow oil, yield: 79%. Eluent for TLC: ethyl acetate:hexane = 1:4, R_f 0.51; IR (neat, cm⁻¹): 1123 (C-O-C), 1441, 1491 (Ph), 3412 (OH). ¹H-NMR (600.1 MHz): δ_H 1.10-1.23, 3.53-3.68, 4.73-4.80 (overlapping multiplets, 9H, OTHP), 1.36 (d, *J*=5.4 Hz, 3H, Me-CH), 1.44 (s, 3H, Me), 2.89 (s, 1H, OH), 3.89-3.97 (m, 2H, CH₂), 7.18-7.32 (m, 5H, Ph). ¹³C-NMR (150.9 MHz) δ_C 15.4 (CH₃), 19.0 (CH₂), 23.3 (CH₃), 25.7 (CH₂), 31.6 (CH₂), 62.6 (CH₂), 71.9 (C), 80.8 (C), 90.0 (C), 91.1 (CH), 96.5 (CH), 120.6-133.0 (Ph). Anal. Calcd. for C₁₇H₂₂O₃: C 74.42, H 8.08; found: C 74.46, H 8.05.

1,3-Diphenyl-1-[1-(tetrahydro-2H-pyran-2-yloxy)-cyclohexyl]-prop-2-yn-1-ol (3c). Pale yellow oil, yield: 65%. Eluent for TLC: ethyl acetate:hexane = 1:4, R_f 0.63; IR (neat, cm⁻¹): 1125 (C-O-C), 1443, 1489 (Ph), 3395 (OH). ¹H-NMR (600.1 MHz): δ_H 1.35-1.65, 3.49-3.79, 5.01-5.07 (overlapping multiplets, 9H, OTHP), 1.71-2.10 (overlapping multiplets, 10H, cyclohexyl), 2.91 (s, 1H, OH), 7.12-7.59 (m, 10H, 2Ph). ¹³C-NMR (150.9 MHz) δ_C 20.8 (CH₂), 23.9 (2xCH₂), 25.0 (CH₂), 25.8 (CH₂), 31.4 (CH₂), 33.1 (2xCH₂), 63.6 (CH₂), 82.1 (C), 84.2 (C), 87.1 (C), 87.8 (C), 99.2

(CH), 123.0-142.4 (2Ph). Anal. Calcd. for C₂₆H₃₀O₃: C 79.97, H 7.74; found: C 80.01, H 7.69.

Synthesis and spectral data of *1,2,4-triphenyl-1-(tetrahydro-2H-pyran-2-yloxy)-but-3-yn-2-ol* **3d** were described in our previous paper [63].

General procedure for synthesis of dimethyl (tetrahydro-2H-pyran-2-yloxy)-alka-1,2-dienephosphonates 5

To a solution of phosphorus trichloride (2.75 g, 20 mmol) and triethylamine (2.23 g, 22 mmol) in dry diethyl ether (60 mL) at -70 °C was added dropwise with stirring a solution of the (tetrahydro-2H-pyran-2-yloxy)-alkynol **3** (20 mmol) in the same solvent (20 mL). After 30 min stirring at the same condition a solution of pyridine (3.16 g, 44 mmol) and of methanol (1.28 g, 40 mmol) in dry diethyl ether (50 mL) were added. The reaction mixture was stirred for an hour at the same temperature and for 12 hours at room temperature. The mixture was then washed with water, 2N HCl, extracted with ether, washed with saturated NaCl, and dried over anhydrous sodium sulfate. After evaporation of the solvent, the residue was chromatographed on a column (silica gel, Kieselgel Merck 60 F₂₅₄) with a mixture of ethyl acetate and hexane as an eluent to give the pure product **5** as an oil, which had the following properties:

Dimethyl 3-methyl-1-phenyl-4-(tetrahydro-2H-pyran-2-yloxy)-buta-1,2-dienephosphonate (5a). Yellow oil, yield: 72%. Eluent for TLC: ethyl acetate:hexane = 1:1, R_f 0.40; IR (neat, cm⁻¹): 1121 (C-O-C), 1263 (P=O), 1445, 1495 (Ph), 1950 (C=C=C). ¹H-NMR (600.1 MHz): δ_H 1.46-1.84, 3.64-3.75, 4.39-4.44 (overlapping multiplets, 9H, OTHP), 2.02 (d, *J*=7.7 Hz, 3H, Me), 3.77 (d, *J*=12.1 Hz, 6H, 2MeO), 4.19-4.33 (m, 2H, CH₂), 7.22-7.80 (m, 5H, Ph). ¹³C-NMR (150.9 MHz) δ_C 15.5 (*J*=5.7 Hz, CH₃), 19.3 (CH₂), 24.9 (CH₂), 29.7 (CH₂), 52.6 (*J*=14.4 Hz, 2xCH₃), 61.7 (CH₂), 68.0 (*J*=5.0 Hz, CH₂), 95.5 (*J*=182.6 Hz, C), 97.4 (CH), 104.5 (*J*=8.3 Hz, C), 117.6-129.7 (Ph), 208.8 (*J*=1.8 Hz, C). ³¹P-NMR (242.9 MHz): δ_P 18.6. Anal. Calcd. for C₁₈H₂₅O₃P: C 61.36, H 7.15; found: C 61.43, H 7.20.

Dimethyl 3-methyl-1-phenyl-4-(tetrahydro-2H-pyran-2-yloxy)-penta-1,2-dienephosphonate (5b). Yellow oil, yield: 77%. Eluent for TLC: ethyl acetate:hexane = 1:1, R_f 0.44; IR (neat, cm⁻¹): 1119 (C-O-C), 1260 (P=O), 1445, 1495 (Ph), 1946 (C=C=C). ¹H-NMR (600.1 MHz): δ_H 1.46 (d, *J*=5.7 Hz, 3H, Me-CH), 1.47-1.58, 3.55-3.71, 4.51-4.62

(overlapping multiplets, 9H, OTHP), 1.85 (d, $J=6.9$ Hz, 3H, Me), 3.76 (d, $J=12.4$ Hz, 6H, 2MeO), 3.89-3.97 (m, 1H, CH), 7.18-7.91 (m, 5H, Ph). $^{13}\text{C-NMR}$ (150.9 MHz) δ_{C} 12.4 ($J=4.5$ Hz, CH_3), 19.7 (CH_2), 20.3 (CH_3), 25.7 (CH_2), 30.8 (CH_2), 53.4 ($J=13.0$ Hz, $2\times\text{CH}_3$), 63.4 (CH_2), 74.6 ($J=4.6$ Hz, CH), 94.0 ($J=185.0$ Hz, C), 95.8 (CH), 106.7 ($J=7.7$ Hz, C), 118.7-129.4 (Ph), 209.7 ($J=2.0$ Hz, C). $^{31}\text{P-NMR}$ (242.9 MHz): δ_{P} 18.9. Anal. Calcd. for $\text{C}_{19}\text{H}_{27}\text{O}_5\text{P}$: C 62.28, H 7.43; found: C 62.34, H 7.47.

Dimethyl 1,3-diphenyl-3-[1-(tetrahydro-2H-pyran-2-yloxy)-cyclohexyl]-propa-1,2-diene-phosphonate (5c). Yellow oil, yield: 73%. Eluent for TLC: ethyl acetate:hexane = 1:1, R_{f} 0.42; IR (neat, cm^{-1}): 1125 (C-O-C), 1258 (P=O), 1447, 1493 (Ph), 1925 (C=C=C). $^1\text{H-NMR}$ (600.1 MHz): δ_{H} 1.30-2.03, 3.51-3.59, 4.38-4.77 (overlapping multiplets, 19H, OTHP, cyclohexyl), 3.78 (d, $J=12.0$ Hz, 6H, 2MeO), 7.18-7.98 (m, 10H, 2Ph). $^{13}\text{C-NMR}$ (150.9 MHz) δ_{C} 18.5 (CH_2), 22.5 ($2\times\text{CH}_2$), 24.4 (CH_2), 25.0 (CH_2), 30.6 (CH_2), 42.5 ($2\times\text{CH}_2$), 51.7 ($J=14.8$ Hz, $2\times\text{CH}_3$), 62.9 (CH_2), 78.7 ($J=4.9$ Hz, C), 95.2 ($J=182.8$ Hz, C), 97.5 (CH), 113.7 ($J=7.8$ Hz, C), 118.0-138.8 (2Ph), 211.5 ($J=1.7$ Hz, C). $^{31}\text{P-NMR}$ (242.9 MHz): δ_{P} 18.5. Anal. Calcd. for $\text{C}_{28}\text{H}_{35}\text{O}_5\text{P}$: C 69.69, H 7.31; found: C 69.63, H 7.28.

Synthesis and spectral data of *dimethyl 1,3,4-triphenyl-4-(tetrahydro-2H-pyran-2-yloxy)-buta-1,2-dienephosphonate 5d* were described in our previous paper [63].

General procedure for synthesis of diphenyl (tetrahydro-2H-pyran-2-yloxy)-alka-1,2-dien-1-yl phosphine oxides 7

To a solution of the (tetrahydro-2H-pyran-2-yloxy)-alkynol **3** (20 mmol) and triethylamine (2.23 g, 22 mmol) in dry diethyl ether (60 mL) at -70 °C, a solution of freshly distilled diphenylchloro phosphine (4.41 g, 20 mmol) in the same solvent (20 mL) was added dropwise with stirring. The reaction mixture was stirred for an hour at the same temperature and for 8 h at room temperature and then washed with water, 2N HCl, extracted with diethyl ether, and the extract was washed with saturated NaCl, and dried over anhydrous sodium sulfate. The solvent was removed using a rotatory evaporator, and the residue was purified by column chromatography on a silica gel (Kieselgel Merck 60 F_{254}) with ethyl acetate-hexane to give the pure product **7** as oil, which had the following properties:

Diphenyl 3-methyl-1-phenyl-4-(tetrahydro-2H-pyran-2-yloxy)-buta-1,2-dien-1-yl phosphine oxide (7a). Yellow oil, yield: 79%. Eluent for TLC: ethyl acetate:hexane = 1:1, R_{f} 0.42; IR (neat, cm^{-1}): 1119 (C-O-C), 1178 (P=O), 1437, 1493 (Ph), 1948 (C=C=C). $^1\text{H-NMR}$ (600.1 MHz): δ_{H} 1.49-1.83, 3.63-3.77, 4.44-4.59 (overlapping multiplets, 9H, OTHP), 2.08 (d, $J=7.6$ Hz, 3H, Me), 4.18-4.40 (m, 2H, CH_2), 7.20-8.02 (m, 15H, 3Ph). $^{13}\text{C-NMR}$ (150.9 MHz) δ_{C} 14.5 (CH_3), 19.3 (CH_2), 25.3 (CH_2), 30.5 (CH_2), 60.8 (CH_2), 66.5 ($J=4.9$ Hz, CH_2), 98.4 ($J=185.9$ Hz, C), 101.5 (CH), 107.5 ($J=7.8$ Hz, C), 128.4-135.2 (3Ph), 209.7 ($J=2.3$ Hz, C). $^{31}\text{P-NMR}$ (242.9 MHz): δ_{P} 31.3. Anal. Calcd. for $\text{C}_{28}\text{H}_{29}\text{O}_3\text{P}$: C 75.66, H 6.58; found: C 75.70, H 6.63.

Synthesis and spectral data of 2-[4-(diphenylphosphinoyl)-1,2,4-triphenyl-but-2,3-dienyloxy]-tetrahydro-2H-pyran **7d** were described in our previous paper [63].

General procedure for synthesis of dimethyl 3-(α -hydroxyalkyl)-alka-1,2-dienephosphonates 8 and diphenyl 3-(α -hydroxyalkyl)-alka-1,2-dienyl phosphine oxides 9

A solution of the dimethyl (tetrahydro-2H-pyran-2-yloxy)-alka-1,2-dienephosphonates **5** or the diphenyl (tetrahydro-2H-pyran-2-yloxy)-alka-1,2-dien-1-yl phosphine oxides **7** (5 mmol) and PPTS (0.5 mmol) in ethanol (10 mL) was stirred at room temperature for 6 h. The mixture was then washed with water, extracted with methylene chloride and dried over anhydrous sodium sulfate. After evaporation of the solvent, the residue was chromatographed on a column (silica gel, Kieselgel Merck 60 F_{254}) with a mixture of ethyl acetate and hexane (3:1) as an eluent to give the pure products **8** or **9** as oils, which had the following properties:

Dimethyl 4-hydroxy-3-methyl-1-phenylbuta-1,2-dienephosphonate (8a). Pale yellow oil, yield: 80%. Eluent for TLC: ethyl acetate:hexane = 1:1, R_{f} 0.58; IR (neat, cm^{-1}): 1258 (P=O), 1447, 1491 (Ph), 1948 (C=C=C), 3376 (OH). $^1\text{H-NMR}$ (600.1 MHz): δ_{H} 1.98 (d, $J=7.5$ Hz, 3H, Me), 2.73 (s, 1H, OH), 3.77 (d, $J=11.8$ Hz, 6H, 2MeO), 5.18-5.26 (m, 2H, CH_2), 7.21-7.79 (m, 5H, Ph). $^{13}\text{C-NMR}$ (150.9 MHz) δ_{C} 15.4 ($J=5.0$ Hz, CH_3), 51.7 ($J=14.9$ Hz, $2\times\text{CH}_3$), 62.5 ($J=4.5$ Hz, CH_2), 94.9 ($J=182.5$ Hz, C), 104.7 ($J=7.8$ Hz, C), 117.1-129.4 (Ph), 209.4 ($J=1.8$ Hz, C). $^{31}\text{P-NMR}$ (242.9 MHz): δ_{P} 18.5. Anal. Calcd. for $\text{C}_{13}\text{H}_{17}\text{O}_4\text{P}$: C 58.21, H 6.39; found: C 58.14, H 6.44.

Dimethyl 4-hydroxy-3-methyl-1-phenylpenta-1,2-dienephosphonate (8b). Yellow oil, yield: 83%. Eluent for TLC: ethyl acetate:hexane = 1:1, R_f 0.61; IR (neat, cm^{-1}): 1262 (P=O), 1443, 1495 (Ph), 1944 (C=C=C), 3420 (OH). $^1\text{H-NMR}$ (600.1 MHz): δ_{H} 1.47 (d, $J=5.5$ Hz, 3H, Me-CH), 1.94 (d, $J=7.0$ Hz, 3H, Me), 2.47 (s, 1H, OH), 3.78 (d, $J=12.1$ Hz, 6H, 2MeO), 4.30-4.39 (m, 1H, CH), 7.18-7.90 (m, 5H, Ph). $^{13}\text{C-NMR}$ (150.9 MHz) δ_{C} 13.1 ($J=4.4$ Hz, CH_3), 19.0 (CH_3), 51.7 ($J=14.0$ Hz, $2\times\text{CH}_3$), 73.2 ($J=4.7$ Hz, CH), 95.1 ($J=184.7$ Hz, C), 107.4 ($J=8.0$ Hz, C), 120.7-129.1 (Ph), 209.3 ($J=1.6$ Hz, C). $^{31}\text{P-NMR}$ (242.9 MHz): δ_{P} 18.6. Anal. Calcd. for $\text{C}_{14}\text{H}_{19}\text{O}_4\text{P}$: C 59.57, H 6.78; found: C 59.61, H 6.83.

Dimethyl 3-(1-hydroxycyclohexyl)-1,3-diphenylpropa-1,2-dienephosphonate (8c). Yellow oil, yield: 85%. Eluent for TLC: ethyl acetate:hexane = 1:1, R_f 0.63; IR (neat, cm^{-1}): 1256 (P=O), 1445, 1493 (Ph), 1933 (C=C=C), 3364 (OH). $^1\text{H-NMR}$ (600.1 MHz): δ_{H} 1.27-1.99 (overlapping multiplet, 10H, cyclohexyl), 2.31 (s, 1H, OH), 3.74 (d, $J=12.1$ Hz, 6H, 2MeO), 7.24-7.71 (m, 10H, 2Ph). $^{13}\text{C-NMR}$ (150.9 MHz) δ_{C} 21.5 ($2\times\text{CH}_2$), 24.7 (CH_2), 39.8 ($2\times\text{CH}_2$), 51.7 ($J=14.8$ Hz, $2\times\text{CH}_3$), 74.1 ($J=5.0$ Hz, C), 97.1 ($J=180.5$ Hz, C), 113.8 ($J=7.9$ Hz, C), 119.1-140.0 (2Ph), 210.0 ($J=1.5$ Hz, C). $^{31}\text{P-NMR}$ (242.9 MHz): δ_{P} 18.6. Anal. Calcd. for $\text{C}_{23}\text{H}_{27}\text{O}_4\text{P}$: C 69.33, H 6.83; found: C 69.37, H 6.86.

Synthesis and spectral data of *dimethyl 4-hydroxy-1,3,4-triphenylbuta-1,2-dienephosphonate 8d* were described in our previous paper [63].

4-(Diphenylphosphinoyl)-2-methyl-4-phenylbuta-2,3-dien-1-ol (9a). Yellow oil, yield: 84%. Eluent for TLC: ethyl acetate:hexane = 1:1, R_f 0.62; IR (neat, cm^{-1}): 1180 (P=O), 1439, 1493 (Ph), 1948 (C=C=C), 3381 (OH). $^1\text{H-NMR}$ (600.1 MHz): δ_{H} 2.07 (d, $J=7.5$ Hz, 3H, Me), 2.71 (s, 1H, OH), 4.71-4.94 (m, 2H, CH_2), 7.32-7.89 (m, 15H, 3Ph). $^{13}\text{C-NMR}$ (150.9 MHz) δ_{C} 14.7 ($J=5.0$ Hz, CH_3), 62.7 ($J=4.6$ Hz, CH_2), 97.4 ($J=184.3$ Hz, C), 110.5 ($J=8.0$ Hz, C), 124.0-139.7 (m, 3Ph), 211.0 ($J=2.0$ Hz, C). $^{31}\text{P-NMR}$ (242.9 MHz): δ_{P} 32.8. Anal. Calcd. for $\text{C}_{23}\text{H}_{21}\text{O}_2\text{P}$: C 76.65, H 5.87; found: C 76.69, H 6.92.

Synthesis and spectral data of *4-(diphenylphosphinoyl)-1,2,4-triphenylbuta-2,3-dien-1-ol 9d* were described in our previous paper [63].

RESULTS AND DISCUSSION

We based our strategy for the synthesis of the phosphorylated 3-(α -hydroxyalkyl)allenes on our

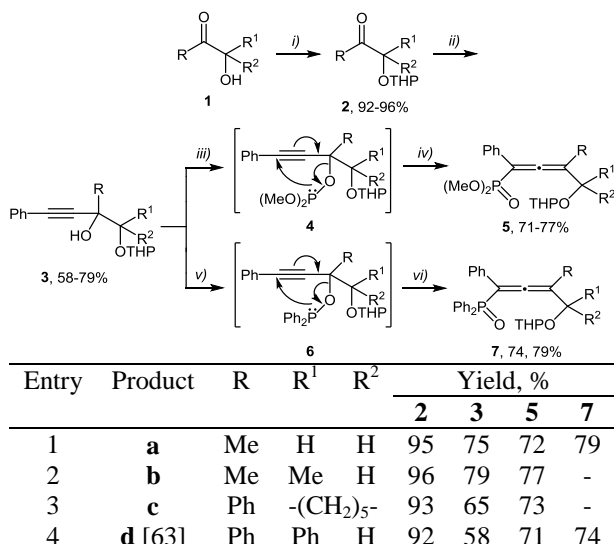
experience in preparation of the phosphorylated 1-(α - [54] and β - [55] hydroxyalkyl)allenes, and relied on the well-precedented [2,3]-sigmatropic shift of propargylic phosphites to allene-phosphonates [40–43] and propargylic phosphinites to allenyl phosphine oxides [46–51]. We were aware of the fact that a precedent exists for such an approach to the synthesis of the diethylphosphono-substituted α -allenic alcohols [52, 53], but as far as we know, a general useful method for regioselective synthesis of phosphorylated (phosphonates and phosphine oxides) 3-(α -hydroxyalkyl)allenes with protected or unprotected hydroxy group with protected or unprotected hydroxy group has not been reported yet.

The main target in our research, and namely 1,3-bifunctionalized allenes, was achieved as a range of the phosphorylated 3-(α -hydroxyalkyl)allenes **5**, **7**, **8**, and **9**, was prepared by applying the following four-step procedure: (i) protection of hydroxy group in the α -hydroxy-alkanones **1**; (ii) subsequent reaction of Grignard reagent and the protected ketones **2** to give the (tetrahydro-2H-pyran-2-yloxy)-alkynols **3** with protected hydroxy group at 4 position; (iii) interaction with dimethyl chlorophosphite or chlorodiphenyl phosphine in the presence of a base; and finally (iv) [2,3]-sigmatropic rearrangement of the mediated hydroxy-protected propargyl phosphites or phosphinites.

The first step in our investigation was to examine the hydroxy group protection in the α -hydroxy-alkanones **1** with 3,4-dihydro-2H-pyran (DHP) in the presence of pyridinium *p*-toluenesulfonate (PPTS) [59–62] (Scheme 1). Thus, the formed (tetrahydro-2H-pyran-2-yloxy)-alkanones **2** were isolated by column chromatography with excellent yield (92–96%). Reaction of the protected alkanones **2** with the *in situ* generated phenylethynylmagnesium bromide from ethyl magnesium bromide and phenylacetylene to give the (tetrahydro-2H-pyran-2-yloxy)-alkynols **3** which are stable and were isolated by column chromatography in 58–79% yield.

Once we had the required alk-1-yn-3,4-diols **3** with protected hydroxy group at 4 position, we were then able to investigate the proposed reactions with the corresponding chloro-containing phosphorus reagents such as dimethyl chlorophosphite and chlorodiphenyl phosphine in the presence of a base and subsequent [2,3]-sigmatropic rearrangement of the mediated propargyl phosphites **4** or phosphinites **6**.

Let us start with the dimethyl (tetrahydro-2*H*-pyran-2-yloxy)-alka-1,2-dienephosphonates **5** that can be easily prepared *via* an atom economical 2,3-sigmatropic rearrangement of the protected propargyl phosphites **4**, intermediate formed by reaction of the alkynols **3** with dimethyl chlorophosphite, *in situ* prepared from phosphorus trichloride in the presence of triethylamine and 2 equiv of methanol and 2 equiv of pyridine, according to Scheme 1.



Reagents and Conditions: *i*) (α -hydroxyalkyl)ketone (**1** eq), DHP (1.5 eq), PPTS (0.1 eq), CH₂Cl₂, rt, 10h, column chromatography; *ii*) dropwise addition of EtMgBr (1 eq) to phenylacetylene (1 eq), THF, reflux, 2h, dropwise addition of prepared ethynylmagnesium bromide to **2** (2 eq), THF, reflux, 16h, column chromatography; *iii*) PCl₃ (1 eq), Et₃N (1.1 eq), Et₂O, -70 °C, 30 min stirring, pyridine (2.2 eq), MeOH (2 eq), Et₂O, -70 °C; *iv*) [2,3- σ]-rearrangement, -70 °C, 1h, rt, 12h, column chromatography *v*) Ph₂PCl (1 eq), Et₃N (1.1 eq), Et₂O, -70 °C; *vi*) [2,3- σ]-rearrangement, -70 °C, 1h, rt, 8h, column chromatography.

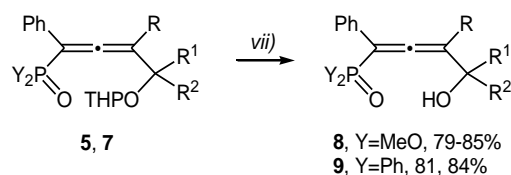
Scheme 1. Synthesis of the 3-(α -hydroxyalkyl)-allene phosphonates **5** and 3-(α -hydroxyalkyl)-allenyl phosphine oxides **7** with protected hydroxy-group.

Next, the reaction of the (tetrahydro-2*H*-pyran-2-yloxy)-alkynols **3** with chlorodiphenyl phosphine in the presence of triethylamine at -70 °C gave the expected diphenyl (tetrahydro-2*H*-pyran-2-yloxy)-alka-1,2-dien-1-yl phosphine oxides **7** in very good yield (74 and 79%) as a result of [2,3]-sigmatropic rearrangement of the protected propargyl phosphinites **6**, according to the reaction sequence outlined in Scheme 1.

A new family of the phosphorylated 3-(α -hydroxyalkyl)allenes with protected hydroxy group **5** and **7** were synthesized *via* an atom economical and regioselective [2,3]-sigmatropic rearrangement of the intermediate formed propargyl phosphites **4**

or phosphinites **6** in the reaction of the alk-1-yn-3,4-diols with protected hydroxy group at 4 position **5** with dimethylchloro phosphite or chlorodiphenyl phosphine in the presence of triethylamine.

Allenic compounds **5** and **7** were stable enough to be handled at ambient temperature. The hydroxy group was deprotected by stirring the ethanol solution of the protected 3-(α -hydroxyalkyl)-allene phosphonates **5** and 3-(α -hydroxyalkyl)-allenyl phosphine oxide **7** in the presence of 0.1 equiv PPTS at room temperature for 6 hours, according to Scheme 2.



Entry	Product	Y	R	R ¹	R ²	Yield, %
1	8a	MeO	Me	H	H	80
2	8b	MeO	Me	Me	H	83
3	8c	MeO	Ph	-(CH ₂) ₅ -		85
4	8d [63]	MeO	Ph	Ph	H	79
5	9a	Ph	Me	H	H	84
6	9d [63]	Ph	Ph	Ph	H	81

Reagents and Conditions: *vii*) PPTS (0.1 eq), EtOH, rt, 6h, stirring, column chromatography.

Scheme 2. Synthesis of the 3-(α -hydroxyalkyl)-allene phosphonates **8** and 3-(α -hydroxyalkyl)-allenyl phosphine oxides **9**

After a conventional work-up, all allenic products **5**, **7**, **8**, and **9** were isolated as stable yellow or orange oils by column chromatography and identified by ¹H, ¹³C, and ³¹P NMR and IR spectra as well as by elemental analysis.

A series of new phosphorylated 3-(α -hydroxyalkyl)allenes with protected (**5** and **7**) and unprotected hydroxy group (**8** and **9**) were synthesized by a convenient, efficient, atom economical and regioselective method.

CONCLUSION

In conclusion, a convenient and efficient regioselective synthesis of a new family of 1,3-bifunctionalized allenes has been explored. Phosphorylated 3-(α -hydroxyalkyl)allenes prepared were derived from [2,3]-sigmatropic rearrangement of the intermediate propargyl phosphites or phosphinites formed in the reaction of protected alkynols with dimethylchloro phosphite or chlorodiphenyl phosphine in the presence of a base.

Further investigations on this potentially important synthetic methodology are currently in progress. At the same time, the synthetic application of the prepared phosphorylated 3-(α -hydroxyalkyl)allenes with protected or unprotected hydroxy group for synthesis of different heterocyclic compounds is now under investigation in our laboratory as a part of our general synthetic strategy for investigation of the scope and limitations of the electrophilic cyclization and cycloisomerization reactions of bifunctionalized allenes. Results of these investigations will be reported in due course. Moreover, results of an initial investigation of the biological activity of the compounds prepared were encouraging, and the antibacterial and antifungal activities of selected compounds as well as potential precursors of effective anticancer drugs are now under investigation in our university.

Acknowledgements: Support from the Research Fund of the Konstantin Preslavsky University of Shumen (Projects Nos. RD-08-109 / 2016 and RD-08-98 / 2017) is acknowledged.

REFERENCES

- R. W. Bates, V. Satcharoen, *Chem. Soc. Rev.*, **31**, 12 (2002).
- N. Krause, A. S. K. Hashmi (Eds.), *Modern Allene Chemistry*, Wiley-VCH, Weinheim, 2004, Vol. 1 & 2.
- S. Ma, *Aldrichimica Acta*, **40**, 91 (2007).
- K. M. Brummond, J. E. DeForrest, *Synthesis*, 795 (2007).
- T. M. V. D. Pinho e Melo, *Curr. Org. Chem.*, **13**, 1406 (2009);
- T. G. Back, K. N. Clary, D. Gao, *Chem. Rev.*, **110**, 4498 (2010).
- M. Enomoto, T. Katsuki, M. Yamaguchi, *Tetrahedron Lett.*, **27**, 4599 (1986).
- S. Phadtare, J. Zemlicka, *J. Am. Chem. Soc.*, **111**, 5925 (1989).
- S. Ma, H. Hou, S. Zhao, G. Wang, *Synthesis*, 1643 (2002).
- J. Ye, S. Li, B. Chen, W. Fan, J. Kuang, J. Liu, Y. Liu, B. Miao, B. Wan, Y. Wang, X. Xie, Q. Yu, W. Yuan, S. Ma, *Org. Lett.*, **14**, 1346 (2012).
- G. P. Boldrini, L. Lodi, E. Tagliavini, C. Tarasco, C. TrombinI, A. Umanl-Ronchi, *J. Org. Chem.*, **52**, 5447 (1987).
- R. W. Hoffman, U. Weldmann, *Chem. Ber.*, **118**, 3966 (1985)
- E. J. Corey, R. Imwinkelried, S. Pikul, Y. B. Xiang, *J. Am. Chem. Soc.*, **111**, 5493 (1989).
- E. J. Corey, C.-M. Yu, D.-H. Lee, *J. Am. Chem. Soc.*, **112**, 878 (1990).
- E. J. Corey, G. B. Jones, *Tetrahedron Lett.*, **32**, 5713 (1991).
- J. Li, W. Kong, C. Fu, S. Ma, *J. Org. Chem.*, **74**, 5104 (2009).
- J. Li, C. Zhou, C. Fu, S. Ma, *Tetrahedron*, **65**, 3695 (2009).
- A. Alexakis, I. Marek, P. Mangeney, J. F. Normant, *Tetrahedron Lett.*, **30**, 2387 (1989).
- A. Alexakis, I. Marek, P. Mangeney, J. F. Normant, *Tetrahedron*, **47**, 1677 (1991).
- J. A. Marshall, K. G. Pinney, *J. Org. Chem.*, **58**, 7180 (1993).
- N. Krause, A. Hoffmann-Röder, J. Canisius, *Synthesis*, **12**, 1759 (2002).
- N. Krause, A. Hoffmann-Röder, *Tetrahedron*, **60**, 11671 (2004).
- J. M. Aurrecochea, M. Solay, *Tetrahedron Lett.*, **36**, 2501 (1995).
- J. M. Aurrecochea, E. Alonso, M. Solay, *Tetrahedron*, **54**, 3833 (1998).
- J. S. Cowie, P. D. Landor, S. R. Landor, *J. Chem. Soc., Chem. Commun.*, 541 (1969).
- J. S. Cowie, P. D. Landor, S. R. Landor, *J. Chem. Soc., Perkin Trans. 1*, 720 (1973).
- M. Nakano, N. Furuichi, H. Mori, S. Katsumura, *Tetrahedron Lett.*, **42**, 7307 (2001).
- C. Darcel, C. Bruneau, P. H. Dixneuf, *J. Chem. Soc., Chem. Commun.*, 1845 (1994).
- C. Darcel, S. Bartsch, C. Bruneau, P. H. Dixneuf, *Synlett*, 457 (1994).
- S. Hoff, L. Brandsma, J. F. Arens, *Rec. Trav. Chim. Pays-Bas*, **87**, 916 (1968).
- S. Hoff, L. Brandsma, J. F. Arens, *Trav. Chim. Pays-Bas*, **87**, 1179 (1968).
- S. Hormuth, H.-U. Reissig, *Synlett*, 179 (1991).
- S. Hormuth, H.-U. Reissig, D. Dorsch, *Liebigs Ann. Chem.*, 121 (1994).
- R. Zimmer, *Synthesis*, 165 (1993).
- J. A. Marshall, Y. Tang, *J. Org. Chem.*, **58**, 3233 (1993).
- V. Mark, The Uncatalyzed Rearrangements of Tervalent Phosphorus Esters, in: *Selective Organic Transformations*, B. S. Thyagarajan (Ed.), John Wiley & Sons, New York, 1970, pp. 319-437.
- P. D. Landor, in: *The Chemistry of the Allenes*, Vol. 1, S. R. Landor (Ed.), Academic Press, New York, 1982, pp. 174-178.
- R. W. Saalfrank, C.-J. Lurz, in: *Methoden der Organischen Chemie (Houben Weyl)*, H. Kropf, E. Scheumann (Eds.), Thieme, Stuttgart, 1993, pp. 2959-3102.
- A. S. K. Hashmi, Synthesis of Allenes, in: *Modern Allene Chemistry*, Vol. 1, N. Krause, A. S. K. Hashmi (Eds.), Wiley-VCH, Weinheim, 2004, pp. 3-50.
- R. S. Macomber, *J. Am. Chem. Soc.*, **99**, 3072 (1977).

41. S. E. Denmark, J. E. Marlin, *J. Org. Chem.*, **56**, 1003 (1991).
42. B. Cai, G. M. Blackburn, *Synth. Commun.*, **27**, 3943 (1997).
43. R. W. Saalfrank, M. Haubner, C. Deutscher, U. Bauer, *Eur. J. Org. Chem.*, 2367 (1999).
44. A. P. Boiselle, N. A. Meinhardt, *J. Org. Chem.*, **27**, 1828 (1962).
45. V. Mark, *Tetrahedron Lett.*, **3**, 281 (1962).
46. K. C. Nicolaou, P. Maligres, J. Shin, E. de Leon, D. Rideout, *J. Am. Chem. Soc.*, **112**, 7825 (1990).
47. M. L. Curfin, W. H. Okamura, *J. Org. Chem.*, **55**, 5278 (1990).
48. J. W. Grissom, D. Huang, *Angew. Chem. Int. Ed.*, **34**, 2037 (1995).
49. C. Darcel, C. Bruneau, P. H. Dixneuf, *Synthesis*, 711 (1996).
50. O. de Frutos, A. M. Echavarren, *Tetrahedron Lett.*, **38**, 7941 (1997).
51. M. Schmittel, J.-P. Steffen, M. Maywald, B. Engels, H. Helten, P. Musch, *J. Chem. Soc., Perkin Trans. 2*, 1331 (2001).
52. V. K. Brel, *Synthesis*, 463 (1999).
53. V. K. Brel, E. V. Abramkin, *Mendeleev Commun.*, **12**, 64 (2002).
54. I. E. Ismailov, I. K. Ivanov, V. Ch. Christov, *Molecules*, **19**, 6309 (2014).
55. I. E. Ismailov, I. K. Ivanov, V. Ch. Christov, *Bulg. Chem. Commun.*, **46**, Special Issue A, 39 (2014).
56. I. E. Ismailov, I. K. Ivanov, V. Ch. Christov, *Molecules*, **19**, 11056 (2014).
57. V. Ch. Christov, I. E. Ismailov, I. K. Ivanov, *Molecules*, **20**, 7263 (2015).
58. V. Ch. Christov, I. E. Ismailov, I. K. Ivanov, *Int. J. Rec. Sci. Res. (IJRSR)*, **6**, 4526 (2015).
59. D. N. Robertson, *J. Org. Chem.*, **25**, 931 (1960).
60. M. Miyashita, A. Yoshikoshi, P. A. Griecolb, *J. Org. Chem.*, **42**, 3772 (1977).
61. M. C. Joshi, P. Joshi, D. S. Rawat, *ARKIVOC*, (xvi), 65 (2006).
62. B. Partha, I. Pimkov, *US Patent 8378123 B2* (2011).
63. V. Ch. Christov, H. H. Hasanov, I. K. Ivanov, *Global J. Pure Appl. Chem. Res.* **3**, 20-36 (2015).
64. H. H. Hasanov, I. K. Ivanov, V. Ch. Christov, *Heteroatom Chem.*, **28**, e21357 (2017).

БИФУНКЦИОНАЛИЗИРАНИ АЛЕНИ. ЧАСТ XX. УДОБЕН И ЕФЕКТИВЕН РЕГИОСЕЛЕКТИВЕН СИНТЕЗ НА ФОСФОРИЛИРАНИ 3-(α -ХИДРОКСИАЛКИЛ)АЛЕНИ

Х. Х. Хасанов, И. К. Иванов, В. Х. Христов*

Катедра по химия, Факултет по природни науки, Шуменски университет „Епископ Константин Преславски“, ул. „Университетска“ 115, 9712 Шумен, България

Постъпила на 08 февруари 2017 г.; Коригирана на 16 март 2017 г.

(Резюме)

Описан е удобен и ефикасен региоселективен синтез на фосфорилирани 3-(α -хидроксиалкил)алени чрез атом-икономична [2,3]-сигматропна прегрупировка на междинно образуваните пропаргилови фосфити или фосфонити, които лесно се получават чрез реакция на (тетрахидро-2*H*-пиран-2-илокси)-алкиноли с диметил хлорофосфит или хлородифенил фосфин съответно в присъствие на база.

Trifunctionalized allenes. Part I. A convenient and efficient regioselective synthesis of 4-phosphorylated 5-hydroxyalka-2,3-dienoates

I. E. Ismailov, I. K. Ivanov, V. Ch. Christov*

Department of Chemistry, Faculty of Natural Sciences, Konstantin Preslavsky University of Shumen, 115 Universitetska St., 9712 Shumen, Bulgaria

Received February 08, 2017; Revised March 16, 2017

Dedicated to Acad. Bogdan Kurtev on the occasion of his 100th birth anniversary

A convenient and efficient regioselective synthesis of 4-phosphorylated 5-hydroxyalka-2,3-dienoates by an atom economical [2,3]-sigmatropic rearrangement of the mediated ethyl 2-(dimethoxyphosphino)oxy- or 2-(diphenylphosphino)oxy-5-(tetrahydro-2*H*-pyran-2-yloxy)-alk-3-ynoates which can be readily prepared *via* reaction of the protected alkyl 2-hydroxy-5-(tetrahydro-2*H*-pyran-2-yloxy)-alk-3-ynoates with dimethyl chlorophosphite or chlorodiphenyl phosphine respectively in the presence of a base is described.

Key words: synthesis; protection of hydroxy group; [2,3]-sigmatropic rearrangement; 4-phosphorylated 5-hydroxyalka-2,3-dienoates

INTRODUCTION

The synthesis and the application of functionalized allenes have been thoroughly explored during the last three decades by the scientists in the preparative organic chemistry field. It is their versatility that attracts scientists' interest. That very specific characteristic makes them key building blocks in organic synthesis and lead to implementation of innovative methods for construction of number of functionalized heterocyclic and carbocyclic systems [1–7].

There are many methods explained by different researchers regarding the construction of alka-2,3-dienoates using Wittig [8–10], Wittig-Horner [11] or the Horner-Wadsworth-Emons [12] olefination of ketenes, iron-catalyzed olefination of ketenes with diazoacetate [13] and other methods [14].

Moreover, there are many methods for the construction of hydroxyallenes, including prototropic rearrangement of propargylic alcohols [15, 16], metal-catalyzed nucleophilic addition of propargylic derivatives to aldehydes [10–16], Cu(I)-catalyzed reaction of propargylic chlorides with Grignard reagents [17, 18], metal-catalyzed reaction of propargylic oxiranes with organometallic compounds [19–23] and ketones [24, 25], reduction of alcohols, ethers, oxiranes *etc.* with aluminium reagents [26–28], Pd(0)-catalyzed reaction of cyclic carbonates with acetylenic compounds [29, 30], S_N2' [31, 32] and A_N [33, 34]

reactions of metallated alkoxy-allenes with oxiranes and ketones [35], and by other methods [36].

On the other hand, there are methods [37–40] for the synthesis of phosphorus-containing allenes (phosphonates [41–44], phosphinates [45, 46], and phosphine oxides [47–52]) including reactions of α -alkynols with chloride-containing derivatives of phosphorus acids followed by [2,3]-sigmatropic rearrangement. Several diethylphosphono-substituted α -allenic alcohols were prepared by Brel [53, 54] directly from alcohols by Horner-Mark rearrangement of unstable propargylic phosphites.

Our research on the chemistry of the trifunctionalized allenes enhanced us to find a convenient method to introduce the phosphonate or phosphine oxide in the fourth-position as well as the α -hydroxy group in the fifth position to the ester group of the allenecarboxylates. The above mentioned groups provoke organic researchers' interest because of their useful functionalities in organic synthesis. It is particularly interesting to explore the applications of these groups as temporary transformers of chemical reactivity of the allenic system in the synthesis of eventually heterocyclic compounds.

Based on our previous research background related to the synthesis of phosphorylated 1-(α -hydroxyalkyl)allenes [61, 63, 64], 1-(β -hydroxyalkyl)allenes [62, 65], 4-hydroxy-1,3,4-triphenylbuta-1,2-dienes [71] and 3-(β -hydroxyalkyl)allenes [72] as well as 4-phosphoryl-substituted

* To whom all correspondence should be sent:
E-mail: vchristo@shu.bg

allene-carboxylates [66] we managed to find a convenient and an efficient regioselective method for synthesis of 4-phosphorylated 5-hydroxyalka-2,3-dienoates by an atom economical [2,3]-sigmatropic rearrangement of the mediated ethyl 2-(dimethoxyphosphino)oxy- or 2-(diphenylphosphino)oxy-5-(tetrahydro-2*H*-pyran-2-yloxy)-alk-3-ynoates formed in the reaction of the protected alkyl 2-hydroxy-5-(tetrahydro-2*H*-pyran-2-yloxy)-alk-3-ynoates with dimethylchlorophosphite or chlorodiphenyl phosphine in the presence of a base.

EXPERIMENTAL

General Information

All new synthesized compounds were purified by column chromatography and characterized on the basis of NMR, IR, and microanalytical data. NMR spectra were recorded on DRX Bruker Avance-250 (Bruker BioSpin, Karlsruhe, Germany) (^1H at 250.1 MHz, ^{13}C at 62.9 MHz, ^{31}P at 101.2 MHz) and Bruker Avance II+600 (Bruker BioSpin GmbH, Karlsruhe, Germany) (^1H at 600.1 MHz, ^{13}C at 150.9 MHz, ^{31}P at 242.9 MHz) spectrometers for solutions in CDCl_3 . All ^1H and ^{13}C NMR experiments were measured referring to the signal of internal TMS and ^{31}P NMR experiments were measured referring to the signal of external 85% H_3PO_4 . J values are given in hertz. IR spectra were recorded with an FT-IRAffinity-1 Shimadzu spectrophotometer (Shimadzu, Tokyo, Japan). Elemental analyses were carried out by the Microanalytical Service Laboratory of Faculty of Chemistry and Pharmacy, University of Sofia, Bulgaria, using Vario EL3 CHNS(O) (Elementar Analysensysteme, Hanau, Germany). Column chromatography was performed on Kieselgel 60 F_{254} (70–230 mesh ASTM, 0.063–0.200 mm, Merck). Et_2O and THF were distilled from Na wire/benzophenone, CH_2Cl_2 was distilled over CaH_2 , and other organic solvents used in this study were dried over appropriate drying agents by standard methods and distilled prior to use. All other chemicals used in this study were commercially available and were used without additional purification unless otherwise noted. Reactions were carried out in oven dried glassware under an argon atmosphere and exclusion of moisture. All compounds were checked for purity on TLC plates Kieselgel F_{254} 60 (Merck). Procedure for the synthesis of the (tetrahydro-2*H*-pyran-2-yloxy)-alkynols **2** (96–98% yield) by protection of

the hydroxy-group by treatment of the alkynol **1** with DHP (3,4-dihydro-2*H*-pyran) in the presence of PPTS (pyridinium *p*-toluenesulfonate) as a catalyst is described in the literature [67–70].

Procedure for synthesis of alkyl 2-hydroxy-5-(tetrahydro-2H-pyran-2-yloxy)-alk-3-ynoates 5

Ethylmagnesium bromide [prepared from magnesium (1.2 g, 50.0 mmol) and ethyl bromide (5.5 g, 50.0 mmol) in dry THF (50 mL)] is added dropwise under stirring to (tetrahydro-2*H*-pyran-2-yloxy)-alkynol **2** (50.0 mmol) and then the mixture is refluxed for 2 h. The solution of the prepared alkynyl magnesium bromides is added dropwise under stirring to alkyl 2-oxoalkanoate (100.0 mmol). The mixture is refluxed for 2 h and after cooling is hydrolyzed with a saturated aqueous solution of ammonium chloride. The organic layer is separated, washed with water, and dried over anhydrous sodium sulfate. Solvent and the excess of the ester are removed by distillation. Purification of the residue is achieved by column chromatography (silica gel, Kieselgel Merck 60 F_{254}) with ethyl acetate-hexane. The pure products **5** had the following properties:

Ethyl 2-hydroxy-2-phenyl-5-(tetrahydro-2H-pyran-2-yloxy)-pent-3-ynoate (5a). Dark orange oil, yield: 89%. Eluent for TLC: ethyl acetate:hexane = 1:3, R_f 0.46; IR (neat, cm^{-1}): 1122 (C–O–C), 1442, 1495 (Ph), 1723 (C=O), 2253 (C≡C), 3418 (OH). $^1\text{H-NMR}$ (250.1 MHz): δ_{H} 1.44 (t, $J=7.1$ Hz, 3H, MeCH_2O), 1.51–1.76, 3.43–3.57, 4.79–4.87 (overlapping multiplets, 9H, OTHP), 4.15–4.23 (m, 2H, OCH_2Me), 4.26–4.36 (m, 2H, CH_2), 4.43 (s, 1H, OH), 7.22–7.51 (m, 5H, Ph). $^{13}\text{C-NMR}$ (62.9 MHz) δ_{C} 13.8 (CH_3), 18.9 (CH_2), 25.4 (CH_2), 30.2 (CH_2), 54.6 (CH_2), 61.3 (CH_2), 63.2 (CH_2), 77.8 (C), 82.4 (C), 83.8 (C), 96.7 (CH), 126.2–136.4 (Ph), 171.8 (C). Anal. Calcd for $\text{C}_{18}\text{H}_{22}\text{O}_5$: C 67.91, H 6.97; found: C 67.96, H 7.01.

Ethyl 2-hydroxy-2-phenyl-5-(tetrahydro-2H-pyran-2-yloxy)-hex-3-ynoate (5b). Yellow oil, yield: 85%. Eluent for TLC: ethyl acetate:hexane = 1:6, R_f 0.53; IR (neat, cm^{-1}): 1123 (C–O–C), 1442, 1493 (Ph), 1725 (C=O), 2250 (C≡C), 3396 (OH). $^1\text{H-NMR}$ (250.1 MHz): δ_{H} 1.21 (t, $J=7.1$ Hz, 3H, MeCH_2O), 1.41–1.83, 3.49–3.77, 4.78–4.90 (overlapping multiplets, 9H, OTHP), 1.53 (t, $J=6.9$ Hz, 3H, MeCH), 4.21 (s, 1H, OH), 4.26–4.33 (m, 2H, OCH_2Me), 4.90–4.96 (m, 1H, CH), 7.22–7.48 (m, 5H, Ph). $^{13}\text{C-NMR}$ (62.9 MHz) δ_{C} 13.8 (CH_3), 15.3 (CH_2), 19.5 (CH_3), 22.4 (CH_2), 31.4 (CH_2), 60.5 (CH), 63.5 (CH_2), 65.9 (CH_2), 76.3 (C), 82.6

(C), 85.2 (C), 96.1 (CH), 124.6-137.6 (Ph), 172.1 (C). Anal. Calcd for C₁₉H₂₄O₅: C 68.66, H 7.28; found: C 68.70, H 7.23.

Methyl 2-hydroxy-5-methyl-2-phenyl-5-(tetrahydro-2H-pyran-2-yloxy)-hex-3-ynoate (5c). Yellow oil, yield: 90%. Eluent for TLC: ethyl acetate:hexane = 1:6, R_f 0.52; IR (neat, cm⁻¹): 1125 (C-O-C), 1440, 1493 (Ph), 1727 (C=O), 2244 (C≡C), 3404 (OH). ¹H-NMR (250.1 MHz): δ_H 1.412-1.74, 3.54-3.69, 4.90-5.01 (overlapping multiplets, 9H, OTHP), 1.58 (s, 6H, Me₂), 3.75 (s, 3H, MeO), 4.18 (s, 1H, OH), 7.21-7.486 (m, 5H, Ph). ¹³C-NMR (62.9 MHz) δ_C 20.4 (CH₂), 25.2 (CH₂), 29.9 (CH₃), 32.4 (CH₂), 53.0 (CH₃), 63.0 (CH₂), 70.1 (C), 774 (C), 80.1 (C), 87.2 (C), 97.0 (CH), 124.3-137.7 (Ph), 173.4 (C). Anal. Calcd for C₁₉H₂₄O₅: C 68.66, H 7.28; found: C 68.61, H 7.32.

Procedure for synthesis of alkyl 4-(dimethoxyphosphoryl)-5-(tetrahydro-2H-pyran-2-yloxy)-alka-2,3-dienoates 7

To a solution of phosphorus trichloride (2.75 g, 20 mmol) and triethylamine (2.23 g, 22 mmol) in dry diethyl ether (60 mL) at -70 °C was added dropwise with stirring a solution of the alkyl 2-hydroxy-5-(tetrahydro-2H-pyran-2-yloxy)-alk-3-ynoate **5** (20 mmol) in the same solvent (20 mL). After 30 min stirring at the same condition a solution of pyridine (3.16 g, 44 mmol) and of methanol (1.28 g, 40 mmol) in dry diethyl ether (50 mL) were added. The reaction mixture was stirred for an hour at the same temperature and for 4 hours at room temperature. The mixture was then washed with water, 2N HCl, extracted with ether, washed with saturated NaCl, and dried over anhydrous sodium sulfate. After evaporation of the solvent, the residue was chromatographed on a column (silica gel, Kieselgel Merck 60 F₂₅₄) with a mixture of ethyl acetate and hexane as an eluent to give the pure product **7** as an oil, which had the following properties:

Ethyl 4-(dimethoxyphosphoryl)-2-phenyl-5-(tetrahydro-2H-pyran-2-yloxy)-penta-2,3-dienoate (7a). Orange oil, yield: 74%. Eluent for TLC: ethyl acetate:hexane = 1:1, R_f 0.58; IR (neat, cm⁻¹): 1121 (C-O-C), 1262 (P=O), 1443, 1491 (Ph), 1723 (C=O), 1942 (C=C=C). ¹H-NMR (600.1 MHz): δ_H 1.30 (t, J=6.9 Hz, 3H, Me), 1.21-1.63, 3.80-3.89, 4.42-4.53 (overlapping multiplets, 9H, OTHP), 3.79 (d, J=12.7 Hz, 6H, 2MeO), 4.21-4.61 (m, 4H, MeCH₂O, CH₂), 7.28-8.18 (m, 5H, Ph). ¹³C-NMR (150.9 MHz) δ_C 14.1 (CH₃), 18.9 (CH₂), 25.9 (CH₂), 29.8 (CH₂), 51.5 (J=13.1 Hz, CH₃), 60.7

(CH₂), 63.0 (CH₂), 66.3 (J=5.8 Hz, CH₂), 94.4 (J=181.5 Hz, C), 96.3 (J=4.4 Hz, CH), 106.5 (J=7.8 Hz, C), 128.5-133.9 (Ph), 169.1 (J=4.0 Hz, C), 218.5 (J=1.3 Hz, C). ³¹P-NMR (242.9 MHz): δ_P 15.4. Anal. Calcd for C₂₀H₂₇O₇P: C 58.53, H 6.63; found: C 58.49, H 6.68.

Ethyl 4-(dimethoxyphosphoryl)-2-phenyl-5-(tetrahydro-2H-pyran-2-yloxy)-hexa-2,3-dienoate (7b). Yellow oil, yield: 72%. Eluent for TLC: ethyl acetate:hexane = 1:1, R_f 0.43; IR (neat, cm⁻¹): 1120 (C-O-C), 1265 (P=O), 1439, 1490 (Ph), 1722 (C=O), 1937 (C=C=C). ¹H-NMR (600.1 MHz): δ_H 1.29 (t, J=7.0 Hz, 3H, MeCH₂O), 1.30-1.66, 3.67-3.77, 4.50-4.62 (overlapping multiplets, 9H, OTHP), 1.44 (dd, J=3.5 Hz, J=6.5 Hz, 3H, Me-CH), 3.78 (d, J=12.5 Hz, 6H, 2MeO), 4.20-4.27 (m, 2H, MeCH₂O), 4.77-4.86 (Me-CH), 7.25-8.11 (m, 5H, Ph). ¹³C-NMR (150.9 MHz) δ_C 14.3 (CH₃), 19.3 (CH₂), 23.6 (J=1.7 Hz, CH₃), 25.6 (CH₂), 30.5 (CH₂), 51.4 (J=12.9 Hz, CH₃), 59.7 (CH₂), 62.6 (CH₂), 67.7 (J=5.9 Hz, CH), 94.2 (J=4.3 Hz, CH), 97.4 (J=183.0 Hz, C), 105.9 (J=7.7 Hz, C), 128.2-134.1 (Ph), 162.3 (J=4.0 Hz, C), 219.6 (J=1.3 Hz, C). ³¹P-NMR (242.9 MHz): δ_P 15.2. Anal. Calcd for C₂₁H₂₉O₇P: C 59.43, H 6.89; found: C 59.37, H 6.92.

Methyl 4-(diisopropoxyphosphoryl)-5-methyl-2-phenyl-5-(tetrahydro-2H-pyran-2-yloxy)-hexa-2,3-dienoate (7c). Orange oil, yield: 75%. Eluent for TLC: ethyl acetate:hexane = 8:1, R_f 0.49; IR (neat, cm⁻¹): 1119 (C-O-C), 1269 (P=O), 1442, 1495 (Ph), 1724 (C=O), 1929 (C=C=C). ¹H-NMR (600.1 MHz): δ_H 1.29 (dd, J=6.1 Hz, J=5.7 Hz, 6H, Me₂CHO), 1.32-1.64, 3.51-3.74, 4.77-4.83 (overlapping multiplets, 9H, OTHP), 1.58 (d, J=3.3 Hz, 6H, Me₂-C), 3.70 (s, 3H, MeO), 4.63-4.75 (m, 2H, 2Me₂CHO), 7.24-8.23 (m, 5H, Ph). ¹³C-NMR (150.9 MHz) δ_C 20.0 (CH₂), 23.9 (J=8.0 Hz, CH₃), 25.5 (CH₂), 30.2 (J=7.8 Hz, CH₃), 30.7 (CH₂), 52.9 (CH₃), 62.1 (CH₂), 67.1 (J=5.0 Hz, CH), 79.9 (J=9.8 Hz, C), 91.3 (J=4.6 Hz, CH), 104.7 (J=184.8 Hz, C), 105.4 (J=7.8 Hz, C), 128.2-135.0 (Ph), 165.3 (J=4.4 Hz, C), 219.1 (J=1.3 Hz, C). ³¹P-NMR (242.9 MHz): δ_P 17.4. Anal. Calcd for C₂₅H₃₇O₇P: C 62.49, H 7.76; found: C 62.56, H 7.71.

Procedure for the synthesis of alkyl 4-(diphenylphosphinoyl)-5-(tetrahydro-2H-pyran-2-yloxy)-alka-2,3-dienoates 9

To a solution of the alkyl 2-hydroxy-5-(tetrahydro-2H-pyran-2-yloxy)-alk-3-ynoate **5** (20 mmol) and triethylamine (2.23 g, 22 mmol) in dry diethyl ether (60 mL) at -70 °C, a solution of

freshly distilled diphenylchloro phosphine (4.41 g, 20 mmol) in the same solvent (20 mL) was added dropwise with stirring. The reaction mixture was stirred for an hour at the same temperature and for 6 h at room temperature and then washed with water, 2N HCl, extracted with diethyl ether, and the extract was washed with saturated NaCl, and dried over anhydrous sodium sulfate. The solvent was removed using a rotatory evaporator, and the residue was purified by column chromatography on a silica gel (Kieselgel Merck 60 F₂₅₄) with ethyl acetate-hexane to give the pure products **9** as an oil, which had the following properties:

Ethyl 4-(diphenylphosphinoyl)-2-phenyl-5-(tetrahydro-2H-pyran-2-yloxy)-penta-2,3-dienoate (9a). Yellow oil, yield: 82%. Eluent for TLC: ethyl acetate:hexane = 1:1, R_f 0.56; IR (neat, cm⁻¹): 1121 (C-O-C), 1177 (P=O), 1439, 1486 (Ph), 1721 (C=O), 1937 (C=C=C). ¹H-NMR (600.1 MHz): δ_H 1.32 (t, *J*=6.8 Hz, 3H, MeCH₂O), 1.30-1.59, 3.64-3.75, 4.49-4.59 (overlapping multiplets, 9H, OTHP), 1.44 (dd, *J*=3.5 Hz, *J*=6.5 Hz, 3H, Me-CH), 3.78 (d, *J*=12.5 Hz, 6H, 2MeO), 4.20-4.28 (m, 2H, MeCH₂O), 4.33-4.46 (CH₂), 7.26-8.14 (m, 15H, 3Ph). ¹³C-NMR (150.9 MHz) δ_C 14.2 (CH₃), 18.8 (CH₂), 25.4 (CH₂), 31.0 (CH₂), 59.4 (CH₂), 62.8 (CH₂), 69.3 (*J*=4.7 Hz, CH₂), 96.8 (*J*=5.8 Hz, CH), 106.1 (*J*=181.5 Hz, C), 111.4 (*J*=7.9 Hz, C), 127.4-136.4 (3Ph), 166.4 (*J*=4.7 Hz, C), 215.4 (*J*=1.6 Hz, C). ³¹P-NMR (242.9 MHz): δ_P 28.5. Anal. Calcd for C₃₀H₃₁O₅P: C 71.70, H 6.22; found: C 71.77, H 6.19.

Ethyl 4-(diphenylphosphinoyl)-2-phenyl-5-(tetrahydro-2H-pyran-2-yloxy)-hexa-2,3-dienoate (9b). Yellow oil, yield: 79%. Eluent for TLC: ethyl acetate:hexane = 1:1, R_f 0.58; IR (neat, cm⁻¹): 1117 (C-O-C), 1176 (P=O), 1439, 1485 (Ph), 1715 (C=O), 1940 (C=C=C). ¹H-NMR (600.1 MHz): δ_H 1.35 (t, *J*=6.9 Hz, 3H, MeCH₂O), 1.37-1.66, 3.57-3.71, 4.53-4.64 (overlapping multiplets, 9H, OTHP), 1.42 (dd, *J*=3.4 Hz, *J*=6.6 Hz, 3H, Me-CH), 4.18-4.27 (m, 2H, MeCH₂O), 4.68-4.82 (m, 1H, Me-CH), 7.21-8.14 (m, 15H, 3Ph). ¹³C-NMR (150.9 MHz) δ_C 14.2 (CH₃), 19.5 (CH₂), 23.2 (*J*=1.6 Hz, CH₃), 25.4 (CH₂), 30.6 (CH₂), 59.4 (CH₂), 63.0 (CH₂), 69.5 (*J*=6.0 Hz, CH), 95.0 (*J*=4.4 Hz, CH), 106.5 (*J*=182.5 Hz, C), 109.6 (*J*=7.9 Hz, C), 128.4-135.7 (3Ph), 165.4 (*J*=4.6 Hz, C), 213.4 (*J*=1.4 Hz, C). ³¹P-NMR (242.9 MHz): δ_P 28.7. Anal. Calcd for C₃₁H₃₃O₅P: C 72.08, H 6.44; found: C 72.04, H 6.49.

Methyl 4-(diphenylphosphinoyl)-5-methyl-2-phenyl-5-(tetrahydro-2H-pyran-2-yloxy)-hexa-2,3-dienoate (9c). Yellow oil, yield: 86%. Eluent for

TLC: ethyl acetate:hexane = 1:1, R_f 0.59; IR (neat, cm⁻¹): 1117 (C-O-C), 1171 (P=O), 1437, 1495 (Ph), 1724 (C=O), 1940 (C=C=C). ¹H-NMR (600.1 MHz): δ_H 1.436-1.71, 3.52-3.75, 4.73-4.80 (overlapping multiplets, 9H, OTHP), 1.56 (d, *J*=3.2 Hz, 6H, Me₂-C), 3.70 (s, 3H, MeO), 7.20-8.18 (m, 15H, 3Ph). ¹³C-NMR (150.9 MHz) δ_C 19.7 (CH₂), 25.4 (CH₂), 29.9 (*J*=7.8 Hz, CH₃), 31.4 (CH₂), 53.2 (CH₃), 63.4 (CH₂), 81.0 (*J*=9.7 Hz, C), 92.9 (*J*=4.6 Hz, CH), 108.1 (*J*=7.8 Hz, C), 114.5 (*J*=185.0 Hz, C), 128.4-136.4 (3Ph), 164.3 (*J*=4.6 Hz, C), 213.4 (*J*=0.9 Hz, C). ³¹P-NMR (242.9 MHz): δ_P 272. Anal. Calcd for C₃₁H₃₃O₅P: C 72.08, H 6.44; found: C 72.13, H 6.48.

Procedure for the synthesis of alkyl 4-(dimethoxyphosphoryl)-5-hydroxy-alka-2,3-dienoates 10 and alkyl 4-(diphenylphosphinoyl)-5-hydroxy-alka-2,3-dienoates 11

A solution of the alkyl 4-(dimethoxyphosphoryl)-5-(tetrahydro-2H-pyran-2-yloxy)-alka-2,3-dienoates **7** or the alkyl 4-(diphenylphosphinoyl)-5-(tetrahydro-2H-pyran-2-yloxy)-alka-2,3-dienoate **9** (5 mmol) and PPTS (0.5 mmol) in ethanol (10 mL) was stirred at room temperature for 5 h. The mixture was then washed with water, extracted with methylene chloride and dried over anhydrous sodium sulfate. After evaporation of the solvent, the residue was chromatographed on a column (silica gel, Kieselgel Merck 60 F₂₅₄) with a mixture of ethyl acetate and hexane as an eluent to give the pure products **10** or **11** as oils, which had the following properties:

Ethyl 4-(dimethoxyphosphoryl)-5-hydroxy-2-phenyl-penta-2,3-dienoate (10a). Yellow oil, yield: 92%. Eluent for TLC: ethyl acetate:hexane = 1:1, R_f 0.42; IR (neat, cm⁻¹): 1265 (P=O), 1440, 1491 (Ph), 1717 (C=O), 1940 (C=C=C), 3428 (OH). ¹H-NMR (600.1 MHz): δ_H 1.34 (t, *J*=7.0 Hz, 3H, Me), 3.21 (s, 1H, OH), 3.79 (d, *J*=12.9 Hz, 6H, 2MeO), 4.19-4.27 (m, 2H, MeCH₂O), 4.57 (d, *J*=14.9 Hz, CH₂), 7.27-8.02 (m, 5H, Ph). ¹³C-NMR (150.9 MHz) δ_C 14.3 (CH₃), 51.4 (*J*=13.8 Hz, CH₃), 59.9 (CH₂), 61.0 (*J*=5.7 Hz, CH₂), 95.1 (*J*=183.0 Hz, C), 107.4 (*J*=7.6 Hz, C), 128.53-133.7 (Ph), 162.1 (*J*=4.3 Hz, C), 217.8 (*J*=1.4 Hz, C). ³¹P-NMR (242.9 MHz): δ_P 16.3. Anal. Calcd for C₁₅H₁₉O₆P: C 55.22, H 5.87; found: C 55.16, H 5.82.

Ethyl 4-(dimethoxyphosphoryl)-5-hydroxy-2-phenyl-hexa-2,3-dienoate (10b). Orange oil, yield: 88%. Eluent for TLC: ethyl acetate:hexane = 1:1,

R_f 0.61; IR (neat, cm^{-1}): 1265 (P=O), 1437, 1489 (Ph), 1723 (C=O), 1939 (C=C=C), 3410 (OH). $^1\text{H-NMR}$ (600.1 MHz): δ_{H} 1.35 (t, $J=7.1$ Hz, 3H, MeCH_2O), 1.42 (dd, $J=3.4$ Hz, $J=6.3$ Hz, 3H, Me-CH), 3.37 (s, 1H, OH), 3.78 (d, $J=13.0$ Hz, 6H, 2MeO), 4.21-4.28 (m, 2H, MeCH_2O), 5.18-5.28 (m, 1H, Me-CH), 7.21-8.10 (m, 5H, Ph). $^{13}\text{C-NMR}$ (150.9 MHz) δ_{C} 14.4 (CH_3), 24.0 ($J=1.8$ Hz, CH_3), 52.0 ($J=13.0$ Hz, CH_3), 60.2 (CH_2), 72.4 ($J=6.1$ Hz, CH), 98.0 ($J=184.0$ Hz, C), 106.4 ($J=7.5$ Hz, C), 127.9-135.0 (Ph), 162.7 ($J=4.2$ Hz, C), 217.4 ($J=1.5$ Hz, C). $^{31}\text{P-NMR}$ (242.9 MHz): δ_{P} 16.4. Anal. Calcd for $\text{C}_{16}\text{H}_{21}\text{O}_6\text{P}$: C 56.47, H 6.22; found: C 56.53, H 6.27.

Ethyl 4-(dimethoxyphosphoryl)-5-hydroxy-2-phenyl-hexa-2,3-dienoate (10c). Yellow oil, yield: 86%. Eluent for TLC: ethyl acetate:hexane = 3:1, R_f 0.55; IR (neat, cm^{-1}): 1268 (P=O), 1441, 1495 (Ph), 1723 (C=O), 1933 (C=C=C), 3418 (OH). $^1\text{H-NMR}$ (600.1 MHz): δ_{H} 1.30 (dd, $J=6.0$ Hz, $J=5.5$ Hz, 6H, Me_2CHO), 1.51 (d, $J=3.4$ Hz, 6H, Me_2C), 3.81 (s, 1H, OH), 4.64-4.78 (m, 2H, $2\text{Me}_2\text{CHO}$), 7.20-8.13 (m, 5H, Ph). $^{13}\text{C-NMR}$ (150.9 MHz) δ_{C} 23.5 ($J=8.0$ Hz, CH_3), 31.4 ($J=7.9$ Hz, CH_3), 53.4 (CH_3), 68.1 ($J=4.5$ Hz, CH), 73.7 ($J=10.1$ Hz, C), 104.3 ($J=185.7$ Hz, C), 106.5 ($J=7.9$ Hz, C), 127.8-133.9 (Ph), 164.0 ($J=4.7$ Hz, C), 215.8 ($J=1.1$ Hz, C). $^{31}\text{P-NMR}$ (242.9 MHz): δ_{P} 12.7. Anal. Calcd for $\text{C}_{20}\text{H}_{29}\text{O}_6\text{P}$: C 60.60, H 7.37; found: C 60.55, H 7.40.

Ethyl 4-(diphenylphosphinoyl)-5-hydroxy-2-phenyl-penta-2,3-dienoate (11a). Orange yellow oil, yield: 94%. Eluent for TLC: ethyl acetate:hexane = 1:1, R_f 0.41; IR (neat, cm^{-1}): 1180 (P=O), 1439, 1485 (Ph), 1721 (C=O), 1934 (C=C=C), 3396 (OH). $^1\text{H-NMR}$ (600.1 MHz): δ_{H} 1.36 (t, $J=6.9$ Hz, 3H, MeCH_2O), 3.18 (s, 1H, OH), 4.19-4.27 (m, 2H, MeCH_2O), 4.64 (d, $J=15.1$ Hz, CH_2), 7.20-8.04 (m, 15H, 3Ph). $^{13}\text{C-NMR}$ (150.9 MHz) δ_{C} 14.3 (CH_3), 60.1 (CH_2), 65.7 ($J=4.8$ Hz, CH_2), 105.7 ($J=182.1$ Hz, C), 110.7 ($J=7.7$ Hz, C), 128.9-136.0 (3Ph), 163.4 ($J=4.7$ Hz, C), 213.5 ($J=1.5$ Hz, C). $^{31}\text{P-NMR}$ (242.9 MHz): δ_{P} 31.3. Anal. Calcd for $\text{C}_{25}\text{H}_{23}\text{O}_4\text{P}$: C 71.76, H 5.54; found: C 71.80, H 5.57.

Ethyl 4-(diphenylphosphinoyl)-5-hydroxy-2-phenyl-hexa-2,3-dienoate (11b). Yellow oil, yield: 92%. Eluent for TLC: ethyl acetate:hexane = 1:4, R_f 0.52; IR (neat, cm^{-1}): 1179 (P=O), 1439, 1485 (Ph), 1717 (C=O), 1944 (C=C=C), 3389 (OH). $^1\text{H-NMR}$ (600.1 MHz): δ_{H} 1.32 (t, $J=7.0$ Hz, 3H, MeCH_2O), 1.40 (dd, $J=3.5$ Hz, $J=6.4$ Hz, 3H, Me-CH), 3.41 (s, 1H, OH), 4.21-4.30 (m, 2H, MeCH_2O), 5.09-5.17 (m, 1H, Me-CH), 7.20-8.10

(m, 15H, 3Ph). $^{13}\text{C-NMR}$ (150.9 MHz) δ_{C} 14.3 (CH_3), 22.9 ($J=1.7$ Hz, CH_3), 60.2 (CH_2), 75.7 ($J=5.8$ Hz, CH), 107.5 ($J=183.2$ Hz, C), 108.4 ($J=8.0$ Hz, C), 127.4-137.1 (3Ph), 163.7 ($J=4.7$ Hz, C), 214.5 ($J=1.5$ Hz, C). $^{31}\text{P-NMR}$ (242.9 MHz): δ_{P} 32.2. Anal. Calcd for $\text{C}_{26}\text{H}_{25}\text{O}_4\text{P}$: C 72.21, H 5.83; found: C 71.27, H 5.87.

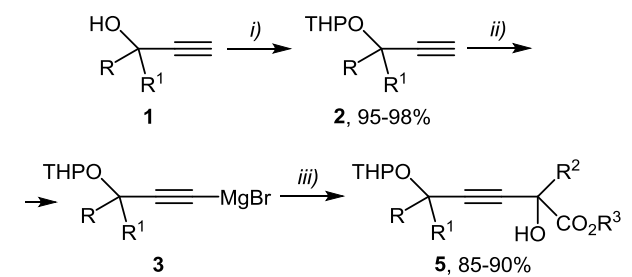
Methyl 4-(diphenylphosphinoyl)-5-hydroxy-5-methyl-2-phenyl-hexa-2,3-dienoate (11c). Yellow oil, yield: 93%. Eluent for TLC: ethyl acetate:hexane = 1:4, R_f 0.60; IR (neat, cm^{-1}): 1170 (P=O), 1437, 1495 (Ph), 1722 (C=O), 1940 (C=C=C), 3396 (OH). $^1\text{H-NMR}$ (600.1 MHz): δ_{H} 1.46 (t, $J=3.5$ Hz, 6H, Me_2C), 3.71 (s, 3H, MeO), 3.94 (s, 1H, OH), 7.20-8.04 (m, 15H, 3Ph). $^{13}\text{C-NMR}$ (150.9 MHz) δ_{C} 30.7 ($J=7.9$ Hz, CH_3), 53.7 (CH_3), 74.8 ($J=10.1$ Hz, C), 110.5 ($J=8.0$ Hz, C), 115.4 ($J=183.2$ Hz, C), 128.2-136.9 (3Ph), 165.0 ($J=4.6$ Hz, C), 211.5 ($J=1.0$ Hz, C). $^{31}\text{P-NMR}$ (242.9 MHz): δ_{P} 29.7. Anal. Calcd for $\text{C}_{26}\text{H}_{25}\text{O}_4\text{P}$: C 72.21, H 5.83; found: C 72.15, H 5.78.

RESULTS AND DISCUSSION

A range of the 4-phosphorylated 5-hydroxy-allenecarboxylates **7**, **9**, **10**, and **11** was prepared by the following four-step procedure including: i) protection of hydroxy group in the alk-3-yn-2-ols; ii) subsequent reaction with Grignard reagent and alkyl 2-oxoalkanoates to give the alkyl 2,5-dihydroxy-alk-3-ynoates with protected hydroxy group at second position; iii) interaction with chloride of phosphorus acid in the presence of a base; and finally iv) [2,3]-sigmatropic rearrangement of the mediated protected ethyl 2-(dimethoxyphosphino)oxy- or 2-(diphenylphosphino)oxy-5-hydroxy-alk-3-ynoates on order to assess the approach applied for 1,1,3-trifunctionalized allenes.

The first thing we examined was the protection of hydroxy group in the alk-3-yn-2-ols **1** with DHP in the presence of PPTS [67–70] (Scheme 1). The formed (tetrahydro-2H-pyran-2-yloxy)-alk-3-yn-2-ols **2** were isolated by column chromatography with excellent yield (96–98%). The reaction of the protected alkynols **2** with ethyl magnesium bromide and subsequent dropwise addition of the *in situ* generated alkynyl magnesium bromide **3** to the alkyl 2-oxoalkanoates **4** and reflux for 2 hours gives the alkyl 2-hydroxy-5-(tetrahydro-2H-pyran-2-yloxy)-alk-3-ynoates **5**, which are stable and were isolated by column chromatography in 85–89% yields as is shown in Scheme 1.

Having already in hand the required alkyl 2,5-dihydroxy-alk-3-ynoates **5** with protected hydroxy group at second position, we were able to investigate the proposed reactions with the corresponding chloro-containing phosphorus reagents such as dimethyl chlorophosphite and chlorodiphenyl phosphine in the presence of a base and subsequent [2,3]-sigmatropic rearrangement of the mediated phosphites **6** or phosphonites **8**.



Entry	Product	R	R ¹	R ²	R ³	Yield, %	
						2	5
1	a	H	H	Ph	Et	95	89
2	b	H	Me	Ph	Et	96	85
3	c	Me	Me	Me	Me	98	90

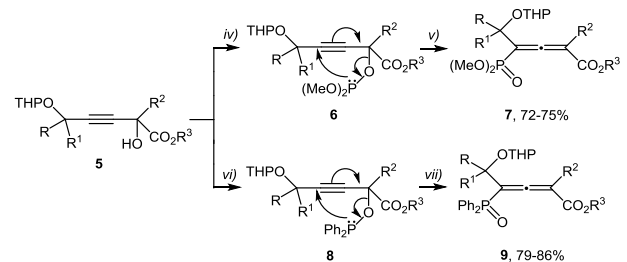
Reagents and Conditions: i) DHP (1.5 eq), PPTS (0.1 eq), CH₂Cl₂, rt, 2h, distillation; ii) EtMgBr (1 eq), THF, reflux, 2h; iii) dropwise addition of **3** to R²C(O)CO₂R³ (**4**) (2 eq), reflux, 2h, column chromatography.

Scheme 1. Synthesis of the alkyl 2-hydroxy-5-(tetrahydro-2H-pyran-2-yloxy)-alk-3-ynoates **5**.

It became obvious that the alkyl 4-(dimethoxyphosphoryl)-5-(tetrahydro-2H-pyran-2-yloxy)-alka-2,3-dienoates **7** can be readily prepared via an atom economical 2,3-sigmatropic rearrangement of the alkyl 2-(dimethoxyphosphino)oxy-5-(tetrahydro-2H-pyran-2-yloxy)-alk-3-ynoates **6**, intermediate formed by reaction of the alkyl 2-hydroxy-5-(tetrahydro-2H-pyran-2-yloxy)-alk-3-ynoates **5** with dimethyl chlorophosphite, prepared *in situ* from phosphorus trichloride and 2 equiv of methanol in the presence of triethylamine, and 2 equiv of pyridine, according to Scheme 2.

Further, reaction of the (tetrahydro-2H-pyran-2-yloxy)-alkynols **5** with chlorodiphenyl phosphine in the presence of triethylamine at -70 °C gave the expected alkyl 4-(diphenylphosphinoyl)-5-(tetrahydro-2H-pyran-2-yloxy)-alka-2,3-dienoates **9** in very good yield (79-82%) as a result of [2,3]-sigmatropic rearrangement of the ethyl 2-(diphenylphosphino)oxy-5-(tetrahydro-2H-pyran-2-yloxy)-pent-3-ynoates **8** for 6 hours at room temperature, according to the reaction sequence outlined in Scheme 2.

It was the 4-phosphorylated 5-hydroxyalka-2,3-dienoates with protected hydroxy group **7** and **9** that were synthesized via an atom economical and regioselective [2,3]-sigmatropic rearrangement of the intermediate formed hydroxy- and carboxy-substituted propargyl phosphites **6** or phosphonites **8** in the reaction of protected hydroxy- and carboxy-substituted alkynols **5** with dimethylchlorophosphite or chlorodiphenyl phosphine in the presence of triethylamine.



Entry	Product	R	R ¹	R ²	R ³	Yield, %	
						7	9
1	a	H	H	Ph	Et	74	82
2	b	H	Me	Ph	Et	72	79
3	c	Me	Me	Me	Me	75	86

Reagents and Conditions: iv) PCl₃ (1 eq), Et₃N (1.1 eq), Et₂O, -70 °C, 30 min stirring, pyridine (2.2 eq), MeOH (2 eq), Et₂O, -70 °C; v) [2,3-σ]-rearrangement, -70 °C, 1h, rt, 4h, column chromatography; vi) Ph₂P(=O)Cl (1 eq), Et₃N (1.1 eq), Et₂O, -70 °C; vii) [2,3-σ]-rearrangement, -70 °C, 1h, rt, 6h, column chromatography.

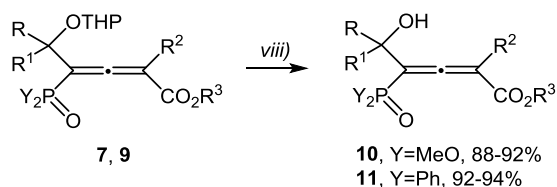
Scheme 2. Synthesis of the alkyl 4-(dimethoxyphosphoryl)-5-(tetrahydro-2H-pyran-2-yloxy)-alka-2,3-dienoates **7** and the alkyl 4-(diphenylphosphinoyl)-5-(tetrahydro-2H-pyran-2-yloxy)-alka-2,3-dienoates **9**.

Compounds **7** and **9** were stable enough to be handled at ambient temperature. The hydroxy group was deprotected by stirring the ethanol solution of the protected alkyl 4-(dimethoxyphosphoryl)- or 4-(diphenylphosphinoyl)-5-(tetrahydro-2H-pyran-2-yloxy)-alka-2,3-dienoates **7** or **9** in the presence of 0.1 equiv PPTS at room temperature for 6 hours to give the alkyl 4-(dimethoxyphosphoryl)-5-hydroxy-alka-2,3-dienoates **10** and the alkyl 4-(diphenylphosphinoyl)-5-hydroxy-alka-2,3-dienoates **11**, according to Scheme 3.

It should be stated that all allenic products **7**, **9**, **10**, and **11** that were isolated as stable yellow or orange oils by column chromatography and identified by ¹H, ¹³C, and ³¹P NMR and IR spectra as well as by elemental analysis.

A series of new 4-phosphorylated 5-hydroxyalka-2,3-dienoates with protected **7** and **9** and unprotected hydroxy group **10** and **11** were

synthesized by a convenient, efficient, atom economical and regioselective method.



Entry	Product	R	R ¹	R ²	R ³	Yield, %	
						10	11
1	a	H	H	Ph	Et	92	94
2	b	H	Me	Ph	Et	88	92
3	c	Me	Me	Me	Me	86	93

Reagents and Conditions: (viii) PPTS (0.1 eq), EtOH, rt, 6h, stirring, column chromatography.

Scheme 3. Synthesis of the alkyl 4-(dimethoxyphosphoryl)-5-hydroxyalka-2,3-dienoates **10** and the alkyl 4-(diphenylphosphinoyl)-5-hydroxyalka-2,3-dienoates **11**.

CONCLUSION

In conclusion, a convenient and efficient method for regioselective synthesis of a new family of 1,1,3-trifunctionalized allenes has been explored. 4-Phosphorylated 5-hydroxyalka-2,3-dienoates prepared were derived from [2,3]-sigmatropic rearrangement of the intermediate hydroxy- and carboxy-substituted propargyl phosphites or phosphinites formed in the reaction of protected hydroxy- and carboxy-substituted alkynols with dimethylchloro phosphite or chlorodiphenyl phosphine in the presence of a base.

Further investigations on this potentially important synthetic methodology are currently in progress. At the same time, the synthetic application of the prepared 4-phosphorylated 5-hydroxyalka-2,3-dienoates with protected or unprotected hydroxy group for synthesis of different heterocyclic compounds is now under investigation in our laboratory as a part of our general synthetic strategy for investigation of the scope and limitations of the electrophilic cyclization and cycloisomerization reactions of trifunctionalized allenes. Results of these investigations will be reported in due course. Moreover, results of an initial investigation of the biological activity of the compounds prepared were encouraging, and the antibacterial and antifungal activities of selected compounds as well as

potential precursors of effective anticancer drugs are now under investigation in our university.

Acknowledgements: Support from the Research Fund of the Konstantin Preslavsky University of Shumen (Projects Nos. RD-08-109 / 2016 and RD-08-98 / 2017) is acknowledged.

REFERENCES

1. R. W. Bates, V. Satcharoen, *Chem. Soc. Rev.*, **31**, 12 (2002).
2. N. Krause, A. S. K. Hashmi (Eds.), *Modern Allene Chemistry*, Wiley-VCH, Weinheim, 2004, Vol. 1 & 2.
3. S. Ma, *Aldrichimica Acta*, **40**, 91 (2007).
4. K. M. Brummond, J. E. DeForrest, *Synthesis*, 795 (2007).
5. T. M. V. D. Pinho e Melo, *Curr. Org. Chem.*, **13**, 1406 (2009);
6. T. G. Back, K. N. Clary, D. Gao, *Chem. Rev.*, **110**, 4498 (2010).
7. M. Enomoto, T. Katsuki, M. Yamaguchi, *Tetrahedron Lett.*, **27**, 4599 (1986).
8. H. J. Bestmann, H. Hartung, *Angew. Chem. Int. Ed. Engl.*, **2**, 214 (1963).
9. G. Aksnes, P. Froeyen, *Acta Chim. Scand.*, **22**, 2347 (1968).
10. R. W. Lang, H.-J. Hansen, *Helv. Chim. Acta.*, **63**, 438 (1980).
11. H. Fillion, A. Hseine, M.-H. Pera, V. Dufaud, B. Refouvelet, *Synthesis*, 708 (1987).
12. K. Tanaka, K. Otsubo, K. Fujii, *Synlett*, 933 (1995).
13. C.-Y. Li, X.-B. Wang, X.-L. Sun, Y. Tang, J.-C. Zheng, Z.-H. Xu, Y.-G. Zhou, L.-X. Dai, *J. Am. Chem. Soc.*, **129**, 1494 (2007).
14. M. Miesch, *Synthesis*, 746 (2003) and references cited therein.
15. S. Phadtare, J. Zemlicka, *J. Am. Chem. Soc.*, **111**, 5925 (1989).
16. S. Ma, H. Hou, S. Zhao, G. Wang, *Synthesis*, 1643 (2002).
17. J. Ye, S. Li, B. Chen, W. Fan, J. Kuang, J. Liu, Y. Liu, B. Miao, B. Wan, Y. Wang, X. Xie, Q. Yu, W. Yuan, S. Ma, *Org. Lett.*, **14**, 1346 (2012).
18. G. P. Boldrini, L. Lodi, E. Tagliavini, C. Tarasco, C. TrombinI, A. UmanI-Ronchi, *J. Org. Chem.*, **52**, 5447 (1987).
19. R. W. Hoffman, U. Weldmann, *Chem. Ber.*, **118**, 3966 (1985).
20. E. J. Corey, R. Imwinkelried, S. Pikul, Y. B. Xiang, *J. Am. Chem. Soc.*, **111**, 5493 (1989).
21. E. J. Corey, C.-M. Yu, D.-H. Lee, *J. Am. Chem. Soc.*, **112**, 878 (1990).
22. E. J. Corey, G. B. Jones, *Tetrahedron Lett.*, **32**, 5713 (1991).

23. J. Li, W. Kong, C. Fu, S. Ma, *J. Org. Chem.*, **74**, 5104 (2009).
24. J. Li, C. Zhou, C. Fu, S. Ma, *Tetrahedron*, **65**, 3695 (2009).
25. A. Alexakis, I. Marek, P. Mangeney, J. F. Normant, *Tetrahedron Lett.*, **30**, 2387 (1989).
26. A. Alexakis, I. Marek, P. Mangeney, J. F. Normant, *Tetrahedron*, **47**, 1677 (1991).
27. J. A. Marshall, K. G. Pinney, *J. Org. Chem.*, **58**, 7180 (1993).
28. N. Krause, A. Hoffmann-Röder, J. Canisius, *Synthesis*, **12**, 1759 (2002).
29. N. Krause, A. Hoffmann-Röder, *Tetrahedron*, **60**, 11671 (2004).
30. J. M. Aurrecoechea, M. Solay, *Tetrahedron Lett.*, **36**, 2501 (1995).
31. J. M. Aurrecoechea, E. Alonso, M. Solay, *Tetrahedron*, **54**, 3833 (1998).
32. J. S. Cowie, P. D. Landor, S. R. Landor, *J. Chem. Soc., Chem. Commun.*, 541 (1969).
33. J. S. Cowie, P. D. Landor, S. R. Landor, *J. Chem. Soc., Perkin Trans. 1*, 720 (1973).
34. M. Nakano, N. Furuichi, H. Mori, S. Katsumura, *Tetrahedron Lett.*, **42**, 7307 (2001).
35. C. Darcel, C. Bruneau, P. H. Dixneuf, *J. Chem. Soc., Chem. Commun.*, 1845 (1994).
36. C. Darcel, S. Bartsch, C. Bruneau, P. H. Dixneuf, *Synlett*, 457 (1994).
37. S. Hoff, L. Brandsma, J. F. Arens, *Rec. Trav. Chim. Pays-Bas*, **87**, 916 (1968).
38. S. Hoff, L. Brandsma, J. F. Arens, *Trav. Chim. Pays-Bas*, **87**, 1179 (1968).
39. S. Hormuth, H.-U. Reissig, *Synlett*, 179 (1991).
40. S. Hormuth, H.-U. Reissig, D. Dorsch, *Liebigs Ann. Chem.*, 121 (1994).
41. R. Zimmer, *Synthesis*, 165 (1993).
42. J. A. Marshall, Y. Tang, *J. Org. Chem.*, **58**, 3233 (1993).
43. V. Mark, The Uncatalyzed Rearrangements of Tervalent Phosphorus Esters, in: Selective Organic Transformations, B. S. Thyagarajan (Ed.), John Wiley & Sons, New York, 1970, pp. 319-437.
44. P. D. Landor, in: The Chemistry of the Allenes, Vol. 1, S. R. Landor (Ed.), Academic Press, New York, 1982, pp. 174-178.
45. R. W. Saalfrank, C.-J. Lurz, in: Methoden der Organischen Chemie (Houben Weyl), H. Kropf, E. Scheumann (Eds.), Thieme, Stuttgart, 1993, pp. 2959-3102.
46. A. S. K. Hashmi, Synthesis of Allenes, in: Modern Allene Chemistry, Vol. 1, N. Krause, A. S. K. Hashmi (Eds.), Wiley-VCH, Weinheim, 2004, pp. 3-50.
47. R. S. Macomber, *J. Am. Chem. Soc.*, **99**, 3072 (1977).
48. S. E. Denmark, J. E. Marlin, *J. Org. Chem.*, **56**, 1003 (1991).
49. B. Cai, G. M. Blackburn, *Synth. Commun.*, **27**, 3943 (1997).
50. R. W. Saalfrank, M. Haubner, C. Deutscher, U. Bauer, *Eur. J. Org. Chem.*, 2367 (1999).
51. A. P. Boiselle, N. A. Meinhardt, *J. Org. Chem.*, **27**, 1828 (1962).
52. V. Mark, *Tetrahedron Lett.*, **3**, 281 (1962).
53. K. C. Nicolaou, P. Maligres, J. Shin, E. de Leon, D. Rideout, *J. Am. Chem. Soc.*, **112**, 7825 (1990).
54. M. L. Curfin, W. H. Okamura, *J. Org. Chem.*, **55**, 5278 (1990).
55. J. W. Grissom, D. Huang, *Angew. Chem. Int. Ed.*, **34**, 2037 (1995).
56. C. Darcel, C. Bruneau, P. H. Dixneuf, *Synthesis*, 711 (1996).
57. O. de Frutos, A. M. Echavarren, *Tetrahedron Lett.*, **38**, 7941 (1997).
58. M. Schmittel, J.-P. Steffen, M. Maywald, B. Engels, H. Helten, P. Musch, *J. Chem. Soc., Perkin Trans. 2*, 1331 (2001).
59. V. K. Brel, *Synthesis*, 463 (1999).
60. V. K. Brel, E. V. Abramkin, *Mendeleev Commun.*, **12**, 64 (2002).
61. I. E. Ismailov, I. K. Ivanov, V. Ch. Christov, *Molecules*, **19**, 6309 (2014).
62. I. E. Ismailov, I. K. Ivanov, V. Ch. Christov, *Bulg. Chem. Commun.*, **46**, Special Issue A, 39 (2014).
63. I. E. Ismailov, I. K. Ivanov, V. Ch. Christov, *Molecules*, **19**, 11056 (2014).
64. V. Ch. Christov, I. E. Ismailov, I. K. Ivanov, *Molecules*, **20**, 7263 (2015).
65. V. Ch. Christov, I. E. Ismailov, I. K. Ivanov, *Int. J. Rec. Sci. Res. (IJRSR)*, **6**, 4526 (2015).
66. I. K. Ivanov, I. D. Parushev, V. Ch. Christov, *Heteroatom Chem.* **24**, 322 (2013).
67. D. N. Robertson, *J. Org. Chem.*, **25**, 931 (1960).
68. M. Miyashita, A. Yoshikoshi, P. A. Griecolb, *J. Org. Chem.*, **42**, 3772 (1977).
69. M. C. Joshi, P. Joshi, D. S. Rawat, *ARKIVOC*, (xvi), 65 (2006).
70. B. Partha, I. Pimkov, *US Patent 8378123 B2* (2011).
71. V. Ch. Christov, H. H. Hasanov, I. K. Ivanov, *Global J. Pure Appl. Chem. Res.* **3**, 20 (2015).
72. H. H. Hasanov, I. K. Ivanov, V. Ch. Christov, *Heteroatom Chem.* **28**, e21357 (2017).

ТРИФУНКЦИОНАЛИЗИРАНИ АЛЕНИ. ЧАСТ I. УДОБЕН И ЕФИКАСЕН
РЕГИОСЕЛЕКТИВЕН СИНТЕЗ НА 4-ФОСФОРИЛИРАНИ 5-ХИДРОКСИАЛКА-2,3-
ДИЕНОАТИ

И. Е. Исмаилов, И. К. Иванов, В. Х. Христов*

*Катедра по химия, Факултет по природни науки, Шуменски университет „Епископ Константин Преславски“,
ул. „Университетска“ 115, 9712 Шумен, България*

Постъпила на 08 февруари 2017 г.; Коригирана на 16 март 2017 г.

(Резюме)

Описан е удобен и ефикасен региоселективен синтез на 4-фосфорилирани 5-хидроксиалка-2,3-диеноати чрез атом-икономична [2,3]-сигматропна прегрупировка на междинно образуваните 2-(диметоксифосфино)окси- или 2-(дифенилфосфино)окси-5-(тетрахидро-2*H*-пиран-2-илокси)-алк-3-иноати, които лесно се получават чрез реакция на защитените 2-хидрокси-5-(тетрахидро-2*H*-пиран-2-илокси)-алк-3-иноати с диметил хлорофосфит или хлоридифенил фосфин съответно в присъствие на база.

Naphthalimide-based platinum(II) and palladium(II) N-heterocyclic carbene complexes: synthesis and structural elucidation

M. Dangalov^{1*}, P. Petrov², N. G. Vassilev¹

¹ Institute of Organic Chemistry with Center of Phytochemistry, Bulgarian Academy of Sciences, Acad. G. Bonchev Str., bl. 9, 1113 Sofia, Bulgaria

² Department of Organic Chemistry, Faculty of Chemistry and Pharmacy, Sofia University St. Kliment Ohridsky, 1 James Bourchier Blvd., 1164, Sofia, Bulgaria

Received February 23, 2017; Revised March 06, 2017

Dedicated to Acad. Bogdan Kurtev on the occasion of his 100th birth anniversary

The synthesis and characterization of five catalytically relevant Pd(II) and Pt(II) complexes involving N-heterocyclic carbenes (NHCs) derived from substituted 1,8-naphthalimides and σ -donor neutral monodentate ligands (DMSO, PPh₃, C₆H₅N and 4-dimethylaminopyridine (DMAP)) is reported. The structure and configuration of the complexes were elucidated on the basis of combination of NMR and DFT studies.

Key words: NHC complexes; ¹H, ¹³C and ¹⁹⁵Pt NMR spectroscopy; DFT calculations

INTRODUCTION

The discovery of N-heterocyclic carbenes (NHCs) by Wanzlick [1–3] and Öfele [4] in the 1960s attracted a significant attention to stable NHCs [5–7] as ancillary ligands in various transition-metal-mediated catalytic reactions such as olefin metathesis [8–10], Pd-catalyzed cross-coupling reactions [11–14] and hydrogenation reactions [15–17]. PEPPSI-typed (Pyridine Enhanced Precatalyst Preparation, Stabilization, and Initiation) complexes are one of the most fertile and well-performed catalysts in various C-C coupling reactions [18, 19]. Recently, Pt(II)-NHC complexes, exceeding their Pt(0) counterparts in air- and moisture-stability, have been increasingly used in homogeneous catalysis especially in hydrosilylation reaction [20–22]. N-heterocyclic carbenes are characterized as strong σ -donors, even stronger than alkyl phosphines; their steric properties are also entirely different than those of phosphines. NHCs also represent less severe environmental risks associated with phosphorus compounds. These advantages define them as favorable ligands for catalysis as well as precatalysts.

1,8-naphthalimide system and its derivatives demonstrate attractive electronic and photoactive properties, their respective fluorescent compounds serve as chemosensors for cations [23, 24],

biosensors [25], optoelectronic materials [26]. 4-amino-3-nitro-1,8-naphthalimides and their 3,4-diamino derivatives as starting compounds for preparation of N-heterocyclic carbene precursors were recently reported by us and their spectroscopic properties were studied [27, 28]. Fusion of imidazole-2-ylidenes to 1,8-naphthalimide moiety to a naphthalimide core affects the aromatic system, providing further attractive features and interesting photo-physical applications of their organometallic complexes. As part of our current interest in carbene complexes, herein we report the synthesis and structural elucidation of new Pt(II) NHC complexes and a palladium PEPPSI-motif complex derived from 5,10-dibutyl-8-(4-methylbenzyl)-4,6-dioxo-4,5,6,10-tetrahydrobenzo[*de*]imidazo[4,5-*g*]isoquinolin-8-ium chloride, *NHC.HCl*, which provide grounds for comparison of metal influences on the spectroscopic properties of the imidazo-naphthalimide ligand system.

EXPERIMENTAL

All reagents purchased from commercial suppliers were used without any further purification. Starting compounds *cis*-[Pt(DMSO)₂(Cl)₂] [29], *trans*-[Pd(Pyr)₂(Cl)₂] [30] and the NHC ligand [28, 31] were prepared according to literature procedures. All of the reactions were performed under inert atmosphere (Ar) using standard Schlenk techniques. The NMR spectra were recorded on a Bruker Avance II+ 600 (600.13 for ¹H NMR, 150.92 MHz for ¹³C NMR,

* To whom all correspondence should be sent:
E-mail: m.dangalov@orgchm.bas.bg

242.92 MHz for ^{31}P NMR and 129.01 MHz for ^{195}Pt NMR), spectrometer with TMS (85% H_3PO_4 for ^{31}P) as internal standard for proton and carbon chemical shifts (δ , ppm). ^{195}Pt NMR spectra are referred to the signal of 1.2M Na_2PtCl_6 in D_2O . ^1H and ^{13}C NMR data are reported as follows: chemical shift, multiplicity (s = singlet, d = doublet, t = triplet, q = quartet, br = broad, m = multiplet), coupling constants J (Hz), integration and identification. The assignment of the ^1H and ^{13}C NMR spectra was made on the basis of DEPT, COSY, HSQC, HMBC and NOESY experiments. Flash chromatography was performed on Silica Gel 60 (0.040–0.063 nm). Elemental analyses were performed by Microanalytical Service Laboratory of Faculty of Chemistry and Pharmacy, University of Sofia, using Vario EL3 CHNS(O) and Microanalytical service Laboratory of the Institute of Organic Chemistry, Bulgarian Academy of Science.

The DFT calculations were carried out on MADARA cluster (<http://madara.orgchm.bas.bg>) using program package GAUSSIAN 09 [32]. Geometry optimizations were performed by using density functional theory [33–35] with B3LYP functionals [36, 37]. As for the basis sets, we used 6-31G(d) sets for C, H, N, O, S, P and Cl [37]. For Pd and Pt, we used LANL2DZ basis sets [38], whose core parts were represented by effective core potentials (ECP). Solvent was included implicitly to the optimizations via the SMD [39] model with the built in solvent parameters. The nature of all critical points was confirmed by means of the vibrational analysis, and ZPV energies were evaluated. The thermal and entropy corrections to Gibbs free energy to 298.15 K have been calculated for all minima from unscaled vibrational frequencies obtained at the same level.

Synthesis of *trans*-[(NHC)Pd(Pyr)(Cl)₂], complex 1:

A Schlenk tube was charged with a magnetic stir bar, **NHC.HCl** (100 mg, 0.2 mmol), *trans*-[Pd(Pyr)₂(Cl)₂] (75 mg, 1.1 eqv.), 2 ml dry THF and finely powdered freshly dried K_2CO_3 (56 mg, 2 eqv.). The mixture was stirred for 2 hours at 40 °C and after cooling to room temperature, the reaction mixture was filtered through a pad of Celite and washed with DCM until the entire product was eluted. After evaporation of all volatiles the product was purified by column chromatography, eluting with petroleum ether/acetone = 4:1. Yield: 90 mg (63%) of pale yellow solid with m.p. decomposition over 120 °C. ^1H NMR (600 MHz, CDCl_3) δ = 0.968

(t, J = 7.4 Hz, 3H, **CH**₃-5-*n*-Bu), 1.204 (t, J = 7.4 Hz, 3H, **CH**₃-10-*n*-Bu), 1.401-1.463 (m, 2H, **CH**₂CH₃-5-*n*-Bu), 1.666-1.717 (m, 2H, **CH**₂CH₂CH₃-5-*n*-Bu), 1.792-1.854 (m, 2H, **CH**₂CH₃-10-*n*-Bu), 2.318 (s, 3H, **CH**₃-*p*-xylyl), 2.301-2.361 (m, 2H, **CH**₂CH₂CH₃-10-*n*-Bu), 4.128-4.154 (m, 2H, **NCH**₂-5-*n*-Bu), 5.546-5.575 (m, 2H, **NCH**₂-10-*n*-Bu), 6.374 (s, 2H, **NCH**₂-*p*-xylyl), 7.189 (d, J = 8.0 Hz, 2H, **H**3,5-*p*-xylyl), 7.402-7.425 (m, 2H, **H**3,5-pyr), 7.559 (d, J = 8.0 Hz, 2H, **H**2,6-*p*-xylyl), 7.827 (dd, J = 1.6, 7.6 Hz, 1H, **H**4-pyr), 7.958 (dd, J = 7.4, 8.5 Hz, 1H, **H**2-naphthyl), 8.508 (s, 1H, **H**7-naphthyl), 8.621 (dd, J = 0.8, 8.5 Hz, 1H, **H**1-naphthyl), 8.687 (dd, J = 0.8, 7.4 Hz, 1H, **H**3-naphthyl), 9.026-9.041 (m, 2H, **H**2,6-pyr). ^{13}C NMR (151 MHz, CDCl_3) δ = 13.84 (**CH**₃-5-*n*-Bu), 13.92 (**CH**₃-10-*n*-Bu), 20.25 (**CH**₂CH₃-5-*n*-Bu), 20.40 (**CH**₂CH₃-10-*n*-Bu), 21.24 (**CH**₃-*p*-xylyl), 30.10 (**CH**₂CH₂CH₃-5-*n*-Bu), 31.17 (**CH**₂CH₂CH₃-10-*n*-Bu), 40.66 (**NCH**₂-5-*n*-Bu), 51.60 (**NCH**₂-10-*n*-Bu), 53.47 (**NCH**₂-*p*-xylyl), 116.62 (**C**7-naphthyl), 119.02 (**Ar**-⁴C), 123.74 (**Ar**-⁴C), 124.68 (**Ar**-⁴C), 124.71 (**C**3,5-pyr), 125.63 (**Ar**-⁴C), 126.74 (**C**1-naphthyl), 127.91 (**C**2,6-*p*-xylyl), 128.18 (**C**2-naphthyl), 129.88 (**C**3,5-*p*-xylyl), 130.17 (**C**3-naphthyl), 131.33 (**Ar**-⁴C), 132.44 (**Ar**-⁴C), 132.54 (**Ar**-⁴C), 138.39 (**C**4-pyr), 138.44 (**Ar**-⁴C), 151.32 (**C**2,6-pyr), 163.30 (⁴**C**6-carbonyl), 163.82 (⁴**C**4-carbonyl), 166.85 (⁴**C**_{NHC}). $\text{C}_{34}\text{H}_{36}\text{Cl}_2\text{N}_4\text{O}_2\text{Pd}$: calcd. C, 57.52; H, 5.11; N, 7.89; found: C, 57.60; H, 5.12; N, 7.63.

Synthesis of *cis*-[(NHC)Pt(DMSO)(Cl)₂], complex 2:

A Schlenk tube was charged with a magnetic stir bar, **NHC.HCl** (250 mg, 0.51 mmol), *cis*-[Pt(DMSO)₂(Cl)₂] (240 mg, 1.1 eqv.), 2 ml dry THF and finely powdered freshly dried K_2CO_3 (140 mg, 2 eqv.). The mixture was stirred for 18 hours at 40 °C and after cooling to room temperature, the reaction mixture was filtered through a pad of Celite and washed with DCM until the entire product was eluted. After evaporation of all volatiles the product was purified by column chromatography, eluting with DCM /ethyl acetate = 4:1. Yield: 350 mg (88%) of pale yellow solid with m.p. decomposition over 120 °C: ^1H NMR (600 MHz, CDCl_3) δ = 0.953 (t, J = 7.4 Hz, 3H, **CH**₃-5-*n*-Bu), 1.139 (t, J = 7.4 Hz, 3H, **CH**₃-10-*n*-Bu), 1.382-1.453 (m, 2H, **CH**₂CH₃-5-*n*-Bu), 1.652-1.701 (m, 2H, **CH**₂CH₂CH₃-5-*n*-Bu), 1.731-1.791 (m, 2H, **CH**₂CH₃-10-*n*-Bu), 2.045-2.131 (m, 1H, a-**CH**₂CH₂CH₃-10-*n*-Bu), 2.267-2.347 (m, 1H, b-

$\text{CH}_2\text{CH}_2\text{CH}_3$ -10-*n*-Bu), 2.305 (s, 3H, CH_3 -*p*-xylyl), 2.981 (s, 3H, CH_3 -DMSO), 3.537 (s, 3H, CH_3 -DMSO), 4.132-4.157 (m, 2H, NCH_2 -5-*n*-Bu), 5.221-5.272 (m, 1H, a- NCH_2 -10-*n*-Bu), 5.333-5.381 (m, 1H, b- NCH_2 -10-*n*-Bu), 5.933 (d, $J = 16.3$ Hz, 1H, a- NCH_2 -*p*-xylyl), 6.478 (d, $J = 16.3$ Hz, 1H, b- NCH_2 -*p*-xylyl), 7.152 (d, $J = 8.2$ Hz, 2H, **H2,6**-*p*-xylyl), 7.212 (d, $J = 8.2$ Hz, 2H, **H3,5**-*p*-xylyl), 7.993 (dd, $J = 7.4, 8.6$ Hz, 1H, **H2**-naphthyl), 8.575 (s, 1H, **H7**-naphthyl), 8.591 (dd, $J = 0.7, 8.6$ Hz, 1H, **H1**-naphthyl), 8.707 (dd, $J = 0.7, 7.4$ Hz, 1H, **H3**-naphthyl). ^{13}C NMR (151 MHz, CDCl_3) $\delta = 13.75$ (CH_3 -5-*n*-Bu), 13.83 (CH_3 -10-*n*-Bu), 20.17 (CH_2CH_3 -10-*n*-Bu), 20.28 (CH_2CH_3 -5-*n*-Bu), 21.08 (CH_3 -*p*-xylyl), 30.01 ($\text{CH}_2\text{CH}_2\text{CH}_3$ -5-*n*-Bu), 30.73 ($\text{CH}_2\text{CH}_2\text{CH}_3$ -10-*n*-Bu), 40.58 (NCH_2 -5-*n*-Bu), 45.21 (CH_3 -DMSO), 45.86 (CH_3 -DMSO), 51.67 (NCH_2 -10-*n*-Bu), 52.06 (NCH_2 -*p*-xylyl), 116.57 (**C7**-naphthyl), 119.41 (**Ar**- ^{13}C), 120.00 (**Ar**- ^{13}C), 123.83 (**Ar**- ^{13}C), 126.01 (**Ar**- ^{13}C), 126.70 (**C1**-naphthyl), 126.89 (**C3,5**-*p*-xylyl), 128.41 (**C2**-naphthyl), 129.87 (**C2,6**-*p*-xylyl), 130.29 (**C3**-naphthyl), 131.11 (**Ar**- ^{13}C), 131.26 (**Ar**- ^{13}C), 132.24 (**Ar**- ^{13}C), 138.40 (**Ar**- ^{13}C), 158.16 ($^{13}\text{C}_{\text{NHC}}$), 163.05 ($^{13}\text{C}_{\text{C4}}$ -carbonyl), 163.60 ($^{13}\text{C}_{\text{C6}}$ -carbonyl). ^{195}Pt NMR (129 MHz, CDCl_3) $\delta = -3542.5$. $\text{C}_{31}\text{H}_{37}\text{Cl}_2\text{N}_3\text{O}_3\text{PtS}$: calcd. C, 46.68; H, 4.68; N, 5.27; S, 4.02; found: C, 46.58; H, 4.76; N, 5.13; S, 4.06.

Synthesis of *cis*-[(NHC)Pt(PPh₃)(Cl)₂], complex 3:

A Schlenk tube was charged with a magnetic stir bar, complex **2** (80 mg, 0.1 mmol), triphenylphosphine (26 mg, 1 mmol) and 2 ml chloroform. The mixture was stirred for 4 hours at 50 °C and after cooling to room temperature, and evaporation of all volatiles, the product was purified by column chromatography, eluting with DCM/ethyl acetate = 5:0.1. Yield: 88 mg (61%) pale yellow solid with m.p. decomposition over 120 °C: ^1H NMR (600 MHz, CDCl_3) $\delta = 0.975$ (t, $J = 7.4$ Hz, 3H, CH_3 -5-*n*-Bu), 1.024 (t, $J = 7.3$ Hz, 3H, CH_3 -10-*n*-Bu), 1.441-1.471 (m, 2H, CH_2CH_3 -5-*n*-Bu), 1.541-1.608 (m, 1H a- CH_2CH_3 -10-*n*-Bu), 1.611-1.651 (m, 1H, b- CH_2CH_3 -10-*n*-Bu), 1.661-1.718 (m, 2H, $\text{CH}_2\text{CH}_2\text{CH}_3$ -5-*n*-Bu), 1694-1.751 (m, 1H, a- $\text{CH}_2\text{CH}_2\text{CH}_3$ -10-*n*-Bu), 2.244 (s, 3H, CH_3 -*p*-xylyl), 2.284-2.359 (m, 1H, b- $\text{CH}_2\text{CH}_2\text{CH}_3$ -10-*n*-Bu), 4.091-4.163 (m, 2H, NCH_2 -5-*n*-Bu), 4.674 (d, $J = 14.8$ Hz, 1H, a- NCH_2 -*p*-xylyl), 4.659-4.699 (m, 1H, a- NCH_2 -10-*n*-Bu), 5.37 (m, 1H, b- NCH_2 -10-*n*-Bu), 6.479 (d, $J = 14.8$ Hz, 1H, b- NCH_2 -*p*-xylyl), 7.034 (d, $J = 8.1$ Hz, 2H, **H2,6**-*p*-

xylyl), 7.181-7.221 (m, 6H, *m*-ArH), 7.292-7.322 (m, 3H, *p*-ArH), 7.496 (d, $J = 8.1$ Hz, 2H, **H3,5**-*p*-xylyl), 7.545-7.614 (s, 6H, *o*-ArH), 7.904 (dd, $J = 7.4, 8.5$ Hz, 1H, **H2**-naphthyl), 8.274 (s, 1H, **H7**-naphthyl), 8.326 (dd, $J = 0.7, 8.5$ Hz, 1H, **H1**-naphthyl), 8.662 (dd, $J = 0.7, 7.4$ Hz, 1H, **H3**-naphthyl). ^{13}C NMR (151 MHz, CDCl_3) $\delta = 13.64$ (CH_3 -5-*n*-Bu), 13.79 (CH_3 -10-*n*-Bu), 20.15 (CH_2CH_3 -10-*n*-Bu), 20.37 (CH_2CH_3 -5-*n*-Bu), 21.16 (CH_3 -*p*-xylyl), 30.05 ($\text{CH}_2\text{CH}_2\text{CH}_3$ -5-*n*-Bu), 30.34 ($\text{CH}_2\text{CH}_2\text{CH}_3$ -10-*n*-Bu), 40.65 (NCH_2 -5-*n*-Bu), 51.50 (NCH_2 -10-*n*-Bu), 52.94 (NCH_2 -*p*-xylyl), 116.52 (**C7**-naphthyl), 118.76 (**Ar**- ^{13}C), 123.71 (**Ar**- ^{13}C), 125.44 (**Ar**- ^{13}C), 126.47 (**C1**-naphthyl), 128.15 (**C2**-naphthyl), 128.30 (**Ar**- ^{13}C), 128.34 (d, $^2J_{\text{C-P}} = 11$ Hz, *m*-ArC), 128.42 (**C3,5**-*p*-xylyl), 129.68 (**C2,6**-*p*-xylyl), 130.12 (**Ar**- ^{13}C), 130.35 (**C3**-naphthyl), 131.27 (brs, *p*-ArC), 131.71 (**Ar**- ^{13}C), 133.97 (d, $^2J_{\text{C-P}} = 11$ Hz, *o*-ArC), 138.58 (**Ar**- ^{13}C), 163.18 ($^{13}\text{C}_{\text{C4}}$ -carbonyl), 163.66 ($^{13}\text{C}_{\text{C6}}$ -carbonyl), 164.54 (brs, $^{13}\text{C}_{\text{NHC}}$). $^{31}\text{P}\{^1\text{H}\}$ NMR (243 MHz, CDCl_3) $\delta = 8.63$ (s, PPh₃). ^{195}Pt NMR (129 MHz, CDCl_3) $\delta = -3993$ (d, $^1J_{\text{Pt-P}} = 3813$ Hz). $\text{C}_{47}\text{H}_{46}\text{Cl}_2\text{N}_3\text{O}_2\text{P}$: calcd. C, 57.49; H, 4.72; N, 4.28; found: C, 57.24; H, 5.31; N, 4.19.

Synthesis of *trans*-[(NHC)Pt($\text{C}_5\text{H}_5\text{N}$)(Cl)₂], complex 4:

A Schlenk tube was charged with a magnetic stir bar, complex **2** (100 mg, 0.125 mmol) and pyridine (2 ml). The mixture was stirred for 18 hours at 50 °C and after cooling to room temperature and evaporation of all volatiles, the product was purified by column chromatography, eluting with DCM/ethyl acetate = 5:0.1. Yield: 95 mg (95%) pale yellow solid with m.p. decomposition over 120 °C: ^1H NMR (600 MHz, CDCl_3) $\delta = 0.972$ (t, $J = 7.4$ Hz, 3H, CH_3 -5-*n*-Bu), 1.187 (t, $J = 7.4$ Hz, 3H, CH_3 -10-*n*-Bu), 1.405-1.468 (m, 2H, CH_2CH_3 -5-*n*-Bu), 1.671-1.722 (m, 2H, $\text{CH}_2\text{CH}_2\text{CH}_3$ -5-*n*-Bu), 1.763-1.825 (m, 2H, CH_2CH_3 -10-*n*-Bu), 2.253-2.311 (m, 2H, $\text{CH}_2\text{CH}_2\text{CH}_3$ -10-*n*-Bu), 2.309 (s, 3H, CH_3 -*p*-xylyl), 4.134-4.159 (m, 2H, NCH_2 -5-*n*-Bu), 5.569-5.597 (m, 2H, NCH_2 -10-*n*-Bu), 6.404 (s, 2H, NCH_2 -*p*-xylyl), 7.176 (d, $J = 8.1$ Hz, 2H, **H3,5**-*p*-xylyl), 7.431-7.455 (m, 2H, **H3,5**-pyr), 7.545 (d, $J = 8.1$ Hz, 2H, **H2,6**-*p*-xylyl), 7.858 (tt, $J = 1.6, 7.6$ Hz, 1H, **H4**-pyr), 7.940 (dd, $J = 7.4, 8.5$ Hz, 1H, **H2**-naphthyl), 8.533 (s, 1H, **H7**-naphthyl), 8.627 (dd, $J = 0.8, 8.5$ Hz, 1H, **H1**-naphthyl), 8.669 (dd, $J = 0.8, 7.4$ Hz, 1H, **H3**-naphthyl), 9.053-9.066 (m, 2H, **H2,6**-pyr). ^{13}C NMR (151 MHz, CDCl_3) $\delta = 13.79$ (CH_3 -5-*n*-Bu), 13.86 (CH_3 -10-*n*-Bu), 20.12

(CH₂CH₃-5-*n*-Bu), 20.35 (CH₂CH₃-10-*n*-Bu), 21.16 (CH₃-*p*-xylyl), 30.05 (CH₂CH₂CH₃-5-*n*-Bu), 31.13 (CH₂CH₂CH₃-10-*n*-Bu), 40.56 (NCH₂-5-*n*-Bu), 50.92 (NCH₂-10-*n*-Bu), 52.65 (NCH₂-*p*-xylyl), 116.67 (C7-naphthyl), 118.74 (Ar-⁴C), 119.03 (Ar-⁴C), 123.63 (Ar-⁴C), 125.03 (C3,5-pyr), 125.63 (Ar-⁴C), 126.82 (C1-naphthyl), 127.59 (C2,6-*p*-xylyl), 127.91 (C2-naphthyl), 129.74 (C3,5-*p*-xylyl), 129.96 (C3-naphthyl), 131.67 (Ar-⁴C), 132.04 (Ar-⁴C), 132.05 (Ar-⁴C), 138.14 (Ar-⁴C), 138.29 (C4-pyr), 151.35 (C2,6-pyr), 155.91 (⁴C_{NHC}), 163.29 (⁴C6-carbonyl), 163.83 (⁴C4-carbonyl). ¹⁹⁵Pt NMR (129 MHz, CDCl₃) δ = -2965 (s). C₃₄H₃₆Cl₂N₄O₂Pt: calcd. C, 51.13; H, 4.54; N, 7.02; found: C, 51.33; H, 4.44; N, 7.19.

Synthesis of *trans*-[(NHC)Pt(DMAP)(Cl)₂], complex 5:

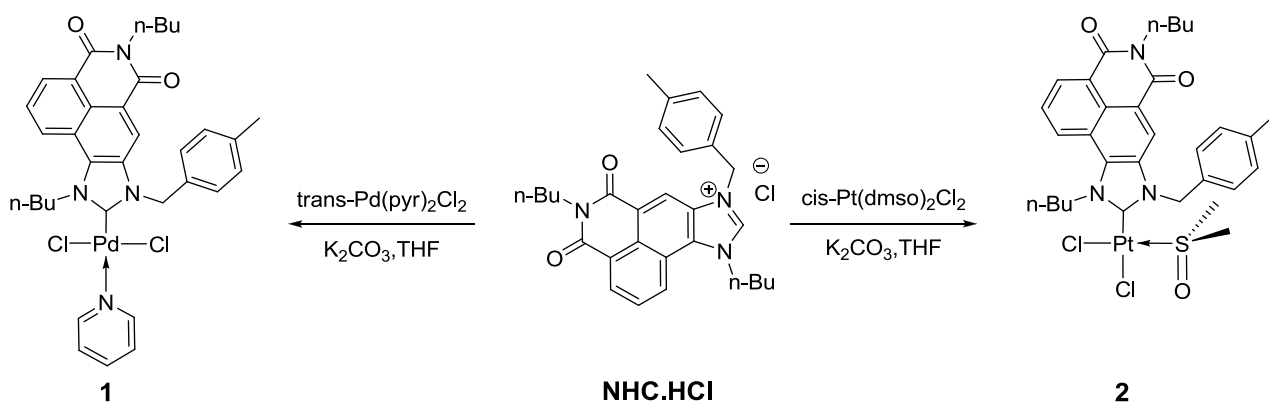
A Schlenk tube was charged with a magnetic stir bar, complex 2 (80 mg, 0.1 mmol), 4-dimethylaminopyridine (15 mg, 1.1 eqv.) and 2 ml chloroform. The mixture was stirred for 18 hours at 50 °C and after cooling to room temperature and evaporation of all volatiles, the product was purified by column chromatography, eluting with DCM/ethyl acetate = 5:0.1. Yield: 50 mg (59%) pale yellow solid with m.p. decomposition over 120 °C: ¹H NMR (600 MHz, CDCl₃) δ = 0.961 (t, *J* = 7.4 Hz, 3H, CH₃-5-*n*-Bu), 1.17 (t, *J* = 7.4 Hz, 3H, CH₃-10-*n*-Bu), 1.395-1.457 (m, 2H, CH₂CH₃-5-*n*-Bu), 1.659-1.711 (m, 2H, CH₂CH₂CH₃-5-*n*-Bu), 1.744-1.806 (m, 2H, CH₂CH₃-10-*n*-Bu), 2.232-2.285 (m, 2H, CH₂CH₂CH₃-10-*n*-Bu), 2.293 (s, 3H, CH₃-*p*-xylyl), 3.044 (s, 6H, CH₃-DMAP), 4.121-4.156 (m, 2H, NCH₂-5-*n*-Bu), 5.567-5.595 (m, 2H, NCH₂-10-*n*-Bu), 6.402 (s, 2H, NCH₂-*p*-xylyl), 6.486 (dd, *J* = 1.6, 6.1 Hz, 2H, H3,5-DMAP), 7.157 (d, *J* = 8.1 Hz, 2H, H3,5-*p*-xylyl), 7.557 (d, *J* = 8.1 Hz, 2H, H2,6-*p*-xylyl), 7.913 (dd, *J* = 7.4, 8.6 Hz,

1H, H2-naphthyl), 8.506 (s, 1H, H7-naphthyl), 8.512 (dd, *J* = 0.9, 6.1 Hz, 2H, H2,6-DMAP), 8.612 (dd, *J* = 0.8, 8.6 Hz, 1H, H1-naphthyl), 8.64 (dd, *J* = 0.8, 7.4 Hz, 1H, H3-naphthyl). ¹³C NMR (151 MHz, CDCl₃) δ = 13.79 (CH₃-10-*n*-Bu), 13.85 (CH₃-5-*n*-Bu), 20.11 (CH₂CH₂CH₃-5-*n*-Bu), 20.35 (CH₂CH₃-5-*n*-Bu), 21.15 (CH₃-*p*-xylyl), 30.05 (CH₂CH₃-10-*n*-Bu), 31.11 (CH₂CH₂CH₃-10-*n*-Bu), 39.26 (CH₃-DMAP), 40.53 (NCH₂-5-*n*-Bu), 50.78 (NCH₂-10-*n*-Bu), 52.56 (NCH₂-*p*-xylyl), 106.89 (C3,5-DMAP), 116.65 (C7-naphthyl), 118.44 (Ar-⁴C), 118.98 (Ar-⁴C), 123.55 (Ar-⁴C), 125.56 (Ar-⁴C), 126.91 (C1-naphthyl), 127.70 (C2,6-*p*-xylyl), 127.76 (C2-naphthyl), 129.68 (C3-naphthyl), 129.83 (C3,5-*p*-xylyl), 131.89 (Ar-⁴C), 132.06 (Ar-⁴C), 132.13 (Ar-⁴C), 137.99 (Ar-⁴C), 149.85 (C2,6-DMAP), 154.46 (C4-DMAP), 158.55 (⁴C_{NHC}), 163.36 (⁴C6-carbonyl), 163.89 (⁴C4-carbonyl). ¹⁹⁵Pt NMR (129 MHz, CDCl₃) δ = -2957 (s). C₃₆H₄₁Cl₂N₅O₂Pt: calcd. C, 51.37; H, 4.91; N, 8.32; found: C, 51.24; H, 5.06; N, 8.49.

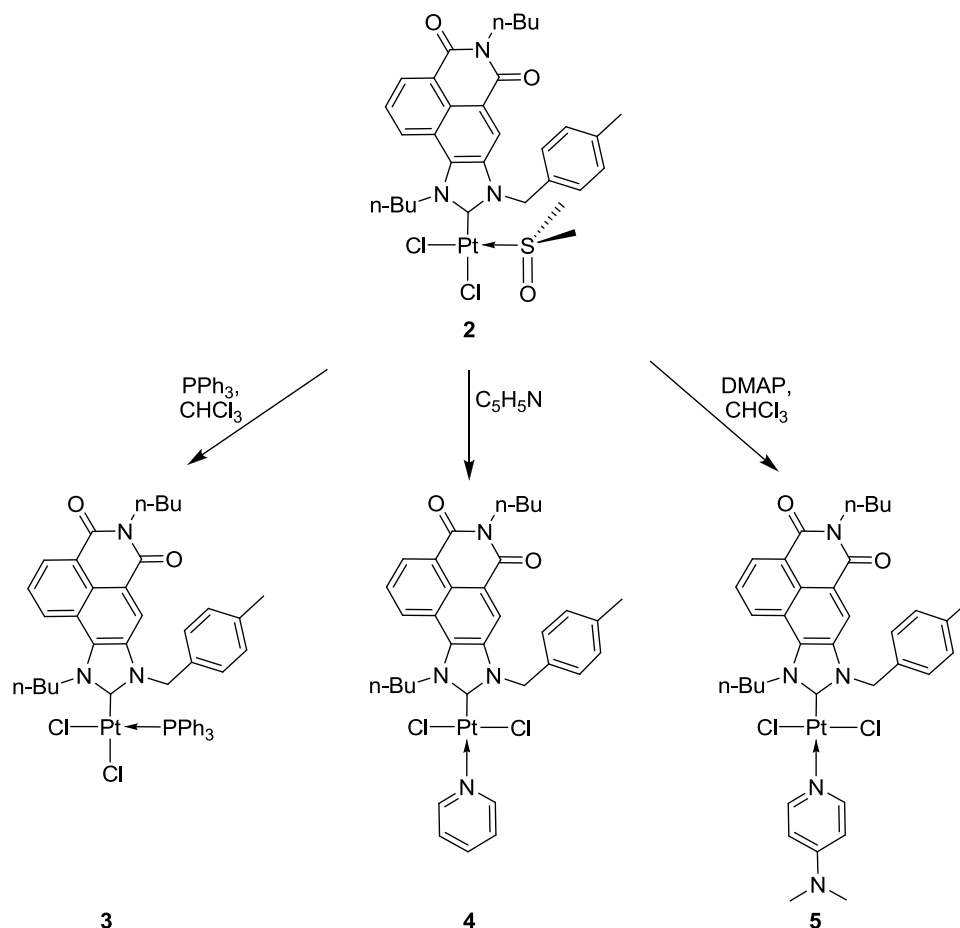
RESULTS AND DISCUSSION

Synthesis and characterization

Palladium complex 1 and platinum complex 2 were synthesized *via in situ* generation of the carbene, by deprotonating the imidazolium salt (NHC.HCl) with the mild base K₂CO₃, in presence of appropriate organometallic precursor in dry THF (Scheme 1), following our previous reported method [31, 40]. The precursor is *trans*-[Pd(Pyr)₂(Cl)₂] in case of complex 1 and respectively *cis*-[Pt(DMSO)₂(Cl)₂] in case of complex 2. N-heterocyclic carbene complexes of type 1, known as PEPSI type could in theory be obtained [18] by reaction of NHC precursors, palladium dichloride, and potassium carbonate in



Scheme 1. Synthesis of complexes 1 and 2.



Scheme 2. Synthesis of platinum(II) complexes **3-5**.

pyridine as a solvent. However, the application of this straightforward protocol for preparation of complex **1** was inappropriate due to generation of high concentrations of carbene and its fast dimerization to a respective ethylenetetramine. A successful workaround was to use a Pd precursor that already contains the pyridine ligand and use the standard $\text{K}_2\text{CO}_3/\text{THF}$ protocol.

Pt(II) complexes **3-5** were prepared by substitution of the labile DMSO ligand in complex **2** with triphenylphosphine, pyridine or 4-dimethylaminopyridine respectively at 50°C (Scheme 2). The new complexes were isolated as pale yellow solids, stable under normal conditions in moderate to high yields.

All new complexes were fully characterized by 1D and 2D ^1H and ^{13}C NMR experiments; complexes **2-5** were additionally studied by ^{195}Pt NMR as well. The ^1H NMR spectrum of palladium complex **1** was influenced by the pyridine ligand coordination, resulting in a downfield shift of the signal for the α -pyridine protons by 0.5 ppm, compared to the same signal of the free pyridine. The carbene atom in complex **1** resonates at 167 ppm in the ^{13}C NMR. The equivalence of the

benzylic CH_2 -protons as consequence of presence of mirror plane confirms *trans*-configuration of complex **1**. In the ^1H NMR spectrum of complex **2**, two singlets are observed for the methyl groups of the DMSO ligand at 2.98 and 3.54 ppm respectively, the coordination of DMSO ligand is additionally confirmed by presence of platinum satellites in ^1H spectrum at 250 MHz for the methyl groups due to $^3J_{\text{H-Pt}}$ coupling constant, which are missing in the ^1H spectrum at 600 MHz due to chemical shift anisotropy (CSA) relaxation (Fig. 1). As magnetic field increases, CSA contribution shortens the ^{195}Pt relaxation times, which broadens the linewidths of platinum satellites. The latter observation and the splitting of the diastereotopic benzylic protons into a doublets support the *cis*-configuration of the complex **2** due to the absence of a mirror plane. The carbene carbon of complex **2** resonates at 158 ppm; the absence of Pt satellites is likely due to low intensity of the signal and CSA effects at high magnetic field, while the ^{195}Pt signal of complex **2** appears at -3543 ppm, a value which is more inherent to the ^{195}Pt chemical shifts of saturated imidazolin-2-ylidene NHC system [41],

which as a “softer” ligand, is a stronger σ -donor causing upfield shift of the ^{195}Pt resonance [42].

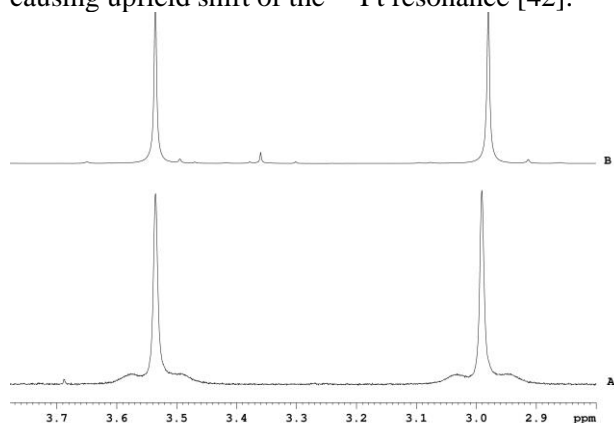


Fig. 1. Expansion of region of DMSO ligand methyl groups in ^1H NMR spectrum of complex **2**. **A:** measured at 250 MHz and showing satellites with $^3J_{\text{H-Pt}}$ coupling; **B:** the same spectrum measured at 600 MHz, in which these satellites are missing due to CSA.

Similarly to complex **2**, platinum complex **3** demonstrates absence of mirror plane as well, as a result of its *cis*-configuration consequently every diastereotopic CH_2 -group shows a pair of distinct signals in the ^1H NMR spectrum. The carbene atom in complex **3** resonates at 164 ppm in the ^{13}C NMR spectrum. The PPh_3 ligand's $^3\text{P}\{^1\text{H}\}$ signal is observed as a singlet at 8.6 ppm with platinum satellites due to $^1J_{\text{P-Pt}}$ coupling constant of 3813 Hz. This value supports the *cis*-configuration of the complex - commonly, values over 3000 Hz are a typical spectral characteristic of *cis*-complexes [43]. The ^{195}Pt signal resonates as a doublet at -3993 ppm and the substitution of the DMSO ligand with a “softer” ligand as PPh_3 shifts the resonance downfield with 450 ppm.

The ^1H -NMR spectrum of **P1** consists of four groups of signals (Fig. 1). The aromatic protons of 7-nitrobenzofurazane (NBD) moieties close to the ring nitrogen atoms and the CH_2 protons adjacent to ring nitrogens appear at 6.53 ppm and between 2.83-2.94 ppm, respectively, while the signals of $\text{C-CH}_2\text{-C}$ protons are around 1.76 ppm.

The ^1H NMR spectra of platinum complexes **4** and **5** demonstrate symmetry of both molecules due to presence of mirror plane, confirming the *trans*-configuration of the complexes. The ^1H NMR spectrum of platinum complexes **4** reveals the same tendency as his palladium analogue for the signal of α -pyridine protons, which is shifted upfield with 0.5 ppm in comparison with the same signal of the free pyridine. The ^{13}C signal for the carbene carbon in complex **4** is observed at 156 ppm, which is

upfield shifted with 11 ppm in comparison with the palladium analogue as result of the more electron-rich properties of platinum and its greater π -backbonding contribution in the carbene-metal bond [31, 44, 45]. The ^{195}Pt chemical shifts of complexes **4** and **5** are observed correspondingly at -2965 and -2957 ppm (Fig. 2).

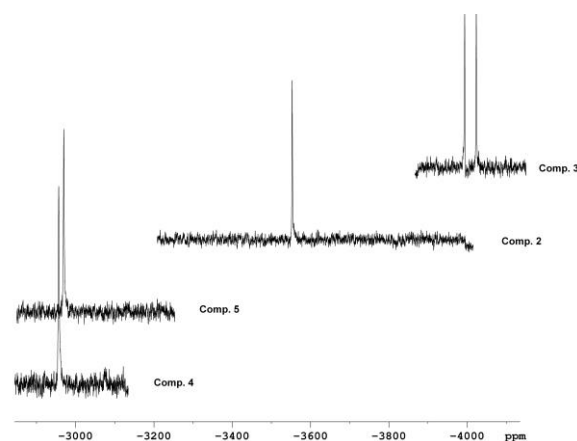


Fig. 2. ^{195}Pt NMR spectra of complexes **2-5**.

DFT study of complexes 1-5

Calculated thermodynamic parameters of complexes **1-5** at standard conditions are compared in Table 1. Calculated relative enthalpy values for *cis* and *trans* configuration at B3LYP/ECP (LanL2DZ for Pd and 6-31G* for other atoms) level including SMD exhibit correct tendency for all investigated complexes **1-5** (Table 1) and are in agreement with the experimentally obtained configuration of complexes which is denoted in Table 1 in bold. The differences in entropy are small and influence insignificantly the position of final thermodynamic equilibrium. The final ΔG° values accumulate computational errors both in enthalpy and in entropy, but the population distributions were predicted very well for all complexes **1-5** at relative low level of theory. From the fact that the obtained configurations of studied complexes are thermodynamically more stable, the conclusion that the studied ligand exchange reaction is carried out under thermodynamic control can be made.

CONCLUSION

Four platinum and one palladium PEPPSI type functionalized new N-heterocyclic carbene complexes were easily synthesized by ligand exchange reaction. The comparison of the ^{13}C NMR carbene resonances of palladium pyridine complex

Table 1. Thermodynamic parameters of *cis* and *trans* configurations of complexes at 298 K. Experimentally determined configurations are denoted in bold.^a

Complex (solvent)	Configuration	ΔH° (kcal mol ⁻¹)	ΔS° (cal K ⁻¹ mol ⁻¹)	ΔG° (kcal mol ⁻¹)	Population (%)
1 (THF)	<i>trans</i>	0.00	0.00	0.00	99.97
	<i>cis</i>	4.88	0.18	4.82	0.03
2 (THF)	<i>trans</i>	2.72	-0.08	2.74	0.97
	<i>cis</i>	0.00	0.00	0.00	99.03
3 (CDCl ₃)	<i>trans</i>	4.49	1.77	3.96	0.12
	<i>cis</i>	0.00	0.00	0.00	99.88
4 (Pyridine)	<i>trans</i>	0.00	0.00	0.00	99.60
	<i>cis</i>	2.61	-2.23	3.27	0.40
5 (CDCl ₃)	<i>trans</i>	0.00	0.00	0.00	99.93
	<i>cis</i>	3.77	-1.79	4.30	0.07

^a Calculated at B3LYP/ECP (LanL2DZ for Pd and 6-31G* for other atoms) level of theory including SMD.

1 and platinum pyridine complex **4** demonstrates the importance of metal center on π -backbonding contribution to the metal-carbene bond. The configuration of all complexes was determined by NMR spectroscopy. The DFT calculated thermodynamic parameters are in agreement with observed stereochemistry of all complexes, which means that the studied ligand exchange reaction is carried out under thermodynamic control.

Acknowledgement: The financial support by the Bulgarian Science Fund (UNA-17/2005, RNF01/0110 and DRNF-02/13) and by the Program for career development of young scientists-BAS (DFNP-130/2016) is gratefully acknowledged.

Electronic Supplementary Data available here.

REFERENCES

- H. W. Wanzlick, E. Schikora, *Angew. Chem.*, **72**, 494 (1960).
- H. W. Wanzlick, H. J. Kleiner, *Angew. Chem.*, **73**, 493 (1961).
- H. W. Wanzlick, *Angew. Chem.*, **74**, 129 (1962).
- K. Öfele, *J. Organomet. Chem.*, **12**, P42 (1968).
- A. J. Arduengo, R. L. Harlow, M. Kline, *J. Am. Chem. Soc.*, **113**, 361 (1991).
- W. A. Herrmann, K. Öfele, M. Elison, F. E. Kühn, P. W. Roesky, *J. Organomet. Chem.*, **480**, c7 (1994).
- A. C. Hillier, W. J. Sommer, B. S. Yong, J. L. Petersen, L. Cavallo, S. P. Nolan, *Organometallics*, **22**, 4322 (2003).
- V. Paradiso, V. Bertolasi, F. Grisi, *Organometallics*, **33**, 5932 (2014).
- A. Peretto, C. Costabile, P. Longo, F. Grisi, *Organometallics*, **33**, 2747 (2014).
- R. D. Savka, H. Plenio, *J. Organomet. Chem.*, **710**, 68 (2012).
- G. Bastug, S. P. Nolan, *Organometallics*, **33**, 1253 (2014).
- Z. Liu, N. Dong, M. Xu, Z. Sun, T. Tu, *J. Org. Chem.*, **78**, 7436 (2013).
- D. Guest, V. H. Menezes da Silva, A. P. de Lima Batista, S. M. Roe, A. A. C. Braga, O. Navarro, *Organometallics*, **34**, 2463 (2015).
- J. C. Bernhammer, N. X. Chong, R. Jothibas, B. Zhou, H. V. Huynh, *Organometallics*, **33**, 3607 (2014).
- P. Hauwert, J. J. Dunsford, D. S. Tromp, J. J. Weigand, M. Lutz, K. J. Cavell, C. J. Elsevier, *Organometallics*, **32**, 131 (2013).
- M. Yoshimura, R. Kamisue, S. Sakaguchi, *J. Organomet. Chem.*, **740**, 26 (2013).
- F. E. Hahn, C. Holtgrewe, T. Pape, M. Martin, E. Sola, L. A. Oro, *Organometallics*, **24**, 2203 (2005).
- J. Nasielski, N. Hadei, G. Achonduh, E. A. B. Kantchev, C. J. O'Brien, A. Lough, M. G. Organ, *Chem. Eur. J.*, **16**, 10844 (2010).
- M. G. Organ, G. A. Chass, D.-C. Fang, A. C. Hopkinson, C. Valente, *Synthesis*, **2008**, 2776 (2008).
- C. Lu, S. Gu, W. Chen, H. Qiu, *Dalton Trans.*, **39**, 4198 (2010).
- M. A. Taige, S. Ahrens, T. Strassner, *J. Organomet. Chem.*, **696**, 2918 (2011).
- J. J. Hu, F. Li, T. S. A. Hor, *Organometallics*, **28**, 1212 (2009).
- I. Grabchev, S. Yordanova, P. Bosch, E. Vasileva-Tonkova, R. Kukeva, S. Stoyanov, R. Stoyanova, *J. Mol. Struct.*, **1130**, 974 (2017).
- S. Yordanova, I. Grabchev, S. Stoyanov, I. Petkov, *J. Photochem. Photobiol. A: Chem.*, **283**, 1 (2014).
- S. Huang, R. Han, Q. Zhuang, L. Du, H. Jia, Y. Liu, Y. Liu, *Biosens. Bioelectron.*, **71**, 313 (2015).
- E. Schab-Balcerzak, M. Siwy, M. Filapek, S. Kula, G. Malecki, K. Laba, M. Lapkowski, H. Janeczka, M. Domanski, *J. Lumines.*, **166**, 22 (2015).

27. S. Stoyanov, P. Petrov, M. Stoyanova, M. Dangalov, B. Shivachev, R. Nikolova, I. Petkov, *J. Photochem. Photobiol. A - Chem.*, **250**, 92 (2012).
28. M. Dangalov, S. Yordanova, M. Stoyanova, D. Cheshmedzhieva, P. Petrov, S. Stoyanov, *J. Mol. Struct.*, **1125**, 705 (2016).
29. J. H. Price, A. N. Williamson, R. F. Schramm, B. B. Wayland, *Inorg. Chem.*, **11**, 1280 (1972).
30. U. Kalinowska, L. Chęcińska, M. Małecka, A. Erxleben, B. Lippert, J. Ochocki, *Inorg. Chim. Acta*, **358**, 2464 (2005).
31. M. Dangalov, P. Petrov, N. G. Vassilev, *J. Organomet. Chem.*, **824**, 104 (2016).
32. M. J. T. Frisch, G. W. Schlegel, H. B. Scuseria, G. E. Robb, M. A. Cheeseman, J. R. Scalmani, G. Barone, V. Mennucci, B. Petersson, G. A. Nakatsuji, H. Caricato, M. Li, X. Hratchian, H. P. Izmaylov, A. F. Bloino, J. Zheng, G. Sonnenberg, J. L. Hada, M. Ehara, M. Toyota, K. Fukuda, R. Hasegawa, J. Ishida, M. Nakajima, T. Honda, Y. Kitao, O. Nakai, H. Vreven, T. Montgomery, Jr., J. A. Peralta, J. E. Ogliaro, F. Bearpark, M. Heyd, J. J. Brothers, E. Kudin, K. N. Staroverov, V. N. Kobayashi, R. Normand, J. Raghavachari, K. Rendell, A. Burant, J. C. Iyengar, S. S. Tomasi, J. Cossi, M. Rega, N. Millam, N. J. Klene, M. Knox, J. E. Cross, J. B. Bakken, V.; Adamo, C.; Jaramillo, J.; Gomperts, R.; Stratmann, R. E. Yazyev, O. Austin, A. J. Cammi, R. Pomelli, C. Ochterski, J. W. Martin, R. L. Morokuma, K. Zakrzewski, V. G. Voth, G. A. Salvador, P. Dannenberg, J. J. Dapprich, S. Daniels, A. D. Farkas, Ö. Foresman, J. B. Ortiz, J. V. Cioslowski, J. Fox, D. J., in: Gaussian, Inc., Wallingford CT, 2009.
33. P. Hohenberg, W. Kohn, *Phys. Rev.*, **136**, B864 (1964).
34. W. Kohn, L. J. Sham, *Phys. Rev.*, **137**, A1697 (1965).
35. R. G. Parr, W. Yang, *Density Functional Theory of Atoms and Molecules*, Oxford Univ Press, Oxford, 1989.
36. A. D. Becke, *J. Chem. Phys.*, **98**, 5648 (1993).
37. C. Lee, W. Yang, R. G. Parr, *Phys. Rev. B*, **37**, 785 (1988).
38. W. R. Wadt, P. J. Hay, *J. Chem. Phys.*, **82**, 284 (1985).
39. A. V. Marenich, C. J. Cramer, D. G. Truhlar, *J. Phys. Chem. B*, **113**, 6378 (2009).
40. M. Dangalov, M. Stoyanova, P. Petrov, M. Putala, N. G. Vassilev, *J. Organomet. Chem.*, **817**, 1 (2016).
41. S. Fantasia, J. L. Petersen, H. Jacobsen, L. Cavallo, S. P. Nolan, *Organometallics*, **26**, 5880 (2007).
42. P. S. Pregosin, *Platinum NMR Spectroscopy*, in: *Annual Reports on NMR Spectroscopy*, G. A. Webb (ed.), Academic Press, 1986, pp. 285.
43. C. P. Newman, R. J. Deeth, G. J. Clarkson, J. P. Rourke, *Organometallics*, **26**, 6225 (2007).
44. W. W. N. O, A. J. Lough, R. H. Morris, *Organometallics*, **29**, 570 (2010).
45. B. Binotti, G. Bellachioma, G. Cardaci, A. Macchioni, C. Zuccaccia, E. Foresti, P. Sabatino, *Organometallics*, **21**, 346 (2002).

НАФТАЛИМИД-БАЗИРАНИ ПЛАТИНОВИ(II) И ПАЛАДИЕВИ(II) N-ХЕТЕРОЦИКЛЕНИ КАРБЕНОВИ КОМПЛЕКСИ: СИНТЕЗ И ДОКАЗВАНЕ НА СТРУКТУРАТА

М. Дангалов^{1*}, П. Петров², Н. Г. Василев¹

¹ *Институт по Органична химия с Център по Фитохимия, Българска Академия на Науките, ул. Акад. Г. Бончев, бл. 9, 1113 София, България*

² *Катедра по органична химия, Факултет по химия и фармация, Софийски университет „Св. Климент Охридски“, ул. Джеймс Баучер 1, 1164 София, България*

Постъпила на 23 февруари 2017 г.; Коригирана на 06 март 2017 г.

(Резюме)

Представен е синтеза и охарактеризирането на пет каталитично приложими Pd(II) и Pt(II) комплекси включващи N-хетероциклени карбени (NHCs) получени от заместени 1,8-нафталимиди и σ -донорни неутрални монодентатни лиганди (DMSO, PPh₃, C₆H₅N и 4-диметиламинопиридин (DMAР)). Структурата и конфигурацията на комплексите е доказана на базата на комбинация от ЯМР и DFT изследвания.

Synthesis and structural characterization of *N*-[2-(diphenylphosphorothioyl)phenyl]-2-(phenylamino)benzamide

R. H. Lyapchev¹, M. G. Dangelov², N. G. Vassilev², P. Y. Petrov^{1*}

¹ Department of Organic Chemistry and Pharmacognosy, Faculty of Chemistry and Pharmacy, Sofia University St. Kliment Ohridsky, James Bourchier 1 blvd., 1164 Sofia, Bulgaria

² Institute of Organic Chemistry with Centre of Phytochemistry, Bulgarian Academy of Sciences, Acad. G. Bonchev street, bl. 9, 1113 Sofia, Bulgaria

Received March 06, 2017; Revised March 29, 2017

Dedicated to Acad. Bogdan Kurtev on the occasion of his 100th birth anniversary

N-(2-(diphenylphosphorothioyl)phenyl)-2-(phenylamino)benzamide with perspective application as a ligand in organometallic homogeneous catalysis was prepared using *N*-phenylanthranilic acid as starting material. Its structure was studied by NMR spectroscopy and X-ray diffraction.

Key words: organophosphorous compounds; one-pot; homogeneous catalysis ligand

INTRODUCTION

Compounds containing phosphorous and nitrogen atom which can coordinate to a transition metal, as well as their respective complexes are subject of research in recent decades [1–4]. Interest in them has increased after discovering of the reactions of Negishi, Heck and Suzuki [5–7], which are catalysed by a palladium complex, usually bearing a phosphine ligand. In this work we present the results of the multistep synthesis and X-ray analysis of a potential (2-aminophenyl)diphenylphosphine sulphide derived ligand. We aimed to obtain an organophosphorus compound, which can be used as a ligand in homogeneous catalysis and as a starting material for the preparation of P-functionalized NHC-precursors.

EXPERIMENTAL

Synthesis

All solvents and chemicals were purchased from commercial suppliers. Petroleum ether was used as received. Dichloromethane was dried over anhydrous CaCl₂ and distilled. Toluene was distilled from sodium/benzophenone and stored under argon. Silica gel 0.035–0.070 mm, 60 A was used for flash chromatography. TLC on silica gel 60 F₂₅₄ on aluminium sheets was used for monitoring of the reactions.

The NMR spectra of (**5**) were recorded on a Bruker Avance II+ 600 (600.13 for ¹H NMR, 150.92 MHz for ¹³C NMR and 242.92 MHz for ³¹P NMR) spectrometer with a reference TMS (85% H₃PO₄ for ³¹P) as internal standard or chemical shifts of residue solvent peaks (δ , ppm). ¹H and ¹³C NMR data are reported as follows: chemical shift, multiplicity (s = singlet, d = doublet, t = triplet, q = quartet, br = broad, m = multiplet), coupling constants J (Hz), integration and identification. The atom numbering follows Fig.1.

In a Schlenk flask equipped with condenser were mixed 0.77 g (3.6 x 10⁻³ mol) *N*-phenylanthranilic acid (**1** on Scheme 1) and 8 ml dry toluene. 0.75 mL (1.028 x 10⁻² mol) of thionyl chloride were added and the mixture was stirred for 15 minutes at room temperature, 25 min at 100 °C, and then 10 minutes at 125 °C. The volatile components of the reaction mixture were removed under reduced pressure to leave the desired chloride (**2** on Scheme 1).

20 ml of dry toluene, 1 g (3.6 x 10⁻³ mol) of 2-(diphenylphosphanyl)aniline (**3** on Scheme 1) and 0.29 ml (3.63 x 10⁻³ mol) of dry pyridine were mixed in a separate Schlenk tube and the resulting solution was degassed.

The prepared acid chloride **2** was dissolved in 8 ml of dry toluene and degassed. The resulting solution was added in one portion to the solution of 2-(diphenylphosphanyl)aniline (**3**) (Scheme 1). The reaction mixture thus obtained was stirred at room temperature until no starting aniline (about 24 hours) remains (TLC). Then 0.127 g (3.97 x 10⁻³ mol) of sulphur was added. The stirring continued

* To whom all correspondence should be sent:
E-mail: ppetrov@chem.uni-sofia.bg

15 hours at room temperature until no more *N*-(2-(diphenylphosphanyl)phenyl)-2-(phenylamino)benzamide (**4** on Scheme 1) could be observed with TLC. The resulting reaction mixture was diluted with an equal volume of ethyl acetate, washed three times with 25 ml portions of brine, dried over anhydrous Na₂SO₄ and the solvent evaporated under reduced pressure. The crude product was purified by flash chromatography on 36 g silica gel, using methylene chloride:petroleum ether = 2:3 as a mobile phase. Yield: 1,4 g (77%) of pale yellow crystals.

¹H NMR (600 MHz, CDCl₃) δ= 6.75 (ddd, J=1.1, 7.0, 8.0 Hz, 1H, **H-C4**), 6.84 (ddd, J=1.3, 7.8, ³J_{P-H}=14.3 Hz, 1H, **H-C15**), 7.01 (tt, J=1.1, 7.3 Hz, 1H, **H-C10**), 7.11 (ddd, J=1.10, 7.60, ⁴J_{P-H}=2.3, 1H, **H-C16**), 7.13 (dd, J=1.1, 8.5 Hz, 2H, **H-C12, H-C8**), 7.23 (ddd, J=1.3, 7.0, 8.4 Hz, 1H, **H-C3**), 7.27 (dd, J=1.1, 8.4 Hz, 1H, **H-C2**), 7.30 (dd, J=7.3, 8.5 Hz, 2H, **H-C11, H-C9**), 7.38-7.42 (m, 6H, **Ar-P**), 7.52 (dd, J=1.3, 8.0 Hz, 1H, **H-C5**), 7.61 (ddd, J=1.3, 7.6, 8.2 Hz, 1H, **H-C17**), 7.70-7.75 (m, 4H, **Ar-P**), 8.08 (ddd, J=1.1, 8.2 Hz, ⁴J_{P-H}=5.0, 1H, **H-C18**), 9.30 (bs, 1H, **N1-H**), 10.31 (s, 1H, **N2-H**).

¹³C-NMR (151, CDCl₃) δ= 115.06 (**C2**), 116.87 (**C6**), 118.03 (**C4**), 120.73 (**C12, 8**), 122.39 (**C10**), 124.31 (d, J=85.5 Hz, **C26, C20**), 124.55 (d, ³J_{C-P}=12.2 Hz, **C16**), 126.39 (d, ³J_{C-P}=6.9 Hz, **C18**), 128.42 (**C5**), 128.73 (d, J=12.9 Hz, **Ar-P**), 129.06 (**C11, 9**), 130.37 (d, J=86.2 Hz, **C19**), 132.33 (**Ar-P**), 132.35 (**Ar-P**), 132.42 (**C15**), 132.70 (**C3**), 132.92 (d, ⁴J_{C-P}=2.1 Hz, **C17**), 141.06 (d, J=4.3 Hz, **C14**), 141.49 (**C7**), 145.86 (**C1**), 167.65 (**C13**).

³¹P NMR (243 MHz, CDCl₃) δ= 40.01 (s, **P1**).

X-ray crystallography

Pale yellow crystals of **5**, suitable for X-ray analysis were obtained by slow evaporation at room temperature from a solution of dichloromethane and petroleum ether.

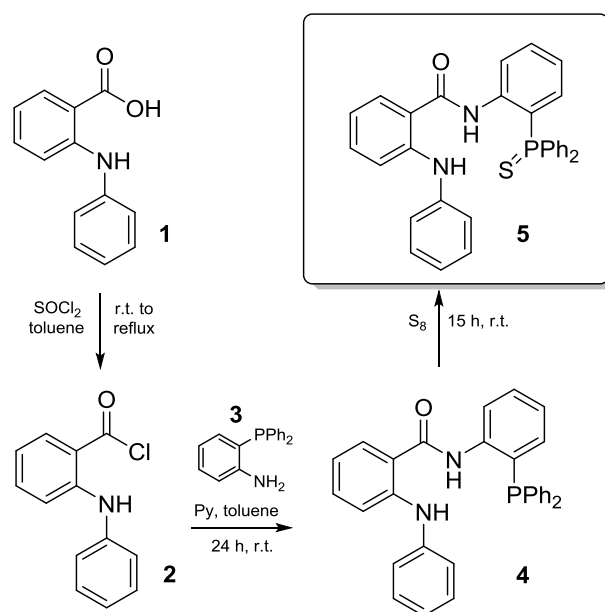
Crystal was mounted with the help of light hydrocarbon oil on Bruker SMART X2S diffractometer and data were collected using graphite monochromated Mo K α radiation ($\kappa=0.71073$ Å). The data integration and reduction were processed with APEX software. An absorption correction was applied [8]. The structure was solved by the direct method using SHELXS-97 and was refined on *F*² by full-matrix least-squares technique using the SHELXL-97 software package [9] and Olex2 [10]. Nonhydrogen atoms were refined anisotropically. In the refinement, hydrogen

atoms were treated as riding atoms using SHELXL default parameters.

RESULTS AND DISCUSSION

Synthesis

The synthesis of the target compound is presented on Scheme 1.



Scheme 1. Synthesis of **5**.

N-phenylanthranilic acid (**1**) was reacted [11] with SOCl₂ in dry toluene in inert Ar atmosphere. After evaporation of the volatiles the acid chloride (**2**) was mixed with 2-(diphenylphosphanyl)aniline [12–14] in the presence of pyridine. The P(III) atom of thus obtained benzamide (**4**) was protected by oxidation to P(V) with elemental sulfur. Finally the target compound (**5**) was purified by column chromatography and obtained with very good overall yield as yellow crystals.

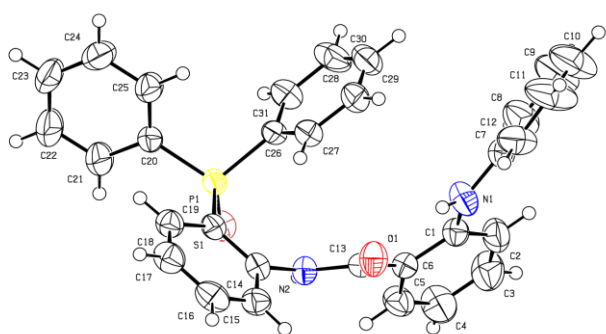
¹H-NMR of *N*-(2-(diphenylphosphorothioyl)phenyl)-2-(phenylamino)benzamide was recorded in deuterated chloroform. The spectrum of (**5**) shows signals at high frequency for the two nitrogen protons, respectively at 9.3 and 10.3 ppm (see Fig. S1 for the actual ¹H, ¹³C and ³¹P NMR spectra), which may be attributed to hydrogen-bond type interactions with S=P and O=C-groups. Signals of the carbon atoms of Ar-P fragment are split due to coupling with the phosphorus atom.

X-ray crystallography

Crystal data and data collection parameters for the compound (**5**) are presented in Table 1.

Table 1. Crystal data and structure refinement for **5**.

Identification code	5
Empirical formula	C ₃₁ H ₂₅ N ₂ OPS
Formula weight	504.56
Temperature/K	300.15
Crystal system	Triclinic
Space group	<i>P</i> -1
<i>a</i> /Å	11.3475(17)
<i>b</i> /Å	11.4393(18)
<i>c</i> /Å	12.429(2)
α /°	106.973(5)
β /°	105.855(5)
γ /°	110.912(5)
<i>V</i> /Å ³	1306.5(4)
<i>Z</i>	2
ρ_{calc} /g/cm ³	1.283
μ /mm ⁻¹	0.212
<i>F</i> (000)	528.0
Crystal size/mm ³	0.4 × 0.3 × 0.05
Radiation	MoK α (λ = 0.71073)
2 θ range for data collection/°	3.78 to 52.632
Index ranges	-13 ≤ <i>h</i> ≤ 14, -14 ≤ <i>k</i> ≤ 14, -14 ≤ <i>l</i> ≤ 15
Reflections collected/independent	9408/5093
Data/restraints/parameters	5093/0/325
Goodness-of-fit on <i>F</i> ²	0.959
Final <i>R</i> indexes [<i>I</i> >= 2 σ (<i>I</i>)]	<i>R</i> = 0.0630, <i>wR</i> = 0.1394
Final <i>R</i> indexes [all data]	<i>R</i> = 0.1422, <i>wR</i> = 0.1831
Largest diff. peak/hole / e Å ⁻³	0.27/-0.38

**Fig. 1.** ORTEP drawing of molecular structure of **5**. The thermal displacement ellipsoids are drawn at the 50% probability.

CCDC 1403430 contains the supplementary crystallographic data for (**5**). These data can be obtained from the Cambridge Crystallographic Data

Centre. ORTEP drawing of molecular structure of (**5**) is depicted on Fig. 1.

Compound (**5**) crystallizes in the triclinic system and space group *P*-1. The bond lengths and angles are shown in Tables 2 and 3.

Table 2. Observed bond lengths in **5**.

Bond	Length Å	Bond	Length Å
P1–S1	1.9698(16)	C7–C8	1.392(6)
P1–C26	1.824(3)	C27–C28	1.380(5)
P1–C19	1.824(3)	C1–C2	1.405(6)
P1–C20	1.808(4)	C15–C16	1.377(6)
O1–C13	1.239(4)	C18–C17	1.378(5)
N2–C14	1.420(5)	C17–C16	1.376(6)
N2–C13	1.380(4)	C25–C24	1.392(6)
N1–C7	1.407(5)	C31–C30	1.390(5)
N1–C1	1.390(5)	C5–C4	1.372(6)
C14–C19	1.408(5)	C28–C29	1.371(6)
C14–C15	1.387(5)	C29–C30	1.370(6)
C26–C27	1.386(5)	C12–C11	1.374(6)
C26–C31	1.390(5)	C24–C23	1.369(6)
C19–C18	1.382(5)	C23–C22	1.377(7)
C13–C6	1.484(6)	C2–C3	1.369(6)
C20–C25	1.379(6)	C8–C9	1.381(6)
C20–C21	1.387(5)	C21–C22	1.380(6)
C6–C1	1.424(5)	C4–C3	1.391(6)
C6–C5	1.394(6)	C11–C10	1.387(7)
C7–C12	1.372(6)	C9–C10	1.348(7)

The carbonyl oxygen and NPh-group are slightly out from the plane of the anthranilic C₆H₄-ring. The geometry at the P atom is tetrahedral; the P=S distance is 1.9681 Å and the average P-C distance is 1.8157 Å. The average C-P-S angle is 112.84° and an average C-P-C angle is 105.9°. The average length of the P-S bond in **5** is longer than that of triphenylphosphine sulfide, due to substituents in the phenyl ring [15]. The average P-C bond and C-P-C angle in **5** and in the reference Ph₃P=S are similar [15]. The crystal structure of **5** shows intramolecular hydrogen bonding interactions between oxygen and hydrogen and between sulphur and hydrogen (Table 4).

Table 4. Details of hydrogen bonds observed in **5**.

<i>D</i> –H... <i>A</i>	<i>D</i> ... <i>A</i> [Å]	H... <i>A</i> [Å]	<i>D</i> –H– <i>A</i> [°]
N1–H...O1	2.739	2.048	136.87
N2–H...S1	3.305	2.698	128.70

Table 3. Observed angles in **5**.

Angle	[°]	Angle	[°]
C26–P1–S1	113.52(14)	C8–C7–N1	123.4(4)
C19–P1–S1	112.12(14)	C28–C27–C26	120.8(4)
C19–P1–C26	105.67(16)	N1–C1–C6	119.2(4)
C20–P1–S1	112.82(14)	N1–C1–C2	123.1(4)
C20–P1–C26	105.74(17)	C2–C1–C6	117.7(4)
C20–P1–C19	106.36(18)	C16–C15–C14	120.0(4)
C13–N2–C14	122.4(3)	C17–C18–C19	121.6(4)
C1–N1–C7	129.7(4)	C16–C17–C18	119.6(4)
C19–C14–N2	121.0(3)	C17–C16–C15	120.5(4)
C15–C14–N2	119.0(3)	C20–C25–C24	121.3(4)
C15–C14–C19	120.1(3)	C30–C31–C26	119.7(4)
C27–C26–P1	123.0(3)	C4–C5–C6	122.7(4)
C27–C26–C31	118.9(3)	C29–C28–C27	119.8(4)
C31–C26–P1	118.0(3)	C30–C29–C28	120.4(4)
C14–C19–P1	120.0(3)	C7–C12–C11	120.8(4)
C18–C19–P1	121.8(3)	C23–C24–C25	119.6(5)
C18–C19–C14	118.2(3)	C24–C23–C22	119.9(5)
O1–C13–N2	121.3(4)	C3–C2–C1	121.2(4)
O1–C13–C6	122.9(3)	C29–C30–C31	120.3(4)
N2–C13–C6	115.8(4)	C9–C8–C7	119.9(5)
C25–C20–P1	121.7(3)	C22–C21–C20	120.7(5)
C25–C20–C21	118.2(4)	C5–C4–C3	118.0(5)
C21–C20–P1	120.2(4)	C2–C3–C4	121.5(5)
C1–C6–C13	120.6(4)	C23–C22–C21	120.3(4)
C5–C6–C13	120.5(3)	C12–C11–C10	120.4(5)
C5–C6–C1	118.9(4)	C10–C9–C8	121.4(5)
C12–C7–N1	118.1(4)	C9–C10–C11	118.8(5)
C12–C7–C8	118.4(4)		

CONCLUSION

The synthesis and detailed structure elucidation of *N*-[2-(diphenylphosphorothioyl)phenyl]-2-(phenylamino)benzamide (**5**) are reported. This compound can serve as both a phosphinotioate and after P-deprotection - as a phosphine ligand as well. The title compound opens further synthetic possibilities to 4-oxo-3,4-dihydroquinazolin-1-ium carbene precursors. The single crystal structure of *N*-(2-(diphenylphosphorothioyl)phenyl)-2-(phenylamino)benzamide (**5**) has been studied, giving insight into its capabilities as a bidentate ligand to accommodate metal atoms. Two different type of hydrogen-acceptor interactions in **5** have been observed as well.

Acknowledgements: Authors acknowledge the Research Fund of Sofia University (project 093/08.05.2014) for financial support, The Laboratory of Molecular Spectroscopy for Structural Analysis, Faculty of Chemistry and Pharmacy, Sofia University St. Kliment Ohridsky and Prof. G. Gencheva.

Electronic Supplementary Data available here.

REFERENCES

1. C. Ansell, M. McPartlin, P. Tasker, M. Cooper, P. Duckworth, *Inorg. Chim. Acta*, **76**, L135 (1983).
2. M. K. Cooper, A. Downes, *J. Chem. Soc. Chem. Commun.*, 381 (1981).

3. V. Yu. Aleksenko, E. V. Sharova, O. I. Artyushin, D. V. Aleksanyan, Z. S. Klemenkova, Yu. V. Nelyubina, P. V. Petrovskii, V. A. Kozlov, I. L. Odinets, *Polyhedron*, **51**, 168 (2013).
4. V. A. Kozlov, V. Yu. Aleksenko, D. V. Aleksanyan, E. V. Sharova, O. I. Artyushin, I. L. Odinets, *Phosphorus, Sulfur Silicon Relat. Elem.*, **188**, 79 (2013).
5. S. Baba, E. Negishi, *J. Am. Chem. Soc.*, **98**, 6729 (1976).
6. R. F. Heck, J. P. Nolley, *J. Org. Chem.*, **37**, 2320 (1972).
7. N. Miyaura, K. Yamada, A. Suzuki, *Tetrahedron Lett.*, **20**, 3437 (1979).
8. G. M. Sheldrick, *SADABS 2.0*, University of Göttingen, Göttingen, Germany, 2000.
9. G. M. Sheldrick, *Acta Cryst. A*, **64**, 112 (2008).
10. O. V. Dolomanov, L. J. Bourhis, R. J. Gildea, J. A. Howard, H. Puschmann, *J. Appl. Cryst.*, **42**, 339 (2009).
11. F. Pin, S. Comesse, A. Daich, *Tetrahedron*, **67**, 5564 (2011).
12. M. K. Cooper, J. M. Downes, P. A. Duckworth, *Inorg. Synth.*, **25**, 129 (1989).
13. M. K. Cooper, J. M. Downes, P. A. Duckworth, E. R. Tiekink, *Aust. J. Chem.*, **45**, 595 (1992).
14. X. Dai, A. Wong, S. C. Virgil, *J. Org. Chem.*, **63**, 2597 (1998).
15. P. W. Coddind, K. A. Kerr, *Acta Cryst. B*, **34**, 3785 (1978).

СИНТЕЗ И СТРУКТУРНО ОХАРАКТЕРИЗИРАНЕ НА N-(2-(ДИФЕНИЛФОСФОРОТИОИЛ)ФЕНИЛ)-2-(ФЕНИЛАМИНО)БЕНЗАМИД

Р. Хр. Ляпчев¹, М. Г. Дангалов², Н. Г. Василев², П. Й. Петров^{1*}

¹ Катедра Органична химия и фармакогнозия, Факултет по химия и фармация, Софийски университет „Св. Климент Охридски“, бул. „Джеймс Баучер“ 1, София 1164, България

² Институт по Органична Химия с Център по Фитохимия, Българска Академия на Науките, ул. Акад. Г. Бончев, бл. 9, 1113 София, България

Постъпила на 06 март 2017 г.; Коригирана на 29 март 2017 г.

(Резюме)

N-(2-(дифенилфосфоротиоил)фенил)-2-(фениламино)бензамид, с перспективно приложение като лиганд в органометалния хомогенен катализ беше получен чрез синтез в няколко стъпки от изходно вещество N-фенилантрапилова киселина. Неговата структура беше изучена чрез ЯМР-спектроскопия и рентгеноструктурен анализ.

Synthesis of bioactive aminoacid derivatives of *trans*-5-aminomethyl-1-benzyl-6-phenylpiperidin-2-one

T. I. Baramov^{1,3}, N. T. Burdzhiev^{1*}, B. T. Pandova², V. Z. Todorova², S. G. Yanev², E. R. Stanoeva¹, C. D. Chanev¹

¹ St. Kliment Ohridski University of Sofia, Faculty of Chemistry and Pharmacy, 1, James Bourchier avenue; 1164 Sofia, Bulgaria

² Bulgarian Academy of Sciences, Institute of Neurobiology, Department of Drug Toxicology, Acad. G. Bonchev Str., Bl. 23, 1113 Sofia, Bulgaria

³ present address: Bachem AG, Hauptstrasse 144, 4416 Bubendorf, Switzerland

Received February 28, 2017; Revised March 24, 2017

Dedicated to Acad. Bogdan Kurtev on the occasion of his 100th birth anniversary

trans-5-Aminomethyl-1-benzyl-6-phenylpiperidin-2-one (**2**) was prepared in high yield *via* Mitsunobu methodology and acylated by means of *N*-protected α -amino acids glycine, L-tryptophan, L-phenylalanine and L-alanine to give new piperidinones with a peptide bond in the side chain to the piperidinone cycle. *N*-Deprotection was carried out and the side chain of the tryptophan derivative **4** was elongated to yield products containing two peptide bonds in it. Mass spectra (EI and/or ESI) of most of the derivatives were taken and some fragmentation patterns were suggested. Tryptophan derivatives **3-5** have been described in a previous paper to possess antihistamine activity. In the present study four peptide derivatives have been tested for ACE inhibitory activity and compounds **13a,b** and **14** have shown a weak ACE inhibitory activity.

Key words: piperidinones; pseudopeptides; ACE inhibition; *N*-deprotection; mass spectrometry

INTRODUCTION

Piperidin-2-ones (δ -lactams) containing amino groups as substituents are intensively investigated because they are regarded as constrained surrogates of dipeptides and are peptidomimetics of the β -turn of the polypeptide chain [1–6]. These peptidomimetics, the so-called Freidinger lactams [7] have shown numerous biological activities, such as ACE- [3] and renin- inhibiting activity [8], serine protease inhibition [9] *etc.* Thus, aminolactams attracted the intensive investigations of different research groups, aiming at both new applications of the compounds as pharmaceuticals and synthons for further synthetic elaboration [10]. 2-Aryl-5-oxopiperidine-3-carboxylic acids and their derivatives have shown antihistaminic and analgesic activity [11, 12]; 2-aryl-3-amino-piperidines such as CP-99,994 (**1**) have shown antagonism against the human neurokinin undecapeptide Substance P (SP) and exhibit effective antiemetic activity [13]. As a neuromediator, SP is responsible for a variety of disorders such as migraine, rheumatoid arthritis and pain [12, 13]. Having in mind the diverse biological activities of amino piperidines [1], we started a

synthetic program on transformation of the carboxylic group of the easily accessible *trans*-1-benzyl-2-phenyl-5-oxopiperidine-3-carboxylic acid **1** [11, 12, 14–17] into amino group [15]. Thus, we published recently on the preparation of piperidines containing a peptide bond in the side chain, *i.e.* *trans*-5-(*N*-acylated amino)-2-oxopiperidines [15]. The present paper is a part of our on-going research program on the introduction of amino substituent onto a lactam ring and it deals with the synthesis of (\pm)-*trans*-5-aminomethyl-1-benzyl-6-phenylpiperidin-2-one **2** from the acid **1**. Amino compound **2** and similarly substituted derivatives can be regarded as reversed analogs of GABA amide [14, 18]. Our purpose is to use the amino group of 5-aminomethyl compound **2** for the introduction of a peptide bond and to obtain new building blocks for biologically active molecules of pseudopeptide type. The α -amino acid residues of glycine, L-tryptophan, L-phenylalanine and L-alanine were selected to be introduced because they are components of the structure of SP. The preliminary biological tests of the newly prepared tryptophan containing pseudopeptide derivatives **3**, **4** and **5** have shown that the compounds exhibit antihistamine activity [17], which is in agreement with literature data [19]. (Fig. 1) From the other

* To whom all correspondence should be sent:
E-mail: nburdzhiev@chem.uni-sofia.bg

hand, other aminopiperidinones, incorporating residues of alanine and glycine [3], or phenylalanine [8] have shown moderate to strong ACE inhibiting activity. Below the synthesis and structural characteristics of amine **2**, its peptide derivatives **3-5** as well as of a series of their peptide analogs **8-15** are described. Some of the peptides were tested for ACE inhibitory activity.

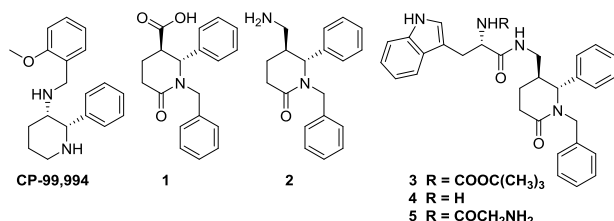


Fig. 1. CP-99,994 and compounds **1-5**; only one diastereomer of compounds **1-5** is shown for the sake of shortness.

EXPERIMENTAL

Synthesis

Melting points were taken on a microhot stage apparatus Boetius PHMK 05 and are uncorrected. IR spectra were recorded on a Specord 75 instrument. ¹H NMR spectra were obtained on Bruker Avance DRX-250 (250.13 MHz) and Bruker Avance III HD (500.13 MHz) spectrometers. The chemical shifts are given in parts per million (ppm; in δ-scale) relative to tetramethylsilane as internal standard. Electron impact mass spectra (EI-MS) were recorded by flow injection of acetonitrile solution into an Agilent 6890 gas chromatograph attached to a mass detector Agilent 5973 at 70 eV. ESI-MS spectra were measured on TCQ Quantum Access MAX, capillary temperature 270 °C and N₂ as a sheath gas. HPLC was performed using apparatus Waters 3000 HPLC with integrator HP 3598, column RP C18 Waters and detector RI. The microanalyses were done with Vario EL III Elemental analyzer in the Faculty of Chemistry and Pharmacy. Thin layer chromatography (TLC) was performed on Merck 1.05554 silica gel 60 F₂₅₄ aluminum plates. Chromatographic filtration and column chromatography were carried out using Fluka 100 silica gel (0.060–0.200 mm), Riedel-de Haën Kieselgel S (0.063–0.200 mm) or Macherey-Nagel Kieselgel 60 (0.063–0.200 mm).

Preparation of (±)-*trans*-2-(1-benzyl-6-oxo-2-phenyl-piperidine-3-yl-methyl)-2H-isoindol-1,3-dione (**7**)

To a stirred solution of alcohol **6** [14] (0.886 g, 3.00 mmol), triphenylphosphine (0.984 g, 3.75 mmol) and phthalimide (0.463 g, 3.15 mmol) in 11.4 mL dry THF under argon, a 40% solution of diethylazodicarboxylate (DEAD) in toluene (1.65 mL, 3.60 mmol) was added dropwise at room temperature. The reaction mixture was irradiated in an ultrasonic bath for 90 min. The completion of the reaction was determined by TLC (hexane/ethyl acetate = 1:1). The solvent was removed *in vacuo* and ethyl acetate was added to the oily residue. The crystals of diethyl 1,2-hydrazinodicarboxylate were filtered off. From the filtrate after column chromatography (hexane/ethyl acetate = 1:1) and recrystallization from ethyl acetate white solid was obtained (75%). Mp 152–154 °C. IR (Nujol): 1700 (CON); 1620 (CON) cm⁻¹. ¹H-NMR δ (250 MHz, CDCl₃): 1.39–1.56 (1H, m, H-4); 1.72–1.90 (1H, m, H-4); 2.36–2.50 (1H, m, H-3); 2.58 (1H, dt, *J* = 6.3, 18.2 Hz, H-5); 2.90 (1H, ddd, *J* = 6.3, 8.2, 18.2 Hz, H-5); 3.33 (1H, d, *J* = 14.7 Hz, NCH₂Ph); 3.45 (1H, dd, *J* = 4.9, 13.9 Hz, CH₂N); 3.74 (1H, dd, *J* = 9.7, 13.9 Hz, CH₂N); 4.27 (1H, d, *J* = 5.2 Hz, H-2); 5.60 (1H, d, *J* = 14.7 Hz, NCH₂Ph); 7.09–7.39 (10H, m, PhH); 7.65–7.82 (4H, m, ArH). EI-MS: *m/z* 424 (M⁺, 14), 333 (31), 186 (42), 172 (26), 160 (65), 159 (78), 117 (22), 106 (82), 104 (24), 91 (100). Anal. Calcd for C₂₇H₂₄N₂O₃ (424.50): C 76.40%, H 5.70%; found C 76.11%, H 5.99%.

Preparation of (±)-*trans*-5-aminomethyl-1-benzyl-6-phenyl-piperidine-2-one (**2**)

A mixture of phthalimide **7** (1.050 g, 2.5 mmol) and 40% aqueous solution of methylamine (28.9 mL, 10.400 g, 33.5 mmol) was refluxed until clear solution was formed (2 h). The completion of the reaction was determined by TLC (hexane/ethyl acetate = 1:1). After cooling down to room temperature, the solution was extracted with dichloromethane (3 x 20 mL). The combined organic layers were dried (Na₂SO₄) and the solvent was removed *in vacuo* to yield the amine **2** as yellowish oil (85%). IR (CHCl₃): 3350 (NH₂); 3250 (NH₂); 1620 (CON) cm⁻¹. ¹H-NMR δ (250 MHz, CDCl₃): 1.33 (2H, br. s, NH₂); 1.46–1.69 (1H, m, H-4); 1.73–1.99 (2H, m, H-4, H-5); 2.50–2.66 (4H, m, H-3, CH₂N); 3.29 (1H, d, *J* = 14.6 Hz, NCH₂Ph); 4.31 (1H, d, *J* = 4.5 Hz, H-6); 5.63 (1H, d, *J* = 14.6 Hz, NCH₂Ph); 7.12–7.42 (10H, m, PhH). EI-MS: *m/z* 294 (M⁺, 7); 277 (42); 276 (26); 264 (13); 249 (17); 186 (13); 174 (66); 117 (15); 106 (60); 91 (100). Anal. Calcd for C₁₉H₂₂N₂O (294.40): C

77.52%, H 7.53%, N 9.52%; found: C 77.60%, H 7.54%, N 9.49%.

Amino acid derivatives of (±)-trans-5-aminomethyl-1-benzyl-6-phenyl-piperidine-2-one **3a,b**, **8a,b**, **13a,b**, **10**, **11**, **15a,b** (General procedure)

To a magnetically stirred solution of amine **2** (0.147 g, 0.5 mmol) and corresponding *N*-protected L-amino acid (0.5 mmol) in dichloromethane (2 mL) cooled to -20 °C, a solution of diisopropylcarbodiimide (DIC, 0.65 mmol) in dichloromethane (2 mL) was added dropwise. The mixture was stirred for 2 h at -10 °C and then 12 h at room temperature. The precipitated urea derivative was filtered and discarded. The filtrate was evaporated under reduced pressure and the resulting oil was dissolved in dichloromethane (10 mL). The solution was successively washed with 10% HCl, water, 10% Na₂CO₃ and brine. Organic layer was dried (Na₂SO₄) and the solvent was removed in vacuo. The residue was purified by means of column chromatography. The following compounds were prepared in this way:

tert-Butyl (*S*)-1-(((2*R*,3*S* and 2*R*,3*S*)-1-benzyl-6-oxo-2-phenylpiperidin-3-yl)methyl)amino)-3-(1*H*-indol-3-yl)-1-oxopropan-2-ylcarbamate (**3a,b**): From amine **2** and *N*-Boc-L-tryptophan. Column chromatography (hexane/ethyl acetate/25% aq. NH₃ = 1:2:0.015) and a subsequent recrystallization from ethyl acetate yielded a white solid of 1:1 mixture of 2*S*,3*R*, α *S*- and 2*R*,3*S*, α *S*-**3a,b** (73%). Mp 138-140 °C. IR (Nujol): 3200-3400 (NH); 1730 (COOC(CH₃)₃); 1680 (CON); 1620 (CON) cm⁻¹. ¹H-NMR δ (250 MHz, CDCl₃): 1.41 (9H, s, COOC(CH₃)₃); 1.44 (9H, s, COOC(CH₃)₃); 1.50-1.60 (2H, m, H-4, H-4*); 1.75-2.00 (4H, m, H-3, H-3*, H-4, H-4*); 2.40-2.50 (4H, m, H-5, H-5*); 2.67-2.81 (2H, m, CH₂NH, CH₂*NH); 2.98-3.30 (8H, m, NCH₂Ph, NCH₂*Ph, CH₂Ind, CH₂*Ind, CH₂NH, CH₂*NH); 3.97 (1H, d, *J* = 5.1 Hz, H-2); 4.02 (1H, d, *J* = 4.9 Hz, H-2*); 4.18 (1H, dt, *J* = 5.8, 7.6 Hz, COCH); 4.29 (1H, dt, *J* = 5.7, 7.7 Hz, COCH*); 4.97 (2H, br.s, NHCO, NHCO*); 5.27 (1H, t, *J* = 6.0 Hz, NHCO); 5.38 (1H, t, *J* = 6.0 Hz, NHCO*); 5.55 (1H, d, *J* = 14.6 Hz, NCH₂Ph); 5.56 (1H, d, *J* = 14.6 Hz, NCH₂*Ph); 6.87-7.41 (28H, m, PhH, PhH*, *H*-ind, *H*-ind*); 7.60 (2H, d, *J* = 7.7 Hz, *H*-ind, *H*-ind*); 8.18 (2H, br.s, NH-ind, NH-ind*). EI-MS: *m/z*: no M⁺; 355 (9); 341 (16); 281 (43); 253 (27); 207 (100); 191 (13); 147 (19); 135 (25); 91 (13); 73 (53). ESI-MS: *m/z* 603 (5, (M+Na)⁺); 582 (22); 581 (64, (M + H)⁺); 525 (15);

482 (29); 481 (100); 465 (6). Anal Calcd for C₃₅H₄₀N₄O₄ (580.73): C 72.39%; H 6.94%; N 9.65%; found: C 72.23%; H 7.04%; N 9.29%.

tert-Butyl (*S*)-1-(((2*S*,3*R* and 2*R*,3*S*)-1-benzyl-6-oxo-2-phenylpiperidin-3-yl)methyl)amino)-1-oxopropan-2-ylcarbamate (**8a,b**): From amine **2** and *N*-Boc-L-alanine. Column chromatography (hexane/ethyl acetate/25% aq. NH₃ = 1:1:0.015) yielded a pale yellow oil (72%) of 1:1 mixture of 2*S*,3*R*, α *S*- and 2*R*,3*S*, α *S*-**8a,b**. IR (CHCl₃): 3420 (NH); 3410 (NH); 1710 (COOC(CH₃)₃); 1680 (CON); 1630 (CON) cm⁻¹. ¹H-NMR δ (250 MHz, CDCl₃): 1.19 (6H, d, *J* = 7.1 Hz, CH₃, CH₃*); 1.42 (9H, s, COOC(CH₃)₃); 1.45 (9H, s, COOC(CH₃)₃*); 1.47-1.60 (2H, m, H-4, H-4*); 1.72-1.91 (2H, m, H-4, H-4*); 2.06-2.20 (2H, m, H-3, H-3*); 2.52-2.66 (4H, m, H-5, H-5*); 2.75-2.95 (2H, m, CH₂NH, CH₂NH*); 3.26 (1H, d, *J* = 14.4 Hz, NCH₂Ph); 3.27 (1H, d, *J* = 14.4 Hz, NCH₂Ph*); 3.31-3.45 (2H, m, CH₂NH, CH₂NH*); 3.79-3.96 (2H, m, COCH, COCH*); 4.16 (1H, d, *J* = 4.2 Hz, H-2); 4.20 (1H, d, *J* = 4.6 Hz, H-2*); 4.76 (1H, d, *J* = 7.0 Hz, NHCO); 4.86 (1H, d, *J* = 7.0 Hz, NHCO*); 5.63 (2H, br. s, CONH, CONH*); 5.68 (2H, d, *J* = 14.4 Hz, NCH₂Ph, NCH₂Ph*); 7.08-7.23 (8H, m, PhH, PhH*); 7.28-7.43 (12H, m, PhH, PhH*). Anal. Calcd for C₂₇H₃₅N₃O₄ (465.59): C 69.65%; H 7.58%; N 9.02%; found: C 70.00%, H 7.83%, N 8.54%.

(*S*)-*N*-(((2*S*,3*R* and 2*R*,3*S*)-1-benzyl-6-oxo-2-phenylpiperidin-3-yl)methyl)-3-phenyl-2-(2,2,2-trifluoro-acetamido)-propanamide (**9a,b**): From amine **2** and *N*-trifluoroacetyl-L-phenylalanine. Column chromatography (hexane/ethyl acetate = 1:3) yielded a pale yellow oil (69%) of 1:1 mixture of 2*S*,3*R*, α *S*- and 2*R*,3*S*, α *S*-**9a,b**. IR (CHCl₃): 3410 (NH); 3400 (NH); 1720 (COOC(CH₃)₃); 1680 (CON); 1620 (CON) cm⁻¹. ¹H-NMR δ (500 MHz, CDCl₃): 1.27-1.36 (2H, m, H-4, H-4*); 1.62-1.73 (2H, m, H-4, H-4*); 1.85-1.93 (1H, m, H-3); 2.00-2.08 (1H, m, H-3*); 2.45-2.58 (4H, m, H-5, H-5*); 2.65-2.72 (1H, m, CH₂NH); 2.77-2.84 (1H, m, CH₂NH*); 2.86-2.95 (2H, m, CH₂Ph, CH₂Ph*); 2.96-3.04 (2H, m, CH₂Ph, CH₂Ph*); 3.18-3.25 (3H, m, CH₂NH, NCHPh, NCHPh*); 3.29 (1H, dt, *J* = 7.0, 13.9 Hz, CH₂NH*); 3.99 (1H, d, *J* = 4.8 Hz, H-2); 4.11 (1H, d, *J* = 4.2 Hz, H-2*); 4.15 (1H, dt, *J* = 5.8, 8.2 Hz, COCH); 4.30 (1H, dt, *J* = 5.8, 8.2 Hz, COCH*); 4.63 (1H, t, *J* = 6.0 Hz, CH₂NH); 4.88 (t, 1H, *J* = 6.0 Hz, CH₂NH*); 5.65 (1H, d, *J* = 14.3 Hz, NCHPh); 5.68 (1H, d, *J* = 14.3 Hz, NCHPh*); 7.00-7.20 (15H, m, NHCOCF₃, NHCOCF₃*, PhH, PhH*); 7.27-7.40 (17H, m, PhH, PhH*). EI-MS: *m/z* 537 (M⁺, 6); 264 (12); 187 (11); 186 (83); 172

(40); 159 (15); 117 (18); 106 (75); 103 (14); 91 (100). Anal. Calcd for $C_{30}H_{30}F_3N_3O_3$ (537.58): C 67.03%, H 5.62%, N 7.82%; found: C 67.02%, H 5.82%, N 8.08%.

Benzyl 2-(((±)-trans-1-benzyl-6-oxo-2-phenylpiperidin-3-yl)methyl)amino)-2-oxoethylcarbamate (10) From amine **2** and *Z*-glycine. Column chromatography purification (ethyl acetate) yielded **10** as a colourless oil (66%). IR ($CHCl_3$): 3420(NH); 3410 (NH); 1720 ($COOCH_2Ph$); 1680 (CON); 1630 (CON) cm^{-1} . 1H -NMR δ (250 MHz, $CDCl_3$): 1.40-1.55 (1H, m, H-4); 1.70-1.88 (1H, m, H-4); 2.00-2.20 (1H, m, H-3); 2.46-2.68 (2H, m, H-5); 2.75-2.95 (1H, m, CH_2NH); 3.24 (1H, d, $J = 14.5$ Hz, NCH_2Ph); 3.29-3.44 (1H, m, CH_2NH); 3.61 (2H, d, $J = 5.6$ Hz, CH_2CO); 4.16 (1H, d, $J = 4.0$ Hz, H-2); 5.11 (2H, s, OCH_2Ph); 5.32 (1H, t, $J = 5.6$ Hz, $NHCO$); 5.56 (1H, br.s, CH_2NH); 5.66 (1H, d, $J = 14.5$ Hz, NCH_2Ph); 7.07-7.45 (15H, m, PhH). EI-MS: m/z No M^+ ; 377 (12); 286 (23); 186 (42); 172 (51); 159 (49); 129 (15); 117 (19); 115 (17); 106 (87); 91 (100). Anal. Calcd for $C_{29}H_{31}N_3O_4$ (485.58): C 71.73%, H 6.43%, N 8.65%; found: C 72.03%, H 6.80, N 8.45%.

tert-Butyl (2-(((±)-trans-1-benzyl-6-oxo-2-phenylpiperidin-3-yl)methyl)amino)-2-oxoethyl carbamate (11): From amine **2** and *N*-Boc-glycine. Column chromatography (hexane/ethyl acetate/25% aq. $NH_3 = 1:2:0.015$) yielded **11** as a pale yellow oil (83%). IR (Nujol): 3200-3400 (NH); 1710 ($COOC(CH_3)_3$); 1660 (CON) cm^{-1} . 1H -NMR (250 MHz, $CDCl_3$): δ 1.49 (9H, s, $COOC(CH_3)_3$); 1.46-1.60 (1H, m, H-4); 1.77-1.91 (1H, m, H-4); 2.07-2.20 (1H, m, H-3); 2.53-2.66 (2H, m, H-5); 2.80-2.95 (1H, m, CH_2NH); 3.26 (1H, d, $J = 14.4$ Hz, NCH_2Ph); 3.38 (1H, td, $J = 6.9$ Hz, $J = 13.5$ Hz, CH_2NH); 3.56 (2H, d, $J = 5.8$ Hz, CH_2CO), 4.17 (1H, d, $J = 4.3$ Hz, H-2); 4.96 (1H, br.s, $CONH$); 5.55 (1H, t, $J = 5.8$ Hz, $NHCO$); 5.68 (1H, d, $J = 14.4$ Hz, NCH_2Ph); 7.10-7.23 (4H, m, PhH); 7.26-7.43 (6H, m, PhH). EI-MS: m/z No M^+ ; 377 (11); 286 (19); 186 (42); 172 (47); 159 (41); 129 (14); 117 (17); 115 (16); 106 (80); 91 (100). Anal. Calcd for $C_{26}H_{33}N_3O_4$ (451.57): C 69.16%, H 7.37%, N 9.31%; found: C 69.12%, H 7.32%, N 9.14%.

tert-Butyl (2-(((S)-1-(((2S,3R and 2R,3S)-1-benzyl-6-oxo-2-phenylpiperidin-3-yl)methyl)amino)-3-(1H-indol-3-yl)-1-oxopropan-2-yl)amino)-2-oxoethyl)carbamate (15a,b): From **4a,b** and *N*-Boc-glycine. Column chromatography purification (hexane/ethyl acetate/25% $NH_3 = 1:2:0.015$) afforded **15a,b** as uncrystallizable oil of 1:1 mixture of *2S,3R,αS*- and *2R,3S,αS*-**15a,b** (73%). IR (Nujol): 3150-3500(NH); 1660

($COOC(CH_3)_3$); 1640 (CON); 1630 (CON); 1620 (CON) cm^{-1} . 1H -NMR δ (250 MHz, $CDCl_3$): 1.30 (18H, s, $C(CH_3)_3$, $C(CH_3)_3^*$); 1.40-1.62 (2H, m, H-4, H-4*); 1.70-1.96 (4H, m, H-3, H-3*, H-4, H-4*); 2.30-2.63 (4H, m, H-5, H-5*); 2.72-2.97 (2H, m, CH_2NH , CH_2NH^*); 3.00-3.18 (4H, m, CH_2 -Ind, CH_2 -Ind*); 3.20-3.37 (4H, m, NCH_2Ph , NCH_2Ph^* , CH_2NH , CH_2NH^*); 3.60-3.72 (4H, m, CH_2CO , CH_2CO^*); 3.97 (1H, d, $J = 5.4$ Hz, H-2); 4.05 (1H, d, $J = 4.6$ Hz, H-2*); 4.49-4.67 (2H, m, $COCH$, $COCH^*$); 5.14 (2H, dd, $J = 5.7$ Hz, $CONH$, $CONH^*$); 5.50 (1H, d, $J = 14.7$ Hz, NCH_2Ph); 5.53 (1H, d, $J = 14.7$ Hz, NCH_2Ph^*); 5.95-6.17 (2H, m, $NHCO$, $NHCO^*$); 6.71 (2H, t, $J = 8.6$ Hz, $NHCO$, $NHCO^*$); 6.90 (2H, s, *H*-Ind, *H*-Ind*); 6.98-7.38 (26H, m, PhH , PhH^* , *H*-Ind, *H*-Ind*); 7.58 (2H, d, $J = 7.7$ Hz, *H*-Ind, *H*-Ind*); 8.38 (1H, s, *NH*-Ind); 8.42 (1H, s, *NH*-Ind*). ESI-MS: m/z 660 (40, $(M+Na)^+$); 638 (7, $(M+H)^+$); 425 (100); 403 (43). Anal. Calcd for $C_{37}H_{43}N_5O_5$ (637.79): C 69.68%, H 6.80%, N 10.98%; found: C 69.29%; H 6.81%, N 11.05.

N-Boc-deprotection of the amides to **4a,b**; **5a,b**, **12a,b** and **14** (General procedure)

A solution of *N*-Boc-protected amide **3a,b**; **8a,b**; **11**; **15a,b** (1 mmol) and trifluoroacetic acid (1.07 mL, 14 mmol) was irradiated in an ultrasonic bath for 15 min. The completion of the reaction was determined by TLC. The reaction mixture was diluted with dichloromethane and the resulting solution was washed with 10% NaOH (2 x 5 mL). The organic layer was dried (Na_2SO_4) and the crude material was purified by column chromatography. The following compounds were prepared in this way:

(*S*)-2-amino-*N*-(((2*S*,3*R* and 2*R*,3*S*)-1-benzyl-6-oxo-2-phenylpiperidin-3-yl)methyl)-3-(1*H*-indol-3-yl)propanamide (**4a,b**): From amide **3a,b**. Column chromatography purification (hexane/isopropanol = 3.5:1) gave a pale yellow oil (78%) of 1:1 mixture of *2S,3R,αS*- and *2R,3S,αS*-**4a,b**. IR (Nujol): 3150-3430 (NH_2 , NH); 1630 (CON); 1620 (CON) cm^{-1} . 1H -NMR δ (250 MHz, $CDCl_3$): 1.35-1.55 (2H, m, H-4, H-4*); 1.66-1.84 (2H, m, H-4, H-4*); 1.94-2.24 (6H, m, NH_2 , NH_2^* , H-3, H-3*); 2.44-2.68 (4H, m, H-5, H-5*); 2.73-2.90 (2H, m, CH_2 -Ind, CH_2 -Ind*); 2.91-3.03 (2H, m, CH_2NH , CH_2NH^*); 3.18-3.40 (6H, m, NCH_2Ph , NCH_2Ph^* , CH_2 -Ind, CH_2 -Ind*, CH_2NH , CH_2NH^*); 3.54-3.64 (2H, m, $COCH$, $COCH^*$); 4.10 (1H, d, $J = 4.5$ Hz, H-2); 4.11 (1H, d, $J = 4.7$ Hz, H-2*); 5.60 (1H, d, $J =$

14.7 Hz, NCH₂Ph); 5.61 (1H, d, *J* = 14.7 Hz, NCH₂Ph*); 6.95-7.42 (30H, m, PhH, PhH*, H-ind, H-ind*, NHCO, NHCO*); 7.62 (1H, d, *J* = 7.8 Hz, H-ind); 7.63 (1H, d, *J* = 7.8 Hz, H-ind*); 8.24 (1H, br.s, NH-ind), 8.28 (1H, br.s, NH-ind*). ESI-MS: m/z 503 (5, (M+Na)⁺); 482 (27); 481 (100, (M+H)⁺). Anal. Calcd for C₃₀H₃₂N₄O₂ (480.61): C 74.97%; H 6.71%; N 11.66%; found: C 74.95%; H 6.90%; N 11.48%.

(*S*)-2-(2-aminoacetyl-amino)-*N*-[[(2*S*,3*R* and 2*R*,3*S*)-1-benzyl-6-oxo-2-phenylpiperidin-3-yl)methyl]-3-(1*H*-indol-3-yl)propanamide (**5a,b**): From amide **15a,b**. Column chromatography purification (hexane/isopropanol/ 25% aq. NH₃ = 1:1:0.02) gave a pale yellow oil (64%) of 1:1 mixture of 2*S*,3*R*, α *S*- and 2*R*,3*S*, α *S*-**5a,b**. IR (Nujol): 3100-3450(NH); 1640 (CON); 1620 (CON) cm⁻¹. ¹H-NMR δ (250 MHz, CDCl₃): 1.20-1.48 (2H, m, H-4, H-4*); 1.44-1.76 (10H, m, H-4, H-4*, NH₂, NH₂*, CH₂Ind, CH₂Ind*); 1.77-1.95 (2H, br. s, H-3, H-3*); 2.35-2.58 (4H, m, H-5, H-5*); 2.74-2.93 (2H, m, CH₂NH, CH₂NH*); 3.00-3.35 (8H, m, NCH₂Ph, NCH₂Ph*, CH₂NH, CH₂NH*, CH₂CO, CH₂CO*); 3.98 (1H, d, *J* = 5.2 Hz, H-2); 4.03 (1H, d, *J* = 4.9 Hz, H-2*); 4.38-4.61 (2H, m, CHCO, CHCO*); 5.44 (1H, br. s, CONH); 5.54 (1H, d, *J* = 14.7 Hz, NCH₂Ph); 5.55 (1H, d, *J* = 14.7 Hz, NCH₂Ph*); 5.62 (1H, br. s, CONH*); 6.88-7.40 (28H, m, PhH, PhH*, H-Ind, H-Ind*); 7.59-7.77 (4H, CONH, CONH*, H-Ind, H-Ind*); 8.03 (2H, br. s, NH-Ind, NH-Ind*). ESI-MS: m/z 560 (20, (M+Na)⁺); 554 (21); 539 (42); 538 (100, (M+H)⁺); 443 (32); 279 (51). Anal. Calcd for C₃₂H₃₅N₅O₃ (537.67): C 71.49%; H 6.56%; N 13.03%; found: C 71.42%; H 6.90%; N 12.79%.

(*S*)-2-amino-*N*-[[(2*S*,3*R* and 2*R*,3*S*)-1-benzyl-6-oxo-2-phenylpiperidin-3-yl)methyl]propanamide (**12a,b**): From amide **8a,b**. Column chromatography purification (hexane/isopropanol/ 25% aq. NH₃ = 1:1:0.015) gave a pale yellow oil (78%) of 1:1 mixture of 2*S*,3*R*, α *S*- and 2*R*,3*S*, α *S*-**12a,b** was obtained. IR (CHCl₃): 3410 (NH₂); 3360 (NH); 3340(NH₂); 1660 (CON); 1620 (CON) cm⁻¹. ¹H-NMR δ (250 MHz, CDCl₃): 1.22 (3H, d, *J* = 6.9 Hz, CH₃); 1.24 (3H, d, *J* = 6.9 Hz, CH₃*); 1.46-1.63 (2H, m, H-4, H-4*); 1.75-1.92 (2H, m, H-4, H-4*); 2.00-2.20 (6H, m, H-3, H-3*, NH₂, NH₂*); 2.46-2.77 (4H, m, H-5, H-5*); 2.87-3.06 (2H, m, CH₂NH, CH₂NH*); 3.27 (2H, d, *J* = 14.6 Hz, NCH₂Ph, NCH₂Ph*); 3.32-3.48 (4H, m, CH₂NH, CH₂NH*, CHCO, CHCO*); 4.15 (1H, d, *J* = 4.8 Hz, H-2); 4.16 (1H, d, *J* = 4.7 Hz, H-2*); 5.63 (2H, d, *J* = 14.6 Hz, NCH₂Ph, NCH₂Ph*); 7.04-7.44 (22H, m, PhH, PhH*, NHCO, NHCO*). EI-MS:

m/z 365 (M⁺, 8); 322 (15); 264 (16); 196 (22); 187 (15); 186 (100); 174 (12); 117 (17); 106 (41); 91 (96). Anal. Calcd for C₂₂H₂₇N₃O₂ (365.47): C 72.30%; H 7.45%; N 11.50%; found: C 71.51%; H 7.50%; N 10.76%.

2-amino-*N*-[[(\pm)-trans-1-benzyl-6-oxo-2-phenylpiperidin-3-yl)methyl]acetamide (**14**): From amide **11**. Column chromatography purification (hexane/isopropanol/25% aq. NH₃ = 2:1:0.015) gave a pale yellow oil of **14** (91%). IR (neat): 3150-3550 (NH, NH₂); 1640 (CON); 1620 (CON) cm⁻¹. ¹H-NMR δ (250 MHz, CDCl₃): 1.45-1.65 (1H, m, H-4); 1.78-1.94 (1H, m, H-4); 1.96-2.20 (3H, m, H-3, NH₂); 2.50-2.77 (2H, m, H-5); 3.00 (1H, dt, *J* = 6.3 Hz, *J* = 13.9 Hz, CH₂NH); 3.19 (2H, s, CH₂CO); 3.30 (1H, d, *J* = 14.4 Hz, NCH₂Ph); 3.39 (1H, dt, *J* = 7.1 Hz, *J* = 13.9 Hz, CH₂NH); 4.17 (1H, d, *J* = 4.9 Hz, H-2); 5.64 (1H, d, *J* = 14.4 Hz, NCH₂Ph); 6.97 (1H, t, *J* = 6.3 Hz, NHCO); 7.07-7.44 (10H, m, PhH). EI-MS: m/z 351 (M⁺, 8); 264 (12); 187 (14); 186 (100); 174 (8); 172 (12); 117 (11); 115 (8); 106 (38); 91 (83). Anal. Calcd for C₂₁H₂₅N₃O₂ (351.45): C 71.77%; H 7.17%; N 11.96%; found: C 71.39%; H 7.16%; N 11.64%.

Preparation of (S)-2-amino-N-([(2S,3R and 2R,3S)-1-benzyl-6-oxo-2-phenylpiperidin-3-yl)methyl]-3-phenylpropanamide (13a,b)

A solution of amide **9a,b** (0.100 g, 0.2 mmol), potassium hydroxide (0.112 g, 1.8 mmol), water (1 mL) and methanol (2 mL) was stirred at room temperature for 24 h, then methanol was removed under reduced pressure. The aqueous residue was extracted with dichloromethane and the combined organic layers were dried (Na₂SO₄). Column chromatography (hexane/ethyl acetate/25% aq. NH₃ = 3:1:0.02) yielded a pale yellow oil (86%) as a 1:1 mixture of 2*S*,3*R*, α *S*- and 2*R*,3*S*, α *S*-**13a,b**. IR (CHCl₃): 3150-3450 (NH, NH₂); 1640 (CON); 1620 (CON) cm⁻¹. ¹H-NMR δ (500 MHz, CDCl₃): 1.40-1.51 (2H, m, H-4, H-4*); 1.67-1.81 (2H, m, H-4, H-4*); 1.99-2.11 (2H, m, H-3, H-3*); 2.46-2.58 (2H, m, H-5, H-5*); 2.59-2.68 (2H, m, H-5, H-5*); 2.68-2.77 (2H, m, CH₂Ph, CH₂Ph*); 2.90-3.02 (2H, m, CH₂NH, CH₂NH*); 3.08-3.18 (2H, m, CH₂Ph, CH₂Ph*); 3.22-3.37 (4H, m, CH₂NH, CH₂NH*, NCHPh, NCHPh*), 3.60-3.77 (2H, m, COCH, COCH*); 4.09 (1H, d, *J* = 5.1 Hz, H-2); 4.11 (1H, d, *J* = 4.8 Hz, H-2*); 5.55 (1H, d, NCHPh, *J* = 14.7 Hz); 5.56 (1H, d, NCHPh*, *J* = 14.8 Hz); 7.06-7.40 (32H, m, PhH, PhH*, NHCO, NHCO*). EI-MS: m/z 441 (M⁺, 6); 350 (18); 322 (13); 264 (12); 196 (17); 187 (11); 186 (66); 120 (89); 106 (30); 91

(100). Anal. Calcd for $C_{28}H_{31}N_3O_2$ (441,57): C 76.16%, H 7.08%, N 9.52%; found: C 75.61%, H 7.08%, N 9.38%

Angiotensin-converting enzyme activity assay

Rabbit serum aliquot was incubated in buffered medium with the ACE substrate analogue Hippuryl-Histidyl-Leucine (HHL). Hippuric acid (HA) as a product of the reaction was extracted with ethyl acetate and then measured by HPLC in isocratic mode at 228 nm. The HPLC was carried out on a Polar-RP 80Å Synergi column (150x4,6 mm, 4 μm, Phenomenex) at flow rate of 1.4 mL/min and mobile phase buffer (0.02 M ammonium acetate adjusted to pH 4.3 with acetic acid)/methanol (95/5). The amount of hippuric acid formed reflects the ACE activity.

Solutions of the piperidinone derivatives **10**, **12a,b**, **13a,b** and **14** in 0.1 M acetic acid were tested for the inhibitory potency in comparison to the inhibitors of ACE Lisinopril and Quinaprilat. The IC_{50} values were determined by non-linear regression analysis of enzyme activity/inhibitor concentrations curves using software package GraphPad Prism 5.0.

RESULTS AND DISCUSSION

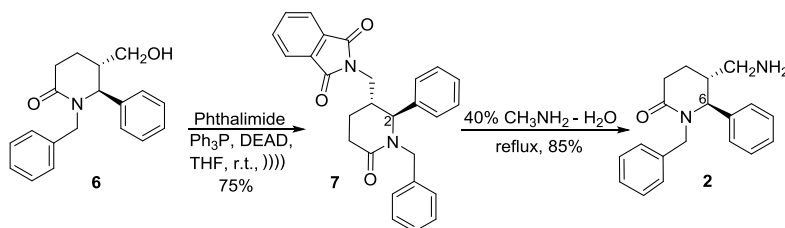
(±)-*trans*-5-Aminomethyl-1-benzyl-6-phenylpiperidine-2-one (**2**) was prepared from the previously synthesized by us alcohol **6** [14] obtained in two steps from (±)-*trans*-1-benzyl-6-oxo-2-phenylpiperidine-3-carboxylic acid **1** [11, 14]. The replacement of the hydroxyl group in **6** for amino group in **2** includes the intermediate formation of phthalimido derivative **7** by means of Mitsunobu methodology [18], followed by cleavage of the phthalimido group (Scheme 1).

The treatment of the alcohol **6** by means of phthalimide in the presence of triphenylphosphine and diethyl azodicarboxylate (DEAD; Mitsunobu step) was carried out overnight at room temperature in analogy to a literature procedure [18]. Alternatively, it was shown that the sonication of the reaction mixture accelerated the reaction, which

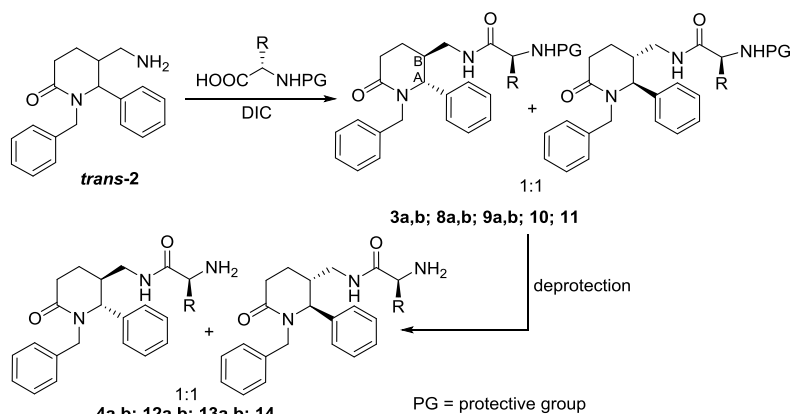
was completed within 1.5 hours to give the phthalimido derivative **7**. The latter compound was separated from the by-products by means of column chromatography and recrystallization in 75% yield. Several reagents were tested for the cleavage of the phthalimido group in **7**. The yields of amine **2** obtained after reflux of the phthalimide **7** in the presence either of ethylenediamine [18] or hydrazine hydrate [20] varied within a broad range in different runs. When **7** was refluxed in an aqueous ethanol solution of CH_3NH_2 [21] the obtained amine **2** tended to retain ethanol, which could not be removed. Best reproducible yield of **2** (85%) was obtained by reflux of phthalimide **7** in 40% aqueous solution of CH_3NH_2 , moreover the product of this reaction showed to be enough pure for the further transformations. This was important since amine **2** is highly polar oil and could not be purified by means of chromatography.

Trans relative configuration of phthalimide **7** and amine **2** was established by comparison of their 1H NMR spectra with the spectra of the starting alcohol **6** [14]. Taking into account the shift of the doublet signal of the proton next to cyclic nitrogen and its 3J , the spectra of compounds **2** and **7** showed similarity to the spectrum of **6**. The doublets of H-2, resp. H-6, in the spectra of **2** and **7** appear in the range of δ 4.27–4.31 ppm with 3J 4.5–5.2 Hz, similarly to the values previously reported [14]. Analogous data of 3J were recently published for *trans*-6-phenyl-5-hydroxypiperidine-2-one, for which the *trans* configuration was confirmed by means of X-ray diffraction analysis [22]. From the other hand, the transformations of the alcohol **6** to the phthalimide **7** and amine **2** do not affect the chiral carbon atoms. On this ground we accepted same *trans* configuration for the newly prepared compounds **2** and **7**. On Scheme 1 we present for shortness only one enantiomer of the racemic compounds **2**, **6** and **7**.

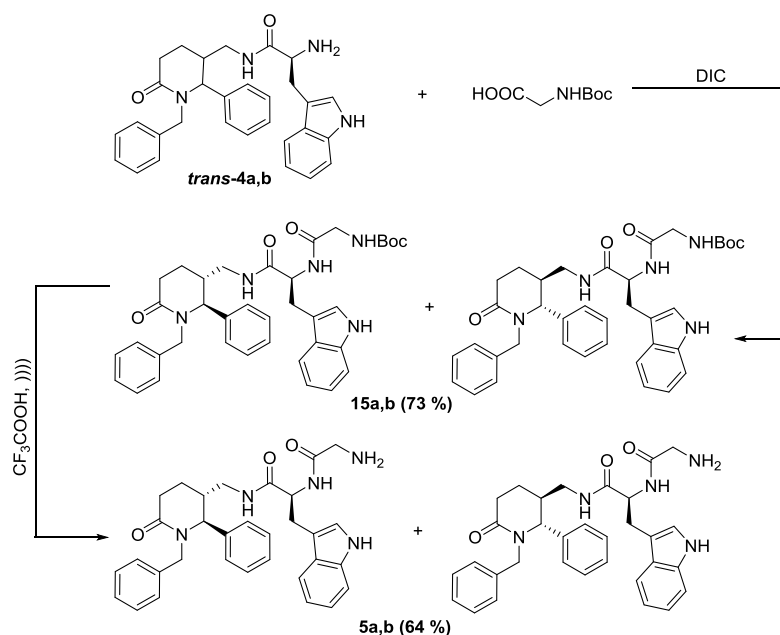
The aminomethyl derivative **2** was converted into the pseudodipeptides **3a,b**, **8a,b**, **9a,b**, **10** and **11** by reaction with the following *N*-protected α -amino acids: *N*-Boc-L-tryptophan, *N*-Boc-L-alanine, *N*-trifluoroacetyl-L-phenylalanine, *N*-Boc-



Scheme 1. Preparation of (±)-*trans*-5-aminomethyl-1-benzyl-6-phenylpiperidine-2-one (**2**) (one enantiomer is shown).



Scheme 2. Synthesis of pseudodipeptides.



Scheme 3. Preparation of pseudotripeptides **5a,b** and **15a,b**.

glycine and *Z*-glycine, resp., in the presence of diisopropylcarbodiimide (DIC) in 69–83% yields after column chromatography purification. (Table 1). *L*-Tryptophan derived *N*-Boc dipeptides **3a,b** were obtained as crystalline product. All the other pseudopeptide derivatives described throughout the paper were obtained as oily products. Gas chromatography analysis of the reaction products **3a,b**, **8a,b** and **9a,b** showed two peaks in 1:1 ratio. Similarly, ¹H NMR spectra of the compounds showed that they are 1:1 mixtures of diastereomers, which could not be separated by means of column chromatography. The diastereomers are designated as “a” and “b”.

The deprotection gave pseudodipeptides with free *N*-terminal group. *N*-Boc-protected pseudodipeptides **3a,b**; **8a,b** and **11** were deprotected by CF₃COOH under sonication [14] to

give pseudopeptides **4a,b**; **12a,b** and **14**, resp. (Scheme 2).

Table 1. Peptide derivatives **3**, **4**, **8–14**.

Compound (Yield, %)	R	PG
3a,b (73)	CH ₂ (Indol-3-yl)	Boc
4a,b (78)	CH ₂ (Indol-3-yl)	H
8a,b (72)	CH ₃	Boc
9a,b (69)	CH ₂ C ₆ H ₅	COCF ₃
10 (66)	H	Z
11 (83)	H	Boc
12a,b (78)	CH ₃	H
13a,b (86)	CH ₂ C ₆ H ₅	H
14 (91)	H	H

N-Trifluoroacetyl group in **9a,b** was cleaved by hydrolysis with potassium hydroxide in methanol-water at room temperature [21] to give pseudopeptide **13a,b**. Yields are given in Table 1.

The tryptophan derivative *trans*-**4a,b** was used for elongation of the peptide chain – it was *N*-acylated by means of *N*-Boc-glycine to give pseudotripeptide *trans*-**15a,b**. Further deprotection of the Boc group as above gave pseudotripeptide *trans*-**5a,b**. (Scheme 3).

Compounds **3**, **4**, **5**, **8**, **9**, **12**, **13** and **15** incorporating amino acid moieties were 1:1 mixtures of α -*S*, (\pm)-*trans*-diastereomers according to their ^1H NMR spectra. In spite of our efforts we could not separate the diastereomeric couples by means of column chromatography. This made difficult the description of ^1H NMR spectral data in the Experimental part, because the signals for the same protons in the different diastereomers are not shifted in one and the same direction. Similar problem was encountered in the course of synthesis of (\pm)-*trans*-5-*N*-acylamino-1-benzyl-6-phenylpiperidin-2-one derivatives published recently by us [15]. For this reason in the Experimental part the signals for the same protons with higher chemical shift are noted with “*” symbol, in analogy to our previous paper [15]. Peptide bond formation did not affect the chiral centers of the piperidinone cycle, as well as the one originating from the L-amino acid. ^1H NMR spectra of the compounds exhibit doublet signals for 2-H in the range of δ 3.97–4.20 ppm with $J_{\text{A,B}}$ 4.0–5.4 Hz. These data are in agreement with *trans* relative configuration of the substituents with respect to the piperidinone cycle, as it was already discussed above.

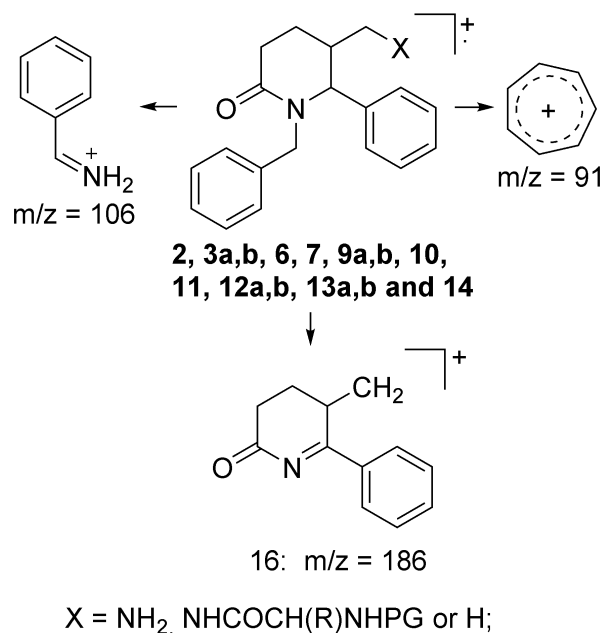
EI-mass spectra (EI-MS) of compounds **2**, **3a,b**, **6**, **7**, **9a,b**, **10**, **11**, **12a,b**, **13a,b**, and **14** were taken. All compounds except for *Z* and Boc protected derivatives **3a,b**, **10** and **11**, showed M^+ with low intensity. The molecular ions of **3a,b**, **10** and **11** were not observed. The most typical fragmentation in EI-MS of the compounds studied was the formation of three fragments: tropylium ion (C_7H_7^+ $m/z = 91$), PhCHNH_2^+ ($m/z = 106$) as well as $m/z = 186$. The latter is probably a result of α -cleavage. [23] (Scheme 4) ESI mass spectra of compounds **3a,b**, **4a,b**, **5a,b** and **15a,b** allowed us to observe the molecular ions $(\text{M}+\text{H})^+$ and $(\text{M}+\text{Na})^+$.

Biological assay

The compounds tested for ACE inhibitory activity were **10**, **12a,b**, **13a,b** and **14**. The significantly modified method of Chiknas [24] was applied for ACE activity determination. Enzyme sources were rabbit serum and a purified enzyme [24]. As referent compounds two well-known inhibitors of ACE with wide therapeutic application

were used – Lisinopril (which does not metabolize and is excreted unchanged in the urine) and Quinaprilat (active metabolite of Quinapril).

Compounds **13a,b** with IC_{50} around 590 ng/ml and **14** with IC_{50} around 530 ng/ml showed a weak ACE inhibitory potency when compared with the inhibitors lisinopril or quinaprilat (with IC_{100} around 20 ng/ml).



Scheme 4. Most typical mass spectral fragmentations in EI-MS

CONCLUSION

A series of new piperidinones with a peptide bond in the side chain to the heterocycle was prepared *via* Mitsunobu methodology and subsequent acylation of the amine **2** by means of selected *N*-protected α -amino acids. Boc deprotection of tryptophan derivatives **3a,b** was carried out and a second peptide bond was introduced *via* protected glycine coupling. Mass spectra of most of the derivatives were taken and fragmentation patterns were suggested for the most abundant ions. The ACE inhibitory activity of four peptide derivatives has been assayed. Compounds **13a,b** and **14** have shown a weak ACE inhibitory activity.

Acknowledgements: The authors are grateful to the FP7 project BeyondEverest. The financial support of National Science Fund of Bulgaria at the Ministry of Education and Science (project TK-X-

1706/07 and project UNION, DO-02-82/2008) as well as of St. Kliment Ohridski University of Sofia (project 142/2006) is acknowledged.

REFERENCES

1. S. Källström, R. Leino, *Bioorg. Med. Chem.*, **16**, 601 (2008).
2. M. Fernandez, A. Diez, M. Rubiralta, E. Montenegro, N. Casamitjana, M. Kogan, E. Giralt, *J. Org. Chem.*, **67**, 7587 (2002).
3. P. Forns, M. Rubiralta, A. Diez, *Contribution to Science*, **2**, 63 (2001).
4. M. Ecija, A. Diez, M. Rubiralta, N. Casamitjana, *J. Org. Chem.*, **68**, 9541 (2003).
5. A. Trabocchi, F. Guarna, A. Guarna, *Curr. Org. Chem.*, **9**, 1127 (2005).
6. E. D. Thorsett, E. E. Harris, S. D. Aster, E. R. Peterson, J. P. Snyder, J. P. Springer, J. Hirschfirdel, E. W. Tristram, A. A. Patchett, E. H. Ulm, T. C. Vassil, *J. Med. Chem.*, **29**, 251 (1986).
7. R. Freidinger, D. Perlow, D. Veber, *J. Org. Chem.*, **47**, 104 (1982).
8. S. E. de Laszlo, B. L. Bush, J. J. Doyle, W. J. Greenlee, D. J. Hangauer, T. A. Halgren, R. J. Lynch, T. W. Schorn, P. K. S. Siegl, *J. Med. Chem.*, **35**, 833 (1992).
9. A. Perdih, D. Kikelj, *Curr. Med. Chem.*, **13**, 1525 (2006).
10. A. Nadin, *Contemp. Org. Synth.*, **4**, 387 (1997).
11. B. Shetty, A. McFadden, P. Hofer, U.S. Patent 4476311 (1984); *Chem. Abstr.*, **102**, 78717h (1985).
12. M. Baroudi, J. Robert, C. Luu-Duc, *Heterocyclic Commun.*, **2**, 255 (1996).
13. P. Datar, S. Srivastava, E. Cautinho, G. Govil, *Curr. Top. Med. Chem.*, **4**, 75 (2004).
14. N. Burdzhiev, E. Stanoeva, *Tetrahedron*, **62**, 8318 (2006).
15. N. Burdzhiev, E. Stanoeva, *C. R. Chimie*, **13**, 1433 (2010).
16. T. Chan, T. M. Kwong, R. Kwok, X. Chen, K. Shi, *J. Inclus. Phenom.*, **6**, 507 (1988).
17. P. Mateeva, N. Burdzhiev, E. Stanoeva, T. Baramov, R. Zamfirova, *Compt. Rend. Bulg. Acad. Sci.*, **63**, 1675 (2010).
18. B. Bonnaud, A. Carlessi, D. Bigg, *J. Heterocycl. Chem.*, **30**, 257 (1993).
19. G. Caliendo, F. Fiorino, P. Grieco, E. Perissutti, V. Santagada, *Il Farmaco*, **52**, 589 (1997).
20. S. K. Davidsen, G. W. Phillips, S. F. Martin, *Org. Synth. Coll. Vol. VIII*, p. 451.
21. T. W. Greene, P. G. Wuts, *Protective Groups in Organic Synthesis*. 2nd Ed. Wiley-Interscience Publication, 1991.
22. J. M. Andres, R. Pedrosa, A. Perez-Encabo, *Tetrahedron Lett.*, **47**, 5317 (2006).
23. J. H. Gross, *Mass Spectrometry*, Springer - Verlag, Berlin Heidelberg, 2004.
24. S. G. Chiknas, *Clin. Chem.*, **25**, 1259 (1979).

СИНТЕЗ НА БИОАКТИВНИ АМИНОКИСЕЛИННИ ПРОИЗВОДНИ НА ТРАНС-5-АМИНОМЕТИЛ-1-БЕНЗИЛ-6-ФЕНИЛПИПЕРИДИН-2-ОН

Т. И. Баръмов^{1,3}, Н. Т. Бурджиев^{1*}, Б. Т. Пандова², В. Ц. Тодорова², С. Г. Янев², Е. Р. Станоева¹, Х. Д. Чанев¹

¹ Софийски университет „Св. Климент Охридски“, Факултет по химия и фармация, Бул. „Джеймс Баучер“ 1, София 1164, България

² Българска академия на науките, Институт по невробиология, Лаборатория по лекарствена токсикология, Ул. „Акад. Г. Бончев, Бл. 23, София 1113, България

³ настоящ адрес: Bachem AG, Hauptstrasse 144, 4416 Bubendorf, Switzerland

Постъпила на 28 февруари 2017 г.; Коригирана на 24 март 2017 г.

(Резюме)

Транс-5-аминометил-1-бензил-6-фенилпиперидин-2-он (**2**) е синтезиран с висок добив по метода на Мицунобу и ацилиран под действието на *N*-защитените α-аминокиселини глицин, L-триптофан, L-фенилаланин и L-аланин до нови пиперидинони с пептидна връзка в страничната верига към пиперидиноновия пръстен. Проведено е отстраняване на *N*-защитните групи, като страничната верига в производното на триптофана **4** е удължена с оглед получаване на съединения съдържащи две пептидни връзки. Снети са мас-спектри (EI и/или ESI) на повечето съединения и са предложени схеми на фрагментация. В предишно съобщение е описана антихистаминовата активност на производните на триптофана **3–5**. В настоящето съобщение е изследвана АСЕ инхибиторната активност на четири пептидни производни. Съединенията **13a,b** и **14** показват слаба АСЕ инхибиторна активност.

Stereoselectivity in the Diels–Alder addition of S-hydroxy-N-methylsuccinimide acrylate to cyclopentadiene: origins and DFT computational models

S. M. Bakalova, J. Kaneti

Institute of Organic Chemistry with Centre of Phytochemistry, Bulgarian Academy of Sciences, Acad. G. Bonchev street, bl. 9, 1113 Sofia, Bulgaria

Received March 02, 2017; Revised March 24, 2017

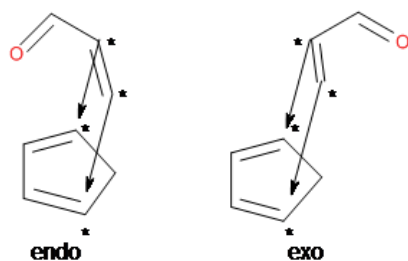
Dedicated to Acad. Bogdan Kurtev on the occasion of his 100th birth anniversary

The title Diels–Alder reaction is used as computational test example of the performance of several DFT functionals at various levels of parameterization. We show that experimental diastereoface selectivities, kinetically corresponding to free activation energy differences of the order of less than 1 kcal.mol⁻¹, can be successfully reproduced by computations using most recent extensively parameterized functionals as M06L, M06-2x and MN12sx, while taking into account the conformational distribution of reactants, in the present case S-hydroxy-N-methylsuccinimide acrylate. Presently computed important contributions to intermolecular interactions between acrylate and cyclopentadiene, governed by dienophile conformation, cannot be assigned only to electrostatic origins in the cases of diastereoface selectivity. In the broader case of *endo:exo* selectivity, contributions of dispersion and longer range repulsion have also been accounted for.

Key words: Diels–Alder stereoselectivity; reactant conformations; transition structures; activation free energies; DFT calculations

INTRODUCTION

The cycloaddition of olefins to dienes, discovered by Diels and Alder in the 1920-ies [1, 2] is still among the most important reactions in organic synthesis. This unabating interest is due to its unique capability to generate up to four chiral centres in a single reaction step, Scheme 1.



Scheme 1. Steric aspects of the [2+4] addition of acrylate to cyclopentadiene. The four prochiral carbon atoms, evolving to chiral centres in the course of DA reaction, are denoted by asterisks.

The latter fact substantiates the continuing effort to elucidate the electronic and steric aspects of its mechanism, reaction rate and stereoselectivity. The development of insights into the Diels–Alder, DA,

mechanism as a [4+2] electrocyclic addition, started with the works of R. Woodward and R. Hoffmann [3], is still based on their ideas and terminology of orbital symmetry.

Interpretations of DA diastereoselectivity are concerned mainly with the *endo vs. exo* selectivity, Scheme 1, with the former usually dominating the reaction outcome [4, 5]. Recent decades of computational studies have witnessed a widening use of density functional theory, DFT [6], treatments of this type of selectivity. However, serious deficiencies in the theoretical predictions have also been revealed [7, 8]. Correct, while still sufficiently robust, computational predictions related to DA stereoselectivity only became possible with recent extensive parameterizations of DFT functionals [8–11]. Thus, the use of DFT computations in the interpretation of DA *endo vs. exo* selectivity is nowadays reliable and theoretically substantiated. The second type of DA selectivity, related to the directionality of the dienophile approach to the planar diastereotopic faces of the diene, is usually modelled by DFT calculations qualitatively correctly. Another computational alternative, namely the use of wavefunction (or MO) theory [12], has also been shown to correctly reproduce the two types of Diels–Alder reaction selectivity using explicit treatment of dynamic electron correlation [8], and

* To whom all correspondence should be sent:

E-mail: bakalova@orgchm.bas.bg;

kaneti@orgchm.bas.bg

can be used as reference, even though at a significantly higher computational cost.

EXPERIMENTAL

Computational details

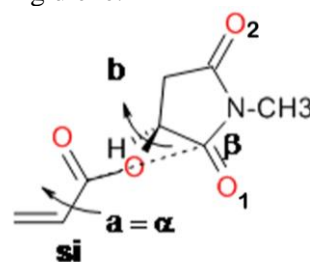
DFT modeling of the reaction is carried out using the GAUSSIAN 09 suite of programs [13]. Several functionals are used in the DFT calculations: PBE0 [14, 15], B97D [16], M06L, M06-2x [9–11]. We also use the recent precisely parameterized Minnesota functionals: M11L [17, 18] and MN12sx [19]. Transition structures, TSs, on the studied diastereoisomeric reaction paths are located using standard optimization techniques and are verified via vibrational analysis to possess a single imaginary frequency, as well as by intrinsic reaction coordinate following [20]. Solvent effects are considered using the PCM approximation [21] in dichloromethane, DCM.

RESULTS AND DISCUSSION

Experiments with acryloyl-*S*-hydroxy-*N*-methyl succinimide, AS, Scheme 2, as the dienophile [22] show low *endo:exo* and diastereoface selectivity of the addition to cyclopentadiene, CPD, in dichloromethane, DCM.

Here, we consider the possible reaction products on the basis of the distribution of existing conformational isomers of the dienophile.

As shown in Fig. 1, rotation from the *s-cis*, center, to the *s-trans*-isomer, left, of the dienophile changes the upper face of the prochiral fragment from **si** to **re**, while virtually leaving the diene approach face, electrostatically assisted by the adjacent carbonyl group, intact. *Vice versa*, a change in the relative orientation of carbonyl groups and dipoles does not alter the configuration of prochiral faces, but changes the attack preference of the incoming diene.



Scheme 2. Conformational degrees of freedom in the dienophile AS with respect to internal rotations around **a** = α and **b**; α determining *s-cis* – *s-trans* isomerism, while the rotation around the ester bond **b** is chosen to determine the dihedral angle β , or $\text{O}=\text{C}---\text{C}=\text{O}_1$, to define the mutual orientation of the two carbonyl bond dipoles at the acrylate fragment and next to the chiral carbon, connected by a dashed line. Carbonyl bonds prefer either the positive, or the negative perpendicular orientation β to each other. [23, 24] As the $\text{OC}---\text{CO}_1$ dihedral angle is equivalent to rotation around a $\text{Csp}^3 - \text{Csp}^3$ bond, the conformation energy profile should possess 3 minima. DFT conformation analysis favors positive β for both *s-cis*- AS (ASC) and *s-trans*- AS (AST) configurations and also reveals two more minima of slightly higher energy with negative β , Table 1.

Table 1. Total (in hartrees) and relative (in kcal.mol^{-1}) energies of *s-cis*-acryloyl-*S*-hydroxy-*N*-methyl succinimide, ASC, and *s-trans*-acryloyl-*S*-hydroxy-*N*-methyl succinimide, AST, conformers of the dienophile, M062x/6-311G(d,p), DCM.

Str.	E(total)	E + ZPE	E + ΔG_{298}	$\Delta\Delta G$	OCCO_1	OCCO_2
ASC1	-665.866542	-665.696842	-665.736794	0.00	103.3	-47.8
ASC2	-665.864483	-665.695181	-665.735680	0.70	-132.5	57.8
ASC3	-665.864480	-665.695118	-665.735600	0.75	-72.9	118.8
AST1	-665.865717	-665.696064	-665.736326	0.29	103.2	-48.0
AST2	-665.863714	-665.694414	-665.735278	0.95	-73.9	116.9
AST3	-665.863965	-665.694633	-665.735235	0.98	-134.1	56.3

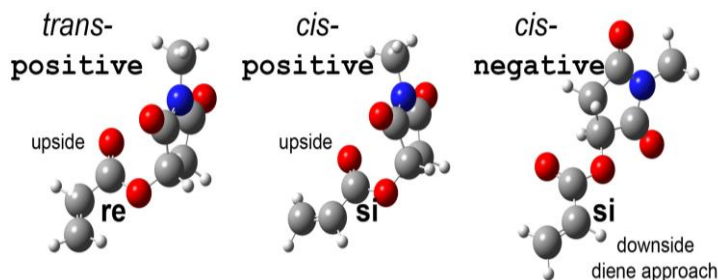
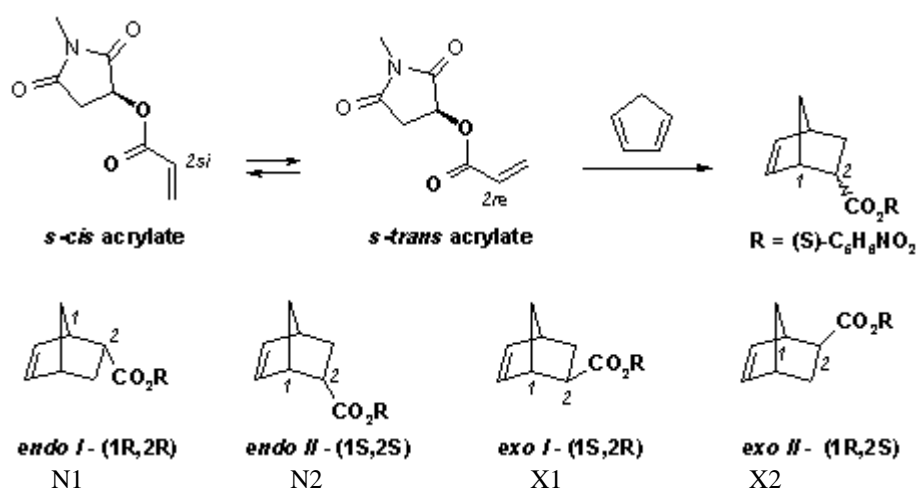


Fig. 1. Conformational effects on prochiral dienophile faces. Configurational designations **re** and **si** refer to the in-plane face. Assuming, for electrostatic reasons, diene approach preference from the side of the adjacent carbonyl group CO_1 , *s-cis* – *s-trans* isomerization directly changes the configuration of the prochiral α -carbon from **re** to **si**, left and center, while positive or negative dihedral angles between acrylate carbonyl and the imide carbonyl group adjacent to the chiral center, center and right, change the preferred direction of attack.

Table 2. Solvent thermodynamics of *s-cis* acryloyl-*S*-hydroxy-*N*-methyl succinimide, ASC, M062x/6-311G++(d,p), along angle β , Scheme 2, $O_{acr} = C \cdots C = O_1$. Stationary point names correspond approximately to the value of β , with TS meaning the respective rotational transition structures.

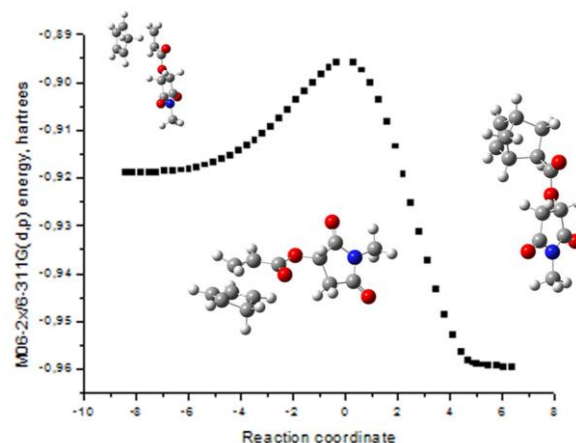
Stationary point	E(total) <i>hartrees</i>	E + ΔG_{298} <i>hartrees</i>	$\Delta\Delta G^\ddagger$ kcal.mol ⁻¹	E + $\Delta G_{(ASC+CPD)}$ <i>hartrees</i>
ASC103	-665.880455	-665.751191	0.00	-859.746234
ASC143TS	-665.867067	-665.737538	8.57	
ASC-133	-665.879063	-665.750244	0.59	-859.745287
ASC-94TS	-665.877827	-665.747966	2.02	
ASC-75	-665.878408	-665.750676	0.32	-859.746540
ASC32TS	-665.866503	-665.736244	9.38	
CPD	-194.061413	-193.995043		

**Scheme 3.** *Endo* and *exo* isomeric products, resulting from the reaction of a single isomer of *S*-hydroxy-*N*-methylsuccinimide acrylate with cyclopentadiene [26, 27]. In transition structures, TSs, acrylate *s-cis* and *s-trans* isomers are possible. In adducts, these isomers cannot be distinguished because of the practically free rotation of the resulting carboxylate group, which is no longer conjugated.

Schemes 1 and 3 outline the origins of four *endo:exo* isomeric product pairs from each of the three conformational isomers of dienophile. Thus, to completely model the reaction in question, we would need to consider computationally 24 diastereoisomeric reaction potential energy paths and obtain the resulting kinetic product distribution from the calculated Gibbs activation free energy differences [25]. However, as the barrier between the two conformers with negative β is less than 2 kcal.mol⁻¹ (Table 2), the corresponding pairs of TSs collapse into each other to give one and only negative- β TS. Thus, the total number of located TS amounts to 16.

Computational results using Pople basis sets, mostly at the 6-311G(d,p) level [28, 29], are listed in Tables 1S and 3. Some of the energetically preferred transition structures are shown in Fig. 3, and the complete product distribution is in Table 3. A general reaction energy profile, *i.e.* the intrinsic reaction coordinate (IRC) for a diastereoisomeric

reaction channel, is shown in Fig. 2: reactants left; product right, separated by a single TS, centre.

**Fig. 2.** A complete electronic energy profile: IRC starting from the TS of the DA addition of CPD to *s-cis* acryloyl-*S*-hydroxy-*N*-methyl succinimide, ASC, M06-2x/6-311G(d,p).

As indicated by computed Gibbs free energies of the 16 diastereoisomeric TSs, there is no single

lowest structure to dominate the stereochemical outcome of the studied [4+2] addition, Table 3. Of the 3 possible $Csp^3 - Csp^3$ rotational isomers, only the positive and one of the two negative isomers produce actual free energies of the located TSs not higher than 3 kcal.mol⁻¹ relative to the generally lowest positive NC1, that is, contributing more than 1% to the final product outcome. Contrary to the Curtin-Hammett principle, the TS and product diastereoisomeric distributions are independent of the ground state equilibrium of dienophile conformers due to the large activation free energy of the reaction, some 3 times higher than computed rotational barriers in AS [30]; Table 2 and Fig. 2.

More detailed inspection of Tables 1S and 3 shows nevertheless that some isomeric TSs are higher by less than 1 kcal.mol⁻¹ than NC1pos, Fig. 3, and contribute 5% or more to the final products. These TSs deserve additional attention to their internal interactions for understanding the overall stereoselectivity. However, TSs and their internal interactions are different with various used functionals. We therefore select the numerical models reproducing most closely the known experimental selectivities [22], namely M06L, M06-2x, and MN12sx, in order to interpret TS internal interactions and the origins of selectivity, Table 3 and Fig. 3.

Energies and selected interatomic distances outlined in Fig. 3 for energetically preferred TSs show close contacts of dienophile carbonyl atoms with hydrogen atoms of the diene in the range of 2.3 to 2.5 Å, which can be interpreted as non-classical hydrogen bonds C=O...H–C in some of these [27]. The abundance of heteroatoms in the chiral auxiliary may be expected to provide a significant number of opportunities for the forming of such stabilizing contacts, and energy preferences thereof, for some of the conformationally possible diastereoisomeric reaction paths. This is also the qualitative explanation of the necessity to consider computationally all of the 16 possible reaction paths in order to obtain a correct prediction of the reaction stereochemical outcome. Three of the most stable TSs shown in Fig. 3 actually have short H...O contacts with carbonyl atoms of the attacking dienophile, and another three have no H...O close contacts. Neither of the shown TSs dominates computed free activation energies, and consequently the reported experimental distribution of stereoisomeric products [22, 26], indicating the dominant role of electrostatic interactions with other dienophiles [27] would be oversimplified in the case of AS reaction with CPD. Indeed, going back to Fig. 1 we see, that positive β prefers N1

Table 3. Percentage product distributions for the reaction of AS and cyclopentadiene, CPD, predicted by DFT calculations at the 6-311G(d,p) gaussian basis set level in dichloromethane, together with predicted selectivities. **Pos** and **neg** refer to positive and negative dihedral angles β between adjacent carbonyl groups, see Scheme 2 and Fig. 1. Also shown are M06-2x^d and MN12sx^d results at the 6-311++G(d,p) basis set level. Experimental product distribution: *endo* DS (N1:N2) = 54:46; *endo:exo* = 4.8, dichloromethane [22].

TS	PBE	B97D	M06L	M06-2x	M06-2x ^d	M11L	MN12sx	MN12sx ^d
NC1 pos	7.15	16.93	42.52	48.53	26.62	31.29	33.37	30.80
NC2 pos	1.84	5.94	17.39	9.54	12.40	24.47	10.39	20.38
XC1 pos	7.25	13.04	13.67	14.36	7.35	13.10	34.12	5.84
XC2 pos	1.02	2.91	5.42	3.50	3.79	6.77	2.50	3.51
NT1 pos	0.19	0.79	1.11	1.53	2.24	1.20	1.04	2.82
NT2 pos	0.83	1.06	2.77	6.20	9.72	4.53	3.18	2.85
XT1 pos	0.07	0.18	0.16	0.11	0.14	0.25	0.12	0.40
XT2 pos	0.55	1.13	1.03	0.33	0.69	0.39	0.05	5.41
NC1 neg	13.22	9.67	4.53	1.64	3.93	2.34	1.54	6.36
NC2 neg	50.96	36.99	6.65	9.75	19.95	9.75	9.85	11.64
XC1 neg	3.39	2.44	0.67	0.39	0.49	1.02	0.36	0.64
XC2 neg	8.97	5.66	2.57	1.38	1.29	3.00	1.74	1.29
NT1 neg	2.62	1.62	1.19	1.73	9.61	1.18	1.41	6.05
NT2 neg	0.69	0.19	0.29	0.66	1.03	0.35	0.10	1.31
XT1 neg	0.97	1.01	0.0	0.28	0.35	0.31	0.16	0.60
XT2 neg	0.28	0.45	0.0	0.08	0.41	0.05	0.05	0.11
<i>endo:exo</i>	77.5:22.5	73.2:26.8	76.5:23.5	79.6:20.4	85.5:14.5	74.5:25.5	60.9:39.1	82.2:17.8
	3.44	2.73	3.25	3.90	5.89	2.92	1.56	4.62
N1:N2	29.9:70.1	39.7:60.3	64.5:35.5	67.1:32.9	49.6:50.4	46.3:53.7	61.4:38.6	56.0:44.0

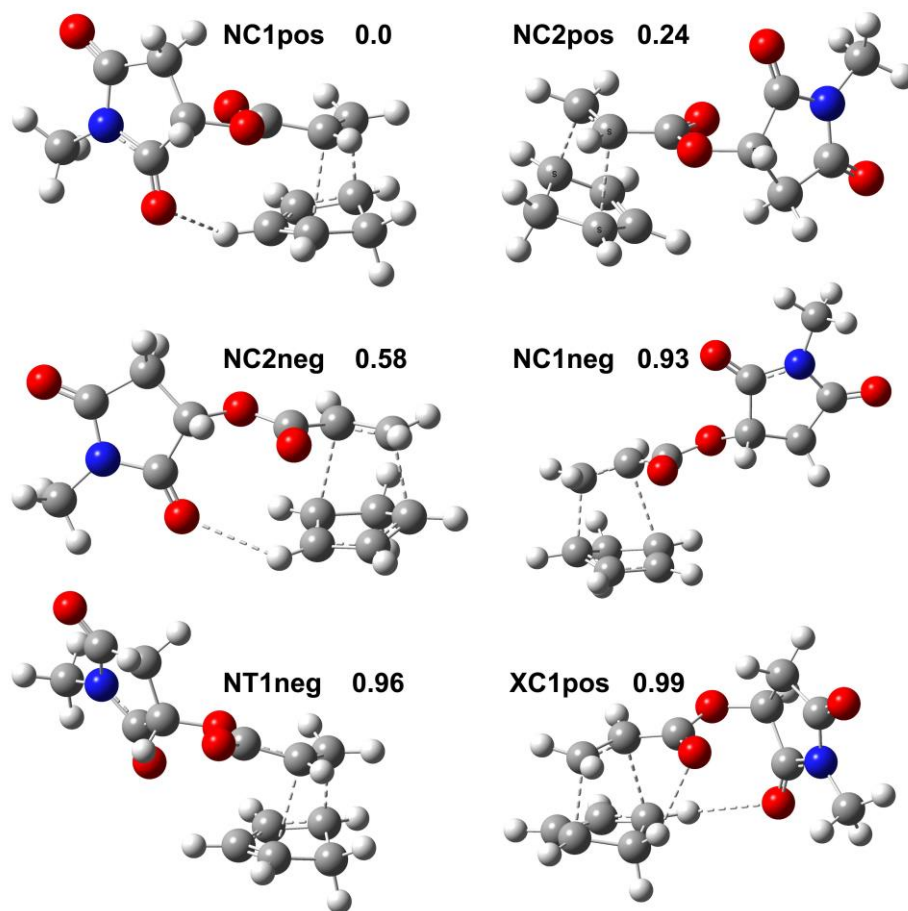


Fig. 3. Energetically preferred transition structures and relative activation free energies at the MN12sx/6-311++G(d,p) level for the [4+2] addition of acryloyl-*S*-hydroxy-*N*-methyl succinimide ASC and cyclopentadiene, CPD, see also Tables 1S and 3. **Pos** and **neg** refer to the respective O=C...C=O dihedral angles β . Short interatomic contacts are outlined as dashed “bonds”: incipient C---C in the range of ca. 2.0 to 2.5 Å; electrostatic contacts C=O...H-C in the range of 2.30 to 2.55 Å.

(*R,R*) selectivity due to the mentioned electrostatic assistance, while negative β prefers N2 (*S,S*) selectivity for the same electrostatic reason. Fig. 3 also shows the 4 most stable *endo* TSs contributing to more than 80% of the predicted population of *endo* TSs. Electrostatic preference to N1 (*R,R*) gives 37%, and to N2 (*S,S*) 32% of the computed total stereochemical outcome, Table 3, which coincides with the observed N1:N2 ratio [22]. It can be seen that in each pair of NC1-NC2 the TSs showing nontraditional hydrogen bonds are more stable than their counterparts. The two diastereoface preferences balance each other to produce the observed low N1:N2 ratio and also contribute to more than 80% of the observed *endo* selectivity. Following in stability are *s-trans* and *exo* TSs, where preferences involve other types of intramolecular interactions along with the electrostatics discussed above, to further complicate

the final experimental stereochemical result. However, as we discuss selectivity changes with the same diene, and *s-cis/s-trans* isomers of the same dienophile, no changes of frontier orbital, or secondary orbital effects, anomeric effects, substituent electronegativity or hyperconjugative aromaticity/antiaromaticity may partake in the present case [31, 32].

CONCLUSION

The reported results show a success of extensively parameterized high-performance functionals as M06L, M06-2x, and MN12sx in the reproduction of observed low diastereoselectivity of the title DA reaction. We find that the full palette of intramolecular interactions, rather than non-traditional H bonds only, govern the diastereofacial

selectivity of the AS + CPD addition, as further substantiated by diffuse basis set M062x/6-311++G(d,p) and MN12sx/6-311++G(d,p) TS optimizations.

Acknowledgements: A part of the reported computations has been carried out on the MADARA HPC cluster, IOCCP, acquired under Project RNF01/0110 (2009-2011) of the National Research Fund of Bulgaria.

Electronic Supplementary Data available here.

REFERENCES

1. O. Diels, K. Alder, *J. Liebig's Ann. Chem.*, **460**, 98 (1928).
2. R. B. Woodward, R. Hoffmann, *Angew. Chem. Int. Ed.*, **8**, 781 (1969).
3. R. Hoffmann, R. B. Woodward, *Science*, **167** (3919), 825 (1970).
4. M. J. S. Dewar, S. Olivella, J. J. P. Stewart, *J. Am. Chem. Soc.*, **108**, 5771 (1986).
5. K. N. Houk, Y. T. Lin, F. K. Brown, *J. Am. Chem. Soc.*, **108**, 554 (1986).
6. E. Goldstein, B. Beno, K. N. Houk, *J. Am. Chem. Soc.*, **118**, 6036 (1996).
7. W. Koch, M. C. Holthausen, *A Chemist's Guide to Density Functional Theory*, 2nd edition, Wiley-VCH, 2001.
8. S. N. Pieniazek, F. R. Clemente, K. N. Houk, *Angew. Chem. Int. Ed.*, **47**, 7746 (2008).
9. Y. Zhao, D. G. Truhlar, *Theor. Chem. Acc.*, **120**, 215 (2008).
10. Y. Zhao, D. G. Truhlar, *Acc. Chem. Res.*, **41**, 157 (2008).
11. Y. Zhao, D. G. Truhlar, *J. Chem. Theory Comput.*, **7**, 669 (2011).
12. W. J. Hehre, L. Radom, P. v. R. Schleyer, J. A. Pople, *Ab Initio MO Theory*, Wiley, NY, 1986.
13. Gaussian 09, Revision D.01: M. J. Frisch, G. W. Trucks, H. B. Schlegel, G. E. Scuseria, M. A. Robb, J. R. Cheeseman, G. Scalmani, V. Barone, B. Mennucci, G. A. Petersson, H. Nakatsuji, M. Caricato, X. Li, H. P. Hratchian, A. F. Izmaylov, J. Bloino, G. Zheng, J. L. Sonnenberg, M. Hada, M. Ehara, K. Toyota, R. Fukuda, J. Hasegawa, M. Ishida, T. Nakajima, Y. Honda, O. Kitao, H. Nakai, T. Vreven, J. A. Montgomery, Jr., J. E. Peralta, F. Ogliaro, M. Bearpark, J. J. Heyd, E. Brothers, K. N. Kudin, V. N. Staroverov, T. Keith, R. Kobayashi, J. Normand, K. Raghavachari, A. Rendell, J. C. Burant, S. S. Iyengar, J. Tomasi, M. Cossi, N. Rega, J. M. Millam, M. Klene, J. E. Knox, J. B. Cross, V. Bakken, C. Adamo, J. Jaramillo, R. Gomperts, R. E. Stratmann, O. Yazyev, A. J. Austin, R. Cammi, C. Pomelli, J. W. Ochterski, R. L. Martin, K. Morokuma, V. G. Zakrzewski, G. A. Voth, P. Salvador, J. J. Dannenberg, S. Dapprich, A. D. Daniels, O. Farkas, J. B. Foresman, J. V. Ortiz, J. Cioslowski, D. J. Fox, Gaussian, Inc., Wallingford CT, 2013.
14. J. P. Perdew, K. Burke, M. Ernzerhof, *Phys. Rev. Lett.*, **77**, 3865 (1996).
15. J. P. Perdew, K. Burke, M. Ernzerhof, *Phys. Rev. Lett.*, **78**, 1396 (1997).
16. S. Grimme, *J. Comp. Chem.*, **27**, 1787 (2006).
17. R. Peverati, D. G. Truhlar, *J. Phys. Chem. Lett.*, **2**, 2810 (2011).
18. R. Peverati, D. G. Truhlar, *J. Phys. Chem. Lett.*, **3**, 117 (2012).
19. R. Peverati, D. G. Truhlar, *J. Chem. Theory and Comput.*, **8**, 2310 (2012).
20. S. S. Shaik, H. B. Schlegel, S. Wolfe, *Theoretical aspects of physical organic chemistry*, Wiley, 1992. H. B. Schlegel, *J. Comp. Chem.* **3**, 214 (1982).
21. J. Tomasi, B. Mennucci, R. Cammi, *Chem. Rev.*, **105**, 2999 (2005).
22. T. Poll, *Neue chirale Auxiliare für die asymmetrische Diels-Alder-Reaktion*, PhD Thesis., Univ. Würzburg, 1988, pp. 133–134; 143–146.
23. M. S. Betson, J. Clayden, H. K. Lam, M. Helliwell, *Angew. Chem. Int. Ed. Engl.*, **44**, 1241 (2005).
24. K. Kahn, T. C. Bruice, *Bioorg. Med. Chem.*, **8**, 1881 (2000).
25. T. H. Lowry, K. S. Richardson, *Mechanism and Theory in Organic Chemistry*, 3rd Edition, Harper International, 1987, pp. 202–229.
26. T. Poll, G. Helmchen, B. Bauer, *Tetrahedron Lett.*, 2191 (1984).
27. S. M. Bakalova, A. G. Santos, *J. Org. Chem.*, **69**, 8475 (2004).
28. W. J. Hehre, R. Ditchfield, J. A. Pople, *J. Chem. Phys.*, **56**, 2257 (1972).
29. T. Clark, J. Chandrasekhar, P. v. R. Schleyer, *J. Comp. Chem.*, **4**, 294 (1983).
30. I. G. Pojarlieff, *Physical Organic Chemistry and Dynamic Stereochemistry* (in Bulgarian), Sofia, 2001, pp. 65–70.
31. B. J. Levandowski, Z. Lufeng, K. N. Houk, *J. Comput. Chem.*, **37**, 117 (2016).
32. B. J. Lewandowski, K. N. Houk, *J. Am. Chem. Soc.*, **138**, 16731 (2016).

СТЕРЕОСЕЛЕКТИВНОСТ НА ДИЛС–АЛДЕРОВОТО ПРИСЪЕДИНЯВАНЕ НА [S]-АКРИЛОИЛ-N-МЕТИЛ СУКЦИНИМИД И ЦИКЛОПЕНТАДИЕН: ПРОИЗХОД И ИЗЧИСЛИТЕЛНО МОДЕЛИРАНЕ В РАМКИТЕ НА ТЕОРИЯТА НА ФУНКЦИОНАЛА НА ПЛЪТНОСТТА

С. М. Бакалова, Х. Канети

¹ *Институт по Органична Химия с Център по Фитохимия, Българска Академия на Науките, ул. Акад. Г. Бончев, бл. 9, 1113 София, България*

Постъпила на 02 март 2017 г.; Коригирана на 24 март 2017 г.

(Резюме)

Изследвана е реакция на Дилс–Алдер с ниска диастереоселективност за сравнение на изчислителните предвиждания от теорията на функционала на плътността с различни нива на параметризация. Показано е, че експерименталната диастереоселективност от 55:45, която отговаря кинетично на разлики между свободните енергии на активация по-малки от 1 ккал.мол⁻¹, може да бъде възпроизведена задоволително от пресмятания с помощта на подобрените по точност функционали M06L, M06-2x и MN12sx в случай, че са подходящо отчетени конформационните разпределения на реагентите. В конкретния изследван случай това е диенофилът *S*-хидрокси-*N*-метилсукцинимид акрилат. Изчислено е, че важните приноси на вътрешно-молекулните и междумолекулните взаимодействия към намерените диастереомерни преходни структури не се дължат предимно на електростатични взаимодействия. Участието на дисперсионни и по-далечни сили в *ендо:екзо* селективността е отчетено от по-новите параметри в пресмятанията.

Synthesis and cytotoxic activity of new heterocyclic analogues of resveratrol, containing benzoxazolone ring

M. S. Gerova¹, E. A. Aleksandrova^{1,2}, Y. B. Ivanova³, D. V. Stanisheva¹, G. Ts. Momekov⁴, O. I. Petrov^{1*}

¹ Department of Pharmaceutical and Applied Organic Chemistry, Faculty of Chemistry and Pharmacy, Sofia University "St. Kliment Ohridski", 1 James Bourchier Blvd, 1164 Sofia, Bulgaria

² Department of General and Clinical Pathology, Medical Faculty, Trakia University, 11 Armeiska Str., 6000 Stara Zagora, Bulgaria

³ Department of Plant Pathology and Chemistry, Faculty of Ecology and Landscape Architecture, University of Forestry, 10 Kliment Ohridsky Blvd, 1756 Sofia, Bulgaria

⁴ Department of Pharmacology, Pharmacotherapy and Toxicology, Faculty of Pharmacy, Medical University-Sofia, 2 Dunav Str., Sofia 1000, Bulgaria

Received March 01, 2017; Revised March 15, 2017

Dedicated to Acad. Bogdan Kurtev on the occasion of his 100th birth anniversary

New heterocycle analogues of resveratrol were designed and synthesized as potential anticancer agents. The compounds contain 3,5-dimethoxy- or 3,5-dihydroxystyryl fragment attached to the C5 or C6 position of a benzoxazolone ring. The compounds were tested for their cytotoxic activity against three human cancer cell lines (HL-60, MGF-7 and MDA-MB-321) and some of them were found to exhibit significant antiproliferative effect. Generally, the obtained 5-styrylbenzoxazolones were more active in compare to the corresponding 6-styrylbenzoxazolone positional isomers.

Key words: resveratrol; benzoxazolone; stilbene; cytotoxicity

INTRODUCTION

Resveratrol (Fig. 1) belongs to a group of naturally occurring polyphenols possessing the *trans*-stilbene scaffold. Found in more than 70 plants, the compound has been shown to exhibit a variety of health-beneficial properties such as antioxidant, anti-inflammatory, anti-diabetic, cardio- and neuroprotective activities [1–5]. Additionally, resveratrol has been recognized as a promising chemopreventive and anticancer agent due to its capability to inhibit tumorigenesis by modulation of several cellular process including apoptosis, cell cycle progression as well as angiogenesis [2, 6–9]. A number of methoxy derivatives of resveratrol have been also reported to exert high cytotoxicity against various human cancer cell lines [10–14]. Some of the synthetic analogues showed better activity compared to the natural compound [10, 11, 14].

In search of new anticancer agents, we have planned the synthesis of a small series of heterocyclic derivatives of resveratrol, in which the 4'-hydroxyphenyl moiety in the parent molecule was replaced with a benzoxazolone (Fig. 1).

Considered to be a "privileged scaffold" in medicinal chemistry, the benzoxazolone heterocyclic system has been extensively used in drug discovery as a phenol and pyrocatechol bioisostere [15]. The 3,5-dihydroxyphenyl fragment of the parent resveratrol molecule was left intact or replaced with a 3,5-dimethoxyphenyl moiety, with the aim to systematically evaluate the role of the isolated fragments on the biological activity of the compounds.

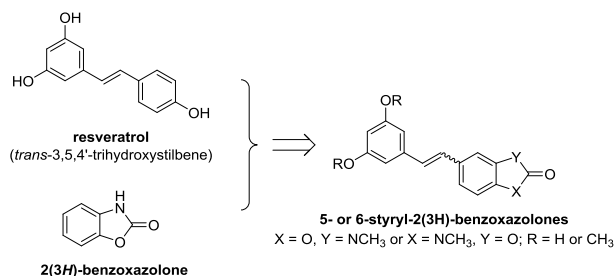


Fig. 1. Chemical structure of resveratrol, 2(3H)-benzoxazolone and target 5- and 6-styryl-2(3H)-benzoxazolones.

Thus, in continuation of our previous studies on the synthesis of heterocyclic stilbenes [16], here we report the preparation of 5- and 6-(3,5-dimethoxy-

* To whom all correspondence should be sent:
E-mail: opetrov@chem.uni-sofia.bg

or 3,5-dihydroxystyryl)-2(3*H*)-benzoxazolones as closely related resveratrol analogues. Their *in vitro* cytotoxicity was examined against three human cancer cell lines.

EXPERIMENTAL

Chemistry

Melting points (mp) were determined on a Boetius hot-stage microscope and are uncorrected. Infrared spectra (IR) were recorded on a Specord 71 spectrometer. ¹H NMR spectra were obtained on a Bruker DRX250 or Bruker DRX400 spectrometers. Chemical shifts were reported in parts per million (ppm, δ) relative to the solvent peak (CDCl₃, 7.26 ppm; DMSO-d₆, 2.50 ppm; acetone-d₆, 2.05 ppm). Elemental analyses (C, H, N) were performed on a Vario III microanalyzer and the obtained results were within 0.4% of theoretical values. All reactions were monitored by thin-layer chromatography (TLC) on silica gel plates (Kieselgel 60 F₂₅₄), using hexane/acetone (2:1 v/v) as eluent. Column chromatography on Merck silica gel 60 (230–400 mesh) was applied for the separation of diastereomers. Phosphonium bromides **1a-b** were synthesized as described previously [16].

General procedure for the synthesis of stilbene derivatives via Wittig reaction

A mixture of appropriate phosphonium bromide **1a-b** (1.51 g, 3 mmol), 3,5-dimethoxybenzaldehyde (0.50 g, 3 mmol), powdered potassium carbonate (1.38 g, 10 mmol) and 18-crown-6 (0.01 g) in THF/DCM (20 mL, 2:1 v/v) was refluxed for 3 h (monitored by TLC). The inorganic salts were filtered off and the filtrate was concentrated under reduced pressure to obtain a mixture of the corresponding *E*- and *Z*-stilbenes and triphenylphosphine oxide. Both diastereomers were isolated by column chromatography using petroleum ether/acetone (10:1 v/v) as eluent.

(*Z*)-5-(3,5-Dimethoxystyryl)-3-methyl-2(3*H*)-benzoxazolone (**2a**)

Yield: 48% (0.48 g), colourless oil. IR (capillary film, cm⁻¹): 1780 (C=O). ¹H NMR (CDCl₃, 250 MHz): δ 3.27 (s, 3H, NCH₃), 3.67 (s, 6H, OCH₃), 6.34 (t, 1H, ArH, *J* = 2.3 Hz), 6.39 (d, 2H, ArH, *J* = 2.3 Hz), 6.57 (s, 2H, =CH), 6.84 (br s, 1H, ArH), 7.04–7.05 (m, 2H, ArH). ¹H NMR (acetone-d₆, 500 MHz): δ 3.29 (s, 3H, NCH₃), 3.65 (s, 6H, OCH₃), 6.36 (t, 1H, ArH, *J* = 2.2 Hz), 6.42 (d, 2H, ArH, *J* = 2.1 Hz), 6.58 (d, 1H, =CH, *J* = 12.2 Hz), 6.65 (d,

1H, =CH, *J* = 12.2 Hz), 7.04–7.06 (m, 2H, ArH), 7.12 (d, 1H, ArH, *J* = 8.0 Hz). Anal. Calcd. for C₁₈H₁₇NO₄ (311.34): C 69.44, H 5.50, N 4.50. Found: C 69.62, H 5.62, N 4.30.

(*E*)-5-(3,5-Dimethoxystyryl)-3-methyl-2(3*H*)-benzoxazolone (**3a**)

Yield: 43% (0.40 g), mp 164–165 °C. IR (nujol, cm⁻¹): 1760 (C=O). ¹H NMR (CDCl₃, 400 MHz): δ 3.44 (s, 3H, NCH₃), 3.84 (s, 6H, OCH₃), 6.41 (t, 1H, ArH, *J* = 2.1 Hz), 6.67 (d, 2H, ArH, *J* = 2.3 Hz), 6.99 (s, 1H, =CH, *J* = 16.2 Hz), 7.08 (s, 1H, =CH, *J* = 16.3 Hz), 7.12 (br s, 1H, ArH), 7.17 (d, 1H, ArH, *J* = 8.3 Hz), 7.23 (dd, 1H, ArH, *J* = 1.0 Hz, *J* = 8.3 Hz). Anal. Calcd. for C₁₈H₁₇NO₄ (311.34): C 69.44, H 5.50, N 4.50. Found: C 69.21, H 5.37, N 4.53.

(*Z*)-6-(3,5-Dimethoxystyryl)-3-methyl-2(3*H*)-benzoxazolone (**2b**)

Yield: 48% (0.48 g), mp 89–91 °C. IR (nujol, cm⁻¹): 1770 (C=O). ¹H NMR (CDCl₃, 250 MHz): δ 3.37 (s, 3H, NCH₃), 3.68 (s, 6H, OCH₃), 6.34 (t, 1H, ArH, *J* = 2.3 Hz), 6.39 (d, 2H, ArH, *J* = 2.3 Hz), 6.54 (s, 2H, =CH), 6.81 (d, 1H, ArH, *J* = 8.4 Hz), 7.09–7.13 (m, 2H, ArH). ¹H NMR (acetone-d₆, 250 MHz): δ 3.38 (s, 3H, NCH₃), 3.67 (s, 6H, OCH₃), 6.37 (t, 1H, ArH, *J* = 2.1 Hz), 6.42 (d, 2H, ArH, *J* = 2.1 Hz), 6.56 (d, 1H, =CH, *J* = 12.2 Hz), 6.64 (d, 1H, =CH, *J* = 12.2 Hz), 7.08 (d, 1H, ArH, *J* = 8.1 Hz), 7.11 (br s, 1H, ArH), 7.16 (dd, 1H, ArH, *J* = 1.1 Hz, *J* = 8.4 Hz). Anal. Calcd. for C₁₈H₁₇NO₄ (311.34): C 69.44, H 5.50, N 4.50. Found: C 69.52, H 5.83, N 4.23.

(*E*)-6-(3,5-Dimethoxystyryl)-3-methyl-2(3*H*)-benzoxazolone (**3b**)

Yield: 35% (0.33 g), mp 164–165 °C. IR (nujol, cm⁻¹): 1770 (C=O). ¹H NMR (CDCl₃, 400 MHz): δ 3.42 (s, 3H, NCH₃), 3.84 (s, 6H, OCH₃), 6.41 (t, 1H, ArH, *J* = 2.2 Hz), 6.66 (d, 2H, ArH, *J* = 2.2 Hz), 6.92–6.99 (m, 2H, =CH, ArH), 7.07 (s, 1H, =CH, *J* = 16.2 Hz), 7.31 (dd, 1H, ArH, *J* = 1.2 Hz, *J* = 8.1 Hz), 7.40 (br s, 1H, ArH). Anal. Calcd. for C₁₈H₁₇NO₄ (311.34): C 69.44, H 5.50, N 4.50. Found: C 69.38, H 5.37, N 4.53.

General procedure for the demethylation of the methoxy groups with BBr₃

Boron tribromide (1.7 M in DCM, 0.53 mL, 0.9 mmol) was added to a stirred solution of corresponding 3,5-dimethoxy-substituted (*E*)-stilbene **3a-b** (0.16 g, 0.5 mmol) in anhydrous DCM (10 mL) at –10 °C. The resulting mixture was stirred for 1 h at –10 °C, allowed to warm to room temperature, and stirred for another 48 h. Then,

water (15 mL) was added and the obtained precipitate was filtered off and air-dried. The product was purified by recrystallization.

(E)-5-(3,5-Dihydroxystyryl)-3-methyl-2(3*H*)-benzoxazolone (**4a**)

Yield: 70% (0.10 g), mp 252–254 °C (ethanol). IR (nujol, cm^{-1}): 3200–3400 (OH), 1720 (C=O). ^1H NMR (DMSO- d_6 , 400 MHz): δ 3.38 (s, 3H, NCH_3), 6.16 (t, 1H, ArH, $J = 2.1$ Hz), 6.43 (d, 2H, ArH, $J = 2.1$ Hz), 7.08 (s, 2H, =CH), 7.29 (s, 2H, ArH), 7.58 (s, 1H, ArH), 9.26 (s, 2H, OH). ^1H NMR (acetone- d_6 , 500 MHz): δ 3.43 (s, 3H, NCH_3), 6.30 (br s, 1H, ArH), 6.57 (d, 2H, ArH, $J = 1.9$ Hz), 7.09 (d, 1H, =CH, $J = 16.3$ Hz), 7.13 (d, 1H, =CH, $J = 16.3$ Hz), 7.21 (d, 1H, ArH, $J = 8.2$ Hz), 7.29 (dd, 1H, ArH, $J = 1.3$ Hz, $J = 8.2$ Hz), 7.47 (br s, 1H, ArH), 8.46 (br s, 2H, OH). Anal. Calcd. for $\text{C}_{16}\text{H}_{13}\text{NO}_4$ (283.28): C 67.84, H 4.63, N 4.94. Found: C 67.54, H 4.81, N 4.71.

(E)-6-(3,5-Dihydroxystyryl)-3-methyl-2(3*H*)-benzoxazolone (**4b**)

Yield: 77% (0.11 g), mp 281–283 °C (acetone/water, 1:1 v/v). IR (nujol, cm^{-1}): 3150–3400 (OH), 1740 (C=O). ^1H NMR (DMSO- d_6 , 400 MHz): δ 3.35 (s, 3H, NCH_3), 6.14 (t, 1H, ArH, $J = 2.1$ Hz), 6.42 (d, 2H, ArH, $J = 2.1$ Hz), 7.05 (d, 2H, =CH), 7.23 (d, 1H, ArH, $J = 8.1$ Hz), 7.42 (dd, 1H, ArH, $J = 1.1$ Hz, $J = 8.1$ Hz), 7.65 (d, 1H, ArH, $J = 1.1$ Hz), 9.23 (s, 2H, OH). ^1H NMR (acetone- d_6 , 500 MHz): δ 3.41 (s, 3H, NCH_3), 6.29 (t, 1H, ArH, $J = 2.0$ Hz), 6.57 (d, 2H, ArH, $J = 2.0$ Hz), 7.05 (d, 1H, =CH, $J = 16.3$ Hz), 7.12 (d, 1H, =CH, $J = 16.3$ Hz), 7.16 (d, 1H, ArH, $J = 8.1$ Hz), 7.40 (dd, 1H, ArH, $J = 1.2$ Hz, $J = 8.1$ Hz), 7.52 (d, 1H, ArH, $J = 1.1$ Hz), 8.43 (br s, 2H, OH). Anal. Calcd. for $\text{C}_{16}\text{H}_{13}\text{NO}_4$ (283.28): C 67.84, H 4.63, N 4.94. Found: C 67.68, H 4.57, N 4.73.

Biology

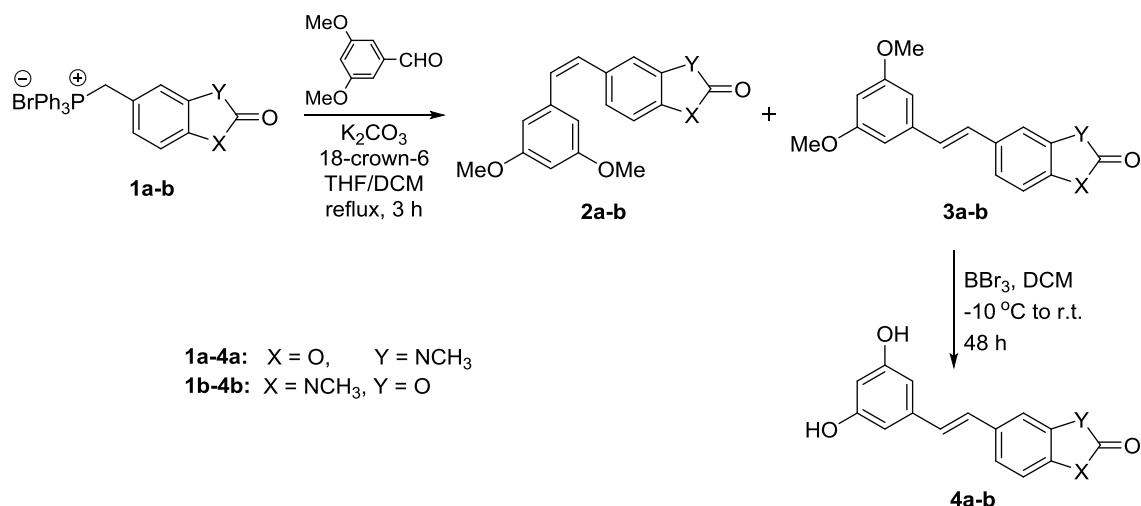
Cytotoxicity tests were carried out on three tumor cell lines with different origin, namely HL-60 (human promyelocytic leukemia), MCF-7 (human breast cancer) and MDA-MB-231 (human breast adenocarcinoma). The cells were maintained as suspension type cultures (leukemia and adenocarcinoma) or as adherent culture (breast cancer) in controlled environment: RPMI-1640 medium, supplemented by 10% FBS and 2 mM L-glutamine at 37 °C in a "Heraeus" incubator with humidified atmosphere and 5% CO_2 . In order to keep cells in log phase, the cultures were refed with fresh RPMI-1640 medium two or three times a week.

Tested compounds were dissolved in DMSO and the solutions were diluted with RPMI-1640 medium to yield the desired final concentrations. Cytotoxicity of the compounds was assessed using the MTT-dye reduction assay [17], with minor modifications [18]. Exponentially growing cells were seeded in 96-well plates (100 μL /well at a density of 1×10^5 cells/mL). After 24 h incubation (37 °C, 5% CO_2 and maximum humidity), they were exposed to various concentrations of the tested compounds (200, 50, 25, 12.5, 6.25 μM) for 72 h. Then, MTT (3-(4,5-dimethylthiazol-2-yl)-2,5-diphenyltetrazolium bromide) solution (10 mg/mL in PBS) was added (10 μL /well). Plates were further incubated for 3 hours at 37 °C. To dissolve the formazan crystals formed, 5% solution of formic acid in isopropanol (100 μL /well) was used. Absorption was measured on an ELISA reader at 580 nm. A mixture of 100 μL RPMI-1640 medium, 10 μL MTT stock and 100 μL 5% formic acid in isopropanol was used as control. For each concentration tested a set of six separate wells was used. The IC_{50} value (the concentration that inhibit 50% of cell growth) for each compound was calculated using OriginLab program.

RESULTS AND DISCUSSION

As depicted in Scheme 1, the synthesis of target stilbene derivatives **2a-b** and **3a-b** was achieved by applying the Wittig methodology on 3,5-dimethoxybenzaldehyde and the appropriate heterocyclic ylide, in turn obtained from the phosphonium bromides **1a-b** in the presence of potassium carbonate and 18-crown-6. The reactions were carried out in THF/DCM at reflux for 3 h and produced the corresponding 3,5-dimethoxystyrylbenzoxazolones as mixtures of π -diastereomers. The pure *Z*- and *E*-stilbenes (**2a-b**, respectively **3a-b**) were separated by column chromatography. As the natural resveratrol is in the *E*-configuration, the obtained methoxy substituted *E*-stilbenes **3a-b** were subjected to a reaction of demethylation with boron tribromide to afford **4a-b** in high yields. The demethylation of the *Z*-isomers **2a-b** in these conditions led to a mixture of products caused by additionally isomerization of the double bond.

The structures of all newly synthesized benzoxazolone-containing stilbene derivatives **2a-b** – **4a-b** were confirmed by ^1H NMR spectroscopy. The geometry of the double bond was assigned on the basis of the coupling constants of the olefinic protons signals ($J = 12.2$ Hz for *Z*-stilbene **2a-b**,



Scheme 1. Synthesis of 5- and 6-styryl-2(3*H*)-benzoxazolones.

and $J = 16.2$ or 16.3 Hz for *E*-stilbene **3a-b** and **4a-b**). Consistent with the coupling constant data, both doublets for the olefinic protons of the *Z*-isomers appeared at 6.54–6.65 ppm whereas those for *E*-stilbenes shifted downfield to 6.99–7.13 ppm.

The synthesized heterocyclic analogues of resveratrol were tested *in vitro* for their cytotoxicity against three human cancer cell lines (HL-60, MCF-7 and MDA-MB-231), using MTT-dye reduction assay. As presented in Table 1, the obtained results showed that most derivatives exert weak antiproliferative effects on the studied cancer cells lines. Compound **2a** bearing (*Z*)-3,5-dimethoxystyryl fragment on C5 position of benzoxazolone ring exhibited the highest activity with IC₅₀ of 19 μM against HL-60, 42 μM against MCF-7 and 76 μM against MDA-MB-231 cells. The corresponding *E*-isomer **3a** was inactive, but the hydroxy substituted *E*-stilbene **4a** exerted a similar cytotoxic potential as **2a**.

Table 1. Cytotoxic effects (expressed as IC₅₀) of compounds **2a-b** – **4a-b** on HL-60, MCF-7 and MDA-MB-231 cell lines.

Compd	IC ₅₀ (μM)±SD		
	HL-60	MCF-7	MDA-MB-231
2a	19±1.1	42±2.1	76±3.2
2b	13±1.3	> 200	> 200
3a	> 200	> 200	> 200
3b	> 200	40±2.2	> 200
4a	38±1.7	42±1.8	105±3.7
4b	> 200	84±2.9	> 200

These results showed that the biological activity of the compounds **2a-b** – **4a-b** was influenced by the position of the styryl fragment in a

benzoxazolone ring as the obtained 5-styrylbenzoxazolones were generally more active in compare to the corresponding 6-styrylbenzoxazolone positional isomers. Disregarding the configuration of the double bond in tested derivatives, the introduction of 3,5-dimethoxystyryl or 3,5-dihydroxystyryl moiety on C5 position of the heterocyclic system led to compounds closely resembling resveratrol.

CONCLUSION

In this study we reported the synthesis of six heterocycle analogues of resveratrol, containing a benzoxazolone ring. Evaluation of the cytotoxicity of the stilbene derivatives on HL-60, MCF-7 and MDA-MB-231 cancer cell lines showed that (*Z*)-3-methyl-5-(3,5-dimethoxystyryl)-2(3*H*)-benzoxazolone (**2a**) and (*E*)-3-methyl-5-(3,5-dihydroxystyryl)-2(3*H*)-benzoxazolone (**4a**) were the most active in the series.

Acknowledgements: The authors are thankful to the Sofia University Scientific Research Fund (grants 85/2009, 99/2011) and the University of Forestry, Sofia, Bulgaria (grant 12/19.01.2016) for the financial support.

REFERENCES

1. F. Wolter, J. Stein, *Drugs Future*, **27**, 949 (2002).
2. P. Saiko, A. Szakmary, W. Jaeger, T. Szekeres, *Mutat. Res.*, **658**, 68 (2008).
3. J. M. Smoliga, J. A. Baur, H. A. Hausenblas, *Mol. Nutr. Food Res.*, **55**, 1129 (2011).

4. C.-F. Wu, J.-Y. Yang, F. Wang, X.-X. Wang, *Chin. J. Nat. Med.*, **11**, 1 (2013).
5. H.-Y. Tsai, C.-T. Ho, Y.-K., Chen, *J. Food Drug Anal.*, **25**, 134 (2017).
6. B. B. Aggarwal, A. Bhardwaj, R. S. Aggarwal, N. P. Seeram, S. Shishodia, Y. Takada, *Anticancer Res.*, **24**, 2783 (2004).
7. F. Brisdelli, G. D'Andrea, A. Bozzi, *Curr. Drug Metab.*, **10**, 530 (2009).
8. M. Athar, J. H. Back, X. Tang, K. H. Kim, L. Kopelovich, D. R. Bickers, A. L. Kim, *Toxicol. Appl. Pharmacol.*, **224**, 274 (2007).
9. J. K. Kundu, Y.-J. Surh, *Cancer Lett.*, **269**, 243 (2008).
10. M. Roberti, D. Pizzirani, D. Simoni, R. Rondanin, R. Baruchello, C. Bonora, F. Buscemi, S. Grimaudo, M. Tolomeo, *J. Med. Chem.*, **46**, 3546 (2003).
11. Y. Schneider, P. Chabert, J. Stutzmann, D. Coelho, A. Fougerousse, F. Gosse J.-F. Launay, R. Brouillard, F. Raul, *Int. J. Cancer*, **107**, 189 (2003).
12. D. Simoni, M. Roberti, F. Paolo Invidiata, E. Aiello, S. Aiello, P. Marchetti, R. Baruchello, M. Eleopra, A. Di Cristina, S. Grimaudo, N. Gebbia, L. Crosta, F. Dielig, M. Tolomeo, *Bioorg. Med. Chem. Lett.*, **16**, 3245 (2006).
13. R. Csuk, S. Albert, B. Siewert, S. Schwarz, *Eur. J. Med. Chem.*, **54**, 669 (2012).
14. J. J. Heynekamp, W. M. Weber, L. A. Hunsaker, A. M. Gonzales, R. A. Orlando, L. M. Deck, D. L. V. Jagt, *J. Med. Chem.*, **49**, 7182 (2006).
15. J. Poupaeert, P. Carato, E. Colacino, *Curr. Med. Chem.*, **12**, 877 (2005).
16. M. S. Gerova, S. R. Stateva, E. M. Radonova, R. B. Kalenderska, R. I. Rusew, R. P. Nikolova, C. D. Chaney, B. L. Shivachev, M. D. Apostolova, O. I. Petrov, *Eur. J. Med. Chem.*, **120**, 121 (2016).
17. T. Mosmann, *J. Immunol. Methods*, **65**, 55 (1983).
18. A. Bakalova, R. Buyukliev, I. Tcholakova, G. Momekov, S. Konstantinov, M. Karaivanova, *Eur. J. Med. Chem.*, **38**, 627 (2003).

СИНТЕЗ И ЦИТОТОКСИЧНА АКТИВНОСТ НА НОВИ ХЕТЕРОЦИКЛЕНИ АНАЛОЗИ НА РЕСВЕРАТРОЛ, СЪДЪРЖАЩИ БЕНЗОКСАЗОЛОНОВ ПРЪСТЕН

М. С. Герова¹, Е. А. Александрова^{1,2}, Й. Б. Иванова³, Д. В. Станишева¹, Г. Цв. Момеков⁴, О. И. Петров^{1*}

¹ Катедра Фармацевтична и приложна органична химия, Факултет по Химия и фармация, Софийски университет "Св. Климент Охридски", бул. Джеймс Баучър 1, София 1164, България

² Катедра Обща и клинична патология, Медицински факултет, Тракийски Университет, ул. Армейска 11, Стара Загора 6000, България

³ Катедра Патология на растенията и химия, Факултет по Екология и ландшафтна архитектура, Лесотехнически университет, бул. Климент Охридски 10, София 1756, България

⁴ Катедра Фармакология, фармакотерапия и токсикология, Фармацевтичен факултет, Медицински университет – София, ул. Дунав 2, София 1000, България

Постъпила на 01 март 2017 г.; Коригирана на 15 март 2017 г.

(Резюме)

Синтезирани са нови хетероцикленни аналози на ресвератрол като потенциални противоракови средства. Съединенията съдържат 3,5-диметокси- или 3,5-дихидроксистирилов фрагмент, въведен в позиция С5 или С6 на бензоксазолонив пръстен. Цитотоксичната активност на съединенията е изследвана върху три туморни клетъчни линии (HL-60, MGF-7 and MDA-MB-321) и получените резултати показват, че някои от тях проявяват добър антипролиферативен ефект. В повечето случаи, 5-стирилбензосазолоните са по-активни в сравнение с техните позиционни изомери, съответните 6-стирилбензосазолони.

Synthesis, characterization and microbiological activity of a Zn(II) complex of a novel benzofurazan derivative

I. Grabchev^{1*}, T. Gajda², S. Yordanova³, S. Purák², E. Vasileva-Tonkova⁴, S. Stoyanov³

¹ Sofia University "St. Kliment Ohridski", Faculty of Medicine, 1407 Sofia, Bulgaria

² Department of Inorganic and Analytical Chemistry, University of Szeged, Dóm tér 7, H-6720 Szeged, Hungary

³ Sofia University "St. Kliment Ohridski", Faculty of Chemistry and Pharmacy, 1164 Sofia, Bulgaria

⁴ Institute of Microbiology and Crystallography, Bulgarian Academy of Sciences, 1113 Sofia, Bulgaria

Received January 31, 2017; Revised February 14, 2017

Dedicated to Acad. Bogdan Kurtev on the occasion of his 100th birth anniversary

Complex formation of Zn(II) and Al(III) ions with a novel 4-nitro-benzofurazan-cyclam conjugate has been investigated by ¹H-NMR and electronic (UV-vis and fluorescence) spectroscopy in dimethylsulfoxide. A stable Zn(II) complex [Zn(**P1**)(NO₃)₂] has been isolated, characterised, and *in vitro* its antimicrobial activity was tested. Good antibacterial activity against several Gram-positive and Gram-negative bacteria and antifungal activity against two yeasts has been observed.

Key words: metal complexes, cyclam, benzofurazane, microbiological, NMR

INTRODUCTION

In recent years, much attention has focused on the synthesis of new metal complexes of biologically important metal ions such as Cu²⁺, Co²⁺, Zn²⁺, Fe²⁺, Fe³⁺ with various organic ligands as potential antimicrobial agents which improve antifungal or antibacterial activity of existing chemotherapeutics [1–5]. On the other hand, the design and synthesis of specific ligands which can coordinate to metal ions is a major goal to many research groups because the biological activity of the metal complexes depend not only on the nature of the metal ions and the chemical structure of the ligands, but also on the type of bonding between them. Although some metal complexes with organic ligands showed very good antimicrobial activity, studies are still in search of new highly active antibacterial and antifungal compounds. This reflects the fact that many of the clinical pathogens quickly become resistant to chemotherapy applied in practice.

Cyclam (1,4,8,11-tetraazacyclotetradecane) is a cyclic polyamine most widely used as a ligand in medical chemistry research which is due to its commercial availability and the easy linking of nitrogen atoms to functional units. In this case the coordination sites of cyclam-cored derivatives are the tertiary amino groups from cyclam ring. The

complexes with biologically important metal ions have been investigated with regard to their potential biomedical applications [6-10]. Recently we have investigated *in-vitro* anticancer, antibacterial and antifungal activity of a new Cu(II) complex of modified cyclam with four 7-nitro-2,1,3-benzoxadiazoles units bonded to its cyclic nitrogen atoms [11].

In this paper we present the Zn(II) complex formation of modified cyclam with four 4-amino-7-nitro-2,1,3-benzoxadiazoles units. The chemical structure, composition and association constants were confirmed and analysed by electronic (UV/Vis and fluorescence), Fourier transform infrared (FTIR), nuclear magnetic resonance (NMR) spectroscopy, and scanning electron microscopy (SEM). The antimicrobial activity of the ligand and its Zn-complex has also been investigated against different pathogens.

EXPERIMENTAL

Materials and Methods

The synthesis of initial ligand **P1** has been described recently [11]. UV/Vis spectrophotometric investigations were performed using a Unicam Helios α spectrophotometer. The fluorescence spectra were taken on a Hitachi F-4500 spectrofluorimeter. All spectra were corrected to dilution, and the fluorescence spectra were also corrected for the inner filter effect using the

* To whom all correspondence should be sent:
E-mail: i.grabchev@chem.uni-sofia.bg

equation $IF_{\text{corr}} = IF_{\text{measured}} \times 10^{(A_{\text{ex}} + A_{\text{em}})/2}$, where IF_{measured} is the measured emitted fluorescence intensity, A_{ex} and A_{em} are the UV-Vis absorption of the solution at the wavelengths of excitation and emission, respectively [12]. All absorption and fluorescence spectra were recorded using 1 cm pathlength synthetic quartz cells at concentration of 2.2×10^{-5} mol l⁻¹. Zn(NO₃)₂·5H₂O and Al(NO₃)₃·9H₂O (Aldrich) were used as a sources of Zn(II) and Al(III) ions respectively. IR spectra were recorded on an Infrared Fourier transform spectrometer (IRAffinity-1 Shimadzu) with the diffuse-reflectance attachment (MIRacle Attenuated Total Reflectance Attachment) at a 2 cm⁻¹ resolution. The ¹H NMR measurements were performed on a Bruker Avance DRX 500 spectrometer. The measurements were carried out in a DMSO-d₆ solution at ambient temperature. The chemical shifts were referenced to a tetramethylsilane (TMS) standard. Electrospray mass spectroscopic measurements were carried out using a Hewlett-Packard Series 110 0 MSD. The surface morphology of P1 and [Zn(P1)(NO₃)₂] was analyzed by scanning electron microscope (SEM) JSM-5510 (JEOL), operated at 10 kV of acceleration voltage. Before imaging, the investigated samples were coated with gold by JFC-1200 fine coater (JEOL).

Synthesis of Zn(II) complex [Zn(P1)(NO₃)₂]

The mixture of P1 (85.2 mg 0.01 mmol) and Zn(NO₃)₂·5H₂O (27.95 mg, 0.01 mmol) in ethanol solution was refluxed for 1 hour and kept overnight at room temperature. The solid complex formed was filtered, washed with ethanol (10 ml, 3 times) and finally dried under vacuum. Yield: 90.7 mg (89.9%). FT-IR (cm⁻¹): 3097, 2948, 2860, 1613, 1540, 1492, 1428, 1276, 1235, 1101, 997, 919, 807, 738; ¹H-NMR (CDCl₃) ppm: 8.61-8.44 (m, 4 Ar-H), 6.94-6.547 (m, 4 Ar-H), 4.49-3.94 (m, 8H, -CH₂-), 3.02-2.89 (m, 8H, -CH₂-), 2.28-1.71 (4 H, -CH₂-). API-ES-MS (positive) m/z: calcd: 1009.73 found 1010.89 (M+H)⁺. Elemental analysis C₃₄H₂₈N₁₈O₁₆Zn: Calc: C- 40.40%; H-2.77%; N-24.95%, Found: C- 40.48%; H-2.71%; N-25.06%.

Antimicrobial assay

The antimicrobial activities of the new compounds, ligand P1 and [Zn(P1)(NO₃)₂] complex, were screened by the agar well diffusion method using DMSO as a solvent. Antibacterial activity was tested against Gram-positive bacteria

Bacillus subtilis, *Bacillus cereus* ATCC 11778 and *Micrococcus luteus*, and Gram-negative bacteria *Pseudomonas aeruginosa*, *Escherichia coli*, *Acinetobacter johnsonii*, *Xanthomonas oryzae* and *Serratia* sp. Antifungal activity was tested against the yeasts *Candida lipolytica* and *Saccharomyces cerevisiae*. The investigated compounds were dissolved in DMSO to obtain stock solution with concentration 5 mg/ml. A lawn of microbial cultures was prepared by spreading aliquots (0.1 ml) of overnight inoculums onto Müller-Hinton agar in Petri plates. Tests were performed using 0.1% and 0.5% of sample solutions, of which equal amount (40 μl) was added into wells (7 mm in diameter) bored into the agar. Simultaneously, gentamicin (G, 10 μg/disc) and nystatin (NS, 100 units/disc) were used as standard antibacterial and antifungal agents, respectively. After incubation of the plates at 25 °C for 24-48 h, the clear inhibition zones around the wells were measured (mm in diameter including well/disc).

RESULTS AND DISCUSSION

In order to study the metal ion binding properties of P1 we applied ¹H NMR, UV-Vis and fluorimetric methods in DMSO solutions.

¹H NMR studies

The ¹H-NMR spectrum of P1 consists of four groups of signals (Fig. 1). The aromatic protons of 7-nitrobenzofurazane (NBD) moieties close to the ring nitrogen atoms and the CH₂ protons adjacent to ring nitrogens appear at 6.53 ppm and between 2.83-2.94 ppm, respectively, while the signals of C-CH₂-C protons are around 1.76 ppm.

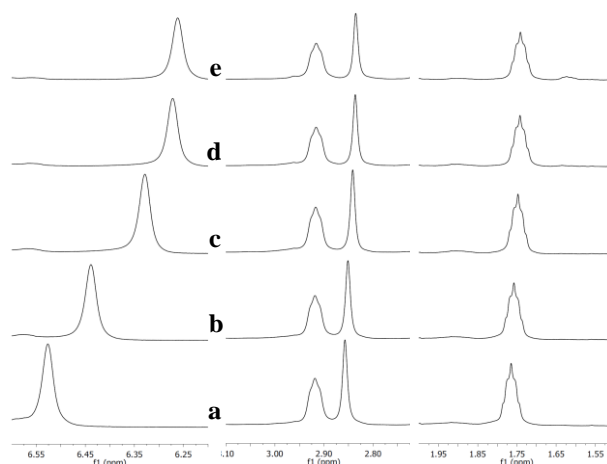


Fig. 1. ¹H NMR spectra of P1 as a function of increasing Zn(II) concentration ([Zn(II)]/[P1] = 0/1 (a), 1/3 (b), 7/10 (c), 1/1 (d), 2/1 (e)), [P1] = 2.5 mM.

Increasing concentration of the diamagnetic Zn(II) ions results upfield shift of the aromatic signals (Fig. 1). This may indicate the involvement of these units in the metal ion binding. The shift of aromatic protons as a function of Zn(II)-to-ligand P1 ratio is depicted in Fig. 1. Since at $[Zn^{2+}]/[P1] = 1$ a sharp breakpoint can be observed (Fig. 2), the stoichiometry of the formed species is clearly 1:1, however based on these data only a lower limit of the stability constant of $[Zn(P1)]^{2+}$ can be estimated ($\log K \geq 5.5$).

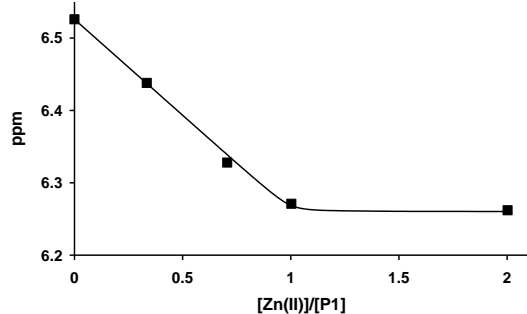


Fig. 2. Shift of the aromatic protons of **P1** as a function of zinc(II)/[**P1**] ratio (see also Fig. 1). The black line is the calculated curve with $\log K = 5.5$.

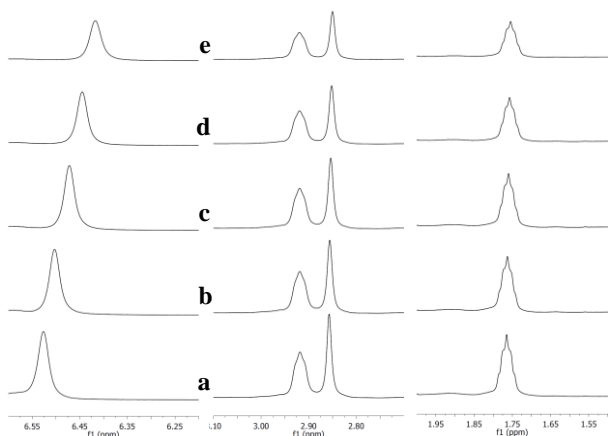
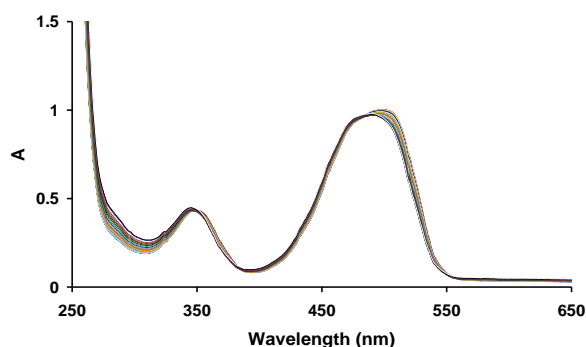


Fig. 3. 1H NMR spectra of **P1** as a function of increasing Al(III) concentration ($[Al(III)]/[P1] = 0/1$ (a), $1/3$ (b), $1/1$ (c), $2/1$ (d), $5/1$ (e), $[P1] = 2.5$ mM).



Similarly to Zn(II), the interaction between ligand **P1** and Al(III) ions results in up field shift of the proton signals (Fig. 3). The effect of increasing Al(III) concentration on the chemical shift of aromatic protons are plotted in Fig. 4. Assuming the formation of a single $[Al(P1)]^{3+}$ species the experimental data can be well reproduced using $\log K_{Al(P1)} = 2.49$.

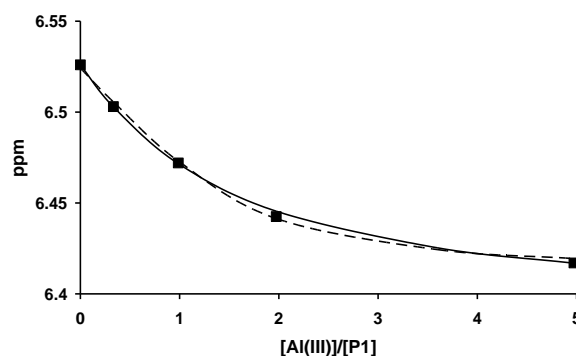


Fig. 4. Shift of the aromatic protons of **P1** as a function of Al(III)/[**P1**] ratio. The solid line is fitted curve with $\log K = 2.49$, for the dashed line see the text.

UV-Vis and fluorescence study

Due to the intense UV-Vis and fluorescence spectra of **P1** these techniques allow to study the metal-ligand interaction at considerably lower concentration range (0.01-0.02 mM) and therefore at much higher metal/ligand ratios than in the case of NMR spectroscopy. Parallel absorption and fluorimetric measurements have been performed in the case of Zn(II). The both methods showed similar change upon increasing concentration of Zn(II): a smaller but well detectable change of intensities up to 1/1 metal to ligand ratio, and a more important change at much higher metal-to-ligand ratio (Fig. 5 and Fig. 6).

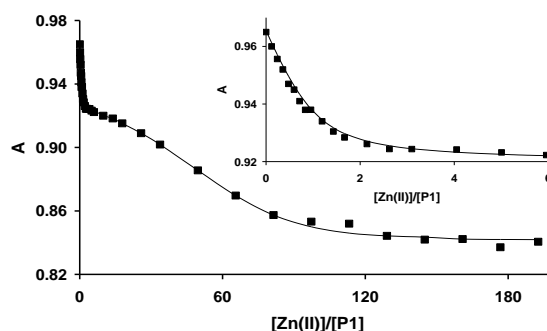


Fig. 5. Absorption spectra (left) and their absorption change at $\lambda_A = 510$ nm (right) of **P1** ($c = 0.022$ mM) at different concentration of Zn (II) ions ($c = 0 - 4.2$ mM); The solid line is fitted curve with $\log K_{Zn(P1)} = 5.3$ and $\log K_{Zn_2(P1)} = 2.6$.

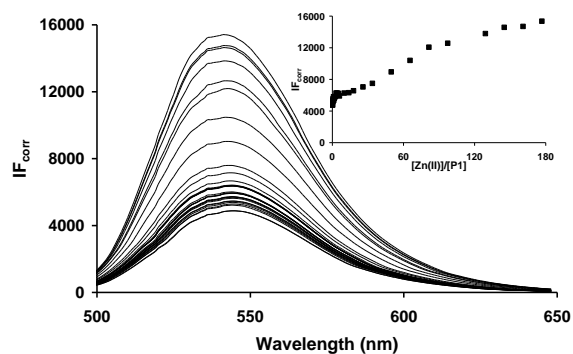


Fig. 6. Fluorescence spectra of the **P1** ($c = 0.022$ mM), as a function of Zn(II) ions concentration ($c = 0$ – 3.9 mM), $\lambda_{\text{ext}} = 480$ nm. The insert shows the intensity change at $\lambda_{\text{F}} = 540$ nm.

These facts indicate the successive formation of two species. The first complex $[\text{Zn}(\text{P1})]^{2+}$ has rather high thermodynamic stability, while the second one has a lower association constant ($[\text{Zn}(\text{P1})]^{2+} + \text{Zn}^{2+} = [\text{Zn}_2(\text{P1})]^{4+}$, $\log K_{\text{Zn}_2(\text{P1})}$). Since the precision of the absorption spectra is much higher than that of the fluorescence spectra, the former was used to derive the stability constants of the Zn(II) complexes ($\log K_{\text{Zn}(\text{P1})} = 5.3 \pm 0.2$ and $\log K_{\text{Zn}_2(\text{P1})} = 2.6 \pm 0.3$, see Fig. 5 right). The stability constant obtained for the species $[\text{Zn}(\text{P1})]^{2+}$ from the UV-Vis data agree well with that calculated based on the NMR measurements (the formation of the dinuclear $[\text{Zn}_2(\text{P1})]^{4+}$ complex was negligible under the conditions used for the NMR study). On the other hand, the formation of dinuclear complex indicates the participation of NBD moieties, too, in the metal ion coordination at higher concentrations of Zn(II) ions.

The increasing concentration of Al(III) also resulted in well-defined changes on the spectral properties. The effect on the UV-Vis spectra was similar to that of Zn(II) (Fig. 7). However, considerable increase on the emission spectra was observed (Fig. 8), even at low Al(III) concentrations. The concentration dependence of the emission intensity at $\lambda_{\text{F}} = 544$ nm is depicted in the insert of Fig. 8. Again, these data can be fitted only by the assumption that two successively formed complexes are present, like in the case of Zn(II). The best fit of the experimental data was obtained by $\log K_{\text{Al}(\text{P1})} = 4.5 \pm 0.2$ and $\log K_{\text{Al}_2(\text{P1})} = 2.8 \pm 0.3$ (Fig. 8). This observation is, however, virtually very different from that obtained by NMR. However, the fluorescence study allowed to collect considerably higher number of experimental points

in a wider range of $[\text{Al(III)}]/[\text{P1}]$ ratios, it provides more complete and therefore more correct description of complex formation equilibria. Indeed, using the latter model, the NMR data can be reproduced very well (within 0.003 ppm, see dashed line in Fig. 4).

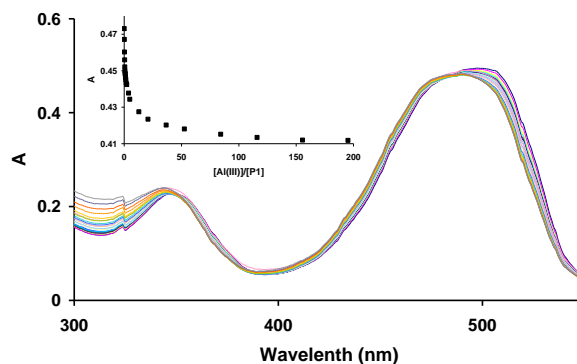


Fig. 7. Absorption spectra of **P1** ($c=0.0104$ mM) in the presence of different concentrations of Al(III) ($c = 0$ – 2.0 mM). The insert shows the changes of absorbance at 510 nm.

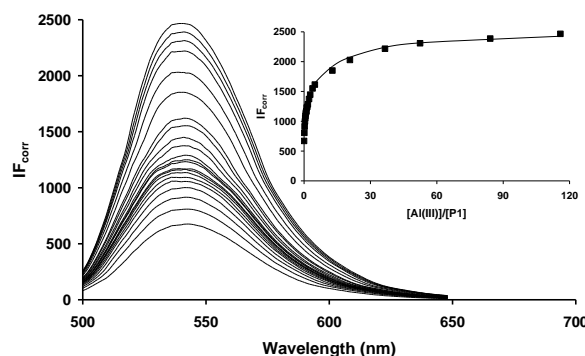
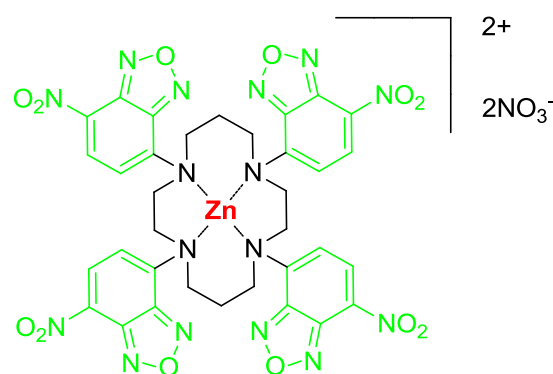


Fig. 8. Fluorescence spectra of **P1** ($c = 0.0104$ mM) in the presence of different concentrations of Al(III) ($c = 0$ – 1.3 mM), $\lambda_{\text{ex}} = 480$ nm); The insert shows the intensity change at $\lambda_{\text{F}} = 540$ nm. The solid line is fitted curve with $\log K_{\text{Al}(\text{P1})} = 4.5$ and $\log K_{\text{Al}_2(\text{P1})} = 2.8$.

FT-IR spectral characteristics of P1 and $[\text{Zn}(\text{P1})(\text{NO}_3)_2]$

In Fig. 9 the IR spectra of ligand **P1** and its Zn(II) complex are plotted. Their comparison shows a significant difference in the spectra of the metal complex where the characteristic peaks for nitrate group ($-\text{NO}_3$) were registered in the 1100–1600 cm^{-1} region. Valence asymmetric vibrations were occurs at 1530–1580 cm^{-1} and the respective symmetrical vibrations are at 1230–1290 cm^{-1} . In this spectral region the characteristic bands assigned to benzofurazan structure are superimposed with those of the nitrate ions, bonded

to the Zn(II) ions. The only differences in the spectrum of the complex are the intensity of the bands. Furthermore, there is no difference in the position of the respective peaks in the spectral region where other functional groups from benzofurazan moiety absorb, what indicates that they do not participate in the formation of coordination bonds with Zn(II). That allows the assumption that, the coordination is realized via the tertiary amine groups in the cyclam ring, as shown in Formula 1.



Formula 1. Chemical structure of [Zn(**P1**)(NO₃)₂].

SEM-analysis

Scanning electron microscopy technique has been used to study the morphological change in **P1** before and after the complex formation with Zn(II). At low amplification an agglomerated morphology has been observed for **P1**. At higher amplification microstructure of **P1** showed compact structure with smaller flakes, however after complex formation the micro structure changes and convert to homogeneous solid with grains as shown in Fig. 10.

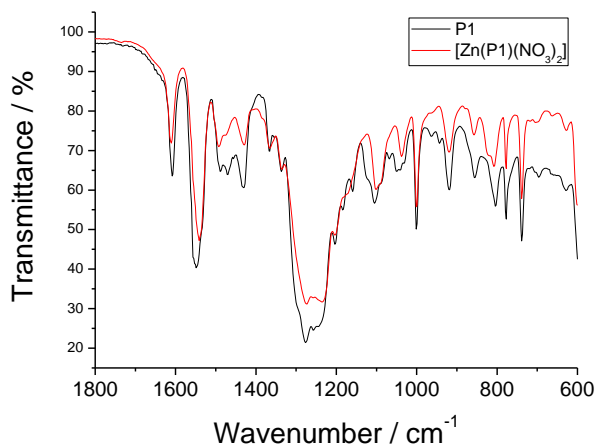


Fig. 9. IR spectra of ligand **P1** and its Zn(II) complex.

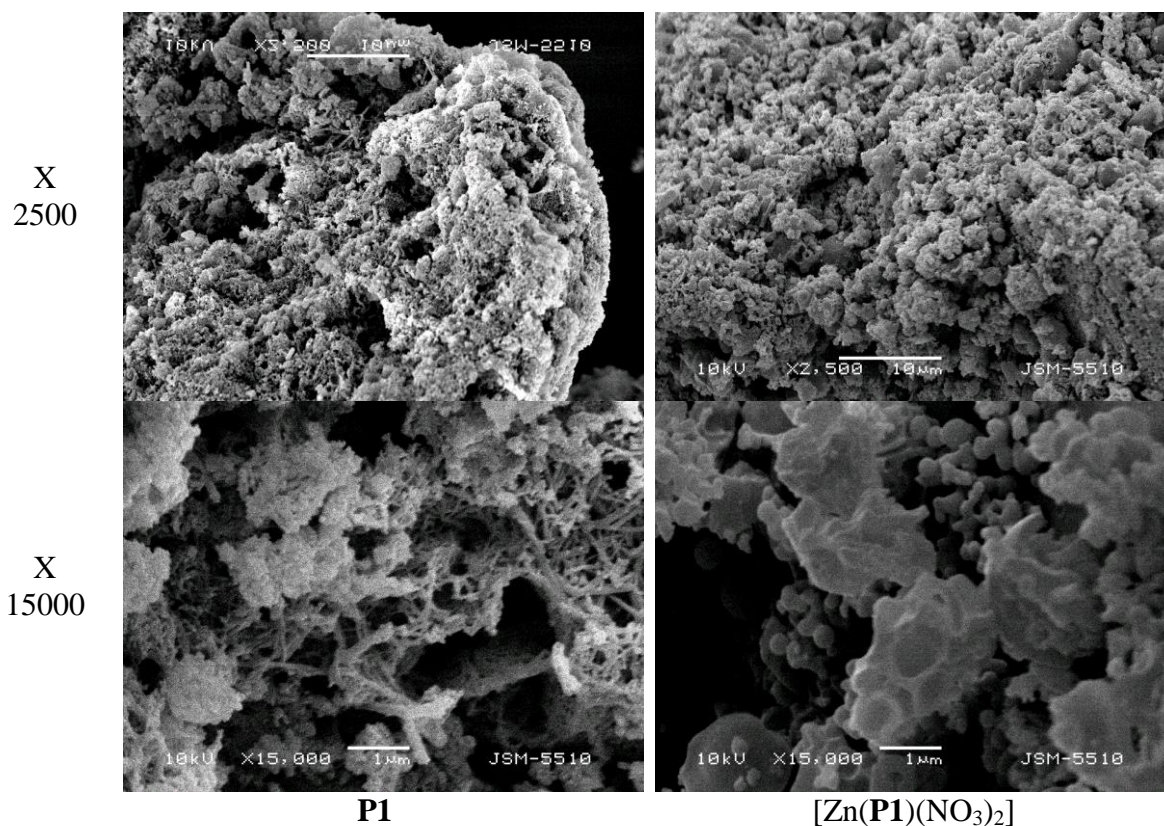


Fig. 10. SEM micrographs of **P1** and [Zn(**P1**)(NO₃)₂] at different amplifications.

The difference is best pronounced at amplification of 15000 where **P1** ligand shows a lattice and reticulation structure while the complex $[\text{Zn}(\text{P1})(\text{NO}_3)_2]$ retains the structure of microspheres. Most probably the interaction of Zn(II) with the cyclam ring causes this change in the morphology.

Antimicrobial activity

The antimicrobial activities of the new compounds were tested *in vitro* against eight bacterial and two yeasts cultures and expressed by the zones of inhibition. Free ligand and its zinc complex showed variable inhibition activity against different test cultures except *P. aeruginosa*, and this activity was differently enhanced on coordination (Fig. 11). The inhibition effect of the complex $[\text{Zn}(\text{P1})(\text{NO}_3)_2]$ was better or comparable to that expressed by the control **P1** against the eight

bacterial test cultures, and about 2.5-fold higher than **P1** against the yeasts *C. lipolytica* (Fig. 11 and Fig. 12). The antimicrobial activity of the zinc complex ranged from good against the yeasts and the test bacteria *B. cereus*, *X. oryzae* and *Serratia* sp. (zones of inhibition in the range 16-20 mm), to moderate against *B. subtilis* and *E. coli* (zones of inhibition 12-13 mm) and weak (zones of inhibition 11 mm) against *M. luteus* and *A. johnsonii*. The obtained results of antimicrobial activity of the zinc complex are similar to those reported for the copper complex [11].

Coordination to biologically active molecules to metal ions can be used as a strategy to enhance their biological activity [2, 3]. The enhancement in biological activity of metal complexes upon coordination can be explained on the basis of Overtone's concept and chelation theory [13].

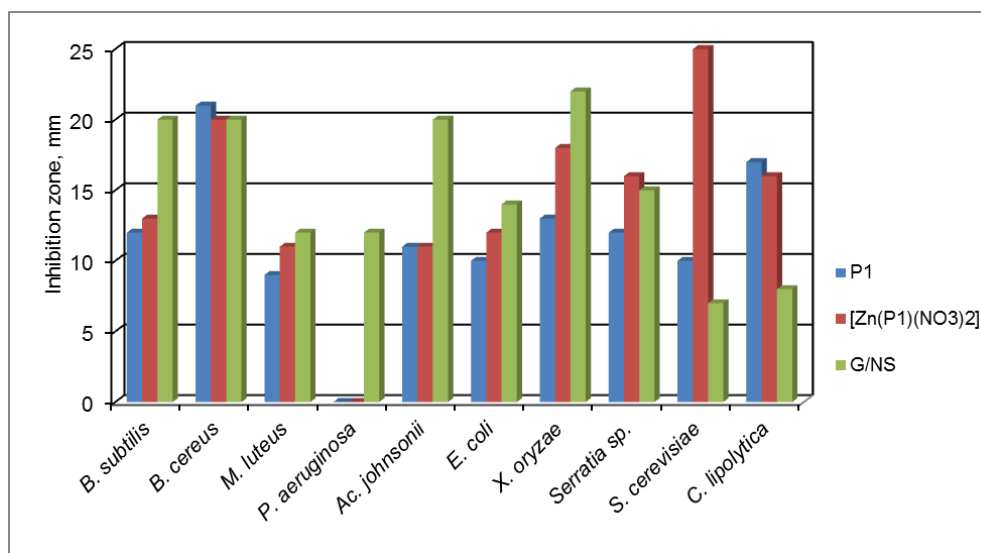


Fig. 11. Inhibition of the growth of test bacteria and yeasts by 0.5% solutions of ligand **P1** and complex $[\text{Zn}(\text{P1})(\text{NO}_3)_2]$. G/NS, Gentamicin/Nystatin was used as a standard antibacterial/antifungal agent.

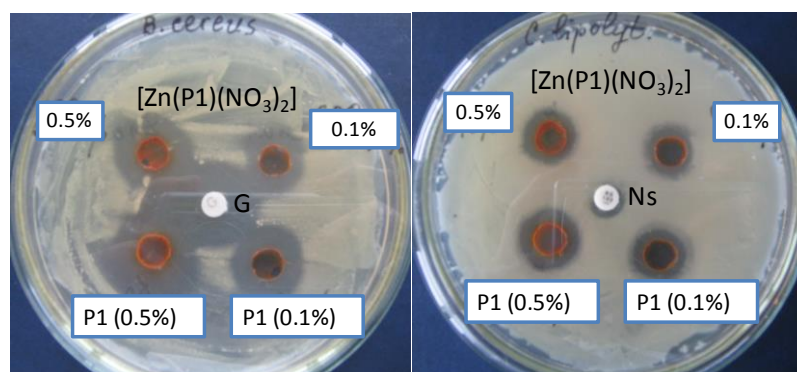


Fig. 12. Zones of inhibition of the growth of *B. cereus* and *C. lipolytica* by 0.1% and 0.5% **P1** and $[\text{Zn}(\text{P1})(\text{NO}_3)_2]$ compounds. Gentamicine (G) and Ns, (Nystatin) were used as a standard antibacterial and antifungal agent, respectively.

CONCLUSION

The effect of Zn(II) and Al(III) ions on the UV-Vis, fluorescence and ¹H NMR spectra of **P1** was studied in DMSO solution and it was shown that cyclam-4-nitro-benzofurazan conjugate may form both mono- and dinuclear complexes. The formation of dinuclear complexes at higher metal-to-ligand ratios indicates the participation of NBD moieties, too, in the metal ion coordination. On the other hand, the relatively strong binding of **P1** to Al(III) may suggest the participation of oxygen atoms of NBD residues. The antimicrobial studies suggested that the ligand is biologically active, and its zinc complex showed enhanced antibacterial and antifungal activity against microbial strains in comparison to the free ligand. Significant activity of the new compounds observed against the test pathogenic *B. cereus* and *C. lipolytica* makes them promising candidates in designing new antimicrobial preparations. Besides, significant activity of the zinc complex against phytopathogenic bacteria *X. oryzae* suggests its potential suitability for use for plant protection.

Acknowledgements: The authors acknowledge Grant No. H 09/03-2016, Fund “Scientific Research”, Ministry of Education and Science of Bulgaria. IG and TG also acknowledge the COST Action MP1304: The Network for the Biology of Zinc (Zinc-Net) for supporting the networking.

REFERENCES

1. I. Sousa, V. Claro, J. L. Pereira, A. L. Amaral, L. Cunha-Silva, B. Castro, M. J. Feio, E. Pereira, P. Gameiro, *J. Inorg. Biochem.*, **110**, 64 (2012).
2. M. O. Agwara, M. D. Yufanyi, J. N. Foba-Tendo, M. A. Atamba, D. T. Ndinteh, *J. Chem. Pharm. Res.*, **3**, 196 (2011).
3. K. L. Haas, K. J. Franz, *Chem. Rev.*, **109**, 4921 (2009).
4. X. Liang, P. J. Sadler, *Chem. Soc. Rev.*, **33**, 246 (2004).
5. E. Aktan, A. B. Gündüzalp, Ü. O. Ozmen, *J. Mol. Struct.*, **1128**, 775 (2017).
6. R. E. Mewis, S. J. Archibald, *Coord. Chem. Rev.*, **254**, 1686 (2010).
7. L. G. Alves, M. Souto, F. Madeira, P. Adão, R. F. Munhá, A. M. Martins, *J. Organomet. Chem.*, **760**, 130 (2014).
8. S. Tan, K. Han, Q. Li, L. Tong, Y. Yang, Z. Chen, H. Xie, J. Ding, X. Qian, Y. Xu, *Eur. J. Med. Chem.*, **85**, 207 (2014).
9. X. Liang, P. J. Sadler, *Chem Soc Rev*, **33**, 246 (2004).
10. F. Liang, S. Wan, Z. Li, X. Xiong, L. Yang, X. Zhou, C. Wu, *Curr. Med. Chem.*, **13**, 711 (2006).
11. I. Grabchev, S. Yordanova, E. Vasileva-Tonkova, M. Cangiotti, A. Fattori, R. Alexandrova, S. Stoyanov, M. F. Ottaviani, *Dyes Pigm.*, **129**, 71 (2016).
12. J. R. Lakowicz, Principles of Fluorescence Spectroscopy, Third Edition, Springer Science Business Media, LLC, 2006.
13. P. B. Pansuriya, M. N. Patel, *J. Enzyme Inhib. Med. Chem.*, **23**, 108 (2008).

СИНТЕЗ, ОХАРАКТЕРИЗИРАНЕ И МИКРОБИОЛОГИЧНА АКТИВНОСТ НА НОВ Zn(II) КОМПЛЕКС С ПРОИЗВОДНО НА БЕНЗОФУРАЗАНА

И. Грабчев^{1*}, Т. Гайда², С. Йорданова³, С. Пурак², Е. Василева-Тонкова⁴, С. Стоянов³

¹ Софийски Университет “Св. Климент Охридски”, Медицински факултет, 1407 София, България

² Департамент по неорганична химия, Университет в Сегет, H-6720 Сегет, Унгария

³ Университет “Св. Климент Охридски”, Факултет по химия и фармация, 1164, София, България

⁴ Институт по микробиология, Българска академия на науките, 1113 София, България, Bulgaria

Постъпила на 31 януари 2017 г.; Коригирана на 14 февруари 2017 г.

(Резюме)

Чрез ¹H ЯМР, UV-Vis и флуоресцентна спектроскопия е проследено образуването на Zn(II) и Al(III) комплекси с използване на модифициран с 4-нитро-бензофуразан циклам като лиганд. Стабилен Zn(II) комплекс [Zn(**P1**)(NO₃)₂] е изолиран, охарактеризиран и неговата антимикробна активност е изследвана *in vitro* спрямо различни грам положителни и грам отрицателни бактерии и два вида дрожди. Установена е добра микробиологична активност спрямо тестваните култури.

Synthesis, characterization and *in vitro* cytotoxic activity of zinc(II), cobalt(II) and nickel(II) complexes with tridentate ONO Schiff base 3-methoxysalicylaldehyde benzoylhydrazone

B. I. Nikolova-Mladenova^{1*}, G. Ts. Momekov²

¹Department of Chemistry, Faculty of Pharmacy, Medical University of Sofia, 2 Dunav, Street, 1000 Sofia, Bulgaria

²Department of Pharmacology, Pharmacotherapy and Toxicology, Faculty of Pharmacy, Medical University of Sofia, 2 Dunav, Street, 1000 Sofia, Bulgaria

Received February 20, 2017; Revised March 15, 2017

Dedicated to Acad. Bogdan Kurtev on the occasion of his 100th birth anniversary

New Zn(II), Co(II) and Ni(II) complexes were synthesized with a cytotoxic ligand 3-methoxysalicylaldehyde benzoylhydrazone. IR, UV-Vis spectroscopy and elemental analysis techniques were applied for characterization. The spectral data of the complexes were interpreted on the basis of comparison with the spectrum of the free ligand. The complexes are mononuclear with 1:2 metal-to-ligand molar ratios. The analysis revealed coordination through phenolic-oxygen, azomethine-nitrogen and amide-oxygen atoms. The new complexes were tested for *in vitro* cytotoxicity against a panel of human leukemic and tumor cell lines by MTT-dye reduction assay. The pharmacological screening showed that the Zn(II) complex causes 50% inhibition of the cellular viability in low micromolar concentrations. The Ni(II) complex is less active, whereas the Co(II) complex is practically devoid of cytotoxic effects.

Key words: 3-methoxysalicylaldehyde; aroylhydrazones; metal complexes; cytotoxic activity

INTRODUCTION

Hydrazones are widely studied biologically active compounds which exhibit an extensive spectrum of activities, such as anti-inflammatory [1, 2], analgesic [2], antituberculosis [3, 4], antibacterial [5], antimicrobial [6], anti-HIV [6, 7] and anticancer [6, 8, 9] activity. The wide variety of the observed pharmacological properties in combination with their relatively easy synthesis has made them attractive ligands. Aroylhydrazones of the type R-CO-NH-N=CH-R', derived by condensation of aromatic aldehydes and acid hydrazides form a series of biologically active ligands used in medicinal chemistry as iron chelators effective in chemotherapy of Fe overload diseases [10–13]. Besides the ability to chelate iron, hydrazones synthesized from salicylaldehyde and its derivatives additionally display an expressed antiproliferative activity [14–19]. Hydrazones obtained from 3-methoxysalicylaldehyde exerted potent antiproliferative effect on a wide spectrum of human tumor cell lines [16, 17]. This activity may be due to the high ability of the hydrazones to chelate Fe(III) from cells, and thereby, to inhibit the proliferation of the neoplastic cells [20]. Salicylaldehyde derived hydrazones are polydentate

ligands that contain many coordination centers and may chelate other metal ions which organisms use in their metabolism. Zinc is one of the most abundant transition metals in the human body that is essential for the structure and function of a large number of macromolecules and for a variety of enzymatic reactions, which mediate a wide range of biochemical and nutritional processes [21, 22]. It interacts with a wide range of organic ligands [23] and participates in the metabolism of RNA and DNA, signal transduction and gene expression. In blood plasma, zinc is bound to and transported by albumin (60%) and transferrin (10%) [24]. Cobalt is valuable for humans because it is a constituent of Vitamin B₁₂ which has a key role in the normal functioning of the brain and nervous system, and for blood formation (hemopoiesis). It is normally involved in the metabolism of all human cells, especially affecting DNA synthesis and regulation, but also fatty and amino acid metabolism [25, 26].

In view of the significant role played by transition metal ions and their complexes in biological systems, here we report the synthesis and characterization of zinc(II), cobalt(II) and nickel(II) complexes with a cytotoxic hydrazine, 3-methoxysalicylaldehyde benzoylhydrazone. The cytotoxic properties of the new complexes were tested by MTT-dye reduction assay on a panel of four different human leukemic cell lines.

* To whom all correspondence should be sent:
E-mail: boriananik@abv.bg

EXPERIMENTAL

Materials and measurements

All chemicals used for the synthesis of the compounds: 3-methoxysalicylaldehyde, benzhydrazone, $\text{Zn}(\text{CH}_3\text{COO})_2 \cdot 2\text{H}_2\text{O}$, $\text{Co}(\text{CH}_3\text{COO})_2 \cdot 4\text{H}_2\text{O}$, $\text{Ni}(\text{CH}_3\text{COO})_2 \cdot 4\text{H}_2\text{O}$, and 96% ethanol were purchased from commercial sources and used without any further purification. All of the other chemicals were of analytical grade. The carbon, nitrogen and hydrogen contents of the compounds were determined by elemental analyses on a "Euro Vector SpA" apparatus. The melting point of the ligand was determined in open capillary tube using a Büchi B-535 apparatus. The thermogravimetric analyses were performed on a Setaram Setsys TG-DSC 15 in air atmosphere with a heating rate of 10 °C/min. The IR spectra were recorded in solid state (in KBr pellets) on a Bruker Tensor 27 spectrophotometer in the range of 4000–400 cm^{-1} . The UV-Vis spectra were recorded on a Hewlett Packard 8452 spectrophotometer in DMSO. The ^1H NMR and ^{13}C NMR spectra of the ligand were recorded on a Bruker Avance DRX 250 in DMSO-d_6 solvent. Chemical shifts (δ) were reported in parts per million (ppm), J values were given in Hz.

The synthesis of the ligand was published in our previous work [16].

3-methoxysalicylaldehyde benzoylhydrazone: Yield 90%; m.p. 126–127 °C; Color: Pale yellow; Anal. Calcd for $\text{C}_{15}\text{H}_{14}\text{O}_3\text{N}_2 \cdot \text{H}_2\text{O}$: C 62.49, H 5.59, N 9.72. Found: C 62.59, H 5.63, N 9.68; IR (KBr) ν (cm^{-1}): 3366 (Ar-OH), 3207 (N-H), 1652 (C=O), 1607 (C=N), 1576 (C-NH), 1247 (C-O); ^1H NMR (250 MHz, DMSO-d_6) δ ppm: 3.81 (s, 3H, -OCH₃), 6.85 (t, 1H, $J = 7.88$ Hz, ArH_{aldehyde}), 7.02 (d, 1H, $J = 8$ Hz, ArH_{aldehyde}), 7.15 (d, 1H, $J = 7.75$ Hz, ArH_{aldehyde}), 7.56 (m, 3H, ArH_{hydrazone}), 7.96 (d, 2H, $J = 8$ Hz, ArH_{hydrazone}), 8.69 (s, 1H, CH=N), 11.08 (s, 1H, NH), 12.15 (s, 1H, OH). ^{13}C NMR (250 MHz, DMSO-d_6) δ ppm: 55.85 (OCH₃), 148.02 (CH=N), 162.98 (C=O).

Synthesis of the complexes

The metal complexes were obtained using the following general procedure: The corresponding metal acetates (1 mmol) were dissolved in 50% ethanol (10 mL) at constant stirring and heating at 30 °C. To avoid the hydrolysis of the metal salt some drops of concentrated CH_3COOH were added. The received solutions were slowly mixed drop-wise with the solution of 3-methoxysalicylaldehyde benzoylhydrazone (2

mmol) in boiling 96% ethanol (15 mL) and immediately precipitates were formed. The mixtures were stirred for 60 min to complete the reaction and then were allowed to stand undisturbed overnight at room temperature. Fine crystals were collected by filtration, washed with ethanol and dried over P_2O_5 in a vacuum desiccator.

Bis-(3-methoxysalicylaldehyde benzoylhydrazone) zinc (II) [$\text{Zn}(\text{C}_{15}\text{H}_{13}\text{O}_3\text{N}_2)_2$]: Yield 95%; Color: Yellow; Anal. Calcd for [$\text{Zn}(\text{C}_{15}\text{H}_{13}\text{O}_3\text{N}_2)_2$]: C 59.66, H 4.34, N 9.28. Found: C 59.55, H 4.51, N 9.17; IR (KBr) ν (cm^{-1}): 3197 (N-H), 1607 (C=O), 1542 (C=N), 518 (Zn-O), 433 (Zn-N).

Bis-(3-methoxysalicylaldehyde benzoylhydrazone) cobalt (II) [$\text{Co}(\text{C}_{15}\text{H}_{13}\text{O}_3\text{N}_2)_2$]: Yield 97%; Color: Bright brown; Anal. Calcd for [$\text{Co}(\text{C}_{15}\text{H}_{13}\text{O}_3\text{N}_2)_2$]: C 60.31, H 4.39, N 9.38. Found: C 59.86, H 4.64, N 9.15; IR (KBr) ν (cm^{-1}): 3194 (N-H), 1601 (C=O), 1541 (C=N), 525 (Co-O), 435 (Co-N).

Bis-(3-methoxysalicylaldehyde benzoylhydrazone) nickel (II) [$\text{Ni}(\text{C}_{15}\text{H}_{13}\text{O}_3\text{N}_2)_2$]: Yield 94%; Color: Dark yellow-greenish; Anal. Calcd for [$\text{Ni}(\text{C}_{15}\text{H}_{13}\text{O}_3\text{N}_2)_2$]: C 60.33, H 4.39, N 9.38. Found: C 60.22, H 4.63, N 9.24; IR (KBr) ν (cm^{-1}): 3196 (N-H), 1602 (C=O), 1540 (C=N), 525 (Ni-O), 438 (Ni-N).

Cell lines and culture conditions

The study was carried out with the following cell lines: HL-60 – human acute myeloid leukemia, established from the peripheral blood of a 35-year-old woman with acute myeloid leukemia; SKW-3 – T-cell leukemia, established from the peripheral blood of a 61-year-old man with T cell chronic lymphocytic leukemia; BV-173 – human B cell precursor leukemia, established from the peripheral blood of a 45-year-old man with chronic myeloid leukemia in blast crisis; K-562 – human chronic myeloid leukemia, established from the pleural effusion of a 53-year-old woman with chronic myeloid leukemia in terminal blast crisis, were purchased from the German Collection of Microorganisms and Cell Cultures (DSMZ, Braunschweig, Germany). The cell lines were cultured under standard conditions – RPMI-1640 liquid medium supplemented with 10% fetal bovine serum (FBS) and 2 mM L-glutamine, in cell culture flasks, housed at 37 °C in an incubator "BB 16-Function Line" Heraeus (Kendro, Hanau, Germany) with humidified atmosphere and 5% CO_2 . Cells were kept in log phase by supplementation with

fresh medium after removal of cell suspension aliquots, two or three times weekly.

Cytotoxicity assessment (MTT-dye reduction assay)

The cell viability after exposure to the tested compounds was assessed using the MTT [3-(4,5-dimethylthiazol-2-yl)-2,5-diphenyltetrazolium bromide] dye reduction assay as described by Mossman [27]. The method is based on the reduction of the yellow tetrazolium salt MTT to a violet formazan product via the mitochondrial succinate dehydrogenase in viable cells. Exponentially growing cells were seeded in 96-well flat-bottomed microplates (100 μL /well) at a density of 1×10^5 cells per ml and after 24 h incubation at 37 °C they were treated to various concentrations of the tested compounds for 72 h. For each concentration a set of 8 wells were used. After the exposure period with the test compounds 10 μL MTT solution (10 mg/mL in PBS) aliquots were added to each well. The microplates were further incubated for 4 h at 37 °C and the MTT-formazan crystals formed were dissolved through addition of 100 μL /well 5% HCOOH in 2-propanol. The MTT-formazan absorption was determined using a microprocessor controlled microplate reader (Labexim LMR-1) at 580 nm.

Bioassay data processing and statistics

The cell survival data were normalized as percentage of the untreated control (set as 100% viability), were fitted to sigmoidal dose response curves and the corresponding IC_{50} values (concentrations causing 50% suppression of cellular viability) were calculated using non-linear regression analysis (GraphPad Prizm Software for PC). The statistical processing of biological data included the Student's t-test whereby values of $p \leq 0.05$ were considered as statistically significant.

DNA fragmentation assay

The characteristic for apoptosis mono- and oligonucleosomal fragmentation of genomic DNA was detected using 'Cell Death Detection' ELISA (enzyme-linked immunosorbent assay) kit following a 24 h exposure to either ligand or Zn(II) and Ni(II) metal complexes. Cytosolic fractions of 1×10^4 HL-60 cells per group (treated or untreated controls) served as an antigen source in a sandwich ELISA, utilizing a primary anti-histone antibody-coated microplate and a secondary peroxidase-conjugated anti DNA-antibody. The photometric

immunoassay for histone-associated DNA-fragments was executed according to the manufacturer's instructions at 405 nm, using a microprocessor-controlled microplate reader (Labexim LMR-1). The results were expressed as a oligonucleosome enrichment factor (representing a ratio between the absorption in the treated versus the untreated control samples). Each test was run in triplicate.

RESULTS AND DISCUSSION

Chemistry

The ligand 3-methoxysalicylaldehyde benzoyl-hydrazone, shown on Fig. 1, was synthesized as previously described [16] by the condensation of 3-methoxysalicylaldehyde and benzhydrazide in ethanol. The complexes were prepared by a direct reaction of the hydrazone and the respective metal acetates in good yields.

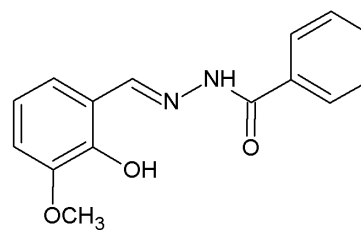


Fig. 1. Structure of the ligand.

The ligand and its Zn(II), Co(II) and Ni(II) complexes were characterized by elemental analysis as a basis for the determination of their empirical formulae. Experimental and calculated C, H, N values reveal molar ratio metal:ligand = 1:2 in the complexes and suggest molecular formula $[\text{M}(\text{L})_2]$ for all complexes. The data from the elemental analysis are summarized in the Experimental section.

The composition derived from the elemental analyses was proved by thermal analysis of the obtained compounds. The TGA and DTA data were used to determine the content of H_2O in the compounds. The thermal decomposition of the hydrazone starts with the stage of dehydration and it comes between 70-115 °C. The experimental mass loss of 6.10% (calc. 6.25%) is due to the loss of one H_2O molecule and it is accompanied by the DTG endo peak at 100 °C. The thermal investigations of the complexes show absence of weight loss up to 190 °C which indicates that the complexes do not contain crystallization water molecules. Above this temperature the complexes began to decompose and at 570-600 °C the decomposition process stopped and stable metal oxides were formed.

The structures of the complexes in the solid state were determined using their IR spectra. The comparative IR spectral study of the ligand and its complexes revealed the coordination mode of the hydrazone during the complex formation. The medium intensity band at 3366 cm^{-1} in the IR spectrum of the ligand due to phenolic OH group had disappeared in the spectra of the complexes. This supports the suggestion for deprotonation of the ligand during the coordination and the displacement of a proton by the metal ion. The band observed at 1607 cm^{-1} in the spectrum of the ligand which is attributed to azomethine C=N group was shifted to lower wave numbers in spectra of the complexes indicating the involvement of N-atom of the azomethine group in the complex formation. An intense band which appears at 1652 cm^{-1} in the spectrum of the ligand is assigned to the stretching vibration of the carbonyl group C=O. In the spectra of the complexes a considerable negative shift is observed showing coordination through the carbonyl-oxygen atom of the free ligands. The NH stretching vibration in the free ligand occurs at 3207 cm^{-1} and remains unaffected after complexation. This precludes the possibility of coordination through imine nitrogen atom. In addition, the appearance of medium bands at $518\text{--}525\text{ cm}^{-1}$ and $433\text{--}438\text{ cm}^{-1}$ in the spectra of the complexes can be assigned to $\nu(\text{M-O})$ and $\nu(\text{M-N})$, respectively.

The characterization of the complexes in solution was performed by UV-Vis spectroscopy. The moderate solubility of the complexes in DMSO was enough for the detection of electronic spectra as the solutions used were much diluted ($10^{-5}\text{--}10^{-6}$ mol/L in DMSO). However, it was difficult to prepare suitable solutions to register NMR-spectra of the complexes. The UV-Vis spectral data for the free ligand and complexes are summarized in Table 1.

Table 1. UV-Vis spectral data for the free ligand and complexes.

Compound	$\lambda_{\text{max}}(\text{nm})$		
Ligand	280	304	-
Zn(II)-complex	260	316	400
Co(II)-complex	262	312	403
Ni(II)-complex	262	306	416

UV-Vis spectrum of the ligand has two intensive bands at 280 nm and 304 nm indicating $n\rightarrow\pi^*$ and $\pi\rightarrow\pi^*$ transitions in phenolic OH- and azomethine C=N- groups, respectively. Upon complexation these bands are slightly shifted

relative to the ligand with maxima at 260–262 nm and 306–316 nm which can be considered as an evidence for the complex formation. The spectra of the complexes additionally exhibited broad band in the visible part of the spectrum at 400–416 nm as a result of d-d transitions responsible for the characteristic colors of the complexes.

The comparison of the IR and UV-Vis spectroscopy data of the Zn(II), Co(II) and Ni(II) complexes with those of the free ligand suggests that 3-methoxysalicylaldehyde benzoylhydrazone act as monoanionic tridentate ligand and coordinate through a deprotonated phenolic-oxygen, azomethine-nitrogen and amide-oxygen atoms forming two chelate rings. The complexes are neutral and mononuclear. Based on the above results, the structure for the transition metal complexes was suggested (Fig. 2).

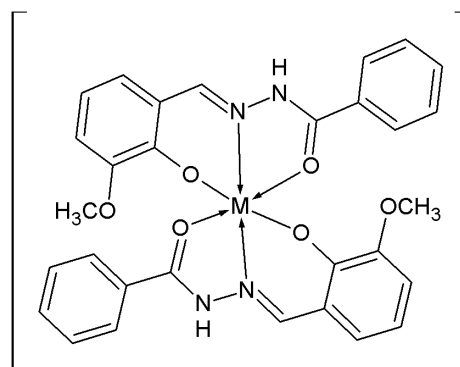


Fig. 2. The suggested structure of the complexes (M= Zn^{2+} , Co^{2+} or Ni^{2+}).

Pharmacology

The new complexes were further tested for *in vitro* cytotoxicity. The cytotoxic activity was assessed by the MTT-dye reduction assay after 72 h incubation against a panel of human leukemic cell lines. The results were fitted to sigmoid dose-response curves and the corresponding IC_{50} values were calculated using non-linear regression (GraphPad Prism software for PC). Throughout the screening investigation the data about the new compounds were compared with the clinically used antineoplastic drugs Cisplatin. The IC_{50} values obtained are summarized in Table 2. Each data point represents the arithmetic mean \pm standard deviation (sd) of at least eight experiments. IC_{50} values were calculated as concentrations of the tested compounds causing 50% decrease of cell survival.

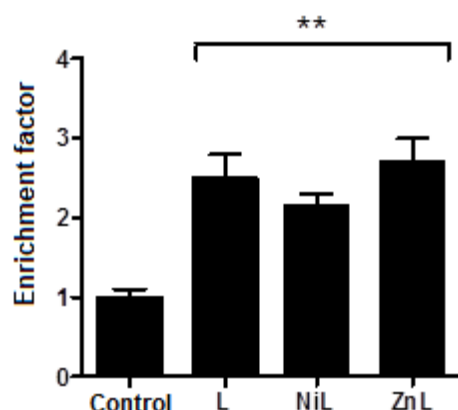
The tested compounds inhibited the growth of tumor cells in a concentration-dependent manner.

Table 2. Cytotoxic activity of 3-methoxysalicylaldehyde benzoylhydrazone and its Zn(II), Ni(II) and Co(II) complexes against a panel of human tumor cell lines after 72 h continuous exposure (MTT-assay).

Compound	IC_{50} ($\mu\text{mol/L}$)			
	HL-60	SKW-3	K-562	BV-173
Ligand	11.3 \pm 2.6	9.8 \pm 3.1	27.0 \pm 2.7	20.8 \pm 4.2
Zn(II)-complex	10.4 \pm 2.6	9.2 \pm 3.3	28.2 \pm 2.4	39.5 \pm 2.1
Co(II)-complex	> 200.0	> 200.0	> 200.0	> 200.0
Ni(II)-complex	32.9 \pm 1.9	11.8 \pm 2.2	50.1 \pm 3.6	19.4 \pm 6.2
Cisplatin	4.7 \pm 3.4	5.2 \pm 3.5	12.5 \pm 4.2	4.2 \pm 2.1

Acute myeloid leukemia HL-60 cell line and T-cell leukemia cell line SKW-3 exhibit the highest sensitivity to the Zn(II) complexes with IC_{50} values slightly lower than these of the ligand. The results showed that the Zn(II)-complex demonstrated superior activity as compared to Ni(II) complex, although its potency was generally inferior to that of the reference agent Cisplatin. The Co(II) complex is devoid of cytotoxic activity against all leukemic cell lines within the tested concentration range (6.25–200 $\mu\text{mol/L}$).

In order to elucidate the mechanistic aspects of the observed effects we evaluated the propensity of ligand 3-methoxysalicylaldehyde benzoylhydrazone and its Ni(II) and Zn(II) complexes to trigger oligonucleosomal DNA-fragmentation, key hallmark of apoptosis. As evident from the data presented in Fig. 3, the 24 h exposure of HL-60 to equieffective concentration of the tested compounds led to statistically a significant increase of the cellular content of histone-associated DNA-fragments. These findings indicate that the cell growth inhibitory effects of metal complexes are at least partly mediated by induction of programmed cell death through apoptosis.

**Fig. 3.** Apoptotic DNA-fragmentation in HL-60 cells after 24 h exposure to ligand and metal complexes. The cytosolic nucleosomal enrichment was determined using a commercially available ELISA kit. Each bar is representative for three experiments.

CONCLUSION

New Zn(II), Co(II) and Ni(II) complexes were synthesized and characterized with elemental analyses, thermal and spectral investigations. The analytical data suggest molecular formula $[M(L)_2]$ and absence of coordinated water in compounds, which was further supported by the thermal analysis. The ligand 3-methoxysalicylaldehyde benzoylhydrazone acted as monoanionic tridentate ligand coordinating to the metal ions through ONO donor sites and thus forming stable six-membered chelates. The preliminary cytotoxicity screening revealed that Zn(II) and Ni(II) complexes induced 50% inhibition of the cell viability at micromolar concentrations. Taking into consideration the superior relative potency of Zn(II) complex, however, as well as its capability to induce programmed cell death we could conclude that Zn(II) complexes with hydrazones deserve further attention in search of anticancer compounds.

REFERENCES

- Z. A. Kaplancikli, M. D. Altintop, A. Ozdemir, G. Turan-Zitouni, S. I. Khan, N. Tabanca, *Let. Drug Des. Discovery*, **9**, 310 (2012).
- W. B. Júnior, M. S. Alexandre-Moreira, M. A. Alves, A. Perez-Rebolledo, G. L. Parrilha, E. E. Castellano, O. E. Piro, E. J. Barreiro, L. M. Lima, H. Beraldo, *Molecules*, **16**, 6902 (2011).
- A. Ozdemir, G. Turan-Zitouni, Z. A. Kaplancikli, G. Revial, *Marm. Pharm. J.*, **14**, 79 (2010).
- B. Koçyiğit-Kaymakçioğlu, E. E. Oruç-Emre, S. Unsalan, S. Rollas, *Med. Chem. Res.*, **18**, 277 (2009).
- T. Govindasami, A. Pandey, N. Palanivelu, A. Pandey, *Int. J. Org. Chem.*, **1**, 71 (2011).
- L. Savini, P. Massarelli, V. Travagli, C. Pellerano, E. Novellino, S. Cosentino, M. B. Pisano, *Eur. J. Med. Chem.*, **39**, 113 (2004).
- P. Vicini, M. Incerti, P. L. Colla, R. E. Loddo, *Eur. J. Med. Chem.*, **44**, 1801 (2009).
- T. B. Chaston, R. N. Watts, J. Yuan, D. R. Richardson, *Clin. Cancer Res.*, **10**, 7365 (2004).

9. D. K. Johnson, T. B. Murphy, N. J. Rose, W. H. Goodwin, L. Pickart, *Inorg. Chim. Acta*, **67**, 159 (1982).
10. P. Ponka, D. Richardson, E. Baker, H. M. Schulman, J. T. Edward, *Biochim. Biophys. Acta*, **967**, 122 (1988).
11. E. Baker, D. R. Richardson, S. Gross, P. Ponka, *Hepatology*, **15**, 492 (1992).
12. D. R. Richardson, P. Ponka, *J. Lab. Clin. Med.*, **131**, 306 (1998).
13. J. L. Buss, E. Arduini, P. Ponka, *Biochem. Pharmacol.*, **64**, 1689 (2002).
14. D. B. Lovejoy, D. R. Richardson, *Blood*, **100**, 666 (2002).
15. D. R. Richardson, K. Milnes, *Blood*, **89**, 3025 (1997).
16. B. Nikolova-Mladenova N. Halachev, R. Iankova, G. Momekov, D. Ivanov, *J. Arzneim.-Forsch.*, **61**, 714 (2011).
17. B. Nikolova-Mladenova, G. Momekov, D. Ivanov, *Pharmacia*, **LVIII (1-4)**, 41 (2011).
18. B. Nikolova-Mladenova, G. Momekov, Ts. Gerasimova, M. Topashka-Ancheva, *J. Med. & Biol. Sci.*, **1**, 44 (2014).
19. B. Nikolova-Mladenova, A. Bakalova, G. Momekov, D. Ivanov, *J. Med. & Biol. Sci.*, **1**, 16 (2015).
20. D. R. Richardson, *Antimicrob. Agents Chemother.*, **41**, 2061 (1997).
21. H. Tapiero, K.D. Tew, *Biomed. Pharmacother.*, **57**, 399 (2003).
22. B. Szewczyk, M. Kubera, G. Nowak, *Prog. Neuropsychopharmacol. Biol. Psychiatry*, **35**, 693 (2011).
23. K. M. Hambidge, N. F. Krebs, *J. Nutr.*, **137**, 1101 (2007).
24. L. Rink, P. Gabriel, *Proc. Nutr. Soc.*, **59**, 541 (2000).
25. K. Yamada, in: *Interrelations between Essential Metal Ions and Human Diseases. Metal Ions in Life Sciences 13*, A. Sigel, H. Sigel; R.K.O. Sigel. Springer, 2013, p. 295.
26. V. Cracan, R. Banerjee, L. Banci In: *Metallomics and the Cell. Metal Ions in Life Sciences 12*, Springer, 2013.
27. T. Mosmann, *J. Immunol. Methods*, **65**, 55 (1983).

СИНТЕЗ, ОХАРАКТЕРИЗИРАНЕ И *IN VITRO* ЦИТОТОКСИЧНА АКТИВНОСТ НА Zn(II), Co(II) И Ni(II) КОМПЛЕКСИ С ТРИДЕНТАТНИЯ ОНО-ЛИГАНД 3-МЕТОКСИСАЛИЦИЛАЛДЕХИД БЕНЗОИЛХИДРАЗОН

Б. И. Николова-Младенова^{1*}, Г. Цв. Момеков²

¹ Катедра Химия, Фармацевтичен Факултет, Медицински Университет – София, ул. Дунав 2, София 1000, България

² Катедра по Фармакология, Фармакотерапия и Токсикология, Фармацевтичен Факултет, Медицински Университет – София, ул. Дунав 2, София 1000, България

Постъпила на 20 февруари 2017 г.; Коригирана на 15 март 2017 г.

(Резюме)

Синтезирани са нови Zn(II), Co(II) и Ni(II) комплекси с активния цитотоксичен лиганд 3-метоксисалицилалдехид бензоилхидразон. Съединенията са охарактеризирани чрез елементарен и термогравиметричен анализ и спектрални методи. Спектралните данни на комплексите са интерпретирани чрез сравнение със спектрите на свободния лиганд. Комплексите са моноядрени с молно съотношение на метала към лиганда 1:2. Анализите доказват, че лигандът е тридентатен и координира металните йони чрез депротонирания фенолен кислороден атом, азотния атом от азометиновата група и кислородния атом от амидната група. Новите комплекси са тествани за *in vitro* цитотоксичност върху спектрът от 4 човешки левкемични клетъчни линии чрез МТТ-тест. Фармакологичните изследвания показват, че Zn(II) комплекс води до инхибиране на 50% от клетъчната жизнеспособност в ниски микромолярни концентрации. Ni(II) комплекс е по-слабо активен, докато Co(II) комплекс практически не проявява цитотоксични ефекти в проучения диапазон от концентрации (6.25–200 µmol/L).

Preparation, characterization, theoretical investigation and cytotoxic activity of new mixed ammine/amine platinum complexes with 3-amino-5-methyl-5-phenylhydantoin

E. Cherneva^{1*}, A. Bakalova¹, R. Michailova², B. Nikolova-Mladenova¹

¹ Department of Chemistry, Faculty of Pharmacy, Medical University - Sofia, 2 Dunav Str., 1000 Sofia, Bulgaria

² Department of Pharmacology, Pharmacotherapy and Toxicology, Faculty of Pharmacy, Medical University - Sofia, 2 Dunav Str., 1000 Sofia, Bulgaria

Received February 08, 2017; Revised February 22, 2017

Dedicated to Acad. Bogdan Kurtev on the occasion of his 100th birth anniversary

New mixed ammine/amine Pt(II) and Pt(IV) complexes with 3-amino-5-methyl-5-phenylhydantoin (L) as carrier ligand were synthesized. The chemical formulas of the complexes *cis*-[Pt(NH₃)LCl₂] and *cis,cis,trans*-[Pt(NH₃)LCl₂(OH)₂] were proved by melting points, elemental analysis and IR spectra. For the prediction of the molecular structures of the ligand and its complexes DFT method was used. Theoretical analysis of the complexes showed the square planar coordination of Pt(II) complex and distorted octahedral coordination of Pt(IV) complex. The theoretical IR spectra were compared to the experimental and a good agreement was found. The cytotoxic activity of the organic compound and its complexes was determined *in vitro* by MTT assay against five human tumor cell lines - Hep-G2, MDA-MB-231, HT-29, HL-60 and REH. The IC₅₀ values of the tested compounds showed that platinum complexes have higher cytotoxic activity than the organic compound.

Key words: Pt complexes; hydantoin; IR spectra; DFT calculations; cytotoxicity

INTRODUCTION

Because of the cisplatin (*cis*-[Pt(NH₃)₂Cl₂]) success in clinical therapy, various new *cis*-Pt(II) complexes have been synthesized and studied by substitution of either chlorine or ammonia ligands with different structures. A new classes of platinum compounds with general formulas *cis*-[Pt(L)(L')(L")₂] and *cis*-[Pt(L)(L')(L")₂(L"')₂], where L and L' are different amines, L" is chloride ions, L"' is hydroxido or carboxylato ions in axial position have been reported to show cytotoxic activity against several tumor cell lines [1]. For example, Pt(II) complexes with chemical formula *cis*-[PtL(NH₃)Cl₂] (L=pyridine, pyrimidine, purine) [2] were reported to show promising antitumor activity. AMD473 (*cis*-[Pt(2-methylpyridine)(NH₃)Cl₂]) was rationally designed in order to reduce the reactivity of glutathione which may be the key to improve responses in resistant tumors [3, 4]. It is active against acquired cisplatin- and oxaliplatin-resistant cell lines [5] and possesses a toxicity profile similar to carboplatin. This promising compound named also picoplatin has been introduced in the treatment of patients with solid tumors. Its clinical trials started in 1997 and

investigations of the picoplatin derivatives continue [6, 7]. Recently new complexes of picoplatin with different organic molecules were prepared and studied for cytotoxicity on some cancer cell lines. The results showed that inclusion complexation may be a promising strategy to design a novel formulation of picoplatin as an anticancer therapy [8, 9].

Platinum(IV) complexes are known to be much more tolerant to ligand substitution reactions than their Pt(II) counterparts [10]. In order to rationally design of new Pt(IV) complexes, correlation between structure, reduction and activity were needed, since it is generally admitted that Pt(IV) compounds must be reduced to be activated [11]. Octahedral Pt(IV) complexes act as prodrugs of their Pt(II) counterparts and represent an important role of recent metal-based anticancer research [12]. Mixed ammine/amine Pt(IV) complexes with equatorial chloride and axial carboxylate or hydroxide ligands also demonstrate cytotoxic activity against cisplatin resistant cells *in vitro*. Some Pt(IV) complexes have shown promising results to enter in clinical trials: Iproplatin (*cis,trans,cis*-[Pt(isopropylamine)Cl₂(OH)₂] [13], Tetraplatin ([Pt(d,l-cyclohexane-1,2-diamine)Cl₄] [14] and Satraplatin (*cis,trans,cis*-[Pt(cyclohexylamine)(NH₃)(OAc)₂Cl₂]) [15]. Satraplatin showed

* To whom all correspondence should be sent:
E-mail: e.d.cherneva@gmail.com

higher activity compared to cisplatin against human cervical, small-cell lung and ovarian carcinoma cell lines [16]. In recent years, satraplatin has emerged as a novel oral platinum analogue with a better toxicity profile than cisplatin. Since satraplatin is more hydrophobic than cisplatin or oxaliplatin, it appears to demonstrate efficacy in cisplatin-resistant cell lines [17].

The goal of the study is to prepare new mixed ammine/amine Pt(II) and Pt(IV) complexes with ligand 3-amino-5-methyl-5-phenylhydantoin and general formulae $cis-[Pt(NH_3)LCl_2]$ and $cis,cis,trans-[Pt(NH_3)LCl_2(OH)_2]$. The complexes were studied by melting points, elemental analysis and IR spectral method. For prediction of molecular structures of the organic compound and its platinum complexes hybrid DFT method was used. The investigated compounds were pharmacologically examined in comparison to clinically applied drug cisplatin.

EXPERIMENTAL

Chemistry

All chemicals were purchased from Fluka (UK) and Sigma-Aldrich. The newly mixed ammine/amine Pt(II) and Pt(IV) complexes were characterized by elemental analysis, melting points and IR spectra. The elemental analysis was carried out on a "EuroEA 3000 – Single", EuroVectorSpA apparatus (Milan, Italy). Corrected melting points were determined, using a Bushi 535 apparatus (BushiLabortechnik AG, Flawil, Switzerland). The IR spectra were recorded on Thermo Scientific Nicolet iS10 spectrophotometer (Thermo Scientific, USA) in the range of 4000-400 cm^{-1} as Attenuated Total Reflection Fourier Transform Infrared Spectroscopy (ATR-FTIR).

The new complexes $cis-[Pt(NH_3)LCl_2]$ (**1**) and $cis,cis,trans-[Pt(NH_3)LCl_2(OH)_2]$ (**2**), where **L** is 3-amino-5-methyl-5-phenylhydantoin (**L**) were prepared by using reported procedure with minor revisions [18, 19]. The synthesis and the structure of 3-amino-5-methyl-5-phenylhydantoin (**L**) were described in details in our previously published work [20].

Synthesis of new mixed Pt(II) and Pt(IV) complexes

Synthesis of cis-3-amino-5-methyl-5-phenylhydantoin-ammine-dichlorido platinum(II) – cis-[Pt(NH₃)LCl₂] (1): An aqueous ethanol solution of (**L**) (0.3216 mmol) was added dropwise to an

aqueous solution of $K[Pt(NH_3)Cl_3]$ (0.5621 mmol) with constant stirring at ambient temperature. The solution was stirred for 5–6 h, concentrated and cooled to 4 °C. A light yellow precipitate was collected by filtration and dried in a vacuum desiccator. The purity was confirmed by TLC with eluent $CH_3COOC_2H_5/C_2H_5OH$ (2:1) and elemental analysis. Yield: 30%; m.p. (dec.) 221 °C.

Synthesis of cis-3-amino-5-methyl-5-phenylhydantoin, ammine, cis-dichlorido, trans-dihydroxidoplatinum(IV) – cis,cis,trans-[Pt(NH₃)LCl₂(OH)₂] (2): 0.1926 mmol of the complex (**1**) and excess of 30% H_2O_2 were mixed. The suspension was stirred for 4-5 h at 50 °C. After 6-7 days from the solution whitish crystals were isolated and dried in vacuum desiccator under P_2O_5 and KOH. The purity was confirmed by TLC with eluent $CH_3COOC_2H_5/C_2H_5OH$ (2:1) and elemental analysis. Yield: 23%; m.p. (dec.) 218 °C.

Calculations

All theoretical calculations were performed using the Gaussian 09 package [21] of programs. Optimization of the structures of the ligand 3-amino-5-methyl-5-phenylhydantoin and possible conformers of Pt(II) and Pt(IV) complexes were carried out by DFT calculations, employing the B3LYP (Becke's three-parameter non-local exchange [22]) and Lee *et al.* correlation [23] hybrid functional and 6-311++G** set for the ligand and LANL2DZ basis set for the platinum complexes. The B3LYP hybrid functional [24, 25] was used because of its high accuracy. The basis set LANL2DZ was chosen to include the pseudopotential of the core electrons in atoms of heavy elements like platinum and it is compatible with all other organic elements (C, N, H, O, Hal).

Pharmacology

The present study describes a comparative evaluation of the cytotoxic effects of the ligand and two newly synthesized platinum complexes. The cytotoxicity of the complexes was compared to metal-free ligand (**L**) and the referent antineoplastic agent cisplatin.

Cell culture conditions

The following cell lines were used for the experiments: (i) Hep-G2 (Human Caucasian hepatocyte carcinoma, isolated from a liver biopsy of a male Caucasian aged 15 years, with a well

differentiated hepatocellular carcinoma), (ii) MDA-MB-231 (human breast cancer cell line, established in 1973 from the pleural effusion of a 51-year-old woman with breast carcinoma), (iii) HT-29 (colon adenocarcinoma, established from the primary tumor of a 44-year-old Caucasian woman with colon adenocarcinoma in 1964), (iv) HL-60 (acute myeloid leukemia, established from the peripheral blood of a patient with acute promyelocyte leukemia), (v) REH (acute lymphoblastic leukemia, established from the peripheral blood of a 15-year-old North African girl with acute lymphoblastic leukemia in 1973). The cell lines were obtained from DSMZ German Collection of Microorganisms and Cell Cultures and were well validated in our laboratory as a proper test system for metal complexes. Their DSMZ catalogue numbers are as follows: Hep-G2 (ACC 180), MDA-MB-231 (ACC 73), HT-29 (ACC 299), HL-60 (ACC 3) and REH (ACC 22).

Cytotoxicity assessment

Cytotoxicity of the compounds was assessed using the MTT [3-(4,5-dimethylthiazol-2-yl)-2,5-diphenyltetrazolium bromide] dye reduction assay as described by Mossman [26] with some modifications [27]. Exponentially growing cells were seeded in 96-well microplates (100 μL /well at a density of 3.5×10^5 cells/mL for the adherent and 1×10^5 cells/mL for the suspension cell lines) and allowed to grow for 24 h prior the exposure to the studied compounds. Stock solutions of the investigated Pt(II) and Pt(IV) complexes were freshly dissolved in DMSO and then promptly diluted in RMPI-1640 growth medium, immediately before treatment of cells. Our

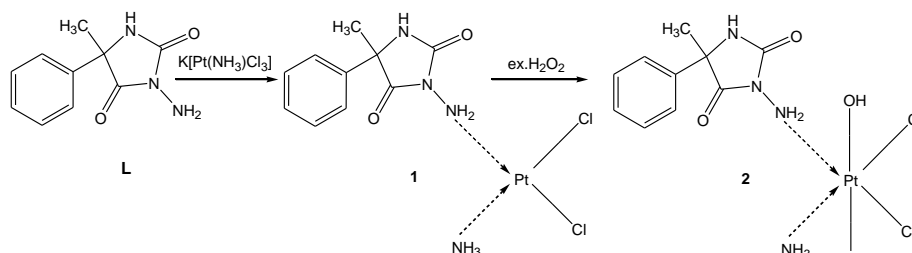
preceding experience with water-insoluble platinum agents, including cisplatin has indicated that the dose-response curves following dissolution in water or stock solution in DMSO (which is then promptly diluted in aqueous phase) overlap and there is no significant modulation of the individual cell lines chemosensitivity. At the final dilutions the solvent concentration never exceeded 0.5%. Cells were exposed to the tested compounds for 72 h, whereby for each concentration a set of 8 separate wells was used. Every test was run in triplicate, *i.e.* in three separate microplates. After incubation with the tested compounds MTT solution (10 mg/mL in PBS) aliquots were added to each well. The plates were further incubated for 4 h at 37 °C and the formazan crystals formed were dissolved by adding 110 μL of 5% HCOOH in 2-propanol. Absorption of the samples was measured by an ELISA reader (UniscanTitertec) at 580 nm. Survival fraction was calculated as percentage of the untreated control. In addition IC_{50} values were calculated from the concentration-response curves. The experimental data was processed using GraphPadPrizm software and was fitted to sigmoidal concentration/response curves *via* non-linear regression.

RESULTS AND DISCUSSION

Calculations

The new platinum complexes were prepared according to the Scheme 1.

The elemental analyses of the complexes (**1**) and (**2**) were in good agreement with the corresponding chemical formulae – *cis*-[Pt(C₁₀H₁₁N₃O₂)(NH₃)Cl₂]



Scheme 1. Synthesis of the complexes (**1**) and (**2**).

Table 1. Physico-chemical data of the newly prepared compounds.

Compound	Molecular formula	MW	Yield ^a (%)	M.p. ^b (dec.) (°C)	Elemental analysis		
					% Calc. (% Found)		
					C	H	N
1	C ₁₀ H ₁₄ N ₄ O ₂ Cl ₂ Pt	487.90	30	221	24.60 (24.72)	2.87 (3.29)	11.48 (11.46)
2	C ₁₀ H ₁₆ N ₄ O ₄ Cl ₂ Pt	521.90	23	218	22.99 (23.47)	3.07 (3.35)	10.73 (10.88)

^aYield of analytically pure product; ^bMp of analytically pure product.

and *cis,cis,trans*-[Pt(C₁₀H₁₁N₃O₂)(NH₃)Cl₂(OH)₂]. The data from elemental analysis and some physical properties are summarized in Table 1.

IR spectra

In the vibrational spectrum of the ligand (**L**), the stretching vibrations of NH₂ and NH groups three bands in the region 3347-3197 cm⁻¹ were observed. While in the spectra of the complexes all amino groups (NH₃, NH₂, NH) were characterized by a broad band appeared at 3400-3280 cm⁻¹. Their corresponding theoretical spectra were presented by several bands at 3560-3100 cm⁻¹. The difference between the experimental and theoretical results is probably due to the formation of some inter- and intra-molecular interactions as H-bonds in solid state.

The C-H stretching vibrations of the CH₃ group and C₆H₅ fragment (theoretical and experimental spectra) were appeared in their usual regions.

In the experimental IR spectra ν (C=O) vibrations of the (**L**), (**1**) and (**2**) were observed as two bands in the area 1787-1700 cm⁻¹ (theoretical bands: 1790–1658 cm⁻¹).

The NH₂ deformation vibrations (theoretical and experimental spectra) were shifted to the lower frequencies with approximately 30 cm⁻¹ in the complexes compared to the ligand. This indicated coordination through the N-atom from the amino group. The results showed a good correlation between theoretical and experimental data.

Geometry

The optimized geometry of the ligand with *R*-configuration and energetically preferred structures of the complexes (**1**), (**2**) and atom numbering were shown on Figs.1-3.

Evaluation of the molecular structures of the (**L**) and complexes (**1**) and (**2**) were carried out by DFT method. The ligand can exist in two stereo configurations – *R* and *S* according to the arrangement of substituents around C₁ atom. In order to establish the geometry of both stereoisomer, full optimization of the molecules was performed at the B3LYP/6-311++G** level of theory. As a result, we found that the stereoisomers are characterized by similar geometry parameters and dipole moments. The hydantoin fragment showed a planar structure as expected. In both cases the molecules were stabilized by formation of a hydrogen bond between the NH₂- and C=O groups

from the hydantoin moiety with identical geometry parameters: N-H...O bond length of 2.87 Å and N-H...O angle of 88.7° respectively.

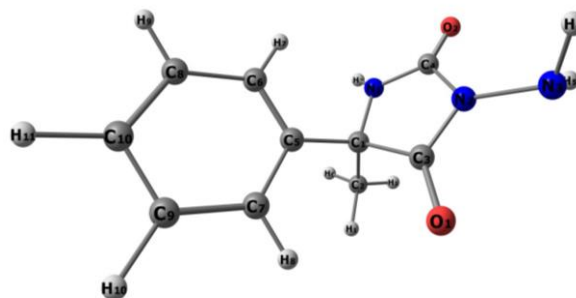


Fig. 1. Optimized structure of the ligand with *R*-configuration.

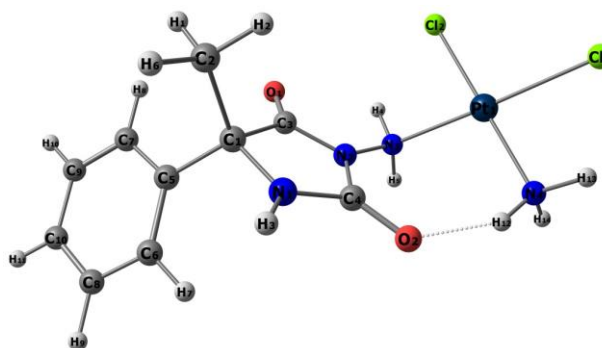


Fig. 2. Optimized structure of the *cis*-[Pt(NH₃)(L)Cl₂].

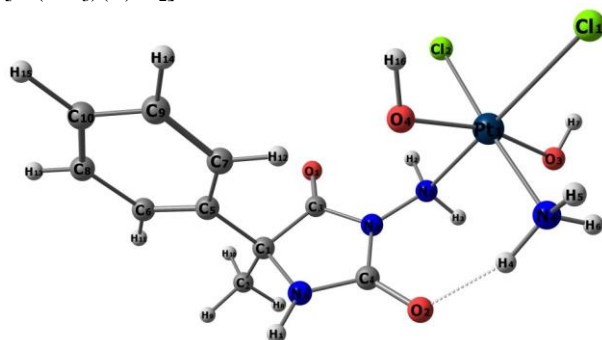


Fig. 3. Optimized structure of the *cis,cis,trans*-[Pt(NH₃)(L)Cl₂(OH)₂].

Taking into account the possible existence of *R* and *S* enantiomers, we carried out analysis on the potential energy surface of all stereoisomer complexes at B3LYP/LAN2DZ level of theory. For each complex, the most probable conformations were constructed and optimized.

It has been found that the complex of Pt(II) with the *R* isomer of the ligand is the preferred structure to complex with the *S* isomer of the ligand with 1.81 kJ/mol.

The coordination around the Pt centre was square planar. In the case of Pt(IV), the complex

with *S* isomer was more favorable than those with *R*-configuration by 1.30 kJ/mol. The platinum centre in Pt(IV) complex was hexacoordinated in a distorted octahedral geometry. The octahedral coordination was formed by two chloride ions, two hydroxyl groups, ammonia and one molecule of the ligand. The complexes were stabilized by an intramolecular N-H...O hydrogen bond of 2.80 Å of Pt(II) and 2.76 Å of Pt(IV) complexes.

The N₂-N₃ bond in the complexes becomes lightly longer than those in the ligand. The coordination leads to small changes in the geometric parameters of the hydantoin fragment as well as of the complexes (Table 2).

The most significant geometric parameters of the ligand and platinum complexes were presented in Table 2.

Pharmacological screening

The ligand (**L**) and the complexes (**1**, **2**) were tested for cytotoxic activity on a panel of human tumor cell lines - hepatocyte carcinoma Hep-G2, human breast cancer cell line MDA-MB-231, colon adenocarcinoma HT-29, acute myeloid leukemia HL-60 and acute lymphoblastic leukemia REH. The tested organic compound (**L**) and complexes (**1**, **2**) exerted cytotoxic effect after 72 h continuous exposure, whereby the individual chemosensitivity varied among the different cell lines. The complexes (**1**) and (**2**) showed higher cytotoxic activity on HT-29, MDA-MB-231 and HL-60 cell lines than the ligand (**L**). Complex (**2**) manifested higher cytotoxic activity than the complex (**1**) and reference cisplatin on the colon adenocarcinoma HT-29 cell line. The results are summarized in Table 3.

Table 2. Calculated geometry parameters of the ligand and its complexes (**1**, **2**) using atom numbering in Figs. 1-3.

Parameters	Ligand(L) <i>R</i>	1	2
μ(D)	2.74	13.66	9.68
Bond lengths (Å)			
Pt-Cl ₁	-	2.42	2.40
Pt-Cl ₂	-	2.39	2.42
Pt-N ₃	-	2.12	2.11
Pt-N ₄	-	2.09	2.08
N ₂ -N ₃	1.39	1.43	1.41
Pt-O ₄	-	-	2.04
Pt-O ₃	-	-	2.05
Angles (°)			
N ₁ -C ₄ -N ₂	106.0	105.5	105.5
N ₁ -C ₁ -C ₃	101.2	100.6	100.3
C ₄ -N ₂ -N ₃	123.4	123.4	123.9
N ₂ -N ₃ -Pt	-	119.9	121.0
N ₃ -Pt-Cl ₂	-	81.1	83.4
N ₄ -Pt-Cl ₁	-	83.6	84.8
N ₃ -Pt-N ₄	-	98.6	97.7
Cl ₁ -Pt-Cl ₂	-	96.4	93.7
O ₃ -Pt-Cl ₁	-	-	97.2
O ₃ -Pt-Cl ₂	-	-	94.4
O ₃ -Pt-N ₃	-	-	79.8
O ₃ -Pt-N ₄	-	-	82.3
O ₄ -Pt-Cl ₁	-	-	92.3
O ₄ -Pt-Cl ₂	-	-	93.2
O ₄ -Pt-N ₃	-	-	90.9
O ₄ -Pt-N ₄	-	-	90.2
Dihedral angles (°)			
C ₄ -N ₂ -C ₃ -C ₁	-3.8	-0.2	-2.6
C ₄ -N ₁ -C ₁ -C ₂	112.7	-	115.4
N ₁ -C ₄ -N ₂ -C ₃	5.7	0.7	3.3
O ₁₂ -C ₄ -N ₂ -N ₃	0.8	-8.9	-11.0
C ₄ -N ₂ -N ₃ -Pt	-	-51.9	-57.0
C ₃ -N ₂ -N ₃ -Pt	-	119.0	109.4
N ₂ -N ₃ -Pt-Cl ₂	-	105.6	-112.9
N ₂ -N ₃ -Pt-N ₄	-	74.9	70.6
N ₂ -N ₃ -Pt-O ₄	-	-	-19.7
N ₂ -N ₃ -Pt-O ₃	-	-	151.3

Table 3. Cytotoxicity of the ligand (**L**) and complexes (**1**, **2**) in comparison with referent drug cisplatin in five human tumour cell lines.

Cell line	IC ₅₀ values/(μM)				
	Hep-G2 ^a	HT-29 ^b	REH ^c	MDA-MB-231 ^d	HL-60 ^e
Compound					
Ligand	> 200	> 200	> 200	> 200	> 200
Complex (1)	> 200	> 200	> 200	143.0	155.7
Complex (2)	-	145.5	> 200	-	> 200
Cisplatin	12.0	170.0	1.07	31.6	8.7

^ahuman hepatocyte carcinoma; ^bcolon adenocarcinoma; ^cacute lymphoblastic leukemia; ^dhuman breast cancer cell line; ^eacute myeloid leukaemia

CONCLUSION

Two new mixed ammine/amine Pt(II) and Pt(IV) complexes with 3-amino-5-methyl-5-phenyl-hydantoin were synthesized and studied. The geometry of the ligand and its platinum complexes were optimized, using the DFT method, employing the B3LYP with 6-311++G** basis set for the ligand and LANL2DZ basis set for the complexes. The metal–ligand binding mode in the new complexes was confirmed by the DFT calculations. In the complexes, platinum ion coordinates in a monodentate manner through the nitrogen atom from the NH₂ group of the hydantoin ring. The computed vibrational frequencies were used for determination of the molecular motions associated with each of observed experimental bands. Experimental frequencies were well reproduced by the theoretical method. The compounds tested exerted concentration-dependent cytotoxicity on a HT-29, MDA-MB-231 and HL-60 human tumor cell lines. The new Pt(IV) complex *cis,cis,trans*-[Pt(NH₃)LCl₂(OH)₂] exhibited higher cytotoxic activity than the Pt(II) complex - *cis*-[PtNH₃(L)Cl₂] and referent drug cisplatin on the colon adenocarcinoma HT-29 cell line.

Acknowledgements: The investigation is supported by the Medical Science Council at the Medical University – Sofia within the Grant № 51/27.05.2016.

REFERENCES

1. C. Gianomenico, W. Blane, E. Wong, Pt(IV) antitumor agent, US Patent 6,413,953 B1 (2002).
2. Y. Chen, Z. Guo, S. Parsons, P. Sadler, *Chem. Eur. J.*, **4**, 672 (1998).
3. J. Holford, S. Sharp, B. Murrer, M. Abrams, L. Kelland, *Br. J. Cancer*, **77**, 366 (1998).
4. F. Raynaud, F. Boxall, P. Goddard, *Clin. Cancer Res.*, **3**, 2063 (1997).
5. L. Kelland, *Expert Opin. Investig. Drugs*, **16**, 1009 (2007).
6. L. Kelland, *Nat. Rev. Cancer*, **7**, 573 (2007).
7. N. J. Wheate, S. Walker, G. E. Craig, R. Oun, *Dalton Trans.*, **39**, 8113 (2010).
8. S. D. Brown, K. D. Trotter, O. B. Sutcliffe, J. A. Plumb, B. Waddell, N. E. Briggs, N. J. Wheate, *Dalton Trans.*, **41**, 11330 (2012).
9. J-Q. Zhang, K. L., Y.-W. Cong, S.-P. Pu, H.-Y. Zhu, X.-G. Xie, Y. Jin, J. Lin, *Carbohydrate Research*, **396**, 54 (2014).
10. L. Drougge, L. Elding, *Inorg. Chim. Acta.*, **121**, 175 (1986).
11. A. Abu-Sarrah, M. Kettunen, *Curr. Med. Chem.*, **13**, 1337 (2006).
12. M. Galanski, *Anti-Cancer Drug Discov.*, **1**, 285 (2006).
13. M. Gordon, S. Hollander, *J. Med.*, **24**, 209 (1993).
14. R. Weiss, M. Christian, *Drugs*, **46**, 360 (1993).
15. M. McKeage, F. Raynaud, J. Ward, C. Berry, D. O'Dell, L. Kelland, M. Murrer, P. Santabarabara, K. Harrap, I. Judson, *J. Clin. Oncol.*, **15**, 2691 (1997).
16. L. Kelland, G. Abel, M. McKeage, M. Jones, P. Goddard, M. Valenti, B. Murrer, K. Harrap, *Cancer Res.*, **53**, 2581 (1993).
17. A. Bhargava, U. N. Vaishampayan, *Expert Opin. Investig. Drugs*, **18**, 1787 (2009).
18. U. Bierbach, Y. Qu, T. W. Hambley, J. Peroutka, H. L. Nguyen, M. Doedee, N. Farell, *Inorg. Chem.*, **38**, 3535 (1999).
19. J. J. Wilson, S. Lippard, *Chem. Rev.*, **114**, 4470 (2014).
20. A. Bakalova, R. Petrova, B. Shivachev, H. Varbanov, *J. Coord. Chem.*, **60**, 1701 (2007).
21. M. J. Frisch, G. W. Trucks, H. B. Schlegel, G. E. Scuseria, M. A. Robb, J. R. Cheeseman, G. Scalmani, V. Barone, B. Mennucci, G. A. Petersson, H. Nakatsuji, M. Caricato, X. Li, H. P. Hratchian, A. F. Izmaylov, J. Bloino, G. Zheng, J. L. Sonnenberg, M. Hada, M. Ehara, K. Toyota, R. Fukuda, J. Hasegawa, M. Ishida, T. Nakajima, Y. Honda, O. Kitao, H. Nakai, T. Vreven, J. A. Montgomery, Jr., J. E. Peralta, F. Ogliaro, M. Bearpark, J. J. Heyd, E. Brothers, K. N. Kudin, V. N. Staroverov, R. Kobayashi, J. Normand, K. Raghavachari, A. Rendell, J. C. Burant, S. S. Iyengar, J. Tomasi, M. Cossi, N. Rega, J. M. Millam, M. Klene, J. E. Knox, J. B. Cross, V. Bakken, C. Adamo, J. Jaramillo, R. Gomperts, R. E. Stratmann, O. Yazyev, A. J. Austin, R. Cammi, C. Pomelli, J. W. Ochterski, R. L. Martin, K. Morokuma, V. G. Zakrzewski, G. A. Voth, P. Salvador, J. J. Dannenberg, S. Dapprich, A. D. Daniels, O. Farkas, J. B. Foresman, J. V. Ortiz, J. Cioslowski, and D. J. Fox, Gaussian 09, Revision A.1, Gaussian Inc., Wallingford CT, 2009.
22. P. J. Stephens, F. J. Devlin, C. F. Chabalowski, M. J. Frisch, *J. Phys. Chem.*, **98**, 11623 (1994).
23. C. T. Lee, W. T. Yang, R. G. Parr, *Phys. Rev.*, **B**, **37**, 785 (1988).
24. A. Becke, *Phys. Rev. A*, **38**, 3098 (1988).
25. A. Becke, *Phys. Rev. A*, **96**, 2155 (1992).
26. T. Mosmann, *J. Immunol. Methods*, **65**, 55 (1983).
27. S. Konstantinov, H. Eibl, M. Berger, *Br. J. Haemat.*, **107**, 365 (1999).

ПОЛУЧАВАНЕ, ОХАРАКТЕРИЗИРАНЕ, ТЕОРЕТИЧНО ИЗСЛЕДВАНЕ И ЦИТОТОКСИЧНА АКТИВНОСТ НА НОВИ СМЕСЕНИ ПЛАТИНОВИ КОМПЛЕКСИ С 3-АМИНО-5-МЕТИЛ-5-ФЕНИЛХИДАНТОИН

Е. Чернева^{1*}, А. Бакалова¹, Р. Михайлова², Б. Николова-Младенова¹

¹ Катедра Химия, Фармацевтичен факултет, Медицински университет - София, ул. Дунав №2, София 1000

² Катедра Фармакология, фармакотерапия и токсикология, Фармацевтичен факултет, Медицински университет - София, ул. Дунав №2, София 1000

Постъпила на 08 февруари 2017 г.; Коригирана на 22 февруари 2017 г.

(Резюме)

Синтезирани са нови смесени комплекси на Pt(II) и Pt(IV) с 3-амино-5-метил-5-фенилхидантоин, използван като носещ лиганд. Химичните формули на комплексите *cis*-[Pt(NH₃)LCl₂] и *cis,cis,trans*-[Pt(NH₃)LCl₂(OH)₂] са доказани чрез точка на топене, елементарен анализ и ИЧ спектроскопия. За предсказване на молекулната структура на лиганда и неговите комплекси е използван ДФТ метод. Теоретичният анализ на комплексите показва плоско-квадратна координация на комплекса на Pt(II) и деформирана октаедрична координация на комплекса на Pt(IV). Установено е добро съответствие между теоретичните и експерименталните данни за ИЧ спектрите. Лигандът и неговите комплекси бяха изследвани за цитотоксична активност *in vitro* с помощта на МТТ тест върху пет човешки туморни клетъчни линии: Hep-G2, MDA-MB-231, HT-29, HL-60 and REN. IC₅₀ стойностите на изследваните съединения показват, че платиновите комплекси проявяват по-висока цитотоксична активност в сравнение с органичното съединение.

Doxylamine/pyridoxine loaded chitosan microspheres as potential nasal drug delivery systems

P. D. Katsarov^{1,4*}, B. A. Pilicheva^{1,4}, Y. I. Uzunova², G. H. Gergov³, M. I. Kassarova^{1,4}

¹ Department of Pharmaceutical sciences, Faculty of Pharmacy, Medical University-Plovdiv, Plovdiv, Bulgaria

² Department of Chemistry and Biochemistry, Faculty of Pharmacy, Medical University-Plovdiv, Plovdiv, Bulgaria

³ Department of Chemistry, Faculty of Pharmacy, Medical University-Sofia, Sofia, Bulgaria

⁴ High-technological Center of Emergency Medicine, Plovdiv, Bulgaria

Received February 14, 2017; Revised March 15, 2017

Dedicated to Acad. Bogdan Kurtev on the occasion of his 100th birth anniversary

Chitosan microspheres loaded with doxylamine and pyridoxine were formulated as potential drug delivery systems intended for nasal administration via spray drying technique. The possibility of incorporating the combination of these two drugs into one polymer matrix was studied. X-ray powder diffraction (XRPD) was applied to investigate possible transformations in the solid state of the drugs. A first-derivative ratio UV-spectrophotometric method for the assay of doxylamine in a binary mixture with pyridoxine was developed. The obtained particles were spherical in shape with median diameter ranging from 3.51 μm to 8.27 μm which is considered appropriate for nasal administration. The production yields (48.06%–66.97%) were recognized as optimum in regard to the spray drying method. The drug entrapment efficiency was high (87.36%–95.67%), indicating a tendency to increase with higher drug/polymer ratio. Drug release studies from the microspheres showed initial burst effect within the first 30 min, followed by a sustained release.

Key words: chitosan microspheres; doxylamine; pyridoxine; drug combination

INTRODUCTION

Drug delivery systems such as microspheres have gained serious popularity in the last few years due to the advantages they offer – enhanced drug stability, high carrier capacity and feasibility of variable routes of administration, including nasal application [1]. Different drugs have already been incorporated in microparticulate structures [2–4]. However, no information concerning microspheres loaded with doxylamine succinate and pyridoxine hydrochloride has been reported so far.

Doxylamine succinate (DOX), a first-generation antihistamine drug, and pyridoxine hydrochloride (PYR), a water-soluble vitamin, are two active substances, which have been well-known and used for the treatment of various pathological conditions. Their combination, on the other hand, is currently gaining serious interest because it is one of the few options on the pharmaceutical market, recently approved by FDA, as safe and effective for the treatment of morning sickness during pregnancy [5, 6]. So far, the drug combination is available only as orally administered dosage forms (tablets and capsules), though this route of administration is not

generally recommended for symptoms such as nausea and vomiting. Nasal administration, on the other hand, has been considered as suitable alternative for achieving good drug absorption and systemic therapeutic effect [7, 8]. For nasal formulations mucoadhesive polymer carriers are often used to ensure optimum deposition of the drugs in the nasal cavity and hence, a more intimate contact with the lining mucosa, which is a prerequisite for improved bioavailability. Chitosan, due to its great mucoadhesive and permeation enhancing properties, is one of the most promising natural polymers used in the pharmaceutical practice. It is also non-toxic, biocompatible and biodegradable, which defines its high potential as a carrier in drug delivery systems [1, 9].

The aim of this study was to formulate and characterize chitosan microspheres loaded with the drug combination DOX/PYR as drug delivery systems intended for nasal administration.

EXPERIMENTAL

Materials

Chitosan (from shrimp shells, low-viscosity, degree of deacetylation >70%), acetic acid,

* To whom all correspondence should be sent:
E-mail: plamen.katsarov@yahoo.com

doxylamine succinate and pyridoxine hydrochloride were purchased from Sigma Aldrich, USA. Phosphate-buffered saline (PBS) with pH 6.8 was prepared according to Ph. Eur. 8 [10]. All of the reagents used for the preparation of the PBS were of analytical grade.

Microspheres formulation

Chitosan microspheres were prepared by spray drying technique using co-current flow type B-290 Mini Spray Dryer (Büchi Labortechnik AG, Flawil, Switzerland). Drug/polymer solutions were prepared by dissolving an accurately weighed amount of chitosan, DOX and/or PYR in 2% (v/v) acetic acid aqueous solution. Drug/polymer ratio was varied. The solutions were further spray-dried through a 0.7 mm nozzle at 600 L/h compressed nitrogen flow rate, 140 °C inlet temperature, 10% pump rate and 95% aspiration. These conditions were experimentally determined as optimum for obtaining satisfactory production yields from the spray-dried solutions.

Microspheres characterization

Shape, size and production yield

The shape and surface morphology of the prepared microspheres were studied using a scanning electron microscope with secondary electrons detection (Philips SEM 515, Eindhoven, the Netherlands). The micrographs were generated at 25 kV accelerating voltage and 5000x magnification. The size of the formulated particles and their size distribution were measured by laser diffraction analyzer (LS 13 320, Beckman Coulter, USA), equipped with a Tornado system for powdered samples. The production yield was calculated on the basis of the obtained particle mass and the total mass of the used polymer and drugs.

Drug loading and entrapment efficiency

Accurately weighed amount of 10 mg microspheres was dispersed into 20 mL acetic acid solution (2% v/v) and sonicated until complete dissolution of the polymer and extraction of the incorporated drugs occurred. The solution was then filtered through a membrane filter (Chromafil Xtra RC, 0.45 µm) and diluted with PBS (pH 6.8). The amount of DOX and PYR was determined spectrophotometrically. Drug loading (*DL*) and entrapment efficiency (*EE*) were calculated and

expressed as average values ± SD after three determinations [11].

UV spectrophotometric assay

The quantitative determination of DOX and PYR was carried out in PBS (pH 6.8) using UV-visible spectrophotometer Evolution 300 (Thermo Fisher Scientific, USA) at wavelengths of 260 nm and 324 nm for DOX and PYR respectively. Due to spectral overlapping, a UV spectrophotometric first-derivative ratio method [12, 13] was developed for the quantitative analysis of DOX in binary mixtures with PYR. The developed methods were validated using mixtures of DOX and PYR and were characterized in terms of the regression parameters: root mean square error of prediction (*RMSEP*), relative error of prediction (*REP*), recovery and coefficient of determination (R^2).

X-ray powder diffraction

X-ray powder diffraction was used to evaluate the solid state structure of the microspheres. The diffractograms were obtained using X-ray powder diffractometer (D2 Phaser, Bruker AXS GmbH, Germany) under the following conditions: Ni-filtered Cu radiation at 30 kV and 10 mA of intensity. Phase analysis using Powder Diffraction; database, (ICDD) was performed for correct interpretation of the studied samples.

FTIR spectroscopy

Infrared spectroscopic study of the formulated microspheres and evaluation of eventual drug/polymer interactions after spray drying was performed using Nicolet iS 10 FTIR spectrometer (Thermo Fisher Scientific, Pittsburgh, PA, USA), equipped with a diamond ATR accessory in the range 650–4000 cm⁻¹.

In vitro drug release

In vitro drug release study was carried out using USP dissolution apparatus I - rotating basket (AT7 Sotax, Allschwil, Switzerland) containing 400 mL medium of PBS (pH 6.8) maintained at temperature of 37±0.5 °C and rotation speed of 50 rpm. Accurately weighed amount of microspheres, equivalent to 10 mg drug content was dispersed into 1 mL medium and transferred in a dialysis membrane bag with the two ends fixed by thread. The bags were then placed in the baskets and were brought into contact with the acceptor medium.

Samples of 5 mL were withdrawn from the solution at fixed time intervals and were replaced with the same amount of fresh PBS. Samples were filtered through a syringe membrane filter (0.45 μm) and analyzed spectrophotometrically for drug content. The release study for each microsphere model was repeated three times.

RESULTS AND DISCUSSION

Microspheres composition and characteristics

Five models of drug loaded microspheres were developed, varying drug concentration and drug/polymer ratio (Table 1). Models D1 and D2 were formulated with DOX, while models P1 and P2 were formulated with PYR. A single model was developed containing the drug combination DOX/PYR (DP). The aim was to investigate the influence of the varied drug concentration (1%–2% w/v) and the drug/polymer ratio (0.5:1 and 1:1 w/w) on the drug incorporation and microsphere characteristics.

SEM micrographs of the obtained microspheres are presented in Fig. 1. The particles had spherical shape and relatively smooth surface. However, a tendency for roughness was observed when the drug concentration of the spray-dried solutions decreased from 2% to 1% w/v (D1, P1).

The different microsphere models had median particle diameter from 3.51 to 8.27 μm (Table 1).

Such size was considered appropriate for nasal administration [14]. Particle size distribution curves of the models are shown in Fig. 2. The presence of structures larger than 20 μm was probably due to particle aggregation.

Production yields varied between 48.06% and 66.97% (Table 1) and were considered as optimum in regard to the typical for the production method extensive losses at laboratory scale [15]. The drug/polymer ratio did not influence the yield of DOX-loaded microspheres (48.06% and 48.12% production yields at ratios 0.5:1 and 1:1 w/w respectively). With the PYR models, however, much higher yield was obtained at higher drug/polymer ratio (1:1 w/w), respectively at higher PYR concentration. When more concentrated solutions were spray dried, larger particles were formed. Larger microspheres were more easily separated and collected as a final product, which diminished losses and resulted in a greater yield. The larger particle size of PYR microspheres (5.12 μm for P1 and 8.27 μm for P2) was probably the reason for the higher production yield of these models in comparison to DOX-loaded microspheres which were much smaller (4.54 μm for D1 and 3.51 μm for D2). The larger size of the PYR microspheres, on the other hand, was probably due to drug crystallization in the particles, which was confirmed by the XRPD analysis.

Table 1. Composition and physicochemical properties of DOX and PYR-loaded chitosan microspheres.

Formulation code	Concentration (% w/v)			Drug/polymer ratio (w/w)	Median particle size ($\mu\text{m}\pm\text{SD}$)*	Yield ($\%\pm\text{SD}$)*
	DOX	PYR	Chitosan			
D1	1	-	2	0.5:1	4.54 \pm 0.48	48.06 \pm 3.27
D2	2	-	2	1:1	3.51 \pm 0.15	48.12 \pm 4.30
P1	-	1	2	0.5:1	5.12 \pm 0.67	60.29 \pm 1.93
P2	-	2	2	1:1	8.27 \pm 1.19	66.97 \pm 1.79
DP	1	1	2	0.5:0.5:1	4.70 \pm 0.72	53.63 \pm 3.42

*n=3

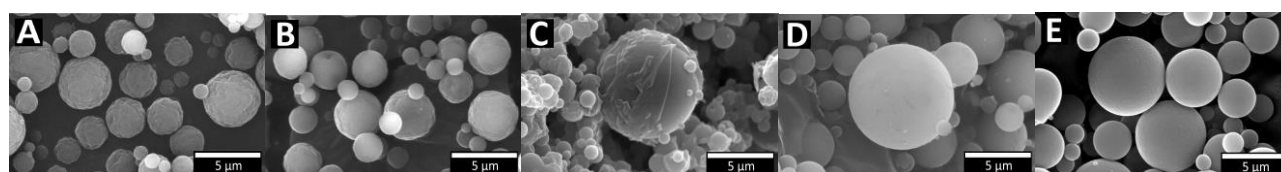


Fig. 1. SEM images of microspheres models: D1 (A), D2 (B), P1 (C), P2 (D), DP (E) (5000x).

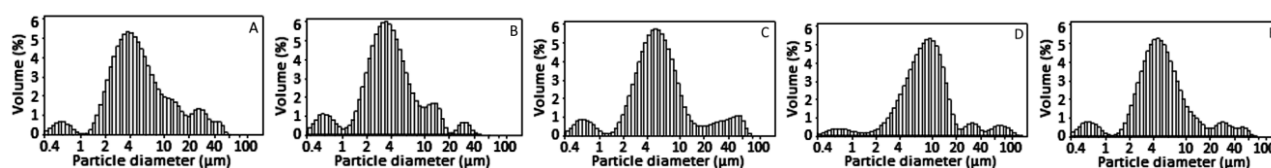


Fig. 2. Particle size distribution of microspheres models D1 (A), D2 (B), P1 (C), P2 (D), DP (E).

Table 2. Drug loading (*DL*) and entrapment efficiency (*EE*) of DOX-, PYR- and DOX/PYR-loaded chitosan microspheres.

Models	Drugs	Theoretical drug content (%)	DL ± SD (%)*	EE ± SD (%)*
D1	DOX	33.33	29.48 ± 0.50	88.43 ± 1.50
D2	DOX	50.00	43.68 ± 0.36	87.36 ± 0.73
P1	PYR	33.33	30.02 ± 0.92	90.09 ± 2.76
P2	PYR	50.00	44.71 ± 0.90	89.41 ± 1.79
DP	DOX + PYR	50.00 (25.00; 25.00)	47.83 ± 0.99 (23.40 ± 0.61; 24.43 ± 0.40)	95.67 ± 1.97 (93.60 ± 2.43; 97.73 ± 1.62)

*n=3;

Drug loading and entrapment efficiency

The obtained microspheres models showed *DL* from 29.48% to 47.83% and *EE* from 87.36% to 95.67% (Table 2). *DL* was strongly influenced by drug/polymer ratio. Increase in that ratio in DOX-loaded microspheres resulted in higher *DL* (from 29.48% in D1 to 43.68% in D2). However, *EE* at different drug/polymer ratios were commensurable (88.43% and 87.36%). Such tendency was also observed for the PYR-loaded microspheres. *DL* increased from 30.02% (P1) to 44.71% (P2) and *EE* was again high (90.09% and 89.41%, respectively). Therefore, for the formulation of DOX/PYR-loaded microspheres drug/polymer ratio of 1:1 rather than 0.5:1 *w/w* was preferred, because it led to higher *DL* for both DOX and PYR.

Beside achieving high *DL*, another challenging issue was to optimize DOX/PYR ratio in solution so that equal amounts of both drugs could be incorporated in the obtained DOX/PYR-loaded microspheres (DP), corresponding to the equal therapeutic doses of the drugs (10 mg DOX and 10 mg PYR) [5, 6]. The models loaded with DOX and PYR separately showed similar *DL* at a particular drug/polymer ratio (29.48% DOX and 30.02% PYR at 0.5:1 *w/w* ratio; 43.68% DOX and 44.71% PYR at 1:1 *w/w* ratio). For that reason, a 1:1 *w/w* DOX/PYR ratio was selected for the preparation of model DP. According to the obtained results for DP model, both drugs were incorporated in the microspheres at equal amounts (23.40% *DL* for DOX and 24.43% *DL* for PYR) which conformed to the primary aim.

As a result, an optimum DOX/PYR/chitosan ratio of 0.5:0.5:1 *w/w/w* was determined for the simultaneous incorporation of DOX and PYR in chitosan microspheres.

UV-spectroscopic quantitative analysis

In binary mixtures of the two drugs, PYR was successfully determined at a wavelength of 324 nm

(PYR absorption maximum) without any interference from DOX, using absorption spectra according to the following equation:

$$Y_1 = 0.0352 \times C_1 + 0.0020$$

where Y_1 is the absorption value at 324 nm and C_1 is PYR concentration in $\mu\text{g mL}^{-1}$.

However, due to intense overlapping of DOX and PYR spectra at 260 nm (DOX absorption maximum), a quantitative method for DOX analysis in binary mixtures with PYR was developed, using first derivative of ratio spectra technique. The recorded spectra of DOX were divided by the normalized absorption spectrum of PYR and first derivative of the ratio spectra were obtained. The amplitudes of the derivative ratio values at 271 nm for DOX were selected and plotted against the corresponding concentration of the standard solutions (Fig. 3).

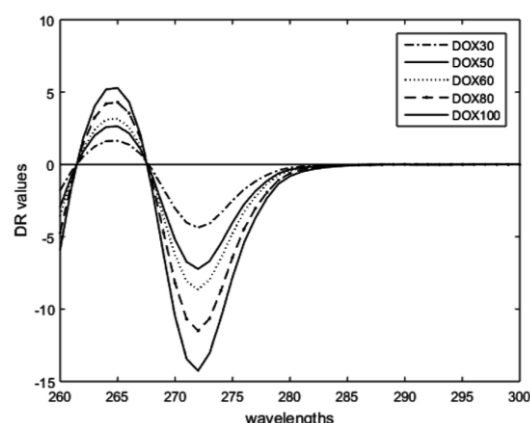


Fig. 3. First derivative ratio spectra of DOX in the range of 30–100 $\mu\text{g mL}^{-1}$ using PYR ($10 \mu\text{g mL}^{-1}$) as divisor.

The normalized spectrum of $10 \mu\text{g mL}^{-1}$ PYR solution was determined as an optimum divisor in the proposed method. The following calibration equation for DOX was calculated:

$$Y_2 = 0.0753 \times C_2 + 0.1338$$

where Y_2 is the peak amplitude at 271 nm and C_2 is DOX concentration in $\mu\text{g mL}^{-1}$.

The proposed quantitative spectrophotometric methods were validated using laboratory-prepared mixtures of DOX and PYR with different concentrations within the determined linearity range of 30–100 $\mu\text{g mL}^{-1}$ for DOX and 10–30 $\mu\text{g mL}^{-1}$ for PYR. The obtained regression parameters were: 1.1679 *RMSEP*, 3.07% *REP*, 101.54±2.41 recovery, 0.9986 R^2 for DOX and 0.1312 *RMSEP*, 0.97% *REP*, 100.57±1.22 recovery, 0.9998 R^2 for PYR.

X-ray powder diffraction analysis

The physical state of DOX and PYR in drug loaded microspheres was evaluated by X-ray powder diffraction. Diffractograms of the pure substances and the formulated microspheres are presented on Fig. 4.

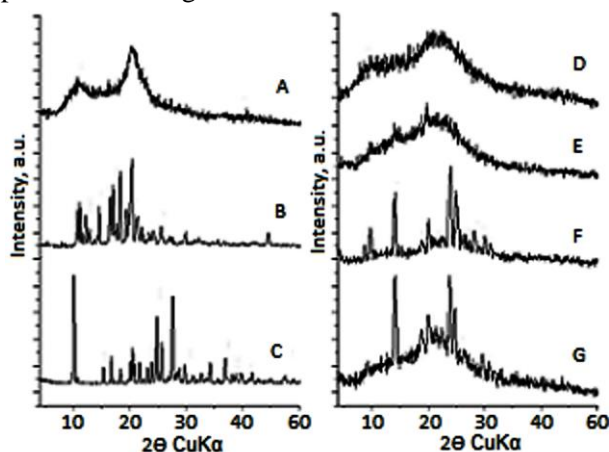


Fig. 4. X-ray powder diffractograms of chitosan (A), DOX (B), PYR (C), chitosan microspheres (D), DOX-loaded chitosan microspheres (E), PYR-loaded chitosan microspheres (F) and DOX-PYR-loaded chitosan microspheres (G).

DOX and PYR diffractograms showed a few characteristic peaks, which proved their crystalline structure. No distinctive peaks were registered in chitosan diffractogram, which indicated its amorphous nature. The microspheres diffractograms revealed that chitosan retained its amorphous structure after spray drying. For the active substances on the other hand, a transition from crystalline into amorphous state was registered. DOX-loaded microspheres diffractograms showed just a few small peaks and amorphous phase corresponding to that of chitosan. PYR-loaded microspheres diffractograms were of a similar pattern. However, a phase corresponding to crystalline PYR and PYR hydrochloride was

registered. Such a phase was also noted in the diffraction spectra of DOX/PYR-loaded microspheres. In the latter model, DOX was amorphous. Therefore, both crystalline drugs underwent transformation into amorphous state after spray drying with PYR partially retaining its crystalline structure.

FTIR spectroscopy

The spectra of the chitosan microspheres loaded with DOX or PYR are shown in Fig. 5. In the spectrum of DOX/PYR-loaded microspheres increased intensity of the absorption peaks at 3000–3600 cm^{-1} was observed due to the overlapping of stretching vibrations of the O-H groups of chitosan and pyridoxine, N-H bonds, and C-H bonds of the aromatic rings. Increased intensity was observed also in the region of 1620–1500 cm^{-1} and 1450–1400 cm^{-1} due to the overlapped vibrations of the aromatic rings of pyridine and benzene with the vibrations of the amide N-H bonds and protonated amino groups of chitosan. In the range 1100–1025 cm^{-1} peaks of symmetric and asymmetric stretching vibrations of C=O, C-O-C and CH₂-OH from the monosaccharide ring were observed, as well as wagging C-H vibrations of the monosaccharide ring of chitosan.

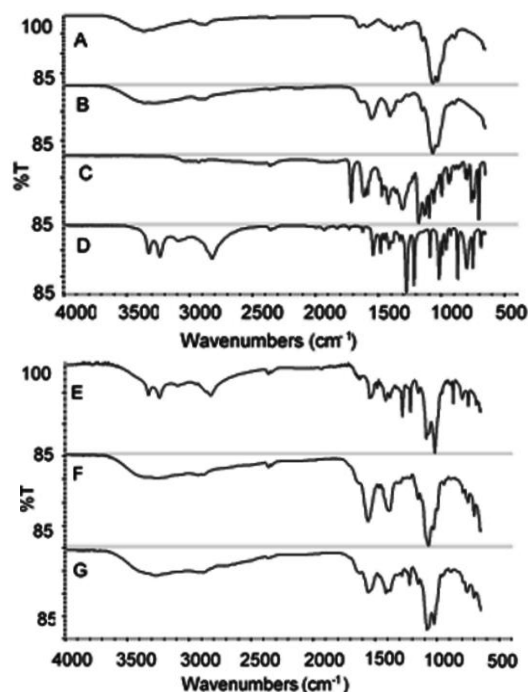


Fig. 5. FTIR-ATR spectra of chitosan (A), chitosan microspheres (B), DOX (C), PYR (D), PYR-loaded chitosan microspheres (E), DOX-loaded chitosan microspheres (F), and DOX-PYR-loaded chitosan microspheres (G).

The observed spectra showed that there were no covalent interactions either between chitosan and DOX or PYR, or between DOX and PYR.

In vitro release study

Dissolution profiles of the microspheres showed that DOX and PYR were released from all of the formulated models in a biphasic way, with initial rapid drug release (burst effect) followed by slower release (Fig. 6). Within the first 30 min 53.32% to 68.96% of the loaded DOX and PYR were released, which was probably due to the immediate dissolution of the molecules incorporated in the particles' periphery. After the initial burst release, prolonged drug release was observed, which was probably due to formation of a gel layer from the swollen chitosan and diffusion of the drugs from the particles core through it [16]. The total drug amount incorporated in the microspheres was completely released within 180 minutes in all investigated formulations. That could be explained with the high aqueous solubility of DOX and PYR [10] and their facilitated diffusion through the swollen polymer matrix and its pores, formed after the initial drug release.

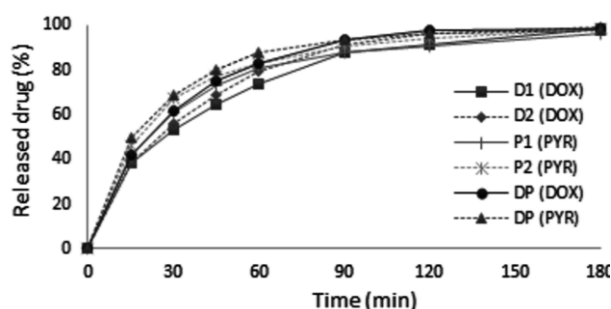


Fig. 6. Dissolution profiles of DOX and PYR from microspheres models D1, D2, P1, P2 and DP. (n=3).

CONCLUSION

Doxylamine and pyridoxine loaded chitosan microspheres of appropriate for nasal administration size were prepared by a conventional spray drying method. The two drugs were incorporated into the obtained particles with high entrapment efficiency. The influence of drug/polymer ratio on the particles drug loading was studied and an optimum model, loaded both with DOX and PYR was proposed as a potential drug delivery system for nasal administration. The registered burst release from the microspheres could be considered as positive, assuring sufficient initial therapeutic drug concentration to alleviate

the treated symptoms. On the other hand, further delay of the drug release should be accomplished, which would be a matter of future studies, in order to reduce the dosage frequency.

Acknowledgements: The authors gratefully acknowledge the financial support from Medical University-Plovdiv through university project SDP-04/2015.

REFERENCES

1. A. Mitra, B. Dey, *Indian J. Pharm. Sci.*, **73**, 355 (2011).
2. Y. Jiao, X. Pang, M. Liua, B. Zhanga, L. Li, G. Zhai, *Colloids Surf., B*, **140**, 361 (2016).
3. T. K. Giri, C. Choudhary, Ajazuddin, A. Alexander, H. Badwaik, D. K. Tripathi, *Saudi Pharm. J.*, **21**, 125 (2013).
4. S. B. Patil, K. K. Sawant, *Curr. Drug Deliv.*, **5**, 312 (2008).
5. S. R. Slaughter, R. Hearn-Stokes, T. van der Vlugt, H. V. Joffe, *N. Engl. J. Med.*, **370**, 1081 (2014).
6. N. Nuangchamngong, J. Niebyl, *Int. J. Womens Health*, **6**, 401 (2014).
7. A. Fortuna, G. Alves, A. Serralheiro, J. Sousa, A. Falcão, *Eur. J. Pharm. Biopharm.*, **88**, 8 (2014).
8. M. Alagusundaram, B. Chengaiah, K. Gnanaprakash, S. Ramkanth, C. M. Chetty, D. Dhachinamoorthi, *Int. J. Res. Pharm. Sci.*, **1**, 454 (2010).
9. V. R. Sinha, A. K. Singla, S. Wadhawan, R. Kaushik, R. Kumria, K. Bansal, S. Dhawan, *Int. J. Pharm.*, **274**, 1 (2004).
10. European Pharmacopoeia Commission, European Pharmacopoeia 8th ed., Council of Europe, Strasbourg, 2014.
11. A. Saigal, W. K. Ng, R. B. Tan, S. Y. Chan, *Int. J. Pharm.*, **450**, 114 (2013).
12. H. A. Merey, *Bull. Fac. Pharm. Cairo Univ.*, **54**, 181 (2016).
13. H. W. Darwish, S. A. Hassan, M. Y. Salem, B. A. El-Zeiny, *Spectrochim. Acta Mol. Biomol. Spectrosc.*, **83**, 140 (2011).
14. B. Pilicheva, P. Zagorchev, Y. Uzunova, M. Kassarova, *Int. J. Drug Delivery*, **5**, 389 (2013).
15. M. Maurya, K. Murphy, S. Kumar, L. Shib, G. Leea, *Eur. J. Pharm. Biopharm.*, **59**, 565 (2005).
16. M. Jelvehgari, D. Hassanzadeh, F. Kiafar, B. D. Loveymi, S. Amiri, *Iran J. Pharm. Res.*, **10**, 457 (2011).

МИКРОСФЕРИ ОТ ХИТОЗАН С ДОКСИЛАМИН И ПИРИДОКСИН – ПОТЕНЦИАЛНИ ЛЕКАРСТВО-ДОСТАВЯЩИ СИСТЕМИ ЗА НАЗАЛНО ПРИЛОЖЕНИЕ

П. Д. Кацаров^{1,4*}, Б. А. Пиличева^{1,4}, Й. И. Узунова², Г. Х. Гергов³, М. И. Касърова^{1,4}

¹ Катедра „Фармацевтични науки“, Фармацевтичен факултет, Медицински Университет-Пловдив, Пловдив, България

² Катедра „Химия и Биохимия“, Фармацевтичен факултет, Медицински Университет-Пловдив, Пловдив, България

³ Катедра „Химия“, Фармацевтичен факултет, Медицински Университет-София, София, България

⁴ Технологичен център за спешна медицина – град Пловдив, Пловдив, България

Постъпила на 14 февруари 2017 г.; Коригирана на 15 март 2017 г.

(Резюме)

Целта на настоящата работа е получаване и охарактеризиране на микросфери от хитозан, натоварени с доксиламин и пиридоксин, като потенциални лекарство-доставящи системи за назално приложение. Проучена е възможността за едновременното включване на двете лекарствени вещества (ЛВ) в обща полимерна матрица. Микросферите са получени по метода разпръсквателно сушене при вариране концентрацията на ЛВ и съотношението ЛВ/хитозан. Съвместимостта и физичното състояние на лекарствените вещества и полимера са проучени чрез инфрачервена спектроскопия и прахова рентгенова дифракция. За определяне количественото съдържание на доксиламин и пиридоксин в смес е разработен спектрофотометричен метод чрез производна спектроскопия. Получените микрочастици имат сферична форма. Средният диаметър е в границите 3.51 μm –8.27 μm и е подходящ за назално въвеждане. Добивът (48.06%–66.97%) се счита за оптимален предвид особеностите на приложената техника на получаване. Ефективността на включване на ЛВ в микросферите е висока (87.36%–95.67%), като се отчита тенденция към повишаване с увеличаване съотношението ЛВ/полимер. Профилите на освобождаване показват „бърст“ ефект през първите 30 мин, последван от забавено освобождаване.

Solution and solid state characterization of “sparteine surrogate” (+)-(1*R*,5*S*,11*aS*)-tetrahydrodeoxocytisine

S. P. Simeonov¹, S. D. Simova¹, B. L. Shivachev², R. P. Nikolova², V. B. Kurteva^{1*}

¹ Institute of Organic Chemistry with Centre of Phytochemistry, Bulgarian Academy of Sciences, Acad. G. Bonchev street, bl. 9, 1113 Sofia, Bulgaria

² Institute of Mineralogy and Crystallography “Acad. Ivan Kostov”, Bulgarian Academy of Sciences, Acad. G. Bonchev street, bl. 107, 1113 Sofia, Bulgaria

Received March 06, 2017; Revised March 16, 2017

Dedicated to Acad. Bogdan Kurtev on the occasion of his 100th birth anniversary

The „sparteine surrogate“ (+)-(1*R*,5*S*,11*aS*)-tetrahydrodeoxocytisine is obtained by two known protocols, direct and two-step procedure, and is characterized in solution and solid state as free base, mono-, and bis-hydrochloride. Unambiguous assignment of the proton and carbon NMR spectra of tetrahydrodeoxocytisine is reported for the first time. X-ray and NMR data are compared and structural preferences in solid state and solution are discussed.

Key words: tetrahydrodeoxocytisine; tetrahydrocytisine; NMR; single crystal XRD

INTRODUCTION

(-)-(1*R*,5*S*)-Cytisine is a nicotinic acetylcholine receptor agonist from Lupin alkaloids' family [1–5], firstly isolated from the seeds of *Cytisus Laburnum Med.* in 19th century [6, 7], which was widely applied to help with smoking cessation. The limitation in the natural sources availability has reasonably provoked extraordinary efforts directed towards developing new protocols for the synthesis of cytisine isomers and derivatives [8–10]. Among its reduced analogues (Fig. 1), tetrahydrocytisine has attracted the most significant attention. It is one of the major alkaloids in *Templetonia biloba* from Western Australia [11], which was firstly isolated from *Thermopsis chinensis* [12]. Several synthetic protocols have been further developed based mainly on applying different catalytic versions for hydrogenation of cytisine and finally, efficient conversion was achieved by using platinum oxide as a catalyst either in acetic acid at atmospheric pressure [13, 14] or in water under increased pressure of hydrogen [15–17].

By contrast, the “sparteine surrogate” tetrahydrodeoxocytisine, which has never been isolated from natural sources, is very poorly studied and is not fully characterized till nowadays. The (+)-isomer has been firstly obtained in 1906 via electrochemical reduction of cytisine in sulfuric acid at a lead cathode and was characterized as bis-hydrochloride and free base by elemental analysis

and optical rotation of the salt [18]. The same isomer has been later obtained by hydrogenation in hydrochloric acid in the presence of platinum oxide as a catalyst [19, 20] and characterized as D-tartrate and dipicrate by elemental analysis and optical rotation of tartrate [21]. Recently, tetrahydrodeoxocytisine has been obtained and used immediately in further step without preliminary purification and characterization [22]. To the best of our knowledge, there are no records in the literature on the NMR and XRD characterization of unsubstituted tetrahydrodeoxocytisine.

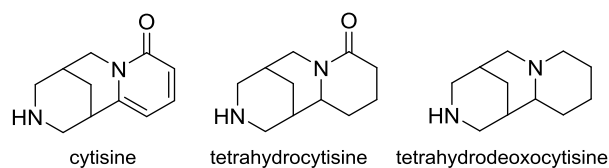


Fig. 1. Cytisine and its reduced derivatives.

Herein, we present a study on solution NMR and single crystal XRD characterization of the “spartein surrogate” (+)-(1*R*,5*S*,11*aS*)-tetrahydrodeoxocytisine as free base, mono- and bis-hydrochloride salts. The solid state structure of tetrahydrocytisine hydrochloride is also reported.

EXPERIMENTAL

Synthesis

All reagents were purchased from Aldrich, Merck and Fluka and were used without any further

* To whom all correspondence should be sent:
E-mail: vkurteva@orgchm.bas.bg

purification. Fluka silica gel/TLC-cards 60778 with fluorescent indicator 254 nm were used for TLC chromatography. The melting points were determined in capillary tubes on SRS MPA100 OptiMelt (Sunnyvale, CA, USA) automated melting point system with heating rate 1 °C/min. The NMR spectra were recorded on a Bruker Avance II+ 600 spectrometer (Rheinstetten, Germany) at 278K, 293K and 323K. The chemical shifts are quoted as δ -values in ppm using as an internal standard tetramethylsilane (TMS) or the solvent signal and the coupling constants are reported in Hz. The assignment of the signals is confirmed by applying 2D COSYDF, NOESY, HSQC and HMBC techniques. The spectra were recorded as 3×10^{-2} M solutions and were processed with Topspin 3.5 pl6 program. The NMR data are listed on Tables 1 and 2 using the numbering presented on Scheme 1. Molecular mechanics calculations were performed by MMFF94 in Spartan08. Specific optical rotation values were measured on Jasco P-2000 polarimeter (Tokyo, Japan) at D line of sodium lamp at 20 °C by using 1 dm quartz cell. The $[\alpha]_D$ are given in $\text{deg. cm}^3 \cdot \text{g}^{-1} \cdot \text{dm}^{-1}$, concentration in $\text{g} \cdot \text{cm}^{-3}$. The IR spectra were recorded on a Bruker Tensor37 FTIR Spectrometer in KBr disks. The frequencies are given in cm^{-1} . The differential thermal analysis (DTA), thermogravimetric analysis (TGA) and gas-mass evolving (MS) were taken on a SETSYS Evolution TGA-DTA/MS (Setaram), up to 300 °C.

*Synthesis of (+)-(1R,5S,11aS)-
tetrahydrodeoxocytisine bis-hydrochloride
(2.2HCl)*

To a solution of cytosine (**1**, 855 mg, 4.5 mmol) in MeOH (25 ml) and 36% aq. HCl (1 ml) platinum(IV) oxide (90 mg, 0.4 mmol) was added and the air was subsequently replaced by argon and hydrogen. The suspension was stirred vigorously under a hydrogen atmosphere overnight. The solid phase was removed by filtration through Celite. The solvent was removed *in vacuo* to afford the crude product (990 mg, 87%) as a colourless bis-hydrochloride salt. The analytically pure **2.2HCl** was obtained by recrystallization from *i*-PrOH: m. p. 274.0–274.2 °C (lit. [18] 282 °C; [20] 260 °C); $[\alpha]_D^{20} +20$ (c=0.5, EtOH) (lit. [18] $+10^\circ 15'$; solvent, concentration, and temperature not indicated). IR (the most intensive bands): 3492, 3363, 2980, 2947, 2796, 1615, 1448, 995 and 470.

*Synthesis of (+)-(1R,5S,11aS)-
tetrahydrodeoxocytisine hydrochloride (2.HCl)*

Tetrahydrocytosine (**3**) was synthesised *via* literature protocol [22] and was converted into hydrochloride salt by saturation of methanol solution with HCl vapours. The analytically pure compound was obtained by recrystallization from *i*-PrOH. To a solution of crude **3** hydrochloride (300 mg, 1.3 mmol) in MTBE (20 ml) LiAlH_4 (230 mg, 6 mmol) was added portion-wise at 0 °C. The suspension was stirred at room temperature under argon atmosphere overnight and was then diluted with MTBE (20 ml). The excess of LiAlH_4 was quenched with water at 0 °C. The solid phase was removed by filtration through Celite. The organic solution was dried over Na_2SO_4 and evaporated to dryness to give crude diamine **2** (159 mg, 68% yield). The latter was dissolved in MTBE (20 ml) and precipitated by slow addition of HCl vapours. The solid phase was filtered off, washed with MTBE and dried in desiccator. The analytically pure **2.HCl** was obtained by recrystallization from *i*-PrOH: m. p. 184.4–184.9 °C; $[\alpha]_D^{20} +24$ (c=0.5, EtOH). IR (the most intensive bands): 3494, 3429, 3066, 2935, 2760, 1640, 1517, 1446, 1124, 1020 and 451.

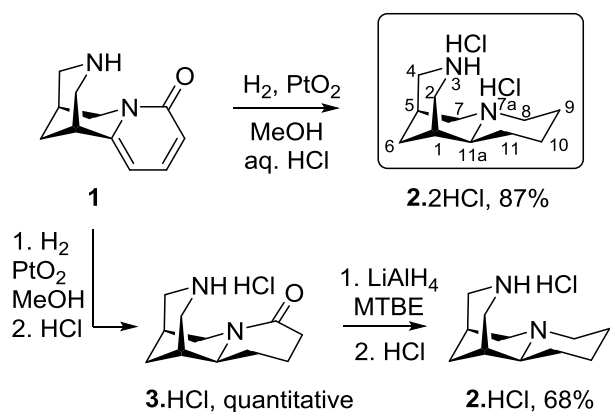
Crystallography

The crystals of **2.2HCl**, **2.HCl** and **3.HCl** were mounted on a glass capillary and all geometric and intensity data were taken from these crystals. Crystallographic measurements were taken on an Agilent SupernovaDual diffractometer equipped with an Atlas CCD detector (**2**) and on an Enraf Nonius CAD4 diffractometer (**3**) using micro-focus Mo $K\alpha$ radiation ($\lambda = 0.71073 \text{ \AA}$) at room temperature. The determination of the unit cell parameters, data collection and reduction were performed with CrysAlispro software for **2** [23] and CAD-4 EXPRESS [24] for **3**. The structures were solved by direct methods and refined by the full-matrix least-squares method on F^2 with ShelxS and ShelxL 2016/6 programs [25]. All non-hydrogen atoms, including solvent molecules, were located successfully from Fourier maps and were refined anisotropically. Hydrogens adjoining N, O and H atoms of chiral centers were positioned from difference Fourier map. The H atoms on $\text{C}_{\text{methylene}}$ were placed in idealized positions ($\text{C}-\text{H} = 0.97 \text{ \AA}$). The hydrogens adjoining N7a, N3, C1, C5 and C11a were freely refined while the remaining H atoms were constrained to ride on their parent

atoms, with $U_{iso}(H) = 1.2U_{eq}(C \text{ or } O)$. The most important crystallographic and refinement indicators are listed on Table S1. Crystallographic data (with structure factors) for the structural analysis have been deposited with the Cambridge Crystallographic Data Centre, No. CCDC-1534860 (**2.HCl**), 1534861 (**2.2HCl**) and CCDC-1534862 (**3.HCl**). Copies of this information may be obtained free of charge from: The Director, CCDC, 12 Union Road, Cambridge, CB2 1EZ, UK. Fax: +44(1223)336-033, e-mail: deposit@ccdc.cam.ac.uk, or www: www.ccdc.cam.ac.uk.

RESULTS AND DISCUSSION

The “spartein surrogate” (+)-tetrahydrodeoxocytisine (**2**) was obtained from natural (-)-(1*R*,5*S*)-cytisine (**1**) *via* two independent protocols, shown on Scheme 1. Platinum oxide catalysed hydrogenation in methanol in the presence of hydrochloric acid at atmospheric pressure led directly to the target product as bis-hydrochloride salt. The two-step procedure ensured the intermediate tetrahydrocytisine (**3**) and the final tetrahydrodeoxocytisine (**2**) as free bases. Both compounds were converted into mono hydrochlorides while trying to grow single crystal phases. The latter provides the opportunity to study the influence of the type of both nitrogen atoms on the structural preferences of cytisine derivatives.



Scheme 1. Synthesis of (+)-(1*R*,5*S*,11*aS*)-tetrahydrodeoxocytisine salts **2.2HCl** and **2.HCl**.

The NMR spectra of cytisine (**1**), tetrahydrodeoxocytisine as free base (**2**) and as hydrochloride (**2.HCl**) and tetrahydrocytisine hydrochloride (**3.HCl**) were recorded in chloroform-*d*, while those of tetrahydrodeoxocytisine bis-hydrochloride (**2.2HCl**) in methanol-*d*₄ due to its very limited solubility in chloroform. The proton spectra of **2.HCl** showed

broad signals for most of the groups in the temperature interval 278–323K without big changes in the chemical shifts. That is why the chemical shift determination was made at the highest temperature 323K where narrow signals for most protons were observed (see Fig. S1). Unambiguous assignment of the proton and carbon signals in the spectra (Tables 1 and 2) was achieved by analysing the specific interactions in homo- and heteronuclear 2D COSY, NOESY, HSQC and HMBC experiments (Figs. S2–S10). For comparison HSQC spectra of **2.2HCl** were also recorded at very low concentration (less than 1×10^{-3} M) in chloroform exacting the chemical shifts from the HSQC spectra.

Based on the known configuration of cytisine (1*R*,5*S*) the absolute configuration of the newly generated chiral centre in the products can be assigned as 11*aS* on the basis of the observed coupling and NOE information. The proton signal for H-11*a* is a doublet with a *J*-coupling bigger than 11 Hz, suggesting its axial position, confirmed by the observed close proximity of H-11*a* to H-1, H-11_{eq}, H-7_{ax}, H-8_{ax}, H-10_{ax} and H-6₁ in the NOESY spectra (Figs. S3, S6, and S8). The fact that the new chiral centre CH-11*a* possesses *S*-configuration is verified also by single crystal XRD.

Crystals suitable for X-ray diffraction analyses were grown from *iso*-propanol solutions by slow evaporation at room temperature for all compounds (**2** and **3**). All three compounds crystallized in non-centrosymmetric groups (Table S1) with one molecule in the asymmetric unit (Fig. 2). The location and positioning of hydrogens adjoining N7*a*, N3, C1, C5 and C11*a* was performed using difference Fourier maps. While for C1, C5 and C11*a* the assignment is unequivocal for all compounds, in the case of mono hydrochloride **2.HCl** the H atom position is more delicate. The following approach has been applied for the correct assignment of hydrogens adjoining nitrogen's. After the location of heavier atoms hydrogens were positioned on calculated positions and four cycles (*e.g.* “l.s. 4” instruction) of anisotropic refinement were performed. In the next step the N7*a* and N3 hydrogen atoms occupancy was set to “zero” and difference Fourier maps were generated based on existing structural parameters (l.s. 0 and “acta” instruction removed). The obtained maps (Fig. 3) show the presence (excess) of electron density (in red) along with the positioning of the H atoms (from chemically sensible positions). One can clearly recognize that in the case of **2.2HCl** there is an excess of electron density near N3 and N7*a*,

Table 1. Chemical shifts, multiplicities^a and coupling constants (in *Italic*) in the ¹H NMR spectra of compounds **1-3**.

proton	1 ^b	2 ^b	2.HCl ^c	2.2HCl ^d	2.2HCl ^e	3 ^b
H-1	2.907 qt 2.6	1.378 bs	1.795 bs	2.25	2.296 bs	1.945 q 3.2
H-2_{ax}	3.059 dd <i>12.1,2.3</i>	2.803 ddd <i>13.8,2.6,1.6</i>	3.178 dd <i>13.3,3.6</i>	3.52	3.343 dd <i>14.2,4.8</i>	3.20 bt
H-2_{eq}	3.002 ddd ov <i>12.5,2.5,1.5</i>	3.298 d <i>13.7</i>	3.663 ddd <i>13.3,3.2,2.3</i>	3.52	3.635 bd <i>14.2</i>	3.790 d <i>13.4</i>
H-4_{ax}		2.999 dt <i>13.4, 2.6</i>	3.328 dt <i>12.9,2.9</i>	3.51 and <i>3.56</i>	3.401 ddd <i>13.5,4.3,1.6</i>	3.28 bt
H-4_{eq}	3.105 dd <i>12.5,2.5</i>	3.120 dt <i>13.4,2.5</i>	3.527 ddd <i>13.0,3.6,2.3</i>		3.518 bd <i>13.3</i>	3.580 d <i>13.1</i>
H-5	2.328 m	1.713 bs	2.120 bs	2.49	2.448 bs	2.24 m
H-6₁	1.962 t	1.73 ov	1.846 m	2.13	2.083 t	1.86 bd
H-6₂	3.3	1.890 dm <i>12.0</i>	1.971 dq <i>13.0,2.8</i>		3.5	2.063 dq <i>13.2, 2.9</i>
H-7_{ax}	3.903 ddd <i>15.6,6.7,1.3</i>	2.425 dt <i>11.2,2.6</i>	2.533 bs	3.26	3.279 bdd <i>13.2,4.0</i>	2.889 d <i>13.6</i>
H-7_{eq}	4.129 d <i>15.6</i>	2.887 dt <i>11.2,2.4</i>	3.025 bd <i>12.4</i>	3.58	3.547 d <i>13.2</i>	4.682 dt <i>13.9,2.1</i>
H-8_{ax}	-	1.75 ov	1.926 vb	3.52 ov.	3.46 d ov	-
H-8_{eq}	-	2.754 dqt <i>11.2,2.1</i>	2.881 d <i>10.9</i>	3.03	3.100 td <i>13.3,2.4</i>	-
H-9_{ax}	6.463 dd <i>9.1,1.5</i>	1.519 qm ov	1.648	2.26	2.324 qt <i>14.2,4.3</i>	2.923 ddd <i>17.0,13.9,6.4</i>
H-9_{eq}		1.60 dm <i>13.1</i>		1.83	1.88 d ov	2.390 ddd <i>17.0,4.9,2.3</i>
H-10_{ax}	7.302 dd <i>9.1, 6.9</i>	1.297 qt <i>12.9,4.0</i>	1.329 qt <i>13.0,4.0</i>	1.69	1.704 qt <i>13.2,4.0</i>	1.675 qdd <i>13.4,4.8,2.9</i>
H-10_{eq}		1.791 d <i>12.0</i>	1.853 m	2.08	1.981 dm <i>13.6,4.0,2.7</i>	1.983 m
H-11_{ax}	6.002 dd <i>6.9,1.5</i>	1.536 qm ov	1.630 m	2.54	2.113 qd <i>12.7,3.7</i>	2.255 qd <i>12.8,3.2</i>
H-11_{eq}		1.430 dm <i>12.7</i>	1.520 dq <i>13.5,3.5</i>	1.89	1.84 d ov	1.762 dqt <i>13.3,3.1</i>
H-11a		2.157 dm <i>11.2</i>	2.334 br	3.37	3.47 d ov	3.464 dt <i>12.0,6.5</i>
NH			10.86 bs	11.46, bs 11.28, bs 10.14, bs		9.79, bs 8.12, bs

^a s – singlet, d – doublet, t – triplet, q – quartet, qt – quintet, b – broad, v – very broad; m – multiplet, and ov – overlapped signals; ^b In CDCl₃ at 293K; ^c In CDCl₃ at 323K; ^d Chemical shifts from HSQC; ^e In CD₃OD at 293K.

Table 2. Chemical shifts in the ¹³C NMR spectra of compounds **1-3**.

Carbon	1 ^a	2 ^a	2.HCl ^b	2.HCl ^c	2.2HCl ^a	2.2HCl ^d	3 ^a
C-1	35.60	34.08	31.58	32.00	30.74	31.76	30.94
C-2	53.98 ^e	47.92	45.83	45.67	39.85	41.42	42.78
C-4	52.99	52.01	49.64	49.57	44.59	46.04	47.34
C-5	27.76	29.68	27.09	27.47	25.89	27.31	25.92
C-6	26.30	34.60	32.28	32.38	28.31	28.49	30.54
C-7	49.75 ^e	61.73	60.68	60.77	56.32	56.99	46.12
C-8	163.69	57.27	56.45	56.67	58.25	58.82	173.01
C-9	116.74	26.03	25.29	25.38	22.75	23.77	33.15
C-10	138.82	24.72	23.91	24.12	22.32	23.74	20.48
C-11	105.02	30.58	29.86	30.06	27.55	28.71	27.41
C-11a	151.07	66.23	65.34	65.65	65.71	66.65	60.10

^a In CDCl₃ at 293K; ^b In CDCl₃ at 278K; ^c In CDCl₃ at 323K; ^d In CD₃OD at 293K; ^e Assignment in [5] is interchanged due to printing error.

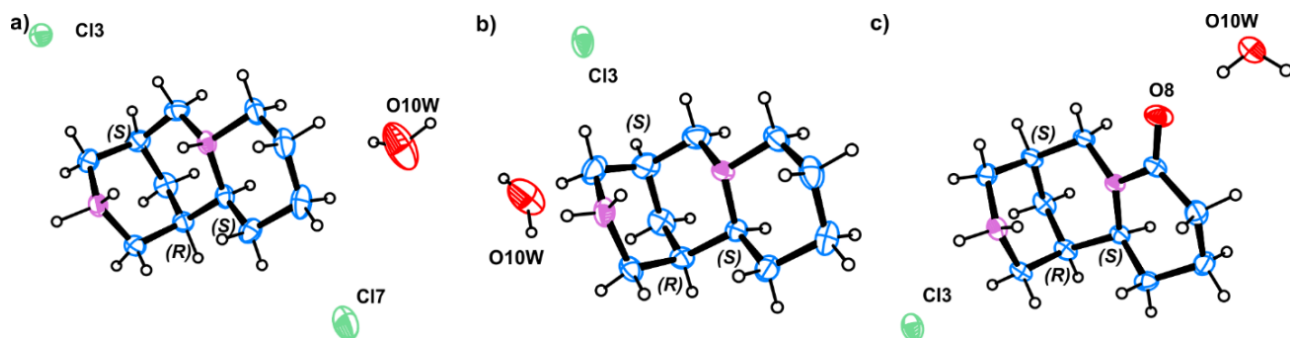


Fig. 2. ORTEP drawings of 2.2HCl (a), 2.HCl (b), and 3.HCl (c) with the atomic numbering scheme (ellipsoids are at 50% probability), the hydrogen atoms are shown as small spheres of arbitrary radii; the atomic numbering is shown on Scheme 1, compound 2.2HCl.

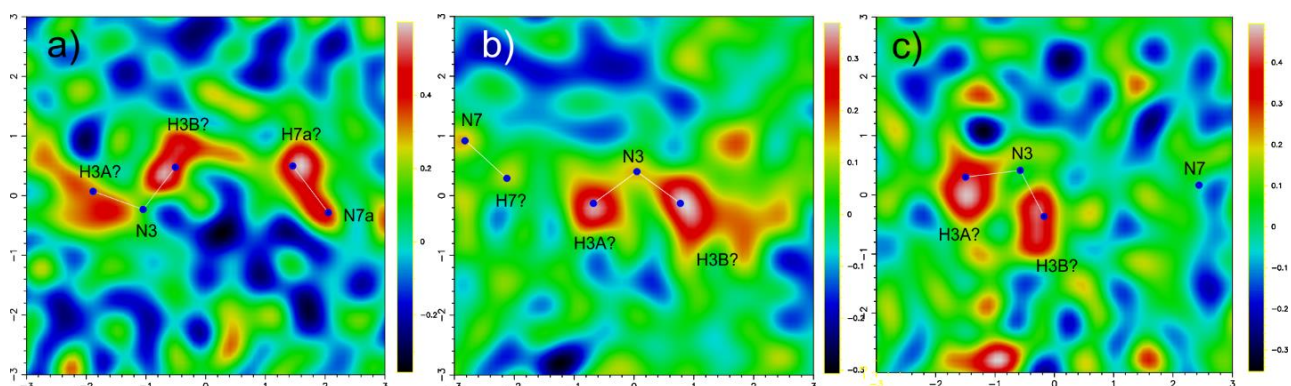


Fig. 3. X-ray difference Fourier maps in the region of N3 and N7a in 2.2HCl (a), 2.HCl (b), and 3.HCl (c) showing the peak (excess of electron density in red) due to the hydrogen.

while in the cases of mono chloride (2.HCl and 3.HCl) the excess is only near N3 and thus only one of the N centres is protonated, which is expected for amide 3.HCl. In addition to the location of the H atoms near the N centres the 2.2HCl structure disclosed one more peculiarity. The initial structure refinement of 2.2HCl did not include a solvent water molecule as the maximum residual electron density in the map was 0.86 e. However the CIF check generated a PLAT094 alert: Ratio of Maximum / Minimum Residual Density 2.16 e.g. “The ratio of the maximum and minimum residual density excursions is unusual. This might indicate unaccounted for twinning or missing atoms (e.g. associated with disordered solvent)”.

Therefore, in order to assess if water was present in 2.2HCl we performed FT-IR (Fig. S11). As the results were inconclusive, due to the overlap of NH^+ , NH_2^+ and water OH vibrations, a DTA-TGA-MS of 2.2HCl was conducted (Fig. S12). The thermal analyses showed an *endo* effect around ~ 70 °C, accompanied by $\sim 2.5\%$ of mass losses while the MS detected the release of water. This indicates the presence of weak bonded water (physisorption or solvent) in the sample. To minimize the residual density, solvent water was introduced in the crystal structure and its occupancy was refined. The

comparison of the values obtained from the structure refinement (O10W occupancy of 29%) and TGA loss are in agreement e.g. 2.4% vs 2.5%.

There are no significant differences in distances or angles within the molecules of the three cytosine derivatives (2.2HCl, 2.HCl and 3.HCl) as can be seen from the overlay of the three molecules (Fig. 4 and Table S2).

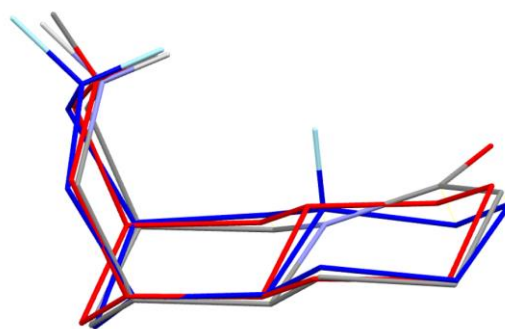


Fig. 4. Relative orientation in 2.2HCl (blue), 2.HCl (red), and 3.HCl (grey); *rmsd* of 0.1498 Å and 0.189 Å for 2.2HCl vs 2.HCl and 2.HCl vs 3.HCl, respectively.

It is interesting to note the geometry of the protonated and deprotonated N7a centre with respect to the plane formed by C7-C8-C11a. The N7a distance to the plane is 0.444, 0.433 and 0.190 Å in 2.2HCl, 2.HCl and 3.HCl respectively. The

observed "flattening" C7-C8-C11a-N7A in **3.HCl** is due to the presence of a carbonyl group (C8=O8) and the resulting conjugation effects. In all structures Cl3 is closer to N3 with distance between Cl3...N3 slightly bigger than 3.0 Å. In **2.2HCl** the second Cl7 is located near N7a (N7a...Cl7 distance of 3.099(5) Å). The solvent water molecules present on all structures interact mainly with chlorine. In **3.HCl** due to the presence of a carbonyl group (strong acceptor) the interaction is Cl...H-O-H...O=C, while in **2.2HCl** and **2.HCl** the interaction is Cl...H-O-H...Cl (Fig. 5). In both **2.2HCl** and **2.HCl** the water position occupancy is not full suggesting that its presence may not be essential for the crystal structure. Indeed, in addition to the typical hydrogen bonding interactions the three-dimensional packing of the molecules is stabilized by several other weak interactions (Table S3).

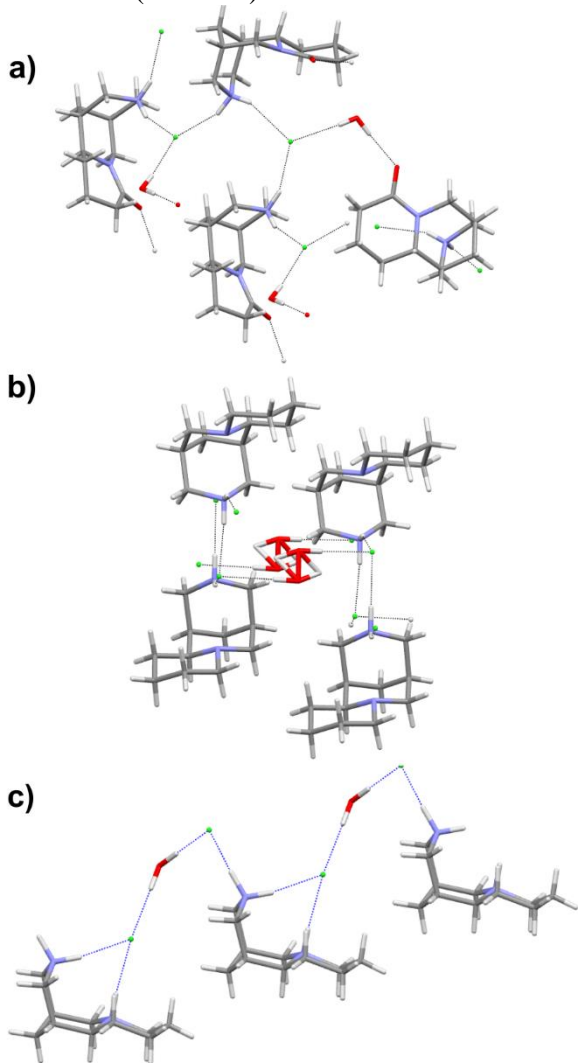


Fig. 5. Observed solvent (water) interactions in a) **3.HCl**, b) **2.HCl**, and c) **2.2HCl**; the water position occupancy in **2.HCl** is 0.41%, while in **2.2HCl** it is 0.29%.

The solution proton and carbon NMR data (Tables 1 and 2) are fully consistent with the X ray observations. It should be, however, noted that while the NMR data for **3.HCl** are compatible with a single conformer, both proton and carbon spectra indicate the presence of more conformers for **2.HCl** and **2.2HCl**. Literature examples [26, 27] predict that the end rings in **2** could principally exist as chair and boat conformation as shown on Fig. 6. Molecular mechanics calculations [28] for **2.HCl** provide evidence that the major conformer constitutes of three chair rings, that corresponds to the X ray structure. Some small amounts of the two possible minor conformers lead to signal broadening that is detected both in the carbon and more pronounced in the proton spectra.

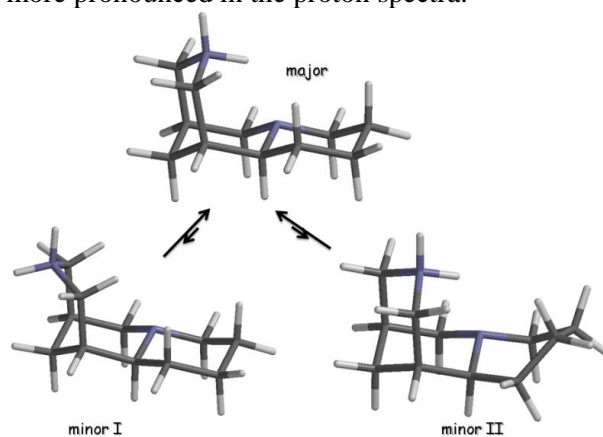


Fig. 6. Possible conformers for **2.HCl**.

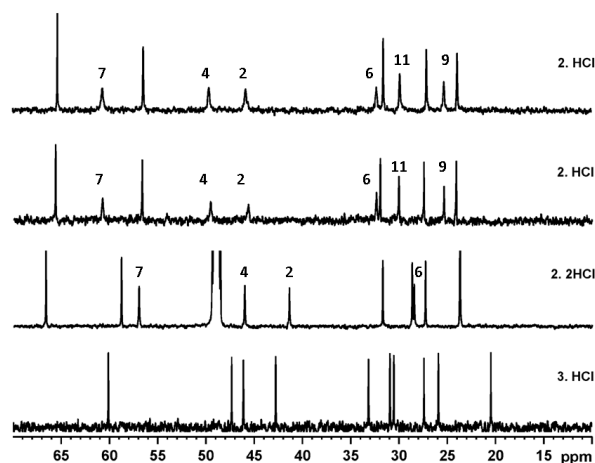


Fig. 7. Aliphatic part of the carbon spectra of the products, ordered from top to bottom: **2.HCl** at 293K, **2.HCl** at 323K, **2.2HCl** at 293K, and **3.HCl** at 293K. The broadened signals in the spectra are indicated.

Inspection of the carbon spectra of the three compounds (Fig. 7) indicates that most broadened signals are observed for **2.HCl**. These signals imply possible presence of two "boat-chair-chair" conformers (denoted as minor I and minor II),

corroborated by the broadened carbon signals for C-7, C-2, C-4, C-6, C-9 and C-11. On the contrary, compound **2**.2HCl does not show any broadening of the C-9 and C-11 signals, indicating exchange only in the N-3 containing ring (minor I conformer). Both salts **2** differ from **3**.HCl, where no signal broadening is observed.

Detailed inspection and comparison of the proton spectra of the compounds studied confirm that the all chair conformer is the major one. Main facts in this respect are some chemical shift differences and coupling patterns. H-11a is a clear doublet with a coupling larger than 10 Hz in all studied compounds, indicating its axial position. A reversal of the usual order of the equatorial-axial protons for H-9 and H-11 is observed, confirming 1,3-*syn* diaxial interaction between hydrogen atoms and N unshared electron pairs [29]. The somewhat broadened signal multiplicities of both H-1 and H-5 does not indicate considerable presence of a boat form, since no big coupling constant as expected for J_{H1H2} and J_{H4H5} in such case is observed.

CONCLUSION

The „sparteine surrogate“ (+)-(1R,5S,11aS)-tetrahydrodeoxocytisine is characterized for the first time by NMR spectroscopy in solution and single crystal XRD in solid state. The detailed analyses of the data indicate only the all chair conformation in solid state and as predominant in solution.

Acknowledgements: The financial support by the Bulgarian Science Fund, infrastructure projects UNA-17/2005, DRNF-02-13/2009, DRNF-02/01, and BG161PO003-1.2.04-0007-C0001, is gratefully acknowledged.

Electronic Supplementary Data available here.

REFERENCES

1. J. P. Michael, *Nat. Prod. Rep.*, **25**, 139 (2008).
2. N. J. Leonard, in: *The Alkaloids, Chemistry and Physiology*, R. H. F. Manske, H. L. Holmes, (eds.), vol. III, Academic Press, New York, NY, 1953, p. 119.
3. S. Ohmiya, K. Saito, I. Murakoshi, in: *The Alkaloids*, G. A. Cordell (ed.), vol. 47, Academic Press, New York, 1995, p 2.
4. K. Saito, I. Murakoshi, in: *Studies in Natural Products Chemistry. Structure and Chemistry* (Part C), Atta-ur-Rahman (ed.), Vol. 15, Elsevier, Oxford, 1995, p 519.
5. S. Berger, D. Sicker, *Classics in Spectroscopy, Isolation and Structure Elucidation of Natural Products*, Wiley-VCH Verlag GmbH & Co., KGaA, Weinheim, 2009, Chapter 1.5, p. 65.
6. A. Husemann, W. Marmé, *Z. Chem.*, **1**, 161 (1865).
7. A. Husemann, T. Husemann, *Die Pflanzenstoffe in Chemischer, Physiologischer, Pharmakologischer und Toxikologischer Hinsicht*, Verlag von Julius Springer, Berlin, 1871, p 64.
8. E. G. Pérez, C. Méndez-Gálvez, B. K. Cassels, *Nat. Prod. Rep.*, **29**, 555 (2012).
9. J. Rouden, M.-C. Lasne, J. Blanchet, J. Baudoux, *Chem. Rev.*, **114**, 712 (2014).
10. D. Bartusik, D. Aebisher, P. Tutka, *Modern Org. Chem. Res.*, **1**, 10 (2016).
11. R. Greinwald, C. Henrichs, G. Veen, J. H. Ross, L. Witte, F.-C. Czygan, *Biochem. Syst. Ecol.*, **23**, 649 (1995).
12. K. Saito, S. Takamatsu, M. Yamazaki, S. Ohmiya, I. Murakoshi, *Tennen Yuki Kagobutsu Toronkai Koen Yoshishu*, **32**, 268 (1990); *CA* **114**, 203603 (1991).
13. F. Bohlmann, E. Winterfeldt, H. Overwien, H. Pagel, *Chem. Ber.*, **95**, 944 (1962).
14. M. J. Johansson, L. Schwartz, M. Amedjkouh, N. Kann, *Tetrahedron: Asymmetry*, **15**, 3531 (2004).
15. F. Galinovsky, O. Vogl, W. Moroz, *Monatsh. Chem.*, **85**, 1137 (1954).
16. A. V. Ivachtchenko, S. E. Tkachenko, Y. B. Sandulenko, V. Y. Vvedensky, A. V. Khvat, *J. Comb. Chem.*, **6**, 828 (2004).
17. Y. B. Sandulenko, A. V. Ivashchenko, D. V. Kravchenko, S. E. Tkachenko, V. Y. Vvedensky, *Russ. Chem. Bull.*, **57**, 1999 (2008).
18. M. Freund, P. Horkheimer, *Ber. Dtsch. Chem. Ges.*, **39**, 814 (1906).
19. F. Galinovsky, E. Stern, *Chem. Ber.*, **77**, 132 (1944).
20. S. Okuda, H. Kataoka, K. Tsuda, *Chem. Pharm. Bull.*, **13**, 491 (1965).
21. F. Galinovsky, O. Vogl, W. Moroz, *Monatsh. Chem.*, **83**, 242 (1952).
22. I. Philipova, G. Stavrakov, N. Vassilev, R. Nikolova, B. Shivachev, V. Dimitrov, *J. Organomet. Chem.*, **778**, 10 (2015).
23. CrysAlis PRO, Agilent Technologies, UK Ltd, Yarnton, England, 2011.
24. XCAD4, Harms & Wocadlo, University of Marburg, Germany, 1995.
25. G. M. Sheldrick, *Acta Cryst.*, **C71**, 3 (2015).
26. A. Gogoll, H. Grennberg, A. Axen, *Magn. Res. Chem.*, **35**, 13 (1997).
27. H.-J. Schneider, L. Sturm, *Angew. Chem. Int. Ed. Engl.*, **15**, 545 (1976).
28. <https://www.wavefun.com/products/spartan.html>.
29. W. M. Golebiewski, *Magn. Res. Chem.*, **24**, 105 (1986).

ОХАРАКТЕРИЗИРАНЕ В РАЗТВОР И ТВЪРДО СЪСТОЯНИЕ НА “СПАРТЕИНОВИЯ СУРОГАТ”
(+)-(1R,5S,11aS)-ТЕТРАХИДРОДЕОКСОЦИТИЗИН

С. П. Симеонов¹, С. Д. Симова¹, Б. Л. Шивачев², Р. Н. Петрова², В. Б. Куртева^{1*}

¹ *Институт по Органична Химия с Център по Фитохимия, Българска Академия на Науките, ул. Акад. Г. Бончев, бл. 9, 1113 София, България*

² *Институт по Минералогия и Кристалография „Акад. Иван Костов“, Българска Академия на Науките, ул. Акад. Г. Бончев, бл. 107, 1113 София, България*

Постъпила на 06 март 2017 г.; Коригирана на 16 март 2017 г.

(Резюме)

„Спартеиновият сурогат“ (+)-(1R,5S,11aS)-тетраhydrodeoxocytisine е синтезиран по две известни процедури, директна и дву-стъпкова, и е охарактеризиран в разтвор и твърдо състояние под формата на свободна база, моно- и ди-хидрохлорид. За първи път е представено еднозначно отнасяне на сигналите в протонните и въглеродни ЯМР спектри на тетраhydrodeoxocytisine. Направен е сравнителен анализ на данните от монокристална рентгенова дифракция и ЯМР спектроскопия и са дискутирани предпочетените структури в твърдо състояние и в разтвор.

Flavonoid glycosides and free radical scavenging activity of Bulgarian endemic *Alchemilla jumrukczalica* Pawl.

A. Trendafilova^{1*}, M. Todorova¹, A. Vitkova²

¹ Institute of Organic Chemistry with Centre of Phytochemistry, Bulgarian Academy of Sciences, Acad. G. Bonchev str., bl. 9, 1113 Sofia, Bulgaria

² Institute of Biodiversity and Ecosystem Research, Bulgarian Academy of Sciences, 2 Gagarin Str., 1113 Sofia, Bulgaria

Received February 14, 2017; Revised March 07, 2017

Dedicated to Acad. Bogdan Kurtev on the occasion of his 100th birth anniversary

The aim of this study was to identify the flavonoid constituents of the Bulgarian endemic *Alchemilla jumrukczalica* Pawl. and evaluate the antiradical scavenging activity of the total extract, fractions and individual compounds. The total MeOH extract exhibited a significant DPPH activity (IC₅₀ 10.7±0.4 µg/ml), while EtOAc fraction obtained after partition of the total extract was found to be the most active radical scavenger (IC₅₀ 5.1±0.1 µg/ml). Catechin and seven flavonoid glycosides (guajaverin, hyperoside, isoquercetin, quercitrin, miquelianin, tiliroside and trifolin) were isolated from EtOAc fraction. Their structures were elucidated on the basis of spectral data. Quercetin glycosides (guajaverin, hyperoside and miquelianin) were found to be better DPPH radical scavengers than kaempferol-3-O-galactoside and catechin.

Key words: *Alchemilla jumrukczalica*; Rosaceae; flavonoid glycosides; DPPH assay

INTRODUCTION

Species of the genus *Alchemilla* L. are valuable medicinal plants referred to the collective name *Alchemilla vulgaris* complex (Lady's mantle). These plants are used in phytotherapy as Herba Alchemillae. The drug possesses astringent, diuretic and antispasmodic properties, and is commonly used in traditional medicine as a cure for excessive menstruation and wounds [1, 2]. Different studies showed that the phenolic compounds (tannins, flavonoids, etc.) presented in the plant are responsible for the pharmacological activity of Lady's mantle [3–9].

The genus *Alchemilla* (Rosaceae) is represented in Bulgarian Flora by 35 species, four of them are Bulgarian and seven - Balkan endemics [10]. The endemic *A. jumrukczalica* Pawl. occurs only in the National Park "Central Balkan" (Stara Planina Mt). The clon-populations can be found along the mountain streams at an altitudinal range between 1600–1800 m a.s.l. and gullies in the subalpine mountain belt [11]. The species was protected as rare and critically endangered one according IUSN criteria and is included in the Red List of Bulgarian vascular plants [12] and Red Data Book of R. Bulgaria [13]. Because of its very limited occurrence, *ex situ* conservation of *A.*

jumrukczalica started a few years ago [14]. It was found that the species could be easily cultivated at places with mountain climate close to that of its natural distribution. The plants grown *ex situ* were larger and more robust than those from natural clone-populations and cultivation did not cause significant changes in the total content of flavonoids and tannins in the aerial parts [14]. All these preliminary results prompted us to continue our investigations on flavonoid constituents of *A. jumrukczalica* and to assess its antioxidant capacity.

EXPERIMENTAL

Plant material

A. jumrukczalica plants with origin of native Bulgarian population (Central Stara planina Mt., 1600 m a.s.l.) cultivated in the experimental field of the Institute of Biodiversity and Ecosystem Research (Vithosha Mt., 1400 m a.s.l.) were used in the experiments.

The aerial parts were collected within phenophase full blossoming, air-dried and kept in dark place.

The voucher specimen (SOM 165678) was deposited in the Herbarium of Institute of Biodiversity and Ecosystem Research, Bulgarian Academy of Sciences, Sofia.

* To whom all correspondence should be sent:
E-mail: trendaf@orgchem.bas.bg

Extraction and isolation

Powdered plant material (70 g) was extracted with CH₃OH (2 x 1 L) at room temperature in an ultrasonic bath for 30 min each and once with 1 L of CH₃OH at room temperature for 24 hrs. After filtration, the solvent from combined extracts was evaporated under vacuum to give total methanolic extract (CH₃OH, 12.71 g). The latter was further dissolved in distilled water (200 ml) and partitioned with petroleum ether (PE, 4 x 80 ml), chloroform (CHCl₃, 4 x 80 ml) and ethyl acetate (EtOAc, 4 x 80 ml) to yield corresponding PE (0.50 g), CHCl₃ (0.50 g) and EtOAc (1.33 g) fractions. The remaining aqueous phase was evaporated to dryness (H₂O residue, 10.28 g).

The total methanolic extract of wild growing *A. jumrukczalica* and the corresponding fractions were obtained from 5 g of dry plant material using the same procedure. TLC comparison was performed on Silica gel (EtOAc/CH₃OH/H₂O, 5:0.8:0.6 and EtOAc/HCOOH/CH₃COOH/H₂O, 100:11:11:26), spraying with NP/PEG reagent and UV visualization at 366 nm [15].

EtOAc extract was dissolved in CH₃OH (15 ml) and filtered through celite in order to remove insoluble parts. Clear methanolic solution was concentrated up to 5 ml and applied to a Sephadex LH-20 column (equilibrated with CH₃OH) to give 2 main fractions A (0.92 g) and B (0.33 g). Flavonoid containing fraction (B) was further applied to MPLC on LiChroprep RP-18 and eluted with increasing concentrations of CH₃OH in H₂O (20 to 70%). Repeated MPLC (LiChroprep RP-18, CH₃OH/H₂O, 50:50) of selected fractions yielded **1** (16 mg), **2** (11 mg), **3** (4 mg), **4** (4 mg), **5** (4 mg), **6** (10 mg), **7** (1 mg) and **8** (6 mg).

Free Radical Scavenging Activity on DPPH radical

DPPH (1,1-diphenyl-2-picrylhydrazyl) radical scavenging method was used for determination of antioxidant capacity of the extracts and individual compounds [16]. Different concentrations of the extracts (2.5–100 µg/ml) and individual compounds (2–20 µM) in CH₃OH were added at an equal volume (2.0 ml) to CH₃OH solution of DPPH[•] (0.1 mM, 2 ml). After 30 min at room temperature and darkness, the absorption values were spectrophotometrically measured at 517 nm and converted into the percentage antioxidant activity using the following equation:

$$\text{DPPH}^{\bullet} (\%) = [1 - (A_{\text{sample}} - A_{\text{blank}}) / A_{\text{control}}] \times 100.$$

CH₃OH (2.0 ml) plus plant extract solution (2.0 ml) was used as a blank, while DPPH[•] solution plus CH₃OH was used as a control. The measurements were performed in triplicate. The results are presented as a mean ± SD. The IC₅₀ values were defined as the concentration of antioxidant necessary to decrease the absorbance of DPPH solution by 50%.

RESULTS AND DISCUSSION

The DPPH scavenging assay is widely used for preliminary evaluation of the antioxidant potential of extracts and individual compounds [15, 16]. In this work, the methanol extract of *A. jumrukczalica* and its fractions obtained after re-extraction with light petroleum (PE), chloroform (CHCl₃), and ethyl acetate (EtOAc), as well as the remaining H₂O residue were studied for their potential to scavenge the stable DPPH radical (Table 1). The total extract exhibited a significant dose dependent inhibition of DPPH activity with a 50% inhibition (IC₅₀) at a concentration of 10.7±0.4 µg/ml. As shown in Table 1, the scavenging activities of the fractions on DPPH increased in the order of PE < CHCl₃ < H₂O < EtOAc. Although the DPPH free radical scavenging ability of the EtOAc fraction (IC₅₀ 5.1±0.2 µg/ml) was less than that of quercetin and ascorbic acid (IC₅₀ 2.4±0.2 and 3.8±0.2 µg/ml, respectively) it was evident that this fraction could serve as free radical inhibitor or scavenger.

Table 1. DPPH radical scavenging activity of *A. jumrukczalica*.

Sample	IC ₅₀ (µg/ml)
total CH ₃ OH extract	10.7±0.4
PE fraction	>200
CHCl ₃ fraction	57.5±0.5
EtOAc fraction	5.1±0.2
H ₂ O residue	7.9±0.3
Quercetin (Reference)	2.4±0.1
Ascorbic acid (Reference)	3.8±0.1

The presence of flavonoids in the most active EtOAc fraction was initially determined by TLC and visualization of the spots with NP/PEG reagent [14]. Two main types of flavonoid glycosides were detected: quercetin (orange coloured spots) and kaempferol (yellow-green coloured spots). The isolation of the individual compounds from EtOAc fraction was achieved by SephadexLH-20 column chromatography and further purification by column chromatography and preparative TLC. Catechin (**1**) [18], guajaverin (**2**) [19], hyperoside (**3**) [20], isoquercetin (**4**) [20], quercitrin (**5**) [21],

miquelianin (**6**) [20], tiliroside (**7**) [22] and trifolin (**8**) [23] (Fig. 1) were identified based on their spectral data (UV, ¹H NMR and MS) compared with those published in the literature.

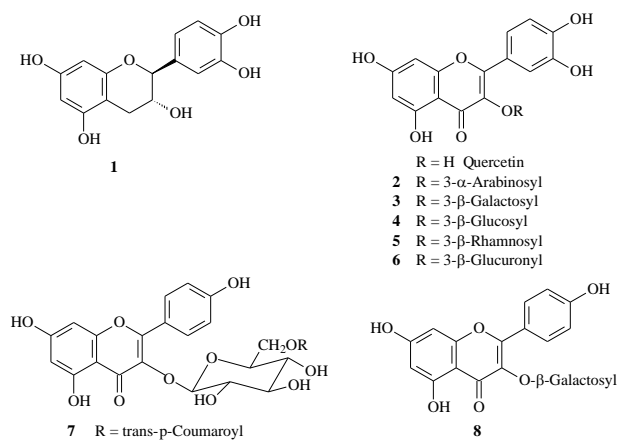


Fig. 1. Structures of the isolated flavonoid glycosides

The obtained in this study results are in accordance with those found previously for the content of quercetin (**2-6**) and kaempferol (**7** and **8**) glycosides in the species of the genus *Alchemilla* [24–27]. In addition, catechin (**1**) has been described as a component of *A. mollis* [26] only.

Selected pure compounds were also studied for their ability to quench the DPPH radical (Table 2) and quercetin was used as reference compound. As can be expected, the radical scavenging activity of the flavonoids depends on the molecular structure and the substitution pattern of hydroxyl groups [17, 28]. Guajaverin (**2**), hyperoside (**3**) and miquelianin (**6**) are quercetin derivatives with free hydroxyl groups at C-3' and C-4' and glycosylated at C-3. The nature of sugar moiety did not affect the activity. They had similar IC₅₀, but lower activity than that of quercetin (7.95±0.10 μ M). Trifolin (**8**), a kaempferol derivative contained only one free hydroxyl group at C-4' in B ring and therefore possessed the lowest activity (31.03±0.49 μ M) [17, 28]. Catechin (**1**) was a weaker antioxidant compared to quercetin and its derivatives because of the absence of C-2/C-3 double bond and carbonyl group at C-4 in its structure [17, 28].

Table 2. DPPH radical scavenging activity of isolated compounds.

Compound	IC ₅₀ (μ M)
Catechin (1)	14.14±0.34
Guajaverin (2)	10.83±0.23
Hyperoside (3)	11.51±0.21
Miquelianin (6)	12.14±0.36
Trifolin (8)	31.03±0.49
Quercetin (Reference)	7.95±0.10

CONCLUSION

TLC comparison of the total extracts and corresponding EtOAc fractions obtained from wild growing and cultivated *A. jumrukczalica* in the presence of isolated compounds did not show any significant qualitative and quantitative differences. The obtained results revealed the possibility to use *ex situ* cultivated *A. jumrukczalica* as a source of secondary metabolites with potential antioxidant activity.

REFERENCES

- I. Ivanov, I. Landjev, G. Neshev, Bilkite v Bulgaria i izpolzvaneto im (Medicinal plants in Bulgaria and their applications), Sofia, 1977.
- N. Bisset, Herbal Drugs and Phytopharmaceuticals, Stuttgart, 1994.
- M. Jonadet, M. T. Meunier, F. Villie, J. P. Bastide, J. L. Lamaison. *J. Pharmacol.*, **17**, 21 (1986).
- J. L. Lamaison, A. Carnat, C. Petitjean-Freytet, A. P. Carnat, *Ann. Pharm. Fr.*, **49**, 186 (1991).
- J. Flipek, *Pharmazie*, **47**, 717 (1992).
- O. Schimmer, M. Lindenbaum, *Planta Med.*, **61**, 141 (1995).
- Alchemillae herba*, ESCOP Herbal Monograph, 2013.
- P. Nedyalkov, M. Kaneva, D. Mihaylova, G. Kostov, S. Kemilev, *Compt. Rend. Bulg. Acad. Sci.*, **68**, 1491 (2015).
- M. Nikolova, I. Dincheva, A. Vitkova, I. Badjakov, *Int. J. Pharm. Sci. Res.*, **3**, 802 (2012).
- I. Assenov, in: Flora of PR Bulgaria, D. Jordanov (Ed.), BAS, Sofia, vol. 5, p. 274, 1973.
- A. Vitkova, L. Evstatieva, D. Peev, *Proceedings of the 7th Conference on Medicinal and Aromatic Plants of Southeast European Countries*, Subotica, Serbia, 14 (2012).
- A. Vitkova, in: Red List of Bulgarian vascular plants, A. Petrova, V. Vladimirov (eds), *Phytol. Balcan.*, **15**, 66 (2009).
- A. Vitkova, in: *Red Data Book of the Republic of Bulgaria*, D. Peev, V. Vladimirov, A. S. Petrova, M. Anchev, D. Temniskova, C. M. Denchev, A. Ganeva, C. Gushev (eds), BAS & MoEW, Sofia, Vol. 1, p. 174, 2015.
- A. Vitkova, A. Gavrilova, M. Delcheva, A. Trendafilova, M. Todorova, *J. App. Hort.*, **15**, 166 (2013).
- H. Wagner, S. Bladt, *Plant Drug Analysis. A Thin Layer Chromatography Atlas*. Second Edition, Springer-Verlag, Brooklyn, New York, 1996.
- P. Molyneux, *Songklanakar J. Sci. Technol.*, **26**, 212 (2004).
- C. D. Zheng, G. Li, H. Q. Li, X. J. Xu, J. M. Gao, A. L. Zhang, *Nat. Prod. Commun.*, **5**, 1759 (2010).
- A. Simic, D. Manolovic, D. Segan, M. Todorovic, *Molecules*, **12**, 2327 (2007).

19. T. Stark, S. Bareuther, T. Hofmann, *J. Agric. Food Chem.*, **53**, 5407 (2005).
20. E. C. Tatsis, S. Boeren, V. Exarchou, A. N. Troganis, J. Vervoort, I. P. Gerotheranassis, *Phytochemistry*, **68**, 383 (2007).
21. M. Jung, M. Park, *Molecules*, **12**, 2130 (2007).
22. I. Matlawska, M. Sikorska, W. Bylka, *Acta Pol. Pharm.*, **56**, 453 (1999).
23. E. Yamazaki, M. Inagaki, O. Kurita, T. Inoue, *Food Chem.*, **100**, 171 (2007).
24. A. Trendafilova, M. Todorova, A. Gavrilova, A. Vitkova, *Biochem. Syst. Ecol.*, **43**, 156 (2012).
25. M. D'Agostino, I. Dini, E. Ramundo, F. Senatore, *Phytotherapy Res.*, **12**, S162 (1998).
26. S. Duckstein, E. Lotter, U. Meyer, U. Lindequist, F. Stintzing, *Z. Naturforsch.*, **67**, 529 (2012).
27. C. Falser, O. Schimmer, *Planta Med.*, **65**, 668 (1999).
28. S. Burda, W. Oleszek, *J. Agric. Food Chem.*, **49**, 2774 (2001).

ФЛАВОНОИДНИ ГЛИКОЗИДИ И АНТИРАДИКАЛОВА АКТИВНОСТ НА БЪЛГАРСКИЯ ЕНДЕМИЧЕН ВИД *ALCHEMILLA JUMRUKCZALICA* PAWL.

А. Трендафилова^{1*}, М. Годорова¹, А. Виткова²

¹ *Институт по органична химия с Център по фитохимия, Българска Академия на Науките, София 1113, България*

² *Институт по биоразнообразие и екосистемни изследвания, Българска Академия на Науките, ул. Гагарин 2, 1113 София, България*

Постъпила на 14 февруари 2017 г.; Коригирана на 07 март 2017 г.

(Резюме)

Целта на настоящето изследване е да се идентифицират флавоноидните съединения в българския ендемичен вид *Alchemilla jumrukczalica* Pawl. и да се определи антирадикаловата активност на тоталния екстракт, фракции и индивидуални съединения. Тоталният метанолен екстракт проявява значителна DPPH активност (IC₅₀ 10.7±0.4 µg/ml), но за етилацетатната фракция (EtOAc) получена след ре-екстракция от тоталния екстракт бе установено, че е най-активният уловител на DPPH радикали (IC₅₀ 5.1±0.1 µg/ml). Катехин и седем флавоноидни гликозиди (гуайаверин, хиперозид, изокверцетин, кверцитрин, микуюелианин, тилирозид и трифолин) бяха изолирани от етилацетатната фракция. Структурите на тези съединения е установена с помощта на спектрални данни. Установено бе, че кверцетиновите гликозиди (гуайаверин, хиперозид и микуюелианин) са по-добри уловители на DPPH радикали от трифолин (кемпферол-3-глюкозид) и катехин.

Content of biologically active compounds in Bulgarian propolis: a basis for its standardization

M. Popova, B. Trusheva, V. Bankova*

Institute of Organic Chemistry with Centre of Phytochemistry, Bulgarian Academy of Sciences, Acad. G. Bonchev str., bl 9, 1113 Sofia, Bulgaria

Received February 23, 2017; Revised March 08, 2017

Dedicated to Acad. Bogdan Kurtev on the occasion of his 100th birth anniversary

In Bulgaria, propolis tincture is among of the most popular home-made remedies. Bulgarian propolis has been studied and it was found to originate from the bud resin of the black poplar *Populus nigra* L.; the chemical constituents responsible for its biological activity are flavonoid aglycones (flavones, flavonols, flavanones, dihydroflavonols), substituted cinnamic acids and their esters. However, the specific quantitative characteristics of Bulgarian poplar propolis have not been studied. Validated spectrophotometric procedures were used to quantify the three main groups of bioactive substances: total phenolics, total flavones/flavonols, total flavanones/dihydroflavonols, in 22 samples of Bulgarian propolis from different regions of the country. Based on the results, we characterized raw poplar propolis in terms of minimum content of its bioactive components (antimicrobial and antioxidant) as follows: 46% resin, 24% total phenolics, 7% total flavones/flavonols; 5.4% total flavanones/dihydroflavonols. These values can be used as a basis for Bulgarian propolis standard. They are somewhat higher than the ones suggested by the International Honey Commission for poplar type propolis. This is a proof that Bulgarian propolis is a valuable bee product of high quality, higher than that of the average poplar propolis samples coming from other regions.

Key words: propolis; Bulgarian propolis; chemical characterization; standardization

INTRODUCTION

Propolis, a sticky material collected by bees and used in their hives as a general purpose sealer, is well known for its diverse and useful biological activities: antimicrobial, antioxidant, anti-inflammatory, immuno-stimulating, and many others [1]. In the last decades, it has become the subject of growing scientific and commercial interest as a major ingredient of health food, cosmetics, food additives, *etc.* Recently, propolis has also been found very useful as a food preservative and as an active agent in food biopackaging materials [2]. A peculiarity of propolis, which is also an obstacle to its wide application in medicine and industry, is its variable chemical composition. Propolis composition depends on the plants available to bees for resin collection/propolis production [3]. Taking into account the fact that bees inhabit almost all ecosystems on Earth, obviously propolis chemistry is very far from constant and thus a universal propolis chemical standard is impossible. On the other hand, in any particular environment, bees have preferred source plants and this provides a good basis for standardization of specific chemical

types of propolis [4].

In Bulgaria, propolis tincture is among of the most popular home-made remedies. Bulgarian traditional medicine applies it for healing of wounds and burns, sore throat, stomach ulcer, *etc.* Bulgarian propolis has been studied and it was found to originate from the bud resin of the black poplar *Populus nigra* L. [5]. Its chemical constituents, which are responsible for its biological activity, and especially for its antimicrobial and antioxidant properties, are well documented. These are flavonoid aglycones: flavones (chrysin, techochrysin), flavonols (galangin, kaempferol), flavanones (pinocembrin, pinostrobin) and dihydroflavonols (pinobanskin, pinobanksin acetate), and other phenolics (mainly substituted cinnamic acids and their esters) [1]. It is important to note that a single propolis batch contains over 100 individual constituents, most of them having proven biological activity. Thus, the quantification of all active ingredients by chromatographic methods would be very inefficient as a routine approach. In addition, it has turned out that it is impossible to connect the bioactivity of propolis (and especially the antimicrobial activity) to one or a few individual propolis constituents [6, 7]. Till

* To whom all correspondence should be sent:
E-mail: bankova@orgchm.bas.bg

now, no individual propolis component was found to possess antimicrobial activity significantly higher than that of the total extract [6, 8]. Moreover, no statistically significant correlation has been found between minimum inhibitory concentration against *S. aureus* and the amounts of various active propolis components [8]. For this reason, earlier we developed and validated a combination of simple and rapid methods for quantification of the main groups of bioactive substances in poplar type propolis: total phenolics; total flavones and flavonols; and total flavanones and dihydroflavonols [9]. Applying it to over 100 poplar samples from all over the world resulted in determining the typical characteristics of poplar propolis in terms of the content of biologically active compounds [10]. However, the specific quantitative characteristics of Bulgarian poplar propolis have not been studied. The aim of the present work is to study the quality of Bulgarian propolis and provide a specific basis for its standardization and quality control.

EXPERIMENTAL

Propolis samples

Propolis samples were kindly supplied by Mr. D. Dimov (Sofia, Bulgaria). The exact sites of collection are given in Table 1. The poplar origin of the samples was confirmed by screening the composition using TLC [11].

Propolis extraction

Frozen propolis (freezer) was grated and 1 g was dissolved in 30 ml 70% ethanol in a 50 mL flask and left for 24 h at room temperature. The extract was filtered and the extraction was repeated. The two extracts were combined and diluted to 100 ml with 70% ethanol in a volumetric flask. This solution was analyzed to determine the total phenolics and flavonoids.

Balsam percentage

From each crude sample, three parallel extracts with 70% ethanol were prepared as described above. Two mL of each were evaporated to dryness *in vacuo* until constant weight, and the percentages of balsam in the extracts were calculated as the ethanol soluble fraction. The mean of the three values was determined.

Flavone and flavonol content

Total flavone and flavonol content was measured by spectrophotometric assay based on aluminum chloride complex formation, as described by Popova et al. [9]. In brief, to 2 mL of the test solution, 20 ml methanol and 1 ml 5% AlCl_3 (wt/vol) were added and the volume made up to 50 ml (volumetric flask). After 30 min, the absorbance was measured at 425 nm. Blank: 2 mL methanol instead of test solution. Every assay was carried out in triplicate. Flavone and flavonol content was estimated using a calibration curve of galangin, concentration range of 4–32 mg/mL.

Flavanone and dihydroflavonol content

For flavanones and dihydroflavonols, the colorimetric method described in DAB9 was used, modified for propolis [9]. In brief, 1 ml of test solution and 2 ml of DNP solution (1g DNP in 2 ml 96% sulfuric acid, diluted to 100 ml with methanol) were heated at 50 °C for 50 min. After cooling to room temperature, the mixture was diluted to 10 ml with 10% KOH in methanol (wt/vol). One ml of the resulting solution was added to 10 ml methanol and diluted to 50 ml with methanol. Absorbance was measured at 486 nm. Blank: 1 ml methanol instead of test solution was used in analogous procedure. Every assay was carried out in triplicate. Flavanone and dihydroflavonol content was estimated using calibration curve of pinocembrin, concentration range of 0.18–1.8 mg/ml.

Total phenolics

The Folin-Ciocalteu method was applied, as described in [9]. In brief, 1 ml of the test solution was transferred to a 50 mL volumetric flask, containing 15 ml distilled water, and 4 ml of the Folin–Ciocalteu reagent and 6 ml of a 20% sodium carbonate solution (wt/vol) were added. The volume was made up with distilled water to 50 ml. After 2 h, the absorbance was measured at 760 nm. Blank solution: 1 ml methanol instead of test solution was used in analogous procedure. Every assay was carried out in triplicate. Total phenolics content was estimated using calibration curve of standard mixture pinocembrin–galangin 2:1, concentration range 37–326 mg/ml.

RESULTS AND DISCUSSION

The study includes 22 Bulgarian propolis samples from all Bulgarian beekeeping regions (Fig. 1). All samples were proven to be of poplar (*P. nigra*) origin by thin layer chromatography

(TLC) test [11], using as references specific marker compounds for poplar propolis [12, 13]. First of all,

the amount of balsam, the extract of crude propolis in 70% ethanol was determined, this being the most

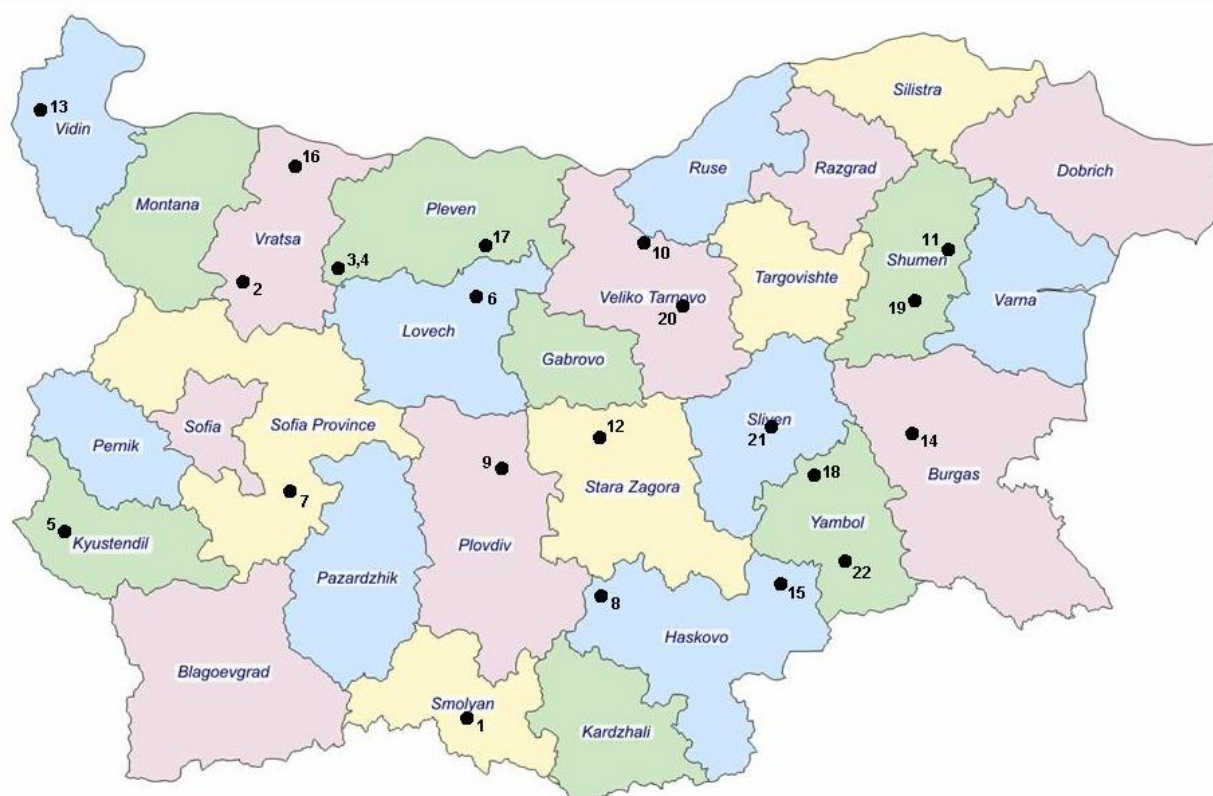


Fig. 1. Locations where propolis samples were collected in Bulgaria (●).

Table 1. Percentage of balsam and main biologically active compounds* in propolis from different regions of Bulgaria.

Sample No	Location of origin	Balsam	Total phenolics	Total flavanones and flavonols	
				Total flavanones and dihydroflavonols	
% in the sample					
1	Smolyan	62	41.9	13.2	9.3
2	Vratsa	77	40.0	12.3	9.4
3	Cherven bryag	65	35.8	11.8	7.3
4	Cherven bryag	82	42.0	13.5	8.6
5	Kyustendil	48	28.0	9.1	5.6
6	Lovech	39	25.7	7.2	6.5
7	Ihtiman	64	40.2	12.2	9.4
8	Gorski Izvor village, Haskovo region	57	30.5	10.4	5.9
9	Prolom village, Plovdiv region	64	34.2	11.0	6.7
10	Polski Trambesh	45	24.3	7.7	5.4
11	Novi Pazar	56	30.5	10.3	6.8
12	Kazanlak	66	24.8	8.8	6.3
13	Kula, Vidin region	38	11.2	3.6	3.5
14	Karnobat	67	40.3	13.2	8.6
15	Topolovgrad	67	39.7	13.0	9.3
16	Krushovitsa village, Vratsa region	48	27.0	9.0	6.4
17	Pelishat village, Pleven region	58	21.2	7.2	5.4
18	Yambol	54	29.7	10.0	8.1
19	Ivanski village, Shumen region	71	36.0	11.8	7.5
20	Kozarevets village, Gorna Oryahovitsa region	33	17.0	4.5	4.1
21	Sliven	46	18.7	2.9	4.5
22	Dobrich village, Yambol region	75	38.2	9.7	6.8

* standard deviations < 6%

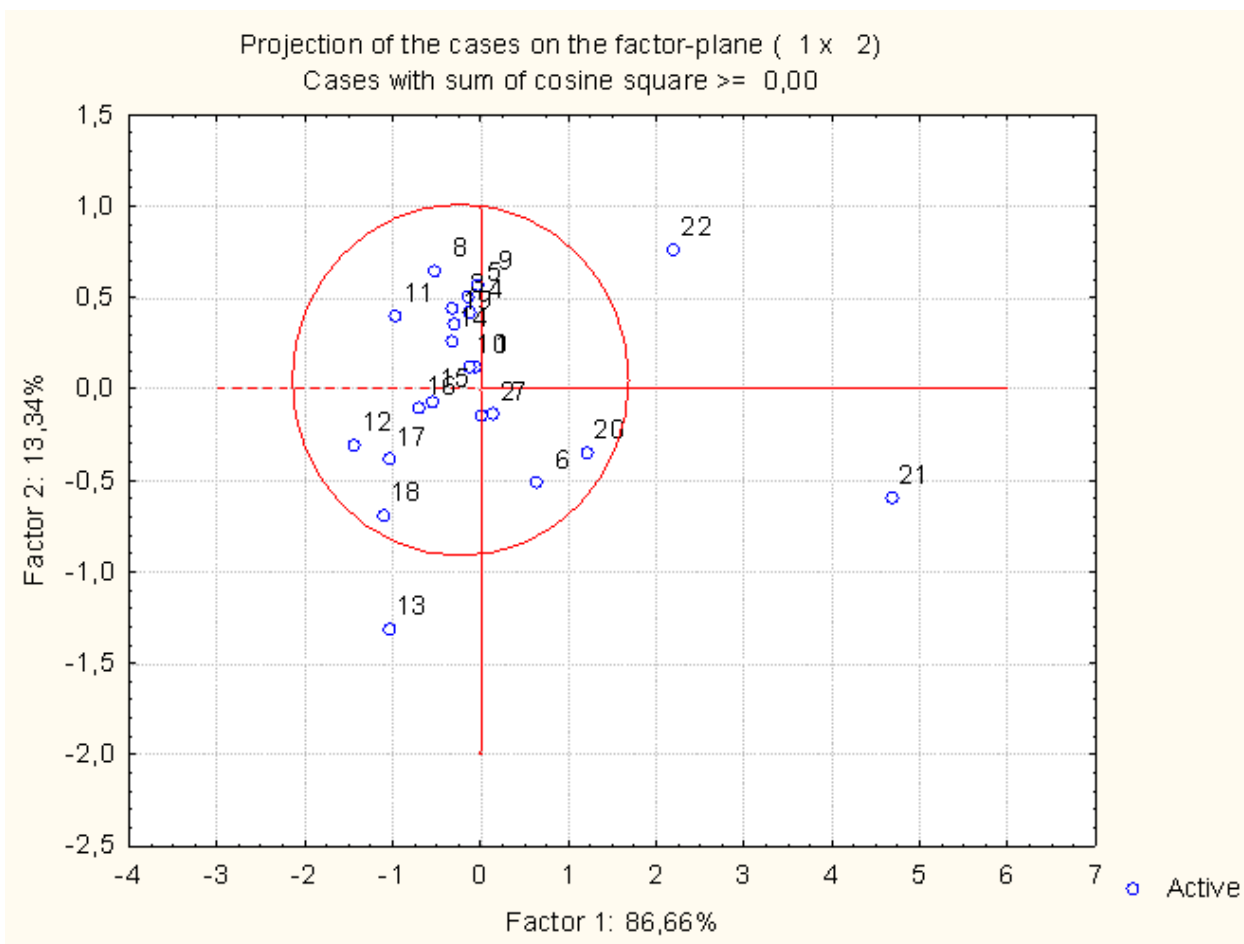


Fig. 2. PCA of propolis chemical composition of propolis samples.

Table 2. Characteristics of Bulgarian propolis samples (based on 22 samples).

Parameter (content, %)	Mean value	Median	Minimum	Maximum	P80*	P20
Balsam	58	60	33	88	67	46
Total phenolics	30.7	30.5	11.2	42	40	24.3
Total flavones and flavonols	9.6	10.2	2.9	13.5	12.3	7.2
Total flavanones and dihydroflavonols	6.8	6.8	3.5	9.4	8.6	5.4

usual way to extract propolis for use in medicine and cosmetics [14]. The balsam percentage is an important characteristic of propolis quality: in general, high percentage of balsam means that propolis contains a low percentage of wax and mechanical impurities, and higher concentration of biologically active components [6].

The values obtained from these measurements and from the spectrophotometric procedures, are presented in Table 1. In general, it is known that the chemical composition of poplar bud exudates is relatively constant; nevertheless, there could be significant variations in the percentage of individual constituents in specific locations or even in different individual plants [12]. However, looking at the data in Table 1, it is hard to make out any specific groups based on geographic origin. In order to analyze the relatively large amount of

analytical data, we applied chemometric approach: the Principal Component Analysis (PCA), using normalized values for the content of the three groups of bioactive compounds. The obtained two-dimensional plot (Fig. 2) covers 100% of the variation. Most samples, except of three, form one well-defined group, despite the fact that they originate from all over the country. Obviously, the Bulgarian poplar trees produce resin of similar quantitative composition, concerning the total content of the three main groups of bioactive constituents. The only exceptions are the samples 21 and 22, characterized by significantly higher amount of total phenolics, and sample 13 with the lowest amount of total phenolics (as percentage of dry extract).

The statistical analysis of the data in Table 1 makes it possible to determine the range of

probable values of the studied parameters and to formulate appropriate limits as a basis for standardization. The results for all of the parameters were analyzed by the Shapiro-Wilk normality test and it was found that the values were not normally distributed. The same was found earlier for poplar type propolis in general [10]. For this reason, we believe it is improper to use mean values as the basis for standardization. Instead, we suggest the 20-th percentile to be used in order to set the minimum values for content of resin and biologically active compounds, as shown in Table 2. According to these results, we suggest the typical characteristics of a Bulgarian propolis sample which can be applied as the basis for standardization and quality control, as follows:

Balsam content: minimum 46 %

Total phenolics: minimum 24 %

Total flavones and flavonols: minimum 7 %

Total flavanones and dihydroflavonols:
minimum 5.4 %

These values are somewhat higher than the ones suggested by the International Honey Commission [15] for poplar type propolis. Especially the value for total phenolics content is 14% higher than the average for poplar type propolis. This fact is important because a statistically significant correlation has been found between total phenolics and antibacterial effect (Minimal Inhibitory Concentration, MIC) of this propolis type: the higher the concentration of total phenolics, the lower the MIC (higher antibacterial activity) [10].

CONCLUSION

The results obtained in this study present a proof that Bulgarian propolis is a valuable bee product of high quality, higher than that of the average poplar propolis samples coming from other regions.

REFERENCES

1. J. M. Sforcin, V. Bankova, *J. Ethnopharmacol.*, **133**, 253 (2011).
2. V. Bankova, M. Popova, B. Trusheva, *Maced. J. Chem. Chem. Eng.*, **35**, 1 (2016).
3. V. Bankova, M. Popova, B. Trusheva, *Chem. Centr. J.*, **8**, 28 (2014).
4. V. Bankova, *J. Ethnopharmacol.*, **100**, 114 (2005).
5. V. Bankova, A. Dyulgerov, S. Popov, L. Evstatieva, L. Kuleva, O. Pureb, Z. Zamjansan, *Apidologie*, **23**, 79 (1992).
6. A. Kujumgiev, I. Tsvetkova, Y. Serkedjieva, V. Bankova, R. Christov, S. Popov, *J. Ethnopharmacol.*, **64**, 235 (1999).
7. A. H. Banskota, Y. Tezuka, S. Kadota, *S. Phytother. Res.*, **15**, 561 (2001).
8. J. S. Bonvehi, F. V. Coll, R. E. Jorda, *J. Am. Oil Chem. Soc.*, **71**, 529 (1994).
9. M. Popova, V. Bankova D. Butovska, V. Petkov, B. Nikolova-Damyanova, A. G. Sabatini, G. L. Marcazzan, S. Bogdanov, *Phytochem. Anal.*, **15**, 235 (2004).
10. M. Popova, V. Bankova, S. Bogdanov, I. Tsvetkova, C. Naydenski, G.- L. Marcazzan, A.-G. Sabatini, *Apidologie*, **38**, 306 (2007).
11. M. Popova, S. Silici, O. Kaftanoglu, V. Bankova, *Phytomedicine*, **12**, 221 (2005).
12. W. Greenaway, T. Scaysbrook, F. R. Whately, *Bee World*, **71**, 107 (1990).
13. V. Bankova, S. L. de Castro, M. C. Marcucci, *Apidologie*, **31**, 3 (2000).
14. W. Greenaway, J. May, T. Scaysbrook, F. R. Whately, *Z.Naturforsch.*, **42c**, 111 (1991).
15. V. Bankova, D. Bertelli, R. Borba, B. J. Conti, I. B. da Silva Cunha, C. Danert, M. N. Eberlin, S. I. Falcão, M. I. Isla, M. I. Nieva Moreno, G. Papotti, M. Popova, K. Basso Santiago, A. Salas, A. C. H. Frankland Sawaya, N. V. Schwab, J. M. Sforcin, M. Simone-Finstrom, M. Spivak, B. Trusheva, M. Vilas-Boas, M. Wilson, C. Zampini, *J. Apicult. Res.* (2016) DOI: 10.1080/00218839.2016.1222661.

СЪДЪРЖАНИЕ НА БИОЛОГИЧНО АКТИВНИ СЪЕДИНЕНИЯ В БЪЛГАРСКИ ПРОПОЛИС – ОСНОВА ЗА СТАНДАРТИЗАЦИЯТА МУ

М. Попова, Б. Трушева, В. Банкова*

Институт по органична химия с Център по фитохимия, Българска академия на науките, ул. Акад. Г. Бончев, бл. 9, 1113 София

Постъпила на 23 февруари 2017 г.; Коригирана на 08 март 2017 г.

(Резюме)

Прополисовата тинктура е сред най-популярните домашно приготвяни лекарства в България. Българският прополис е изследван и е установено, че той произхожда от смолата на пъпките на черната топола *Populus nigra* L., като химичните съединения, отговорни за биологичната му активност са флавоноидни аглиconi (флаволи, флавоноли, флаванони и дихидрофлавоноли), заместени канелени киселини и техни естери. Все още обаче не са изследвани специфичните количествени характеристики на българския тополов прополис. Използвахме валидирани спектрофотометрични процедури за количествено определяне на трите основни групи биологично активни вещества: тотални феноли, тотални флаволи и флавоноли, тотални флаванони и дихидрофлавоноли в 22 проби прополис от различни райони на България. Въз основа на получените резултати можахме да охарактеризираме суровия български прополис по отношение на минимално съдържание на биологичноактивни вещества (антимикробиялни и антиоксидантни), както следва: 46% балсам, 24% тотални феноли, 7% тотални флаволи и флавоноли, 5,4% тотални флаванони и дихидрофлавоноли. Тези стойности могат да се използват като основа за стандартизация на българския прополис. Те надвишават минималните стойности, предложени от Международната комисия по меда за тополов тип прополис. Този факт доказва, че българският прополис е ценен пчелен продукт с високо качество, по-високо от средното за тополов прополис от други географски райони.

Content of steviol glycosides in stevia (*Stevia Rebaudiana* B.) genotypes cultivated in Bulgaria

P. N. Denev^{1*}, I. I. Uchkunov², V. I. Uchkunov², M. G. Kratchanova¹

¹ Institute of Organic Chemistry with Centre of Phytochemistry, Bulgarian Academy of Sciences, Laboratory of Biologically Active Substances, 139 "Ruski" blvd., 4000 Plovdiv, Bulgaria

² Agricultural Institute, Shumen, 3 "Simeon Veliki" blvd., 9700 Shumen, Bulgaria

Received February 06, 2017; Revised February 24, 2017

Dedicated to Acad. Bogdan Kurtev on the occasion of his 100th birth anniversary

Current study presents data on the content of steviol-glycosides (stevioside and rebaudioside A) in twenty four genotypes of (*Stevia Rebaudiana* B.), cultivated in Bulgaria. The HPLC analysis showed that the content of stevioside in the separate groups reached 6.80 g/100 g dry mass and that of rebaudioside A – 8.27 g/100 g dry weight. These results allow us to make a conclusion that trough the path of individual selection, it is possible to develop stevia genotypes with high content of steviol-glycosides, under the climatic conditions of Bulgaria.

Key words: Stevia (*Stevia Rebaudiana* B.) leaves; HPLC determination; steviol glycosides; stevioside, rebaudioside A

INTRODUCTION

Stevia (*Stevia Rebaudiana* B.) is a perennial shrub of the *Asteraceae* (*Compositae*) family, growing naturally in Paraguay and Brazil. Dried stevia leaves are a rich source of ent-kaurene-type diterpene glycosides, called steviol-glycosides and the most abundant of them is stevioside [1]. Being 300 times sweeter than sucrose, stevioside is considered as one of the strongest natural sweeteners [2]. The content of stevioside in stevia leaves is in the range 4–20% and depends on the cultivar and on growth conditions [3]. Other glycosides in the leaves are rebaudioside A (about 3%); rebaudioside C, D, E, F and dulcoside A (totally about 2%). Minor quantities of steviolbioside, rubusoside, and rebaudioside were found as well [4–7]. There are evidences that other steviol-glycosides such as steviolbioside and rebaudioside B could be formed by partial hydrolysis during the extraction process of steviol-glycosides [8, 9]. Except steviol-glycoside, stevia leaves contain variety of biologically active substances such as flavonoids, alkaloids, chlorophylls, xanthophylls, hydroxycinnamic acids, oligosaccharides, free sugars, amino acids, lipids and trace elements [10] and it is suggested that stevia extracts exert beneficial effects on human health, including anti-hypertensive anti-hyperglycemic and anti-human rotavirus activities [11–13].

For many years, food industry has traditionally used sugar as the main sweetening agent but in the last century many synthetic and natural sweeteners were released on the market as well. Nowadays, in response mainly to the consumer preferences, there is increasing demand for natural sweeteners. Among the mandatory requirements for the sweeteners such as lack of toxicity, consumers prefer sweeteners that are low in calories and have sugar-like taste profile. On the other hand, food industry requires sweeteners that are heat and pH stable. Steviol-glycosides being noncaloric and high potency sweetener fulfill these requirements and meet customer's preferences, and therefore subject of enormous interest in the recent years. The commercial exploration of Stevia has become stronger since the 70's, when Japanese researchers developed a series of processes for the extraction and refining of the leaf sweeteners. It was claimed that stevioside had a 20% of market share of low-calorie sweeteners in Japan [14]. Nowadays, steviol glycosides (stevioside and rebaudioside A) are approved for general food use in Australia, Argentina, Brazil, China, European Union, India, Israel, Japan, New Zealand, Paraguay, Russia, South Korea and few other countries. In the USA, rebaudioside A and highly purified steviol glycosides received status "generally recognized as safe". Presently stevia is recognized as a plant with a significant economic value [15, 16] and is being cultivated in different countries worldwide. Not surprisingly many countries conduct their own research directed to the selection of high steviol-

* To whom all correspondence should be sent:
E-mail: petkodenev@yahoo.com

glycosides cultivars and development of extraction and separation techniques for these natural sweet compounds [17].

Stevia is a relatively plastic culture. The development of the plant is influenced by the region and geographical latitudes [18]. The high plasticity of the plant is significantly influenced by the unique conditions of the area where it is cultivated [19]. The climate of Paraguay is subtropical and characteristic with variable temperatures and high amount of rainfalls. *Stevia* is thermophilic culture and it was found that temperatures below +12 °C suppress plant development. The plant is highly sensitive to low temperatures and genotypes, developed in Bulgaria freeze at 1-2 °C [18]. Therefore, under the climatic conditions of Bulgaria *stevia* can be grown as annual crop. The purpose of the current study was to determine the content of steviol-glycosides in 24 genotypes of *Stevia* (*Stevia Rebaudiana* B.), cultivated in Bulgaria. Such a comparative study is the initial step in the development of *Stevia* cultivar with high content of steviol-glycosides.

EXPERIMENTAL

Plant Materials

Stevia plants from different genotypes were cultivated on the experimental fields of the Agricultural Institute, Shumen on carbonate chernozem soils, under irrigation. Altogether twenty four *stevia* genotypes were studied. Genetic material used is included in the breeding program of the Institute and plants were derived and adapted in tissue culture laboratory. Ten individual plants of each origin were evaluated. Plants were harvested in the autumn and fresh leaves were collected from the stem. Leaves were dried in shade at room temperature. Dry leaves were stored in paper bags prior to analysis. The dry matter and the content of steviol-glycosides were analyzed in each sample.

Extraction of Steviol-glycosides

Dry *stevia* leaves were ground with a coffee mill to a homogeneous powder mass. About 1g of the ground mass was weighed accurately and extracted with 100 ml water at water bath (95 °C) for 30 min. The mixture was cooled to room temperature and filtrated through filter paper. The filtrate was separated and the residue was subjected to a second extraction under the same conditions. Both supernatants were combined and the volume was adjusted to 200 ml with distilled water.

Extracts purification through solid-phase extraction

Stevia extracts were subjected to purification by solid-phase extraction. For this purpose, 3 ml of the extract was passed through a column Oasis C-18, activated with pure methanol. Impurities in the sample were eluted first with 5 ml water and then with 5 ml 40% methanol (v:v). Steviol-glycosides, were eluted from the column using 5 ml of 70% methanol (v:v). The resulting fraction was used to determine the steviol-glycosides by high performance liquid chromatography (HPLC).

High performance liquid chromatography (HPLC) of steviol-glycosides

To determine the content of stevioside and rebaudioside A in *stevia* extracts an Agilent 1220 chromatographic system equipped with a UV-Vis detector Agilent 1220 was used. The elution was isocratic with a mobile phase acetonitrile:water (80:20). The separation of steviol glycosides, was performed on chromatographic column Agilent Zorbax Carbohydrate (4.6 x 150 mm, 5 µm) at room temperature and flow rate of the mobile phase, 1 ml/min at a wavelength of $\lambda = 210$ nm. External standards (stevioside and rebaudioside A) were used to quantify the content steviol-glycosides. All analyses were performed two times and their content was expressed in g/100 g dry leaf mass.

RESULTS AND DISCUSSION

As already mentioned the natural habitat of *S. rebaudiana* is located in the subtropics, but it was shown that the plant is worthy for cultivation in European countries [20, 21]. The increment of steviol-glycosides is the main goal in different breeding programs of *stevia* (*Stevia Rebaudiana* B.). It is known that long day conditions promote the vegetative growth and even increase steviol-glycosides in *stevia* [22]. This is an advantage of the European latitudes, compared to the shorter days in Paraguay and Brazil. It was proposed that the cultivation of *Stevia rebaudiana* could be economical feasible in Czech Republic [23] and Germany [24]. To our knowledge, the current study is the first report on the content of steviol glycosides in *Stevia* genotypes, cultivated in Bulgaria.

In our study, we investigated 24 *stevia* genotypes from the genetic bank of the Agricultural Institute – Shumen for their content of steviol-

glycosides. The highest yield of a single plant has been found in genotype 2304, where the excess of the mean value for the group reached 37.5%. Genotypes 2101 and 2110 are characteristic with relatively equal results and with an excess of 28.7% and 30.2% respectively (Table 1).

Table 1. Content of dry matter in stevia leaves from different genotypes.

Genotype	Dry matter content, g	Relative value to the mean, %
2001	18.2	55.5
2002	31.8	97.0
2003	18.1	55.2
2101	42.2	128.4
2102	28.5	86.9
2204	31.5	96.1
2205	33.7	102.8
2206	26.9	82.1
2207	34.4	104.9
2210	42.7	130.2
2211	33.2	101.3
2212	37.2	113.5
2213	36.5	111.3
2301	29.5	90.0
2302	40.1	122.3
2303	31.9	97.3
2304	45.1	137.5
2305	25.3	77.2
2306	27.4	83.6
2401	27.5	83.9
242	31.7	96.7
2403	40.5	123.5
2404	31.1	104.0
2405	38.7	118.1
Mean	32.8	100

The HPLC method used by us allowed rapid and precise determination of steviol glycosides presented in the samples with very good separation of stevioside from rebaudioside A (Fig. 1).

From the data for individual stevioside content in the investigated selection materials, it is evident that the average stevioside content in the investigated genotypes was 6.38 g/100 g dry matter (Fig. 2). Genotypes 2304 and 2401 are characteristic with excess above the mean annual content in the range 39.5%–44.2%. It was found that the content of rebaudioside A, varies

significantly among the investigated samples with average content 5.65 g/100 g dry weight. For example, genotype 2205 contains 3.3 g/100 g rebaudioside A, whereas its content in genotype 2303 reaches 16.5 g/100 g dry weight. The total content of sweet substances in the dry mass is a composite indicator comprising the amount of the two steviol-glycosides. Our results show that the average annual content of steviol-glycosides reaches 12.03 g/100 g. This parameter varies in relatively narrow range, indicating that to a larger extent this is a conservative feature. The highest content of total steviol-glycosides was recorded in genotype 2305, where the excess over the mean for the group was 83.7%, followed by genotype 2302 with 21.9 g/100 g (18.1%). These results allow us to make a conclusion that through the path of individual selection it is possible to develop stevia genotypes with relatively high content of steviol-glycosides.

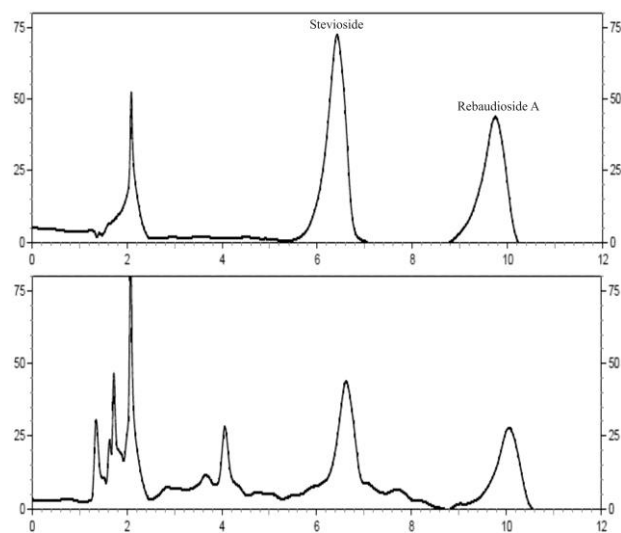


Fig. 1. HPLC chromatogram of 0.5 mg/ml pure steviol glycosides (upper panel) and extract from sample 2204 (lower panel).

Fig. 3 presents the average data for the groups of the studied genotypes. The highest stevioside content (average 6.71 g/100g) possess the material of origin 2400, whereas rebaudioside A content is the highest in the genotypes of group 2300 (8.27 g/100 g).

Rebaudioside A is the most desirable component due to its sweetening potency and superior taste profile [25]. Responding to this challenge, new cultivars with significantly higher concentration of rebaudioside A have been reported [26]. The native ratio stevioside:rebaudioside A in stevia leaves is usually about 2. As a result of the higher content, stevioside imparts a characteristic bitter after-taste

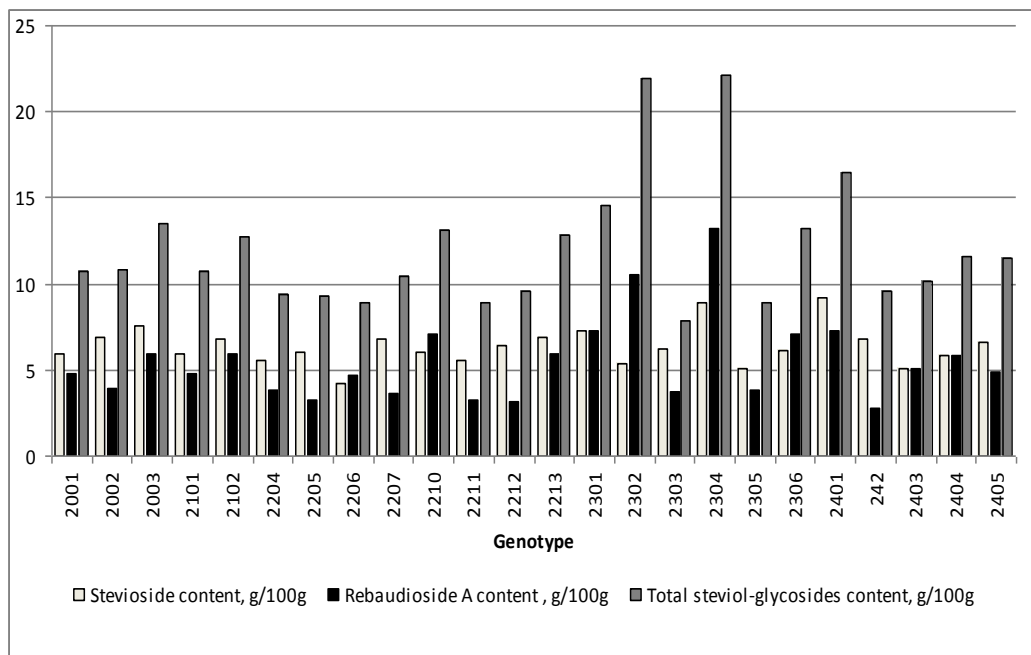


Fig. 2. Stevioside, rebaudioside A and total steviol-glycosides content in the leaves of different stevia genotypes.

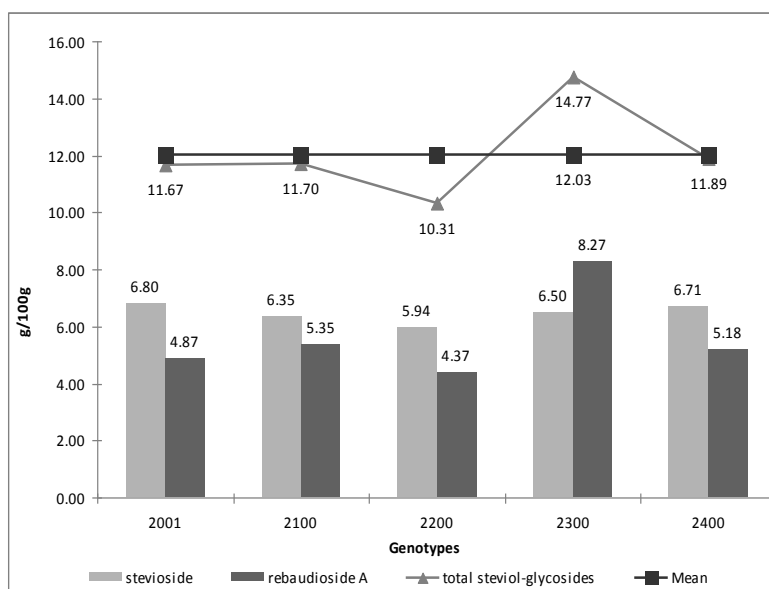


Fig. 3. Average content of stevioside, rebaudioside A and total steviol-glycosides content in the groups of the investigated genotypes.

to the crude extracts. Conversely, the most valuable extracts are those that have rebaudioside A as the major component, because of its organoleptic and physicochemical features (the best taste profile relative and the best solubility in water) [25], what permits a greater variety of formulations. Therefore, the phytochemical characterization of new genotypes and varieties of stevia with higher levels of total steviol-glycosides and particularly of rebaudioside A the main goal to research groups

dealing with the improvement and utilization of this source of natural sweeteners. In our study the ratio between stevioside and rebaudioside A reached 1.13.

CONCLUSION

We investigated 24 stevia genotypes from the genetic bank of the Agricultural Institute – Shumen for their content of steviol-glycosides (stevioside and rebaudioside A). Genotypes with relatively

high stevioside (2101 – 9.2 g/100 g) and rebaudioside A (2304 – 13.2 g/100 g) content were selected. The content of steviol-glycosides in the selection materials of genotype 2300 reaches 14.77 g/100 g dry weight. These results allow us to make a preliminary conclusion that under the climatic conditions of Bulgaria, it is possible to obtain stevia genotypes with relatively high content of steviol-glycosides. This opens the possibility to develop stevia cultivar in Bulgaria rich in steviol-glycosides and particularly in rebaudioside A.

REFERENCES

1. M. Bridel, R. Lavieille, *J. Pharm. Chim.*, **14**, 99 (1931).
2. D. D. Soejarto, C. M. Compadre, P. J. Medon, S. K. Kamath, A. D. Kinghorn, *Econom. Bot.*, **37**, 71 (1983).
3. J. M. C. Geuns, *Recent Res. Dev. Phytochem.*, **4**, 75 (2000).
4. H. C. Makapugay, N. P. D Nanyakkara, A. D. Kinghorn, *J. Chromatogr.*, **283**, 390 (1984).
5. S. Shizhen, *Sci. Agric. Sin.*, **28**, 37 (1995).
6. A. Y. Leung, S., Foster, *Encyclopedia of common natural ingredients used in food, drugs and cosmetics* (2nd ed.), John Wiley and Sons, Inc., New York, 1996, p. 478.
7. J. M. C. Geuns, *Phytochem.*, **64**, 913 (2003).
8. S. H. Kim, G. F. Dubois, in: *Handbook of sweeteners*, S. Marie and J. R. Piggott (eds), Blackie A&P, Glasgow, 1991, p 116.
9. I. Prakash, G. E. DuBois, J. F. Clos, K. L. Wilkens, L. E. Fosdick, *Food Chem. Toxicol.*, **46**, S75 (2008).
10. N. F. Komissarenko, A. I. Derkach, I. P. Kovalyov, N. P. Bublik, *Rast. Res.*, **1**, 53 (1994).
11. P. Chan, B. T. Linson, Y. Chen, J. Liu, M. Hsieh, J. Cheng, *Brit. J. Clin. Pharmacol.*, **50**, 215 (2000).
12. K. G. Lee, T., Shibamoto, *Food Chem. Toxicol.*, **39**, 1199 (2001).
13. P. B. Jeppesen, S. Gregersen, K. K. Alstrup, K. Hermansen, *Phytomedicine*, **9**, 9 (2002).
14. H. Kikuchi, *Food Sci. (Japan)*, **85**, 52 (1985).
15. A. D. Kinghorn, in: *Stevia, the Genus of Stevia medicinal and aromatic plants-industrial profiles*, A. D. Kinghorn (ed), Taylor and Francis, London. 2002, p. 1.
16. K. Ramesh, V. Singh, N. W. Megeji, *Adv. Agron.*, **89**, 137 (2006).
17. A. K. Yadav, S. Singh, D. Dhyani, P. S. Ahuja, *Can. J. Plant Sci.*, **91**, 1 (2011).
18. M. Vurbanov, K. Slavov, L., Hristova, K., Uchkunova, *Proceedings of the Jubilee Scientific Session "25 years Shumen University"*, 1996, p. 129.
19. I. Krumov, K. Slavov, Y. Slavova, *Reports of the State Comity for Science and Technical progress*, **1**, 73 (1984).
20. R. Pude, M. Schmitz-Eiberger, G. Noga, *Z. Arz. Gew. Pfla.*, **10**, 37 (2005).
21. C. Lankes, R. Pude, in: *Proceedings of the 2nd Stevia symposium*, Leuven, Belgium, 2008.
22. J. Metivier, A. M. Viana, *J. Exp. Bot.*, **30**, 1211 (1979).
23. A. Nepovim, H. Drahosova, P. Valicek, T. Vanek, *Pharm. Pharmacol. Lett.*, **8**, 19 (1998).
24. U. Woelwer-Rieck, C. Lankes, A. Wawrzun, M. Wust, *Eur. Food Res. Technol.*, **231**, 581 (2010).
25. B. Crammer, R. Ikan, *Chem. Br.*, **22**, 915 (1986).
26. J. Brandle, *Can. J. Plant Sci.*, **79**, 85 (1999).

СЪДЪРЖАНИЕ НА СТЕВИОЛ ГЛИКОЗИДИ В ГЕНОТИПОВЕ СТЕВИЯ (*STEVIA REBAUDIANA* V.), КУЛТИВИРАНИ В БЪЛГАРИЯ

П. Н. Денев^{1*}, И. И. Учкунув², В. И. Учкунув², М. Г. Крачанова¹

¹ *Институт по Органична Химия с Център по Фитохимия, Българска Академия на Науките, Лаборатория по Биологично Активни Вещества, бул. „Руски“ 139, 4000 Пловдив, България*

² *Земеделски Институт гр. Шумен, бул. „Симеон Велики 3, 9700 Шумен, България*

Постъпила на 06 февруари 2017 г.; Коригирана на 24 февруари 2017 г.

(Резюме)

Настоящото изследване представя данни за съдържанието на стевиол гликозиди (стевиозид и ребаудиозид А) в двадесет и четири генотипа стевия (*Stevia rebaudiana* V.), отглеждани в България. Посредством високоефективна течна хроматография бе установено, че съдържанието на стевиозид в отделните групи достига 6.80 g/100 g суха маса, а това на ребаудиозид А – 8.27 g/100 g сухо тегло. Тези резултати позволяват да се направи заключение, че при климатичните условия в България, посредством пътя на индивидуален подбор е възможно селектиране на генотипове стевия с високо съдържание на стевиол гликозиди.

Super-critical carbon dioxide extraction as an effective green technology for production of high quality rose hip oil

S. Taneva, A. Konakchiev, I. Totzeva, M. Kamenova-Nacheva, Y. Nikolova, S. Momchilova*, V. Dimitrov

Institute of Organic Chemistry with Centre of Phytochemistry, Bulgarian Academy of Sciences, Acad. G. Bonchev street, bl. 9, 1113 Sofia, Bulgaria

Received March 09, 2017; Revised March 21, 2017

Dedicated to Acad. Bogdan Kurtev on the occasion of his 100th birth anniversary

The application of super-critical carbon dioxide extraction of rose hip (*Rosa canina* L.) seeds for production of high quality oil was explored. For the purpose, main oil characteristics as fatty acids composition, tocopherols and carotenoids contents, as well as the oil oxidative stability were evaluated. The results revealed that technological conditions as pressure (350–450 bar) and particles size of the milled seeds (0.4, 1 mm) did not practically affect the fatty acids composition. However, increasing the pressure from 350 to 400 bar caused slight increasing of tocopherols and carotenoids contents whereas decreasing of particles size reduced their amounts. The higher quantity of these antioxidants insured better oxidative stability of the rose hip oil and thence its high quality.

Key words: rose hip oil; extraction with super-critical carbon dioxide; fatty acids; oxidative stability; tocopherols; carotenoids

INTRODUCTION

Rose hip oil is obtained from the seeds of *Rosa canina* L. fruits. Being a rich source of healthy biologically active substances as essential fatty acids, strong antioxidants as tocopherols and carotenoids, *etc.*, that oil improves lipid metabolism and possesses anticancerogenic effects along with a positive influence on dermatoses, ulcers and other skin problems [1]. Therefore the use of rose hip oil as a healthy dietary supplement and valuable cosmetic ingredient increases significantly in recent years and that requires development of effective and harmless procedures for its production.

Among the methods for extraction of oils from seeds that with super-critical carbon dioxide (CO₂) exceeds the others in the use of non-toxic, non-corrosive, non-flammable, eco-friendly and cheap solvent which can be recovered without damaging the substrate and extract. Also, the low extraction temperatures prevent thermal damage of labile compounds [2]. In recent years the application of super-critical CO₂ extraction expands significantly and put it among the leading “green” technologies.

The information published about super-critical CO₂ extraction of the oil from rose hip seeds is deficient, fragmentary and even discrepant.

Therefore the aim of our work was to elucidate the effects of some technological conditions on the composition and stability of the oil and thus to reveal the potential of that “green” method for production of rose hip oil of high quality. For the purpose, basic oil features as fatty acid composition, tocopherols and carotenoids contents, as well as its oxidative stability, were investigated.

EXPERIMENTAL

Samples and reagents

Seeds of rose hip (*Rosa canina* L.) were provided by the Foundation Information and Nature Conservation [3]. Reagents and solvents used for methylation and oxidative stability determination were of analytical grade (Merck). The solvents used as mobile phase components were of HPLC grade (Merck). Reference fatty acid methyl esters, alpha- and gamma-tocopherols, and beta-carotene were from Sigma-Aldrich, Inc., delta-tocopherol was from Supelco. Carbon dioxide was 99.95% purity (Messer Ltd., Bulgaria).

Extraction of oil

Air-dried rose hip seeds (with moisture content 3.2%, determined by Electronic Moisture Analyser KERN DBS 60-3) were ground in a hammer-mill

* To whom all correspondence should be sent:
E-mail: svetlana@orgchm.bas.bg

with 1 mm sieve and then were sorted using respective sieves to 0.4 and 1 mm particles size powders. The oil was extracted by super-critical carbon dioxide (super-critical CO₂) in SEPAREX (France) high pressure extractor equipped with extraction vessel of 5 L and working pressure up to 1000 bar. Experiments were carried out at 350, 400 and 450 bar. Effects of particles size were tested at 350 bar. After extraction at 60 °C for 120 min the respective samples were decanted to separate oil and eject the water. Then the oil was filtered under vacuum and stored in dark at 4 °C prior to analysis. Another portion of the seeds was subjected to extraction with hexane in Soxhlet apparatus for 8 hours [4] and that sample was used as a reference. The selection of all experimental conditions was based on literature data.

Analysis of fatty acids composition

Fatty acids composition of the rose hip oil was determined by gas chromatography (GC) of methyl esters (FAME). For the purpose, about 50 mg oil were transmethylated with 1% sulfuric acid in methanol [5]. The FAME were purified by preparative silica gel G thin-layer chromatography (TLC) using hexane-acetone (100:6, v/v) as a mobile phase. GC was performed on Shimadzu 17A (Shimadzu, Japan) gas chromatograph equipped with flame ionization detector and Supelcowax-10 column (100 m x 0.25 mm x 0.25 µm, SUPELCO). The column temperature was programmed from 160 °C to 270 °C with 4 °C/min and held at this temperature for 20 min. The injector and detector temperatures were 260 °C and 280 °C, respectively. Helium was the carrier gas at flow rate of 1.1 mL/min; sample size 15 µg, split 1:50. The peaks identification was according to retention times of the reference FAME. Analyses were performed in triplicate and the results were presented as relative percent of each fatty acid.

Analysis of tocopherols and carotenoids

Tocopherols and beta-carotene were analyzed directly by HPLC using Agilent 1100 liquid chromatograph equipped with an autosampler injector, column oven (25 °C) and diode-array detector at 292 nm (for *alpha*-tocopherol), 298 nm (for *gamma*- and *delta*-tocopherols [6]) and 450 nm (for *beta*-carotene [7]). Analyses were carried out on 250 mm x 4.6 mm Nucleosil 100-5 column including an EC 4/3 Nucleosil 100-5 guard column (Macherey-Nagel). Tocopherols were eluted by

mobile phase of hexane-tetrahydrofuran (96:4, v/v) at 1 mL/min flow rate (400 µg sample size) whereas beta-carotene was eluted by hexane at 0.8 mL/min flow rate (400 µg sample size). Identification was by comparison of retention times with that of reference individual isomers. Quantitation was done using respective calibration curves obtained as follows: (i) stock solution of 0.1 mg/mL *alpha*-, *gamma*- and *delta*-tocopherol, respectively, in hexane was diluted to work solutions with concentrations in the range 0.025 – 0.05 mg/mL; (ii) stock solution of 25 mg/L beta-carotene in hexane/2-propanol mixture (10:1 v/v), stored under nitrogen at -20 °C in dark, was diluted to work solutions with concentrations in the range 0.25–2.5 mg/L. Measurements were done in triplicate and the results were presented as [mg/kg oil].

Total carotenoids were determined spectrophotometrically using Cecil Series 8000 UV/VIS double beam scanning spectrophotometer (Cecil Instruments Ltd., UK) at 445 nm [8]. A calibration curve was prepared using solutions of *beta*-carotene in cyclohexane with concentrations in the range 0.5–10 mg/L. The measured samples contained about 1.2000 g oil dissolved in 25 mL cyclohexane (volumetric flask) with careful keeping of all these solutions in dark. Measurements were performed in triplicate and the results were presented as beta-carotene content [mg/kg oil].

Determination of oxidative stability

The Acid value (AV, presented as mg KOH/g) was determined by titration with ethanolic KOH [9]. Free fatty acids (FFA, given as % oleic acid) were measured titrimetrically using ethanolic NaOH [10]. The Peroxide value (PV, expressed as mEq/kg) was estimated by modified iodometric method [11]. The Induction period (IP, in hours) was found out by the following procedure: oil sample (2 g) was oxidized at 100 °C by blowing air at 50 mL/min flow rate. Aliquots were taken in fixed time intervals and the degree of oxidation was estimated by iodometric determination of the peroxide value (PV). Then kinetic curves of PV accumulation were plotted, all of them representing the mean value of three independent experiments. The Induction period (IP) was determined by the method of tangents to two parts of the kinetic curves [12]. Linear relationship between parameters investigated was obtained using the Linear fit tool of Origin software (OriginLab Corporation, MA, USA).

Statistics

The results are presented as mean values of three measurements \pm standard deviation and have been compared by Student's *t*-test (Microsoft Excel software).

RESULTS AND DISCUSSION

Fatty acids composition

Rose hip oil is one of the several seed oils which are abundant in the essential *omega*-3 (linolenic) fatty acid. With its about 23% linolenic (18:3) acid, 50% linoleic (18:2), 16% oleic (18:1) and 9% saturated (18:0 and 16:0) fatty acids the oil analyzed here (Table 1) was similar to those produced by different methods in Turkey [13–16], Romania [17], Hungary [18, 19], Poland [20]. Regarding fatty acids composition of rose hip oils obtained by super-critical CO₂ the data are scarce and inconsistent. Among four studies found in the literature [18, 19, 21, 22] only one [21] investigated effects of super-critical CO₂ extraction conditions (pressure, temperature, flow rate) on the fatty acids amounts. It was interesting that such effects were observed for 16:0, 18:0 and 18:3 only but not for 18:2. It should be noted that 18:1 was not mentioned among the results. Moreover, the unidentified components varied between 4 and 18% but these analytical flaws were not taken into account by the authors. The other three papers [18, 19, 22] compared fatty acids composition of oils obtained by super-critical CO₂ and by the standard Soxhlet extraction. According to one of them [19] there were differences in 16:0, 18:1 and 18:2 (but not in 18:3 and 18:0) amounts depending on the extraction method. The other two papers [18, 22] did not report any influence of the method of extraction on the FA composition of rose hip oil.

Table 1 presents our results about fatty acids composition of oil samples obtained by super-

critical CO₂ at different conditions and by Soxhlet extraction. As can be seen, practically no differences are observed. Thus, super-critical CO₂ extraction can be successfully used for production of rose hip oil with preserved essential fatty acids.

Tocopherols and carotenoids

Tocopherols and carotenoids are important biologically active substances. They are strong and effective natural antioxidants and for that reason higher their amounts are desirable feature of all oils and fats. Especially for rose hip oil which is highly unsaturated (Table 1) their contents are crucial for its stability. Unfortunately, significant part of them could be lost during oil production and that depends on both the method used and the applied technological conditions.

According to results found in the literature about tocopherols in rose hip oil (Table 2) cold-pressed oils have quite high tocopherols levels compared to other technologies, with total amounts above 1000 mg/kg oil. To the best of our knowledge, no data for tocopherols in rose hip oil extracted with super-critical CO₂ have been published yet, thence the investigations presented here reveal new and useful information.

Our results are given in Table 3. As can be seen, two isomers (*alpha*- and *gamma*-) were measured at that *gamma*-tocopherol was above five times more than the *alpha*-isomer. *Beta*-tocopherol was not expected to be present in measurable levels (Table 2), whereas *delta*-tocopherol was not detected in oil samples. Total amounts of tocopherols were above 1100 mg/kg which exceeded the best results achieved by other extraction methods. Concerning the production conditions, increasing of CO₂ pressure to 400 bar slightly increased the *gamma*-tocopherol amount. On the other hand, decreasing the particles size from 1 to 0.4 mm reduced amounts of both *alpha*- and *gamma*-isomers.

Table 1. Fatty acids composition (rel.%) of rose hip oil obtained by super-critical carbon dioxide extraction (SC-CO₂) and in Soxhlet apparatus.

Fatty acids	SC-CO ₂ 350bar/1mm	SC-CO ₂ 350bar/0.4mm	SC-CO ₂ 400bar/1mm	SC-CO ₂ 450bar/1mm	Soxhlet extraction
16:0	5.3 \pm 0.7*	5.3 \pm 0.7	5.2 \pm 0.8	5.3 \pm 0.6	5.3 \pm 0.9
16:1	0.1 \pm 0.01	0.1 \pm 0.01	0.1 \pm 0.01	0.1 \pm 0.01	0.1 \pm 0.01
18:0	3.6 \pm 0.3	3.5 \pm 0.4	3.4 \pm 0.4	3.5 \pm 0.3	3.4 \pm 0.5
18:1	15.8 \pm 0.6	15.6 \pm 0.5	15.5 \pm 0.7	15.8 \pm 0.7	15.9 \pm 0.9
18:2	50.3 \pm 1.8	50.7 \pm 1.7	50.6 \pm 1.9	50.4 \pm 2.0	50.7 \pm 2.3
18:3	23.2 \pm 0.9	23.1 \pm 1.1	23.5 \pm 1.1	23.2 \pm 1.2	23.0 \pm 1.5
20:0	1.3 \pm 0.1	1.3 \pm 0.1	1.3 \pm 0.1	1.3 \pm 0.1	1.2 \pm 0.1
20:1	0.3 \pm 0.06	0.3 \pm 0.01	0.3 \pm 0.0	0.3 \pm 0.01	0.3 \pm 0.01
22:0	0.1 \pm 0.01	0.1 \pm 0.02	0.1 \pm 0.01	0.1 \pm 0.01	0.1 \pm 0.01

* Within each row, no statistically significant difference between values was found (at P=0.95).

Table 2. Data found in literature about tocopherols content in rose hip oil obtained by different methods (average values).

[Ref. No.] Extraction method	α -tocopherol (mg/kg)	β -tocopherol (mg/kg)	γ -tocopherol (mg/kg)	δ -tocopherol (mg/kg)	total tocopherols (mg/kg)
[16] cold-pressing	58	5	1060	4	1125
[20] cold-pressing	120-150	nd*	630-780	230-260	1000-1200
[23] hexane	170	nd	900	30	1100
[14] hexane	8	nd	nd	nd	-
[18] subcritical CO ₂ -propane	57	nd	92	27	180
[24] Soxhlet	16	1.5	nd	nd	17.5

* nd - not detected

Table 3. Tocopherols, carotenoids contents and oxidative stability parameters of rose hip oil obtained by super-critical CO₂ extraction at different conditions.

	SC-CO ₂ 350bar/1mm	SC-CO ₂ 350bar/0.4mm	SC-CO ₂ 400bar/1mm	SC-CO ₂ 450bar/1mm
tocopherols				
α -tocopherol (mg/kg)	180 ± 10 ^{a*}	150 ± 10 ^b	200 ± 10 ^a	190 ± 10 ^a
γ -tocopherol (mg/kg)	1040 ± 20 ^a	980 ± 20 ^b	1160 ± 20 ^c	1180 ± 20 ^c
total tocopherols (mg/kg)	1220 ^{**}	1130 ^{**}	1360 ^{**}	1370 ^{**}
carotenoids				
total carotenoids (as β - carotene, mg/kg)	16.6 ± 0.6 ^a	14.1 ± 0.6 ^b	18.4 ± 0.6 ^c	18.0 ± 0.5 ^c
β -carotene (mg/kg)	9.0 ± 0.3 ^a	3.5 ± 0.2 ^b	11.5 ± 1.0 ^c	12.5 ± 0.8 ^c
oxidative stability				
AV (mg KOH/g)	6.6 ± 0.8 ^a	6.1 ± 0.7 ^a	2.8 ± 0.5 ^b	3.2 ± 0.5 ^b
FFA (% oleic acid)	3.5 ± 0.4 ^a	3.2 ± 0.3 ^a	1.5 ± 0.3 ^b	1.7 ± 0.3 ^b
PV (mEq/kg)	9.0 ± 0.4 ^a	7.2 ± 0.4 ^b	6.1 ± 0.3 ^c	5.9 ± 0.3 ^c
IP (hours)	4.9 ± 0.3 ^a	5.6 ± 0.3 ^b	6.7 ± 0.5 ^c	6.6 ± 0.4 ^c

* Different letters within each row indicate statistically significant difference between the mean values (at P=0.95).

** Sum of the values for *alpha*- and *gamma*-isomers.

However, even the lowest tocopherols contents are comparable to the best results obtained by other extraction methods (cold-pressing, hexane extraction, etc.).

Carotenoids and specially *beta*-carotene in rose hip oil are presented in several publications. Depending on the producing technology, their amounts vary from 40 to 150 mg/kg for total carotenoids [15, 19, 20, 23] and from 0.2 to 2 mg/kg for *beta*-carotene [14, 18, 23]. According to our results (Table 3), super-critical CO₂ extraction at the investigated conditions ensured rose hip oil with 14–18 mg/kg total carotenoids and 4–13 mg/kg *beta*-carotene. Comparing to the results mentioned above, total carotenoids were far less but the *beta*-carotene content was significantly higher than the available data. As with the tocopherols, increasing the pressure from 350 to 400 bar caused slight increasing of carotenes contents whereas decreasing of particles size reduced their amounts. Comparing to other methods, the extraction with super-critical CO₂ ensures rose hip oil rich in *beta*-carotene along with tocopherols.

Oxidative stability

The oxidative stability of oils depends mainly on their fatty acids composition and the presence of antioxidants. Because of its high content of linolenic acid the rose hip oil is expected to have rather low oxidative stability. In literature have been found data only about acid value (AV) and peroxide value (PV) of two cold-pressed rose hip oils, in the range respectively 0.1–0.6 mg KOH/g and 1.2–2.1 mEq/kg [20]. Our results about oxidative stability are given in Table 3. Concerning AV and PV, the values of oil produced by super-critical CO₂ (2.8–6.6 mg KOH/g and 5.9–9.0 mEq/kg) are higher than cold-pressed rose hip oils cited above. Nevertheless, AV and free fatty acids (FFA) are below the maximum values permitted for virgin olive oil [25]. The induction periods (IP) of tested rose hip oils (4.9–6.7 hours) are typical for oils with similar unsaturation, e.g. linseed oil [26]. Regarding conditions for super-critical CO₂ extraction and samples content discussed in the previous sections, it should be expected decreasing

of AV, FFA and PV and respective increasing of IP with increasing of the CO₂ pressure because of the same trends in the main antioxidants along with no alteration in fatty acids (Tables 1 and 3). Indeed, the results for oxidative stability of rose hip oil samples (Table 3) confirm that assumption. So, pressures above 400 bar could be recommended for production by super-critical CO₂ extraction of rose hip oil with higher stability, *i.e.* of higher quality.

CONCLUSION

The extraction of rose hip seeds with super-critical CO₂ enables production of high quality glyceride oil containing significant amounts of unchanged essential fatty acids and natural antioxidants (mainly tocopherols and carotenoids). Extraction conditions such as pressure (350–450 bar) and particles size of the milled seeds (0.4, 1 mm) do not practically affect the fatty acids composition. On the other hand, increasing the pressure from 350 to 400 bar causes slight increasing of tocopherols and carotenes contents whereas decreasing of particles size reduced their amounts. The higher quantity of these antioxidants insures better oxidative stability of the rose hip oil and thence its high quality.

Acknowledgements: Financial and technical support from the Foundation Information and Nature Conservation (project “Municipal Model for Medicinal and Aromatic Plants Conservation and Sustainable Use (www.herbvaluebg.org)” funded by TFCSP of the Bulgarian-Swiss Cooperation Programme, and by the Project BG161PO003-1.2.04-0007-C0001 “Upgrading of the IOCCP equipment for utilization of medicinal and aromatic plants through green technologies”, OP “Development of the Competitiveness of the Bulgarian Economy”, was gratefully acknowledged.

REFERENCES

1. C. Chrubasik, B. D. Roufogalis, U. Muller-Ladner, S. Chrubasik, *Phytoter. Res.*, **22**, 725 (2008).

2. R. K. Saini, Y.-S. Keum, *Food Res. Intern.*, **82**, 59 (2016).
3. <http://ecologybg.com/index.html>
4. ISO 659:2009, Oilseeds – Determination of oil content (Reference method), p. 12 (2009).
5. W. W. Christie, *Lipid Analysis*, The Oily Press, Bridgwater, England, 2003.
6. ES ISO 9936:2012, Animal and vegetable fats and oils – Determination of tocopherol and tocotrienol contents by HPLC.
7. G. Panfili, A. Fratianni, M. Irano, *J. Agric. Food Chem.*, **52**, 6373 (2004).
8. British Standard Methods of Analysis – B.S.684, Section 2.20:1997, Determination of Carotene in Vegetable Oils.
9. AOCS Official method Cd 3d-63.
10. AOCS Official method Ca 5a-40.
11. N. Yanishlieva, A. Popov, E. Marinova, *Compt. Rend. Acad. Bulg. Sci.*, **31**, 869 (1978).
12. B. Le Tutour, D. Guedon, *Phytochem.*, **31**, 1173 (1992).
13. M. Ozkan, *J. Med. Food*, **5**, 137 (2002).
14. S. Kazaz, H. Baydar, S. Erbas, *Czech J. Food Sci.*, **27**, 178 (2009).
15. H. Ilyasoglu, *Int. J. Food Prop.*, **17**, 1591 (2014).
16. M. Topkafa, *Anal. Methods*, **8**, 4220 (2016).
17. N. Ionescu (Bordei), G.-C. Ivopol, M. Neagu, M. Popescu, A. Meghea, *U.P.B. Sci. Bull., Series B* **77**, 39 (2015)
18. V. Illes, O. Szalai, M. Then, H. Daood, S. Perneckzi, *J. Supercrit. Fluids*, **10**, 209 (1997).
19. K. Szentmihalyi, P. Vinkler, B. Lakatos, V. Illes, M. Then, *Biores. Technol.*, **82**, 195 (2002).
20. M. Grajzer, A. Prescha, K. Korzonek, A. Wojakowska, M. Dziadas, A. Kulma, H. Grajeta, *Food Chem.*, **188**, 459 (2015).
21. S. Machmudah, Y. Kawahito, M. Sasaki, M. Goto, *J. Supercrit. Fluids*, **41**, 421 (2007).
22. U. Salgin, S. Salgin, D. D. Ekici, G. Uludag, *J. Supercrit. Fluids*, **118**, 194 (2016).
23. M. Fromm, S. Bayha, D. R. Kammerer, R. Carle, *J. Agric. Food Chem.*, **60**, 10733 (2012).
24. L. Barros, A. M. Carvalho, I. C. F. R. Ferreira, *Food Res. Intern.*, **44**, 2233 (2011).
25. Codex Standard for Named Vegetable Oils (CODEX-STAN 210 - 1999).
26. E. Rudnik, A. Szczucinska, H. Gwardiak, A. Szulc, A. Winiarska, *Thermochim. Acta*, **370**, 135 (2001).

ЕКСТРАКЦИЯТА СЪС СУПЕР-КРИТИЧЕН ВЪГЛЕРОДЕН ДИОКСИД КАТО ЕФЕКТИВНА „ЗЕЛЕНА“ ТЕХНОЛОГИЯ ЗА ПОЛУЧАВАНЕ НА ВИСОКОКАЧЕСТВЕНО ШИПКОВО МАСЛО

С. Танева, А. Конакчиев, И. Тоцева, М. Каменова-Начева, Я. Николова, Св. Момчилова*, Вл. Димитров

Институт по Органична Химия с Център по Фитохимия, Българска Академия на Науките, ул. Акад. Г. Бончев, бл. 9, 1113 София, България

Постъпила на 09 март 2017 г.; Коригирана на 21 март 2017 г.

(Резюме)

Изследвано е приложението на екстракцията със супер-критичен въглероден диоксид за получаване на висококачествено масло от семки на шипка (*Rosa canina* L.). За целта са определени основните характеристики на маслото като мастно-киселинен състав, съдържание на токофероли и каротеноиди, както и окислителната му стабилност. Резултатите показват, че технологични условия като налягането (350–450 бара) и размер на частиците на смлените семки (0.4, 1 мм) не влияят върху мастно-киселинния състав. Обаче, повишаване на налягането от 350 до 400 бара предизвиква леко увеличение в токоферолното и каротеноидно съдържание, докато намаляване размера на частиците води до намаляване на количеството токофероли и каротеноиди. Повисокото съдържание на тези антиоксиданти осигурява по-висока окислителна стабилност на шипковото масло и така повишава неговото качество.

Structural basis for the inactivation of *Candida rugosa* lipase in the presence of amino acid ionic liquids

M. Guncheva^{1*}, D. Yancheva¹, P. Ossowicz², E. Janus²

¹ Institute of Organic Chemistry with Centre of Phytochemistry, Bulgarian Academy of Sciences, Sofia, Bulgaria

² Institute of Organic Chemical Technology, West Pomeranian University of Technology Szczecin, Szczecin, Poland

Received February 24, 2017; Revised March 13, 2017

Dedicated to Acad. Bogdan Kurtev on the occasion of his 100th birth anniversary

The aim of this study is to evaluate the interactions between a lipase from *Candida rugosa* (CRL) with ionic liquids (ILs) consisting of cholinium [Chol] or 1-ethyl-3-methylimidazolium [emim] cation, and anions of amino acids with uncharged non-polar or polar side chains. The effect of the ILs on the enzyme activity was followed in a spectrophotometric assay using 4-nitrophenyl acetate as a substrate. The compounds were tested in a wide concentration range. Added to the reaction mixture at concentrations up to 0.025 mM, all cholinium-based ILs, except cholinium glycinate, enhanced or had no effect on CRL activity. Large influence of the anion and a clear trend in the order Leu>Trp>Thr>Val>Met>Ile>Gly of decreased activity was observed for the two series. The effects induced of [emim] were stronger than those observed for [Chol]. FTIR spectroscopy was applied to be monitored IL-induced changes in the secondary structure of CRL. A correlation between the activities of CRL in presence of ILs and the changes in the enzyme structure was established.

Key words: *Candida rugosa* lipase; ionic liquids; hydrolytic activity; protein secondary structure

INTRODUCTION

Lipases [EC 3.1.1.3] are hydrolytic enzymes that catalyze the hydrolysis of ester bonds in triacylglycerols, which results in formation of di-, monoacylglycerols, glycerol and fatty acids [1]. Despite of their origin, lipases share common structural organization (α/β fold) and have the same catalytic centre [1]. They differ in their substrate specificity and biochemical properties, which is a key factor for their versatile applications as biocatalysts for various industrial processes, diagnostic tools or food supplements in medicine, biosensors for pesticide detection, etc. [2–6].

Microbial enzymes are of great commercial interest, which is due to their advantages over the enzymes of plant and animal origin. For example, they are obtained at lower production costs, they can be easily isolated and genetically manipulated, they are relatively more stable, etc. [7, 8].

Lipase from *Candida rugosa* (CRL) has a broad specificity and is used as catalyst in biodiesel production, reactions of enantioselective hydrolysis and/or esterification, modifications of natural products, etc. [9–12]. Yet, biocatalysts remain relatively expensive and less stable in comparison

to the conventional catalysts and despite of their higher selectivity their industrial usage is not high.

It is noteworthy to be mentioned that most of the bacterial lipases exhibit good activity in organic solvents, while some of enzymes are alkaline-, acid- or salt-tolerant [13, 14]. Media engineering is an easy-to-perform and an effective strategy to enhance activity, improve stability and/or tuning the lipases selectivity [15, 16]. In some cases adding of a surfactant to the reaction media or pre-treatment of lipases with organic solvents may alter their specificity or may have an effect on their activity [17, 18]. In last two decades scientists have focused their attention on the possible application of ionic liquids (ILs) as solvents or co-solvents for enzyme-catalyzed reactions [19]. ILs are mixtures of organic cations and/or anions that melt below 100 °C [20]. Up to date there is no systematic knowledge on the interactions of ILs with lipases, in particular CRL, although many papers have been published on this topic. For example, CRL exhibited higher thermal stability in 1-methyl-3-octyl-imidazolium hexafluorophosphate [omim][PF₆] than in hexane [21]. Li *et al.* reported that CRL chemically-modified with IL based on PEGylated imidazolium cation and dihydrogen phosphate anion have also enhanced thermal stability catalytic activity and is tolerant toward polar organic solvents in comparison to the native

* To whom all correspondence should be sent:
E-mail: maia@orgchem.bas.bg

CRL [22]. In addition, Cabrera-Padilla *et al.* found that adding of 1-butyl-3-methylimidazolium bis-(trifluoromethylsulfonyl) imide [bmim][NTf₂] to the enzyme loading solution facilitated CRL adsorption on eco-friendly organic polymer, which resulted in 3-fold increase of the immobilization yield [23]. Shah and Gupta reported a highly enantioselective transesterification of (±)-1-phenylethanol in [bmim][PF₆] catalyzed by CRL [24]. Enhanced enantioselectivity of CRL in [bmim][PF₆] was reported by other authors [25, 26]. On the other hand, CRL did not exhibit any activity in the reaction of acylation of flavonoid glycosides in 1-butyl-3-methylimidazolium tetrafluoroborate [bmim][BF₄] and [bmim][PF₆] [27]. Low enantioselectivity was reported also for the CRL-catalyzed esterification of ibuprofen with 1-propanol in ILs containing imidazolium or phosphonium cation and organosulfate anion [28].

The activity of CRL in presence of ILs containing amino acid anions has not been evaluated yet. Such ionic liquids have relatively low toxicity and are considered as biocompatible and easily biodegradable [29]. In this research, we tested the activity of CRL in presence of IL containing 1-ethyl-3-methylimidazolium [emim] or cholinyl [Chol] cation and non-polar amino acids as anions. The results from the enzymatic activity assays are correlated with the induced by ILs changes in protein structure.

EXPERIMENTAL

Materials

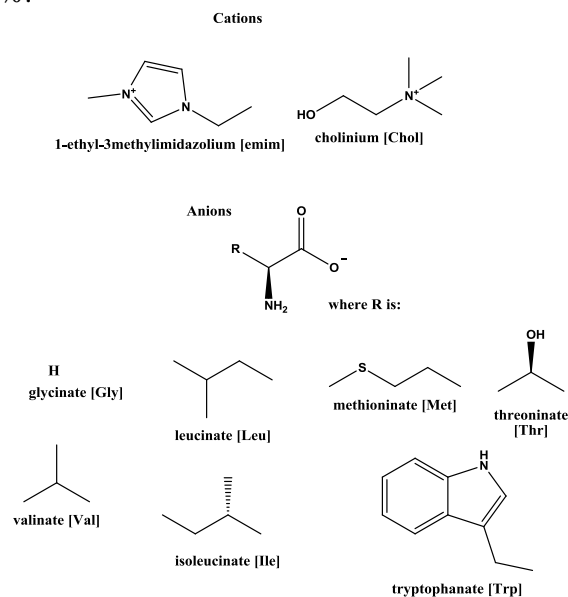
Lipase from *Candida rugosa* (CRL) (MW 64 kDa, 30 U/mg (olive oil as a substrate), 10% (w/w) protein content) was purchased by Amano Pharmaceutical Co., Japan. 4-Nitrophenyl acetate was obtained from Sigma. 1-Ethyl-3-methylimidazolium amino acids [emim][AA] and cholinium amino acids [Chol][AA] (Scheme 1) were synthesized, purified and characterized as previously described [30, 31].

Hydrolytic activity assay

Prior to be tested, 20 µL of CRL stock solutions (20 mg/mL in 0.05 M sodium phosphate buffer, pH 7.0) were mixed with 20 µL of solutions of ILs in water (0.01–0.5 M). Then, aliquots of 0.01 mL IL-treated CRL were withdrawn and were added to a reaction mixture consisting of 1.65 mL sodium phosphate buffer (0.05 M, pH 7.0) and 0.04 mL of 0.02 M 4-nitrophenyl acetate in DMSO. The release

of 4-nitrophenol with the time was monitored spectrophotometrically at 410 nm (ϵ molar = 14 200 M⁻¹ cm⁻¹). Spontaneous hydrolysis was taken into account in control experiments without an enzyme but in presence of the corresponding amount of IL (or water). The activity of CRL-IL complexes is expressed as relative activity in comparison to the activity of native CRL, which is taken for 100%.

All experiments were performed in triplicate and the mean values were reported. The relative standard deviation for each experiment was up to 5%.



Scheme 1. Structures of the tested compounds.

Fourier transform infrared spectroscopy (FTIR)

For the measurements, solutions of 40 mg/mL CRL in 5% (w/v) ionic liquid or water were prepared. Infrared spectra of the CRL-IL complexes were recorded on Bruker Tensor 27 spectrometer, equipped with deuterated triglycine sulphate detector (DTGS). Each sample was deposited onto a diamond crystal (ATR element) and a 64 scan interferogram was collected in a single beam mode, with 2 cm⁻¹ resolution from 4000–600 cm⁻¹. Reference spectra containing the corresponding IL in the same concentration were recorded. A baseline correction was performed in the amide I region (1600–1700 cm⁻¹) assuming a linear baseline. In order to enhance the component peaks contributing to Amide I band the spectra were treated by Fourier-self deconvolution using Opus software version 5.5. Second derivative spectra were obtained using the Savitzky-Golay algorithm based on 25 smoothing points. In the fitting, the number of components and the initial values of their position were set as determined from the

second derivative spectra. The initial bandwidth of all components was set to 11 cm^{-1} and the components were approximated by mixed Lorentzian/Gaussian functions. The curve-fitting was performed according to the Local Least Squares algorithm. The assignment of the Amide I band positions to secondary structure was done according to the literature data [32].

RESULTS AND DISCUSSION

Activity of CRL in presence of [emim][AA] and [Chol][AA]

ILs containing amino acid anions with uncharged non-polar or polar side chains were selected for this study. All compounds were tested in a concentration range between 0.025 and 0.25 mM. We found that both the structure of the cation and the anion of the ILs have an effect on the CRL hydrolytic activity (Fig. 1A and 1B).

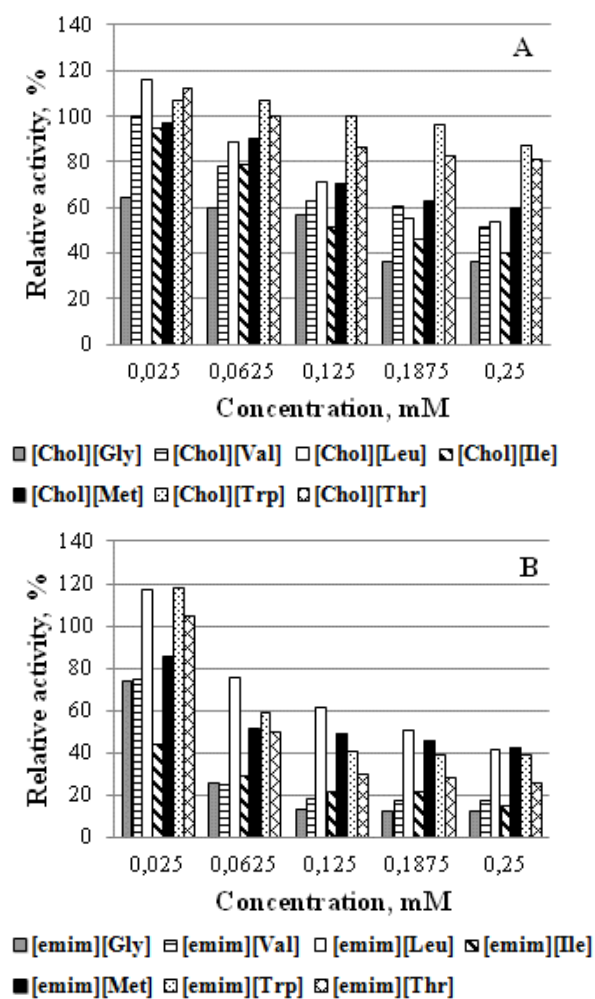


Fig. 1. Hydrolytic activity of *Candida rugosa* lipase in presence of cholinium-based amino acids (A) and 1-ethyl-3-methylimidazolium-based amino acids (B).

Significant decrease of the hydrolytic activity of CRL was observed in presence of all [emim]AAs, except for the most dilute solutions of [emim][Leu], [emim][Trp] and [emim][Thr]. On the other hand, CRL is relatively stable in presence of [Chol][Trp] and [Chol][Thr] at the all tested concentrations. In contrast, the hydrolysis rate of 4-nitrophenyl acetate tends to decrease in presence of the other cholinium amino acids in a dose-dependent manner. In comparison, Deive *et al.* reported for a downward shifts of the thermal unfolding of a lipase from *Thermomyces lanuginosus* in the presence of cholinium alaninate, cholinium glycinate and cholinium lysinate [33]. It was assumed that the examined salts induce also some changes in the lipase conformation, which resulted in its increased lipolytic activity [33]. In addition, higher yield of the target fatty acid esters *i.e.* enhanced esterification activity was reported for CRL pre-coated with tetraethylammonium 1-histidinate and tetraethylammonium 1-asparaginate [34]. To the best of our knowledge, beside the above two papers, there is no systematic research on the effect of amino acid-based ILs on the activity and/or structure of lipases. Large influence of the anion and a clear trend in the order $\text{Leu} > \text{Trp} \geq \text{Thr} > \text{Val} \geq \text{Met} > \text{Ile} > \text{Gly}$ of decreased activity was observed for the two series.

Conformational changes in CRL molecules in presence of [emim][AA] and [Chol][AA]

We recorded FTIR spectra of the CRL-IL complexes that exhibited an enhanced, unaltered and/or deteriorated catalytic performance in comparison to the activity of the native CRL in order to assess the changes in the enzyme secondary structures that were induced by the amino acid salts. There are several main secondary structures that were observed in the following frequency intervals: α -helical structures at $1650\text{--}1659\text{ cm}^{-1}$, β -sheet structures at $1625\text{--}1635\text{ cm}^{-1}$, random coils at $1640\text{--}1647\text{ cm}^{-1}$, β -turns at $1670\text{--}1688\text{ cm}^{-1}$, as well as aggregated or antiparallel β -sheets at $1609\text{--}1614\text{ cm}^{-1}$, and vibrations of tyrosine residues comprising the protein molecule at $1600\text{--}1606\text{ cm}^{-1}$. The estimated elements of the secondary structure are summarized in Table 1. A decrease in α -helix and β -structures in favor of unordered and aggregated structures has been found in the FTIR spectra of the two CRL-glycinate complexes. In addition, an increase in the proportion of the band, characteristic for the amino acid side-chains (mainly benzene ring of tyrosyl

Table 1. Main secondary structure elements of *Candida rugosa* lipase obtained by FTIR-spectroscopy in water solution of ILs.

Solvent	Relative area, %					
	α -helix	β -sheet	β -turn	random coils/unordered structures	antiparallel β -sheets/aggregated strands	Tyr-residues
water	27.2	34.9	20	–	–	5.1
[Chol][Gly]	16.5	20.6	18.3	26.5	7.8	17.2
[emim][Gly]	16.2	16.9	10.5	19.7	18.4	18.2
[Chol][Met]	25.8	16.5	11.9	28.5	17.3	–
[emim][Met]	25.2	18.6	10.7	25.5	20.1	–
[Chol][Val]	41.7	28.9	16.2	–	13.2	–
[emim][Val]	24.3	21.8	11.3	20.7	21.8	–
[Chol][Thr]	22.0	27.3	12.7	15.6	17.5	–
[emim][Thr]	25.3	20.7	13.1	25.1	–	14.9

Complexes were prepared by mixing of CRL (40 mg/mL, 0.62 mM) with water solutions of 100 mM [Chol][AA] or [emim][AA].

residues) can be seen, which means that these hydrophobic residues, which in the native lipase are buried in the interior of the protein molecule, in presence of [Chol][Gly] and [emim][Gly] become more exposed to the solvent. All this implies a partial unfolding of the CRL in presence of the two glycinate anions and correlates with the observed reduction in the enzyme hydrolytic activity.

At the lowest tested protein-to-IL ratio, [Chol][Met] and [Chol][Val] have no effect on the CRL activity, while [emim][Met] and [emim][Val] have weak inhibitory effect. No unfolding was noticed in the FTIR spectra of CRL in presence of these four ILs. However, in this case a significant rearrangement in the protein molecule was observed. Interestingly, the two IL with methionine anions induced the same structural changes in the CRL conformation and the effect of the cation is neglectable. On the other hand, both [Chol][Val] and [emim][Val] suppressed the aggregation and/or unfolding and the lipase folds into more coiled and compact conformation. In addition, an 1.5-fold increase in the α -helix content of CRL was observed in the presence of cholinium valinate. This change, however, probably did not occur near the enzyme active centre, thus the enzyme activity remained preserved. In contrast, the two ILs with the threonine anion induced reorganization in CRL molecules which probably makes the active site more accessible to the substrate and resulted in the enzyme activation.

CONCLUSION

Ionic liquids that contain anions of amino acids with medium or large size hydrophobic side-chain residues have a stimulatory effect on *Candida rugosa* lipase, when added to the reaction mixture in quantities up to 100-times higher than the

concentration of the lipase. In general, such ILs do not promote unfolding, but induce rearrangement in the protein molecule and possibly the enzyme active site becomes more accessible to the substrate. On the other hand ILs with glycinate anion initiate processes of denaturation and aggregation which results in decreased enzyme activity.

Acknowledgements: COST action CM1206 “EXIL” is gratefully acknowledged.

REFERENCES

1. L. Casas-Godoy, S. Duquesne, F. Bordes, G. Sandoval, A. Marty in *Lipases and Phospholipases, Methods in Molecular Biology*, G. Sandoval (ed.), V. 861, Humana Press, 2012, p.3-30.
2. R. Gupta, N. Gupta, P. Rathi, *Appl. Microbiol. Biotechnol.*, **64**, 763 (2004).
3. F. Hasan, A. A. Shah, A. Hameed, *Enz. Microb. Tech.*, **39**, 235 (2006).
4. C. Anobom, A. Pinheiro, R. De-Andrade, E. Aguieiras, G. Andrade, M. Moura, R. V. Almeida, D. Freire, *Biomed. Res. Int.*, Article ID 684506 (2014).
5. B. Rachman, *Clin. Nutr. Ins.*, **5**, 1 (1997).
6. N. Zehani, R. Kherrat, S. V. Dzyadevych, N. Jaffrezic-Renault, *Intern. J. Environ. Anal. Chem.*, **95**, 466 (2015).
7. P. Anbu, S. Gopinath, A. C. Cihan, B. P. Chaulagain, *Biomed. Res. Int.*, Article ID 204014 (2013).
8. B. Andualema, A. Gessesse, *Biotechnol.*, **11**, 100 (2012).
9. W. Parawira, *Crit. Rev. Biotechnol.*, **29**, 82 (2009).
10. M. Kapoor, M. N.Gupta, *Proc. Biochem.*, **47**, 555 (2012).
11. A. Intra, A. Bava, G. Nasini, S. Riva, *J. Mol. Cat. B: Enzym.*, **29**, 95 (2004).

12. I. Antonopoulou, S. Varriale, E. Topakas, U. Rova, P. Christakopoulos, V. Faraco, *Appl. Microbiol. Biotechnol.*, **100**, 6519 (2016).
13. A. Salihu, Md. Z. Alama, *Proc. Biochem.*, **50**, 86 (2015).
14. R. Schmid, R. Verger, *Angew. Chem. Int. Ed.*, **37**, 1608 (1998).
15. U. Bornscheuer, C. Bessler, R. Srinivas, S. Hari Krishna, *Trends Biotechnol.*, **20**, 433 (2002).
16. Y. Khmel'nitsky, A. Levashov, N. Klyachko, K. Martinek, *Enzym. Microb. Technol.*, **10**, 710 (1988).
17. V. Stepankova, S. Bidmanova, T. Koudelakova, Z. Prokop, R. Chaloupkova, J. Damborsky, *ACS Catal.*, **3**, 2823 (2013).
18. E. Abaházi, Z. Boros, L. Poppe, *Molecules*, **19**, 9818 (2014).
19. F. van Rantwijk, R. M. Lau, R. A. Sheldon, *TRENDS Biotechnol.*, **21**, 133 (2003).
20. T. Welton, *Chem. Rev.*, **99**, 2071 (1999).
21. O. Ulbert, K. Belafi-Bako, K. Tonova, L. Gubicza, *Biocatal. Biotransfor.*, **23**, 177 (2005).
22. X. Li, C. Zhang, S. Li, H. Huang, Y. Hu, *Ind. Eng. Chem. Res.*, **54**, 8072 (2015).
23. R. Cabrera-Padilla, M. Lisboa, M. Pereira, R. T. Figueiredo, E. Franceschi, A. Fricks, Á. S. Lima, D. Silva, C. Soares, *Bioprocess Biosyst. Eng.*, **38**, 805 (2015).
24. S. Shah, M. Gupta, *Bioorg. Med. Chem. Lett.*, **17**, 921 (2007).
25. Y. Yuan, S. Bai, Y. Sun, *Food Chem.*, **97**, 324 (2006).
26. D.-H. Zhang, S. Bai, M.-Y. Ren, Y. Sun, *Food Chem.*, **109**, 72 (2008).
27. M. Katsoura, A. Polydera, L. Tsironis, A. Tselepis, H. Stamatis, *J. Biotechnol.*, **123**, 491 (2006).
28. Y. Hongwei, W. Jinchuan, C. C. Bun, *Chirality*, **17**, 16 (2005).
29. A. Yazdani, M. Sivapragasam, J.-M. Levêque, M. Moniruzzaman, *J Microb Biochem Technol.*, **8**, 415 (2016).
30. M. Guncheva, K. Paunova, P. Ossowicz, Z. Rozwadowski, E. Janus, K. Idakieva, S. Todinova, Y. Raynova, V. Uzunova, S. Apostolova, R. Tzoneva, D. Yancheva, *Int. J. Biol. Macromol.*, **82**, 798 (2016).
31. M. Guncheva, K. Paunova, P. Ossowicz, Z. Rozwadowski, E. Janus, K. Idakieva, S. Todinova, Y. Raynova, V. Uzunova, S. Apostolova, R. Tzoneva, D. Yancheva, *RSC Adv.*, **5**, 63345 (2015).
32. A. Barth, *Biochim. Biophys. Acta*, **1767**, 1073 (2007).
33. F. J. Deive, D. Ruivo, J. V. Rodrigues, C. M. Gomes, M. Á. Sanromán, L. P. N. Rebelo, J. M. S. S. Esperança, A. Rodríguez, *RSC Adv.*, **5**, 3386 (2015).
34. M. B. A. Rahman, K. Jumbri, N. A. M. A. Hanafiah, E. Abdulmalek, B. A. Tejo, M. Basri, A. B. Salleh, *J. Mol. Catal. B: Enzym.*, **79**, 61 (2012).

ОБЯСНЕНИЕ НА РАЗЛИКИТЕ В АКТИВНОСТТА НА ЛИПАЗА ОТ *CANDIDA RUGOSA* В ПРИСЪСТВИЕ НА ЙОННИ ТЕЧНОСТИ НА ОСНОВАТА НА АМИНОКИСЕЛИНИ ЧРЕЗ ПРОМЕНИ В ПРОТЕИНОВАТА КОНФОРМАЦИЯ

М. Гунчева^{1*}, Д. Янчева¹, П. Осовиц², Е. Янус²

¹ Институт по органична химия с Център по фитохимия, Българска Академия на Науките, София, България

² Институт по органична химична технология, Западно Померански технологичен университет на Шчечин, Полша

Постъпила на 24 февруари 2017 г.; Коригирана на 13 март 2017 г.

(Резюме)

Във фокуса на настоящото изследване са взаимодействията на липаза, изолирана от *Candida rugosa* (CRL), с йонни течности, съдържащи холин [Chol] или 1-етил-3-метил имидазолиев [emim] катион и аниони – незаредени аминокиселини. Ефектът на йонните течности (ЙТ) върху ензимната активност беше изследван за всички съединения в широк концентрационен интервал в моделна реакция спрямо субстрат 4-нитрофенил ацетат. С изключение на глицината, всички останали ЙТ от холиновата серия нямат ефект или повишават активността на CRL, добавени в ниски концентрации към реакционната смес. За двете серии ЙТ се наблюдава зависимост на ензимната активност от структурата на аниона, макар че тенденцията е по-ясно изразена при серията, съдържаща [emim] катион. С помощта на ИЧ спектроскопия бяха проследени промените във вторичната структура на CRL, индуцирани от ЙТ. Направена е корелация между възникналите промени в структурата на ензима и отчетената активност в присъствие на ЙТ.

DFT study on the radical scavenging capacity of apocynin with different free radicals

D. Y. Yancheva^{1*}, S. S. Stoyanov¹, E. A. Velcheva¹, B. A. Stamboliyska¹, A. Smelcerovic²

¹ Institute of Organic Chemistry with Centre of Phytochemistry, Bulgarian Academy of Sciences, Acad. G. Bonchev Str., build. 9, 1113 Sofia, Bulgaria

² Department of Chemistry, Faculty of Medicine, University of Nis, Blv. Dr Zorana Djindjica 81, 18000 Nis, Serbia

Received March 07, 2017; Revised March 11, 2017

Dedicated to Acad. Bogdan Kurtev on the occasion of his 100th birth anniversary

Apocynin is known as a nicotinamide adenine dinucleotide phosphate oxidase inhibitor and has been used as one of the most promising drugs in experimental models in vascular, inflammatory and neurodegenerative pathologies where the regulation of reactive oxygen species (ROS) plays a crucial role. Different possible mechanisms such as hydrogen atom transfer (HAT), single-electron transfer (SET-PT), sequential proton loss electron transfer (SPLET) were studied by DFT computations of the respective reaction enthalpies in polar and nonpolar solvents. The reactivity against various free radicals was accounted by analysing the thermodynamic data of apocynin reactions with hydroxyl, hydroxyperoxyl, alkoxyl and alkoxyperoxyl radicals. According to the calculations, the SPLET mechanism is preferred in ionization supporting solvents such as water. In this relation, the formation of oxyanion of apocynin was carried out in DMSO, and the structural and spectral changes arising from the conversion were followed by IR methods and DFT computations.

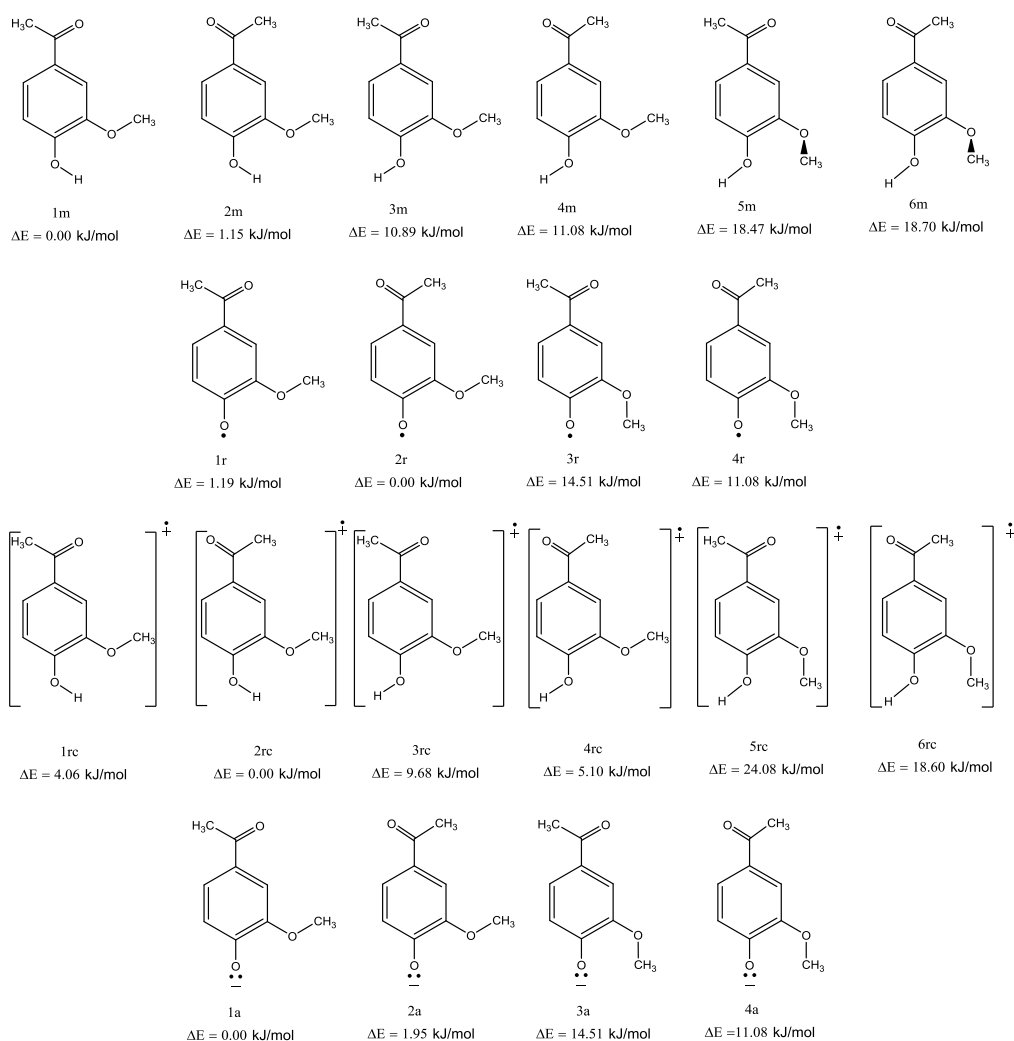
Key words: apocynin; DFT; radical scavenging capacity; vibrational spectra; anion

INTRODUCTION

Imbalance between reactive oxygen species (ROS) synthesis and normal production of oxidants in the body causes many inflammatory and neurodegenerative pathologies. Atherosclerosis, osteoarthritis or rheumatoid arthritis, ischemia-reperfusion lung injury, brain injury *etc.* are all associated to excessive production of ROS. Nicotinamide adenine dinucleotide phosphate oxidase (NADPH oxidase, NOX) is the enzyme that triggers the ROS production, and inhibition of this enzyme represents a successful strategy in the treatment of many diseases. Apocynin (Scheme 1, other trivial names: 4-hydroxy-3-methoxyacetophenone, acetovanillone), a plant phenol – the biologically active substance in the roots of *Picrorhiza kurroa* growing in alpine Hymalaya, has been established as effective and nontoxic inhibitor of NADPH oxidase [1, 2]. Plant extract from *Picrorhiza kurroa* have been used in India and Sri Lanka for the preparation of ethnical medicines since long ago [3, 4]. Extracts of this plant are commercialized in the USA for treatment of liver disease and other conditions related to severe oxidative damage. Due to its inhibitory activity to NADPH oxidase, apocynin exhibit potent anti-inflammatory effect. The high effectiveness and

low toxicity of apocynin make it very promising lead compound and its clinical effects were documented in various models of neurodegenerative diseases, including Alzheimer and Parkinson's disease [4] and cardiovascular diseases [5]. On the other hand, there are reports suggesting that apocynin is not actually inhibitor of vascular NADPH oxidase, but an antioxidant [6]. It was suggested that apocynin only inhibits NADPH oxidase in leukocytes, whereas in endothelial and vascular smooth muscle cells, it predominantly acts as an antioxidant. The authors demonstrated that apocynin selectively deactivates hydroxyl and hydroxyperoxyl radicals [6]. Oxidative side effects of apocynin were also reported due to pro-oxidant activity of its radical [7]. Despite the variety of experimental data supporting the radical-scavenging efficiency of apocynin [8, 9], there are no reports on the anticipated mechanism of its action. Therefore, the purpose of the present study is to investigate the possible mechanisms of antioxidant action taking into account the influence of the medium polarity. Different possible mechanisms such as hydrogen atom transfer (HAT), single-electron transfer (SET-PT), and sequential proton loss electron transfer (SPLET) will be studied by DFT computations of the respective reaction enthalpies in polar and nonpolar solvents. In order to estimate the reactivity against

* To whom all correspondence should be sent:
E-mail: deni@orgchem.bas.bg



Scheme 1. Conformers of neutral apocynin (**1m-6m**), its radical (**1r-4r**), radical cation (**1rc-6rc**) and oxyanion (**1a-4a**), the relative energies ΔE are given in $\text{kJ}\cdot\text{mol}^{-1}$ with respect to the most stable conformers.

various free radicals the enthalpies of the reactions between apocynin and hydroxyl, hydroperoxyl, alkoxy and alkoxyperoxyl radicals will be analysed.

EXPERIMENTAL

Apocynin (98% purity) was purchased from Sigma-Aldrich Co and applied without further purification. CD_3OD (99% at. enrichment) was purchased from Merck and used to obtain CD_3ONa by reacting it with Na. Spectral quality CDCl_3 and DMSO-d_6 were purchased from Sigma-Aldrich Co.

The corresponding anion was obtained by adding $0.08 \text{ mol}\cdot\text{l}^{-1}$ DMSO-d_6 solution of the parent compound to excess of dry CD_3ONa . The reaction mixture was filtered to remove the remains of solid CD_3ONa and put immediately into a spectroscopic cell to record the IR spectra. The conversion was

practically complete (no bands of the parent compound were seen in the spectrum after metalation). The IR spectra in DMSO-d_6 solution were recorded on Bruker Tensor 27 FT spectrometer in a 0.129 mm CaF_2 sample cell at a resolution of 2 cm^{-1} and 64 scans.

The quantum chemical calculations were performed using the Gaussian 09 package [10] of programs. Geometry of the species studied was performed by analytical gradient technique without any symmetry constraint. The results were obtained using the density functional theory (DFT), employing the M05-2X [11] in conjunction with 6-311++G(3df,3dp) basis set. To establish the stability order for the neutral, radical and ionic species in solvent we used the Integral Equation Formalism Polarizable Continuum Model (IEF-PCM) [12] on the same level of theory.

The preferred geometry of the molecule of apocynin, its anion, radical and radical cation was found by constructing and optimizing the most probable conformers with planar and nonplanar geometry and different mutual orientations of the carbonyl, methoxyl and hydroxy group at M05-2X/6-311++G(3df,3dp) level of theory. For every structure, the stationary points found on the molecular potential energy hypersurfaces were characterized using standard analytical harmonic vibrational analysis. The absence of imaginary frequencies, as well as of negative eigenvalues of the second-derivative matrix, confirmed that the stationary points correspond to minima on the potential energy hypersurface.

Dissociation enthalpy (BDE), ionization potential (IP), proton dissociation enthalpy (PDE), proton affinity (PA), and electron transfer enthalpy (ETE) of the most stable conformers were calculated according [13].

$$\begin{aligned} BDE &= H(\text{ArO}^\bullet) + H(\text{H}) - H(\text{ArOH}) \\ IP &= H(\text{ArOH}^+) + H(e^-) - H(\text{ArOH}) \\ PDE &= H(\text{ArO}^\bullet) + H(\text{H}^+) - H(\text{ArOH}^+) \\ PA &= H(\text{ArO}^-) + H(\text{H}^+) - H(\text{ArOH}) \\ ETE &= H(\text{ArO}^\bullet) + H(e^-) - H(\text{ArO}^-) \end{aligned}$$

All reaction enthalpies were calculated for 298 K. The enthalpies of hydrogen atom, $H(\text{H})$, proton, $H(\text{H}^+)$, and electron, $H(e^-)$, for each solvent were obtained by the same method and basis set. Solvation enthalpy of electron was determined as:

$$H(e^-)_{\text{solv}} = H(\text{DMSO}^-)_{\text{solv}} - H(\text{DMSO})_{\text{solv}} - H(e^-)_{\text{gas}},$$

where $H(e^-)_{\text{gas}}$ is $3.145 \text{ kJ}\cdot\text{mol}^{-1}$ following the procedure already applied in similar studies [14, 15].

Theoretical IR spectra were calculated for the most stable conformers of the neutral and anion species at B3LYP/6-311++G(2df,p) theory level [16, 17].

RESULTS AND DISCUSSION

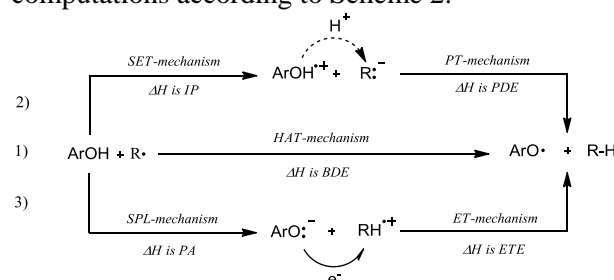
Conformational isomers

Structures of the most probable conformational isomers of apocynin, its anion, radical and radical cation were optimized using density functional theory M05-2X/6-311++G(3df,3dp) in gas phase and different media. Earlier optimization of apocynin in gas phase yielded *s-cis* (with carbonyl group oriented towards the methoxyl group – conformer **1m**) as the most stable form, followed by *s-trans* (with carbonyl group oriented opposite

to the methoxyl group – conformer **2m**) [18]. Our optimization in benzene, water and DMSO provided that the same conformers are the most favourable in these solvents as well. The optimized geometries of the conformers are shown in Scheme 1. The most stable form of the neutral molecule is stabilized by the formation of an intramolecular hydrogen bond with the participation of H-atom from the hydroxyl group and the O-atom from the methoxyl group. The most unfavourable conformations are those with methoxyl groups out of the plane of phenyl ring. All conformations of the radical, radical cation and oxyanion of apocynin show planar structure with *s-cis* form being more favourable for the oxyanion, while *s-trans* form – for the radical and radical cation (Scheme 1).

Radical scavenging properties of apocynin

Three possible mechanisms – hydrogen atom transfer (HAT), single-electron transfer (SET-PT), sequential proton loss electron transfer (SPLET) were studied by M05-2X/6-311++G(3df,3dp) computations according to Scheme 2.



Scheme 2. Possible mechanisms of apocynin reaction with free radicals.

The ability of apocynin to form radical, radical cation and oxyanion as well as the transformation of its radical cation and oxyanion into radical, were estimated in polar and nonpolar medium. The corresponding bond dissociation enthalpies (BDE), ionization potentials (IP), proton dissociation enthalpies (PDE), proton affinities (PA), and electron transfer enthalpies (ETE) of apocynin are collected in Table 1. These enthalpies were analysed in order to estimate whether the apocynin is prone to react via HAT, SET-PT or SPL-ET in polar and nonpolar medium.

In gas phase and benzene, *i.e.* the nonpolar (lipid) phase, the apocynin would preferably inactivate free radicals by directly transferring a hydrogen atom to free radicals and forming an apocynin radical. The energy needed to transfer an electron or a proton to free radicals is much higher and it can be concluded that HAT would be the

Table 1. DFT bond dissociation enthalpy (BDE), ionization potential (IP), proton dissociation enthalpy (PDE), proton affinity (PA), and electron transfer enthalpy (ETE) values of apocynin and vanillin in kJ/mol.

compound	BDE	IP	PDE	PA	ETE	miLogP
<i>Gas Phase</i>						
apocynin	376.9	789.3	901.6	1420.7	270.2	1.18
vanilin	378.9	806.3	886.7	1409.4	283.6	1.07
<i>Benzene (2.28)^a</i>						
apocynin	372.4	673.6	129.2	432.2	360.6	
vanilin	375.1	682.2	123.3	442.2	373.3	
<i>Water (80.10)^a</i>						
apocynin	365.8	508.9	71.7	218.3	362.4	
vanilin	369.0	517.1	66.8	211.3	372.6	

Table 2. DFT reaction enthalpies (in kJ/mol) of apocynin and vanillin with various free radicals according to Scheme 2.

Compound	Radical	ΔH_{BDE}	ΔH_{IP}	ΔH_{PDE}	ΔH_{PA}	ΔH_{ETE}
<i>Gas phase</i>						
apocynin	OH	-116.3	-434.9	308.1	-148.3	107.0
	OCH ₃	-58.2	-255.1	198.8	-183.0	126.6
	OOH	20.9	-240.6	261.5	-158.5	179.4
	OOCH ₃	28.4	-156.0	184.4	-141.1	169.5
	L	36.0	-50.1	86.1	-196.7	232.7
	OL	-60.4	-59.0	-1.4	-141.0	80.6
	OOL	-3.9	-72.4	101.6	-115.3	144.4
vanilin	OH	-114.3	-417.9	293.1	-234.9	120.6
	OCH ₃	-56.4	-238.1	183.8	-194.3	140.0
	OOH	23.0	-223.6	246.6	-169.8	192.8
	OOCH ₃	30.5	-139.0	169.5	-152.4	182.9
	L	38.0	-33.1	71.1	-208.2	246.2
	OL	-58.3	-42.0	-16.3	-152.5	94.2
	OOL	-2.1	-55.5	86.6	-126.8	158.0
<i>Benzene</i>						
apocynin	OH	-123.5	-352.8	229.3	-148.3	24.8
	OCH ₃	-62.1	-202.4	140.3	-135.9	73.8
	OOH	14.7	-177.9	192.6	-99.5	114.2
	OOCH ₃	16.6	-116.0	132.7	-259.3	275.9
	L	31.9	-35.4	67.3	-191.4	223.3
	OL	-64.6	-54.4	-10.2	-120.9	56.2
	OOL	23.6	-67.1	90.7	-93.8	117.4
vanilin	OH	-120.8	-344.2	223.4	-158.3	37.5
	OCH ₃	-59.3	-193.8	134.5	-145.9	86.5
	OOH	17.4	-169.2	186.7	-109.5	126.9
	OOCH ₃	19.4	-107.4	126.8	-269.3	288.7
	L	34.6	-26.8	61.4	-201.4	236.0
	OL	-61.9	-45.8	-16.1	-130.8	68.9
	OOL	26.3	-58.5	84.8	-103.8	130.1
<i>Water</i>						
apocynin	OH	-133.5	-292.8	148.9	-102.0	-33.1
	OCH ₃	-71.3	-165.0	139.9	-103.6	32.3
	OOH	5.8	-134.1	93.7	-61.7	67.5
	OOCH ₃	13.9	-136.2	150.0	-60.6	74.4
	L	24.7	-23.7	46.7	-188.6	211.7
	OL	-72.9	-40.8	-32.0	-98.6	25.7
	OOL	17.3	-64.1	81.4	-68.8	86.1
vanilin	OH	-130.3	-284.7	144.0	-109.0	-22.9
	OCH ₃	-68.1	-156.9	135.0	-110.5	42.5
	OOH	9.0	-126.0	88.8	-68.7	77.7
	OOCH ₃	17.1	-128.0	145.1	-67.6	84.7
	L	27.9	-15.5	41.8	-195.6	222.0
	OL	-69.6	-32.7	-36.9	-105.5	35.9
	OOL	20.6	-56.0	76.5	-75.8	96.3

only mechanism of radical scavenging exerted in lipid phase. Regarding the relative activity for apocynin compared to vanillin, based on the similar BDE values the two compounds are predicted to show similar activity via HAT. The IP calculated in water is higher than the water BDE of apocynin, but significantly lower than the IP calculated in benzene due to the favourable solvation of the charged species involved in the reactions. The ability of apocynin to donate an electron is found to be greater than those of vanillin in agreement with the reported oxidation potentials determined by electrochemical measurements [9].

According to the calculations, in water the proton affinity of apocynin becomes considerably lower than its BDE and IP values which favours the deprotonation and transfer of the proton to free radical (first step of SPLET mechanism). The second step of the SPLET requires subsequent transfer of an electron from apocynin to the cation produced from the free radical. This process is described by ETE and the calculated value shows that this step too can be achieved more easily than HAT. Deprotonation of apocynin is predicted as slightly more difficult in comparison to vanillin.

The oxidation processes in biological systems involve various free radicals. Among the ROS, hydroxyl radicals, $\cdot\text{OH}$, are the most reactive and show little selectivity towards the possible sites of attack [20]. Hydroperoxyl radicals, $\cdot\text{OOH}$, are less reactive, but they can diffuse into remote cellular locations [21] and initiate the lipid peroxidation [22]. The lipid alkoxy radicals, $\cdot\text{OR}$, are formed from the reduction of peroxides and are less reactive than $\cdot\text{OH}$, but significantly more reactive than the lipid peroxy radicals $\cdot\text{OOR}$ [23, 24]. Different reactivity of free radicals is connected with different scavenging capacity of the antioxidants. The reactivity of apocynin against different free radicals was evaluated by including the free radicals in the reactions (Scheme 1) and calculating the respective reaction enthalpies according to the following equations:

$$\Delta BDE = BDE(\text{ArOH}) - BDE(\text{ROH})$$

$$\Delta IP = IP(\text{ArOH}) - IP(\text{ROH})$$

$$\Delta PDE = PDE(\text{ArOH}) - PDE(\text{ROH})$$

$$\Delta PA = PA(\text{ArOH}) - PA(\text{ROH})$$

$$\Delta ETE = ETE(\text{ArOH}) - ETE(\text{ROH})$$

The free radicals ($\text{R}\cdot$) included in the study were as follows: $\cdot\text{OH}$; $\cdot\text{OCH}_3$; $\cdot\text{OOH}$; $\cdot\text{OOCH}_3$; $\cdot\text{R}$; $\cdot\text{OR}$; and $\cdot\text{OOR}$, where $\text{R} = (\text{Z})\text{-hex-2-ene-4-yl}$. The

calculation results (Table 2) show that the enthalpies required for each of these reactions are of a very different magnitude, which enable to judge on ability of apocynin to scavenge particular type of free radicals. In nonpolar phase apocynin and vanillin would react exothermically with $\cdot\text{OH}$ and alkoxy ($\cdot\text{OCH}_3$ and $\cdot\text{OR}$) radicals via HAT mechanism with resulting negative ΔH_{BDE} value, but not peroxy ($\cdot\text{OOH}$, $\cdot\text{OOCH}_3$ and $\cdot\text{OOR}$) and alkyl radicals ($\cdot\text{R}$). Taking into account the negative water ΔH_{PA} and ΔH_{ETE} – negative or positive, but smaller than ΔH_{PA} , it seems that apocynin would readily scavenge $\cdot\text{OH}$ and alkoxy ($\cdot\text{OCH}_3$ and $\cdot\text{OL}$) radicals via SPLET mechanism in water. Scavenging of $\cdot\text{OOH}$ by apocynin would only be possible via SET-PT mechanism in water according to the calculated ΔH_{IP} .

Comparable relative activity for apocynin and vanillin, found by the theoretical estimation of BDE values, is in good accordance with the experimental data from crocin bleaching inhibition [9]. Apocynin and vanillin were tested also in oxygen radical absorbance assay (ORAC) which utilizes AAPH-derived hydroperoxyl radical to mimics the lipid peroxy radicals involved in the lipid peroxidation chain reaction *in vivo* [8]. In this test apocynin and vanillin exhibited comparable activity as well. In a cell-based antioxidant assay - oxidative haemolysis inhibition assay (OxHLIA), where oxidation of erythrocyte membranes is induced by AAPH-derived hydroperoxyl radical, apocynin showed superior activity compared to vanillin [8], but those result was attributed to superior lipophilicity of apocynin and higher resulting access to lipophilic biomembrane of erythrocytes in OxHLIA [8].

Since the SPLET mechanism, preferred in water, involves deprotonation product of apocynin, it was worthwhile to generate the corresponding oxyanion of apocynin and characterize it in more details. Therefore, the apocynin was converted into oxyanion and the spectral, structural, and electronic changes resulting from the conversion were followed by experimental IR methods and DFT computations.

IR spectra of apocynin and its anion

The IR spectra of apocynin in DMSO- d_6 and its oxyanion are shown in Fig. 1. Numerical values of experimental vibrational frequencies and band intensities in region 1800–1100 cm^{-1} are compared with the theoretical ones in Table 3. For a better corresponding between experimental and calculated

Table 3. Theoretical and experimental vibrational frequencies and IR integrated intensities of apocynin and its oxyanion.

No	Theoretical data			Experimental data ^a			
	$\nu_{\text{theor.}}$ ^b	A ^c	Approximate description ^d	DMSO-d ₆		CDCl ₃	
				ν_{exp}	A ^e	ν_{exp}	A ^e
<i>Apocynin molecule</i>							
1.	1638	378.1	$\nu(\text{C}=\text{O})$	1668	s	1674	s
2.	1581	32.6	$\nu_{\text{Ph}}(\text{C}=\text{C})$	1599	sh	1608	m
3.	1570	389.1	$\nu_{\text{Ph}}(\text{C}=\text{C})$	1590	s	1596	m
4.	1489	238.3	$\nu_{\text{Ph}}(\text{C}=\text{C})$	1520	m	1519	m
5.	1449	85.8	$\delta^{\text{as}}(\text{CH}_3)$	1466	w	1465	m
6.	1438	14.0	$\delta^{\text{as}}(\text{CH}_3)$	} 1455	vw	1455	w
7.	1438	7.9	$\delta^{\text{s}}(\text{CH}_3)$				
8.	1422	14.6	$\delta^{\text{as}}(\text{CH}_3)$				
9.	1417	25.1	$\delta^{\text{as}}(\text{CH}_3)$	- ^f	- ^f	- ^f	- ^f
10.	1410	189.2	$\nu_{\text{Ph}}(\text{C}=\text{C})$	1424	m	1429	m
11.	1367	86.1	$\delta(\text{C}-\text{OH})$	1397	w	1389	w
12.	1341	56.3	$\delta^{\text{s}}(\text{CH}_3)$	1360	w	1358	w
13.	1277	2.3	$\delta_{\text{Ph}}(\text{CH})$	1291	sh	- ^f	- ^f
14.	1253	813.9	$\nu(\text{C}-\text{CO}), \nu(\text{C}-\text{OCH}_3)$	1281	vs	1283	vs
15.	1234	48.7	$\nu(\text{C}-\text{OH}), \delta_{\text{Ph}}(\text{CH})$	1263	sh	1261	w
16.	1197	169.5	$\nu(\text{C}-\text{OCH}_3), \delta_{\text{Ph}}(\text{CH})$	1228	m	1218	m
17.	1178	454.7	$\delta_{\text{Ph}}(\text{CH}), \delta(\text{C}-\text{OH})$	1177	w	1172	w
18.	1157	29.2	$\delta_{\text{Ph}}(\text{CH}), \delta(\text{C}-\text{OH})$	1138	w	1138	w
19.	1136	1.2	$\gamma(\text{CH}_3)$	- ^f	- ^f	- ^f	- ^f
20.	1114	78.8	$\delta_{\text{Ph}}(\text{CH})$	1128	w	1119	w
21.	1054	56.0	$\delta_{\text{Ph}}(\text{CH})$	- ^f	- ^f	1071	w
22.	1015	2.6	$\gamma(\text{CH}_3)$	- ^f	- ^f	1032	w
<i>Apocynin oxyanion</i>							
23.	1584	57.3	$\nu(\text{C}=\text{O})$	1628	m		
11.	1537	594.2	$\nu_{\text{Ph}}(\text{C}=\text{C})$	1573	s		
12.	1494	23.5	$\nu_{\text{Ph}}(\text{C}=\text{C})$	1528	sh		
13.	1479	1812.0	$\nu(\text{C}-\text{O})$	1517	s		
14.	1450	100.7	$\delta^{\text{as}}(\text{CH}_3)$	1466	w		
15.	1435	10.5	$\delta^{\text{as}}(\text{CH}_3)$	1455	w		
16.	1433	81.1	$\delta^{\text{s}}(\text{CH}_3)$	1455	w		
17.	1424	12.4	$\delta^{\text{as}}(\text{CH}_3)$	1434	w		
18.	1421	14.2	$\delta^{\text{s}}(\text{CH}_3)$	- ^f	- ^f		
19.	1415	145.5	$\delta^{\text{as}}(\text{CH}_3)$	- ^f	- ^f		
20.	1364	877.0	$\delta_{\text{Ph}}(\text{CH})$	1376	s		
21.	1334	41.1	$\delta^{\text{s}}(\text{CH}_3)$	- ^f	- ^f		
22.	1284	3.2	$\delta_{\text{Ph}}(\text{CH})$	1310	w		
23.	1265	1069.8	$\nu(\text{C}-\text{CO}), \delta_{\text{Ph}}(\text{CH})$	1288	m		
24.	1200	201.9	$\delta_{\text{Ph}}(\text{CH}), \nu(\text{C}-\text{CO})$	1233	m		
25.	1186	430.0	$\nu(\text{C}-\text{OCH}_3), \gamma(\text{CH}_3)$	1213	m		
26.	1152	145.4	$\gamma(\text{CH}_3), \nu(\text{C}-\text{OCH}_3)$	1177	m		
27.	1134	1.6	$\gamma(\text{CH}_3)$	1130	w		
28.	1111	259.0	$\delta_{\text{Ph}}(\text{CH})$	1113	w		
29.	1048	138.2	$\gamma(\text{CH}_3)$	- ^f	- ^f		
30 ^g .	1011		$\nu(\text{O}-\text{CH}_3)$	- ^f	- ^f		

^aMeasured after having decomposed the complex bands into components. ^bScaled infrared frequencies [cm^{-1}]. ^cPredicted intensities [$\text{km}\cdot\text{mol}^{-1}$]. ^dVibrational modes: ν , stretching; δ , in-plane bending; γ , out of plane bending; superscripts: s – symmetrical, as – asymmetrical, Ph - phenyl; ^eRelative intensities: vw, very weak; w, weak; m, moderate; s, strong; vs, very strong; sh, shoulder. ^fThese bands were not detected in the IR spectrum.

value the native theoretical IR frequencies of the neutral molecule and anion were scaled according to the following equation:

$$\nu^{\text{sc}} = 1.0195 \cdot \nu^{\text{native}} - 51.4 \text{ (cm}^{-1}\text{)}$$

obtained from the linear correlation between the experimental and calculated native frequencies of the neutral compound **1**. The correlation coefficient R was 0.9961, standard deviation S. D. = 34.2 cm^{-1} ; number of data points $n = 16$. The mean absolute

deviation $MAD = n^{-1} \sum |(\rho v_i^{theor.(native)} + b) - v_i^{exp.}|$ was used as a measure for the deviation between the theoretical and experimental values. After scaling the native theoretical frequencies according to the above-mentioned equation, MAD of 10.9 cm^{-1} was obtained for neutral apocynin and 10.5 cm^{-1} – for the anion. These values are lower than the MADs reported by Velcheva *et al.* [25]. This better result should be explained with the higher theory levels and with solvation model which were used.

The highest frequency vibration in the spectrum of the molecule is the hydroxyl stretching. In solid state the position of the bands is 3303 cm^{-1} . In CDCl_3 it appears as moderate sharp band at 3553 cm^{-1} . This frequency is shifted down by 40 cm^{-1} , compared with that of 4-hydroxy-acetophenone in the same solution. These data indicated that the OH group is intramolecular hydrogen bonded *i.e.* conf. **1m** and **2m** are predominant in this solution. The IR spectra measured in DMSO and DMSO-d_6 solutions have different appearance. A multiplet broad band is present between 3400 and 2700 cm^{-1} , due to the formation of hydrogen bonds of the apocynin mainly with the solvent.

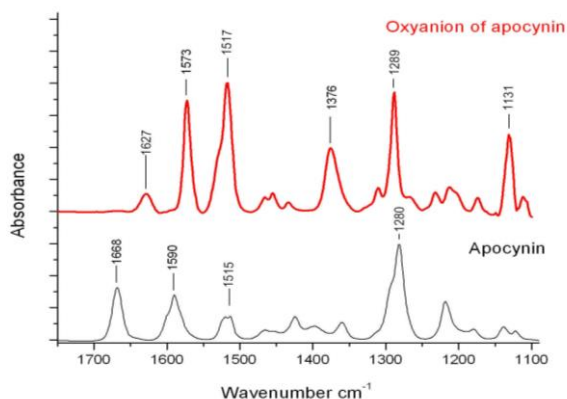


Fig. 1. Infrared spectra of apocynin and of its oxyanion (with counter ion Na^+) in DMSO-d_6 .

The strongest band in the IR spectrum of apocynin in DMSO/DMSO-d_6 at 1281 cm^{-1} corresponds to $\nu(\text{C-CO})$. The band for the carbonyl stretch is found at 1668 cm^{-1} with strong intensity. The C-O vibrations (No 14-18) are greatly mixed with $\delta_{\text{Ph}}(\text{CH})$, including the one associated with the C-OH bond at 1263 cm^{-1} . The bands characterizing the benzene ring appear at their typical positions.

The conversion of apocynin molecule into the oxyanion causes:

- a strong decrease in the $\nu(\text{C=O})$ frequency: predicted 54 cm^{-1} , and observed 40 cm^{-1} (Table 3 and Fig. 1);

- a strong decrease in integral intensity $A_{\text{C=O}}$ of the $\nu(\text{C=O})$ band. This result is not typical, as the intensity of carbonyl band usually increases by the conversion of carbonyl compounds into anions. The result is, however not surprising, as it was previously observed in other acetophenones containing electron-releasing substituents in the phenyl ring [26];
- essential intensities increases of the aromatic skeletal bands $\nu_{\text{Ph}}(\text{C=C})$ similarly to [25, 26];
- a very strong frequency increase of the phenoxyl vibration: predicted 245 cm^{-1} , and observed 256 cm^{-1} .

CONCLUSION

DFT calculations in gas phase, benzene and water were used to study the reactivity of apocynin against different free radicals via hydrogen atom transfer, single-electron transfer, sequential proton loss electron transfer mechanisms. It was found that in nonpolar medium the preferred mechanism of the antioxidant action is direct hydrogen atom transfer, while in polar medium – SPLET related to the formation of an oxyanion. Therefore the oxyanion of apocynin was generated in DMSO-d_6 solution and characterized in more details. The spectral, structural, and electronic changes resulting from the conversion were followed by experimental IR methods and DFT computations.

Acknowledgements: The financial support by the National Science Fund of Bulgaria (Contract RNF01/0110) is gratefully acknowledged.

REFERENCES

1. M. S. Petrônio, M. L. Zeraik, L. M. da Fonseca, V. F. Ximenes, *Molecules*, **18**, 2821 (2013).
2. J. Stefanska, R. Pawliczak, *Mediat. Inflamm.*, **2008**, Article ID 106507 (2008).
3. F. Engels, B. F. Renirie, B. A. Hart, R. P. Labadie, F. P. Nijkamp, *FEBS Lett.*, **305**, 254 (1992).
4. B. Hart, S. Copray, I. Philippens, *Biomed. Res. Intern.*, **2014**, ID 298020 (2014).
5. J. Yu, M. Weiwer, R. J. Linhardt, J. S. Dordick, *Curr. Vasc. Pharmacol.*, **6**, 204 (2008).
6. S. Heumüller, S. Wind, E. Barbosa-Sicard, H. H. Schmidt, R. Busse, K. Schröder, R. P. Brandes, *Hypertension*, **51**, 211 (2008).
7. L. R. G. Castor, K. A. Locatelli, V. F. Ximenes, *Free Radic. Biol. Med.*, **48**, 1636 (2010).
8. A. Tai, T. Sawano, F. Yazama, *Biosci. Biotechnol. Biochem.*, **75**, 2346 (2011).

9. R. Bortolomeazzi, N. Sebastianutto, R. Toniolo, A. Pizzariello, *Food Chem.*, **100**, 1481 (2007).
10. M. Frisch, G. Trucks, H. Schlegel, G. Scuseria, M. Robb, J. Cheeseman, G. Scalmani, V. Barone, B. Mennucci, G. Petersson, H. Nakatsuji, M. Caricato, X. Li, H. Hratchian, A. Izmaylov, J. Bloino, G. Zheng, J. Sonnenberg, M. Hada, M. Ehara, K. Toyota, R. Fukuda, J. Hasegawa, M. Ishida, T. Nakajima, Y. Honda, O. Kitao, H. Nakai, T. Vreven, J. Montgomery, Jr., J. Peralta, F. Ogliaro, M. Bearpark, J. Heyd, E. Brothers, K. Kudin, V. Staroverov, R. Kobayashi, J. Normand, K. Raghavachari, A. Rendell, J. Burant, S. Iyengar, J. Tomasi, M. Cossi, N. Rega, J. Millam, M. Klene, J. Knox, J. Cross, V. Bakken, C. Adamo, J. Jaramillo, R. Gomperts, R. Stratmann, O. Yazyev, A. Austin, R. Cammi, C. Pomelli, J. Ochterski, R. Martin, K. Morokuma, V. Zakrzewski, G. Voth, P. Salvador, J. Dannenberg, S. Dapprich, A. Daniels, O. Farkas, J. Foresman, J. Ortiz, J. Cioslowski, D. Fox, Gaussian 09, Revision A.1, Gaussian Inc., Wallingford CT, 2009.
11. Y. Zhao, D. G. Truhlar, *Theor. Chem. Acc.*, **120**, 241(2008).
12. J. Tomasi, B. Mennucci, E. Cancès, *J. Mol. Struct. (THEOCHEM)*, **464**, 211 (1999).
13. E. Klein, V. Lukes, M. Ilcin, *Chem. Phys.*, **336**, 51 (2007).
14. Z. Markovic, D. Amic, D. Milenkovic, J. M. Dimitric-Markovic, S. Markovic, *Phys. Chem. Chem. Phys.*, **15**, 7370 (2013).
15. E. Klein, V. Lukes, *J. Phys. Chem. A*, **110**, 12312 (2006).
16. A. D. J. Becke, *J. Chem. Phys.*, **98**, 5648 (1993).
17. C. Lee, W. Yang, G. R. Parr, *Phys. Rev.*, **37B**, 785 (1988).
18. J. E. Cocinero, F. J. Basterretxea, P. Ecija, A. Lesarri, J. A. Fernandez, F. Castano, *Phys. Chem. Chem. Phys.*, **13**, 13310 (2011).
19. E. Wilhelm, R. Battino, *Chem. Rev.*, **73**, 1 (1973).
20. A. Samuni, J. Aronovitch, M. Chevion, *Life Chem. Rep.*, **2**, 39 (1983).
21. L. J. Marnett, *Carcinog.*, **8**, 1365 (1987).
22. J. Aikens, T. A. Dix, *J. Biol. Chem.*, **266**, 15091 (1991).
23. J. R. León-Carmona, A. Galano, *J. Phys. Chem. B*, **115**, 4538 (2011).
24. R. E. Huie, P. Neta, in: *Reactive Oxygen Species in Biological Systems: An Interdisciplinary Approach*, D. L. Gilbert, C. A. Colton (eds.), Kluwer Academic Publishers, New York/Boston/Dordrecht/London/Moscow, 2002, p. 33.
25. E. Velcheva, B. Stamboliyska, *Spectrochim. Acta A*, **60**, 2013 (2004).
26. P. J. Vassileva-Boyadjieva, E. A. Velcheva, Y. I. Binev, *Bulg. Chem. Commun.*, **37**, 313 (2005).

ТЕОРЕТИЧНО ИЗСЛЕДВАНЕ НА РАДИКАЛ-УЛАВЯЩАТА СПОСОБНОСТ НА АПОЦИНИН СПРЯМО РАЗЛИЧНИ СВОБОДНИ РАДИКАЛИ

Д. Я. Янчева^{1*}, С. С. Стоянов¹, Е. А. Велчева¹, Б. А. Стамболийска¹, А. Шмелцерович²

¹ *Институт по органична химия с Център по фитохимия, Българска академия на науките, ул. „Акад. Г. Бончев“, бл. 9, 1113 София, България*

² *Катедра по химия, Медицински факултет, Университет в Ниш, бул. „Д-р Зоран Джинджич“ 81, 18000 Ниш, Сърбия*

Постъпила на 07 март 2017 г.; Коригирана на 11 март 2017 г.

(Резюме)

Апоцининът е добре известен инхибитор на ензима никотинамид-аденин-динуклеотид-фосфат оксидаза и се използва като едно от най-обещаващите лекарствени средства в експериментални модели на сърдечно-съдови, възпалителни и невродегенеративни патологични състояния, където регулацията на реактивни кислородни частици играе решаваща роля. Различни вероятни механизми на радикал-улавящото действие на апоцинина като директен пренос на водород (НАТ), пренос на единичен електрон (SET-PT) и пренос на протон последван от електронен пренос (SPLET) бяха изследвани чрез пресмятане на енталпите на съответните реакции с използване на теория на плътностния функционал (DFT) в полярни и неполярни разтворители. Реактивоспособността спрямо различни свободни радикали беше оценена чрез анализ на термодинамичните данни за реакциите на апоцинина с хидроксилни, хидроксипероксидни, алкоксилни и алкоксипероксидни радикали. Въз основа на изчисленията, беше установено, че SPLET механизмът е предпочетен в полярни разтворители, благоприятстващи йонизацията, например вода. В тази връзка оксианионът на апоцинина беше получен в разтвор на диметилсулфоксид и спектралните и структурни промени, породени от превръщането, бяха проследени с ИЧ спектроскопия и DFT пресмятания.

Conformational analysis of oligomers of non-ionic thermoresponsive polymers containing amide groups

P. Ivanov^{1*}, Ch. Tsvetanov²

¹ Institute of Organic Chemistry with Centre of Phytochemistry, Bulgarian Academy of Sciences, Acad. G. Bonchev street, bl. 9, 1113 Sofia, Bulgaria

² Institute of Polymers, Bulgarian Academy of Sciences, Acad. G. Bonchev str., bloc 103, 1113 Sofia, Bulgaria

Received February 27, 2017; Revised March 27, 2017

Dedicated to Acad. Bogdan Kurtev on the occasion of his 100th birth anniversary

The conformations of oligomers of 2-isopropyl-2-oxazoline (**IPOZ**) and N-isopropylacrylamide (**NIPAM**) were studied with molecular mechanics. Preferred geometries and inherent energy balances were determined. The computed data present significant differences in the conformational distributions of oligomers of **IPOZ** and **NIPAM** with the same degree of polymerization (hexamers). Only a few conformations of **IPOZ-6** have most of the computed population, whereas more than hundred conformations of **NIPAM-6** are in equilibrium. Two orders of magnitude larger number of conformations belong to the lowest-energy cluster of **NIPAM-6** compared with **IPOZ-6**. The intramolecular hydrogen bonds in **NIPAM-6** are the decisive factor for its preferred conformations.

Key words: oligomers of thermoresponsive polymers; conformations; molecular mechanics; cluster analysis

INTRODUCTION

The development of synthetic building blocks that can selectively interact in water with a given substrate or self-assemble to yield highly responsive functional materials is a topic of increasing significance. Water-soluble oligomers have acquired importance due to the demand for water-based instead of the traditional solvent-based technological processes [1]. The non-ionic thermoresponsive oligomers are building units of polymeric nanoparticles possessing thermosensitive core and functional outer shell that manifest *smart* behavior – the inner core of the aggregates is sensitive to temperature variations and can solubilize and deliver hydrophobic substances, mostly biologically active compounds (*e.g.* drugs) under external stimuli. Such *stimuli-sensitive* systems (due to changes in temperature, pH, solvent, light, *etc.*) may have macroscopic properties that could be controlled at the macroscopic level by modifying the structure and organization of the polymeric chain. Besides, in particular, some of them could be considered also as candidates for thermo-driven single-molecule motors [2] and many other advanced applications.

Most of the synthetic macromolecules become more soluble when heated. There are, however, water soluble polymers that separate from solution

upon heating (*inverse temperature-dependent solubility*) above the phase transition temperature (*lower critical solution temperature*, LCST). This phenomenon is explained to result from the balance between the enthalpic contribution from the energy stabilization due to hydrogen bonding of the polymer with the water molecules and the entropy gain of the system at higher temperature that outweighs the enthalpic preference at lower temperatures. Hydrogen bonding between the polymer and the water molecules lowers the free energy of dissolution. This effect becomes less important at higher temperature and accordingly, entropy effects become more important [1].

Polymers containing amide groups constitute the largest group among the thermoresponsive polymers. The most examined thermoresponsive polymers are poly (2-isopropyl-2-oxazoline) [**PIPOZ**] and poly(N-isopropylacrylamide) [**PNIPAM**], both isomeric to poly(leucine) (Fig. 1). The two polymers, **PIPOZ** and **PNIPAM**, could be considered as simplified, but appropriate models of a protein. Substantial difference between **PIPOZ** and **PNIPAM** from one side, and poly (leucine) from the other, is that poly(leucine) contains amide groups in the main chain and has nonpolar side-chain substituents; the main chain of **PNIPAM** is nonpolar with amide group in the side fragment, whereas **PIPOZ** is with polar backbone and amide group in the side chain. The amide groups of **PNIPAM** can be proton donors as well as proton

* To whom all correspondence should be sent:
E-mail: ivanov@bas.bg

acceptors, whereas the amide groups of **PIPOZ** can be only proton acceptors.

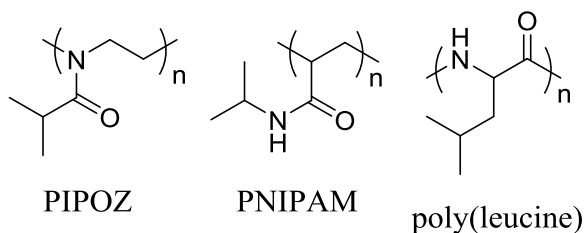


Fig. 1. Schematic structures of **PIPOZ**, **PNIPAM** and poly(leucine).

We report here results from molecular mechanics conformational search studies on the conformations of hexamers of 2-isopropyl-2-oxazoline (**IPOZ-6**) and N-isopropylacrylamide (**NIPAM-6**) with the aim to elucidate at atomistic level differences in the conformational distributions of the oligomers that may have effect on the particle's behavior at the macroscopic level. A dodecamer was studied also for one of the cases (**IPOZ-12**) in order to ascertain the effect of increasing the chain length on the preferred conformations of the oligomer.

Oligomers of different length (up to 50-units) of PNIPAM have been studied by molecular dynamics simulations below and above its LCST [3–7]. The expected behavior has been observed where the backbone folds onto itself above the LCST in order to minimize the amount of hydrophobic surface in contact with water [3, 7]. The decisive interactions in the isolated oligomer constitute an extensive intra-chain hydrogen bonding, responsible for the adoption of more compact structures. Isolated water molecules buried inside the polymer contribute to stabilize the conformation of chain fragments [3]. Computational studies on oligomers of PIPOZ are not known to us.

COMPUTATIONAL DETAILS

Two problems are of particular importance when molecular mechanics is used for modelling conformations of large molecules: (i) the proper choice of a force field for modelling the system under study; (ii) reliable and effective conformational search of low-energy conformations when many degrees of freedom for intramolecular rotations determine the conformational flexibility of the molecule. The force field used in the present study is MMFF94 [8–14], whereas conformational search approach [15, 16], implemented in CONFLEX version 5.0 Rev. A.2 and version 6.89

[17] was applied for searching for low-energy conformations. The CONFLEX algorithm was specifically developed for searching conformations of macro-rings, but it has also an efficient module for stepwise rotations to generate new rotamers during the conformational search. Thirty rotatable bonds were detected for the two hexamers by the 'rotatable bond finder' procedure in CONFLEX, and twice as much for **IPOZ-12**. These were, accordingly, the bonds with rotations about which was searched for low-energy conformations and used also for conformation comparison when eliminating identical conformers. The default values of the options were used when the steric energies and the dihedral angles were compared in the redundancy test. A gradual increase to a search limit of 10.0 kcal mol⁻¹ determined the energy range from which the initial structures for the search were selected [15, 16]. The full-matrix Newton-Raphson minimization procedure was used. Electrostatic interactions were estimated with the value 1.0 of the dielectric parameter as recommended for the MMFF94 force field. The searches ended with 4546, 10280 and 14947 conformations stored with relative energies less than 25.0 kcal mol⁻¹, for **IPOZ-6**, **IPOZ-12** and **NIPAM-6**, respectively.

The complete sets of conformations (4552, 15378, 14947, respectively) were subjected to a cluster analysis [18]. The single linkage clustering method was used with torsional distance as similarity (distance) index, distance threshold 10.0°, and distance definitions (number of torsions for the clustering) 17, 34 and 10 for **IPOZ-6**, **IPOZ-12** and **NIPAM-6**, respectively. The main chain torsional angles were used for the clustering in all cases. Populations of conformations within a cluster and distribution (population) of clusters were estimated at 300 K following Boltzmann distribution. Computed data for some low-energy clusters are presented in Table S1 in Supplementary Data. An identity number has been given to each conformation designating the sequential number of appearance of a new conformation during the conformational search (Fig. S1 and Table S1).

RESULTS AND DISCUSSION

The computed data are indicative for differences in the conformational distributions of the oligomers that originate from the inherent properties of the monomeric building blocks. Only one conformation was found for the monomeric unit of **IPOZ** whereas four conformations of **NIPAM-1** have the

Table 1. Conformational energies (in kcal mol⁻¹) of oligomers of thermo-responsive polymers.

Energy range	Steric energy		Gibb's free energy	
	Number of conformations	Population	Number of conformations	Population
IPOZ-1				
1. 0.0 – 0.5	1	1.00	1	1.00
IPOZ-6				
1. 0.0 – 0.5	1	0.38	2	0.25
2. 0.5 – 1.0	0	-	4	0.17
3. 1.0 – 1.5	3	0.13	6	0.10
4. 1.5 – 2.0	6	0.12	18	0.13
5. 2.0 – 2.5	12	0.10	39	0.11
6. 2.5 – 3.0	25	0.10	67	0.08
7. 3.0 – 3.5	33	0.05	108	0.06
8. 3.5 – 4.0	42	0.03	83	0.04
9. 4.0- 10.0	3584	0.09	3457	0.06
IPOZ-12				
1. 0.0 – 0.5	1	0.72	2	0.51
2. 0.5 – 1.0	0	-	2	0.14
3. 1.0 – 1.5	0	-	3	0.12
4. 1.5 – 2.0	3	0.12	5	0.07
5. 2.0 – 2.5	3	0.06	9	0.06
6. 2.5 – 3.0	6	0.04	16	0.04
7. 3.0 – 3.5	6	0.02	20	0.02
8. 3.5 – 4.0	8	0.01	29	0.01
9. 4.0- 10.0	1451	0.03	1729	0.03
NIPAM-1				
1. 0.0 – 0.5	2	0.77	2	0.84
2. 0.5 – 1.0	2	0.20	1	0.11
3. 1.0 – 1.5	0	-	1	0.05
4. 1.5 – 2.0	1	0.02	0	-
NIPAM-6				
1. 0.0 – 0.5	10	0.14	8	0.07
2. 0.5 – 1.0	30	0.17	51	0.19
3. 1.0 – 1.5	76	0.20	100	0.19
4. 1.5 – 2.0	129	0.15	282	0.22
5. 2.0 – 2.5	236	0.12	433	0.14
6. 2.5 – 3.0	398	0.09	696	0.10
7. 3.0 – 3.5	595	0.06	855	0.05
8. 3.5 – 4.0	875	0.03	875	0.01
9. 4.0- 10.0	7790	0.04	8468	0.03

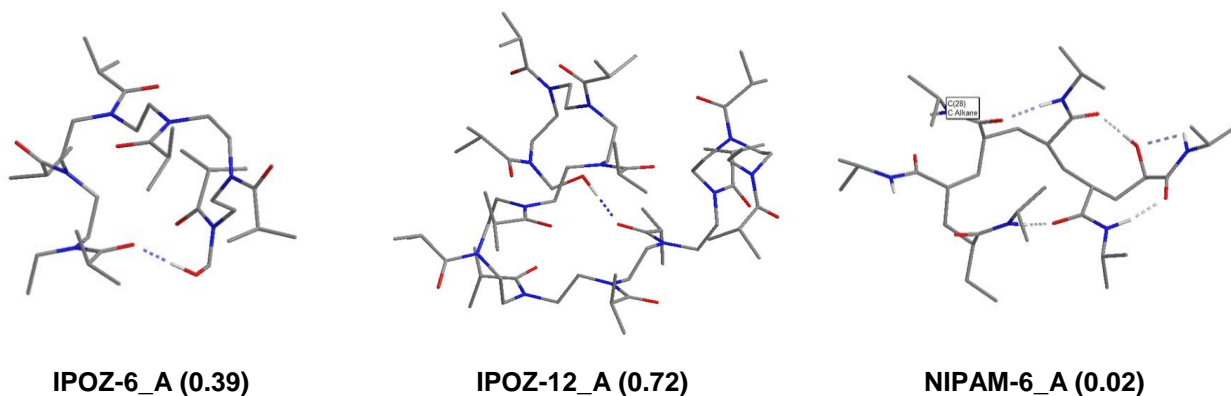


Fig. 2. Optimized geometries of the lowest-energy conformations of the most populated clusters of **IPOZ-6**, **IPOZ-12** and **NIPAM-6** (populations of conformers are given in parenthesis).

Table 2. Different energy contributions to the total steric energy of the lowest energy conformations of oligomers of thermo-responsive polymers (in kcal mol⁻¹).

Energy term	Total steric energy					Steric energy per monomer unit		
	IPOZ-1	IPOZ-6	IPOZ-12	NIPAM-1	NIPAM-6	IPOZ-6	IPOZ-12	NIPAM-6
Stretch	1.3	11.9	24.1	1.0	9.6	2.0	2.0	1.6
Bend	4.4	26.2	53.6	1.3	15.8	4.4	4.5	2.6
Torsion	-3.1	-13.1	-24.6	-4.1	-10.1	-2.2	-2.1	-1.7
van der Waals	13.4	73.9	140.4	9.8	63.1	12.3	11.7	10.5
Electrostatic	-24.1	-149.9	-244.0	-27.6	-189.7	-25.0	-20.3	-31.6
Total steric	-7.7	-48.3	-45.0	-19.6	-110.2	-8.1	-3.7	-18.4

total of 97% population (Table 1). Accordingly, 50% of the steric energy population of **IPOZ-6** is given by four conformations, whereas the same population in **NIPAM-6** is distributed over 116 local minima conformations. The conformational preference in **IPOZ** shifts further to a strongly populated conformation with increasing the chain length. Thus, in comparison with **PIPOZ**, the **PNIPAM** oligomers should have better pronounced conformational changes upon temperature variations. At the same time, the larger number of hydrogen bonds in **NIPAM-6**, in comparison with **IPOZ-6** (Fig. 2), as well as the greater number of conformations representing the lowest-energy cluster **A** of **NIPAM-6** (Table S1 in Supplementary Data; 4764 for **NIPAM-6** vs. 55 for **IPOZ-6**), makes the **PNIPAM** chain less amenable to deformations upon external stimuli. The values for the number of clusters and the maximum size of cluster provide clear indications for the completely different conformational distributions in the two species (Table S1 in Supplementary Data).

The energy contributions per monomer unit, related to the intramolecular coordinates - stretch, bend and torsion, become more disadvantageous with increasing the number of monomer units, whereas the non-bonded terms (van der Waals and electrostatic) have more complex behavior (Table 2; compare data for monomers, **IPOZ-1** and **NIPAM-1**, with averages for monomer units of **IPOZ-6** and **NIPAM-6**, respectively). The van der Waals interactions become more favourable for **IPOZ-6**, and less advantageous in **NIPAM-6** with increasing the chain length and this originates from the differences in the hydrogen bonding patterns in the two systems – the hydrogen bonding is at the expense of worsening the van der Waals interactions (Fig. 2). Hydrogen bonding interactions in the MMFF94 force field are considered as being essentially electrostatic in nature and are modeled by adjusting key van der Waals and electrostatic parameters to better fit scaled intermolecular interaction energies and geometries obtained from HF/6-31G* calculations [9].

The electrostatic energy contributions manifest trend opposite to the van der Waals interactions, in a way as the contributions from the two intramolecular interactions balance each other. Additivity of the contributions from different energy terms is evident from comparing the steric energy components of **IPOZ-6** and **IPOZ-12** (Table 2). The **IPOZ-6** and **NIPAM-6** have substantially different conformational distributions and this may reflect on differences in flexibility in water of the two polymeric chains.

Fig. 2 presents the lowest-energy conformations of the most populated clusters (**A**) of the three oligomers. The lowest-energy local minima of some other less populated clusters are given in Fig. S1 in the Supplementary Data. The end OH group in the most populated conformation of cluster **A** (39%) of **IPOZ-6**, **IPOZ-6_A**, closes 21-membered hydrogen bonded ring with the carbonyl at the other end of the chain. All side fragments point outwards from the macroring thus being exposed for interaction with the solvent molecules. The macroring presents opened cavity. The representative conformations of clusters **B** and **C** closely resemble the one of cluster **A** (21-membered hydrogen bonded rings), the macroring in **B** being more elongated. 18-ring with the carbonyl of the 5th-monomer unit is formed in cluster **D**. Clusters **E**, **G**, **I** and **J** are similar to cluster **A** with regard to the type and size of the 21-membered hydrogen bonded ring. A 15-membered ring is formed with the carbonyl of the 4th monomer unit in cluster **F**, with a side fragment to the macroring composed of two monomer units. The last presented cluster, **IPOZ-6_K** is similar to cluster **D**. There is clearly expressed tendency for forming the largest possible hydrogen bonded macroring – the most favourable appears the largest 21-membered ring, next comes the 18-membered ring, followed by a 15-membered ring, representing hydrogen bonding of the end hydroxyl group with the carbonyls of the 6th, of the 5th and of the 4th monomer units, respectively.

How changes the situation when increasing the chain length with additional six monomer units, **IPOZ-12**? Enhances the population of the preferred cluster **A** - 72% population is computed for the lowest-energy conformation. The backbone acquires helix-like form with a 30-membered hydrogen bonded ring closed by O—H ... O=C hydrogen bond between the end hydroxyl and the carbonyl of the 9th monomer unit. Three monomer units constitute a side fragment to the macroring. The geometries of the conformations of clusters **B** and **C** are also characterized by the presence of 30-membered hydrogen bonded rings. Completely different geometry presents cluster **D**. The O—H ... O=C hydrogen bonding is with participation of the carbonyl of the 7th monomer unit and the side fragment contains five monomer units bent over the macroring. The overall shape of the macroring is boat-like.

Two kinds of hydrogen bonds can be formed in the model structure of the **NIPAM** hexamer - O—H ... O=C and N—H ... O=C. Thus variety of hydrogen bonds could be formed that determine large manifold of different clusters. The highest computer population of a cluster is less than 5%. Five hydrogen bonds characterize cluster **A**. The 1st and the 5th monomer units close 14-membered N—H ... O=C hydrogen bonded ring, which is further stabilized by additional two N—H ... O=C bonds between the 3rd and the 4th, and the 5th and the 6th monomer units, plus two consecutive N—H ... O—H ... O=C bonds with participation of the side chains of the 4th and the 6th monomer units and the end hydroxyl group. As a result, two 8-membered hydrogen bonded rings are formed. 14-membered hydrogen bonded ring is formed also in cluster **B**. Five more hydrogen bonds are present that constitute interrelated system connecting residues 2-3-4-6-5. The 4th and the 6th monomer units here are also connected by N—H ... O—H ... O=C bonds. Thus in addition to the 14-membered ring are formed one 9-membered, three 8-membered and one small 5-membered rings, *i.e.* in comparison with cluster **A**, one 8-membered ring is present in addition. Cluster **C** displays extended backbone stabilized by six N—H ... O=C hydrogen bonds. Three of them are between 1,3-monomer units closing three ten-membered rings. The end OH-group participates in a 9-membered O—H ... O=C ring with the 3rd residue. 8-membered ring (N—H ... O=) is formed between the first and the second monomer units.

CONCLUSION

We examined with the aid of molecular mechanics the conformations of oligomers of 2-isopropyl-2-oxazoline (**IPOZ-6**, **IPOZ-12**) and N-isopropylacrylamide (**NIPAM-6**) with the purpose to gain insight into their preferred geometries and inherent energy balances that may have effect on the particle's behavior at the macroscopic level. The computed data are indicative for significant differences in the conformational distributions of oligomers of **IPOZ** and **NIPAM** with the same degree of polymerization. Only a few conformations of **IPOZ-6** have most of the computed population whereas more than hundred conformations of **NIPAM-6** are in equilibrium. Two orders of magnitude larger number of conformations belongs to the lowest-energy cluster of **NIPAM-6** compared with **IPOZ-6**. The larger number of intramolecular hydrogen bonds in **NIPAM-6** is the decisive factor for its preferred conformations, and determines most probably different responses of the two molecules when merged in water.

The intrachain hydrogen bonds in PNIPAM will greatly influence the mode of solution-dissolution process in PNIPAM aqueous medium below and upon phase transition temperature, which leads to crucial difference with PIPOZ [19].

Acknowledgements: The financial support is from the National Science Fund within the projects TK01/0167 and RNF01/0110.

Electronic Supplementary Data available here.

REFERENCES

1. I. Dimitrov, B. Trzebicka, A. H. E. Müller, A. Dworak, Ch. B. Tsvetanov, *Prog. Polym. Sci.*, **32**, 1275 (2007).
2. X. Ch. Pang, Sh. X. Cui, *Langmuir*, **29**, 12176 (2013).
3. G. Longhi, F. Lebon, S. Abbate, S. L. Fornili, *Chem. Phys. Lett.*, **386**, 123 (2004).
4. J. Walter, V. Ermatchkov, J. Vrabec, H. Hasse, *Fluid Phase Equil.*, **296**, 164 (2010).
5. S. A. Deshmukh, S. K. R. S. Sankaranarayanan, K. Suthar, D. C. Mancini, *J. Phys. Chem. B*, **116**, 2651 (2012).
6. A. K. Tucker, M. J. Stevens, *Macromolecules*, **45**, 6697 (2012).
7. L. J. Abbot, A. K. Tucker, M. J. Stevens, *J. Phys. Chem. B*, **119**, 3837 (2015).
8. T. A. Halgren, *J. Comput. Chem.*, **17**, 490 (1996).

9. T. A. Halgren, *J. Comput. Chem.*, **17**, 520 (1996).
10. T. A. Halgren, *J. Comput. Chem.*, **17**, 553 (1996).
11. T. A. Halgren, R. B. Nachbar, *J. Comput. Chem.*, **17**, 587 (1996).
12. T. A. Halgren, *J. Comput. Chem.*, **17**, 616 (1996).
13. T. A. Halgren, *J. Comput. Chem.*, **17**, 720 (1996).
14. T. A. Halgren, *J. Comput. Chem.*, **17**, 730 (1996).
15. H. Goto, E. Osawa, *J. Am. Chem. Soc.*, **111**, 8950 (1989).
16. H. Goto, E. Osawa, *J. Chem. Soc. Perkin Trans. 2*, 187 (1993).
17. H. Goto, K. Ohta, T. Kamakura, S. Obada, N. Nakayama, T. Matsumoto, E. Osawa, Conflex corp., Tokyo-Yokohama, Japan, CONFLEX Version 5.0, Rev. A.2 (2004) and Version 6.89 (2011).
18. E. Osawa, H. Goto, T. Hata, E. Deretey, *J. Mol. Struct. (Theochem)*, **398-399**, 239 (1997).
19. E. Haladjova, N. Toncheva-Moncheva, M. D. Apostolova, B. Trzebicka, A. Dworak, P. Petrov, I. Dimitrov, S. Rangelov, Ch. B. Tsvetanov, *Biomacromolecules*, **15**, 4377 (2014).

КОНФОРМАЦИОНЕН АНАЛИЗ НА ОЛИГОМЕРИ НА НЕЙОНОГЕННИ ТЕРМОЧУВСТВИТЕЛНИ ПОЛИМЕРИ СЪДЪРЖАЩИ АМИДНИ ГРУПИ

П. Иванов^{1*}, Хр. Цветанов²

¹ *Институт по Органична Химия с Център по Фитохимия, Българска Академия на Науките, ул. Акад. Г. Бончев, бл. 9, 1113 София, България*

² *Институт по полимери, Българска Академия на Науките, ул. Акад. Г. Бончев, блок 103, 1113 София, България*

Постъпила на 27 февруари 2017 г.; Коригирана на 27 март 2017 г.

(Резюме)

С молекулна механика са изследвани конформациите на олигомери на 2-изопропил-2-оксазолин (**ИРОЗ**) и N-изопропил акриламид (**НИРАМ**). Определени са предпочетени геометрии на конформери и енергетични баланси на вътрешномолекулни взаимодействия. Изчислените данни представят значителни разлики в конформационните разпределения на олигомери на **ИРОЗ** и **НИРАМ** с една и съща степен на полимеризация (хексамери). Изчислената конформационна населеност при **ИРОЗ-6** е свързана с малък брой структури, докато над сто конформации са в равновесие при **НИРАМ-6**. В сравнение с **ИРОЗ-6**, на два порядъка по-голям брой конформации определят клъстера с най-ниска енергия на **НИРАМ-6**. Вътрешномолекулните водородни връзки са определящ фактор за предпочетеността на конформациите на **НИРАМ-6**.

Geochemical appraisal of hydrocarbon generative potential of Bulgarian part from the Thrace Basin: I. Linear biomarkers

G. Meracheva¹, M. Stefanova^{2*}, S. P. Marinov², E. Zaneva-Dobranova¹

¹ Faculty of Geology and Exploration, University of Mining and Geology “St. Ivan Rilski”, Sofia 1700, Bulgaria

² Institute of Organic Chemistry with Centre of Phytochemistry, Bulgarian Academy of Sciences, Sofia 1113, Bulgaria

Received January 25, 2017; Revised March 06, 2017

Dedicated to Acad. Bogdan Kurtev on the occasion of his 100th birth anniversary

Bulgarian part from the Thrace Basin is recognized as its NW flank. Hydrocarbon generation for some formations in the Bulgarian part, analogue to Turkish ones with already proven generative abilities, is expected. In order to assess source rocks and to foresee exploration activities in the region, eleven samples from the prospective formations, *i.e.* seven well samples and four outcrops samples, are evaluated by geochemical proxies. Extractable organic matter (OM), the so-called “free” bitumens, and extracted after demineralization (“bound” bitumens), are characterized. A broad range of biomarkers is considered. In this study linear structures, *i.e.* *n*-alkanes, regular isoprenoids, *n*-alkan-2-ones, *n*-alcohols, fatty acids, etc. will be considered. Rock Eval data and component analysis determine immature Type III and mixed Type II/III kerogen. *n*-Alkanes are dominant in all bitumen extracts. Their distributions are complex, depth dependent and give a hint for more mature OM redeposition. The cross-plots of regular isoprenoids in Pr/*n*C₁₇ vs. Ph/*n*C₁₈ diagram implies immature mixed Type II/III kerogen. Pr/Ph ratios, argue for immature OM deposited in anoxic/sub-oxic environment. The cross-plots of TOC vs. P_{aq} argue for at least two pools of *n*-alkanes: (i) short chain homologous from algal/bacterial contribution; (ii) and, mid-chain, from submerged/floating macrophytes wax. Fatty acids, *n*C₁₂-*n*C₃₄ with “even” numbered dominance and changes with depth, are identified only in the “bound” bitumens. A similarity in possible origin with *n*-alkanes is assumed. Dicarboxylic fatty acids, *n*C₁₈-*n*C₃₀, maximizing at *n*C₂₆, *n*C₂₈, *n*C₃₀ are recognizable as well.

Key words: Thrace Basin; oil/gas generative potential; geochemical proxies

INTRODUCTION

Thrace Basin spreads through the European part of Turkey, the most NE part of Greece and SE part of Bulgaria. It is one of the largest natural gas and oil producing basins in Turkey [1]. Generative potential of source rocks from the Turkish part of the Thrace Basin with proven potential for oil/gas generation is described [1–3].

The studied area is situated within the Early-Palaeogene Madjarovo foreland depression, which formed along the intensively faulted eastern part of the Rhodope massif [4]. Rocks of different age and compositions were outcropped on the surface of the studied area and question of interest for oil/gas exploration was the clastic rocks of the sediment sequence with Tertiary (Eocene and Oligocene) age. Information from well investigations is limited as the deepest one reaches 1754 m. In the Turkish part of the Basin these intervals with Eocene and Oligocene age are the major reservoirs for the hydrocarbon accumulations [1].

Shally intervals of the terrigenous-limestone-

shale fm., and shales and mudstones of shale-marl fm. are considered the most promising seals in the reservoir systems in the Bulgarian part of the basin [5]. These intervals are further characterized by a good generative potential for hydrocarbons as well.

Current study is inspired by the renewed interest to Mezardere Fm. as a potential oil resource for hydrocarbons supply in Turkey [3]. The aim of the present investigation is to assess by geochemical proxies the hydrocarbon generative potential of samples from the perspective Fms. in the Bulgarian part of the Thrace Basin. Search for a similarity with Fms. in the Turkish part of the Basin is under special concern.

EXPERIMENTAL

Tectonic scheme of the Bulgarian part of the Thrace Basin in comparison with Turkish part and lithostratigraphy of the area under study are shown in Supplementary Material (Fig. S1).

The following set of samples was studied (Table 1): (i) core samples G1-G5 were from the shally intervals of shale-marl Fm., analogue to Yenimuhacir group in Turkey; (ii) core and outcrop

* To whom all correspondence should be sent:
E-mail: maia@orgchm.bas.bg

samples G6-G10 were from the rocks analogue of Ceylan Fm. (Turkey). Outcrops are commonly weathered, resulting in altered OM. Therefore, special attention was paid to collect them from fresh cuts at positions with low dips; (iii) and, sample G11, G12 with Neogene age from shale rock outcrops. All samples were crushed, grounded, sieved to $< 0.25\text{mm}$. Firstly, they were characterized by Rock Eval pyrolytic technique [5]. Preliminary data and parameters definition could be found in [6].

For lipids isolation about 40g of each sample were subjected to exhaustive Soxhlet extraction with chloroform. By this protocol "free" bitumens were prepared. The residue in the thimble after extraction was treated by 10% HCl for demineralization. Cl⁻ ions in the filter cakes were removed by copious washing. Later on they were dried at ambient temperature, grounded and transferred into thimbles for subsequent extraction with chloroform for "bound" bitumen isolation. Solvents of the highest purity were used. Extracts were concentrated at reduced pressure. The yields of bitumens, *i.e.* "free" and "bound", were calculated in wt. %. Asphaltenes in bitumens were precipitated by pouring samples solutions in a high excess of chilly *n*-hexane (1:50, v/v). Asphaltenes were filtered and dried to constant weights.

Bitumen fractional compositions were determined by column adsorption chromatography on mini-columns (10×100mm) filled with Kieselgel 60, 0.2-0.5 mm (Merck). The following eluents were used: hexane - for elution of neutrals; dichloromethane (DCM) - for aromatics and slightly polars; and acetone - for nitrogen, oxygen and sulfur containing (NOS) components. The neutrals were treated by Cu turnings for removal of elemental sulfur.

GC-MS study was carried out on a Hewlett-Packard 6890 GC system plus HP 5973 MSD equipped with a HP-5 MS column (0.25mm×30m×0.25 μ film thickness) with flame ionization detector (300°C). A split/splitless capillary injector (300°C) is used in the splitless mode (valve reopened 1 min after injection). After 0.5 min isothermal period at 85°C the oven temperature was increased to 200°C at 20°/min and then to 320°C at 5°/min. The MSD was operated in the electron impact (EI) mode with energy of 70 eV and scan range from 50 to 650 Daltons. The data were acquired and processed with the HP software. Individual compounds were determined by comparison of mass spectra (MS) with literature and library data, comparison of MS and GC

retention times with those of authentic standards or interpretation of mass spectra [7, 8]. For MS spectra tracking Xcalibur software was used. MS were quantitatively interpreted by inner standards application, *i.e.* deuterated $n\text{C}_{24}$ for the neutral fraction, and triethylbenzene for the aromatic slightly polar fraction. Amounts were normalized in $\mu\text{g/gC}_{\text{org}}$.

The distribution patterns and relative amounts of *n*-alkanes were tracked by single ion monitoring (SIM) of m/z 85. Based on *n*-alkanes separations carbon preference index (CPI) value was calculated [7, 9]. Some specific fragments were used for SIM tracking: m/z 183 for regular isoprenoids, *i.e.* pristane (Pr) and phytane (Ph); m/z 58 for linear alkan-2-ones; m/z 111 for linear alcohols; m/z 74 and 88 for esters of linear fatty acids (FAs).

RESULTS AND DISCUSSION

For some samples Rock Eval data in Table 1 indicate total organic carbon (TOC) above 0.5% (G1-G5, G12). For samples with TOC $< 0.5\%$ (G7, G9-G10) data for T_{max} are doubtful and are omitted. The relationship TOC vs. HI demonstrates linear correlation with $R^2=0.755$, giving us a confidence to keep TOC data for G2 and G6 in Table 1.

A tendency for decrease in T_{max} (from 437.5°C to 428.5°C) for the shallowest samples is recognizable. These data evoke more mature OM for the shallowest interval. Registered decrease in T_{max} is rather narrow. However it is indicative for redeposition of more mature OM and this possibility should be consider in the further appraisal by geochemical proxies.

Based on the TOC values, the samples range from "poor" to "fair" generative potential (Fig. 1A), a view supported by the Rock Eval data (Table 1). The highest TOC (2.31%) was determined for sample G5. Such magnitude is characteristic for source rocks with "good to very good" hydrocarbon generative potential as is visible in Fig. 1A, where S_1+S_2 were correlated with TOCs [10]. According to this diagram TOCs values were high for samples from the Shale-marl formation corresponding to Mezardere Fm. in the Turkish part of the Basin. On this base they were depicted as perspective and received special attention in further study.

Yields of bitumens and their fractional compositions, *i.e.* neutrals, aromatics/slightly polars, NOS and asphaltenes, are shown in Table 2. Oily fractions, first and second ones, are studied by GC/MS. Table 3 summarizes the total amounts of *n*-alkanes, normalized to TOC ($\mu\text{g/gC}_{\text{org}}$).

Table 1. Rock Eval data of samples.

Sample	Depth (m)	Rock Eval data							
		S ₁	S ₂	S ₃	T _{max}	TOC (%)	MINC(%)	HI	
Well	G1	266.5	0.010	2.455	0.790	437.0	1.295	1.975	189.5
	G2	363.7	0.000	0.135	0.990	437.5	0.475	2.635	28.5
	G3	443.3	0.025	3.345	1.025	430.5	1.825	2.050	183.5
	G4	495.6	0.005	1.290	0.745	431.5	1.275	1.385	101.0
	G5	553.0	0.015	3.390	1.035	428.5	2.310	0.650	147.0
	G6	816.8	0.000	0.010	0.230	428.5	0.235	5.525	4.0
	G7	1685.3	0.005	0	0.115	n.d.	0.100	2.780	0
Outcrop	G9	-	0.010	0	0.330	n.d.	0.065	3.565	0
	G10	-	0.010	0	0.165	n.d.	0.035	3.185	0
	G11	-	0.000	0	0.575	n.d.	0.070	1.860	0
	G12	-	0.040	0.065	0.590	418.0	1.035	1.080	103.0

n.d. – not determined.

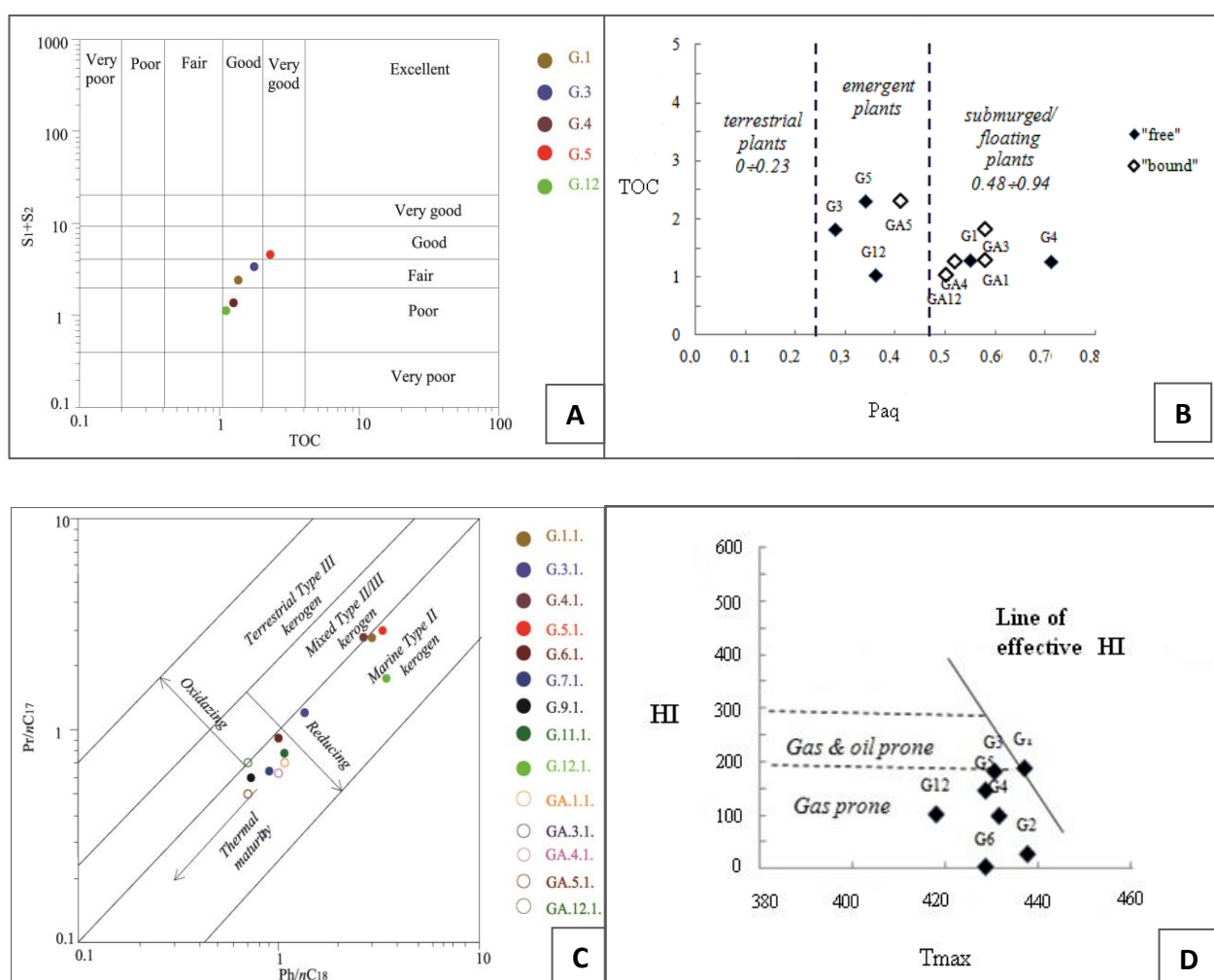


Fig. 1. Correlations of Rock Eval data and biomarker parameters. A) Plots S_1+S_2 vs. TOC for appraisal of generative potential; B) Relationship P_{aq} vs. TOC distinguishing different pools of *n*-alkanes contributions after Ficken *et al.* [11]; C) Cross-plots of Pr/nC_{17} vs. Ph/nC_{18} for kerogen type assignment after Hunt [15] (● – “free” bitumen; ○ – “bound” bitumen); D) Plots of HI vs. T_{max} highlighting the increase in HI prior to the onset of oil expulsion after Sykes and Snowdon [19].

Lipid distributions are visualised as histograms in Fig. 2. Relative amounts of short-, mid- and long- chain *n*-alkanes are presented in Table 4.

Portions of long chain homologous in “free” bitumens constitute >60% of the *n*-alkanes, except for sample G4, which is extremely enriched in short

chain members. For TOC rich samples, *i.e.* G3, G5, G12, a tentative shift of *n*-alkanes signature to mid-chain members is recognizable (Fig. 2). The trend is accompanied by a decrease in CPI values (Table 3). Lower CPI ratios might be indicative for the

subordinated incorporation of plant-wax *n*-alkanes into the “bound” bitumens.

At a certain extent *n*-alkanes distributions could assign a mixture of immature and mature OM. In fact, the *n*-alkane distributions for some samples

Table 2. Yields of bitumens and their fractional compositions, in %.

Sample	Yields (%)		Fractional composition, %										
	"Free"	"Bound"	"Free" bitumen					"Bound" bitumen					
			Neutrals	Aromatics/ slightly polars	NSO	Asphaltenes	Losses	Neutrals	Aromatics/ slightly polars	NSO	Asphaltenes	Losses	
Well	G1	0.17	0.13	5.6	16.8	26.1	47.3	4.2	3.7	5.1	19.5	58.6	13.1
	G2	0.12	0.06	1.2	3.0	14.5	72.8	8.5	6.5	6.5	20.4	58.7	7.9
	G3	0.17	0.09	2.5	18.1	21.1	50.3	8.0	7.8	6.1	37.7	38.1	10.3
	G4	0.15	0.07	3.9	7.7	33.7	51.2	3.5	12.2	10.5	42.9	32.4	2.0
	G5	0.14	0.08	13.0	15.2	24.1	43.2	4.5	15.4	11.5	36.5	32.3	4.3
	G6	0.05	0.03	7.2	11.2	16.4	57.9	7.3	11.5	11.5	26.5	39.8	10.7
	G7	0.05	0.03	4.0	4.5	13.1	75.0	3.4	tr.	9.3	30.5	49.2	11.0
Outcrop	G9	0.03	0.04	4.8	10.6	25.2	50.0	9.4	10.1	8.0	25.4	55.8	0.7
	G10	0.08	0.03	0.3	6.4	7.8	84.3	1.2	10.6	12.6	31.7	44.2	0.9
	G11	0.06	0.05	5.6	9.7	20.9	58.8	5.0	7.1	7.1	28.4	50.6	6.8
	G12	0.11	0.06	12.9	14.4	37.1	34.7	0.9	18.8	11.9	27.3	41.5	0.5

Table 3. Amounts of *n*-alkanes in mg/g sample, regular isoprenoids in $\mu\text{g/gC}_{\text{org}}$ and CPI values.

Sample	Σ <i>n</i> -alkanes, (mg/g)	Pr ($\mu\text{g/gC}_{\text{org}}$)	Pr/ <i>n</i> C ₁₇	Ph ($\mu\text{g/gC}_{\text{org}}$)	Ph/ <i>n</i> C ₁₈	Pr/Ph	CPI*	
"Free" bitumen	G1	7.50	11.55	2.83	12.47	3.01	0.93	4.59
	G3	3.98	3.91	1.26	3.25	1.44	1.20	2.31
	G4	4.02	31.00	2.81	37.80	2.72	0.82	2.28
	G5	22.48	80.18	3.02	81.25	3.42	0.99	1.57
	G6	2.06	17.26	0.92	12.25	1.00	1.41	1.16
	G7	2.17	1.04	0.64	0.60	0.91	1.73	1.11
	G9	1.96	0.97	0.60	0.70	0.72	1.39	1.13
	G11	2.35	0.74	0.78	0.40	1.10	1.85	1.43
	G12	3.53	2.79	1.80	7.11	3.60	0.39	1.43
"Bound" bitumen	G1	2.36	0.85	0.72	0.40	1.16	2.13	1.26
	G3	4.54	1.14	0.33	0.27	0.83	4.22	0.98
	G4	2.79	3.70	0.63	1.66	1.00	2.23	1.19
	G5	5.87	5.02	0.50	2.46	0.71	2.04	0.95
	G12	5.63	1.05	0.69	1.96	0.69	0.54	0.90

$$*CPI = \frac{\Sigma[(nC_{23} \div nC_{31})_{\text{odd}} + \Sigma(nC_{25} \div nC_{33})_{\text{odd}}]}{2 \Sigma(nC_{24} \div nC_{32})_{\text{even}}}$$

Table 4. *n*-Alkanes distributions in TOC rich samples, in rel.% and calculated P_{aq} values.

Sample	<i>n</i> -Alkanes, in rel. %*						P_{aq} value**	
	"Free" bitumens			"Bound" bitumens			"Free"	"Bound"
	Short-	Mid-	Long-	Short-	Mid-	Long-		
G1	9.7	28.5	61.7	12.6	41.2	46.2	0.55	0.58
G3	15.3	23.7	61.0	18.7	52.0	29.3	0.28	0.58
G4	53.5	32.0	14.5	15.7	41.0	43.3	0.71	0.52
G5	16.7	22.3	61.0	5.0	28.4	66.6	0.34	0.41
Outcrop G12	9.5	26.9	63.6	9.8	39.1	51.1	0.36	0.50

*Short chain *n*-alkanes $\Sigma (nC_{16} - nC_{20})$, Mid-chain *n*-alkanes $\Sigma (nC_{21} - nC_{25})$, Long chain *n*-alkanes $\Sigma (nC_{26} - nC_{34})$,

** $P_{aq} = (nC_{23} + nC_{25}) / (nC_{23} + nC_{25} + nC_{29} + nC_{31})$ after Ficken *et al.* [12].

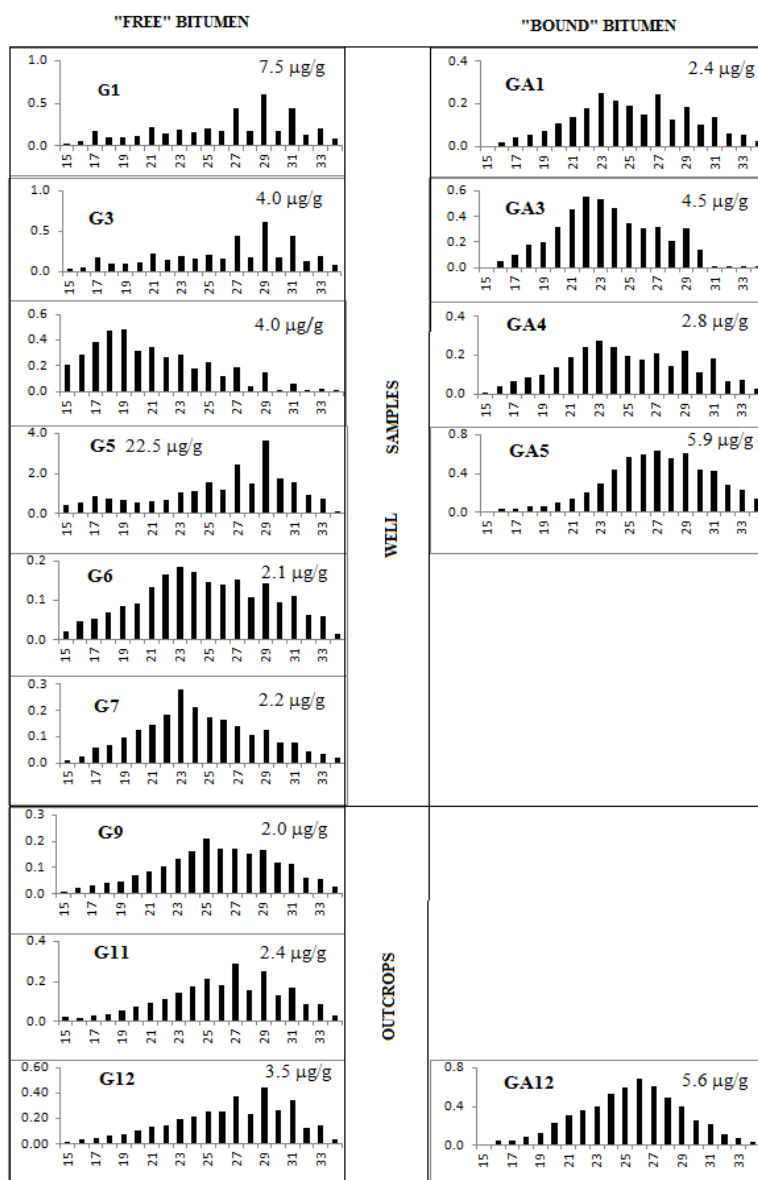


Fig. 2. Histograms of *n*-alkanes distributions (numbers correspond to carbon atoms).

strongly resemble that in oils (G4), suggesting contribution from redeposited mature OM. *n*-Alkanes distribution for sample G4 is typical for Type I kerogen. At low maturity levels even the mid-chain *n*-alkanes are characterized by odd-over-even predominance, *i.e.* high CPI. A possibility for mature OM deposition is discussed in the second part of the study devoted to the cyclic biomarkers.

Ficken *et al.* [11] have proposed P_{aq} ratio with the aim to discriminate macrophytes and emergent terrestrial plant. The proxy takes into account the fact that submerged/floating species are rich in mid-chain *n*-alkanes while higher plants are enriched in longer homologous. Respectively, the P_{aq} ratio distinguishes macrophytes of terrestrial plants from the other supply. This proxy is often used to assess the impact of hydrological changes in peat transitions from wet fen to dry periods [12]. The cross-plots of TOC *vs.* P_{aq} in Fig. 1B argue for at least two pools of *n*-alkanes [13]: (i) short chain homologous from algal/bacterial contribution; (ii) and, mid-chain, from submerged/floating macrophytes wax. According to Ficken *et al.* [11] P_{aq} values in the range of 0.01-0.23 are linked to terrestrial plant wax, whereas values in the range 0.48-0.94 are associated with submerged/floating species of macrophytes. P_{aq} values in Table 4 point to a mixed *n*-alkanes origin, namely, from higher plant/macrophyte wax and algal or bacterial contributions. Interestingly, P_{aq} values for the “free” bitumens are lower as compared to the magnitudes calculated for the “bound” bitumens. On the other hand, the lowest values are calculated for samples with the highest TOC contents. This is a hint that the increase in TOCs can be attributed to a substantial input of emergent plants to the palaeoenvironment (Fig. 2B). Relatively close values of ~ 0.50 are calculated for the “bound” bitumens. This evokes submerged/floating macrophytes OM input. The tendency is additionally confirmed by the data for CPI in Table 3 where systematically higher values for the “free” bitumens ratios comparing to the “bound” ones are calculated.

The acyclic regular isoprenoids, *i.e.* Pr and Ph, are registered in all studied samples. Their amounts, together with Pr/Ph, Pr/*n*C₁₇ and Ph/*n*C₁₈ ratios are shown in Table 3. Ph concentrations are higher than *n*C₁₈, thus giving distinctively high Ph/*n*C₁₈ ratios, especially for TOC rich samples. Ratios Ph/*n*C₁₈ are in the range of 3.0-3.6 for the “free” bitumens, while for the “bound” bitumens total amounts of isoprenoids and calculated ratios are lower.

The Pr/Ph ratio is frequently used to assess depositional environment. However it is well known that isoprenoids/*n*-alkanes ratios generally suffer from two main problems: (i) Pr and Ph may originate not only from the phytyl side chain of chlorophyll- α , but also from tocopherols and bacterial lipids. (ii) Isoprenoids and *n*-alkanes are strongly influenced by the maturity and Pr is preferentially formed during maturation. In the meantime, *n*-alkanes experience thermal degradation and cracking, which introduces great uncertainties in calculating the ratios. Nevertheless the ratios are still often used with the proviso that the data should be considered as biased.

Pr/Ph values > 3 are attributed to OM from land plants (oxidising conditions of deposition), while values < 1.0 indicate anoxic conditions. Magnitudes in the interval 1.0-3.0 suggest intermediate conditions of deposition (sub-oxic condition) [14]. Pr/Ph ratios in Table 3 were moderate and have denoted that source rocks were deposited in sub-oxic conditions. Hunt [15] proposed to plot the ratios in the Pr/*n*C₁₇ *vs.* Ph/*n*C₁₈ diagram (Fig. 1C). Therein samples with high TOCs are located at the zone of immature kerogen almost on the demarking line for Type II and Type II/III kerogen. Actually such plots tolerate deposition in sub-oxic conditions and have sustained assumption based on Pr/Ph ratios. Cross-plots for “bound” bitumens in Fig. 1C were somehow dispersed, and typical for more mature Type II kerogen. These results were in agreement with the patterns of *n*-alkane distributions illustrated in Figure 2, where macrophyte contribution from submerging/floating vegetation to “bound” bitumens formation has been depicted.

According to Pr/*n*C₁₇ *vs.* Ph/*n*C₁₈ diagram mixed Type II/III kerogen is characteristic for high TOCs samples with “good” hydrocarbon generative potential (Fig. 1C). It comprises “gas-prone” source rocks as has been already assumed based on Rock Eval data [5]. This view is additionally strengthened by HI *vs.* T_{max} correlation, assigning “gas prone” source rocks for TOC rich samples (Fig. 1D). As far as similarity with Mezardere Fm. in the Turkish part was already assumed (Fig. S2), it was supposed that the source rocks under study will be capable to generate biogenic gas at appropriate burial and thermal palaeoenvironmental conditions of deposition.

Long-chain acyclic *n*-alkan-2-ones *n*C₁₃-*n*C₃₃, maximizing at *n*C₂₉, 2-nonacosanone, M⁺422, were present in aromatic/slightly polars. Highly abundant

was C₁₈ isoprenoid ketone, a clue for a microbial activity, as it has been supposed to be derived from the microbial degradation of phytol [16]. In all separations “odd” numbered *n*-alkan-2-ones have prevailed over the “even” numbered homologues. Distribution signatures for long-chain *n*-alkanes and *n*-alkan-2-ones were similar as both series have maximized at the long chain “odd” members. This resemblance has admitted a product-precursor relationship [14].

Thereinafter “even” carbon numbered *n*-alkanols, *n*C₂₂-*n*C₂₈ (C_{max} *n*C₂₆) were identified, accompanied by two esters of 9-hexadecenoic acid, *i.e.* C₃₄ and C₃₆ (C_{16:1}-C₁₈ and C_{16:1}-C₂₀). Alkyl esters were often major constituents of the natural waxes of microorganism, plants and animals [17]. Alkan-2-ones, *n*-alkanols and alkyl esters are common in the plant kingdom and attest land plants in the studied area [14, 18].

Fatty acids (FAs) were registered only in the “bound” bitumens, where they have represented significant portions of the fractions (Table 2). Their distribution covered a broad span of homologous, *n*C₁₂-*n*C₃₄, with “even” numbered dominance. FAs signatures were characterized by two maxima, at the ubiquitous *n*C₁₆ and at long chain member, *n*C₂₈. Proportions of the two groups of FAs have varied. With depth the relative amount of the short chain FAs has increased and *i*-, *ai*-FAs have appeared. A similarity in possible origins with *n*-alkanes was admitted. In “bound” bitumens dicarboxylic fatty acids (di-FAs), *n*C₁₈-*n*C₃₀ were identified as well. FAs distribution pattern has denoted at least two possible sources – from ester hydrolysis of diagenetically reduced cutins, suberins or of glycerides from cell membranes for the shorter members and from the hydrolysis of epicuticular waxes. FAs distribution, like in the case of *n*-alkanes, has admitted mixed kerogen origin, from higher plant/macrophyte wax and from algal or bacterial contributions.

CONCLUSION

The study of linear biomarkers in samples from the Bulgarian part of the Thrace Basin reveals the advantage of combining bulk and organic geochemical proxies for source rocks evaluation. The following observations are of special importance:

(i) *n*-Alkanes distributions are complex and give molecular evidences for variation in palaeovegetation and palaeohydrological conditions of deposition. Signatures for the “free” bitumens

are characterized by long homologous dominance and high CPI values. “Bound” bitumens are enriched in mid-chain members. The cross-plots of TOC rich samples in Pr/*n*C₁₇ vs. Ph/*n*C₁₈ diagram imply immature to slightly mature Type II/III kerogen. Pr/Ph ratios argue for immature OM deposition in anoxic/sub-oxic environment. However this point should be considered rather biased inasmuch as it is possible that some regular isoprenoids are still in “bound” state. *n*-Alkanes distributions admit mixed origin, namely, from higher plant/macrophyte wax and algal or bacterial contributions. Lower P_{aq} values are denoted for the “free” bitumens comparing to the “bound” ones. This is a hint that an increase in TOCs for “free” bitumens can be attributed to emergent/terrigenous supply. Comparable P_{aq} values of 0.50 calculated for “bound” bitumens argue for submerged/floating macrophytes OM input;

(ii) Patterns of distributions for long-chain *n*-alkanes and *n*-alkan-2-ones are similar as both series maximize at the long chain “odd” member homologues. The similarity admits a product-precursor relationship. Fatty acids (FAs) with a broad span of homologous, *n*C₁₂-*n*C₃₄, and “even” numbered dominance are registered only in the “bound” bitumens. A similarity in possible origins with *n*-alkanes is evident.

The decrease in T_{max} and *n*-alkane distributions for the shallowest samples evokes more mature OM redeposition. However, the assumption needs verification by additional data and will be considered in the study of cyclic structures.

Acknowledgements: The authors would like to express their gratitude to the reviewer for his contribution to improve the manuscript.

Electronic Supplementary Data available here.

REFERENCES

1. O. Huvaz, N. Karahanoglu, V. Ediger, *J. Petr. Geol.*, **30**, 3 (2007).
2. H. M. Hoşgörmez, N. Yalcin, B. Cramer, P. Gerling, U. Mann, *Chem. Geol.*, **214**, 179 (2005).
3. K. Gürgey, *J. Petr. Sci. Eng.*, **133**, 543 (2015).
4. S. Yovchev, A. Atanasov, I. Boiadjiev, Tectonic structure of Bulgaria, Technika, 1971) (in Bulgarian).
5. G. Palakarcheva, M. Stefanova, *Ann. Univ. Mining Geol.*, **56**, 86 (2013) (article in Bulgarian with an abstract in English).

6. J. Espitalié, J. L. LaPorte, M. Madec, F. Marquis, P. Leplat, J. Paulet, A. Boutefeu, *Rev. l'Inst. Fr. Pétrole* **32**, 23 (1977) (article in French).
7. R. P. Philp, Fossil Fuel Biomarkers. Application and Spectra. Methods in Geochemistry and Geophysics 23, Elsevier, Amsterdam, Oxford, New York, Tokyo, 1985.
8. D. W. Waples, T. Machihara, Biomarkers for Geologists - A Practical Guide to the Application of Steranes and Triterpanes in Petroleum Geology, AAPG Methods in Exploration 9, Tulsa, Oklahoma, USA, 1991.
9. E. E. Bray, E. D. Evans, *Geochim. Cosmochim. Acta*, **22**, 2 (1961).
10. K. E. Peters, *AAPG Bull.*, **70**, 318 (1986).
11. K. J. Ficken, B. Li, D. L. Swain, G. Eglinton, *Org. Geochem.*, **31**, 745 (2000).
12. R. A. Andersson, P. Kuhry, P. Meyers, Y. Zebühr, P. Crill, M. Mörth, *Org. Geochem.*, **42**, 1065 (2011).
13. P. A. Cranwell, *Prog. Lipid Res.*, **21**, 271 (1982).
14. B. M. Didyk, B. R. T. Simoneit, S. C. Brassell, G. Eglinton, *Nature*, **272**, 216 (1978).
15. J. M. Hunt, Petroleum Geochemistry and Geology, Second ed., Freeman, San Francisco, New York, 1995.
16. C. Deport, L. Lemée, A. Amblès, *Org. Geochem.*, **37**, 649 (2006).
17. P. A. Cranwell, J. K. Volkman, *Chem. Geol.*, **32**, 29 (1981).
18. P. A. Cranwell, in: Lake Sediments and Environmental History, E. Y. Haworth and J.W.G. Lund (Eds.), Leicester Univ. Press, 1984, p. 69.
19. R. Sykes, L. R. Snowdon, *Org. Geochem.*, **33**, 1441 (2002).

ГЕОХИМИЧНА ОЦЕНКА НА ВЪГЛЕВОДОРОД ГЕНЕРИРАЦИЯ ПОТЕНЦИАЛ НА БЪЛГАРСКАТА ЧАСТ ОТ ТРАКИЙСКИЯ БАСЕЙН: I. ЛИНЕЙНИ БИОМАРКЕРИ

Г. Мерачева¹, М. Стефанова^{2*}, С. П. Маринов², Е. Занева-Добранова¹

¹ Минно-геоложки Университет „Св. Ив. Рилски“, София 1700, България

² Институт по органична химия с Център по фитохимия, Българска Академия на Науките, София 1113, България

Постъпила на 25 януари 2017 г.; Коригирана на 06 март 2017 г.

(Резюме)

Частта от Тракийския Басейн, намираща се на територията на България, се определя като негов северозападен фланг. Данните за въглеродородния потенциал на този регион за момента са ограничени. Очаква се някои формации, аналози на такива от турската част на басейна, за които са доказани добри генериращи способности за въглеродороди, да имат нефто/газоносни свойства. С цел оценка перспективността на района чрез методи на органичната геохимия, подробно са изучени 11 проби (7 сондажни и 4 разкрития). Под формата на „свободен“ и „свързан“ битуми е изследвано екстрахируемото органично вещество. Чрез Rock Eval и GC-MS е изучена широка гама от органични съединения, някои от които биомаркери. В настоящото изследване обект на изучаване са линейните биомаркери: *n*-алкани, изопреноиди, мастни киселини и др. Rock Eval данните и компонентният състав определят органичното вещество като незряло от Тип III и от смесен Тип II/III. Във всички екстракти преобладават *n*-алкани. Разпределението им по дължина на алкиловата верига се променя с дълбочината на сондажа. Има и данни за преотлагане на по-зряло органично вещество. Позициите на изследваните проби в Pr/*n*C₁₇ vs. Ph/*n*C₁₈ диаграма определя керогена на потенциално нефто/газогенериращите скали като незрял, от смесен Тип II/III. Отношението Pr/Ph е характерно за слабо преобразувано органично вещество, отложено в редукционна и/или променяща се палеообстановка. Само в „свързаните“ битуми са установени мастни киселини, *n*C₁₂-*n*C₃₄, с преобладаващи четни хомолози и разпределение повлияно от дълбочината на залагане. За тях се предполага произход като на *n*-алканите Установени са и дикарбоксилови киселини, *n*C₁₈-*n*C₃₀, като максимални са *n*C₂₆, *n*C₂₈, *n*C₃₀.

Geochemical appraisal of hydrocarbon generative potential of Bulgarian part from the Thrace Basin: II. Cyclic biomarkers

G. Meracheva¹, M. Stefanova^{2*}, S. P. Marinov², E. Zaneva-Dobranova¹

¹ Faculty of Geology and Exploration, University of Mining and Geology "St. Ivan Rilski", Sofia 1700, Bulgaria

² Institute of Organic Chemistry with Centre of Phytochemistry, Bulgarian Academy of Sciences, Sofia 1113, Bulgaria

Received January 25, 2017; Revised March 06, 2017

Dedicated to Acad. Bogdan Kurtev on the occasion of his 100th birth anniversary

Assemblages of cyclic components in bitumens help to verify some assumption based of linear structures interpretation and supply relevant information for the generative potential of the region and palaeoenvironment of deposition. Hopanes and steranes determine immature Type III to mixed Type II/III kerogen for the Bulgarian part of the Thrace Basin. The view for Type III kerogen is additionally supported by the signatures for triterpenoids (TTs) abundance. In bitumen fractions monounsaturated, aromatized, C-3 functionalised or partly destructed TTs are identified. All these components unequivocally attest angiosperm taxa contribution to the palaeoenvironment. Consistent with the composition of the products from TTs destruction or aromatization it is assumed that oleanane type TTs strongly prevail ursane/lupane structures. Saturated diterpenoids were practically absent in bitumen extracts. Cross-plots of Pr/Ph vs. C₂₉/C₂₇ regular steranes attest deposition in anoxic/sub-oxic environment. Positions of samples in the diagram confirm the assumption for mixed type of OM (algae/bacteria and from land plants). Plots of steranes in tertiary diagram depict OM formation in open water environment (bay or estuarine) in lacustrine-fluvial/deltaic environments. A decrease in MPI-3 values with depth parallel to T_{max} changes was observed. It might be a hint for redeposition of more mature OM. This surmise was not supported by the changes in biomarker parameters, *i.e.* T_s/(T_s+T_m), hopane ratio, homohopane index, sterane C₂₉ ββ/(αα+ββ) and C₂₉ 20S/(20S+20R) ratios and positions in Pr/nC₁₇ vs. Ph/nC₁₈ diagram, all attesting maturity increase with depth. More samples and additional study are needed to verify this assumption. Rock Eval data and cyclic biomarker assemblages give us a confidence to denote that samples from the shale interval of the shale-marl formation in the Bulgarian territories and analogues to the Yenimuhacir group in the Turkish part of the Thrace Basin, can be regarded as "gas-prone" source rocks capable to generate biogenic gas. Although based on limited number of samples, some of them with low total organic carbon content, the current study is informative for a region where geochemical data are practically absent.

Key words: Thrace Basin; generative potential; cyclic biomarkers

INTRODUCTION

The hydrocarbon accumulations in the Thrace Basin are associated with structural and stratigraphic traps in the Eocene to Oligocene clastic and carbonate reservoir rocks. Since the first discovery, numerous studies considering the source rocks from the sedimentary sequence in the Turkish part of the basin are published [1–8].

The sedimentary succession in the central part of the Thrace basin is more than 9000 m thick, while in the Bulgarian part the maximum thickness of the whole succession is around 2500 m. Nevertheless, based on their lithological and stratigraphic characteristics, the sediment formations are very well correlated [9]. In the Bulgarian part of the Basin, these rocks exhibit similar reservoir properties as in the hydrocarbon fields in Turkey.

The sandstone intervals of the shale-marl fm., is proposed to be analogue of one of the major reservoir units Oligocene Yenimuhacir group, which are characterized by porosity values between 9-25% and a permeability of 2-6mD [4]. Therefore, there are indications that the area of the Basin in the Bulgarian territory could be regarded as its NW flank and detailed evaluation of sediments as potential source rocks for future exploration activities is necessary.

Present study continues previous investigation on the linear biomarkers from the same provenance. Herein data on biomarker assemblage will be enriched with results for cyclic components with the aim to determine depositional environment from the perspective formations from the Bulgarian part of the Thrace Basin. The study will proceed with attempts to look for analogy with Turkish sequences of the basin with already proven oil/gas accumulations.

* To whom all correspondence should be sent:
E-mail: maia@orgchm.bas.bg

EXPERIMENTAL

Samples characteristics, scheme of separation and Rock Eval data were published in a previous paper dedicated to the linear structures in bitumen extracts [9]. Briefly, the following set of samples was studied: (i) core samples G1-G5 were from the shaly intervals of shale-marl fm., analogue to Yenimuhacir group in Turkey; (ii) core and outcrop samples G6-G10 were from the rocks analogue of Ceylan fm. (Turkey); (iii) G11 and G12 from shale rock outcrops.

GC-MS study was carried out on a Hewlett-Packard 6890 GC system plus HP 5973 MSD equipped with a HP-5 MS column (0.25 mm×30 m×0.25 μ film thickness) with flame ionization detector (300 °C). A split/splitless capillary injector (300 °C) is used in the splitless mode (valve reopened 1 min after injection). After 0.5 min hold at 85 °C the oven temperature was increased to 200 °C at 20 °/min and then to 320 °C at 5°/min. The MSD was operated in the electron impact (EI) mode with energy of 70 eV and scan range from 50 to 650 Daltons. The data were acquired and processed with the HP software. Individual compounds were determined by comparison of MS with literature and library data, comparison of MS and GC retention times with those of authentic standards or interpretation of mass spectra. For MS spectra tracking Xcalibur software was used. MS were quantitatively interpreted by inner standards application, i.e. deuterated nC_{24} for the neutral fraction, and triethylbenzene for the aromatic/slightly polar fraction. Amounts were normalized to TOC and are presented in μg/gC_{org}.

The following cyclic biomarkers were MS tracked: steranes (m/z 217), diasteranes (m/z 259), tri-, tetra-, pentacyclic terpanes of hopane type, benzohopanes, hopanoic acids (m/z 191). Based on peak areas some biomarker parameters for hopane (H) and steranes (S) were calculated. The following ratios were determined: (i) $T_s/(T_s+T_m)$; (ii) $H_{30\alpha\beta}/H_{29\alpha\beta}$; (iii) $S/(S+R)$ stereo isomers at C-22 carbon atom in homohopane $H_{31\alpha\beta}$; (iv) $\beta\beta/(\alpha\beta+\beta\alpha+\beta\beta)$ hopanes; (v) and, regular sterane $S/(S+R)$ stereo isomers at C-20. Parameters definitions and applications are described in Peters and Moldowan [10]. Specific fragments were used for homologous and individual compounds tracking: m/z 123 for diterpenoids (DTs); m/z 203 and m/z 218 for TTs; m/z 231 for 4-Me steranes; m/z 424 for 3-keto-TTs; m/z 274 for products of TTs destruction and aromatization.

RESULTS AND DISCUSSION

In the studies of fossil materials pentacyclic TTs are divided into two main groups - hopanoids (hopanes, H) and non-hopanoids [11–13]. Hopanes in Fig. 1 comprise the series C_{27} - C_{33} (C_{28} absent) with their $\alpha\beta$, $\beta\alpha$ and $\beta\beta$ isomers and some benzohopanes, C_{32} - C_{34} . Hopanoids are indicators for microbial activity in the sediments. The contribution of microorganism during the diagenetic transformation of the parent OM supplies hopanes. However, some of them might be derived from lower plants like ferns [10]. Distributions of regular hopanes in Fig. 1 maximize at $C_{30\alpha\beta}$. Some variations with depth in hopanes parameters are obvious in Table 1 and in Fig. S1. In Fig. 1 anoxicity marker $17\alpha(H)$ -28,30-bisnorhopane M⁺284 is absent, an indication that the samples were deposited in terrestrial or lacustrine environment under oxic or sub-oxic conditions [10]. This assumption contradicts a bit with correlations Pr/Ph vs. C_{29}/C_{27} regular steranes discussed later in the text where definitively anoxic conditions were depicted. Low amount of $17\alpha(H)$ -28,30-bisnorhopane below the detection limit of GC-MS might be one possible explanation for the discrepancy. In the samples sequence G6-G9, with depth increasing tricyclic terpanes (C_{25} , C_{28}) have appeared. One $17,21$ -seco-hopane, C_{24} , M⁺330 is detectable as well. All listed tri-/tetra terpanes are characteristic components for petroleum and petroleum source rocks [10]. For “bound” bitumens, hopanes assemblages are similar to the “free” ones, except appearance of hopanes ($C_{27:1\alpha}$, $C_{30:1\alpha\beta}$). They are indicators for hopanes still attached to the kerogen OM.

By m/z 191 tracking in aromatics/slightly polar fractions were identified hopanoid acids (as methyl esters), maximizing at $C_{32\beta\beta}$, (Table 2). They are hopanes biological precursors and are common in the bitumens from immature fossils. Functionalized hopanes with carbonyl/hydroxyl group at the C-3 position are determined as well, i.e. hop-22(29)-en-3-one, M⁺ 424, m/z 189 (100%) and diplopterol M⁺ 426. The last one is a functionalized diploptene, highly abundant in the neutrals fractions and one of the possible hopane precursors. Diploptene (peak D, in Fig. 1) is common in all hopanoid-producing bacteria and represents likely source for hopanes with < C_{30} carbon atoms.

Some biomarker parameters based of hopanes distributions are calculated and shown in Table 1. Values for $T_s/(T_s+T_m)$ ratios for well samples are somehow dispersed, 0.21–0.53. It is known that T_s and T_m are sensitive to maturity, type of OM and

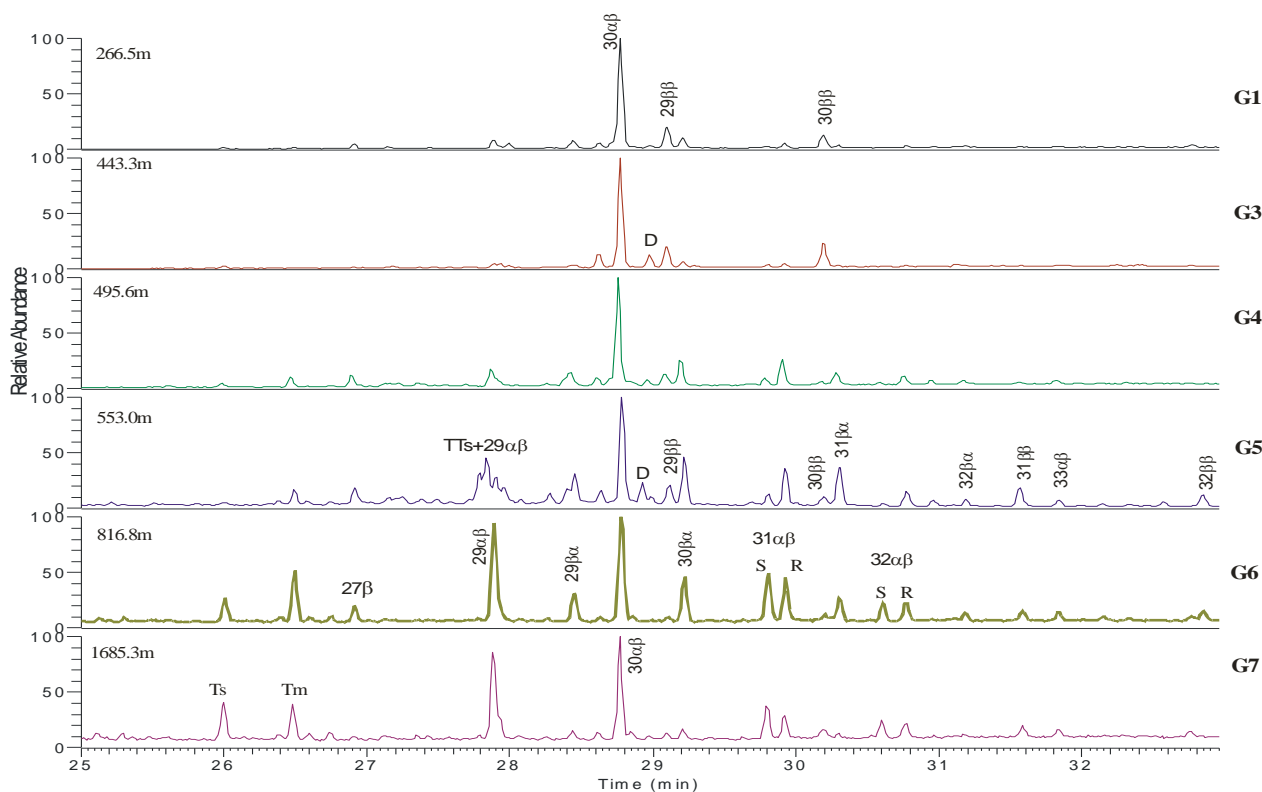


Fig. 1. Variations in hopanes distributions with depth increase tracked by m/z 191. (Abbreviations in Table 1; TT – non-hopanoid triterpenoids; D- diploptene).

Table 1. Variations in hopanes distributions with depth increase tracked by m/z 191.

Sample	Hopanes (H)					Steranes (S)			$\alpha\alpha$ Steranes (20R), rel. %		
	$T_s/(T_s+T_m)$ ratio	Mor/H ratio	H ratio	HomoH index	DiaS/S	$\beta\beta/(\alpha\alpha+\beta\beta)$	S/(S+R)	27	28	29	
"Free" bitumen											
Well	G1	-	0.09	0.08	0.1	0.4	0.27	0	36.2	20.9	42.9
	G3	-	0.05	0	0.1	n.d.	n.d.	0	n.d.	n.d.	n.d.
	G4	-	0.24	0.24	0.18	0.56	0.34	0	35	23.4	41.6
	G5	0.21	0.41	0.3	0.22	0.52	0.34	0	33.3	24.8	41.9
	G6	0.31	0.36	0.9	0.54	0.50	0.43	0.34	42.7	23.9	33.4
	G7	0.53	0	1.08	0.6	0.89	0.52	0.34	40.2	29	30.8
Outcrop	G9	0.81	0	0.75	0.63	n.d.	n.d.	n.d.	n.d.	n.d.	n.d.
	G11	0.34	0.3	0.45	0.47	0.3	0.3	0.1	31	29	40
	G12	0.48	0.11	0.98	0.11	0.25	0.25	0.09	23	27	50
"Bound" bitumen											
Well	GA1	0.47	0.28	0.2	0.45	0.23	0.43	0.16	34.6	23.5	41.9
	GA3	0.56	0.08	0.12	0.48	0.4	0.22	0.07	28.8	26	45.2
	GA4	0.3	0.27	0.36	0.28	0.42	0.35	0.1	29.1	25.1	45.8
	GA5	0.28	0.38	0.39	0.3	0.45	0.32	0.1	28.3	25	46.7
	Outcrop	GA12	0.49	0.13	0.14	0.57	0.41	0.41	0.21	38	21

n.d. – not determined

T_s - 18 α (H)22,29,30-Trisnorhopane

Moretane/Hopane ratio (Mor/H) = H30 $\beta\alpha$ /H30 $\alpha\beta$

Homohopane index (HomoH) = H31 $\alpha\beta$ S/(S+R)

Diasterane/Sterane ratio (DiaS/S) = $\beta\alpha$ -Dia-C27(S+R)/ $\alpha\alpha$ C27(S+R)

Sterane $\beta\beta/(\alpha\alpha+\beta\beta)$ = C29 $\beta\beta$ (S+R)/[C29 $\alpha\alpha$ (S+R) + C29 $\beta\beta$ (S+R)]

T_m - 17 α (H)22,29,30-Trisnorhopane

Hopane ratio (H) = H29 $\alpha\beta$ /H30 $\alpha\beta$

Sterane S/(S+R) = C29 $\alpha\alpha$ S/(S+R)

Table 2. Compounds and homologous series identified in G5 sample, expressed in $\mu\text{g/g}$ sample and normalized to $\mu\text{g/g C}_{\text{org}}$.

Series or compound classes	Bitumen							
	"Free"				"Bound"			
	Neutrals		Aromatics/Slightly polars		Neutrals		Aromatics/Slightly polars	
	$\mu\text{g/g}$	$\mu\text{g/g C}_{\text{org}}$	$\mu\text{g/g}$	$\mu\text{g/g C}_{\text{org}}$	$\mu\text{g/g}$	$\mu\text{g/g C}_{\text{org}}$	$\mu\text{g/g}$	$\mu\text{g/g C}_{\text{org}}$
<i>n</i> -Alkanes and isoprenoids	31.2	1351	-	-	8.2	355	-	-
<i>n</i> -Alkan-2-ones	-	-	1.92	83.1	tr.	tr.	tr.	tr.
C ₁₈ <i>iso</i> -ketone	0	0	0.1	4.3	0	0	0.07	3
Diterpenoids	1.8	77.9	0	0	tr.	tr.	tr.	tr.
Polar aromatic diterpenoids	0	0	0.05	2.2	0	0	0.03	1.3
Triterpenoid (TTs)	1.9	82.3	0	0	0.25	10.8	0	0
Products of TTs destruction	1.8	77.9	0.11	4.8	0.44	19.1	0	0
Aromatized TTs	0	0	1.36	58.9	0	0	0.4	17.3
Polar TTs	0	0	0.03	1.3	0	0	0.05	2.2
Perylene	0	0	0.27	11.7	0	0	0.02	0.9
Hopanes and benzohopanes	5.2	225.2	0	0	0.62	26.8	0	0
Hopanoic acids, methyl esters	0	0	0	0	0	0	0.52	22.5
Fatty acid, methyl esters	0	0	0	0	0	0	3.96	171.5
Dicarboxylic fatty acids, dimethyl esters	0	0	0	0	0	0	0.47	20.4
Total	41.9	1814.3	3.84	166.3	9.51	411.7	5.52	239.1

samples lithology [14]. With maturation T_m is gradually transferred into T_s . In our samples set G1-G7 in parallel with the increase in burial depth the ratios $T_s/(T_s+T_m)$ rise (Table 1 and Fig. S1), attesting increase in maturity. With increasing depth the magnitudes for hopane ratios and homohopane index also increase. Homohopane index for sample G9 is 0.63 (Table 1) and argues for a high sample maturity. In hopane distributions $\alpha\beta$ hopanes are more prominent than $\beta\alpha$ isomers, reflecting in varying moretane ratios, the highest calculated for OM rich samples, ~ 0.4 . Hopanes distribution of G5 "free" bitumen (Fig. 1) permits determination of the relative portion of $\beta\beta$ hopanoids ("bio"-hopanoids) from the total sum of regular hopanes. It is known that during diagenesis $\beta\beta$ hopanoids are progressively transferred into "geo"-hopanoids ($\alpha\beta$ and $\beta\alpha$ epimers). The ratio "bio"/"geo" hopanes for G5 "free" bitumen is 0.16 and almost alike, 0.17, for the "bound" bitumen. The m/z 191 separations in Fig. 1 and calculated parameters (Table 1) argue for immature OM comprising considerable portion of $\beta\beta$ homologues.

Triterpenoids of non-hopanoid type are unambiguous biomarkers for angiospermous floral input, where oleananes have proven to be the most commonly cited [15]. These cyclic alkanes are identified in many oils and shales with terrestrial

source rock provenance. By tracking m/z 203, m/z 218 and M^+ 410 olean-13(18)-ene, olean-12-ene, olean-18-ene (β -olean-12-ene maximal) were identified. These compounds are intermediates in the classical diagenetic transformation of 3-oxygenated triterpenoids to chrysene and pyrene via the pathway proposed by Murrey *et al.* [16]. The scheme is additionally validated by the presence of C-3 functionalized oleanane/ursane type TTs with M^+ 424, *i.e.* α/β amyrones (all present in the aromatic/slightly polar fractions, Table 2). Oxygenated TTs abundance is a convincing proof for the considerable terrigenous input. All compounds and homologous series identified in G5 sample, expressed in $\mu\text{g/g}$ sample and normalized to $\mu\text{g/g C}_{\text{org}}$, are shown in Table 2.

In the first fractions (neutrals) were determined des-A-oleanane/ursane and their mono-/di-unsaturated homologues. Des-A-lupane, M^+ 330, m/z 123 was in negligible content. There were several attempts to use des-A-TTs as biomarkers for paleoenvironmental reconstruction [17–19]. Commonly they have related des-A-TTs formation and accumulation to wetter climate, high water table and anaerobic environment. Respectively, such conditions might be assumed for the palaeoenvironment.

In the aromatics/slightly polar fractions products of α/β -amyrin aromatization were depicted, *i.e.* dimethyl- (M^+ 310) and trimethyl (M^+ 324) substituted tetrahydropicenes. They are the end products of TTs destruction and aromatization [16].

By M^+ 274 tracking three components were visualized: (i) with m/z 218 (100%) for oleanane type TTs; (ii) with m/z 259 (100%) for ursane type TTs; (iii) and, with m/z 231 (100%) for lupane type TTs [20]. Ratios for the three groups were 46:3:1. Therefore, on the base of the TTs products of destruction and aromatization, oleanane type TTs seems to have been strongly predominant in the floral assemblage. Generally, TTs biomarkers do not specify palaeovegetation. They simply assign angiosperm contribution to the kerogen formation. However, studies in this field are in progress as potential TTs precursor assignment will considerably increase chemotaxonomic value of angiosperms for sedimentary environmental reconstruction [21].

No saturated DTs were detected by m/z 123 tracking. Only aromatized DTs, *i.e.* simonellite and retene, were identified. These two components are the end products of diterpenoids diagenetic transformation [22–24]. Likewise DTs provide evidences for the subordinate gymnosperms presence in palaeovegetation and for advance in maturation.

Absolute amounts of the regular steranes in the studied samples are very low, which prohibits their quantitative determination. Hence, regular steranes were only qualitatively interpreted and distributions in rel. % are shown in Table 1. Signature of regular steranes in terrigenous OM is very simple: (i) dominated by C_{29} steranes; (ii) and, the ratio regular sterane/hopane is very low [25]. In a case of OM mixed input to the source rocks it is more complicated. Another feature of the regular sterane distribution is the presence of diasteranes. Recent studies have provided evidences that maturation, oxic-type environment and the catalytic role of clays tolerate rearrangement with diasteranes formation [10]. The ratios diasterane/regular sterane for the well samples were in the range 0.4–0.5 and have increased to ~ 0.9 with depth, parallel with maturation (Table 1). An attempt to make a correlation with lithology has not been done.

According to the number of carbon atoms in their molecules regular steranes are grouped in C_{27} , C_{28} , C_{29} and distributions are plotted in Fig. 2 [26]. Commonly, C_{27} steranes are related to algal contribution while C_{29} steranes point to land plants input. This approach for steranes interpretation is

rather simplistic for general use as it is known that phytoplankton could also contribute to C_{29} sterols [27]. However, the diagram is often used for oil/source rocks correlations. The plots of samples in Fig. 2 indicate OM formation in open water environment (bay or estuarine) and imply that most likely the kerogen has been formed in lacustrine-fluvial/deltaic environments. The proportion C_{27}/C_{29} steranes varies with a depth. The algal supply, respectively the relative content of C_{27} steranes, increases with depth to $\sim 40\%$, while TOC rich samples (at shally intervals) are enriched in C_{29} steranes. Variations in sterane distributions for samples G1, G3 and G5 might be contributed to the changes in the sedimentary environment, namely low water table and terrigenous input. Generally, regular sterane signature confirms the assumptions based on *n*-alkane distributions [10] - mixed origin for OM, *i.e.* aquatic and terrestrial, in different proportions depending on the depth. Variations in C_{27}/C_{29} steranes ratios with depth give a picture for hydrological oscillations at different periods - arid (0.79–0.84, for shally intervals of shale-marl fm. analogue to Yenimuhacir group, Turkey) and humid (~ 1.3 , for intervals analogue of Ceylan fm., Turkey).

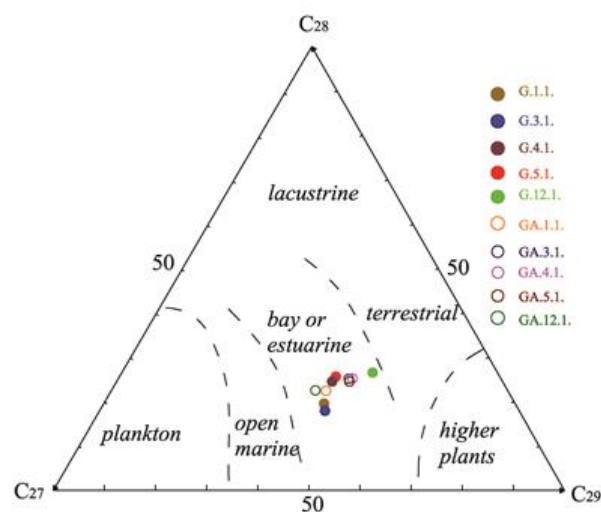


Fig. 2. Plots of steranes distributions in C_{27} , C_{28} , C_{29} ternary diagram after Huang and Meinschein [26].

In all samples by SIM m/z 231 4-methyl steranes, *i.e.* C_{28} , C_{29} , C_{30} , were identified. They were interpreted as dinosteranes attesting dinoflagellates presence and microbial activity in the palaeoenvironment [10].

In samples studied polycyclic aromatic hydrocarbons (PAHs) with 2–4 condensed aromatic rings, *i.e.* naphthalene, phenanthrene (highly present), pyrene (tentatively identified) and their alkylated homologous, *i.e.* C_1 – C_4 derivatives, were

determined. It is impossible PAHs quantification due to their low concentrations. However, it was feasible to calculate MPI-3 maturity index. It is based on distribution of methyl phenanthrene isomers. The definition, application and limits were explained by Radke *et al.* [28]. Methyl phenanthrenes (m/z 192) are the most commonly found in separations and their distributions comprise peaks of 2-, 3-, 4+9-, and 1-methyl phenanthrenes. MPI-3 calculated values for well samples vary in the range 1.42–1.60, while for the outcrops samples they are in the range of 1.35–1.65. There is not an appreciable change of MPI-3 ratios with depth (1.61 to 1.43). However, a tendency for a decrease in MPI-3 values parallel to T_{\max} decrease in Rock Eval parameters is recognizable [9]. It might be a hint for redeposition of more mature OM. The assumption is not supported by parameters calculated on the base of cyclic biomarkers where unequivocal proves for increase in maturation with depth were obtained (Supplementary Material 1). More samples are needed to clarify the item.

MPI-3 ratios are not calculated for “bound” bitumens as in GC-MS separations methyl phenanthrenes have overlapped with elemental sulphur. Highly substituted phenanthrenes were less abundant, except 1-Me-7-*i*-Pr-phenanthrene, M^+ 234, retene.

Perylene ($11.7 \mu\text{g/gC}_{\text{org}}$) was present in G5 aromatic/slightly polar fraction (Table 2). Previous researches proved that its precursors could be fungi, wood-degrading fungi, terrestrial sources [29]. A diagenetic product of perylene is registered predominantly in humid, terrestrial OM rich environments.

GENERAL DISCUSSION

Data in Table 1 and Fig. S1 demonstrate that the ratio $22\text{S}/(22\text{S}+22\text{R})$ for $\text{C}_{31}17\alpha(\text{H}),21\beta(\text{H})$ -hopanes is depth dependent and from 0.10 gradually increases to 0.60, attesting that at 1685.3 m hopane epimer equilibrium is already attained. The magnitudes for sterane $\text{C}_{29} 20\text{S}/(20\text{S}+20\text{R})$ ratios are very low. In m/z 217 track of some samples 20S epimers were virtually absent reflecting in $\text{S}/(\text{S}+\text{R}) = 0$ (Table 1, Fig. S1). With depth increasing 20S epimer became visible and the ratio reached 0.34. The magnitudes for outcrop samples and “bound” bitumens are also low (0.07–0.21, Table 1) and argue for kerogen immature stage. Some relationship for sterane $\text{C}_{29} \beta\beta/(\alpha\alpha+\beta\beta)$ vs. depth are recognizable as well (Fig. S1). The

values vary in the range 0.3–0.5 (Table 1), for well samples they increased with depth, attesting advance in maturation. A correlation of two maturity parameters, $\text{C}_{29}20\text{S}/(\text{S}+\text{R})$ for regular steranes and $\text{C}_{31} 22\text{S}/(\text{S}+\text{R})$ for hopanes, is shown in Fig. 3. The cross-plots unequivocally argue for kerogen immature stage. Only G6 and G7 (deeper well samples) are shifted to kerogen of “early mature stage”. None of the samples is plotted in the “oil window” area.

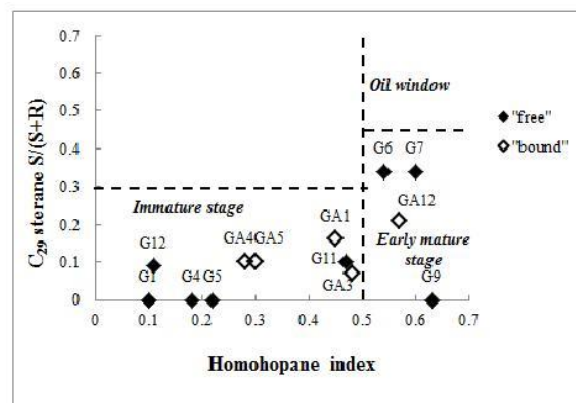


Fig. 3. Estimation of kerogen maturity by homohopane index vs. C_{29} steranes $\text{S}/(\text{S}+\text{R})$ ratios correlations after Peters and Moldowan [10].

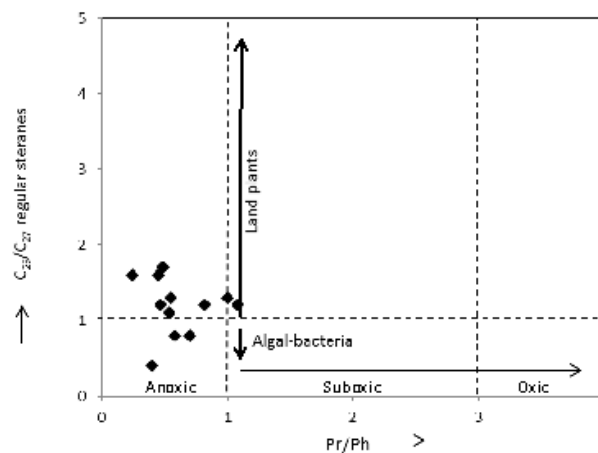


Fig. 4. Cross-plots of Pr/Ph vs. $\text{C}_{29}/\text{C}_{27}$ regular steranes ratios suggesting samples anoxic/sub-oxic conditions of depositions after Hakimi *et al.* [31]

Cross-plots of Pr/Ph vs. $\text{C}_{29}/\text{C}_{27}$ regular steranes are illustrated in Fig. 4 [30, 31]. On the base of Pr/Ph ratios in the previous paper an assumption for OM deposition in anoxic/sub-oxic environment has been done [9]. Positions of samples in Pr/Ph vs. $\text{C}_{29}/\text{C}_{27}$ regular steranes diagram (Fig. 4) confirm it. The cross-plots depict a mixed type of OM input (from algae/bacteria and from land plants) and deposition in anoxic-sub-oxic environment.

Estimates regarding the generative potential of the samples on the base of biomarkers are in a good coherency with Rock Eval data. The fractional compositions and biomarker assemblages of TOC-rich samples evaluate moderate OM contents. According to these parameters the rocks can be classified as source rocks with “fair” to “good” potential. Kerogen is defined as immature of mixed Type II/III capable to generate biogenic gas. These main conclusions fit well with the data published for the Turkish part of the Thrace Basin [3, 5–7, 32, 33]. Therein, for Thrace sediments is assumed oil/gas potential based on the data from oil/gas to source rocks correlations and basin modeling.

CONCLUSION

The study highlights the relevance of biomarkers for source rocks and depositional environment appraisal. Assemblages of cyclic components help to verify some assumption based of linear structures interpretation and supply information for the generative potential of the region. The following observations are of particular importance: (i) Ratios sterane/hopane for TOC rich samples are very low and attest kerogen with considerable terrigenous input. Plots of regular steranes in ternary diagram depict OM formation in lacustrine-fluvial/deltaic environment in agreement with Pr/Ph ratios, 0.3–1.1. According to these geochemical data samples most likely have been deposited under oxygen-deficient, but not at completely anoxic conditions; (ii) Plots $C_{29}20S/(S+R)$ steranes vs. $C_{31}22S/(S+R)$ hopanes denote immature to early mature OM; (iii) Geochemical proxies determine immature mixed Type II/III kerogen with considerable supply of microbially reworked OM. Variety of TTs in sample G5, *i.e.* monounsaturated, aromatized or C-3 functionalized as ketones and alcohols, partly destructed, *etc.*, admits Type III kerogen and indicates floral supply dominated by angiosperm taxa. Based on the compositions of products from TTs destruction/aromatization, oleanane precursors preponderance over ursane/lupine structures is assumed; (iv) MPI-3 index and T_{max} values gave a hint for redeposition of more mature OM. On the other hand this surmise was not supported by the changes in biomarker parameters with depth, *i.e.* $T_s/(T_s+T_m)$, hopane ratio, homohopane index, sterane $C_{29} \beta\beta/(\alpha\alpha+\beta\beta)$ and $C_{29} 20S/(20S+20R)$ ratios and positions in Pr/ nC_{17} vs. Ph/ nC_{18} diagram. More extensive survey is required to test the validity of this assumption. Finally, for some

samples of the shaley intervals of the shale-marl Fm. a similarity with Yenimuhacir group in the Turkish part of the Thrace Basin is admitted. These successions are resolved as potential “gas-prone” source rocks capable to generate biogenic gas. However, further work on the Bulgarian part of the Basin using densely sampled Fms. is needed to confirm or reject this point.

Acknowledgements: *The authors are greatly indebted to the reviewer for the useful comments and propositions on the earlier version of the manuscript which helped us a lot to improve it.*

Electronic Supplementary Data available here.

REFERENCES

1. S. Turgut, G. Eseller, *Marine Petr. Geol.*, **17**, 61 (2000).
2. S. Turgut, M. Türkaslan, D. Perinçek, in: Generation, Accumulation, and Production of Europe's Hydrocarbons, A. M. Spencer (ed.), Special Publication of European Association of Petroleum Geoscientists, London, 1991, p.415.
3. M. Siyako, O. Huvaz, *Sed. Geol.*, **198**, 75 (2007).
4. O. Huvaz, N. Karahanoglu, V. Ediger, *J. Petr. Geol.*, **30**, 3 (2007).
5. Ş. Şen, *Energy Sour., Part A*, **33**, 1005 (2011).
6. Ş. Şen, S. Yillar, *AAPG Bull.*, **93**, 357 (2009).
7. Ş. Şen, S. Yillar, I. E. Kerey, *J. Petr. Sci. & Eng.*, **64**, 55 (2009).
8. K. Gürgey, *J. Petr. Sci. & Eng.*, **133**, 543 (2015).
9. G. Meracheva, M. Stefanova, S.P. Marinov, E. Zaneva-Dobranova, *Bulg. Chem. Com.* (2017) (submitted to this volume).
10. K. E. Peters, J. M. Moldowan, *The Biomarker Guide: Interpreting Molecular Fossils in Petroleum and Ancient Sediments*. Englewood Cliffs, N. J. 1993.
11. R. P. Philp, *Fossil Fuel Biomarkers. Application and Spectra. Methods in Geo-chemistry&Geophysics 23*, Elsevier, Amsterdam, Oxford, NY, Tokyo, 1985.
12. A. Bechtel, R. Sachsenhofer, I. Kolcon, R. Gratzner, A. Otto, W. Püttmann, *Int. J. Coal Geol.*, **51**, 31 (2002).
13. A. Bechtel, R. F. Sachsenhofer, M. Markic, R. Gratzner, A. Lücke, W. Püttmann, *Org. Geochem.*, **34**, 1277 (2003).
14. J. M. Moldowan, W. K. Seifert, E. J. Gallegos, *Bull. Am. Assoc. Petr. Geol.*, **69**, 1255 (1985).
15. J. K. Volkman, in: *Lacustrine Petroleum Source Rocks*, A. J. Fleet, K. Kelts, M. R. Talbot (eds.), Geol. Soc., London Spec. Publ. **40**, 103 (1988).
16. A. P. Murray, I. B. Sosrowidjojo, R. A. Alexander, R. Kagi, C. M. Morgate, R. E. Summons, *Geochim. Cosmochim. Acta*, **61**, 1261 (1997).

17. J. Jacob, J. Disnar, M. Boussafir, A. Albuquerque, A. Sifeddine, B. Turcq, *Org. Geochem.*, **38**, 180 (2007).
18. X. Huang, S. Xie, L. Zhang, D. Jiao, J. Huang, J. Yu, F. Jin, Y. Gu, *Org. Geochem.*, **39**, 1765 (2008).
19. Y. Zheng, W. Zhou, Z. Lin, Q. M. Chen, X. Yu, X. D. M. Liu, *Chin. Sci. Bull.*, **55**, 2275 (2010).
20. S. G. Wakeham, C. Schaffner, W. Giger, *Geochim. Cosmochim. Acta*, **44**, 415 (1980).
21. G. Schnell, P. Schaeffer, H. Tardivon, E. Motsch, J. Connan, D. Ertlen, D. Schwartz, N. Schneider, P. Adam, *Org. Geochem.*, **66**, 107 (2014).
22. B. R. T. Simoneit, *Adv. Space Res.*, **33**, 1255 (2004).
23. B. R. T. Simoneit, *Mass Spec. Rev.*, **24**, 719 (2005).
24. M. Stefanova, K. Markova, S. P. Marinov, B. R. T. Simoneit, *Bull. Geosci.*, **80**, 93 (2005).
25. A. S. Mackenzie, in: *Advances in Petroleum Geochemistry*, J. Brooks, D. Welte (eds.), Acad. Press Inc. London, 1984, 115.
26. W. Y. Huang, W. G. Meinschein, *Geochim. Cosmochim. Acta*, **43**, 739 (1979).
27. J. K. Volkman, *Org. Geochem.*, **9**, 83 (1986).
28. M. Radke, D. H. Welte, H. W. Willsch, *Org. Geochem.*, **10**, 51 (1986).
29. L. Marynowski, J. Smolarek, A. Bechtel, M. Phillippe, S. Kurkiewicz, B. R. T. Simoneit, *Org. Geochem.*, **59**, 143 (2013).
30. M. H. Hakimi, W. H. Abdullah, *Marine Petr. Geol.*, **45**, 304 (2013).
31. M. H. Hakimi, W. H. Abdullah, M. R. Shalaby, G. A. Alramisy, *Marine Petr. Geol.*, **50**, 185 (2014).
32. H. M. Hoşgörmez, N. Yalcin, B. Cramer, P. Gerling, U. Mann, *Chem. Geol.*, **214**, 179 (2005).
33. K. Gürgey, *J. Petr. Sci. & Eng.*, **133**, 543 (2015).

ГЕОХИМИЧНА ОЦЕНКА НА ВЪГЛЕВОДОРОД ГЕНЕРИРАЦИЯ ПОТЕНЦИАЛ НА БЪЛГАРСКАТА ЧАСТ ОТ ТРАКИЙСКИЯ БАСЕЙН: II. ЦИКЛИЧНИ БИОМАРКЕРИ

Г. Мерачева¹, М. Стефанова^{2*}, С. П. Маринов², Е. Занева-Добранова¹

¹ Минно-геоложки Университет „Св. Ив. Рилски“, София 1700, България

² Институт по органична химия с Център по фитохимия, Българска Академия на Науките, София 1113, България

Постъпила на 25 януари 2017 г.; Коригирана на 06 март 2017 г.

(Резюме)

Наборът от цикличните биомаркери дава възможност да се проверят някои вече направени заключения на базата на състава и разпределението на линейните структури и предоставя допълнителна информация относно генериращия потенциал на региона и палеообстановката на отлагане. Хопаните и стераните определят керогена от българската част от Тракийския басейн като незрял от Тип III и/или от смесен Тип II/III. Представата за Тип III кероген се потвърждава и от широкото разпространение на тритерпеноиди. Във всички изследвани битуми присъстват мононенаситени, ароматни, C-3 заместени с функционални групи или частично деструктурирани производни на тритерпеноиди. Всички те са недвусмислено указание за присъствие в палеоблатото на широколистна растителност. В съгласие със състава на продукти от разграждане и ароматизация на тритерпеноиди се предполага, че олеановите структури доминират над урсанови или лупанови такива. В битумите практически липсват наситени дитерпеноиди. Зависимостта Pr/Ph vs. C₂₉/C₂₇ стерани допуска отлагане в променяща се обстановка като позициите на пробите в диаграмата потвърждават схващането за смесен тип на органичното вещество (водорасли/бактерии и наземна растителност). Разпределенията на стераните, оформено в тройна диаграма, допуска формиране на органичното вещество в открити води (залив или устие на река) в езерна-речна или делтова обстановка. Установено бе, че стойностите за MPI-3 намаляват паралелно с тези за T_{max}, което допуска преотлагане на по-зряло органично вещество. Това твърдение не се подкрепя от измененията на някои биомаркери с удълбочаване на пробата, а именно T_s/(T_s+T_m), отношението на хопаните, индекса на хомохопаните, отношенията C₂₉ ββ/(αα+ββ) и C₂₉ 20S/(20S+20R), позициите в Pr/nC₁₇ vs. Ph/nC₁₈ диаграма. Всички те утвърждават повишение на зрялостта с удълбочаване. Тези експериментални данни показват, че твърдението следва да се провери с анализа на по-голям брой проби. Данните от Rock Eval и съставът на цикличните биомаркери дават основание да се допусне, че пробите от шистовия интервал на глинесто-мергелната задруга на българска територия са аналог на Йенимухачир групата от Турската част на Басейна и могат да се разглеждат като перспективни газоносни скали за продуциране на биогенен газ при залягане при подходящи термобарични условия. Независимо, че настоящото изследване е проведено с ограничен брой проби, някои от които са с ниско съдържание на общ въглерод, то дава информация за геохимичната обстановката в регион, за който практически липсват сведения.

Copper, zinc and manganese spinel ferrites hosted in activated carbon from waste biomass as catalysts for hydrogen release from methanol

T. S. Tsoncheva^{1*}, G. S. Issa¹, A. B. Mileva¹, R. N. Ivanova¹, M. D. Dimitrov¹, I. P. Spassova², D. G. Kovatcheva², D. G. Paneva³, N. I. Velinov³, B. G. Tsyntsarski¹, N. V. Petrov¹

¹ Institute of Organic Chemistry with Centre of Phytochemistry, Bulgarian Academy of Sciences, 1113 Sofia, Bulgaria

² Institute of General and Inorganic Chemistry, Bulgarian Academy of Sciences, 1113 Sofia, Bulgaria

³ Institute of Catalysis, Bulgarian Academy of Sciences, 1113 Sofia, Bulgaria

Received February 13, 2017; Revised March 06, 2017

Dedicated to Acad. Bogdan Kurtev on the occasion of his 100th birth anniversary

Activated carbon was prepared from peach stones and used as a host matrix of nanosized MFe_2O_4 ($M = Cu, Zn, Mn$) spinel ferrites. The obtained composites were characterized by Nitrogen physisorption, XRD, UV-Vis, FTIR, Moessbauer spectroscopy and TPR with hydrogen. Their catalytic behaviour was tested in methanol decomposition with a potential application as hydrogen carrier. Activated carbon based catalysts revealed higher catalytic activity but relatively low selectivity to syngas formation than their analogues hosted in mesoporous silica matrix. $ZnFe_2O_4$ is more appropriate active phase for the activated carbon support, while $CuFe_2O_4$ has higher activity on the silica matrix. The role of different supports on the state of catalytic active phase was discussed in detail.

Key words: activated carbon from waste biomass; spinel ferrites; methanol decomposition

INTRODUCTION

Recently, the energy crisis and the increased environmental problems forced the development of fuel cell technology. However, due to the limitation of the hydrogen storage technologies, the interest towards the development of integrated fuel processors, supplied with liquid fuel, which can release hydrogen in case of need, gains a considerable attention [1–3]. Methanol possesses more advantages, such as high H/C ratio, compatibility with the present gasoline infrastructures and possibility to be produced by well developed technologies from different sources, including waste and renewable ones [2, 4]. Among the various reforming processes, methanol decomposition is the simplest one producing syngas [2, 5 and refs therein]. In our previous study we demonstrated that spinel ferrites could be effective catalysts for methanol decomposition at relatively low temperatures [6–10]. Spinel ferrites can be described by the general formula AB_2O_4 , where A and B stand for tetrahedral and octahedral cation sites in a close cubic packing of oxygen. In normal spinel ferrite structure, M^{2+} ions occupy tetrahedral (A) sites, while the majority of Fe^{3+} cations occupy the octahedral (B) ones, as it is the case of $ZnFe_2O_4$ [11]. In an inverse spinel structure, like $CuFe_2O_4$,

half of Fe^{3+} ions occupy tetrahedral sites, while the M^{2+} ions together with the rest Fe^{3+} ions are situated in octahedral positions. In partially inverse spinel ferrites, like $MnFe_2O_4$, M^{2+} and Fe^{3+} occupy both tetrahedral and octahedral position in different proportion [3]. The ferrite structure offers close connectivity between the cations responsible for their interesting magnetic, electric, catalytic and photocatalytic properties, which are strongly influenced by the cationic distribution [12].

A reliable approach to produce cheaper and more active catalysts is their usage in nanoscale by deposition on suitable supports. Activated carbon (AC) can be used for this purpose due to its high surface area, special surface reactivity and porous structure [13]. The main drawback of the activated carbon based technologies, which make them costly and with restricted applicability, is the use of non-renewable and relatively expensive raw materials (such as coal and wood) for their production. Nowadays to attain better economic viability, the application of low-cost AC, derived from renewable materials, such as biomass, is preferred [14]. In our pioneer investigations we reported the role of AC texture and functional characteristics on the formation of highly dispersed and catalytic active copper, iron, manganese and cobalt nanoparticles [15, 16]. We also stressed on the reductive activity of AC support on the regulation of oxidative state of metal species both during the

* To whom all correspondence should be sent:
E-mail: tsoncheva@orgchm.bas.bg

preparation procedure and the catalytic process, which often leads to fast catalyst deactivation. The facile effect of binary systems, like ZnFe₂O₄ spinel ferrite, on the stabilization of highly active metal species was demonstrated in [17]. This study is focused on the understanding the role of metal ion in supported on activated carbon MFe₂O₄ spinel ferrites on their catalysts behaviour in methanol decomposition. For the purpose, AC derived from waste biomass (peach stones), was compared with mesoporous silica type KIT-6 as a host matrix of CuFe₂O₄, MnFe₂O₄ and ZnFe₂O₄ spinel ferrites.

EXPERIMENTAL

The activated carbon, denoted as ACP, was obtained by carbonization of peach stones in nitrogen atmosphere at 873 K and subsequent activation of the obtained product in flow of water vapour at 1123 K. The carbons were modified by incipient wetness impregnation with methanol solutions of Fe(NO₃)₃·9H₂O and Zn(NO₃)₂·6H₂O, Mn(NO₃)₂·4H₂O or Cu(NO₃)₂·3H₂O (total metal content - 8 wt%; Fe/M = 2 (M = Zn, Mn or Cu)). The precursor decomposition was carried out in nitrogen flow at 773 K. For comparison similar modifications of mesoporous silica type KIT-6 [19] were obtained. The samples are denoted as CuFe/S, MnFe/S and ZnFe/S, where S stands for ACP or KIT-6 support.

The texture characteristics were determined by low-temperature nitrogen adsorption in a Quantachrome Instruments NOVA 1200e (USA) apparatus. Powder X-ray diffraction patterns were collected on Bruker D8 Advance diffractometer with Cu K α radiation and LynxEye detector. The UV-Vis spectra were recorded on the powder samples using a Jasco V-650 apparatus. The IR spectra (KBr pellets) were recorded on a Bruker Vector 22 FTIR spectrometer. The Mossbauer spectra were obtained in air at room temperature

with a Wissel (Wissenschaftliche Elektronik GmbH, Germany) electromechanical spectrometer using ⁵⁷Co/Rh source and α -Fe standard. The TPR/TG analyses were performed on a Setaram TG92 instrument in a flow of 50 vol% H₂ in Ar (100 cm³ min⁻¹) and heating rate of 5 K min⁻¹.

Methanol conversion was carried out in a fixed bed flow reactor (0.055 g of catalyst), argon being used as a carrier gas (50 cm³.min⁻¹). The methanol partial pressure was 1.57 kPa. The catalysts were tested under conditions of a temperature-programmed regime within the range of 350–770 K with heating rate of 1 K.min⁻¹. On-line gas chromatographic analyses were performed on HP apparatus equipped with flame ionization and thermo-conductivity detectors, on a PLOT Q column, using an absolute calibration method and a carbon based material balance.

RESULTS AND DISCUSSION

Texture and structure characterization

Nitrogen physisorption isotherms of parent and ferrite modified ACP are of type I-IV according to the IUPAC classification which is typical of materials with well developed micro-mesoporous texture (not presented). The calculated parameters (Table 1) reveal that all ACP based materials are characterized with high surface area (960–1260 m².g⁻¹) and pore volume of 0.4–0.6 cm³.g⁻¹, mainly determined by the presence of micropores (V_{mes}/V_{mic} is about 0.3). The significant decrease in the BET surface area and pore volume of ACP after the modification evidences pore blocking due to metal particles deposition. The slight decrease in the V_{mes}/V_{mic} for CuFe/ACP and ZnFe/ACP as compared to pure ACP (Table 1) indicates a preferable location of metal species into the mesopores, while blocking of micropores in higher extent is considered for MnFe/ACP.

Table 1. Nitrogen physisorption data: S_{BET} (specific surface area), S_{mi} (specific surface area of micropores), V_t - total pore volume, V_{mi} - micropore volume, D_{av} - average pore diameter).

Sample	S_{BET} , m ² /g	S_{mi} , m ² /g	V_t , cm ³ /g	V_{mi} , cm ³ /g	D_{av} nm	ΔS_{BET} , %	ΔV_{tot} , %	V_{mes}/V_{mic}
ACP	1258	1116	0.61	0.44	1.9			0.35
CuFe/ACP	994	885	0.49	0.37	1.9	21	20	0.32
MnFe/ACP	1004	893	0.49	0.35	1.9	20	20	0.40
ZnFe/ACP	965	866	0.46	0.35	1.9	23	24	0.31
KIT-6	872	278	1.23	0.14	8.1			7.78
CuFe/KIT-6	744	197	1.07	0.10	5.8	15	13	9.70
ZnFe/KIT6	561	108	0.80	0.05	5.7	36	35	15.00
MnFe/KIT-6	800	106	1.20	0.05	6.0	8	2	23.00

For comparison, the nitrogen physisorption isotherms of KIT-6 silica are of IV type with well pronounced step in the 0.6–0.8 partial pressure range and type I hysteresis loop (not shown), which reveals presence of cylindrical and almost uniform mesopores (Table 1). The changes in the textural parameters after KIT-6 modification are indication for some differences in the location of metal species within the silica porous structure. Almost random blocking of micro and mesopores could be assumed for CuFe/KIT-6, while preferable location into the micropores seems to be realized for ZnFe/KIT-6, and even in higher extent for MnFe/KIT-6 (Table 1).

The XRD patterns of parent ACP and its modifications (Fig. 1a) contains well defined reflections at about 25° and 45° 2θ which according to *Liou and Wu* [20] are due to the turbostratic structure in AC. The preservation of the reflections after the modification reveals absence of significant structural collapse of the support, which is in agreement with the nitrogen physisorption data (Table 1). All additional reflections at 30.1° , 35.3° , 42.6° , 52.9° , 56.7° and 62.7° in the pattern of ZnFe/ACP could be indexed to (220), (311), (400), (422), (511) and (440) planes of cubic ZnFe_2O_4 ferrite (pdf 089-1010) with average crystallite size of about 7 nm. The XRD pattern of parent KIT-6 (Fig. 1b, inset) represents two well-distinguished reflections in the small-angle region, which could be assigned to the (211) and (220) planes of 3-D cubic structure of high quality material. The preservation of these main reflections after the modification procedures (not presented) reveals absence of structural collapse with the silica support. The XRD pattern of ZnFe/KIT-6 represents reflections of $\alpha\text{-Fe}_2\text{O}_3$ and ZnFe_2O_4 phases with average crystallite size of 11–13 nm (Fig. 1b). Taking into account the nitrogen physisorption data (Table 1), one could be assumed that the blocking of micropores of silica support during the active phase deposition renders difficult the formation of ferrite phase and leads to segregation of relatively large hematite and ferrite particles on the external surface or nearby the pore openings. The broad reflections at about 34.6° , 35.9° , 37.1° , 41.6° , 43.6° , 58.0° , 62.0° , 63.8° and 74.7° 2θ in the pattern of CuFe/ACP (Fig. 1a) could be indexed as (103), (211), (202), (004), (220), (321), (224), (400) and (413) diffractions of cubic CuFe_2O_4 (pdf 077-0427) with average crystallite size of 8 nm. An addition, impurity peaks of metallic Cu (pdf 085-1326) with average crystallite

size of 2 nm is also distinguished, probably due to the reduction activity of carbon support during the preparation procedure. On contrary, the absence of any reflections in CuFe/KIT-6 pattern (Fig. 1b) reveals higher dispersion of loaded metal oxide phase in the silica matrix, probably due to its stabilization into the support mesopores (Table 1). The broad diffraction reflections in the pattern of MnFe/ACP correspond to face centered cubic MnFe_2O_4 (pdf 074-2403) with average crystallite size of 4 nm. It seems that the blocking of active phase into the micropores of silica support (Table 1, Fig. 1b) provokes the formation of highly dispersed amorphous phase in MnFe/KIT-6.

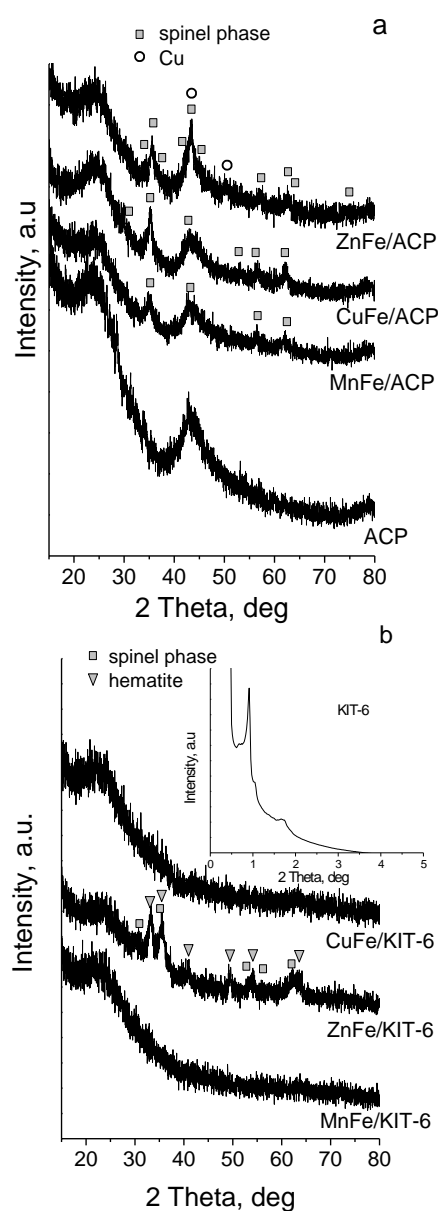


Fig. 1. XRD patterns of ACP (a) and KIT-6 (b) based samples before the catalytic test. Inset: low angle XRD pattern of KIT-6.

Spectroscopic measurements

FTIR spectra (Fig. 2) and Boehm method [17] are used for the characterization of AC surface functionality. The bands at *c.a.* 1360 cm^{-1} and 3000–2800 cm^{-1} could be assigned to asymmetric and symmetric $-\text{C}-\text{H}$ stretching vibrations in aliphatic groups, while the strong band at around 1552 cm^{-1} is assigned to the vibrations in $-\text{C}-\text{C}-$ aromatic bonds and $\text{C}-\text{O}-\text{O}-$ structures [14].

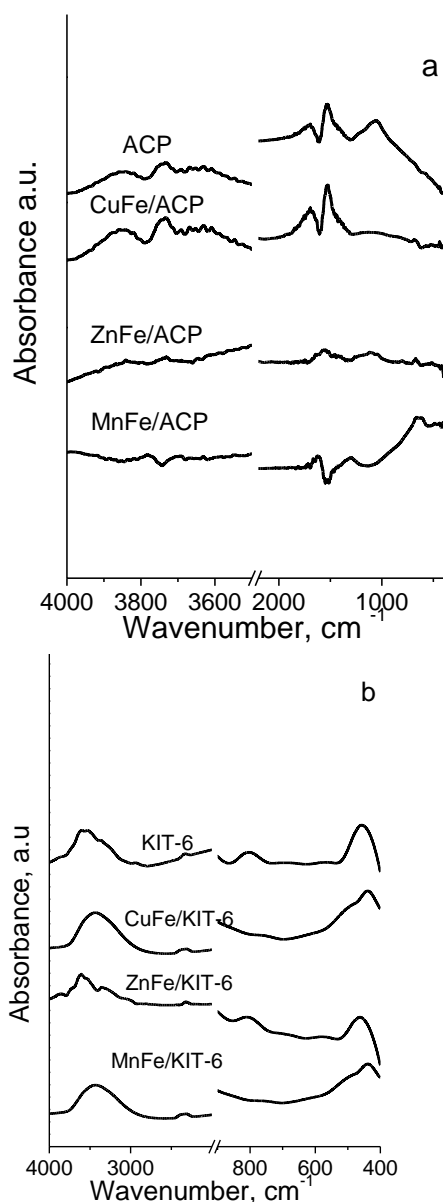


Fig. 2. FTIR spectra of ACP (a) and KIT-6 (b) ferrite modifications.

The band at *c.a.* 1044 cm^{-1} represents $\text{C}-\text{O}$ stretching vibrations and the existence of a shoulder to the main peak is usually assigned to the positional differences among these functional

groups. The observed decrease in the intensity of the absorption band at around 1550 cm^{-1} for CuFe/ACP and MnFe/ACP and at 1044 cm^{-1} for ZnFe/ACP could be due to the interaction of metal oxide species with π -electron structure and oxygen groups of carbon structure, respectively [21]. The band at 800–600 cm^{-1} can be attributed to $\text{C}-\text{C}$ bending vibrations in aromatic and non-aromatic structures. The broad absorbance in the region 3644–3026 cm^{-1} is associated to residual water or $-\text{O}-\text{H}$ stretching vibration mode of hydrogen bonded hydroxyl groups [14, 22]. The additional study by Boehm method reveals predominant presence of surface basic groups (1.04 mmol/g) as well as carbonyl (1.07 mmol/g) and hydroxyl (0.04 mmol/g) acidic ones. The appearance of two well pronounced bands at *c.a.* 600–500 cm^{-1} and 400–430 cm^{-1} in the FTIR spectra of CuFe/ACP and ZnFe/ACP (Fig. 2a) could be due to $\text{M}-\text{O}$ stretching vibrations of metal ions in tetrahedral and octahedral positions in ferrite phase, respectively [22]. In case of MnFe/ACP, the presence of only one and broad band at *c.a.* 566 cm^{-1} slightly doubt the formation of ferrite phase and we'll return to this point with the Moessbauer spectroscopic study. For comparison, well pronounced bands, typical of ferrite phase, could be distinguished in the FTIR spectra of CuFe/KIT-6 and MnFe/KIT-6 (Fig. 2b). In consistence with the XRD data, the increased absorption at *c.a.* 566 cm^{-1} in the spectrum of ZnFe/KIT-6 could be ascribed to the co-existing of hematite and spinel phases [23]. The UV-Vis spectra of CuFe/KIT-6, ZnFe/KIT-6 and MnFe/KIT-6 represent absorption edges at 386, 518 and 391 nm, respectively which could be assigned to the presence of the corresponding ferrite particles. The significant deviation of the values for ZnFe/KIT-6 from the reported in the literature ones [24] could be assigned to the presence of impurities of Fe_2O_3 , in consistence with the XRD and FTIR data (see above). Unfortunately the UV-Vis spectra of ACP based materials are not sufficiently representative. In order to obtain more information for the state of loaded ferrite phase in the parent materials and the changes with it during the catalytic test, room temperature Moessbauer spectra are collected and presented in Figs. 3a and 3b, respectively. The characteristic parameters: isomer shift (IS), quadruple splitting (QS), effective internal magnetic field (H_{eff}), the line width (FWHM) and the relative weight of each component (G), are presented in Table 2. The Moessbauer spectrum of parent CuFe/ACP (Fig. 3a. Table 2) represents superposition of doublet (Db)

and 3 sextets (Sx). The parameters of Sx1 and Sx2 correspond to tetrahedral and octahedral coordination of iron ions in magnetite structure, respectively. However, the presence of quadruple splitting, especially for octahedral coordinated iron (Sx2), shows that the magnetite is copper substituted. The third sextet component (Sx3) with low hyperfine field and broad line width might be attributed to additive effects of smaller magnetite particles, Fe^{3+} ions at the interface of non-structured CuFe_2O_4 and/or Fe^{3+} ions surrounded by more vacancies (and/or Cu^{2+} ions) [25]. The Db part of the spectrum indicates presence of finely dispersed (below 10–12 nm) Fe^{3+} containing nanoparticles with superparamagnetic (SPM) behavior. Obviously the carbon support promotes segregation of reduced phases (Cu^0 and $\text{Cu}_x\text{Fe}_{3-x}\text{O}_4$) and restricts the formation of stoichiometric copper ferrite phase and (Fig. 3a) this is also confirmed by the XRD analyses (Fig. 1b). After the catalytic test (Fig. 3b, Table 2), new sextet component attributable to Fe_3C appears. On the base of relative weight of each component, phase transformations with the highly defective $\text{Cu}_x\text{Fe}_{3-x}\text{O}_4$ particles under the influence of the reductive reaction medium could be assumed. For comparison, the Moessbauer spectrum of $\text{CuFe}/\text{KIT-6}$ represents only doublet. This tendency of stabilization of more finely dispersed phase into the micro/mesopores of silica support is confirmed with the XRD and nitrogen physisorption measurements. Note that no changes with the active phase could be mentioned after the

catalytic test (Fig. 3b, Table 2). The spectrum of parent MnFe/ACP is well fitted with two sextets (Fig. 3a, Table 2). The broadening of both sextets could be explained with presence of particles with different size [25]. Formation of MnFe_2O_4 phase is also detected by XRD (Fig. 1a). The relatively high Db part in the Moessbauer spectrum of MnFe/ACP (about 78%) reveals presence of finely dispersed (below 10–12 nm) Fe^{3+} containing species. This is not surprised, taking account that these species are blocked predominantly into the micropores of ACP support (Table 1). This tendency is more pronounced for the MnFe/KIT sample, where the Moessbauer spectrum consists only of Db component. After the catalytic test (Fig. 3b, Table 2), the ferrite phase in parent MnFe/ACP , corresponding to the Sx component in the spectrum, is almost fully decomposed to magnetite. Just the opposite, no changes with the active phase could be assumed for $\text{MnFe}/\text{KIT-6}$. The spectrum of parent ZnFe/ACP (Fig. 3a, Table 2) represents a quadruple doublet with hyperfine parameters characteristic for $\text{Zn}_x\text{Fe}_{3-x}\text{O}_4$ ferrite with relatively high Zn content ($x > 0.8$) [26]. The preservation of the spectrum after the catalytic test (Fig. 3b, Table 2) indicates stability of the ferrite phase under the reaction medium. For comparison, the Moessbauer spectrum of $\text{ZnFe}/\text{KIT-6}$ (Fig. 3a, Table 2) is superposition of 3 sextets. The parameters of Sx1 with relative weight of 15% correspond to Fe_2O_3 [26], in consistent with XRD data. The other two

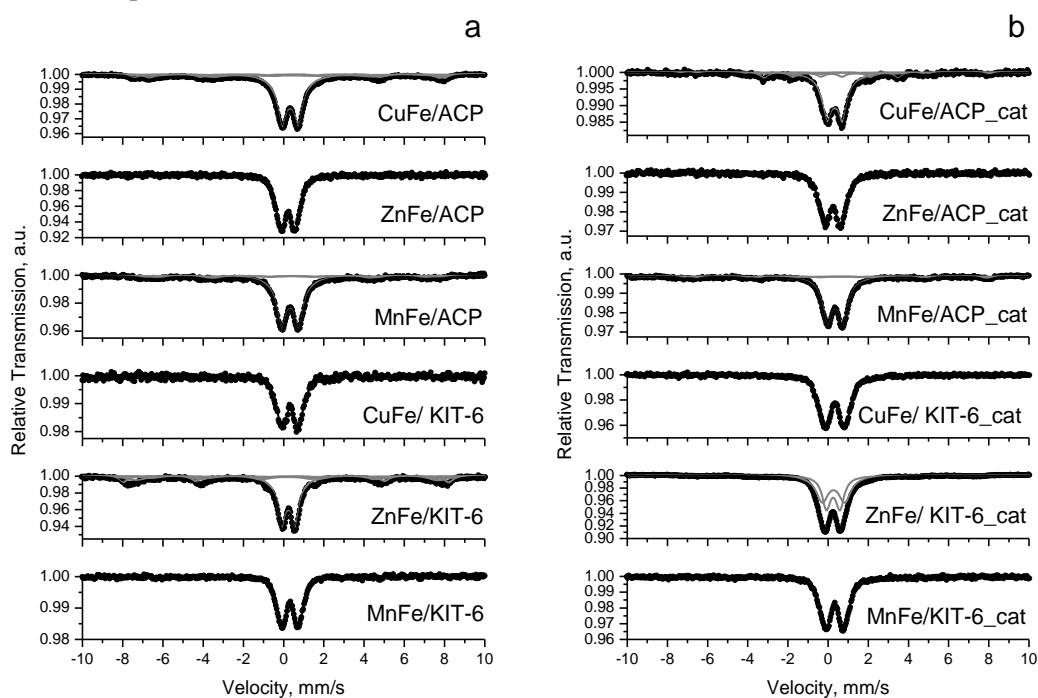


Fig. 3. Moessbauer spectra of all modifications before (a) and after (b) the catalytic test.

Table 2. Moessbauer parameters of ACP and KIT-6 modifications before and after (cat) the catalytic test.

Sample	Components	IS, mm/s	QS, mm/s	H _{eff} , T	FWHM, mm/s	G, %
CuFe/ACP	Sx1-Fe ³⁺ _{tetra} , Cu _x Fe _{3-x} O ₄	0.30	-0.03	48.0	0.53	8
	Sx2-Fe ^{2.5+} _{octa} , Cu _x Fe _{3-x} O ₄	0.58	-0.10	44.8	0.58	9
	Sx3-Cu _x Fe _{3-x} O ₄	0.40	0.06	40.2	1.80	18
	Db- SPM	0.33	0.81	-	0.62	65
ZnFe/ACP	Db - Fe ³⁺ _{octa} , Zn _x Fe _{3-x} O ₄	0.35	0.74	-	0.58	100
MnFe/ACP	Sx1-Fe ³⁺ _{tetra} , MnFe ₂ O ₄	0.44	0.00	45.9	0.90	9
	Sx2-Fe ³⁺ _{octa} , MnFe ₂ O ₄	0.40	0.00	41.0	0.90	13
	Db-SPM	0.32	0.86	-	0.62	78
CuFe/ KIT-6	Db-SPM	0.32	0.82	-	0.60	100
ZnFe/KIT-6	Sx1 - Fe ³⁺ _{octa} - α-Fe ₂ O ₃	0.33	-0.11	50.4	0.50	15
	Sx2 - Fe ³⁺ _{tetra} - Zn _x Fe _{3-x} O ₄	0.30	0.00	46.6	1.00	21
	Sx3 - Fe ^{2.5+} _{octa} - Zn _x Fe _{3-x} O ₄	0.64	0.00	43.5	1.20	10
	Db - Zn _y Fe _{3-x} O ₄	0.34	0.67	-	0.51	54
MnFe/KIT-6	Db-SPM	0.32	0.84	-	0.55	100
CuFe/ACP_cat	Sx1-Fe ³⁺ _{tetra} , Fe _{3-x} O ₄	0.28	0.00	47.5	0.45	4
	Sx2-Fe ^{2.5+} _{octa} , Fe _{3-x} O ₄	0.80	0.00	45.4	0.45	5
	Sx3-Fe ₃ C	0.16	0.00	20.7	0.47	17
	Db- SPM	0.34	0.76	-	0.65	74
CuFe/ KIT-6_cat	Db-SPM	0.34	1.00	-	0.68	100
ZnFe/ACP_cat	Db - Fe ³⁺ _{octa} , Zn _x Fe _{3-x} O ₄	0.34	0.80	-	0.64	100
ZnFe/ KIT-6_cat	Db1 - Fe ³⁺ _{octa} , Zn _x Fe _{3-x} O ₄	0.36	0.68	-	0.50	46
	Db2 - SPM	0.37	1.12	-	0.73	54
MnFe/ACP_cat	Sx1-Fe ³⁺ _{tetra} , Fe _{3-x} O ₄	0.28	0.00	46.4	0.50	5
	Sx2-Fe ^{2.5+} _{octa} , Fe _{3-x} O ₄	0.74	-0.03	45.2	0.54	8
	Db- SPM	0.36	0.79	-	0.61	87
MnFe/KIT-6_cat	Db-SPM	0.33	0.92	-	0.62	100

sextets with relatively high FWHM and G = 31 % could be assigned to non-stoichiometric Zn_xFe_{3-x}O₄ ferrite with relatively low Zn content [26]. The parameters of Db part of the spectrum are typical of ferrite phase with high degree of Zn substitution. The changes in the spectrum after the catalytic test (Fig. 3b, Table 2) reveal reduction transformation of the active phase under the reaction medium with the formation of finely dispersed iron oxides and/or carbides (Table 2).

TPR study

The TPR method is a feasible, but sometimes difficult for the interpretation, approach to characterize the oxidative state of metallic ions and the defectiveness of metal oxide crystal lattice. In Fig. 4 are presented TPR-TG and TPR-DTG profiles of all ACP and KIT-6 modifications. The reduction decomposition of CuFe/KIT-6 to Cu⁰ and magnetite starts at 450 K followed by fast magnetite reduction to metallic iron [27]. The appearance of only one reduction effect with a maximum at 593 K confirms the facilitated reduction of magnetite due to the spillover of

activated on copper species hydrogen [28]. The reduction profile of CuFe/ACP exhibits two well distinguished peaks indicating complex composition of the loaded metal phase. This result well corresponds to the XRD and Moessbauer data (Fig. 1, Table 2) for the co-existence of Cu and partially reduced Cu_xFe_{3-x}O₄ and confirms the obstructive role of AC support for the stoichiometric copper ferrite formation. The reduction decomposition of MnFe₂O₄ to MnO and magnetite and its further reduction to metallic iron is about 130 K shifted to higher temperatures as compared to CuFe/KIT-6. The absence of well distinguished additional low temperature effects and the symmetry of the main TPR-DTG effect clearly indicate the uniformity of the loaded into the micropores of silica support MnFe₂O₄ species, as was also seen from the nitrogen physisorption, XRD and Moessbauer data. The TPR-TG profile of MnFe/ACP demonstrates not only easier reduction decomposition of loaded MnFe₂O₄ phase, but also some significant changes with the AC above 700 K, most probably promoted by the formation of metallic Fe⁰. Contrary to other KIT-6 loaded ferrites, TPR-DTG profile of ZnFe/KIT-6 consists

of two overlapping effects, which in consistent with the XRD and Moessbauer measurements, could be due to the reduction of a mixture of Fe_2O_3 and ZnFe_2O_4 . The reduction transformation of ZnFe_2O_4 seems to be facilitated on the ACP support and similarly to MnFe/ACP and CuFe/ACP , here significant changes with ACP occur above 700 K.

Catalytic tests

In Fig. 5a is presented the evolution of methanol decomposition on various modifications with the temperature increase. All materials exhibit catalytic activity above 600 K and CO, CH_4 and CO_2 in different proportion (Fig. 5b) are the only detected carbon-containing products. Among the KIT-6 based materials, the best catalytic activity with relatively high selectivity to CO and CH_4 is detected for CuFe/KIT-6 . According to the XRD, Moessbauer and nitrogen physisorption measurements (Fig. 1, Tables 1 and 2) this could be assigned to the formation of finely dispersed CuFe_2O_4 particles, almost randomly distributed in the micro-mesopores of the silica matrix. The latter stabilizes them also against phase transformations under the reaction medium as was illustrated by the Moessbauer analyses (Fig. 3b, Table 2). We could speculate that the preferable location of copper ions on the most exposed to the reactants octahedral positions in the inverse CuFe_2O_4 spinel structure provokes the activity of $\text{Cu}^{2+}\text{-Cu}^{1+}$ redox pairs, which ensure high catalytic activity at relatively low temperature. However the Cu-Fe modification does not exhibit high catalytic activity when ACP is used as a host matrix. In accordance with the physicochemical measurements, this could be due to the limited formation of CuFe_2O_4 on the support with high reduction ability, like ACP. Here, during the catalyst preparation procedure, segregation of relatively large and low active Cu^0 and defective $\text{Cu}_x\text{Fe}_{3-x}\text{O}_4$ nanoparticles, which also change under the reaction medium to Fe_3C (Fig. 3b, Table 2), is observed. Obviously, the predominant location of Zn^{2+} ions on tetrahedral positions of normal ZnFe_2O_4 spinel provides the activity of $\text{Fe}^{3+}\text{-Fe}^{2+}$ redox pairs, situated on the octahedral position. The predominant location of metal oxide species into the mesopores of ACP seems to facilitate their intimate contact leading to the formation of finely dispersed ZnFe_2O_4 (Figs.1 and 3a, Tables 1 and 2). More over, the significantly low reduction ability of this ferrite phase (Fig. 4) ensures its preservation against decomposition under the reduction reaction medium even in the presence of carbon support and

this is well illustrated by the Moessbauer spectra after the catalytic test (Fig. 3b, Table 2). This provides extremely high catalytic activity for ZnFe/ACP (Fig. 5). In accordance with the nitrogen physisorption, Moessbauer and XRD measurements (Tables 1 and 2 and Figs. 1 and 3a), it could be concluded that the blocking of active phase in the micropores of KIT-6 support renders difficult the formation of ZnFe_2O_4 phase and provokes segregation of less active individual Fe_2O_3 . In case of mixed MnFe_2O_4 spinel ferrite (Fig. 5), the partial substitution of Mn^{2+} ions in tetrahedral position forces the migration of Fe^{2+} ions in octahedral one, which ensures the activity of $\text{Fe}^{2+}\text{-Fe}^{3+}$ redox pairs.

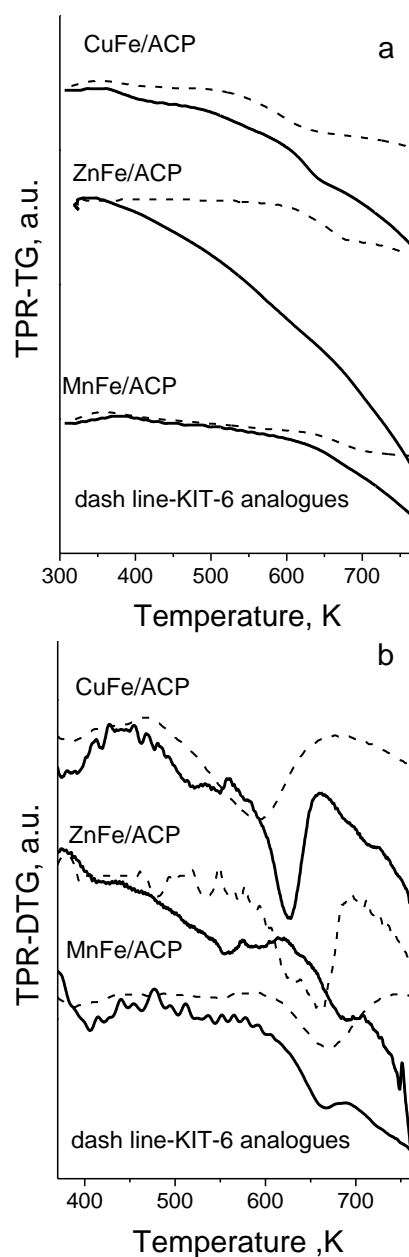


Fig. 4. TPR-TG (a) and TPR-DTG (b) data for ACP and KIT-6 modifications.

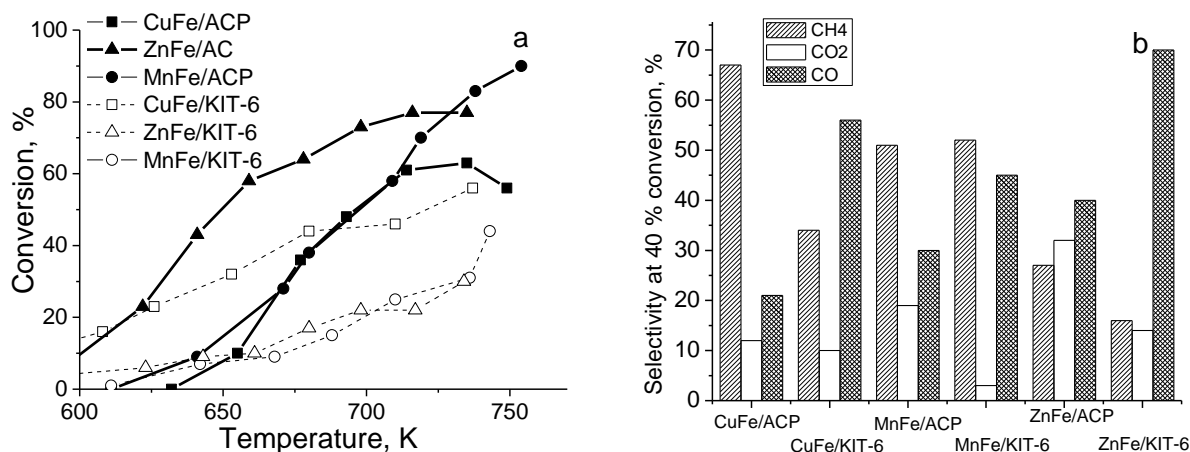


Fig. 5. Temperature dependency of methanol conversion (a) and products distribution at 40% conversion (b) for various samples.

On contrary to ZnFe_2O_4 , we expect that the substitution with larger Mn^{2+} ions expands the spinel lattice, which suppresses the electron exchange in the Fe^{2+} - Fe^{3+} redox pairs and leads to lower catalytic activity and some differences in the selectivity. The significantly lower catalytic activity of MnFe_2O_4 species, hosted in the KIT-6 as compared to ACP is probably provoked by their lower accessibility for the reactant molecules due to the predominant location in the micropores of silica matrix (Table 1).

CONCLUSION

Activated carbon obtained from agriculture residues (peach stones) could be suitable host matrix for the stabilization of finely dispersed ferrite nanoparticles. Their formation is strongly controlled by the texture characteristics and the reduction properties of carbon support. ZnFe_2O_4 is appropriate ferrite phase for the preparation of highly active catalysts for methanol decomposition.

Acknowledgements: Financial support Bulgarian Scientific Fund, project FNI E02/2/2014, is acknowledged.

REFERENCES

1. A. Pohar, D. Belavi, G. Dolan, S. Hocevar, *J. Power Sources*, **256**, 80 (2014).
2. S. T. Yong, C. W. Ooi, S. P. Chai, X. S. Wu, *Int. J. Hydrogen Energy*, **38**, 9541 (2013).
3. A. Evdou, V. Zaspalis, L. Nalbandian, *Fuel*, **165**, 367 (2016).
4. M. Santiago, K. Barbera, C. Ferreira, D. Curulla-Ferré, P. Kolb, J. Pérez-Ramírez, *Catal. Commun.*, **21**, 63 (2012).
5. M. Pori, B. Likozar, M. Marinšek, Z. C. Orel, *Fuel Proc. Technol.*, **146**, 39 (2016).
6. E. Manova, T. Tsoncheva, D. Paneva, J. L. Rehspringer, K. Tenchev, I. Mitov, L. Petrov, *Appl. Catal. A: General*, **317**, 34 (2007).
7. T. Tsoncheva, E. Manova, N. Velinov, D. Paneva, M. Popova, B. Kunev, K. Tenchev, I. Mitov, *Catal. Commun.*, **12**, 105 (2010).
8. E. Manova, T. Tsoncheva, D. Paneva, M. Popova, N. Velinov, B. Kunev, K. Tenchev, I. Mitov, *J. Solid State Chem.*, **184**, 1153 (2011).
9. N. Velinov, E. Manova, T. Tsoncheva, C. Estournès, D. Paneva, K. Tenchev, V. Perkova, K. Koleva, B. Kunev, I. Mitov, *Solid State Sci.*, **14**, 1092 (2012).
10. N. Velinov, K. Koleva, T. Tsoncheva, E. Manova, D. Paneva, K. Tenchev, B. Kunev, I. Mitov, *Catal. Commun.*, **32**, 41 (2013).
11. H. Xue, Z. Li, X. Wang, X. Fu, *Mater. Lett.*, **61**, 347 (2007).
12. D. H. K. Reddy, Y.-S. Yun, *Coord. Chem. Rev.*, **315**, 90 (2016).
13. M. S. Podder, C. B. Majumder, *Ground water Sust. Devel.*, **2-3**, 53 (2016).
14. K.-W. Jung, B. Hyun Choi, M.-J. Hwang, T.-U. Jeong, K.-H. Ahn, *Biores. Technol.*, **219**, 185 (2016).
15. T. Tsoncheva, I. Genova, D. Paneva, M. Dimitrov, B. Tsyntsarski, N. Velinov, R. Ivanova, G. Issa, D. Kovacheva, T. Budinova, I. Mitov, N. Petrov, *Solid State Sci.*, **48**, 286 (2015).
16. B. Tsyntsarski, I. Stoycheva, T. Tsoncheva, I. Genova, M. Dimitrov, B. Petrova, D. Paneva, Z. Cherkezova-Zheleva, T. Budinova, H. Kolev, A. Gomis-Berenguer, C. O. Ania, I. Mitov, N. Petrov, *Fuel Process. Technol.*, **137**, 139 (2015).

17. T. Tsoncheva, A. Mileva, D. Paneva, D. Kovacheva, I. Spassova, D. Nihtianova, P. Markov, N. Petrov, I. Mitov, *Micropor. Mesopor. Mater.*, **229**, 59 (2016).
18. T. Tsoncheva, I. Genova, M. Stoyanova, M. Pohl, R. Nickolov, M. Dimitrov, E. Priboczki, M. Mihaylov, D. Kovacheva, K. Hadjiivanov, *Appl. Catal. B: Env.*, **147**, 684 (2014).
19. H. P. Boehm, Chemical Identification of Surface Groups, *Adv. Catal. Related Subjects*, **16**, 179 (1966).
20. T. H. Liou, S. J. Wu, *J. Hazard. Mater.*, **171**, 693, (2009).
21. F. Rodriguez-Reinoso, *Carbon*, **36**, 159 (1998).
22. S. Briceño, W. Escamilla, P. Silva, J. García, H. Del Castillo, M. Villarroel, J. P. Rodriguez, M. A. Ramos, R. Morales, Y. Diaz, *J. Magnet. Magnet. Mater.*, **360**, 67 (2014).
23. M. Florea, M. Alifanti, V. I. Parvulescu, D. Mihaila-Tarabasanu, L. Diamandescu, M. Feder, C. Negri, L. Frunza, *Catal. Today*, **141**, 361 (2009).
24. X. Li, Y. Hou, Q. Zhao, L. Wang, *J. Coll. Int. Sci.*, **358**, 102 (2011).
25. R. Olar, M. Badea, L. Diamandescu, E. Cristurean, D. Marinescu, D. Mihaila-Tarabasanu, N. Stanica, M. Brezeanu, *J. Alloys Comp.*, **363**, 262 (2004).
26. J. A. Zawicki, H. A. Allsop, *J. Nuclear. Mater.*, **240**, 22 (1996).
27. N. Thouchprasitchai, A. Luengnaruemitchai, S. Pongstabodee, *J. Ind. Eng. Chem.*, **19**, 1483 (2013).
28. Z. H. Chonco, L. Lodya, M. Claeys, E. van Steen, *J. Catal.*, **308**, 363 (2013).

КАТАЛИЗАТОРИ ЗА ОСВОБОЖДАВАНЕ НА ВОДОРОД ОТ МЕТАНОЛ НА ОСНОВАТА НА МЕДЕН, ЦИНКОВ И МАНГАНОВ ШПИНЕЛНИ ФЕРИТИ, НАНЕСЕНИ ВЪРХУ АКТИВЕН ВЪГЛЕН ОТ ОТПАДНА БИОМАСА

Т. С. Цончева^{1*}, Г. С. Исса¹, А. Б. Милева¹, Р. Н. Иванова¹, М. Д. Димитров¹, И. П. Спасова², Д. Г. Ковачева², Д. Г. Панева³, Н. И. Велинов³, Б. Г. Цинцарски¹, Н. В. Петров¹

¹ *Институт по органична химия с Център по фитохимия, Българска академия на науките, 1113 София, България*

² *Институт по обща и неорганична химия, Българска академия на науките, 1113 София, България*

³ *Институт по катализ, Българска академия на науките, 1113 София, България*

Постъпила на 13 февруари 2017 г.; Коригирана на 06 март 2017 г.

(Резюме)

Активен въглен, получен от костилки от праскови, е използван като носител на наноразмерни MFe_2O_4 ($M = Cu, Zn, Mn$) шпинелни ферити. Получените композити са характеризирани с физисорбция на азот, рентгеноструктурен анализ, УВ, ФТИР и Мьосбауерова спектроскопии и ТПР с водород. Каталитичното поведение на образците е изследвано в разлагане на метанол, с оглед потенциалното му приложение като носител на водород. Катализаторите, получени на основата на активен въглен, показват по-висока активност, но по-ниска селективност до синтез газ, в сравнение с аналозите им, получени при използването на мезопорест силикат. $ZnFe_2O_4$ е най-подходяща активна фаза върху активен въглен, докато $CuFe_2O_4$ показва най-висока активност върху силикатен носител. Дискутирана е подробно ролята на различните носители върху формирането на каталитично активната фаза.

Total oxidation of ethyl acetate on nanostructured manganese-cerium oxide catalysts supported on mesoporous silica

R. N. Ivanova*, T. S. Tsoncheva

Institute of Organic Chemistry with Centre of Phytochemistry, Bulgarian Academy of Sciences, 1113 Sofia, Bulgaria

Received February 21, 2017; Revised March 08, 2017

Dedicated to Acad. Bogdan Kurtev on the occasion of his 100th birth anniversary

Current investigation is focused on the texture effect of mesoporous silica support on the structure, redox and catalytic properties of hosted in it nanosize mono- and bi-component manganese-cerium oxides. Mesoporous silicas type SBA-15 and KIT-6 with uniform cylindrical mesopores, packed in 2D- and 3D-symmetry respectively, was used as a support. A complex of physicochemical techniques, such as nitrogen physisorption, X-ray diffraction, UV-Vis spectroscopy and temperature-programmed reduction with hydrogen were used for the samples characterization. The potential application of the composites as catalysts for ethyl acetate combustion was studied. It was demonstrated that SBA-15 and KIT-6 could be good host matrix for the stabilization of highly dispersed manganese-ceria oxide particles. Strong effect of mesoporous silica support topology, which also depends on the samples composition, on the formation of catalytic active sites was established.

Key words: manganese-cerium oxides; SBA-15 and KIT-6 mesoporous silica; ethyl acetate oxidation

INTRODUCTION

Volatile organic compounds (VOCs) are considered as one of the major pollutants emitted from the industrial processes, transport and human activity and most of them are identified as carcinogenic and teratogenic [1]. Nowadays, the increasing political, social and economic attention on the environment and the quality of life has enforced the strict monitoring of VOCs emission and the development of efficient technologies for their elimination. The catalytic total oxidation has been recognized as more economic process even when VOCs were emitted in low concentrations [2–7]. It works at relatively lower operation temperatures and with higher efficiency compared to thermal combustion techniques, avoiding the supplementary use of fuel and reducing air contamination due to NO_x formation [1, 8]. Despite noble metals are commonly used catalysts owing to their high catalytic activity, transition metal oxides could be also good alternative due to their low cost, accessibility and stability to different pollutants [1]. During the last decade the efforts have been directed to the increase in their catalytic activity by the miniaturization in nanoscale and mesoporous silicas were considered as a suitable host matrix for the preparation and stabilization of metal oxide

nanoparticles. It was reported that ceria-based catalysts exhibit high activity in VOCs oxidation due to their unique high oxygen storage capacity associated with facile Ce⁴⁺/Ce³⁺ redox transition [8, 9]. Manganese oxide materials are also known as efficient catalysts for various redox processes due to the multivalent state of Mn ions [1, 10]. Obviously, this provides good catalyst potential of Ce–Mn mixed oxides and their behaviour has already been tested in number of catalytic processes, such as complete oxidation of ethanol [3], formaldehyde, hexane [11], selective catalytic reduction (SCR) of NO with NH₃ [12] catalytic oxidation of diesel soot [13] *etc.* In this study, we focused our attention on the development of nanostructured Mn–Ce mixed oxides by their deposition on mesoporous silica support. The pore topology effect on the control of phase composition and catalytic behaviour of Mn–Ce oxides was studied using mesoporous silicas with almost uniform cylindrical pores arranged in 2D- (SBA-15) or 3D- (KIT-6) structure as a support. The catalytic activity of the obtained composites was tested in ethyl acetate combustion.

EXPERIMENTAL

Materials

SBA-15 and KIT-6 mesoporous silicas were prepared by hydrothermal synthesis at 373K using

* To whom all correspondence should be sent:
E-mail: rivanova@orgchm.bas.bg

Pluronic P123 triblock-co-polymer (EO₂₀PO₇₀EO₂₀) as structure-directing agent according to the procedures described in [14] and [15], respectively. The silica modification was carried out by incipient wetness impregnation technique using 1.2 M aqueous solution of Mn(NO₃)₂·4H₂O and/or Ce(NO₃)₂·6H₂O. The impregnated samples were dried at room temperature for 24 h and then treated in air at 773K for 2 h for precursor decomposition. The metal content in all modifications was set to be 6 wt.%. The obtained materials were denoted as xMnyCe/S, where x/y represents the Mn/Ce ratio and S is the silica support used (SBA-15 or KIT-6).

Methods of characterization

The nitrogen physisorption data were obtained by nitrogen adsorption at 77 K on Quantachrome NOVA 1200 apparatus. S_{BET} was calculated applying the Brunauer, Emmet and Teller (BET) equation for N₂ relative pressure in range of 0.05/P/P₀ < 0.30, and the pore size distribution was determined by the DFT method applied to the adsorption branch of the isotherm. The t-plot method was used for the estimation of micropores parameters. The powder X-ray diffraction spectra were recorded within the range from 1° to 80° 2 θ with on a Bruker D8 Advance diffractometer with Cu K α radiation. The UV-Vis spectra were recorded on the powder samples using a Jasco V-650 UV-Vis spectrophotometer equipped with a diffuse reflectance unit. The TPR/TG (temperature-programmed reduction/thermo-gravimetric) analyses were performed on a Setaram TG92 instrument in a flow of 50 vol% H₂ in Ar (100 cm³/min⁻¹) and heating rate of 5 K/min⁻¹. The catalytic experiments were performed in a flow type reactor (0.030 g of catalyst) with a mixture of ethyl acetate (1.21 mol%) in air with WHSV – 335 h⁻¹. Gas chromatographic (GC) analyses were carried out on HP5850 apparatus using carbon-based calibration. The samples were pretreated in Ar at 423K for 1 h and then the temperature was raised with a rate of 2K/min in the range of 423–773K.

RESULTS AND DISCUSSION

Nitrogen physisorption measurements were conducted in order to elucidate the textural properties of the studied samples. In Fig. 1 are presented nitrogen physisorption isotherms for both SBA-15 and KIT-6 silica supports and their mono-

and bi-component Mn-Ce modifications. The texture parameters are listed in Table 1.

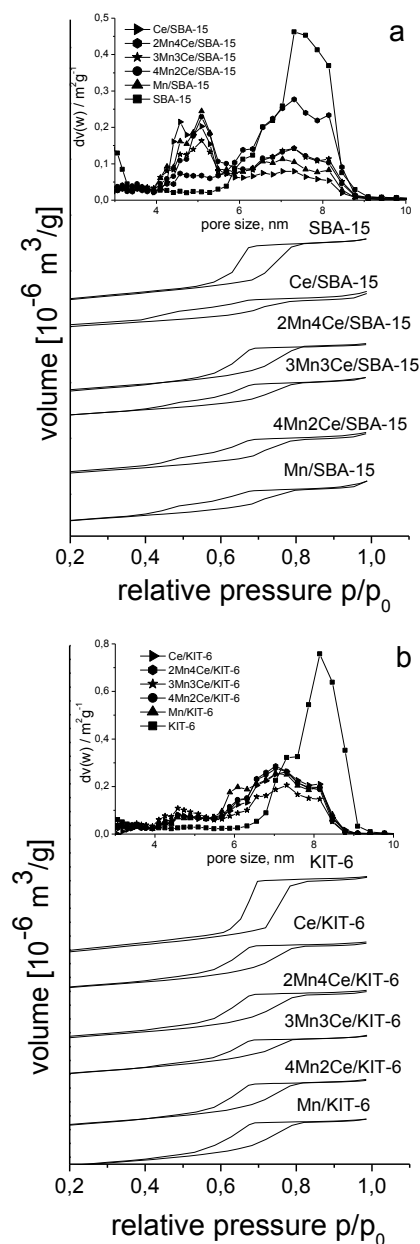


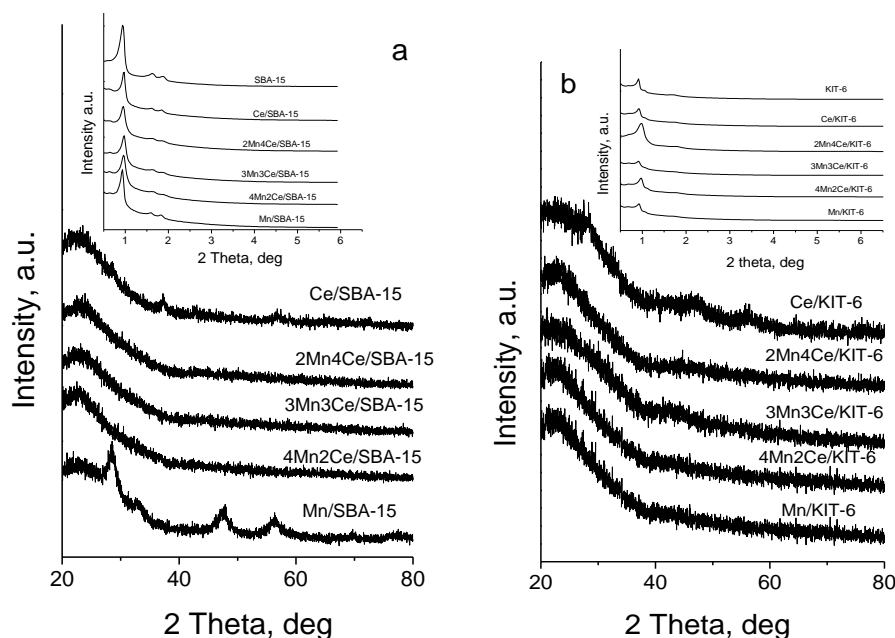
Fig. 1. Nitrogen physisorption isotherms with pore size distributions (inset) for the studied samples.

Nitrogen physisorption isotherms of SBA-15 and KIT-6 materials are of type IV with H1 hysteresis loop in the 0.4–0.8 P/P₀ region, which is typical of ordered mesoporous materials with uniform cylindrical mesopores. Note, that both supports possess almost similar BET surface area (800–850 m²/g), total pore volume (1–1.2 cm³/g) and average pore diameter of about 7–8 nm. The preservation of the isotherms after the modification indicates absence of structure collapse of the silica matrix.

Table 1. Texture characteristics of the obtained materials.

Sample	S_{BET} , m^2/g	V_{tot} , cm^3/g	V_{mic} , cm^3/g	V_{mes} , cm^3/g	$D_{\text{av,p}}$, nm
SBA-15	799	1.03	0.08	0.95	7.3
Ce/SBA-15	540	0.61	0.05	0.56	4.5
2Mn4Ce/SBA-15	629	0.79	0.05	0.74	5.0
3Mn3Ce/SBA-15	518	0.64	0.03	0.61	4.9
4Mn2Ce/SBA-15	575	0.68	0.03	0.65	4.7
Mn/SBA-15	528	0.67	0.03	0.64	5.1
KIT-6	872	1.23	0.14	1.09	8.2
Ce/KIT-6	664	0.79	0.04	0.75	7.3
2Mn4Ce/KIT-6	635	0.79	0.05	0.74	5.0
3Mn3Ce/KIT-6	593	0.68	0.04	0.64	4.6
4Mn2Ce/KIT-6	628	0.78	0.04	0.74	4.9
Mn/KIT-6	654	0.80	0.05	0.75	7.0

S_{BET} - specific surface area; V_{tot} - total pore volume; V_{mic} and V_{mes} - micro and mesopore volume, $D_{\text{av,p}}$ - average pore diameter

**Fig. 2.** XRD patterns of the studied samples in small (inset) and wide angle region.

The observed change in the shape of the desorption branch for all modifications as compared to the parent materials, which is more pronounced for the 2D- based ones, evidences pore blocking probably due to the deposition of metal oxide particles in them. This assumption was also confirmed with the observed decrease in the BET surface area and pore volume after the modification procedure (Table 1), again being more visible for the SBA-15 supported samples. The decrease in the maximum of pore size distribution peaks (Fig. 1 inset) combined with its shift to lower values clearly indicates location of manganese and ceria nanoparticles within the mesopore structure.

XRD patterns of parent and modified mesoporous materials are presented in Fig. 2.

In the small angle region (Fig. 2 inset), two diffraction peaks, indexed as (211) and (222) planes of cubic mesoporous structure, and three well resolved reflections, assigned to (100), (110) and (200) planes of hexagonally ordered mesopores, were registered for KIT-6 and SBA-15 materials, respectively [16]. These results indicate that the silica supports exhibit high quality ordered porous texture with 3D- and 2D-topology. After the impregnation, preservation of the ordered mesoporous structure was observed. The decrease in the intensities of the reflections could be due to a decrease in the electron density contrast upon introduction of metal oxide species into the silica host matrix. XRD pattern in the wide angle region of Ce/SBA-15 represents low intensive diffraction

peaks at 28.6° , 33.0° , 47.0° and 56.0° 2θ , corresponding to highly dispersed CeO_2 particles (JCPDS 43-1002). In the case of Mn/SBA-15 the appearance of weak diffraction peaks at 28.6° , 37° , 43.0° and 56.0° 2θ could be assigned to highly dispersed $\alpha\text{-MnO}_2$ (JCPDS 44-0141). The absence or the appearance of very broad reflections in the patterns of mixed manganese-ceria modifications indicates high dispersion of metal oxide phase on both silica supports, the effect being more pronounced for KIT-6.

UV-Vis analysis (Fig. 3) has been used to obtain information for the coordination and oxidative state of metal ions.

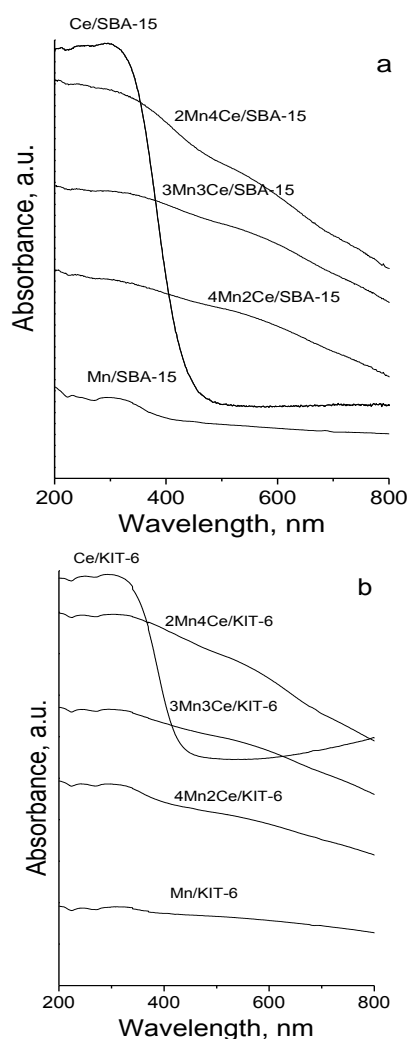


Fig. 3. UV-Vis spectra of SBA-15 and KIT-6 modifications.

The spectra of monocomponent ceria samples show well pronounced absorption peaks at about 265 and 300 nm, corresponding to charge transfer (CT) of O^{2-} to Ce^{3+} and O^{2-} to Ce^{4+} , respectively [17]. The absorption edge is significantly red-shifted for Ce/KIT-6 as compared to the Ce/SBA-

15, which could be associated with the formation of more finely dispersed CeO_2 crystallites in the former material. Among the monocomponent manganese modifications, the observed absorption in the region 350–500 nm, could be due to the $\text{O}^{2-} \rightarrow \text{Mn}^{3+}$ CT transitions. The observed absorption at about 330 nm can be associated with the presence of Mn^{4+} ions in octahedral coordination [16] and this is in consistent with the XRD data. An increased absorption above 450 nm in the spectra of bi-component samples demonstrates changes in the environment and/or oxidation state of manganese ions.

Additional information for the redox properties of the studied materials was obtained by temperature-programmed reduction (TPR) with hydrogen (Fig. 4).

Data for the initial temperature of the reduction, the position of the maximum in DTG curves and the calculated reduction degree are presented in Table 2. The reduction of monocomponent ceria samples initiates above 650 K and the calculated reduction degrees for $\text{Ce}^{4+} \rightarrow \text{Ce}^{3+}$ transition [3] in the entire temperature region are 36 and 57% for Ce/SBA-15 and Ce/KIT-6, respectively. In accordance with data from XRD and UV-Vis analysis, the observed differences in the reduction degree can be attributed to the presence of more finely dispersed CeO_2 crystallites in the KIT-6 sample compared to its SBA-15 analogue. The TPR-DTG profiles of monocomponent Mn modifications show two reduction effects, which are generally assigned to step-wise reduction of MnO_2 or Mn_2O_3 to Mn_3O_4 and then to MnO [19, 20]. The reduction peaks of Mn/SBA-15 are narrower which could be associated to the presence of more uniform well crystallized particles and this is in consistency with the XRD data. The reduction degree for Mn/SBA-15 is lower than the expected theoretic one for the reduction of $\text{Mn}^{4+}/\text{Mn}^{3+}$ to Mn^{2+} (Table 2) which could be due to the: (1) predominant presence of manganese ions in lower oxidation state (Mn^{2+} and Mn^{3+}); (2) strong interaction of manganese species with the silanol groups of the support and/or (3) less accessibility of manganese species into the porous host matrix. The latter assumption is also confirmed by the nitrogen physisorption data (Table 1), where a significant decrease in the BET surface area is observed. For the 3D- based analogue, the experimental weight loss is higher than the calculated one for the Mn^{3+} to Mn^{2+} transition which indicates significant presence of Mn^{4+} ions. The reduction profiles for the binary materials are shifted to higher

temperatures in comparison with the corresponding pure Mn modifications, which reveal changes with the manganese phase. In case of SBA-15 binary samples the reduction degree preserves almost similar to that one for Mn/SBA-15. However significant decrease in the reduction degree occurs for all binary KIT-6 modifications. This could be due to the existence of strong interaction between the individual oxides which is controlled by the pore topology of silica support.

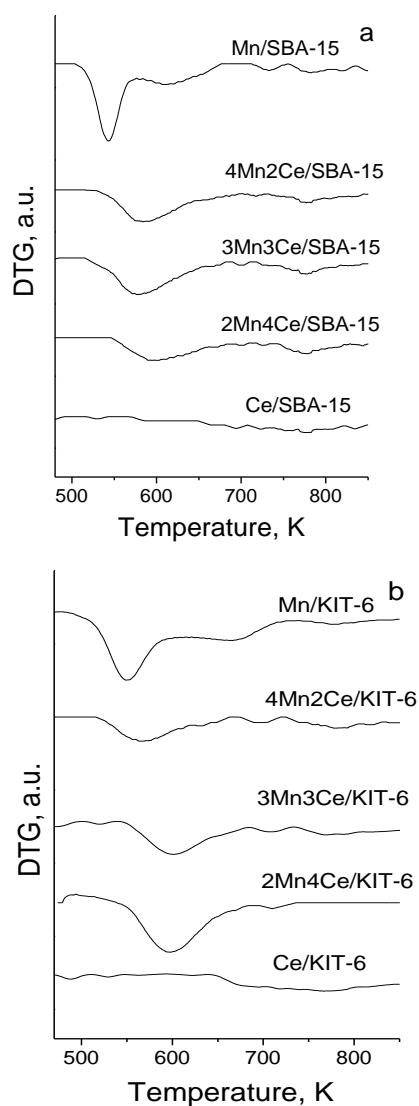


Fig. 4. TPR-DTG profiles of all manganese-ceria modifications.

The temperature dependencies of EA conversion within the range of 450–650 K are presented in Fig. 5a. All materials represent notable catalytic activity above 550 K and 80–100% conversion is achieved at 600–620 K. The main product of the conversion is CO₂, but ethanol (Et), acetaldehyde (AA) and acetic acid (AcAc) in different proportion are also registered as by-products. The changes in the

selectivity in all investigated temperature interval are presented in Fig. 5b and the products distribution at 30% conversion is listed in Table 3. Among various modifications the highest catalytic activity combined with high selectivity to CO₂ is registered for Mn/KIT-6. Taking into account the physicochemical data, this could be assigned to higher dispersion of manganese oxide phase in 3D-silica support as compared to pure Mn/SBA-15.

Moreover, here domination of MnO₂ was assumed on the base of TPR and XRD data, which evidences the high activity of Mn⁴⁺-Mn³⁺ redox pairs in total oxidation of EA. For comparison, the individual CeO₂ modified materials exhibit lower catalytic activity and high selectivity to ethanol formation. This could be understood taking into account that the EA oxidation typically proceeds as a step-wise process, starting with the hydrolysis to Et and AcAc and their further oxidation by Mars van Krevelen mechanism [21]. Obviously, the higher surface acidity of CeO₂ provokes the facile hydrolysis of EA. All binary materials possess lower catalytic activity than mono-component manganese ones but improved selectivity to CO₂ formation compared to ceria modifications. This could be provoked by the substitution of Mn⁴⁺ ions by Ce⁴⁺ and/or increase in the number of Ce and Mn ions in lower oxidation state leading to the formation of oxygen vacancies. This ensures the activity of new type of active redox pairs and changes the acidic-base and redox properties of the solid. This assumption is confirmed by the significant changes in the UV-Vis spectra (Fig. 3) and the decrease in the reduction ability for the binary materials (Fig. 4), despite the improved dispersion as compared to the individual oxides (Fig. 2).

The more pronounced changes in the catalytic activity with the samples composition combined with higher selectivity to CO₂ for the KIT-6 based binary materials urge the authors to assume higher extent of interaction between the individual oxides in the more opened 3D-structure. The absence of simple relation between the catalytic activity of the samples and their composition (Table 3) evidences that pore topology of silica support controls not only the phase composition but also the accessibility of the active species for the reactant molecules.

CONCLUSION

Ordered mesoporous silica type SBA-15 and KIT-6 can be good host matrix for the stabilization of highly dispersed manganese-ceria oxide particles by their predominant location into the mesopores.

The more opened porous structure of KIT-6 facilitates the interaction between the individual oxides. The increase in the ceria content in binary materials results in a decrease in the catalytic

activity but preservation of relatively high selectivity to CO₂, and this effect could be successfully controlled by the pore topology of silica support.

Table 2. Data from temperature-programmed reduction

Sample	T _{ini} , K	T _{max} , K	Total weight loss, mg (510–770 K)	Theoretic weight loss, mg	Reduction degree, %
Ce/SBA-15	522	770	0.05		36
Ce/KIT-6	653	780	0.08	0.14	57
2Mn4Ce/SBA-15	535	596	0.18	0.20(0.32)	90(56)
2Mn4Ce/KIT-6	530	597	0.25		125(71)
3Mn3Ce/SBA-15	553	586	0.24	0.25(0.42)	96(26)
3Mn3Ce /KIT-6	560	600	0.14		56(33)
4Mn2Ce/SBA-15	555	580	0.25	0.28(0.51)	89(47)
4Mn2Ce/ KIT-6	540	560	0.16		57(32)
Mn/SBA-15	505	543,610	0.30	0.35(0.70)	86(43)
Mn/KIT-6	517	549,668	0.43		122(61)

T_{ini} - initial reduction temperature, T_{max} - maximum of the reduction peak; reduction degree calculated for Mn³⁺ to Mn²⁺ or Mn⁴⁺ to Mn²⁺ (in brackets) transition.

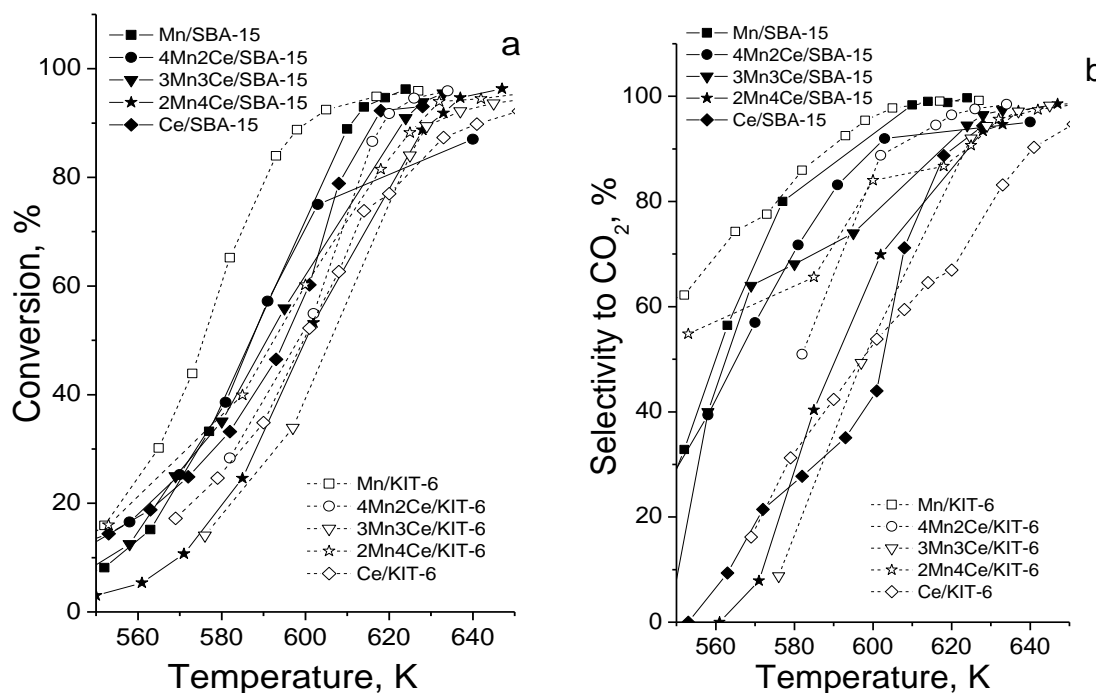


Fig. 5. Catalytic activity (a) and selectivity to CO₂ (b) in ethyl acetate oxidation over SBA-15 and KIT-6 manganese-ceria modifications.

Table 3. Products distribution (wt.%) at 30% conversion for all studied samples.

Sample composition	SBA-15 modifications					KIT-6 modifications				
	Selectivity, %				Conversion at 590 K, %	Selectivity, %				Conversion at 590 K, %
	AA	Et	AcAc	CO ₂		AA	Et	AcAc	CO ₂	
CeO ₂	23	39	10	28	42	17	32	7	44	34
2Mn ₄ Ce	16	33	10	41	31	11	16	3	70	46
3Mn ₃ Ce	8	14	3	75	48	10	12	2	76	27
4Mn ₂ Ce	11	23	8	58	55	3	11	3	83	38
Mn _x O _y	5	12	3	80	55	3	6	1	90	78

Acknowledgements: Financial support by Program for career development of young scientists, BAS (project DFNP 145 /12.05.2016) is gratefully acknowledged.

REFERENCES

1. G. Picasso, R. Cruz, M. del Rosario Sun Kou, *Mater. Res. Bull.*, **70**, 621 (2015).
2. T. Tsoncheva, R. Ivanova, M. Dimitrov, D. Paneva, D. Kovacheva, J. Henych, P. Vomáčka, M. Kormunda, N. Velinov, I. Mitov, V. Štengl, *Appl. Catal. A Gen.*, **528**, 24 (2016).
3. D. Delimaris, T. Ioannides, *Appl. Catal. B: Environ.*, **89**, 295 (2009).
4. P. Papaefthimiou, T. Ioannides, X. Verykios, *Appl. Therm. Eng.*, **18**, 1005 (1998).
5. C. Hu, *Chem. Eng. J.*, **168**, 1185 (2011).
6. P. Heynderickx, J. Thybaut, H. Poelman, D. Poelman, G. Marin, *J. Catal.*, **272**, 109 (2010).
7. T. Tsoncheva, G. Issa, T. Blasco, M. Dimitrov, M. Popova, S. Hernández, D. Kovacheva, G. Atanasova, J. M. López Nieto, *Appl. Catal. A Gen.*, **453**, 1 (2013).
8. W. Li, J. Wang, H. Gong, *Catal. Today*, **148**, 81 (2009).
9. S. Todorova, A. Naydenov, H. Kolev, K. Tenchev, G. Ivanov, G. Kadinov, *J. Mater. Sci.*, **46**, 7152 (2011).
10. Y. Yang, J. Huang, S. Wang, S. Deng, B. Wang, G. Yu, *Appl. Catal. B Environ.*, **142-143**, 568 (2013).
11. G. Picasso, M. Gutiérrez, M. P. Pina, J. Herguido, *Chem. Eng. J.*, **126**, 119 (2007).
12. G. Qi, R. Yang, R. Chang, *Appl. Catal. B Environ.*, **51**, 93 (2004).
13. X. Wu, F. Lin, H. Xu, D. Weng, *Appl. Catal. B Environ.*, **96**, 101 (2010).
14. M. Choi, W. Heo, F. Kleitz, R. Ryoo, *Chem. Commun.*, 1340 (2003).
15. F. Kleitz, S. H. Choi, R. Ryoo, *Chem. Commun.*, 2136 (2003).
16. T. Tsoncheva, G. Issa, J. M. Nieto, T. Blasco, P. Concepcion, M. Dimitrov, G. Atanasova, D. Kovacheva, *Micropor. Mesopor. Mat.*, **180**, 156 (2013).
17. A. Kambolis, H. Matralis, A. Trovarelli, Ch. Papadopoulou, *Appl. Catal. A Gen.*, **377**, 16 (2010).
18. Q. Tang, S. Hu, Y. Chen, Z. Guo, Y. Hub, Y. Chen, Y. Yang, *Micropor. Mesopor. Mater.*, **132**, 501 (2010).
19. Y. Liao, M. Fu, L. Chen, J. Wu, B. Huang, D. Ye, *Catal. Today*, **216**, 220 (2013).
20. H. Pérez, P. Navarro, J. J. Delgado, M. Montes, *Appl. Catal. A Gen.*, **400**, 238 (2011).
21. P.-O. Larsson, A. Andersson, *Appl. Catal. B Environ.*, **24**, 175 (2000).

ПЪЛНО ОКИСЛЕНИЕ НА ЕТИЛАЦЕТАТ ВЪРХУ НАНОСТРУКТУРИРАНИ МАНГАН-ЦЕРИЕВО ОКСИДНИ КАТАЛИЗАТОРИ НАНЕСЕНИ ВЪРХУ МЕЗОПОРЕСТИ СИЛИКАТИ

Р. Н. Иванова*, Т. С. Цончева

Институт по Органична Химия с Център по Фитохимия, БАН, София, България

Постъпила на 21 февруари 2017 г.; Коригирана на 08 март 2017 г.

(Резюме)

Настоящото изследване е насочено към ефекта от текстурата на мезопорести силикати върху структурните, редокс и каталитични свойства на нанесени наноразмерни моно- и би-компонентни манган-цериеви оксиди. Мезопорести силикати тип SBA-15 и KIT-6 с еднакви цилиндрични мезопори подредени в 2D- и 3D- симетрия, бяха използвани като носители. Комплекс от физикохимични техники, като азотна физисорбция, прахова рентгенова дифракция, UV-Vis спектроскопия и температурно-програмирана редукция с водород бяха използвани за характеризиране на образците. Беше изследвано потенциалното приложение на композитите като катализатори за окисление на етилацетат. Беше демонстрирано, че SBA-15 и KIT-6 могат да бъдат добра матрица за стабилизирането на високо дисперсни манган-цериево оксидни частици. Беше установен силен ефект от топологията на мезопорестия носител, който също зависи и от състава на образците, върху формирането на каталитично активните фази.

The photodegradation of Methylene Blue and Methyl Orange dyes and their mixture by ZnO obtained by hydrothermally activated precipitates

V. N. Blaskov¹, I. D. Stambolova^{1*}, K. I. Milenova², K. L. Zaharieva², L. D. Dimitrov³, D. D. Stoyanova¹, A. E. Elias²

¹ Institute of General and Inorganic Chemistry, BAS, Acad. G. Bonchev St, bl.11, 1113 Sofia, Bulgaria

² Institute of Catalysis, BAS, Acad. G. Bonchev St, bl.11, 1113 Sofia, Bulgaria

³ Institute of Mineralogy and Crystallography "Acad. Ivan Kostov" BAS, Acad. G. Bonchev bl. 107, 1113, Sofia, Bulgaria

Received January 25, 2017; Revised February 24, 2017

Dedicated to Acad. Bogdan Kurtev on the occasion of his 100th birth anniversary

Zinc oxide sample was obtained by precipitation followed by hydrothermal treatment. The sample was characterized by PXRD, BET method and TG-DTA methods. Thermal treatment at 170°C results in formation of well crystallized wurtzite phase. The BET analysis revealed prevailing quantity of mesopores (15 - 50 nm). The hysteresis loop of the adsorption-desorption isotherms implies the presence of cylindrical pores. The photocatalytic degradation of two types of dyes, namely hetero- polyaromatic (Methylene Blue, MB) and azoic (Methyl Orange, MO) dye and the simultaneous photodegradation of the mixture of MO and MB dyes in aqueous solution under UV irradiation have been studied. The rate of degradation of MB and the mixture MO+MB is higher than those of MO dye.

Key words: ZnO, photocatalysis; Methyl Orange; Methylene Blue

INTRODUCTION

The environmental problems associated with toxic water pollutants have attracted much attention. Wastewater from textile, paper, and some other industrial processes contain residual dyes, which are nonbiodegradable, toxic and carcinogenic. Various chemical, physical and biological processes (coagulation/flocculation, reverse osmosis, etc.) have been developed in order to remove the color from textile effluents. [1]. However, these techniques are nondestructive, since they only transfer the nonbiodegradable matter into sludge. Among advanced oxidation processes (AOPs), heterogeneous photocatalysis has appeared as an emerging destructive technology leading to the total mineralization of most organic pollutants [2].

Several semiconductors such as TiO₂, WO₃, SrTiO₃, Fe₂O₃ and ZnO have energies of their band gap sufficient for catalysing a wide range of redox reactions. ZnO is the most extensively studied semiconductor found from the literature [3] because it is inexpensive, non-toxic, highly photoactive. It has been found to be the most promising for photocatalytic destruction of organic pollutants.

Methyl orange is one of the representative azo

dyes, which are the most important class of synthetic organic dyes used in the textile industry. The absorption spectrum shows two absorption peaks at ~ 270 and 463 nm. Methylene blue is a heterocyclic aromatic chemical compound with maximum absorption of light around 670 nm. P. Wongkalasin *et al.* have studied the photocatalytic degradation of mixtures of two azo dyes – Acid Yellow (AY) monoazo dye and Acid Black (AB) diazo dye by using a mesoporous-assembled TiO₂ nanocrystal photocatalyst [4]. According to the best of our knowledge, the photocatalytic degradation of dye mixtures by ZnO particles has been not studied yet. Therefore, in the present work we have investigated the photocatalytic degradation of single dyes MO and MB and their mixture over ZnO powders, prepared by precipitation followed by hydrothermal activation.

EXPERIMENTAL

Preparation and Characterization

Zinc acetate was dissolved in deionized water in order to obtain 0.2 M solution (sol A). Urea aqueous solution (0.6 M) was added dropwise to sol A under vigorous stirring. The pH of solution was adjusted to 7. The resultant mixture was transferred into an autoclave and subjected to hydrothermal at

* To whom all correspondence should be sent:
E-mail: stambolova@yahoo.com

90 °C for 12 h, then the autoclave was left to cool to room temperature. The final product was washed several times and dried in oven at 100 °C. Finally, the sample were thermally treated in programmable oven at 170 °C for 3 hours.

The X-ray diffraction (XRD) patterns were carried out on a Bruker D2 Phaser diffractometer using Cu K α radiation ($\lambda = 0.154056$ nm). The specific surface area measurement and the pore size distribution were accomplished on an automated apparatus NOVA Win – CFR Quantachrom – Gas Sorption System. The calculation of the surface area was done using the BET equation, whereupon the pore size distribution, as well as the average pore diameter were evaluated by DFT method assuming a cylindrical model of the pores. The total pore volume was estimated in accordance with the rule of Gurvich at relative pressure of 0.96. The differential thermal analysis has been accomplished on a combined DTA/TG apparatus LABSYSEVO 1600 (SETARAM Company; France). Synthetic air was used as carrier gas, with flow rate of 20 ml/min, heating rate 10K/min up to 350 °C.

The photocatalytic degradation experiments were performed in a glass reactor. Single MO or MB dyes (10 ppm) and mixed bi-component MO and MB dye solutions (1:1) were freshly prepared and used for the photocatalytic activity testing. A desired amount (150 mg) of the synthesized photocatalyst was suspended in 150 ml aqueous solutions of both single and mixed dyes under various reaction conditions by using a magnetic stirrer. Prior to the photocatalytic activity testing, the continuously suspended mixture was left for 30 min in a dark. The photocatalytic reaction was started by exposing the mixture in the reactor to UV light irradiation (maximum emission at wavelength 365 nm 2.6 mW/cm²). Feed air stream was passing continuously bubbling through the suspension saturating the contaminated water in dissolved oxygen (semi-batch reactor). The suspension was periodically withdrawn for analysis from the reactor, and the sample was then centrifuged to remove the photocatalyst powder. The course of the oxidative discoloration reaction was monitored by UV-Vis absorbance spectrophotometer UV-1600PC within the wavelength range from 200 to 800 nm. The photocatalytic decolorization efficiency D (%) was evaluated by the following equation:

$$D = (C_0 - C) / C_0 \times 100 \quad (1)$$

where C_0 is the initial dye concentration and C is the dye concentration after irradiation at selected

time interval. Equation (1) is based on the pseudo-first order kinetics, assuming the dissolved oxygen concentration to be constant (air stream – semi-batch reactor) – in this approximation the conversion degree is function only of the dye concentration.

RESULTS AND DISCUSSION

The XRD pattern of ZnO sample after thermal treatment possesses well crystallized wurtzite phase with predominant peaks, corresponding to (100) and (101) planes (Fig. 1). The average crystallite size about 17 nm. The application of urea precipitant promotes the crystallization of wurtzite phase [5].

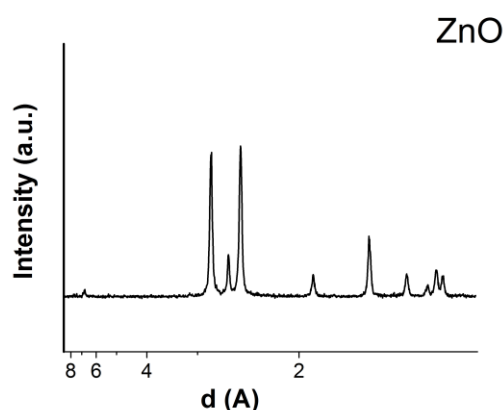


Fig. 1. X-ray diffractogram of ZnO powder.

The adsorption-desorption isotherm is identified as type IV, while the hysteresis loop is type I according to IUPAC nomenclature, revealing the type of mesoporous structure (Fig. 2). The hysteresis loop is in the relative pressure range 0.8–0.9, which is a confirmation of the existence of cylindrical pores [6]. It is also visible that the adsorption-desorption isotherm loop is closed at a relative pressures of about 0.5–0.6, which is typical of mesoporous structures (as is the case with our ZnO sample) having prevailing cylindrical pores or close to cylindrical shape pores [7]. The inset of Fig.2 represents the pore size distribution. It is seen that the sample consist of mesopores with size within in the range 15 nm - 50 nm. Similar distributions of pores have obtained by another researchers for zinc oxide powders [8]. The specific surface area and average pore volume of ZnO are evaluated to be approximately 42 m²/g and 0.27 cm³/g, respectively.

Fig. 3 represents TG and DTA curves of the precipitate, dried at 100 °C. One endothermic peak is observed on the pattern with maximum at 244 °C, which corresponds to the zinc acetate

decomposition. The corresponding weight loss is 21.5%. Other research groups have registered that the decomposition of zinc acetate occurred nearly this temperature [8].

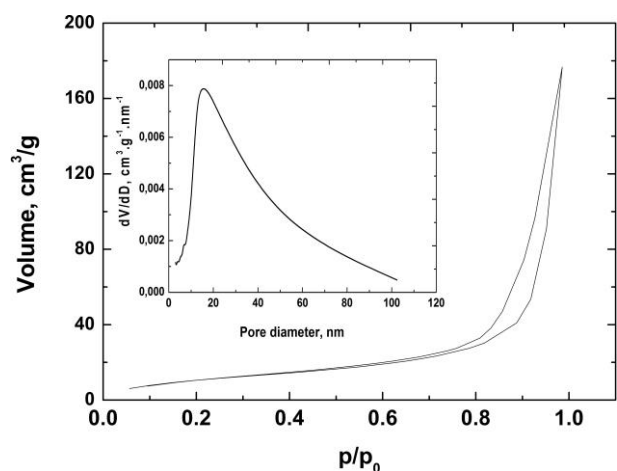


Fig. 2. Adsorption-desorption isotherm of the sample.

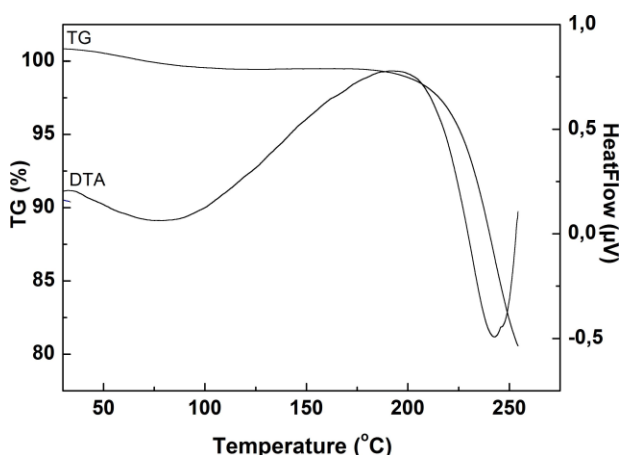


Fig. 3. DTA/TG analysis of the precipitate, dried at 100 °C.

The UV–visible spectra profiles of MO and MB and their mixture are shown comparatively in Fig. 4. From the figure, the absorption maxima of MO and MB dyes are 464 and 664 nm, respectively. It is clear that these values are not changed upon their mixing.

The photocatalytic properties of ZnO nanoparticle on decolorization of Methyl Orange were studied (Fig. 5). Extent of photocatalytic degradation was determined by the reduction in absorbance of the solution. During the first stage of photodecolorization, methylene blue was decayed with fast decolorization rate, followed by the second stage, which was characterized by a rather slow decolorization rate. Similar trend is registered for the mixture MB+MO. The slow kinetics of methylene blue decolorization in the second stage

of decolorization might be due to the difficulty in converting the N-atoms of the dye into oxidized nitrogen compounds [9]. In addition the accumulated intermediates in the first stage decrease the rate of oxidative photocatalytic reaction. The experiments show also that the decolorization rate of MB is higher than those of MO (Table 1). This could be explained by the easier loss of π -electrons and disruption of the conjugated double-bond and single-bond, propagating on a larger carbon atom skeleton and better delocalization in comparison to single benzene rings in the MO dye.

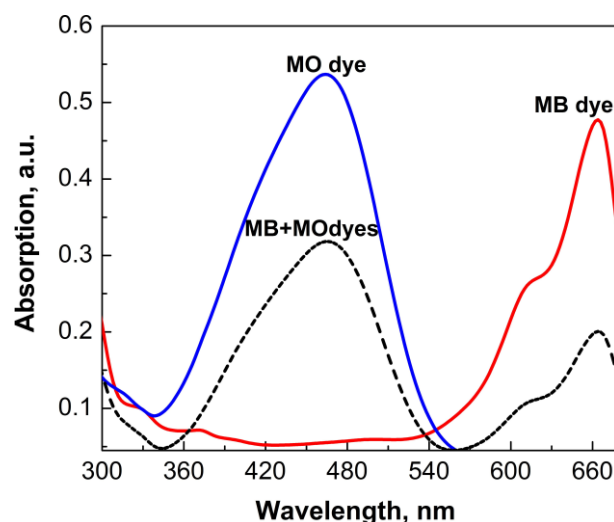


Fig. 4. Absorption spectra of MO dye, MB dye and mixture MO+MB.

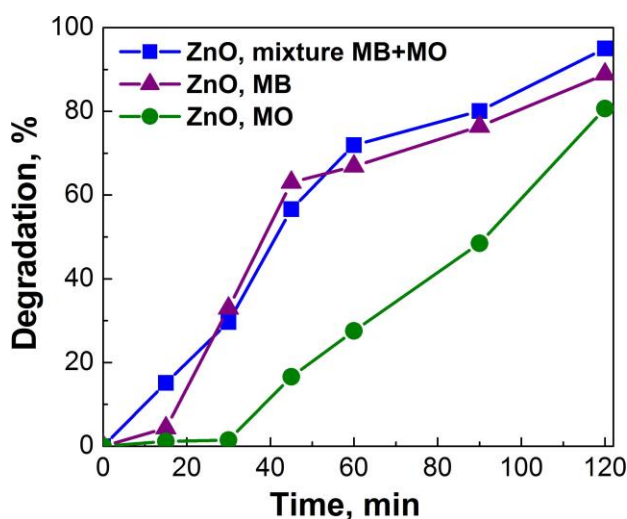


Fig. 5. Decolorization of model dye solutions over ZnO powder.

The adsorption capacity of the sample is presented in Table 1. It is seen in the Table that the photocatalytic activity does not follow the changes of the sorption properties. ZnO surface is positively

charged below pH 9 based on their $zpc=9.0$, whereupon this anionic dye MO has stronger adsorption affinity in comparison to the cationic dye MB under our experimental conditions (pH factor 6.8). Similar results were obtained for photocatalytic degradation of Acid Brown 14 for ZnO powders [3].

Table 1. Adsorption capacity and rate constants of oxidative decolorization process of ZnO sample.

Type of solution	Adsorption capacity, mg/g	k ($\times 10^{-3}$, min ⁻¹)
MB dye	0.028	17.4
MO dye	0.072	9.7
Mixture MB+MO dyes, evaluated by the strongest absorption peak of MB dye	0.105	21.6

CONCLUSION

Zinc oxide sample was obtained by combination of precipitation and hydrothermal treatment. Mesopores in the range (15 - 50 nm) were registered. The large specific surface area, pore volume, greater share of mesopores and high degree of crystallinity contribute to high photocatalytic efficiency of the ZnO powders. The photocatalytic decolorization rates of Methylene Blue (MB) and the bi-component mixture MB and Methyl orange (MO) are faster than MO dye under UV irradiation. During the first stage of photodecolorization, methylene blue was decayed with fast decolorization rate, which could be explained by the easier disruption of the conjugated double-bond and single-system. Methyl orange

decolorizes slower due to the difficult destruction of single benzene rings.

Acknowledgements: The authors gratefully acknowledge financial support by National Science Fund, Ministry of Education and Sciences of Bulgaria (Contracts DFNI – T-02-16 and DFNI-E02/2/2014), contract “Heterogeneous catalytic and photocatalytic destruction of organic and pharmaceutical contaminants in the nature by multicomponent systems” EBR SANI.

REFERENCES

1. V. Gomez; M. Larrechi, M. Callao, *Chemosphere*, **69**, 1151 (2007).
2. S. Kansal, M. Singh, D. Sud, *J. Hazard. Mater.*, **141**, 581 (2007)
3. S. Sakthivel, B. Neppolian, M. V. Shankar, B. Arabindoo, M. Palanichamy, V. Murugesan, *Solar Energy Mater. Solar Cells*, **77**, 65 (2003).
4. P. Wongkalasin, S. Chavadeja, T. Sreethawong, *Coll. Surf. A*, **384**, 519 (2011).
5. S. Hussain, T. Liu, B. Miao, M. Kashif, N. Aslam, M. Rashad, W. Zen, X. Peng, *Ceram Intern.*, **41**, 4861 (2015).
6. K. S. W. Sing, D. H. Everett, R. A. W. Haul, L. Moscou, R. A. Pierotti, J. Rouquerol, T. Siemieniewska, *Pure Appl. Chem.*, **57**, 603 (1985).
7. S. J. Gregg, K. S. W. Sing, Adsorption, surface area and porosity, London, Academic Press, 1991.
8. Y. Miao, H. Zhang, S. Yuan, Z. Jiao, X. Zhu, *J. Colloid Interface Sci.*, **462**, 9 (2016).
9. S.-H. Hu, Y.-C. Chen, C.-C. Hwang, C.-H. Peng, D.-C. Gong, *J. Mater. Sci.*, **45**, 5309 (2010).

ФОТОКАТАЛИТИЧНО РАЗГРАЖДАНЕ НА МЕТИЛЕНОВО СИНЬО И МЕТИЛ
ОРАНЖЕВО БАГРИЛА И ТЯХНАТА СМЕС ЧРЕЗ ZnO, ПОЛУЧЕН ОТ
ХИДРОТЕРМАЛНО АКТИВИРАНА УТАЙКА

В. Н. Блъсков¹, И. Д. Стамболова^{1*}, К. И. Миленова², К. Л. Захариева², Л. Д.
Димитров³, Д. Д. Стоянова¹, А. Е. Елиаз²

¹ *Институт по обща и неорганична химия, Българска академия на науките, ул. „Акад. Г. Бончев“, бл. 11, 1113
София, България*

² *Институт по катализ, Българска академия на науките, ул. „Акад. Г. Бончев“, бл. 11, 1113 София, България*

³ *Институт по минералогия и кристалография “Акад. Иван Костов”, ул. „Акад. Г. Бончев“, бл. 107, 1113
София, България*

Постъпила на 25 януари 2017 г.; Коригирана на 24 февруари 2017 г.

(Резюме)

Образец от цинков оксид беше получен чрез утаяване и последваща хидротермална обработка. Той бе охарактеризиран посредством прахова рентгенова дифракция, BET метод и ТГ – ДТА анализи. Беше регистрирано формирането на добре кристализирала вюрцитна фаза след термичната обработка при 170 °С. С помощта на BET метода беше установено наличието на преобладаващи мезопори (15-50 nm). От вида на хистерезисните примки, наблюдавани в адсорбционна – десорбционните изотерми на образеца, съдим за присъствие на цилиндрични пори. Изследвано беше фотокаталитичното разлагане на два вида багрила – хетерополиароматно (Метиленово Синьо) и азо багрило (Метил Оранжево), както и фотокаталитичното обезцветяване на багрилата при съвместното им присъствие във воден разтвор, под действие на ултравиолетова светлина. Установено беше, че скоростта на разграждане на Метиленовото синьо, както и на сместа от Метиленово синьо и Метил оранжево е по-висока, отколкото скоростта на разлагане на метил оранжевото багрило.

Thermal behavior of some germanates with non-olivine structure

I. Koseva^{1*}, V. Nikolov¹, A. Yordanova¹, P. Tzvetkov¹, N. Petrova²

¹ Institute of General and Inorganic Chemistry, Bulgarian Academy of Sciences, 1113 Sofia, Bulgaria

² Institute of Mineralogy and Crystallography, Bulgarian Academy of Sciences, 1113 Sofia, Bulgaria

Received January 26, 2017; Revised February 01, 2017

Dedicated to Acad. Bogdan Kurtev on the occasion of his 100th birth anniversary

Single phase germanates LiAlGeO_4 , LiGaGeO_4 and Zn_2GeO_4 with hexagonal structure (space group, S. G., R3), $\text{Li}_2\text{CaGeO}_4$ with tetragonal structure (S. G. I-42m), $\text{Ca}_5\text{Ge}_3\text{O}_{11}$ with monoclinic structure (S. G. C1) and $5\text{LiAlGeO}_4 \cdot 4\text{Zn}_2\text{GeO}_4$ with cubic structure were obtained by solid-state synthesis. The thermal behavior of these germanates was studied with a view to finding out the most appropriate method and conditions for growing single crystals from them, which, after doping with Cr^{4+} , can be used as matrices for lasers with a broad emission spectrum in the range from 1.0 to 1.6 μm . By means of powder X-ray diffraction and DTA/TG analysis, the melting temperatures, the type of melting (with or without decomposition), the type of the phases crystallizing after decomposition, as well as the presence (or lack) of polymorphic transitions in the vicinity of the melting temperature, were studied. Most of the data on the thermal behavior of these germanates are reported here for the first time. It is found that four of the synthesized germanates (LiAlGeO_4 , Zn_2GeO_4 , $\text{Ca}_5\text{Ge}_3\text{O}_{11}$, and $5\text{LiAlGeO}_4 \cdot 4\text{Zn}_2\text{GeO}_4$) are melting congruently (without decomposition) and do not display phase transitions. Unlike the germanates with olivine structure, which are examined in more details for the same purpose, single crystals from non-olivine germanates could be directly grown from their own solutions (by the methods of Czochralski, Bridgman-Stockbarger or Kyropoulos) instead of using the flux method, which is characterized by a considerably lower rate of growing and a limited crystal size.

Key words: germanates, melting temperature, phase transitions, X-ray diffraction analysis, DTA analysis

INTRODUCTION

Single crystals of complex oxides doped with ions of transition 3d elements with different oxidation states are of particular interest as laser media. These single crystals display a broad emission range as tunable lasers [1, 2] and may also be used as media for femtosecond lasers [3, 4]. Of particular importance are the Cr^{4+} doped media emitting in the range from 1.1 to 1.6 μm . Lasers emitting in this range find increasing application in medicine, ecology and telecommunications [5, 6]. The most popular Cr^{4+} doped single crystals are those of Mg_2SiO_4 (forsterite) and $\text{Y}_3\text{Al}_5\text{O}_{12}$ (garnet). Both of these single crystals have, however, several drawbacks. For example, a severe problem is caused by nonradiative transitions, as a result of which the quantum efficiency amounts to about 9% for forsterite and 14-22% for YAG [7, 8]. Another problem is the undesired presence of Cr^{3+} along with Cr^{4+} . As a rule, only a small percentage of chromium is in the desired Cr^{4+} state [8]. Owing to the issues mentioned, novel Cr^{4+} doped laser matrices are still looked for. Most promising among

the novel crystal matrices studied so far seem to be the Cr^{4+} doped germanates having Ge^{4+} in the tetrahedral environment preferred by Cr^{4+} as the ionic radii of Ge^{4+} and Cr^{4+} are very close – 0.41 and 0.39 Å [9], respectively. From this point of view, substitution of Ge^{4+} by Cr^{4+} is significantly facilitated up to high concentrations of Cr^{4+} . Favorable fact is that the existence of chromium as Cr^{3+} or Cr^{2+} in these germanates is highly improbable.

Suitable class of single crystal matrices is that of germanates with olivine structure (S. G. Pnma) with the general formulas: Me_2GeO_4 (Me=Mg, Ca); $\text{Li}_2\text{MeGeO}_4$ (Me=Mg, Zn); LiMeGeO_4 (Me= Sc, In, Y), as well as the compound Li_4GeO_4 . Our study of the thermal behavior of these germanates revealed that most of them are melting with decomposition (incongruently) or display phase transitions. The only exception is Mg_2GeO_4 . Its melting temperature is, however, too high (1885 °C) and considerable amounts of GeO_2 evaporate. Hence, the flux method from high-temperature solutions is the only option of growing crystals from these compounds. The crystal growth should be performed below the decomposition temperature or the temperature of phase transition. A major drawback of this method compared with the growth from the own melt

* To whom all correspondence should be sent:
E-mail: ikosseva@svr.igic.bas.bg

(methods of Czochralski, Bridgman-Stockbarger or Kyropoulos) is the considerably lower rate of growing. This explains the search for other germanates which possess the advantages of the olivine-group ones (tetrahedral environment of germanium, close ionic radii of Ge^{4+} and Cr^{4+}) and melt with no decomposition or phase transitions.

According to the literature data, LiAlGeO_4 , LiGaGeO_4 and Zn_2GeO_4 are isostructural and belong to the same structural group (S. G. R3) [10-15]. Germanium participates in this structure in two tetrahedra differing by size and deformation degree; lithium and aluminium (lithium and gallium), as well as zinc in Zn_2GeO_4 are also in tetrahedral positions. The structural differences between these three compounds are due to the different Ge-O and Me-Ge distances, where Me is Li, Al, Ga or Zn. There is no information on their thermal behavior before melting (presence or lack of transitions).

$\text{Li}_2\text{CaGeO}_4$ has tetragonal structure (S. G. I-42m), in which germanium and lithium are in tetrahedral environment, while calcium is in dodecahedral coordination [16]. Although this compound, doped with rare earth elements (Er, Tb, Dy), has been examined as a phosphorescent substance, there are no data about its thermal behavior. The phase $\text{Ca}_5\text{Ge}_3\text{O}_{11}$ has monoclinic structure in which germanium participates in three tetrahedra differing by size and deformation degree, while calcium is in a dodecahedral occupation [17, 18]. There is no data about the thermal behavior of this compound either.

According to the pseudobinary diagram of LiAlGeO_4 - Zn_2GeO_4 [19], the compound $5\text{LiAlGeO}_4:4\text{Zn}_2\text{GeO}_4$ ($\text{Li}_5\text{Al}_5\text{Zn}_8\text{Ge}_4\text{O}_{36}$) exists and has a temperature of congruent decomposition about 1080°C with no polymorphic transitions up to this temperature.

All the above mentioned six germanates possess Ge^{4+} in a tetrahedral position, therefore they are suitable for Cr^{4+} doping as the already investigated germanates with olivine structure.

The main purpose of this work was to study the thermal behavior (melting temperatures, type of phases obtained by eventual decomposition, presence or lack of polymorphic transitions) of the above mentioned six germanates. The thermal behavior strongly determines the method and conditions of single crystals growth.

EXPERIMENTAL

The studied germanates were obtained by solid-state synthesis using the following reagents: CaCO_3

(99.9), Li_2CO_3 (99.99), ZnO (99.0), Al_2O_3 (99.99), Ga_2O_3 (99.9) and GeO_2 (99.999). Stoichiometric amounts of the starting reagents for the corresponding germanate were weighed with a precision of ± 0.01 g and were mixed and ground in an agate mortar. The reaction mixtures were thermally pretreated at 900°C for 2 h for decomposition of the carbonates present. After a further homogenization, the mixture was heated for 16 h, with two intermediate grindings, at different temperatures until the minimal temperature was established, which was sufficient for obtaining a well-crystallized pure germanate product with no admixtures of unreacted reagents or side compounds. After synthesis at different temperatures the following optimal temperatures for solid-state synthesis were found: 1050°C for LiAlGeO_4 , 1100°C for LiGaGeO_4 , 1150°C for Zn_2GeO_4 , 1050°C for $\text{Li}_2\text{CaGeO}_4$, 1200°C for $\text{Ca}_5\text{Ge}_3\text{O}_{11}$ and 1050°C for $5\text{LiAlGeO}_4:4\text{Zn}_2\text{GeO}_4$.

Structural characterization was carried out by powder X-ray diffraction (XRD) using a Bruker D8 Advance powder diffractometer with Cu K α radiation and SolX detector. XRD spectra were recorded at room temperature. Data were collected in the 2θ range from 10 to $80^\circ 2\theta$ with a step of $0.048 2\theta$ and counting time of 1 s/step. XRD spectra were identified using the Diffractplus EVA program.

Differential thermal analysis was carried out on a DTA-TG analyzer SETSYS Evolution 2400, SETARAM in static air atmosphere with a heating rate of $10^\circ\text{C min}^{-1}$ and 15-20 mg sample weight.

Additional experiments were performed in order to establish the melting type (congruent or incongruent). For this purpose a sample of about 2 g was placed in a platinum crucible and was heated in a furnace with a MoSi_2 heater with controllable temperature ($\pm 1^\circ\text{C}$) up to a temperature by 20-30 $^\circ\text{C}$ above the melting temperature established by DTA. After holding for 30 min, the sample was withdrawn from the hot area and was briskly cooled on a cold copper plate. The sample cooled down to room temperature for 10-15 s. The briskly crystallized sample was subjected to XRD analysis for identification of the crystallized phases.

RESULTS AND DISCUSSION

Figs. 1 and 2 present the powder XRD patterns of germanates obtained by solid-state synthesis, compared to the corresponding PDF data. No additional phases can be distinguished and the patterns are consistent with the literature data.

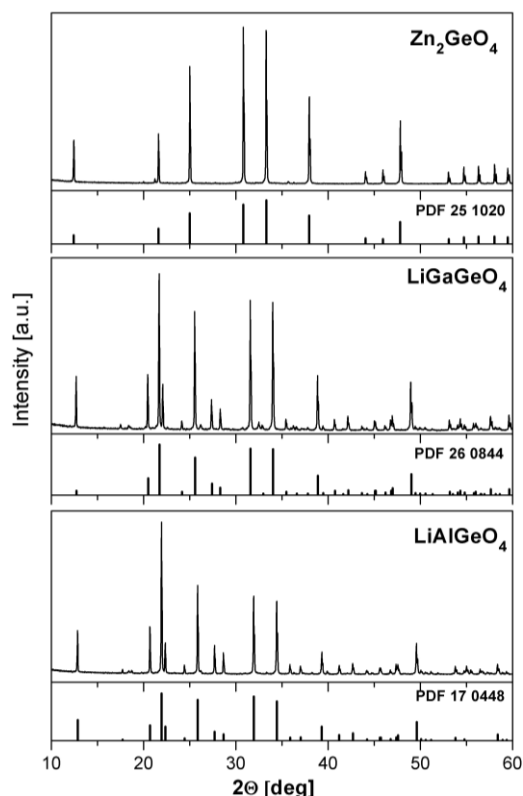


Fig. 1. Powder XRD patterns of the LiAlGeO_4 , LiGaGeO_4 and Zn_2GeO_4 obtained by solid-state synthesis, compared to the corresponding PDF data.

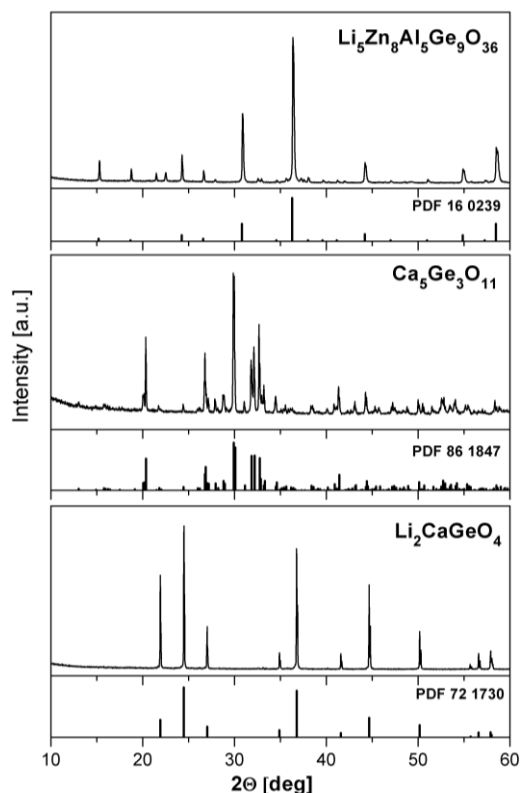


Fig. 2. Powder XRD patterns of the $\text{Li}_2\text{CaGeO}_4$, $\text{Ca}_5\text{Ge}_3\text{O}_{11}$ and $\text{Li}_5\text{Zn}_8\text{Al}_5\text{Ge}_9\text{O}_{36}$ obtained by solid-state synthesis, compared to the corresponding PDF data.

The DTA/TG curves of the samples are shown in Fig. 3. As can be seen, none of the germanates displays phase transitions in the vicinity of the melting temperature. The established melting temperatures are: 1190 °C for LiAlGeO_4 , 1147 °C for LiGaGeO_4 , 1505 °C for Zn_2GeO_4 , 1120 °C for $\text{Li}_2\text{CaGeO}_4$, 1560 °C for $\text{Ca}_5\text{Ge}_3\text{O}_{11}$ and 1160 °C for $5\text{LiAlGeO}_4 \cdot 4\text{Zn}_2\text{GeO}_4$. Except for the melting temperature of Zn_2GeO_4 , these data differ from those given in the literature. Thus, for LiAlGeO_4 the temperature 1150 °C is given in [13] (1190 °C in this work); for LiGaGeO_4 -1200 °C [20] (1147 °C in this work); for Zn_2GeO_4 -1502 °C [12] (1505 °C in this work); no data are available for $\text{Ca}_5\text{Ge}_3\text{O}_{11}$ and $\text{Li}_2\text{CaGeO}_4$; while the temperature 1080 °C is given for $5\text{LiAlGeO}_4 \cdot 4\text{Zn}_2\text{GeO}_4$ according to the phase diagram [19], (1160 °C in this work).

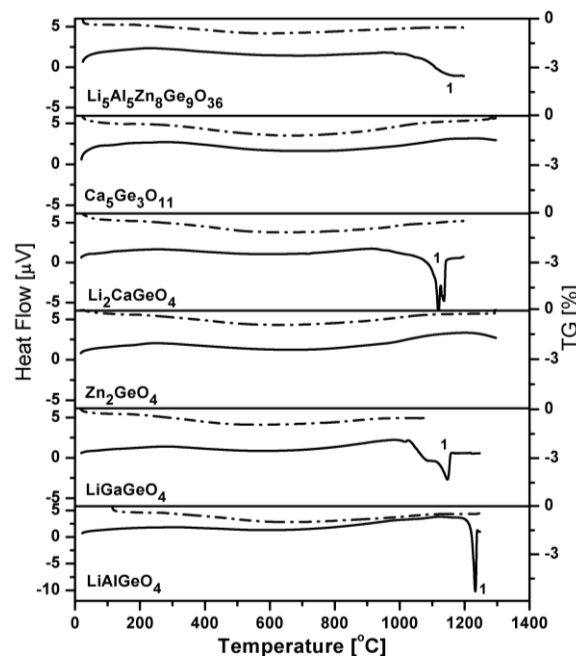


Fig. 3. DTA/TG curves of LiAlGeO_4 , LiGaGeO_4 , Zn_2GeO_4 , $\text{Li}_2\text{CaGeO}_4$, $\text{Ca}_5\text{Ge}_3\text{O}_{11}$ and $\text{Li}_5\text{Zn}_8\text{Al}_5\text{Ge}_9\text{O}_{36}$ up to the melting temperature. 1 – melting temperature.

The results of the experimental study of the type of melting of the germanates and the phases crystallizing from the melts are presented in Fig. 4. As can be seen, the XRD pattern of the products after melting of LiAlGeO_4 and subsequent brisk cooling, does not contain any peaks different from those of LiAlGeO_4 and matches very well the one given in the literature (PDF-270289), *i.e.* LiAlGeO_4 is melting congruently at 1160 °C. Similar behavior is displayed by Zn_2GeO_4 , $\text{Ca}_5\text{Ge}_3\text{O}_{11}$ and $5\text{LiAlGeO}_4 \cdot 4\text{Zn}_2\text{GeO}_4$. The congruent melting of these four germanates (LiAlGeO_4 , Zn_2GeO_4 , $\text{Ca}_5\text{Ge}_3\text{O}_{11}$ and $5\text{LiAlGeO}_4 \cdot 4\text{Zn}_2\text{GeO}_4$) is of great

significance as crystal growth is concerned, because single crystals of these germanates could be grown from their own melts by methods characterized by technological simplicity and high growing rate.

Fig. 4 illustrates the thermal behavior of LiGaGeO_4 after melting. Differently from the published assertion [10] that this compound melts congruently, our studies revealed that it melts at 1147°C with decomposition, the main decomposition product being Li_2GeO_3 . Fig. 4 also presents the thermal behavior of $\text{Li}_2\text{CaGeO}_4$ which melts with decomposition to Ca_2GeO_4 and Li_2GeO_3 .

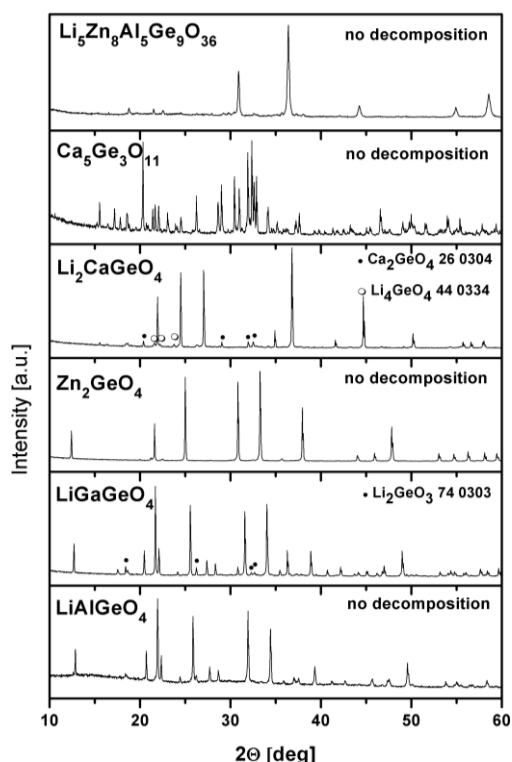


Fig. 4. Powder XRD patterns of the products after melting of LiAlGeO_4 , LiGaGeO_4 , Zn_2GeO_4 , $\text{Li}_2\text{CaGeO}_4$, $\text{Ca}_5\text{Ge}_3\text{O}_{11}$ and $\text{Li}_5\text{Zn}_8\text{Al}_5\text{Ge}_9\text{O}_{36}$. Additional phases in the cases of incongruent melting are marked.

As was already said, none of the examined germanates displays phase transitions.

CONCLUSION

The germanates examined in the present study are considerably more appropriate for crystal growth than the germanates with olivine structure. Our former studies revealed that out of nine germanates with olivine structure, none could be directly grown from its own melt. Unlike the olivine-type germanates, four of the germanates in the present study (LiAlGeO_4 , Zn_2GeO_4 , $\text{Ca}_5\text{Ge}_3\text{O}_{11}$ and $5\text{LiAlGeO}_4 \cdot 4\text{Zn}_2\text{GeO}_4$) are melting congruently without phase transitions. Hence, methods for

single crystal growth from the own melt can be applied (Czochralski, Bridgman-Stockbarger and Kyropoulos). It should be kept in mind, however, that two of these germanates (Zn_2GeO_4 and $\text{Ca}_5\text{Ge}_3\text{O}_{11}$) are melting at relatively high temperatures (1505°C and 1560°C , respectively), which would hamper the crystal growth due to some evaporation of GeO_2 . The thermal behavior of the other two germanates (LiAlGeO_4 and $5\text{LiAlGeO}_4 \cdot 4\text{Zn}_2\text{GeO}_4$) is perfectly suited for single crystal growth from their own melts. The compounds LiGaGeO_4 and $\text{Li}_2\text{CaGeO}_4$ are melting with decomposition and crystal growth from them could be realized only by the flux method, as in the case of the germanates of the olivine group.

REFERENCES

1. E. V. Zharikov, V. A. Smirnov, *Wide Gap Luminescent Materials: Theory and Applications*, Kluwer Academic, Nowell, MA, 1997.
2. S. Kück, *Appl. Phys. B*, **72**, 515 (2001).
3. M. J. Hayduk, S. T. Johns, M. F. Krol, *Laser focus world*, **32**, 73 (1996).
4. S. Spälter, M. Böhm, M. Burk, B. Mikulla, R. Fluck, I.D. Jung, G. Zhang, U. Keller, A. Sizmann, G. Leuchs, *Appl. Phys. B*, **65**, 335 (1997).
5. Y. Kalisky, *Prog. Quant. Electron.*, **28**, 249 (2004).
6. A. Sennaroglu, *Prog. Quant. Electron.*, **26**, 287 (2002).
7. C. R. Pollock, D. B. Barber, J. L. Mass, S. Margraf, *IEEE J. Sel. Topics Quantum Electron.*, **1**, 62 (1995).
8. A. G. Okhrimchuk, A. V. Shestakov, *Opt. Mater.*, **3**, 1 (1994).
9. R. T. Shannon, *Acta Crystallogr. A*, **32**, 751 (1976).
10. M. E. Fleet, *Z. Kristallogr.*, **180**, 63 (1987).
11. G. Blasse, *J. Inorg. Nucl. Chem.*, **25**, 743 (1963).
12. P. G. Bruce, A. R. West, *Mat. Res. Bull.*, **15**, 379 (1980).
13. K. A. Subbotin, V. A. Smirnov, E. V. Zharikov, A. V. Gaister, I. A. Shcherbakov, L. D. Iskhakova, *Opt. Spectrosc.*, **89**, 56 (2000).
14. K. A. Soubbotin, V. A. Smirnov, S. V. Kovaliov, H. J. Scheel, E. V. Zharikov, *Opt. Mater.*, **13**, 405 (2000).
15. K. A. Soubbotin, V. A. Smirnov, E. V. Zharikov, I. A. Shcherbakov, *Advanced Solid State Lasers*, Optical Society of America, 2002.
16. J. A. Gard, A. R. West, *J. Solid State Chem.*, **7**, 422 (1973).
17. G. J. Redhammer, G. Roth, G. Amthauer, *Acta Crystallogr. C*, **62**, i94 (2006).
18. J. Barbier, D. Levy, *Z. Kristallogr.*, **212**, 519 (1997).
19. R. K. Datta, *J. Am. Ceram. Soc.*, **50**, 384 (1967).
20. M. Behruzi, Th. Hahn, *Z. Kristallogr.*, **133**, 405 (1971).

ТЕРМИЧНО ПОВЕДЕНИЕ НА НЯКОИ ГЕРМАНАТИ С НЕОЛИВИНОВА СТРУКТУРА

Й. Косева^{1*}, В. Николов¹, А. Йорданова¹, П. Цветков¹, Н. Петрова²

¹ *Институт по обща и неорганична химия, Българска Академия на Науките, 1113 София, България*

² *Институт по минералогия и кристалография, Българска Академия на Науките, 1113 София, България*

Постъпила на 26 януари 2017 г.; Коригирана на 01 февруари 2017 г.

(Резюме)

Чрез твърдофазен синтез бяха получени монофазни германати от съединенията с хексагонална структура LiAlGeO_4 , LiGaGeO_4 и Zn_2GeO_4 (S.G. R3), от съединението с тетрагонална структура $\text{Li}_2\text{CaGeO}_4$ (S.G. I-42m), от съединението с моноклинна структура $\text{Ca}_5\text{Ge}_3\text{O}_{11}$ (S.G. C1') и от съединението с кубична структура $5\text{LiAlGeO}_4 \cdot 4\text{Zn}_2\text{GeO}_4$. Беше изследвано термичното поведение на тези германати от гледна точка да се намерят най-подходящия метод и условия за израстване от тях на монокристали, които след дотиране с Cr^{4+} , могат да бъдат използвани като лазерни матрици за лазери с широк спектър на излъчване в областта от 1.0 до 1.6 μm . Температурите на топене, вида на стапяне (с разлагане или без разлагане), вида на кристализиращите фази след разлагане, както и наличието или липсата на полиморфно превръщане близко до температурата на топене бяха изследвани чрез рентгенов фазов анализ и диференциален термичен анализ. Голяма част от данните за термичното поведение на тези германати се публикуват за първи път. Установено е, че четири от синтезираните германати (LiAlGeO_4 , Zn_2GeO_4 , $\text{Ca}_5\text{Ge}_3\text{O}_{11}$, и $5\text{LiAlGeO}_4 \cdot 4\text{Zn}_2\text{GeO}_4$) се топят конгруентно (без разлагане) и не показват наличие на фазов преход. За разлика от германатите с оливинова структура, които бяха изследвани по-детайлно за същите цели, монокристали от неоливиновите германати могат да бъдат израствани директно от тяхната собствена стопилка (по методите на Чохралски, Бриджман-Стокбаргер или Киропулос) вместо да се използва флакс метода, който се характеризира със значително по-малка скорост на израстване и ограничение за размера на израствания кристал.

Doped with Cu and Mn zinc oxide catalysts for oxidation of CO in noxious gas emissions

K. I. Milenova^{1*}, I. A. Avramova², P. M. Nikolov³, N. A. Kasabova³, G. M. Ivanov²

¹ Institute of Catalysis, Bulgarian Academy of Sciences, Acad. G. Bonchev St., bl. 11, 1113 Sofia, Bulgaria

² Institute of General and Inorganic Chemistry, Bulgarian Academy of Sciences, Acad. G. Bonchev St., Bl. 11, 1113 Sofia, Bulgaria

³ University of Chemical Technology and Metallurgy, 8 Kliment Ohridski, 1756, Sofia, Bulgaria

Received January 30, 2017; Revised February 16, 2017

Dedicated to Acad. Bogdan Kurtev on the occasion of his 100th birth anniversary

In the present work doped with Cu and Mn zinc oxide is investigated as catalyst for oxidation of CO. The doped zinc oxide samples are synthesized from carbonate, acetate and nitrate precursors and from activated doped ZnO. The content of Mn and Cu in the catalyst compositions is less than 1 wt %. For structural, textural and morphological characterization of the samples trivial methods were used: Atomic Absorption Spectroscopy (AAS), X-ray Diffraction (XRD), BET surface area analysis, X-ray Photoelectron Spectroscopy (XPS). Measurements of the catalytic activity were performed. A correlation between the type of precursor used for ZnO synthesis and the catalytic conversion has been established. The conversion reaches the highest values of 50% at 290 °C and 95% at 320 °C for Cu doped sample when activated ZnO is used as a carrier. ZnO synthesized by trivial method from carbonate precursor has 50% conversion at about 35 °C higher temperature than the activated sample. The results of recent investigation show high perspective of the catalysts, synthesized from activated carbonate precursors.

Key words: zinc oxide; manganese; copper; doping; carbon monoxide oxidation

INTRODUCTION

The accelerated development of energy and chemical industries leads to serious contamination of the environment. The existence of noxious emissions in the air such as CO, NO_x, H₂S and hydrocarbons from the internal combustion engines and the industry is a serious ecological problem. The catalytic disposal is one of the effective way for downgrading these contaminations [1–5]. Carbon monoxide can be removed by complete catalytic oxidation, achieved by catalysts with high efficiency and stable at dynamic variable conditions [6–8]. Precious metals based catalysts have widespread application in purification of waste gases [6–12]. These catalysts used in industrial practice have a number of disadvantages. They are expensive, due to the use of active components with high price, as well as the use of complex technological methods for production of the active phases. The searching of catalytic compounds with optimal composition and parameters is still actual question [1]. Another widespread catalytic group is that with high content of oxides and compounds of 3d transition metals [2, 10]. There is enhanced interest to the recently synthesized catalysts

consisting low per cent content of active phases Cu and Mn [8, 10, 13]. The choice of the precursor for the synthesis of active catalyst is essential. In some cases the change of the synthesis route can change the structure of materials, which is useful for practical application [8]. In the field of catalysis basic properties such as activity and selectivity are seriously influenced by the nanostructure of materials, which highly depends on the synthesis conditions [7, 9–12]. During the last years there is increasing interest to ZnO, obtained from different precursors. This is due to the specific chemical, surface and microstructure properties of this oxide, depending on the synthesis conditions and various methods of preparation. Participation of dopants in ZnO based catalysts leads to changes in the structure and texture characteristics, higher catalytic activity and stability and better performance in practice [6, 14–17]. That is why doped and activated ZnO is promising material because of its relatively low price and wide scale application as catalyst [12, 13, 18].

The aim of the present work is synthesis of ZnO based phases from different precursors (nitrate, acetate, carbonate) doped with Cu and Mn (<1 wt.%) and investigation of their catalytic activity. The content of Cu and Mn is lower than 1 wt.% and

* To whom all correspondence should be sent:
E-mail: kmilenova@ic.bas.bg

the obtained samples are from nitrate, acetate and carbonate precursor solutions.

EXPERIMENTAL

Several samples were obtained and named as follows:

A) From nitrate precursor: *MnZnO nitrate and CuZnO nitrate*

From acetate precursor: *MnZnO acetate and CuZnO acetate*

From carbonate precursor: *MnZnO carbonate and CuZnO carbonate*

Doped with Mn and Cu samples of ZnO were obtained from zinc nitrate, acetate and carbonate precursors.

Zn(NO₃)₂·4H₂O and Zn(CH₃COO)₂·2H₂O solutions were thermally decomposed for the preparation of ZnO. Small amounts of solutions of respective dopants - Mn(NO₃)₂·6H₂O or Cu(NO₃)₂·3H₂O were also added in defined ratio. For preparation of ZnO from carbonate, solutions of 0.8M Na₂CO₃, 0.4M ZnSO₄·7H₂O and Mn(NO₃)₂·6H₂O or Cu(NO₃)₂·3H₂O were used in defined ratio. For preparation of the catalysts, the corresponding precursors were heated for 3 h at 400 °C in air.

B) From carbonate precursor by deposition: *CuZnO deposition*

Previously obtained carbonate precursor was treated by aqueous solutions of Cu(NO₃)₂·3H₂O to lay the active phase by deposition method.

C) Previously activated Zinc oxide: *MnZnO activated, CuZnO activated*

Precursor of activated ZnO was prepared using method described in Bulgarian patent № 28915/1979. The active, Cu and Mn (~ 0.2 wt.%) phases of the supported catalysts were synthesized using deposition method. Definite quantities of the aqueous solutions of the corresponding metal salts MnSO₄·H₂O or CuSO₄·5H₂O were used. The samples were finally calcined at 400 °C for 3 h in air.

Chemical composition of the samples was determined using Atomic Absorption Analysis FAAS - SOLAAR M5 spectrometer.

The X-ray diffraction (XRD) analysis was carried out on a Siemens powder diffractometer model D500 using CuK α radiation within a 2 θ angle of diffraction interval of 10 ÷ 60 degrees. The identification of the phases was done by means of the JCPDS database of the International Center of Powder Diffraction Data. The particle size was determined by Scherrer's formula.

The determination of the specific surface area of the samples was carried out by nitrogen adsorption at the boiling temperature of liquid nitrogen (77.4 K) using a conventional volume measuring apparatus.

The X-ray photoelectron spectroscopy (XPS) studies were performed in a VG Escalab II electron spectrometer using AlK α radiation with energy of 1486.6 eV under base pressure 10⁻⁷ Pa and a total instrumental resolution 1eV. The binding energies (BE) were determined utilizing the C1s line (from an adventitious carbon) as a reference with energy of 285.0 eV. The accuracy of the measured BE was 0.2 eV. The C1s, Zn2p, O1s, Mn2p and Cu2p photoelectron lines were recorded and corrected by subtracting a Shirley-type background and quantified using the peak area and Scofield's photoionization cross-sections.

The catalytic activity of the samples was studied in an isothermal plug flow reactor enabling operation under steady-state conditions without temperature gradients.

The size of the catalyst particles (0.3 ÷ 0.6 mm) was chosen taking into account the reactor diameter (6.0 mm) and the hourly space velocity (20 000 h⁻¹) in order to reduce diffusion effects. The gas feed flow rate was 4.4 l/h, the catalyst bed volume was 0.2 cm³ and the mass of the catalyst charge was 0.5 ÷ 0.6 g. The catalytic oxidation of CO was performed at the temperature interval 200 ÷ 400 °C, the oxidizing agent used being oxygen from air (gas mixture: 21% O₂ and 79% N₂). The preliminary treatment of the catalyst included heating in air flow at 120 °C for 1 hour. The flow of CO was fed into the reactor by an Ismatex M62/6 pump (Switzerland).

The initial concentration of CO was 0.5 vol.%. The carrier gas was air (a mixture of 21% O₂ and 79% N₂). A Maihak (O₂/CO/CO₂) gas analyser was used to measure the CO and CO₂ concentrations with an accuracy of ±0.1 ppm, while the oxygen measurement accuracy was ±100 ppm.

RESULTS AND DISCUSSION

It is of interest to establish and to compare catalytic activity of doped with Mn and Cu zinc oxide. MnZnO and CuZnO catalysts obtained from carbonate, acetate and nitrate precursors as well as from doped pre-activated ZnO have been obtained and investigated. The values of specific surface areas of compounds obtained from different precursor are shown in Table 1.

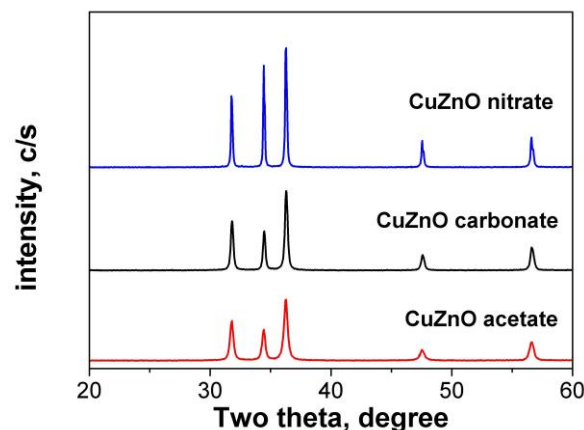
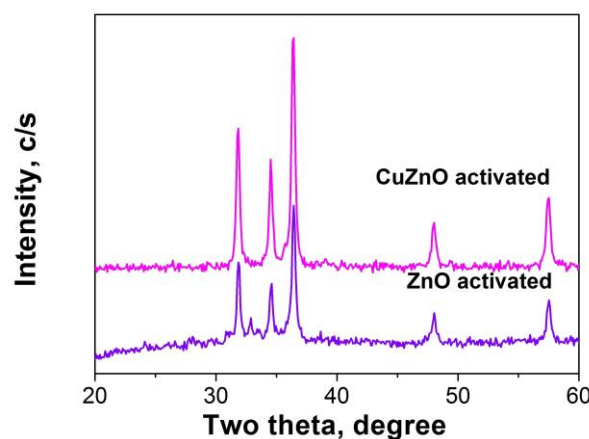
Table 1. Dopant content, crystallites size and specific surface area (A_{BET}) of Mn-doped and Cu-doped ZnO.

Sample	Dopant content, Wt.%	Crystallites size, nm	A_{BET} , m^2/g
MnZnO acetate	0.16	39	9
CuZnO acetate	0.19	36	10
MnZnO nitrate	0.14	68	1
CuZnO nitrate	0.17	57	1
MnZnO carbonate	0.15	31	23
CuZnO carbonate	0.18	27	23
CuZnO deposition	0.15	25	24
ZnO activated	-	25	44

It is evident that the specific surface area highly depends on the kind of used precursor, and from the doped element and the doping process, and also from the pre-activation of the obtained ZnO. That was expected, because the precursor decomposition also depends on their chemical composition. Lowest value of the specific surface area ($1 \text{ m}^2/\text{g}$) was measured for MnZnO nitrate and CuZnO nitrate samples. Possible explanation is the fact that the decomposition process passes in molten state. The samples obtained from carbonate precursor have the highest value of the specific area. All samples obtained have nanoscale sizes. Most fine crystals are observed for samples, obtained from basic zinc carbonate. It was observed tendency that Cu doping leads to lower sizes of oxide crystallites compared to Mn doping. XRD analysis of oxide samples (Figs. 1 and 2) show formation of hexagonal wurzite structure of ZnO (JCPDS 36-1451) observed for all samples. Diffractograms show only existence of ZnO phase, due to low content of the dopants Cu and Mn in it [18]. Probably the dopants are included in the lattice of ZnO leading to differences in the nanosize scale. The peak intensity is in correlation with investigated specific surface area. The width of diffraction lines also increases in the row: nitrate < acetate < carbonate in accordance with their specific area and the crystallinity. The obtained results correlate with the parameters of the precursor of ZnO.

XPS spectroscopy analysis of CuZnO and MnZnO samples was carried out. Fig. 3 and Fig. 4 present the observed Zn2p, O1s, Cu2p and Mn2p

lines. The results from investigation of Cao *et al.* of ZnO films doped with 1.5 wt.% Al and 0.2 wt.% Mn, shows that Mn^{2+} induce formation of more oxygen vacancies and this has been verified by O 1s XPS results [19].

**Fig. 1.** X-ray diffractograms of CuZnO carbonate, CuZnO acetate and CuZnO nitrate samples.**Fig. 2.** X-ray diffractograms of CuZnO activated and activated pure ZnO samples.

From XPS results was made estimation of manganese and copper contents and their chemical states, as Cu^{1+} and Mn^{2+} . The O1s peaks of Figs. 3 and 4 can be deconvoluted into three peaks corresponding to the low binding energy (LP), middle binding energy (MP), and high binding energy (HP) components centered at 530.30 ± 0.1 , 531.41 ± 0.11 , and 532.45 ± 0.05 eV, respectively. The first one is attributed to O^{2-} ions surrounded by Zn in the ZnO compound system. This peak is the indication of the amount of oxygen atoms in a fully oxidized, stoichiometric environment [20]. The middle peak centered at around 531.5 eV can be associated with the existence of O^x ions where $x < 2$ in the oxygen deficient region in the ZnO matrix and is related to the presence of oxygen vacancies [21].

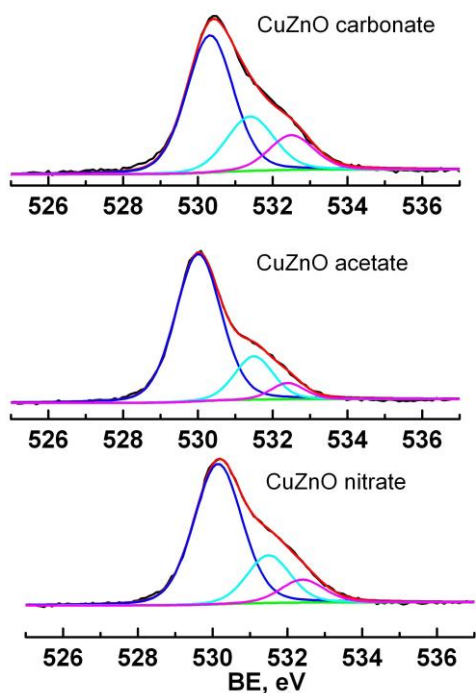


Fig. 3. XPS spectra of O1s for CuZnO samples obtained from nitrate, carbonate and acetate precursors.

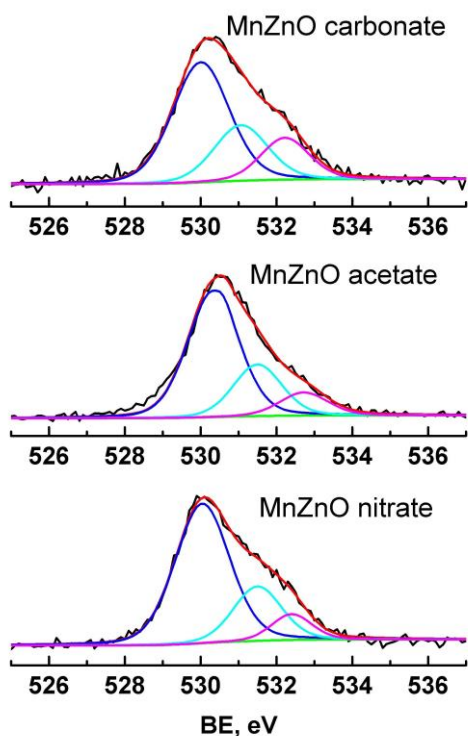


Fig. 4. XPS spectra of O1s for MnZnO samples obtained from nitrate, carbonate and acetate precursors.

The last higher binding energy peak is related to chemisorbed oxygen, dissociated oxygen, or OH⁻ groups on the surface. The area ratio of MP/(LP+MP+HP) for all investigated samples was

calculated. The MP/(LP+MP+HP) ratio for MnZnO samples is higher for the MnZnO (acetate), equal to 0.32, while the higher value for the CuZnO samples was evaluated for the CuZnO (carbonate), equal to 0.24. Obviously the higher the concentration of Cu and Mn atoms on the surface of the studied samples the higher the number of oxygen vacancies in them are. It is worth to notice here that the presence of Mn²⁺ into the ZnO introduce more oxygen vacancies than Cu⁺ into the ZnO independently of the used precursors.

The XPS investigation on Mn and Cu doped previously activated ZnO have been done too. The obtained and fitted results of the O1s photoelectron line are shown in Fig. 5. The area ratios of MP/(LP+MP+HP) for both samples have been calculated and were evaluated to be 0.29 for the Mn doped and 0.33 for the Cu doped one. The intensity of the HP and MP peak are almost equal, which indicates coexistence of oxygen vacancies and chemisorbed oxygen. The obtained result shows that the advanced procedure of activation ZnO is most probably due to the transfer of the oxygen atoms, oxygen vacancies and chemisorbed oxygen come forth simultaneously as dominant defects.

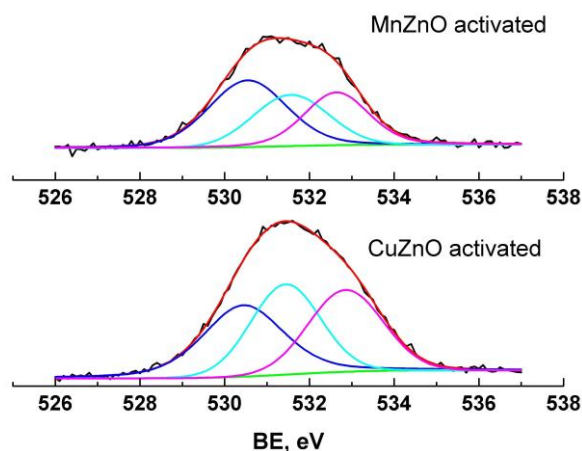


Fig. 5. XPS spectra of O1s for investigated samples after advanced activation of ZnO obtained from carbonate precursors.

The catalytic activity of CO oxidation reaction for different MnZnO and CuZnO samples is shown in Figs. 6a and 6b. The composition of the model gas used in the investigation is similar to those of the gases emitted by the automotive transport. Regarding CO oxidation it can be concluded, that the precursor of zinc oxide carrier is of great importance and the observed catalytic activity is in the row: carbonate > nitrate > acetate. It was also found that copper doping has better performance than manganese one when compare the samples

from the same precursor [22]. For the doped activated ZnO regardless of the kind of the dopant is observed higher activity in comparison with all other samples. Doping with Cu leads to 50% conversion at 290 °C, and full conversion is observed at about 330 °C. Doping with Mn of activated ZnO sample has lower effect over catalytic activity, respectively the temperatures for conversion are shifted to higher values - at temperatures between 360 °C and 370 °C a full conversion is achieved.

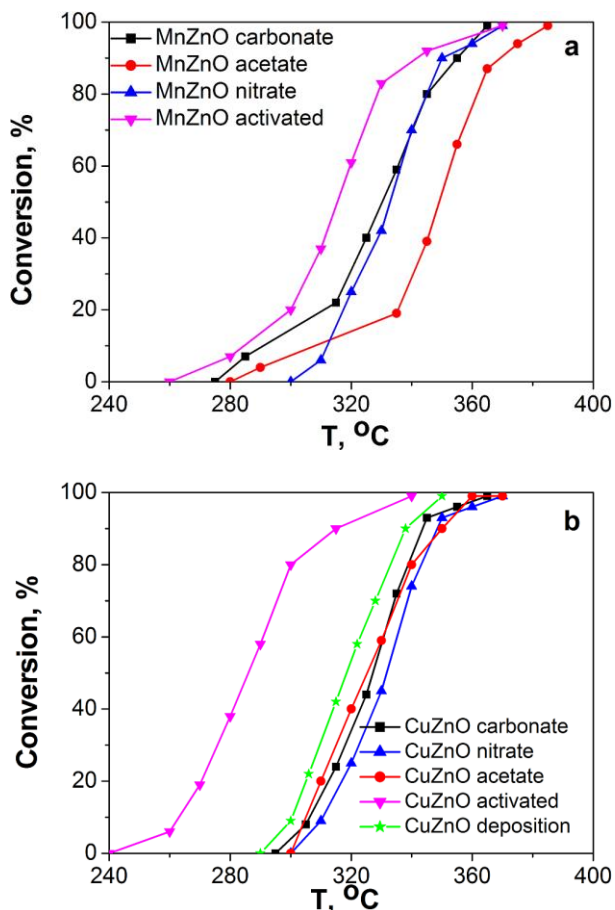


Fig. 6. Conversion of CO transformed to CO₂ of: a) MnZnO samples and b) CuZnO samples.

CONCLUSION

ZnO based catalysts doped with Cu and Mn (up to 0.2 wt.%) were synthesized from three different precursor solutions and the measured catalytic activity for CO oxidation reaction in waste gas emissions is ranged in the row: carbonate > acetate > nitrate. The presence of Cu as a dopant in catalytic compositions irrespective of used zinc oxide precursor provides higher catalytic activity toward investigated reaction. Activated zinc oxide

doped with Cu provides full conversion of CO at lowest temperature due to simultaneous role of oxygen vacancies and the oxygen absorbed on the surface of the catalyst. The obtained doped phases based on activated ZnO are perspective materials for industrial purification of gas fluids from CO.

REFERENCES

1. I. Didenkulova, Synthetic Ceramic Catalysts for Oxidation of CO to CO₂: Kinetics and Mechanism (in Russian). PhD Thesis, Nizhny Novgorod, 2008.
2. Y. Gou, X. Liang, B. Chen, *J. Alloy Comp.*, **574**, 181 (2013).
3. A. Łamacz, A. Krzton, G. Djéga-Mariadassou, *Appl. Catal. B Environ.*, **142-143**, 268 (2013).
4. X. Zhang, G. Dou, Z. Wanga, L. Li, Y. Wang, H. Wang, Z. Hao, *J. Hazard. Mater.*, **260**, 104 (2013).
5. A. Liu, T. Zhu, X. Lu, L. Song, *Appl. Energy*, **111**, 383 (2013).
6. X. Liu, M. H. Liu, Y. C. Luo, C. Y. Mou, S. D. Lin, H. Cheng, J. M. Chen, J. F. Lee, T. S. Lin, *J. Am. Chem. Soc.*, **134**, 10251 (2012).
7. P. Kundu, N. Singhanian, G. Madras, N. Ravishankar, *Dalton Trans.*, **41**, 8762 (2012).
8. T. Reina, S. Ivanova, M. Dominguez, M. Centeno, J. Odriozola, *Appl. Catal. A Gen.*, **419-420**, 58 (2012).
9. H. Noei, A. Birkner, K. Merz, M. Muhler, Y. Wang, *J. Phys. Chem. C*, **116**, 11181 (2012).
10. S. Pongstabodee, S. Monyanon, A. Luengnaruemitchai, *Int. J. Hydrogen. Energy*, **37**, 4749 (2012).
11. E. Castillejos, R. Bacsá, A. Guerrero-Ruiz, I. Rodríguez-Ramos, L. Datas, P. Serp, *Nanoscale*, **3**, 929 (2011).
12. Y. W. Chen, D. S. Lee, H. J. Chen, *Int. J. Hydrogen. Energy*, **37**, 15140 (2012).
13. Y. Yoshida, Y. Mitani, T. Itoi, Y. Izumi, *J. Catal.*, **287**, 190 (2012).
14. J. P. Auffredic, A. Boulitif, J. Langford, D. Louer, *J. Amer. Cer. Soc.*, **78**, 323 (1995).
15. N. Audebrand, J. Auffredic, D. Louer, *Chem. Mater.*, **10**, 2450 (1998).
16. Y. Zhang, K. Yu, S. Ouyang, Z. Zhu, *Phys. B Condens. Matter.*, **382**, 76 (2006).
17. L. Yang, G. Wang, C. Tang, H. Wang, L. Zhang, *Chem. Phys. Lett.*, **409**, 337 (2005).
18. Q. Xiao, L. Ouyang, *J. Alloy Comp.*, **479**, L4 (2009).
19. H. Cao, Z. Pei, J. Gong, C. Sun, R. Huang, L. Wen, *J. Solid State Chem.*, **177**, 1480 (2004).
20. B. J. Coppa, R. F. Davis, R. J. Nemanich, *Appl. Phys. Lett.*, **82**, 400 (2003).
21. P. T. Hsieh, Y. C. Chen, K. S. Kao, C. M. Wang, *Appl. Phys. A Mater. Sci. Process*, **90**, 317 (2008).
22. K. Milenova, I. Avramova, A. Eliyas, V. Blaskov, I. Stambolova, N. Kassabova, *Environ. Sci. Pollut. Res.*, **21**, 12249 (2014).

ДОТИРАНИ С Cu И Mn ЦИНКОВО ОКСИДНИ КАТАЛИЗАТОРИ ЗА ОКИСЛЕНИЕ НА CO ВЪВ ВРЕДНИ ГАЗОВИ ЕМИСИИ

К. И. Миленова^{1*}, И. А. Аврамова², П. М. Николов³, Н. А. Касабова³, Г. М. Иванов²

¹ *Институт по катализ, Българска академия на науките, ул. „Акад. Г. Бончев“, бл. 11, 1113 София, България*

² *Институт по обща и неорганична химия, Българска академия на науките, ул. „Акад. Г. Бончев“, бл. 11, 1113 София, България*

³ *Химикотехнологичен и Металургичен Университет, бул. "Св. Климент Охридски" No 8, 1756 София, България*

Постъпила на 30 януари 2017 г.; Коригирана на 16 февруари 2017 г.

(Резюме)

В настоящата работа дотиран с Cu и Mn цинков оксид е изследван като катализатор за окисление на CO. Дотираните проби от цинков оксид са получени от карбонатен, ацетатен и нитратен прекурсори и от активиран дотиран ZnO. Съдържанието на Mn и Cu в каталитичните композиции е под 1 wt %. За структурно, текстурно и морфологично охарактеризиране на пробите са използвани тривиални методи: Атомно Абсорбционна Спектроскопия (AAS), Рентгенофазов Дифракционен анализ (XRD), BET анализ на повърхността, Рентгенова Фотоелектронна Спектроскопия (XPS). Изследвана е и каталитичната активност. Съществува корелация между вида прекурсор, използван за синтеза на ZnO и каталитичното превръщане. Най-висока конверсия се наблюдава за Cu дотираната проба върху носител активиран ZnO: 50% конверсия при 290 °C и 95% при 320 °C. ZnO, синтезиран по стандартен метод от прекурсор карбонат претърпява 50% конверсия при около 35 °C по-висока температура, отколкото активираната проба. Резултатите от настоящото изследване показват висока перспектива на катализатори, получени от активирани карбонатни прекурсори.

Oxygen Radical Absorbance Capacity of Bulgarian fruits, vegetables, herbs and mushrooms. A review

P. N. Denev*

Institute of Organic Chemistry with Centre of Phytochemistry, Bulgarian Academy of Sciences, Laboratory of Biologically Active Substances, 139 "Ruski" blvd., 4000 Plovdiv, Bulgaria

Received February 13, 2017; Revised March 07, 2017

Dedicated to Acad. Bogdan Kurtev on the occasion of his 100th birth anniversary

In search of novel sources of antioxidants in the recent years, traditional plant foods have been extensively studied for their antioxidant activity. Investigation of natural products is a research field with great potential and is especially important in countries possessing great biodiversity, like Bulgaria. About 600 plant species from Bulgarian flora are recognized as medicinal and are traditionally used in ethnopharmacology and phytotherapy. Given the huge interest in antioxidants, the large number of methods developed to give a quantitative assessment of antioxidant action is not surprising. Dozens of methods for determination of antioxidant activity in food and biological samples have been developed. The results reported in following sections are part of a long-term study of the Laboratory of biologically active substances, Institute of Organic Chemistry with Centre of Phytochemistry – Bulgarian Academy of Sciences, on antioxidant activity of Bulgarian fruits, vegetables, herbs and mushrooms. Results are obtained by the Oxygen Radical Absorbance Capacity (ORAC) method in which the inhibition time and inhibition degree can be measured. The ORAC method is relevant for biological samples, since it assesses the radical scavenging activity of the sample against peroxy radicals, which physiologically are the most important ones. Besides, oxidation process is performed in water media, at physiological pH and temperature. Current review compiles data for antioxidant activity of 90 raw materials, including unpublished results for ORAC value of 11 mushrooms, 4 vegetables and 2 herbs.

Key words: ORAC - Oxygen Radical Absorbance Capacity; Bulgarian plants, fruits, vegetables, herbs, mushrooms

INTRODUCTION

Life on earth is inconceivable without oxygen (O_2) but in higher concentration this vital element is toxic to aerobes. Most of the damaging effects of O_2 are due to oxygen radicals which embrace superoxide ($O_2^{\cdot-}$), hydroperoxyl (HOO^{\cdot}), hydroxyl (HO^{\cdot}), peroxy (ROO^{\cdot}) and alkoxy (RO^{\cdot}) radicals [1]. These, together with the non-radicals hydrogen peroxide (H_2O_2), ozone (O_3) and singlet oxygen (1O_2) constitute the so called reactive oxygen species (ROS). ROS together with the nitrogen reactive species (RNS): nitric oxide (NO), peroxynitrite ($ONOO^{\cdot}$), peroxynitrate, *etc.* are constantly produced in our bodies through numerous physiological reactions and processes [2]. Experimental evidence has directly or indirectly suggested that there are six major reactive species causing oxidative damage in human body. These species are superoxide anion, hydrogen peroxide, peroxy radicals, hydroxyl radical, singlet oxygen and peroxynitrite. Superoxide is formed *in vivo* by NADPH oxidase in phagocytic cells, by other enzymes like xanthine

oxidase and xanthine dehydrogenase which reduce O_2 to $O_2^{\cdot-}$ and by the auto-oxidation of many biomolecules like glyceraldehydes, FMNH₂, FADH₂, adrenalin, noradrenalin and dopamine [3]. The most important source of $O_2^{\cdot-}$ *in vivo* is the mitochondrial electron transport chain and hemoglobin in human erythrocytes also could be a source of superoxide radicals [4]. Hydroxyl radicals are the most potent oxidants among ROS. Physiologically they are being produced mainly through Fenton-like reactions catalyzed by transition metal ions, UV-induced homolytic cleavage of H_2O_2 [5], γ -rays-assisted homolytic fission of water and hypochlorous acid reacting with $O_2^{\cdot-}$ [6]. Peroxy and alkoxy radicals are good oxidizing agents which can easily abstract hydrogen atom from different biomolecules. *In vivo* they are formed through the reaction of carbon-centered radicals with O_2 or by decomposition of organic peroxides [7]. Hydrogen peroxide is continuously produced in many tissues *in vivo* and mitochondria are the biggest contributors to its generation both by monoamine oxidases and by dismutation of $O_2^{\cdot-}$ [1]. Singlet oxygen is often generated by photosensitization reactions and its detrimental

* To whom all correspondence should be sent:
E-mail: petkodenev@yahoo.com

effect is expressed mainly in skin and eyes damages. Peroxynitrite is generated by the reaction of NO with superoxide radical and the biggest contributors for NO generation are the nitric oxide synthase enzymes. To counteract the assault of all ROS and RNS, living cells had elaborated a complex biological defense system composed of enzymatic and non-enzymatic antioxidants that convert ROS/RNS to harmless species. The term antioxidant is defined as any substance that in low concentrations compared to those of an oxidizable substrate, significantly delays or prevents oxidation of the substrate [1]. By the mechanism of action, antioxidants are divided to preventive and chain-breaking antioxidants. Preventive antioxidants act as the first line defense by suppressing the formation of ROS and RNS. These antioxidants remove active species rapidly before they attack biologically essential molecules. For example, superoxide radical is converted to oxygen and hydrogen peroxide by superoxide dismutase (SOD) and hydrogen peroxide can be converted to water and oxygen by catalase. In contrast, no enzymes are known to counteract $ROO\cdot$, $HO\cdot$, 1O_2 and $ONOO^-$ [8]. Therefore, the burden of defense relies on a variety of nonenzymatic antioxidants such as vitamins C and E and many phytochemicals such polyphenols that have the property to scavenge oxidants and free radicals. These scavenging antioxidants act as the second line defense *in vivo*. Usually, there is balance between the antioxidants and the prooxidants *in vivo* but several factors like stress, radiation, nutrition, polluted atmosphere and smoking disrupt the oxidative balance leading to the so called oxidative stress. Oxidative stress is a physiological state which is believed to be a prerequisite for the development of many diseases including cardiovascular disease (CVD), stroke, and neurodegenerative disorders such as Alzheimer disease and Parkinson disease [9–11]. The injury caused by oxidative stress can affect all organ systems. For example, LDL oxidation is the initial step to the arteriosclerosis development, leading to cardiovascular diseases and oxidized DNA basis are mutagenic and are involved in the carcinogenesis. In case of oxidative stress it is necessary to accept exogenous antioxidants with the diet. Most of the antioxidants taken with the diet are of plant origin and the richest sources are herbs, fruit and vegetables. Polyphenol substances, carotenoids, vitamin C and vitamin E are the biggest contributors to the antioxidant properties of these raw materials. A growing amount of evidences indicates that the consumption of plant

foods is correlated with a lower risk from development of atherosclerosis and oxidative stress-related diseases [12]. In contrast, diets poor in plant-based foods and rich in animal products and ingredients are related to increased risk for CVD and certain types of cancer [13]. In the last decades, polyphenolic compounds gained a lot of attention and are subject to thorough research because of their antioxidant properties and beneficial effect beyond vitamin action. They are the most abundant antioxidants taken with the diet [14] with over 8000 known compounds which makes them one of the largest groups in plant kingdom. By definition polyphenols are compounds that have more than two phenolic hydroxyl group attached to one or more benzene rings. Natural polyphenols are structurally diverse and vary from single molecules, for example some phenolic acids to highly polymerized structures like tannins [15].

Taking into consideration the diversity of substances with antioxidant activity and that of ROS and RNS, the challenge for the development of a standard universal method for measuring antioxidant activity is high. The situation is complicated additionally by the different physico-chemical characteristics of antioxidants and the fact that antioxidants react differently towards different radicals or oxidants. For example, carotenoids which are poor radical scavengers are very good inhibitors of singlet oxygen. Due to the different mechanisms and reaction characteristics, none of the known methods described in the literature does not accurately reflect all aspects of antioxidant activity against the variety of ROS and RNS, and there is still no consensus for a universal standardized method for determination of antioxidant activity of natural products [16]. The antioxidant activity is defined as the ability of a compound to reduce prooxidant agents. Given the huge interest in antioxidants, the large number of methods developed to give a quantitative assessment of the antioxidant action is not surprising. Dozens of methods for determination of antioxidant activity in food and biological samples have been developed. Typically, the samples analyzed are composed of a large number of individual compounds, which makes difficult the quantitative assessment of their antioxidant action and therefore, most methods measure the common antioxidant activity of the sample. Different methods are based on the generation of different radicals, acting through different mechanisms and still lacks a unified standard method which provides an assessment of the antioxidant properties of a

given compound against all radicals. None of the methods invented do fully cover the antioxidant activity, because it expresses the antioxidant properties of a given compound against a given oxidant under defined conditions. Therefore, no method gives "total" evaluation of these properties and it is correct whenever talking about antioxidant activity to note the method by which it is measured [16]. Still the most employed concept for antioxidant action is associated with antioxidants as radical scavengers. Based on the chemical mechanism by which this is done, the methods for the determination of antioxidant activity are divided into two categories: based on hydrogen atom transfer (HAT), and based on a single electron transfer (SET). Those based on SET include redox reaction with the oxidant, which is also the indicator of the reaction. They reflect the ability of the potential antioxidant to transfer single electron, and reduce the oxidant. TBA-based methods measure the ability of an antioxidant to scavenge free radicals by donation of a hydrogen atom. Therefore, HAT-based methods provide a more accurate assessment of the ability of antioxidants to interrupt free radical chain reactions. Because peroxy radicals are the most physiologically important and are involved in lipid oxidation, it is believed that HAT methods with greater reliability reflect the mechanism by which antioxidants act *in vivo*. However, none of the methods invented do not reflect the total antioxidant activity of a given sample, neither reflect the bioavailability of antioxidants [16].

OXYGEN RADICAL ABSORBANCE CAPACITY OF BULGARIAN FRUITS, VEGETABLES, HERBS AND MUSHROOMS

In search of novel sources of antioxidants in the last years, traditional plant foods have been extensively studied for their antioxidant activity. The ingestion of fresh fruit, vegetables and teas rich in natural antioxidants has been associated with prevention of cancer and cardiovascular diseases [17]. The higher intake of plant foods correlates with lower risk of mortality from these diseases [18]. Approximately 60% of the commercially available anti-tumoral and anti-infective agents are of natural origin [19]. Investigation of natural products is a research field with great potential and is especially important in countries possessing great biodiversity, like Bulgaria. About 600 plant species from the Bulgarian flora are recognized as medicinal and are traditionally used in

ethnopharmacology and phytotherapy [20, 21]. The results reported in the following sections are part of a long-term investigation performed in the Laboratory of biologically active substances, Institute of Organic Chemistry with Centre of Phytochemistry – Bulgarian Academy of Sciences on antioxidant activity of fruits, vegetables and herbs grown in Bulgaria. Results are obtained by the Oxygen Radical Absorbance Capacity (ORAC) in which the inhibition time and inhibition degree are measured as the oxidation reaction goes to completion [22]. The ORAC method is relevant for biological samples, since it assesses the radical scavenging activity of the sample against peroxy radicals, which physiologically are the most important ones. Besides, oxidation process is performed in water media at physiological pH and temperature [8, 16, 23]. It was found that ORAC method is more sensitive than other methods, thus indicating antioxidant properties in samples with very low quantities of polyphenols [24]. The accumulation of biologically active substances in plants depends on several genetic and environmental factors including cultivar, climate, fertilization, irrigation, sun exposure, *etc.* Ou *et al.* [25] reported variable results even for samples from one species depending on the variety, place of origin, and harvest time. Therefore, it is of a particular interest to evaluate the antioxidant activity of local natural products, since they are the most consumed by the Bulgarian population. The presented results are part of a long-term investigation, aiming the development of a database with antioxidant capacities of Bulgarian raw materials. The development of such database will identify the major contributors to the antioxidant potential of our daily diet. In the literature, similar ORAC databases are already reported for common foods in the USA [26] and fruits produced in south Andes region of South America [27].

Bulgarian Fruits

Fresh fruits are a good source of antioxidants and their use in human nutrition is of fundamental importance. To encourage fruit consumption among the population it is important to recognize which fruits have the highest antioxidant activity and to promote their regular consumption. In a recent study, we evaluated the ORAC antioxidant activity of 26 fruits of Bulgarian origin and results are shown in Table 1 [28]. Since polyphenols contribute significantly to the antioxidant activity of plant materials, their content in the investigated fruits is given in the table, as well.

Table 1. ORAC antioxidant activity and polyphenol content of Bulgarian fruits according to Denev *et al.*, 2013 [28]. Results are expressed as means \pm standard deviations on a fresh weight basis.

Fruits	ORAC, $\mu\text{mol TE/g}$	Total polyphenols, GAE/100g
Apple	13.8 \pm 2.6	126.0 \pm 5.6
Apricot	7.2 \pm 1.0	44.4 \pm 0.4
Black currant	96.0 \pm 3.2	835.1 \pm 19.1
Blackberry	74.2 \pm 3.5	688.2 \pm 19.0
Blackthorn	79.1 \pm 3.9	858.3 \pm 19.4
Blueberry	98.8 \pm 7.1	819.5 \pm 9.7
Cherry	25.8 \pm 1.2	118.4 \pm 6.7
Chokeberry	160.8 \pm 4.8	1 817.8 \pm 34.8
Cornel cherry	49.0 \pm 3.5	624.6 \pm 1.3
Cranberry	70.0 \pm 1.9	705.5 \pm 17.9
Elderberry	205.4 \pm 15.2	1 148.0 \pm 11.9
Fig	13.6 \pm 1.6	98.7 \pm 2.8
Hawthorn	153.6 \pm 9.1	1 184.4 \pm 15.7
Honeydew melon	2.3 \pm 0.1	40.4 \pm 1.1
Peach	6.2 \pm 1.5	41.1 \pm 1.4
Plum	10.8 \pm 1.1	64.5 \pm 1.7
Pomegranate	19.7 \pm 3.1	195.1 \pm 8.0
Pumpkin	4.9 \pm 0.5	14.6 \pm 0.9
Raspberry	38.9 \pm 2.0	369.1 \pm 1.7
Red grapes	26.8 \pm 3.4	195.5 \pm 8.9
Rosehip	201.1 \pm 14.6	1 934.3 \pm 4.3
Rowanberry	80.9 \pm 6.2	733.6 \pm 7.4
Sour cherry	58.6 \pm 5.8	529.9 \pm 10.0
Strawberry	47.2 \pm 3.1	386.5 \pm 15.2
Watermelon	3.8 \pm 0.5	39.8 \pm 0.8
White grapes	6.3 \pm 1.3	112.1 \pm 0.3

The total antioxidant activity varied considerably among the investigated fruits. For example, on the basis of fresh weight, elderberry and rosehip showed the highest antioxidant capacity - (205.38 \pm 15.24 $\mu\text{mol TE/g}$) and (201.14 \pm 14.59 $\mu\text{mol TE/g}$), respectively. Pumpkin, watermelon and honeydew melon revealed the lowest ORAC antioxidant activity (4.92 \pm 0.47, 3.80 \pm 0.47 and 2.33 \pm 0.12 $\mu\text{mol TE/g}$, respectively). The beneficial properties of elderberry, rosehip and hawthorn are well known to the Bulgarian population as they have been widely used in ethnopharmacology and traditional medicine since ancient times. Another fruit with high antioxidant activity, chokeberry is of North American origin and was introduced to Bulgaria about 60 years ago. Nowadays it is cultivated successfully as an industrial crop and deserves attention, because it is recognized as an especially beneficial medicinal plant. There are many papers attempting to rank the antioxidant properties of different plant materials *via* different methods [29, 30] including ORAC [25, 26, 31]. When comparing

the results with other published data it is seen that Bulgarian fruits reveal different antioxidant properties. Our results 47.2 $\mu\text{mol TE/g}$ and 98.8 $\mu\text{mol TE/g}$ for strawberries and blueberries are 18.5% and 37% higher than the results reported by Wu *et al.* [26] for the same plant species. On the other hand, results reported from the same authors for raspberry are 26% higher than the results in our study. The accumulation of biologically active substances in plants depends on several genetic and environmental factors including cultivar, climate, fertilization, irrigation, sun exposure, *etc.* Therefore, it is of a particular interest to evaluate the antioxidant activity of local natural products. In one of the first attempts to quantify dietary antioxidant needs of the body Prior *et al.* [32] demonstrated that consumption of certain berries and fruits such as blueberries, mixed grape and kiwifruit was associated with increased ORAC plasma antioxidant capacity in the postprandial state and consumption of an energy source of macronutrients containing no antioxidants was associated with a decline in plasma antioxidant capacity. The authors estimated that according to the energy intake of the diet, 5000 – 15000 $\mu\text{mol TE}$ are necessary to cover human daily antioxidant needs. Therefore, comparative studies such as the current are interesting not only from research point of view, but also for the consumers and nutritionists. The obtained results are a good tool for the medical professionals to promote the consumption of fruits with high antioxidant activity as a part of a healthy diet. For example, the consumption of only 25–75 g elderberries or briers, or 30–90 g chokeberries will cover the necessary antioxidant units per day. In contrast, approximately 2170–6500 g of honeydew melons will provide the same amount of ORAC units.

Bulgarian Vegetables

Vegetables are among the major antioxidant sources in our daily diet, and therefore the estimation of daily antioxidant capacity intake from these foods is beneficial [9]. Vegetables are known to possess a variety of antioxidant effects and properties. Flavonols (such as quercetin, myricetin, kaempferol) and flavones (e.g. apigenin, luteolin) in plant materials are closely associated with their antioxidant function mainly due to their redox properties exerted by various possible mechanisms: free-radical scavenging activity, transition-metal-chelating activity, and/or singlet-oxygen-quenching capacity [33, 34].

Our study in 2010 was the first reporting antioxidant activity of Bulgarian vegetables [24]. These vegetables are commonly consumed by the Bulgarian population as an important constituent of their traditional food [24]. The total polyphenol content of these selected vegetables was measured as well, so as to evaluate its contribution to their total antioxidant function. The objective of the study was to supply both new methodological background for the food quality control in food industry and new information on the antioxidant function of selected vegetables for nutritionists and public. Results are shown in Table 2.

Table 2. ORAC antioxidant activity and polyphenol content of Bulgarian vegetables according to Ciz *et al.*, 2010 [24]. Results are expressed as means \pm standard deviations on fresh weight basis.

Vegetables	ORAC, $\mu\text{mol TE/g}$	Total polyphenols, GAE/100g
Beans *	20 \pm 1.8	98.2 \pm 4.3
Broccoli	16.1 \pm 1.2	102.1 \pm 5.9
Capsicum	19.9 \pm 1.4	286.7 \pm 5.1
Carrot	4.8 \pm 1.1	35.2 \pm 2.0
Celery leaves	113.5 \pm 6.1	605.6 \pm 9.4
Celery root	15.3 \pm 1.2	43.8 \pm 2.3
Chick peas *	28 \pm 2.1	107.6 \pm 5.6
Chilli pepper	36.1 \pm 6.5	298.6 \pm 1.8
Cucumber	1.2 \pm 0.2	24.2 \pm 2.4
Dill	10.5 \pm 1.1	150.4 \pm 0.9
Eggplant	16.2 \pm 2.0	102.9 \pm 4.7
Goathorn pepper	30.6 \pm 1.4	260.5 \pm 5.0
Green beans	14.5 \pm 1.2	101.5 \pm 3.3
Green onion	14.7 \pm 1.5	92.7 \pm 0.9
Green pepper	5.6 \pm 0.3	80.7 \pm 3.6
Gumbo	14.6 \pm 0.8	89.8 \pm 4.0
Lentils *	49 \pm 3.7	254.3 \pm 8.4
Lovage	57.3 \pm 5.0	267.0 \pm 2.1
Parsley	108.6 \pm 13.1	599.7 \pm 0.4
Potato	10.3 \pm 1.3	65.5 \pm 1.1
Radish	23.6 \pm 1.7	89.9 \pm 1.7
Red beet	12.6 \pm 1.6	81.5 \pm 1.6
Red pepper	9.3 \pm 0.9	115.7 \pm 1.5
Soybean *	99 \pm 5.2	589.6 \pm 32.1
Tomato	5.4 \pm 0.3	41.3 \pm 2.2
Vegetable marrow	2.9 \pm 0.3	20.0 \pm 1.7

* Unpublished results

The total phenolic content in the vegetable analyzed was in the range of 605.6 to 20.0 mg GAE/100g fresh weight and there was a direct relationship between the total phenolic content and ORAC antioxidant activity with correlation coefficient $r = 0.95$. As we have shown, aromatic vegetable such as parsley, dill and lovage with high polyphenol content and high ORAC values could

be excellent sources of antioxidant and should be a part of everyday diet.

Bulgarian Herbs

In search of novel sources of antioxidants in the last years, medicinal plants have been extensively studied for their antioxidant activity. From ancient times, herbs have been used in many areas, including nutrition, medicine, flavoring, beverages, cosmetics, *etc.* It is of particular interest to investigate the antioxidant properties of medicinal plants, especially those traditionally used in folk medicine. Prior to our study, there was just scarce information on antioxidant activity of Bulgarian herbs with methods like DPPH and ABTS [35, 36]. In our study, we investigated medicinal plants, which were chosen based on their use in traditional medicine [37]. Table 3 shows the ORAC antioxidant activity of the investigated medicinal plants. The greatest ORAC value of 2917 $\mu\text{mol TE/g}$ was found for peppermint. This study was the first one reporting ORAC antioxidant activity for several medicinal plants, such as: wild basil (*Clinopodium vulgare*) leaves, birch (*Betula pendula*) leaves, caltrop (*Tribulus terrestris*) aerial parts, mountain tea (*Sideritis scardica*) aerial parts, hop (*Humulus lupulus*) flowers, marigold (*Calendula officinalis*) flowers and greater burdock (*Arctium lappa*) roots.

Bulgarian Mushrooms

Mushrooms are another common food for the Bulgarian population. Therefore, we investigated antioxidant activity of the following 11 mushrooms of Bulgarian origin: black chanterelle (*Craterellus cornucopioides*), Caesar's mushroom (*Amanita caesarea*), champignon (*Agaricus bisporus*), chanterelle (*Cantharellus cibarius*), edible boletus (*Boletus edulis*), fairy ring mushroom (*Marasmius oreades*), honey mushroom (*Armillaria mellea*), Judas's ear fungus (*Auricularia auricular*), Oyster mushroom (*Pleurothus ostreatus*), shiitake (*Lentinus edodes*), yellow foot (*Cantharellus aurora*). These results are unpublished and are depicted on Fig. 1. From the results it is evident that edible boletus distinct among other mushrooms with ORAC value of 113.9 $\mu\text{mol TE/g}$ dry weight followed by fairy ring mushroom and Judas's ear fungus. These results indicate that mushrooms are not very rich source of antioxidants but could contribute the total antioxidant value of our daily diet.

Table 3. ORAC antioxidant activity and polyphenol content of Bulgarian herbs according to Kratchanova et al., 2010 [37]. Results are presented as means \pm SD based on dry weight.

Herb	ORAC, $\mu\text{mol TE/g}$	Total polyphenols, mg/100g
Basil (<i>Ocimum basilicum</i>) leaves	402 \pm 40	2391 \pm 38
Birch (<i>Betula pendula</i>) leaves	1185 \pm 73	5542 \pm 201
Caltrop (<i>Tribulus terrestris</i>) aerial parts	819 \pm 56	5681 \pm 200
Camomile (<i>Matricaria chamomilla</i>) flowers	814 \pm 72	4665 \pm 137
Chicory (<i>Cichorium intybus</i>) aerial parts	398 \pm 22	1821 \pm 63
Common balm (<i>Melissa officinalis</i>) leaves	1121 \pm 60	11885 \pm 109
Dandelion (<i>Taraxacum officinale</i>) aerial parts	381 \pm 16	2206 \pm 58
Dandelion (<i>Taraxacum officinale</i>) roots *	193 \pm 12	1210 \pm 72
Fenugreek (<i>Trigonella foenum-graecum</i>) seeds	327 \pm 28	1692 \pm 105
Greater burdock (<i>Arctium lappa</i>) roots	365 \pm 31	2742 \pm 112
Hawthorn (<i>Crataegus monogyna</i>) leaves and flowers	2163 \pm 89	7104 \pm 111
Hop (<i>Humulus lupulus</i>) flowers	749 \pm 62	5728 \pm 262
Laurel leaves (<i>Laurus nobilis</i>) leaves	837 \pm 81	7081 \pm 299
Lime (<i>Tilia cordata</i>) flowers	1020 \pm 88	9296 \pm 427
Liquorice (<i>Glycyrrhiza glabra</i>) roots	670 \pm 48	3452 \pm 98
Marigold (<i>Calendula officinalis</i>) flowers	407 \pm 57	2141 \pm 115
Mountain tea (<i>Sideritis scardica</i>) aerial parts	778 \pm 77	3984 \pm 201
Nettle (<i>Urtica dioica</i>) leaves	162 \pm 11	958 \pm 43
Nettle (<i>Urtica dioica</i>) roots *	23 \pm 1.8	345 \pm 18
Peppermint (<i>Mentha piperita</i>) leaves	2917 \pm 52	20216 \pm 359
Raspberry (<i>Rubus idaeus</i>) leaves	1156 \pm 80	7759 \pm 216
Sage (<i>Salvia officinalis</i>) leaves	966 \pm 69	5295 \pm 148
Spearmint (<i>Mentha spicata</i>) leaves	748 \pm 57	4522 \pm 102
St. John's worth (<i>Hypericum perforatum</i>) aerial parts	1141 \pm 93	11283 \pm 74
Thyme (<i>Thymus vulgaris</i>) aerial parts	1637 \pm 59	11409 \pm 171
Wild basil (<i>Clinopodium vulgare</i>) aerial parts	1437 \pm 60	9468 \pm 128
Yarrow (<i>Achillea millefolium</i>) flowers	842 \pm 80	5728 \pm 232

* Unpublished results

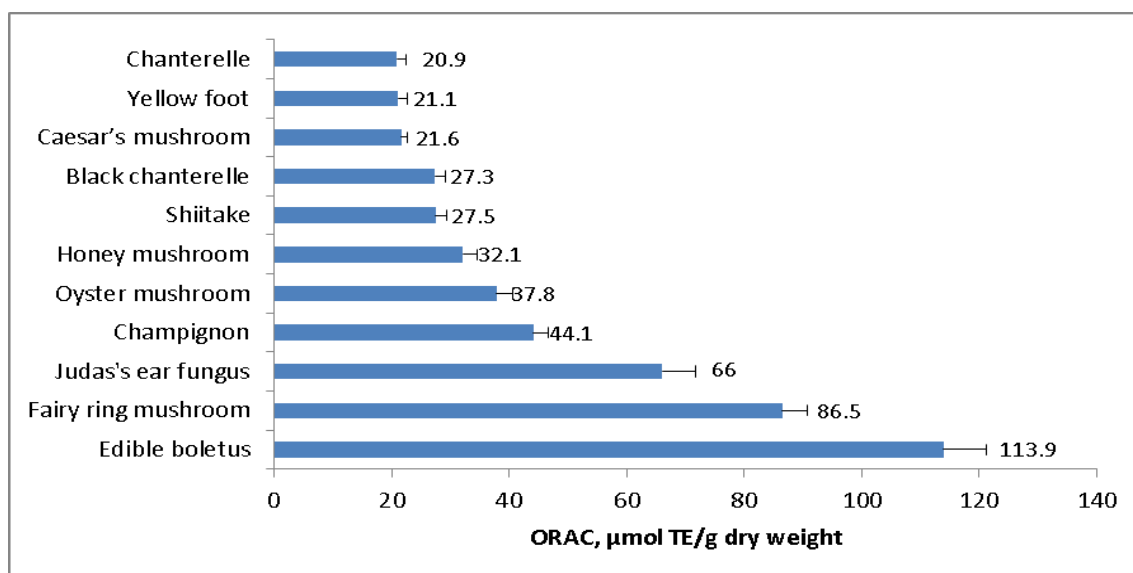


Fig. 1. ORAC antioxidant activity of Bulgarian mushrooms.

FINAL REMARKS

The results for the antioxidant activity of selected Bulgarian fruits, vegetables, herbs and mushrooms are a good tool for the medical

professionals to promote the consumption of foods with high antioxidant activity as a part of a healthy diet. Such kind of information is useful to not only doctors and nutritionists, but also to food scientist

and technologists for the development of functional foods, rich in natural antioxidants. These results enrich the national database for antioxidant activity in foods helping the identification of the major contributors to the antioxidant potential of Bulgarian daily diet.

REFERENCES

1. B. Halliwell, J. Gutteridge, Free radicals in biology and medicine 4th ed., Oxford Univ. Press. New York, 2007.
2. P. Denev, Ch. Kratchanov, M. Ciz, A. Lojek, M. Kratchanova, *Compr. Rev. Food Sci. F.*, **11**, 471 (2012).
3. M. Kirsch, *J. Biol. Chem.*, **278**, 24481 (2003).
4. J. Rifkind, *Antiox. Redox. Sign.*, **6**, 657 (2004).
5. C. von Sonntag, The chemical basis of radiation biology, Taylor and Francis, London, 1987.
6. L. K. Folkes, L. P. Candeias, P. Wardman, *Arch. Biochem. Biophys.*, **323**, 120 (1995).
7. L. G. Forni, R. L. Willson, *Biochem. J.*, **240**, 897 (1986).
8. D. Huang, B. Ou, R. L. Prior, *J. Agric. Food. Chem.*, **53**, 1841 (2005).
9. K. J. Davies, *IUBM Life*, **50**, 279 (2000).
10. T. Fenkel, N.J. Holbrook, *Nature*, **408**, 240 (2000).
11. L. M. Sayre, G. Perry, M. A. Smith, *Chem. Res. Toxicol.*, **21**, 172 (2008).
12. I. Ellingsen, E. Hjerkin, I. Seljeflot, H. Arnesen, S. Tonstad., *Brit. J. Nutr.*, **99**, 674 (2008).
13. T. Rissanen, S. Voutilainen, J. Virtanen, B. Venho, M. Vanharanta, J. Mursu, J. Salonen, *J. Nutr.*, **133**, 199 (2003).
14. J. A. Ross, C. M. Kasum, *Annu. Rev. Nutr.*, **22**, 19 (2002).
15. J. B. Harborne, N. W. Simmonds, Biochemistry of phenolic compounds, London: Acad. Press, London, 1964, p 101.
16. R. L. Prior, X. Wu, K. Schaich, *J. Agric. Food Chem.*, **53**, 4290 (2005).
17. J. K. Willcox, S. L. Ash, G. L. Catignani, *Crit. Rev. Food Sci. Nutr.*, **44**, 275 (2004).
18. I. T. Johnson: in Antioxidants in food, Woodhead Publishing Ltd, Cambridge, 2001, p. 100.
19. G. M Cragg, D. J. Newman, R. B. Weiss, *Semin. Oncol.*, **24**, 156 (1997).
20. P. Dimkov, Bulgarska Narodna Medicina, BAN, Sofia, 1979, p. 677.
21. V Petkov, Modern Phytotherapy, Meditzina, Sofia, 1982, p 516.
22. B. X., Ou, M. Hampsch-Woodill, R. L. Prior, *J. Agric. Food Chem.*, **49**, 4619 (2001).
23. C. C. Wang, C. Y. Chu, K. O. Chu, K. W. Choy, K. S. Khaw, M. S. Rogers, C. P. Pang, *Clin. Chem.*, **50**, 952 (2004).
24. M. Číž, H. Čížová, P. Denev, M. Kratchanova, A. Slavov, A. Lojek, *Food Control*, **21**, 518 (2010).
25. B. Ou, D. Huang, M. Hampsch-Woodill, J. A. Flanagan, E. K. Deemer, *J. Agric. Food Chem.*, **50**, 3122 (2002).
26. X. Wu, L. Gu, J. Holden, D. Haytowitz, S. Gebhardt, G. Beecher, R. L. Prior, *J. Food Compos. Anal.*, **1**, 407 (2004).
27. H. Speisky, C. López-Alarcón, M. Gómez, J. Fuentes, C. Sandoval-Acuña. *J. Agric. Food Chem.*, **60**, 8851 (2012).
28. P. Denev, A Lojek, M. Ciz, M. Kratchanova, *Bulg. J. Agric. Sci.*, **19**, 22 (2013).
29. Y. Velioglu, G. Mazza, L. Gao, B. Oomah, *J. Agric. Food Chem.*, **46**, 4113 (1998).
30. N. Pellegrini, M. Serafini, B. Colombi, D. Del Rio, S. Salvatore, M. Bianchi, F. Brighenti. *J. Nutri.*, **133**, 2812 (2003).
31. H. Wang, G. Cao, R. L. Prior, *J. Agric. Food Chem.*, **44**, 701 (1996).
32. R. L. Prior, H. Hoang, L. Gu, X. Wu, J. R. Jacob, G. Sotoudeh, A. Kader, R. Cook, *J. Am. Coll. Nutr.*, **269**, 170 (2007).
33. S. B. Lotito, B. Frei, *Free Rad. Biol. Med.*, **41**, 1727 (2006).
34. B. Shan, Y. Z. Cai, M. Sun, H. Corke, *J Agric. Food Chem.*, **53**, 7749 (2005).
35. D. Ivanova, D. Gerova, T. Chervenkov, T. Yankova, *J. Ethnopharm.*, **96**, 145 (2005).
36. Y. Kiselova, D. Ivanova, T. Chervenkov, D. Gerova, B. Galunska, T. Yankova, *Phytother. Res.*, **20**, 961 (2006).
37. M. Kratchanova, P. Denev, M. Ciz, A. Lojek, A. Mihailov, *Acta Biochim. Pol.*, **57**, 229 (2010).

ORAC АНТИОКСИДАНТНА АКТИВНОСТ НА БЪЛГАРСКИ ПЛОДОВЕ, ЗЕЛЕНЧУЦИ, БИЛКИ И ГЪБИ. ОБЗОР

П. Н. Денев*

Институт по Органична Химия с Център по Фитохимия, Българска Академия на Науките, Лаборатория по Биологично Активни Вещества, бул. „Руски“ 139, 4000 Пловдив, България

Постъпила на 13 февруари 2017 г.; Коригирана на 07 март 2017 г.

(Резюме)

В търсене на нови източници на антиоксиданти през последните години, растителните храни са обект на задълбочени изследвания по отношение на тяхната антиоксидантна активност. Изучаването на природни продукти е научно направление с голям потенциал и е особено важно за страни, които притежават богато биологично разнообразие, като България. Около 600 вида растения от българската флора са признати като лечебни и се използват традиционно в етнофармакологията и фитотерапията. Като се има предвид огромния интерес към антиоксидантите, не е изненадващ и големия брой методи, разработени, за да се направи количествена оценка на тяхното антиоксидантно действие. В резултат са разработени десетки методи за определяне на антиоксидантна активност в хранителни и биологични проби. Резултатите, представени в настоящия обзор са част от дългогодишно изследване в Лаборатория по биологично активни вещества, Институт по органична химия с Център по фитохимия - Българска Академия на Науките върху антиоксидантната активност на български плодове, зеленчуци, билки и гъби. Резултатите са получени чрез Oxygen Radical Absorbance Capacity метода, при който окислителната реакция протича практически до край отчитайки и времето, и степента на инхибиране. Установено е, че ORAC методът е подходящ за биологични проби, тъй като измерва радикало-улавящата способност на антиоксидантите срещу пероскилни радикали, които са физиологически най-значими. Освен това, окислителната реакция протича във водна среда при физиологични стойности на рН и температура. Настоящият обзор обобщава данните за антиоксидантната активност на 90 български суровини, включвайки и непубликувани до момента резултати за ORAC стойността на 11 гъби, 4 зеленчука и 2 билки.

BULGARIAN CHEMICAL COMMUNICATIONS

Instructions about Preparation of Manuscripts

General remarks: Manuscripts are submitted in English by e-mail or by mail (in duplicate). The text must be typed double-spaced, on A4 format paper using Times New Roman font size 12, normal character spacing. The manuscript should not exceed 15 pages (about 3500 words), including photographs, tables, drawings, formulae, etc. Authors are requested to use margins of 3 cm on all sides. For mail submission hard copies, made by a clearly legible duplication process, are requested. Manuscripts should be subdivided into labelled sections, e.g. **Introduction, Experimental, Results and Discussion, etc.**

The title page comprises headline, author's names and affiliations, abstract and key words.

Attention is drawn to the following:

a) **The title** of the manuscript should reflect concisely the purpose and findings of the work. Abbreviations, symbols, chemical formulas, references and footnotes should be avoided. If indispensable, abbreviations and formulas should be given in parentheses immediately after the respective full form.

b) **The author's** first and middle name initials, and family name in full should be given, followed by the address (or addresses) of the contributing laboratory (laboratories). **The affiliation** of the author(s) should be listed in detail (no abbreviations!). The author to whom correspondence and/or inquiries should be sent should be indicated by asterisk (*).

The abstract should be self-explanatory and intelligible without any references to the text and containing not more than 250 words. It should be followed by key words (not more than six).

References should be numbered sequentially in the order, in which they are cited in the text. The numbers in the text should be enclosed in brackets [2], [5, 6], [9–12], etc., set on the text line. References, typed with double spacing, are to be listed in numerical order on a separate sheet. All references are to be given in Latin letters. The names of the authors are given without inversion. Titles of journals must be abbreviated according to Chemical Abstracts and given in italics, the volume is typed in bold, the initial page is given and the year in parentheses. Attention is drawn to the following conventions:

a) The names of all authors of a certain publications should be given. The use of "*et al.*" in the list of references is not acceptable.

b) Only the initials of the first and middle names should be given.

In the manuscripts, the reference to author(s) of cited works should be made without giving initials, e.g. "Bush and Smith [7] pioneered...". If the reference carries the names of three or more authors it should be quoted as "Bush *et al.* [7]", if Bush is the first author, or as "Bush and co-workers [7]", if Bush is the senior author.

Footnotes should be reduced to a minimum. Each footnote should be typed double-spaced at the bottom of the page, on which its subject is first mentioned.

Tables are numbered with Arabic numerals on the left-hand top. Each table should be referred to in the text. Column headings should be as short as possible but they must define units unambiguously. The units are to be separated from the preceding symbols by a comma or brackets.

Note: The following format should be used when figures, equations, etc. are referred to the text (followed by the respective numbers): Fig., Eqns., Table, Scheme.

Schemes and figures. Each manuscript (hard copy) should contain or be accompanied by the respective illustrative material as well as by the respective figure captions in a separate file (sheet). As far as presentation of units is concerned, SI units are to be used. However, some non-SI units are also acceptable, such as °C, ml, l, etc.

The author(s) name(s), the title of the manuscript, the number of drawings, photographs, diagrams, etc., should be written in black pencil on the back of the illustrative material (hard copies) in accordance with the list enclosed. Avoid using more than 6 (12 for reviews, respectively) figures in the manuscript. Since most of the illustrative materials are to be presented as 8-cm wide pictures, attention should be paid that all axis titles, numerals, legend(s) and texts are legible.

The authors are asked to submit **the final text** (after the manuscript has been accepted for publication) in electronic form either by e-mail or

mail on a 3.5" diskette (CD) using a PC Word-processor. The main text, list of references, tables and figure captions should be saved in separate files (as *.rtf or *.doc) with clearly identifiable file names. It is essential that the name and version of the word-processing program and the format of the text files is clearly indicated. It is recommended that the pictures are presented in *.tif, *.jpg, *.cdr or *.bmp format, the equations are written using "Equation Editor" and chemical reaction schemes are written using ISIS Draw or ChemDraw programme.

The authors are required to submit the final text with a list of three individuals and their e-mail addresses that can be considered by the Editors as potential reviewers. Please, note that the reviewers should be outside the authors' own institution or organization. The Editorial Board of the journal is not obliged to accept these proposals.

EXAMPLES FOR PRESENTATION OF REFERENCES

REFERENCES

1. D. S. Newsome, *Catal. Rev.–Sci. Eng.*, **21**, 275 (1980).
2. C.-H. Lin, C.-Y. Hsu, *J. Chem. Soc. Chem. Commun.*, 1479 (1992).
3. R. G. Parr, W. Yang, *Density Functional Theory of Atoms and Molecules*, Oxford Univ. Press, New York, 1989.
4. V. Ponec, G. C. Bond, *Catalysis by Metals and Alloys* (Stud. Surf. Sci. Catal., vol. 95), Elsevier, Amsterdam, 1995.
5. G. Kadinov, S. Todorova, A. Palazov, in: *New Frontiers in Catalysis* (Proc. 10th Int. Congr. Catal., Budapest, 1992), L. Guzzi, F. Solymosi, P. Tetenyi (eds.), Akademiai Kiado, Budapest, 1993, Part C, p. 2817.
6. G. L. C. Maire, F. Garin, in: *Catalysis. Science and Technology*, J. R. Anderson, M. Boudart (eds), vol. 6, Springer-Verlag, Berlin, 1984, p. 161.
7. D. Pocknell, *GB Patent 2 207 355* (1949).
8. G. Angelov, PhD Thesis, UCTM, Sofia, 2001.
9. JCPDS International Center for Diffraction Data, *Power Diffraction File*, Swarthmore, PA, 1991.
10. *CA* **127**, 184 762q (1998).
11. P. Hou, H. Wise, *J. Catal.*, in press.
12. M. Sinev, private communication.
13. <http://www.chemweb.com/alchem/articles/1051611477211.html>.

CONTENTS

<i>I. Pojarlieff</i> , Professor Bogdan Jordanov Kurtev, Member of BAS - Builder of Modern Organic Chemistry in Bulgaria	5
<i>I. Zagranyarska, K. Kostova, A. Chimov, V. Dimitrov</i> , Diastereoselective addition of functionalized organolithium compounds to (-)-menthone – synthesis of chiral ligands for enantioselective addition of diethylzinc to aldehydes	10
<i>A. Petrova, M. Pancheva, K. Kostova, I. Zagranyarska, M. Tavlinova-Kirilova, V. Dimitrov</i> , Stereoselective functionalization strategy of 2,5-diketopiperazine derived from L-proline and glycine	18
<i>H. H. Hasanov, I. K. Ivanov, V. Ch. Christov</i> , Bifunctionalized allenes. Part XX. A convenient and efficient regioselective synthesis of phosphorylated 3-(α -hydroxyalkyl)allenes	25
<i>I. E. Ismailov, I. K. Ivanov, V. Ch. Christov</i> , Part I. A convenient and efficient regioselective synthesis of 4-phosphorylated 5-hydroxyalka-2,3-dienoates	33
<i>M. Dangelov, P. Petrov, N. G. Vassilev</i> , Naphthalimide-based platinum(II) and palladium(II) N-heterocyclic carbene complexes: synthesis and structural elucidation	42
<i>R. H. Lyapchev, M. G. Dangelov, N. G. Vassilev, P. Y. Petrov</i> , Synthesis and structural characterization of <i>N</i> -[2-(diphenylphosphorothioyl)phenyl]-2-(phenylamino)benzamide	50
<i>T. I. Baramov, N. T. Burdzhiev, B. T. Pandova, V. Z. Todorova, S. G. Yanev, E. R. Stanoeva, C. D. Chaney</i> , Synthesis of bioactive amino acid derivatives of <i>trans</i> -5-aminomethyl-1-benzyl-6-phenylpiperidin-2-one	55
<i>S. M. Bakalova, J. Kaneti</i> , Stereoselectivity in the Diels–Alder addition of <i>S</i> -hydroxy- <i>N</i> -methylsuccinimide acrylate to cyclopentadiene: origins and DFT computational models	64
<i>M. S. Gerova, E. A. Aleksandrova, Y. B. Ivanova, D. V. Stanisheva, G. Ts. Momekov, O. I. Petrov</i> , Synthesis and cytotoxic activity of new heterocyclic analogues of resveratrol, containing benzoxazolone ring	71
<i>I. Grabchev, T. Gajda, S. Yordanova, S. Purák, E. Vasileva-Tonkova, S. Stoyanov</i> , Synthesis, characterization and microbiological activity of a Zn(II) complex of a novel benzofurazan derivative	76
<i>B. I. Nikolova-Mladenova, G. Ts. Momekov</i> , Synthesis, characterization and <i>in vitro</i> cytotoxic activity of zinc(II), cobalt(II) and nickel(II) complexes with tridentate ONO Schiff base 3-methoxysalicylaldehyde benzoylhydrazone	83
<i>E. Cherneva, A. Bakalova, R. Michailova, B. Nikolova-Mladenova</i> , Preparation, characterization, theoretical investigation and cytotoxic activity of new mixed ammine/amine platinum complexes with 3-amino-5-methyl-5-phenylhydantoin	89
<i>P. D. Katsarov, B. A. Pilicheva, Y. I. Uzunova, G. H. Gergov, M. I. Kassarova</i> , Doxylamine/pyridoxine loaded chitosan microspheres as potential nasal drug delivery systems	96
<i>S. P. Simeonov, S. D. Simova, B. L. Shivachev, R. P. Nikolova, V. B. Kurteva</i> , Solution and solid state characterization of “sparteine surrogate” (+)-(1 <i>R</i> ,5 <i>S</i> ,11 <i>aS</i>)-tetrahydrodeoxocytisine	103
<i>A. Trendafilova, M. Todorova, A. Vitkova</i> , Flavonoid glycosides and free radical scavenging activity of Bulgarian endemic <i>Alchemilla jumrukczalica</i> Pawl.	111
<i>M. Popova, B. Trusheva, V. Bankova</i> , Content of biologically active compounds in Bulgarian propolis: a basis for its standardization	115
<i>P. N. Denev, I. I. Uchkunov, V. I. Uchkunov, M. G. Kratchanova</i> , Content of steviol glycosides in stevia (<i>Stevia Rebaudiana</i> B.) genotypes cultivated in Bulgaria	121
<i>S. Taneva, A. Konakchiev, I. Totzeva, M. Kamenova-Nacheva, Y. Nikolova, S. Momchilova, V. Dimitrov</i> , Super-critical carbon dioxide extraction as an effective green technology for production of high quality rose hip oil	126
<i>M. Guncheva, D. Yancheva, P. Ossowicz, E. Janus</i> , Structural basis for the inactivation of <i>Candida rugosa</i> lipase in the presence of amino acid ionic liquids	132
<i>D. Y. Yancheva, S. S. Stoyanov, E. A. Velcheva, B. A. Stamboliyska, A. Smelcerovic</i> , DFT study on the radical scavenging capacity of apocynin with different free radicals	137
<i>P. Ivanov, Ch. Tsvetanov</i> , Conformational analysis of oligomers of non-ionic thermoresponsive polymers containing amide groups	145
<i>G. Meracheva, M. Stefanova, S. P. Marinov, E. Zaneva-Dobranova</i> , Geochemical appraisal of hydrocarbon generative potential of Bulgarian part from the Thrace Basin: I. Linear biomarkers	151
<i>G. Meracheva, M. Stefanova, S. P. Marinov, E. Zaneva-Dobranova</i> , Geochemical appraisal of hydrocarbon generative potential of Bulgarian part from the Thrace Basin: II. Cyclic biomarkers	159
<i>T. S. Tsoncheva, G. S. Issa, A. B. Mileva, R. N. Ivanova, M. D. Dimitrov, I. P. Spassova, D. G. Kovatcheva, D. G. Paneva, N. I. Velinov, B. G. Tsyntsarski, N. V. Petrov</i> , Copper, zinc and manganese spinel ferrites hosted in activated carbon from waste biomass as catalysts for hydrogen release from methanol	167
<i>R. N. Ivanova, T. S. Tsoncheva</i> , Total oxidation of ethyl acetate on nanostructured manganese-cerium oxide catalysts supported on mesoporous silica	176
<i>V. N. Blaskov, I. D. Stambolova, K. I. Milenova, K. L. Zaharieva, L. D. Dimitrov, D. D. Stoyanova, A. E. Eliyas</i> , The photodegradation of Methylene Blue and Methyl Orange dyes and their mixture by ZnO obtained by	183

hydrothermally activated precipitates	188
<i>I. Koseva, V. Nikolov, A. Yordanova, P. Tzvetkov, N. Petrova</i> , Thermal behavior of some germanates with non-olivine structure	188
<i>K. I. Milenova, I. A. Avramova, P. M. Nikolov, N. A. Kasabova, G. M. Ivanov</i> , Doped with Cu and Mn zinc oxide catalysts for oxidation of CO in noxious gas emissions	193
<i>P. N. Denev</i> , Oxygen Radical Absorbance Capacity of Bulgarian fruits, vegetables, herbs and mushrooms. A review	199
INSTRUCTIONS TO THE AUTHORS	207

СЪДЪРЖАНИЕ

<i>И. Пожарлиев</i> , Професор Богдан Йорданов Куртев, Академик на БАН – Строител на модерната органична химия в България	5
<i>И. Загранярска, К. Костова, А. Чимов, В. Димитров</i> , Диастереоселективно присъединяване на функционализирани органолитиеви съединения към (-)-ментон – синтез на хирални лиганди за енантоселективно присъединяване на диетилцинк към алдехиди	10
<i>А. Петрова, М. Панчева, К. Костова, И. Загранярска, М. Тавлинова-Кирилова, В. Димитров</i> , Стратегия за стереоселективно функционализиране на 2,5-дикетопиперазин получен от l-пролин и глицин	18
<i>Х. Х. Хасанов, И. К. Иванов, В. Х. Христов</i> , Бифункционализирани алени. Част XX. Удобен и ефективен региоселективен синтез на фосфорилирани 3-(α -хидроксиалкил)алени	25
<i>И. Е. Исмаилов, И. К. Иванов, В. Х. Христов</i> , Трифункционализирани алени. Част I. Удобен и ефикасен региоселективен синтез на 4-фосфорилирани 5-хидроксиалка-2,3-диеноати	33
<i>М. Дангалов, П. Петров, Н. Г. Василев</i> , Нафталимид-базирани платинови(II) и паладиеви(II) N-хетероциклени карбенови комплекси: синтез и доказване на структурата	42
<i>Р. Хр. Ляпчев, М. Г. Дангалов, Н. Г. Василев, П. Й. Петров</i> , Синтез и структурно охарактеризиране на N-(2-(дифенилфосфоритоил)фенил)-2-(фениламино)бензамид	50
<i>Т. И. Баръмов, Н. Т. Бурджиев, Б. Т. Пандова, В. Ц. Тодорова, С. Г. Янев, Е. Р. Станоева, Х. Д. Чанев</i> , Синтез на биоактивни аминокиселинни производни на <i>транс</i> -5-аминометил-1-бензил-6-фенилпиперидин-2-он	55
<i>С. М. Бакалова, Х. Канети</i> , Стереоселективност на Дилс–Алдеровото присъединяване на [S]-акрилоил-N-метил сукцинимид и циклопентадиен: произход и изчислително моделиране в рамките на теорията на функционала на плътността	64
<i>М. С. Герова, Е. А. Александрова, Й. Б. Иванова, Д. В. Станишева, Г. Цв. Момеров, О. И. Петров</i> , Синтез и цитотоксична активност на нови хетероциклени аналози на ресвератрол, съдържащи бензоксазолонов пръстен	71
<i>И. Грабчев, Т. Гайда, С. Йорданова, С. Пурак, Е. Василева-Тонкова, С. Стоянов</i> , Синтез, охарактеризиране и микробиологична активност на нов Zn(II) комплекс с производно на бензофуразана .	76
<i>Б. И. Николова-Младенова, Г. Цв. Момеров</i> , Синтез, охарактеризиране и <i>in vitro</i> цитотоксична активност на Zn(II), Co(II) И Ni(II) комплекси с тридентатния ONO-лиганд 3-метоксисалицилалдехид бензоилхидразон	83
<i>Е. Чернева, А. Бакалова, Р. Михайлова, Б. Николова-Младенова</i> , Получаване, охарактеризиране, теоретично изследване и цитотоксична активност на нови смесени платинови комплекси с 3-амино-5-метил-5-фенилхидантоин	89
<i>П. Д. Кацаров, Б. А. Пиличева, Й. И. Узунова, Г. Х. Гергов, М. И. Касърова</i> , Микросфери от хитозан с доксиламин и пиридоксин – потенциални лекарство-доставящи системи за назално приложение	96
<i>С. П. Симеонов, С. Д. Симова, Б. Л. Шивачев, Р. Н. Петрова, В. Б. Куртева</i> , Охарактеризиране в разтвор и твърдо състояние на “спартеиновия сурогат” (+)-(1R,5S,11aS)-тетрахидродеоксоцитизин	103
<i>А. Трендафилова, М. Тодорова, А. Виткова</i> , Флавоноидни гликозиди и антирадикалова активност на българския ендемичен вид <i>Alchemilla jurtukczalica</i> Pawl.	111
<i>М. Попова, Б. Трушева, В. Банкова</i> , Съдържание на биологично активни съединения в български прополис – основа за стандартизацията му	115
<i>П. Н. Денев, И. И. Учкунув, В. И. Учкунув, М. Г. Крачанова</i> , Съдържание на стевиол гликозиди в генотипове стевия (<i>Stevia Rebaudiana</i> V.), култивирани в България	121
<i>С. Танева, А. Конакчиев, И. Тоцева, М. Каменова-Начева, Я. Николова, Св. Момчилова, Вл. Димитров</i> , Екстракцията със супер-критичен въглероден диоксид като ефективна „зелена“ технология за получаване на висококачествено шипково масло	126
<i>М. Гунчева, Д. Янчева, П. Осовиц, Е. Янус</i> , Обяснение на разликите в активността на липаза от <i>Candida rugosa</i> в присъствие на йонни течности на основата на аминокиселини чрез промени в протеиновата конформация	132
<i>Д. Я. Янчева, С. С. Стоянов, Е. А. Велчева, Б. А. Стамболийска, А. Шмелцерович</i> , Теоретично изследване на радикал-улавящата способност на апоцинин спрямо различни свободни радикали	137
<i>П. Иванов, Хр. Цветанов</i> , Конформационен анализ на олигомери на нейногенни термочувствителни полимери съдържащи amidни групи	145
<i>Г. Мерачева, М. Стефанова, С. П. Маринов, Е. Занева-Добранова</i> , Геохимична оценка на въглеродород генериращия потенциал на българската част от тракийския басейн: I. Линейни биомаркери	151
<i>Г. Мерачева, М. Стефанова, С. П. Маринов, Е. Занева-Добранова</i> , Геохимична оценка на въглеродород генериращия потенциал на българската част от тракийския басейн: II. Циклични биомаркери	159
<i>Т. С. Цончева, Г. С. Исса, А. Б. Милева, Р. Н. Иванова, М. Д. Димитров, И. П. Спасова, Д. Г. Ковачева, Д. Г. Панева, Н. И. Велинов, Б. Г. Цинцарски, Н. В. Петров</i> , Катализатори за освобождаване на водород от	167

метанол на основата на меден, цинков и манганов шпинелни ферити, нанесени върху активен въглен от отпадна биомаса	
<i>Р. Н. Иванова, Т. С. Дончева</i> , Пълно окисление на етилацетат върху наноструктурирани манган-цериево оксидни катализатори нанесени върху мезопорести силикати	176
<i>В. Н. Блъсков, И. Д. Стамболова, К. И. Миленова, К. Л. Захариева, Л. Д. Димитров, Д. Д. Стоянова, А. Е. Елиаз</i> , Фотокаталитично разграждане на метиленово синьо и метил оранжево багрила и тяхната смес чрез ZnO, получен от хидротермално активирана утайка	183
<i>Й. Косева, В. Николов, А. Йорданова, П. Цветков, Н. Петрова</i> , Термично поведение на някои германати с неоливинова структура	188
<i>К. И. Миленова, И. А. Аврамова, П. М. Николов, Н. А. Касабова, Г. М. Иванов</i> , Дотирани с Cu и Mn цинково оксидни катализатори за окисление на CO във вредни газове емисии	193
<i>П. Н. Денев</i> , ORAC антиоксидантна активност на български плодове, зеленчуци, билки и гъби. Обзор	199
ИНСТРУКЦИЯ ЗА АВТОРИТЕ	207